

THE JOURNAL OF PHYSICAL CHEMISTRY

(Registered in U. S. Patent Office)

CONTENTS

A. C. Andrews and J. S. Cantrell: Dehydration Kinetics of 2-Butanol over a Copper-Chromium Oxide Catalyst.	1089	patrick: The Kinetics of the Reactions of Aromatic Hydrocarbons in Sulfuric Acid. III. Mesitylene.	1189
A. E. Simchen: The Fusion Point and the Thermal Decomposition of $KClO_4$	1093	F. Holtzberg and A. Reisman: Sub-Solidus Equilibria in the System $Nb_2O_5-Ta_2O_5$	1192
R. E. Thoma, C. F. Weaver, H. A. Friedman, H. Insley, L. A. Harris and H. A. Yakel, Jr.: Phase Equilibria in the System $LiF-YF_3$	1096	Robert H. Linnell and A. Kaczmarczyk: Ultraviolet Spectra of $-N=C-C=N-$ Compounds.	1196
J. L. Ryan: Anion Exchange and Non-Aqueous Studies of the Anionic Nitrate Complexes of the Hexavalent Actinides.	1099	Pranjivan V. Popat and Norman Hackerman: Electrical Double Layer Capacity of Passive Iron and Stainless Steel Electrodes.	1201
Karol J. Mysels, Michael C. Cox and John D. Skewis: The Measurement of Film Elasticity.	1107	Richard J. Neddenriep and John E. Willard: The Radiolysis of Normal Propyl Bromide.	1206
J. de D. Lopez-Gonzales, F. G. Carpenter and V. R. Deitz: Adsorption of Nitrogen and Argon on Mineralogical Graphite and Diamond.	1112	David A. Aikens and James W. Ross, Jr.: Effect of Chloride on the Kinetics of Electro-Oxidation of Chromium(II) in Acidic Perchlorate Medium.	1213
Akiyoshi Wada, Masamichi Tsuboi and Emiko Konishi: Optical Rotatory Dispersion of the β -Form of the Polypeptide Chain.	1119	Robert E. Connick and Armine D. Paul: The Fluoride Complexes of Silver and Stannous Ions in Aqueous Solution.	1216
S. Ruven Smith and Alvin S. Gordon: A Study of the Pyrolysis of Cyclohexene.	1124	H. R. Bronstein and M. A. Bredig: The Electrical Conductivity of Solutions of Metals in their Molten Halides. II. Sodium-Sodium Iodide, Potassium-Potassium Iodide, and Potassium-Potassium Fluoride.	1220
R. P. Gupta: Nuclear Magnetic Resonance Study of some Liquid-containing Poly-(hexamethylene adipamides).	1128	Mario Ciampolini and Piero Paoletti: Thermochemical Studies. V. Heats of Stepwise Neutralization of Ethylenediamine and Diethylenetriamine.	1224
Ralph A. Zingaro and Richard M. Hedges: Phosphine Oxide-Halogen Complexes: Effect on P-O and P-S Stretching Frequencies.	1132	K. Nishikawa, D. Patterson and G. Delmas: Critical Phenomena in Thin Films Using the Bragg-Williams Approximation.	1226
James B. Ifft, Donald H. Voet and Jerome Vinograd: The Determination of Density Distributions and Density Gradients in Binary Solutions at Equilibrium in the Ultracentrifuge.	1138	Joshua Jortner, Raphael Levine, Michael Ottolenghi and Gabriel Stein: The Photochemistry of the Iodide Ion in Aqueous Solution.	1232
Marvin F. L. Johnson and John S. Meik: Dealkylation of <i>t</i> -Butylbenzene by Cracking Catalysts.	1146	Ivan E. Lichtenstein and Thomas L. Allen: The Nature of the Chromium(VI)-1,5-Diphenylcarbohydrazide Reaction. II. The Chromium-(II)-Diphenylcarbazone Reaction.	1238
E. W. Balson: Some Aspects of Molecular Effusion.	1151	Ricci J. Larese and William J. Canady: Thermodynamics of Solution of Hippuric Acid in Water and in Various Sodium Chloride Solutions.	1240
Remolo Ciola and Robert L. Burwell, Jr.: Hydrogenation of 3,3-Dimethyl-1,4-pentadiene on Nickel Catalysts. A Test of the Degree of Diffusional Control in Catalytic Hydrogenations.	1158	R. H. Stokes: The Conductance of Hydrochloric Acid at 25°.	1242
Hyung Kyu Shin and J. Calvin Giddings: Validity of the Steady-State Approximation in Unimolecular Reactions.	1164	N. Sutin, J. K. Rowley and R. W. Dodson: Chloride Complexes of Iron(III) Ions and the Kinetics of the Chloride-Catalyzed Exchange Reaction between Iron(II) and Iron(III) Ions in Light and Heavy Water.	1248
H. D. Fisher, W. J. Lehmann, and I. Shapiro: Trifluoroboroxine: Preparation, Infrared Spectrum, and Structure.	1166	Mitsugi Senda, Hideo Imai and Paul Delahay: Faradaic Rectification and Electrode Processes. II.	1253
Elliott Greenberg, Jack L. Settle, Harold M. Feder and Ward N. Hubbard: Fluorine Bomb Calorimetry: I. The Heat of Formation of Zirconium Tetrafluoride.	1168	S. W. Rabideau and B. J. Masters: Kinetics of the Reaction Between Pu(VI) and Sn(II) in Chloride-Perchlorate Solution.	1256
W. L. Medlin: Thermoluminescence in Aragonite and Magnesite.	1172	P. E. Eberly, Jr.: Measurement of Adsorption Isotherms and Surface Areas by Continuous Flow Method.	1261
Emilio Gallegos and Robert W. Kiser: Electron Impact Spectroscopy of Ethylene Sulfide and Ethylenimine.	1177	Edward P. Egan, Jr., Zachary T. Wakefield and Basil B. Luff: Low Temperature Heat Capacity, Entropy and Heat of Formation of Crystalline and Colloidal Ferric Phosphate Dihydrate.	1265
M. K. Chappurey and P. H. Emmett: Study of the Hydrogenation of Ethylene over Homogenized Cu-Ni Alloy Films.	1182		
Michael Hoch and Herrick L. Johnston: The Heat Capacity of Aluminum Oxide from 1000 to 2000° and of Thorium Dioxide from 1000 to 2500°.	1184	NOTES	
R. B. Ellis, J. E. Smith, W. S. Wilcox, and E. H. Crook: The System Potassium Bromide-Cadmium Chloride. I. Surface Tension.	1186	Arnulf J. Maeland and Thomas R. P. Gibb, Jr.: X-Ray Diffraction Observations of the Pd-H ₂ System Through the Critical Region.	1270
Martin Kilpatrick, Max W. Meyer and Mary L. Kil-		Rameshwar Prasad and Arun K. Dey: Adsorption of Congo Red by Hydrous Thorium Oxide.	1272

THE JOURNAL OF PHYSICAL CHEMISTRY

(Registered in U. S. Patent Office)

W. ALBERT NOYES, JR., EDITOR

ALLEN D. BLISS

ASSISTANT EDITORS

A. B. F. DUNCAN

EDITORIAL BOARD

A. O. ALLEN
C. E. H. BAWN
J. BIGEISEN
D. D. ELEY

D. H. EVERETT
S. C. LIND
F. A. LONG
K. J. MYSELS

J. E. RICCI
R. E. RUNDLE
W. H. STOCKMAYER
A. R. UBBELOHDE

E. R. VAN ARTSDALEN
M. B. WALLENSTEIN
W. WEST
EDGAR F. WESTRUM, JR.

Published monthly by the American Chemical Society at 20th and Northampton Sts., Easton, Pa.

Second-class mail privileges authorized at Easton, Pa. This publication is authorized to be mailed at the special rates of postage prescribed by Section 131.122.

The *Journal of Physical Chemistry* is devoted to the publication of selected symposia in the broad field of physical chemistry and to other contributed papers.

Manuscripts originating in the British Isles, Europe and Africa should be sent to F. C. Tompkins, The Faraday Society, 6 Gray's Inn Square, London W. C. 1, England. Manuscripts originating elsewhere should be sent to W. Albert Noyes, Jr., Department of Chemistry, University of Rochester, Rochester 20, N. Y.

Correspondence regarding accepted copy, proofs and reprints should be directed to Assistant Editor, Allen D. Bliss, Department of Chemistry, Simmons College, 300 The Fenway, Boston 15, Mass.

Business Office: Alden H. Emery, Executive Secretary, American Chemical Society, 1155 Sixteenth St., N. W., Washington 6, D. C.

Advertising Office: Reinhold Publishing Corporation, 430 Park Avenue, New York 22, N. Y.

Articles must be submitted in duplicate, typed and double spaced. They should have at the beginning a brief Abstract, in no case exceeding 300 words. Original drawings should accompany the manuscript. Lettering at the sides of graphs (black on white or blue) may be pencilled in and will be typeset. Figures and tables should be held to a minimum consistent with adequate presentation of information. Photographs will not be printed on glossy paper except by special arrangement. All footnotes and references to the literature should be numbered consecutively and placed in the manuscript at the proper places. Initials of authors referred to in citations should be given. Nomenclature should conform to that used in *Chemical Abstracts*, mathematical characters be marked for italic, Greek letters carefully made or annotated, and subscripts and superscripts clearly shown. Articles should be written as briefly as possible consistent with clarity and should avoid historical background unnecessary for specialists.

Notes describe fragmentary or incomplete studies but do not otherwise differ fundamentally from articles and are subjected to the same editorial appraisal as are articles. In their preparation particular attention should be paid to brevity and conciseness. Material included in Notes must be definitive and may not be republished subsequently.

Communications to the Editor are designed to afford prompt preliminary publication of observations or discoveries whose value to science is so great that immediate publication is imperative. The appearance of related work from other laboratories is in itself not considered sufficient justification for the publication of a Communication, which must in addition meet special requirements of timeliness and significance.

Their total length may in no case exceed 1000 words or their equivalent. They differ from Articles and Notes in that their subject matter may be republished.

Symposium papers should be sent in all cases to Secretaries of Divisions sponsoring the symposium, who will be responsible for their transmittal to the Editor. The Secretary of the Division by agreement with the Editor will specify a time after which symposium papers cannot be accepted. The Editor reserves the right to refuse to publish symposium articles, for valid scientific reasons. Each symposium paper may not exceed four printed pages (about sixteen double spaced typewritten pages) in length except by prior arrangement with the Editor.

Remittances and orders for subscriptions and for single copies, notices of changes of address and new professional connections, and claims for missing numbers should be sent to the American Chemical Society, 1155 Sixteenth St., N. W., Washington 6, D. C. Changes of address for the *Journal of Physical Chemistry* must be received on or before the 30th of the preceding month.

Claims for missing numbers will not be allowed (1) if received more than sixty days from date of issue (because of delivery hazards, no claims can be honored from subscribers in Central Europe, Asia, or Pacific Islands other than Hawaii), (2) if loss was due to failure of notice of change of address to be received before the date specified in the preceding paragraph, or (3) if the reason for the claim is "missing from files."

Subscription rates (1961): members of American Chemical Society, \$12.00 for 1 year; to non-members, \$24.00 for 1 year. Postage to countries in the Pan-American Union \$0.80; Canada, \$0.40; all other countries, \$1.20. Single copies, current volume, \$2.50; foreign postage, \$0.15; Canadian postage \$0.10; Pan-American Union, \$0.10. Back volumes (Vol. 56-64) \$30.00 per volume; foreign postage, per volume \$1.20, Canadian, \$0.40; Pan-American Union, \$0.80. Single copies: back issues, \$3.00; for current year, \$2.50; postage, single copies: foreign, \$0.15; Canadian, \$0.10; Pan-American Union, \$0.10.

The American Chemical Society and the Editors of the *Journal of Physical Chemistry* assume no responsibility for the statements and opinions advanced by contributors to THIS JOURNAL.

The American Chemical Society also publishes *Journal of the American Chemical Society*, *Chemical Abstracts*, *Industrial and Engineering Chemistry*, International Edition of *Industrial and Engineering Chemistry*, *Chemical and Engineering News*, *Analytical Chemistry*, *Journal of Agricultural and Food Chemistry*, *Journal of Organic Chemistry*, *Journal of Chemical and Engineering Data*, *Chemical Reviews*, *Chemical Titles* and *Journal of Chemical Documentation*. Rates on request.

M. Judith Schmelz, M. Ann Gertrude Hill, and Columba Curran: Electric Moments of some Addition Compounds of Zinc Chloride with Organic Bases	1273
Irving M. Klotz and Joel W. Russell: The Effect of Urea on the Configuration of Polyvinylpyrrolidone	1274
V. J. Lyons and V. J. Silvestri: The Dissociation Pres-	

sure of GaAs	1275
R. H. Stokes: The Soret Effect as a Source of Error in Conductance Measurements	1277
Marriner K. Norr: The Lead Salt-Thiourea Reaction	1278
R. A. Robinson and V. E. Bower: The Ionization Constant of Hydroxylamine	1279

THE JOURNAL OF PHYSICAL CHEMISTRY

(Registered in U. S. Patent Office) (© Copyright, 1961, by the American Chemical Society)

VOLUME 65

JULY 26, 1961

NUMBER 7

DEHYDRATION KINETICS OF 2-BUTANOL OVER A COPPER-CHROMIUM OXIDE CATALYST

By A. C. ANDREWS AND J. S. CANTRELL¹

Department of Chemistry of Kansas State University, Manhattan, Kansas

Received July 16, 1960

When the temperature range of 500 to 700°K. was investigated the principal reaction of 2-butanol in the presence of a mixed copper-chromium oxide catalyst at temperatures between 600 and 700°K. was dehydration. The rate of water production, measured by a modified Karl Fischer reagent, was first order with respect to water produced. The heterogeneous gas-solid reaction was studied using a flow system and the flow rate equation of Neish. The specific reaction rate constant, k , ranged from 0.013 sec.⁻¹ at 498°K. to 0.945 sec.⁻¹ at 730°K. The activation energy was 13,000 cal. per mole, and the entropy of activation was -41.6 ± 0.3 e.u. at 600°K.

Introduction

Two reactions have been observed when vaporized 2-butanol was passed over a catalyst composed of copper oxide and chromium oxide mixed together.² One reaction was dehydration and the other was dehydrogenation. Dehydration was slight below 500°K., but was found to be the principal reaction at temperatures above 600°K. A kinetic study of the over-all reaction seemed warranted because of the predominance of this dehydration reaction at higher temperatures. The rate of water production was determined by analyzing the products for water utilizing a modified^{3c,4} form of the Karl Fischer (K.F.R.) reagent.

Experimental

The 2-butanol, Eastman, was dried over calcium carbide and then distilled through a six-inch Vigreux column. The fraction distilling at 98 and 100° was collected and mixed with approximately 10% by weight of the copper-chromium oxide catalyst to remove possible catalyst poisons. After a week the alcohol was filtered and redistilled and the same fraction was retained for use.

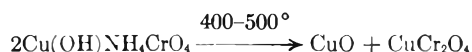
The catalyst, prepared according to the method of Connor, Folkers and Adkins^{2a} (37-KAF), was the same as that employed by Griebstein^{2b} in vapor phase dehydrogenation

kinetic studies of 2-butanol. Griebstein's values were reproduced for comparison during the course of this work. The catalyst is here referred to as copper-chromium oxide.² Stroupe^{2c} has given X-ray diffraction evidence for the presence of two oxides, CuO and CuCr₂O₄, in the catalyst.

This catalyst was produced as follows^{2b}: a solution was prepared by dissolving 31.3 g. (0.12 mole) of barium nitrate in 100 ml. of boiling distilled water. Then 261 g. (1.03 moles) of cupric nitrate trihydrate was added, diluted to 900 ml. with boiling distilled water, and the temperature held constant at 80° until all of the cupric nitrate had dissolved.

A second solution was prepared by adding 151.2 g. (0.6 mole) of ammonium dichromate to 225 ml. (3.33 moles) of concentrated ammonium hydroxide solution, stirred until all of the ammonium dichromate had dissolved, then diluted to 900 ml. with cold distilled water. The hot solution of cupric nitrate and barium nitrate was added slowly with stirring to the second solution. The heavy yellow-brown precipitate of basic copper ammonium chromate which formed immediately was filtered from the warm solution, and dried overnight at 75°. The resulting hard, dry mass was pulverized until it would pass a 20-mesh screen.

Portions of the yellow-brown precipitate were carefully heated. This decomposition of the chromate evolved considerable heat and the reaction became uncontrollable if the heat was not dissipated by stirring. Overheating would lead to a greenish colored product with very little catalytic activity. Controlled decomposition gave a finely divided brownish-black powder. This was stirred into 600 ml. of a 10% acetic acid solution, allowed to stand for 30 minutes, filtered, washed six times with 100-ml. portions of distilled water and dried overnight at 125°. Thorough washing with dilute acetic acid and water was necessary to remove residual undecomposed basic copper ammonium chromate from the catalyst. Six preparations, combined to give a yield of 1074 g., were made and mixed together by pulverizing to give the catalyst used in these dehydration studies.



(1) Abstracted in part from a Thesis submitted for the degree of Master of Science at Kansas State University.

(2) (a) R. Connor, K. Folkers and H. Adkins, *J. Am. Chem. Soc.*, **54**, 1138 (1932); (b) W. J. Griebstein, Ph.D. Dissertation, Kansas State University, 1953; (c) J. D. Stroupe, *J. Am. Chem. Soc.*, **71**, 569 (1949).

(3) J. Mitchell, Jr., and D. M. Smith, "Aquametry," Interscience Publishers, New York, N. Y., 1948; (a) p. 86; (b) p. 94; (c) p. 147; (d) p. 121.

(4) G. Wernimont and F. J. Hopkinson, *Ind. Eng. Chem., Anal. Ed.*, **15**, 272 (1943).

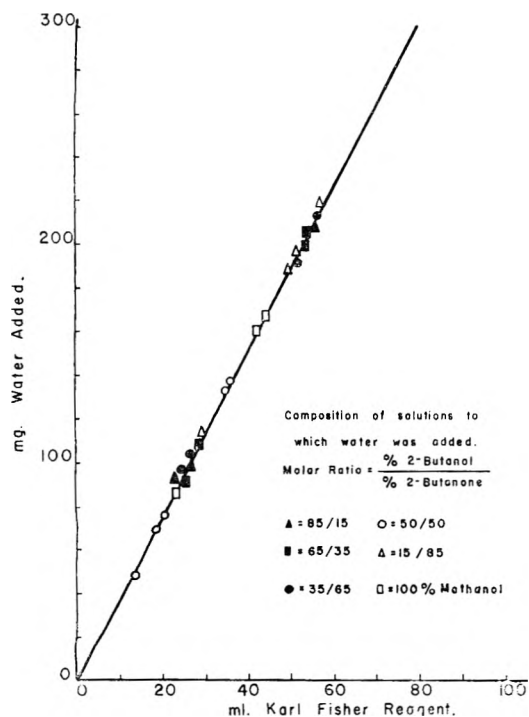


Fig. 1.—Calibration of the modified Karl Fischer reagent in the kinetic system.

Barium nitrate is used to replace 10% of the cupric nitrate in order to make the catalyst more resistant to loss of activity on use.^{2a} The chemicals: barium nitrate, cupric nitrate and ammonium dichromate, were all J. T. Baker Analyzed Reagents and used as purchased.

The procedure outlined by Thomas⁵ for determination of the active surface area of a catalyst by titration with KOH was employed here. Five grams of the catalyst was shaken with 200 ml. of previously standardized, 0.1 *N* KOH. A 20-ml. aliquot was taken and titrated with standard, 0.1 *N* HCl using three different indicators, methyl orange, methyl red and phenolphthalein. For nine determinations the average amount of base neutralized by the catalyst was 6.0 milliequivalents. Assuming the active sites to be Lewis acid in nature, the milliequivalents of base titrated correspond to the number of active sites on the surface of the 5 g. of catalyst used. The number of active sites calculated by this method is 3.61×10^{21} , $\pm 0.06 \times 10^{21}$.

The modified K.F.R.^{3c} (M.K.F.R.) of Wernimont and Hopkinson⁴ was employed. It contained 87.4 g. of iodine, 920 ml. of pyridine, 30 ml. of methyl alcohol and 45 ml. of liquid sulfur dioxide. The pyridine was Baker Analyzed Reagent (water less than 0.05%), and the iodine was Baker, U.S.P. resublimed. The methanol which contained less than 0.1% water was Mallinckrodt, Reagent Grade. The sulfur dioxide was 99.5% pure from Matheson Co. and had less than 0.5% water. The water equivalence of this M.K.F.R., expressed in mg. water per ml., was determined by adding known amounts of water to a sample of the reaction condensate and titrating the resulting mixture with the M.K.F.R. Carbonyl compounds have been shown^{3c} to interfere with this water titration; this interference is characterized by a rapidly fading end-point and subsequent high apparent water content. Carbonyl compounds tend to form acetals and ketals with the methanol present. In order to overcome this interference the standard^{3a} K.F.R. was modified so as to greatly reduce the methanol and increase the pyridine content. K.F.R.^{3d,6} has been reported to have virtually no tendency to react with unsaturated compounds. There was no measurable interaction between the M.K.F.R. and reaction products. A series of different mixtures ranging from 15 to 85 mole % 2-butanol in 2-butanone was prepared and the results are shown in Fig. 1. Varying amounts of water, ranging from 40 to 230 g., were

added to each of these mixtures. The precision of these water determinations was four parts per thousand. This M.K.F.R. was standardized at the start and at the finish of every change in temperature or feed rate, always within a period of four hours.

The kinetic rate measurements were calculated from known amounts of 2-butanol vapor introduced into the catalyst chamber, the amounts of water produced by the reaction, and the temperature of the catalyst bed. The apparatus was essentially that of Komarewsky and Riesz,⁷ except that the input portion consisted of a motor driven hypodermic syringe connected to a preheater. A variable speed motor advanced the plunger of a syringe at a constant rate. The delivery rate in ml. per second of the syringe was calibrated from the weight of mercury discharged. The temperature was measured by a platinum-iridium thermocouple fixed in a well located in the center of the catalyst bed. The thermocouple was calibrated using the freezing point and boiling point of water and the melting point of potassium dichromate as standardizing temperatures.

Vapor products of the dehydration reaction were bubbled into an electrolysis cell filled with 50 ml. of M.K.F.R. and the vapors titrated conductometrically to a dead stop end-point.^{3b} Mitchell and Smith^{3a} have referred to this procedure as the back titration. This back titration method gave a sharp, reproducible end-point with a precision three times better than when the titration was made in the forward direction.

Calculations.—The concentration of water produced, in moles per liter, was calculated from known values of the water equivalence, the volume of M.K.F.R., and the molecular weight of water. A zero order was found for this reaction when the quantity of water produced was plotted against the corresponding time of its production. If the velocity of the reaction is controlled by the decomposition of the catalyst-product complex, Schwab⁸ and Hinshelwood⁹ have concluded the order of the reaction should be either zero or reciprocal first order. The true order of the reaction will be the one corresponding to the average time a 2-butanol molecule spends in the catalyst bed before it reacts. This average time of residence in the catalyst bed by reactant molecules will be referred to as the time of reaction. In calculating the time of reaction it is assumed that the reaction occurs throughout the length of, and only in, the catalyst bed. The average time of reaction was found by dividing the volume available for vapor in the catalyst bed by the volume of vapor passing through it per sec. The volume of 2-butanol vapor entering the catalyst bed per second is given by the expression¹⁰

$$GV_0[(N+n)/N]dt$$

where G is the number of moles of 2-butanol entering the catalyst bed per second and V_0 is the specific volume of 2-butanol corrected by the mole fraction, $(N+n)/N$. For each molecule of 2-butanol reacted two molecules of product were formed, *i.e.*, a molecule of water and a molecule of 1- or 2-butene. The volume of void space, V , in the catalyst bed was found by integrating from the entrance to the exit of the bed, *i.e.*

$$\int_0^x A dx = V$$

(7) V. I. Komarewsky and C. A. Riesz, *Oil and Gas J.*, **42**, no. 7, 91 (1943).

(8) G. Schwab, "Catalysis," trans. by H. S. Taylor and R. Spence, D. Van Nostrand Co., New York, N. Y., 1937, p. 221.

(9) C. N. Hinshelwood, "Kinetics of Chemical Change in Gaseous Systems," 3rd Ed., Oxford, England, 1933.

(10) A. C. Neish, *Can. Research*, **23B**, 55 (1945).

(5) C. L. Thomas, *Ind. Eng. Chem.*, **41**, pt. 2, 2564 (1949).

(6) (a) K. Fisher, *Angew. Chem.*, **48**, 394 (1937); (b) C. D. McKimsey, Jr., and R. T. Hall, *Ind. Eng. Chem., Anal. Ed.*, **15**, 460 (1943).

where V is the volume available for vapor, and A is the area of void space in an incremental length of the bed, dx . Because a gas occupies all of the space available in its container, the void space equals the volume of vapor passing through in unit time. Equating the volume of 2-butanol vapor entering the catalyst bed to the volume of void space gives¹⁰

$$GV_0 \int_0^t [(N+n)/N] dt = \int_0^x A dx$$

This void space, V , measured by the displaced volume of an inert solvent (benzene), was equal to 6.2 ml. for 5 g. of catalyst. To integrate the left side of the above equation, a substitution of $n/N = 1 - e^{kt}$ (from the integrated first-order rate equation) was made for the mole fraction term, $1 + (n/N)$. The equation becomes:

$$V_0G \int_0^t (1 + 1 - e^{kt}) dt = V$$

which upon integration gives

$$V = V_0G \{2t + nt/(N \ln [(N-n)/N])\}$$

V_0G is the volume of reactant vapor delivered to the catalyst per second. The equation, solved for t , and with V_0G replaced by $N'RT/P$ from the ideal gas equation, becomes: $t(\text{sec.}) = 2.263P/N'TB$, where $B = 1 - n/[4.606 N \log \{N/(N-n)\}]$. Again rearranging the Neish¹⁰ equation and substituting for dt gives the specific reaction rate constant, k , as

$$k/\text{sec.} = (2N'RT/PV) \{ \ln [N/(N-n)] - n/2N \}$$

where k has the units of reciprocal seconds, N is the moles per liter of 2-butanol entering the catalyst bed, and n is the moles per liter of water being formed. N' is the number of moles per second of alcohol being delivered to the catalyst. This equation was used to calculate the data shown in Fig. 2.

The apparatus was not designed for work above 700°K.; however the catalyst was stable to 800°K. Two techniques were employed to determine the order of the reaction. The first method, that of plotting $2.303 \log [N/(N-n)] - n/2N$ against $PV/2N'RT$, is shown in Fig. 2. The linear relation, shown by this graph, classifies this process as a first-order reaction. The second method of assigning the reaction order was based on the constancy of k calculated from the first-order equation¹⁰ for feed rate changes of more than 100%. The specific reaction rate constant, k , was found to be 0.166 sec.⁻¹ at 576°K. The rate constant of the first-order dehydration of 2-butanol varied from 0.013 sec.⁻¹ at 498°K. to 0.945 sec.⁻¹ at 730°K., as shown in Fig. 3.

An activation energy of 13,000 cal. per mole was calculated from the slope of the straight line, shown in Fig. 3. The intercept of this plot gave a value for the Arrhenius frequency factor, A , of $8.32 \times 10^3 \text{ sec.}^{-1}$. Writing the Arrhenius equation in its final form by substituting the values calculated from the data gives $k(\text{sec.}^{-1}) = 8.32 \times 10^3 \exp(13,000/RT)$. This equation was then written in the absolute reaction rate form to permit calculation of entropy of activation

$$k = \kappa (k'T/h) \exp(\Delta S^*/R) \exp(-\Delta H^*/RT)$$

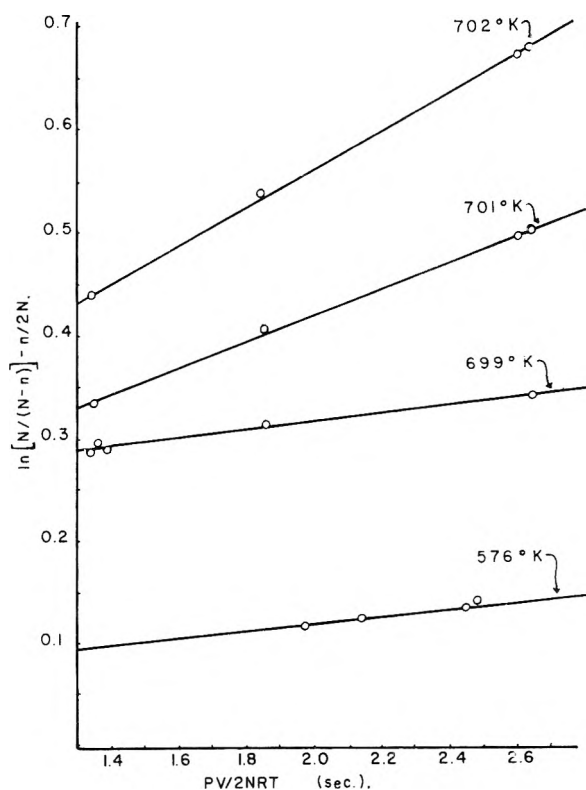


Fig. 2.—Treatment of data from the rate experiments. $\ln [N/(N-n)] - n/2N$ is plotted vs. $PV/2N'RT$ in seconds. The slope is $1/k$, which is the reciprocal of the specific reaction rate constant.

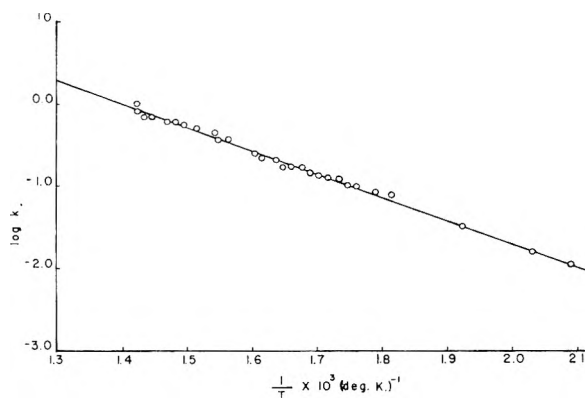


Fig. 3.—Effect of temperature on the dehydration reaction.

where ΔS^* is the entropy of activation and k is the specific reaction rate constant. T is the temperature in °K. and k' is the Boltzmann constant. The activation energy, E_a , is taken as ΔH^* . Assuming the transmission coefficient, κ , to be unity the equation was solved for ΔS^* and these values are assembled in Table I along with specific reaction rate constants and corresponding temperatures.

Discussion

The initial step of the dehydration reaction can best be explained in terms of chemical combination, rather than physical adsorption, because of the temperatures employed.¹¹ Copper or chromium ions present in the surface are considered to be "active sites" of the catalyst. Chemical adsorp-

tion will be described here as the formation of a coordinate covalent bond¹¹ between available electron pairs on the hydroxyl oxygen of 2-butanol with the vacant orbitals of the exposed metals ions. This bond formation may also be discussed in terms of Lewis acids and bases,¹² the complexes being formed between metals serving as electron acceptors and organic molecules serving as electron donors.

TABLE I

KINETIC AND THERMODYNAMIC DATA FOR THE DEHYDRATION REACTION OF 2-BUTANOL OVER COPPER-CHROMIUM OXIDE CATALYST

T, °K.	k (sec. ⁻¹)	ΔS*, e.u. ± 0.3 e.u.
500	0.020	-41.5
525	.036	-41.5
550	.068	-41.5
575	.110	-41.7
600	.178	-41.7
625	.269	-41.8
650	.439	-41.9
675	.575	-41.9
700	.920	-41.9

In determining whether water or hydrogen is produced, the primary factor to be considered is the availability of sufficient energy to break the appropriate bonds. This energy must come from the catalyst. When the catalyst complex is formed, the electron density around the oxygen is decreased. Hence, the hydroxyl hydrogen of the complexed alcohol becomes acidic and can react with the hydrogen on the adjacent carbon thus forming molecular hydrogen. Ketone is simultaneously produced. The bond between carbon and oxygen is polarized during complex formation and the carbon-oxygen bond can dissociate producing water and butene. The hydrogen on the carbon adjacent to the hydroxyl group is assumed to be involved in both dehydration and dehydrogenation. Our work has shown that only 2% of the 2-butanol had reacted to form water^{2b} between 500 and 550° K. Almost no hydrogen was produced at 700° K. and the production of water accounted for 99% of the reacted 2-butanol. The predominance of dehydration over dehydrogenation at higher temperatures is the result of a higher energy requirement for dehydration.

The activation energy for dehydration, determined experimentally here, is 13 kcal. This value is too small to account for the energies required to break the bonds¹³ described previously. Better agreement was found between this experimental value of 13 kcal. and the dissociation energy of the complex formed between products and catalyst. These complexes are formed by water coordinating

with Cu⁺⁺ or Cr₂O₃. The dissociation energy¹⁴ for Cu⁺⁺ (aq.) is 15.39 kcal. and for Cr₂O₃ (aq.) is 2.5 kcal. The 13 kcal. measured here is in agreement with the work of Kälberer and Dohse.¹⁵ They measured the heat of chemisorption of water on a similar catalyst. If one step in a reaction mechanism is significantly slower than the others, it will control the kinetics of the over-all process. Assuming that the rate-controlling step is the dissociation of the reaction products complexed to the catalyst, these values account for the activation energy. The experimentally determined first-order rate of reaction is in agreement with this assumption.

The large negative entropy of activation (-41.6 e.u. for dehydration and -49.7 e.u. for dehydrogenation^{2b}) can be explained in terms of chemical adsorption of the reacting molecules on the catalyst sites.¹⁶ The reactant has three degrees of translational freedom, plus rotation, which are probably lost in formation of the activated complex.^{11,16} This indicates a considerable loss of entropy accompanying the formation of the complex state. The entropy of activation is estimated¹⁶ to be -56 e.u. per mole for an immobile adsorption followed by dissociation of the adsorbed complex. The process of adsorption in forming the immobile layer produces a theoretical change of entropy of at least -110 e.u. per mole.¹⁶ Therefore, the increase in entropy contributed by dissociation of the complexed product is about +54 e.u. The entropy increase resulting from the other product (butene) which is not complexed to the catalyst is approximately +16 e.u. Adding this +70 e.u. to the -110 e.u. leaves a resultant entropy value of about -40 e.u. This agrees with our measured entropy of -41.6 e.u.

The main contribution to the over-all entropy of activation does not seem to come from the rate-controlling step. It is necessary to assume the velocity of the adsorption step to be the most rapid one as did Taylor,¹⁷ who qualitatively justified this assumption by consideration of the availability of active sites on the catalyst surface. A catalyst surface, congested by complexed molecules, will sterically hinder the approach of molecules to the catalyst sites. Steric hindrance is practically eliminated as a factor in retarding the reaction if there is a large excess of available sites, as would be the case if the rate of flow of the reactant is kept below the catalyst's maximum efficiency. Diffusion controlled reactions generally involve small entropy changes. The diffusion effect on the reaction rate should be evaluated, especially if the catalyst was of variable particle size. The same catalyst, which had a homogeneous particle size, was used throughout this work so that the diffusion effect is considered negligible.

Titration of the catalyst gave 3.61×10^{21} active sites on the surface of 5 grams of the powdered catalyst. In the present work 0.62×10^{-4} mole

(11) P. H. Emmett, "Catalysis, Fundamental Principles," Pt. 1, Reinhold Publ. Corp., New York, N. Y., 1954; (b) D. A. Dowden, *J. Chem. Soc.*, 24 (1950); (c) K. Huang and G. Wyllie, *Disc. Faraday Soc.*, 8, 24 (1950); (d) D. D. Eley, *ibid.*, 8, 34 (1950); (e) K. J. Laidler, *ibid.*, 8, 47 (1950); (f) T. Kwan, *Advances in Catalysis*, VIII, 100 (1954); (g) J. H. de Boer, *ibid.*, VI, 18 (1954).

(12) (a) Pines and Haag, *J. Am. Chem. Soc.*, 82, 2471 (1960); (b) C. Walling, *ibid.*, 72, 1164 (1950); (c) H. A. Benesi, *ibid.*, 78, 5490 (1956); (d) M. W. Tamele, *Faraday Soc. Disc.*, 8, 270 (1950); (e) T. Milliken, G. A. Mills and A. C. Oblad, *ibid.*, 8, 279 (1950).

(13) T. L. Cottrell, "The Strengths of Chemical Bonds," Academic Press, New York, N. Y., 1954.

(14) "Selected Values of Chemical Thermodynamic Properties," Nat. Bureau of Standards Circular No. 500, 1952.

(15) Dohse and Kälberer, *Z. physik. Chem.*, 5B, 131 (1929).

(16) S. Glasstone, K. Laidler and H. Eyring, "The Theory of Rate Processes," McGraw-Hill Book Co., Inc., New York, N. Y., 1941, pp. 347-399.

(17) H. S. Taylor, *Chem. Revs.*, 9, 1 (1931).

of water was formed at 703°K . from 1.11×10^{-4} mole of 2-butanol in every second. The calculated residence time in the catalyst bed of an average reactant molecule then becomes about one second. Thus for every second, 3.73×10^{19} molecules of 2-butanol are dehydrated by 3.61×10^{21} sites, and accordingly one in 100 sites is actually in use at any instant. Because of the excess of available active sites, the complexed molecules do not inter-

fer appreciably with the approach of entering molecules.

Acknowledgment.—This investigation was supported in part by a research grant PHS E-1354(C5) from the Department of Health, Education, and Welfare of the Public Health Service, and in part by a Frederick Gardner Cottrell Grant from the Research Corporation. The authors wish to thank both of these sponsors.

THE FUSION POINT AND THE THERMAL DECOMPOSITION OF POTASSIUM PERCHLORATE

BY A. E. SIMCHEN

Scientific Department, Ministry of Defense, P.O.B. 7063, Tel Aviv (Israel)

Received September 12, 1960

When heated isothermally above 570° , pure KClO_4 undergoes first a partial decomposition in the solid state, then the resulting solid mixture melts while continuing to lose oxygen and solidifies again when the KClO_3 intermediately formed has disappeared, and the KCl content approaches about 60 mole %; the still remaining KClO_4 continues to decompose until pure KCl remains. The detailed kinetics of the decomposition is complicated because of consecutive, simultaneous and reverse chemical reactions: (1) $\text{KClO}_4 \rightarrow \text{KClO}_3 \rightarrow \text{KCl}$; (2) simultaneously with the simple decomposition, there are the reactions between KClO_4 and KCl ; between KClO_4 and KClO_3 ; (3) $4\text{KClO}_3 \rightarrow 3\text{KClO}_4 + \text{KCl}$. The initiation of the decomposition is considered to be a monomolecular process at germs distributed throughout the volume of the substance, and then propagated by a branching chain of oxygen atoms migrating through the crystal lattice or through the melts.

1. General Description of Phenomena Obtained on Heating KClO_4 .—For the fusion point of KClO_4 several different values are quoted: 525 – 530° ,⁵ $588^{11,12}$ and $610 \pm 10^\circ$.⁴ On the other hand, partial decomposition on heating, giving KCl and KClO_3 , has been known for more than a century.^{14,15} In view of the practical importance of the thermal decomposition of KClO_4 as a source of oxygen in solid rocket propellant formulations, it seemed of interest to have a clearer picture of the phenomena in question. The vacuum decomposition apparatus in which the data reported below were obtained, has been described in a previous paper.⁷

The essential fact emerging from this study is that KClO_4 has no congruent fusion point. The substance remaining after the resolidification of the fused mass is *not* KClO_4 . When heating KClO_4 at a constant and sufficiently high temperature, and waiting for a sufficient time, it undergoes first a partial decomposition in the solid state^{2,3,7,20};

the solid salt mixture thus obtained undergoes further chemical reactions accompanied by the complete fusion of the sample. The fused mass, too, decomposes, its chemical composition continues to change and in the long run a re-solidification of the mass sets in at a (more or less) constant temperature (the exothermal effects of the chemical reactions¹¹ and of crystallization being balanced by the temperature-regulating mechanism of the apparatus and by the heat transfer to the surroundings).

The chemical reactions preceding^{3,20} and accompanying fusion are dependent on time and temperature, and so is the heating up of the sample and of the glass support. This leads to a time-temperature dependency of the fusion which is given in Table I.

TABLE I

TIMES OF BEGINNING FUSION AT DIFFERENT TEMPERATURES, OF 100-MG. SAMPLES OF PURIFIED ANALYTICAL KClO_4 (INCLUDING HEAT-UP TIMES)

Temp., °C.	Time, min.	Mole % KCl in residue after isothermal re-solidification
570	120	23.3 mole % in 1 residue; 2.2 mole % in a 2nd sample that had not melted
580	33
590	24	52.5; 52.9; 53.8
600	20
610	16	56.7
620	15	57.1

The re-solidified, partially decomposed residue still contains appreciable quantities of KClO_4 , but almost no KClO_3 if one waits until the evolution of gaseous O_2 has died down. The composition of the residue is not exactly reproducible, perhaps due to a different extent of the decomposition in samples

- (1) Benrath and Braun, *Z. anorg. Chem.*, **244**, 348 (1940).
- (2) Bircumshaw and Phillips, *J. Chem. Soc.*, 703 (1953).
- (3) Cabané and Bénard, *C.R. Ac. Sc.*, **250**, 128, 331 (1960).
- (4) Carnelley and Carleton-Williams, *J. Chem. Soc.*, **37**, 125 (1880).
- (5) Duerre, Dissertation, Giessen, 1907.
- (6) Frankland and Dingwall, *J. Chem. Soc.*, **51**, 2747 (1887).
- (7) Glasner and Simchen, *Bull. soc. chim. France*, **18**, 233 (1951).
- (8) "Gmelins Handbuch der anorganischen Chemie," 8th edn., "Chlor," and fol., Verlag Chemie, 1927, p. 395.
- (9) Harvey, Edmison, Jones, Seybert and Catto, *J. Am. Chem. Soc.*, **76**, 3270 (1954).
- (10) Hodgman, "Handbook of Chemistry and Physics," 41st edn., Chemical Rubber Publishing Co., Cleveland, Ohio, 1959, p. 627.
- (11) Markowitz, *J. Phys. Chem.*, **61**, 505 (1957).
- (12) Markowitz, *ibid.*, **62**, 827 (1958).
- (13) Marignac, *Bibl. Univ.*, **45**, 353 (1843).
- (14) Millon, *Ann. phys.*, [3] **7**, 334 (1843).
- (15) Millon, *Lieb. Ann.*, **46**, 281 (1843).
- (16) Otto and Fry, *J. Am. Chem. Soc.*, **45**, 1138 (1923).
- (17) Rodgers and Wassink, Univ. of Arkansas, Final Summary Report, 1 Sept. 54–31 Jan. 58, Contract No. DA-23-072-ORD-1049.
- (18) J. C. Schumacher, "Perchlorates," Am. Chem. Soc. Monograph, Reinhold Publ. Corp., New York, N. Y., 1960, pp. 37–38.
- (19) Scobai, *Z. physik. Chem.*, **44**, 328 (1903).
- (20) Simchen and Glasner, *Bull. soc. chim. France*, **20**, 127 (1953).

TABLE II
COMPOSITION OF ISOTHERMALLY RE-SOLIDIFIED RESIDUES, IN MOLE % KCl

Description of the KClO ₄	540	550	560	570	580	590	610	610	620°
1 Commercial I (traces of Cu)	33.3	43.3	52.7	57.7	60.0	..	60.5	60.5	..
			52.8	60.0			61.0	62.1	
2 Commercial II (traces of Pb)	..	31.0	..	50.0	..	55.0	..	58.9	..
3 J. T. Baker Analyzed (traces of Fe)	..	4.4	2.2	41.0	52.3	50.2	53.9	56.7	..
				43.0		50.8			
4 Recrystallized from Baker Analyzed (No. 3)	2.2	..	52.5	..	56.7	57.1
				23.3	..	52.9	..		
						53.8			

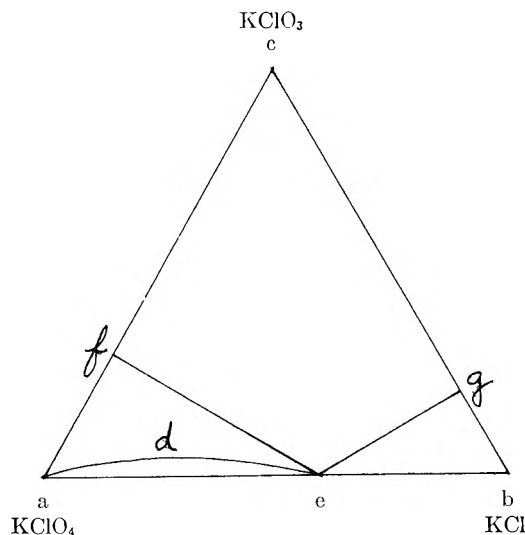


Fig. 1.—Evolution of the chemical composition of decomposing KClO₄. The reaction path is: a-d-e-b; e-point of re-solidification. The KClO₄-content of the re-solidified mass is given by e-g, the KCl-content by e-f (schematic).

differently distributed in the glass spoon, differences in the distribution of the grain size of the sample before fusion, or other causes. The composition of the residue and the temperature of incipient fusion are strongly influenced by the degree of impurity of the sample, and the quality of the impurities present. The results are given in Table II.

A tendency to a higher KCl content in the residues of fusion at higher temperatures is clearly visible, with a limit of about 60 mole % of KCl; this may represent the solubility of KCl in the fused mass. If the heating is interrupted after various times without regard for oxygen evolution and the cooled mass submitted to chemical analysis, a continuous change of chemical composition may be noticed, as exemplified in Table III (see below). The KClO₃ that first appears in the mass together with KCl (the first mention of KClO₃ in the thermal decomposition products of KClO₄ go back to 1843 (!),^{14,15} disappears later leaving a mixture of KCl and KClO₄. The remaining KClO₄ decomposes entirely and pure KCl is obtained. The lower temperature limit for carefully purified KClO₄ undergoing fusion accompanied by decomposition has been found to be about 570°. This temperature coincides with the eutectic temperature of the KCl-KClO₄ mixture reported by Benrath and Braun¹ and by Harvey and co-workers⁹

who disregarded the instability of the mixture. In the ternary system KClO₄-KClO₃-KCl, the fusion point of KCl at 771°² is the only one to be considered as accurate; the other fusion points are to be treated with reserve, and the same may be said about the above mentioned eutectic temperature of KClO₄-KCl. If we neglect in a first approximation the thermal effect accompanying the fusion or the decomposition in the above system, then all changes of the chemical composition can be regarded as the displacement of a representative point inside the triangular diagram having the three components KClO₄, KClO₃ and KCl at its summits. For the decomposition of KClO₄, the representative point will leave the KClO₄ corner of the diagram and will follow a path directed toward the KCl corner, but approaching somewhat the KClO₃ corner on its way (Fig. 1).

TABLE III

CHEMICAL COMPOSITION OF RESIDUES OF 100-MG. SAMPLES OF KClO₄ (RECRYSTALLIZED FROM ANALYTICAL KClO₄)

HEATED ISOTHERMALLY FOR DIFFERENT TIMES

A. Heating at atm. pressure: A.1 580 ± 1°

Time, min.	15	30	50	70	100	150
Mole % KCl	1.39	12.85	33.60	47.0	65.3	96.9
Mole % KClO ₃	0.60	4.71	3.40	1.20	0.80	0.00
Mole % KClO ₄	98.0	82.44	63.0	51.4	33.9	3.1

A.2 600 ± 1°

Time, min.	15	30	45	60
Mole % KCl	2.63	11.2	91.97	99.4
Mole % KClO ₃	2.68	4.74	0.98	0.43
Mole % KClO ₄	94.69	84.06	7.03	0.17

B. Heating at 600 ± 1° in a maintained vacuum. Initial pressure: 1 μ, and always less than 0.2 mm.

Time, min.	10	18	25	35	45	60
Mole % KCl	5.45	13.82	37.06	62.00	74.32	80.12
Mole % KClO ₃	2.88	4.95	3.28	1.40	1.00	0.43
Mole % KClO ₄	91.67	81.23	59.66	36.60	24.50	19.45

At the point where this curve of the reaction path meets the solidus of the system, the fused mass will begin to solidify. The part which is still liquid will continue to lose oxygen at a characteristic rate v_1 ; the part already solidified decomposes at a different and much slower rate v_2 .^{9,20} Finally the mass solidifies entirely and loses the remaining oxygen at a rate of the order of magnitude of v_2 only, until pure KCl remains. The time of re-solidification of the fused mass depends, like the time of beginning fusion, upon several factors such as the quantity of material undergoing decomposition, and the heat transfer between the reacting mass and the furnace. The difference in the decomposition rates in the solid state and in the fused state can be understood easily if the dif-

ferent modes of the transport of oxygen in both cases are considered. In a crystal the oxygen must make its way through the interstices and/or defects of the crystal lattice, or perhaps through the inter-mosaic fissure; even the "frozen" lattice, ignoring the thermal vibrations, affords the space necessary for the interstitial movement of oxygen which may also move by jumps from anion to anion.⁷ In the liquid on the other hand, there is, in addition to the above, diffusion of oxygen, and the movement of gas bubbles ascending through the liquid and giving a more efficient mode of mass transport.

2. The Decomposition Reactions.—The decomposition reactions of KClO_4 at high temperature have been investigated several times since 1816.²¹ The principal difficulty arises from the strong reactivity of KClO_4 at high temperature and from its sensitivity to impurities.²⁰ Qualitatively, the action of copper, iron or cobalt salts in catalyzing the thermal decomposition of KClO_4 has been known for a long time.¹¹

It may be that heavy metal perchlorates form and decompose subsequently into oxides oscillating between higher and lower states of oxidation.

Even in analytical grade KClO_4 heavy metal traces are present and can be identified easily. At the high temperatures investigated, there is a clear difference between analytical KClO_4 , and the same product after 2–3 recrystallizations (compare Table II, the results at 570°). The presence of KClO_3 in partially decomposed KClO_4 has been reported a number of times since its first discovery by Millon in 1843,^{6,9,14,15,19,22,23,24} and contested by others.^{13,18} A systematic investigation of KClO_3 and of KCl , as a function of heating time, in the resolidified residues of 100-mg. samples of carefully purified KClO_4 , *in vacuo* (less than 200μ) and at atmospheric pressure, gave the results represented in Table III.

The continuous loss of oxygen seems to proceed by successive steps: $\text{KClO}_4 \rightarrow \text{KClO}_3 \rightarrow \text{KCl}$. The kinetics of the system are not simple; besides the consecutive decomposition reactions mentioned above, there are simultaneous reactions: the reaction between KCl and KClO_4 ,^{7,20} and perhaps others, and besides the decomposition reactions leading to compounds poorer in oxygen, there is the well-known inverse reaction: $4\text{KClO}_3 = 3\text{KClO}_4 + \text{KCl}$. The fused mass decomposes with loss of oxygen, simultaneously becoming richer in KCl . After re-solidification of the mass the velocity of the gas evolution diminishes to a low value and remains low as long as the temperature is not raised. The higher diffusion velocity in the liquid mass is again replaced by the slower travelling through the crystal lattice, and the bulk movement of the oxygen bubbles rising through the melt to its surface and collecting the dissolved oxygen in their path, ceases altogether.

3. The Kinetics of the Decomposition.—Previous work reported elsewhere^{7,20} has led us to consider the thermal decomposition of KClO_4 as

composed of two different basic processes. One of them is relatively slow and corresponds to the initiation of the decomposition, while the other process, up to 500 times more rapid, represents the propagation of the decomposition by a branched chain mechanism.⁷ The latter is the result of the differences between the velocity of oxygen transport from a ClO_x -group ($x = 1$ to 4), with one oxygen atom possessing the necessary energy of activation, to a neighboring ClO_y -group ($y = 0$ to 3) on the one hand, and the velocity of activating the ClO_x -group once the favorable conditions are obtained, *i.e.*, if a ClO_n -ion poorer in oxygen is created spatially adjacent to a ClO_x -ion which is richer in oxygen.

If the activation velocity is smaller than the transport velocity, a vacant place on a ClO_y -group may remain open for a time in which an oxygen on more than one adjacent ClO_x -group is activated, and branching may result. Such a reasoning implies the possible existence of at least two distinct modes of oxygen transport through the crystal lattice: (1) the diffusion of oxygen between the ions of the crystal lattice and/or the defects of the lattice, through the cracks, fissures, etc., of the macrocrystals; (2) the movement, by jumps, of oxygen from the ClO_x -ions to neighboring ClO_y -ions (x greater than y), with a time of arrest at the different stations; (3) possibly a combination of (1) and (2) above, part of the movement being between the lattice constituents, and part by jumps from anion to anion. Now if the spacing of the ions in the KClO_4 is sufficiently loose to permit the transport of oxygen, it is even looser in the molten mass, and the "interstitial" movement of oxygen is possible for both. It seems to-day unnecessary to postulate as we did previously,⁷ a chain initiation from germs on the exterior crystal surface. Such a hypothesis led to a term proportional to the $2/3$ power of mass in the expression for the velocity of gas formation, which should rather be replaced by a term proportional to the mass present if the initiation of decomposition at lattice defects is accepted; these defects are distributed through the bulk of the crystals.

In the molten mass the initiation throughout the volume can be observed visually. If the initiation of the decomposition takes place in the bulk rather than on the surface of the crystals, then the grain size and its distribution should be irrelevant to the thermal decomposition (unless the strains accompanying *commixtion* lead to some preferential distribution of lattice defects or dislocations; our samples were 80 to 100 mesh BSS). Thus, instead of

$$dy/dt = jy(a - y) + j_1(a - y)^{2/3} \quad (1)$$

for initiation on the surface of the crystals, we have

$$dy/dt = jy(c - y) + j_1(a - y) \quad (2)$$

for initiation in the mass of the crystals ($a =$ maximum quantity of oxygen gas obtainable from the sample up to the solidification of the melt; $y =$ oxygen pressure at time t ; j_1 and $j =$ velocity constants for the initiation of the reaction and for the branched chain reaction, respectively). The value of a depends on the conditions in each experiment

(21) Stadion, *Gilbert's Ann.*, **52**, 213 (1816).

(22) Teed, *Proc. Chem. Soc.*, **2**, 141 (1886).

(23) Teed, *Chem. News*, **53**, 56 (1886).

(24) Teed, *J. Chem. Soc.*, **51**, 282 (1887).

and on its fusion and re-solidification phase. An approximation may be found for a by graphically integrating the experimental curves of gas evolution velocity *vs.* time, from the beginning of the experiment to the (extrapolated) virtual cessation of gas evolution at solidification. The further calculations are derived from the integration of the equation

$$dx/dt = kx(1-x) + k_1(1-x) \quad (3)$$

obtained by dividing both sides of eq. 2 by a ; we have

$$x = y/a; k_1 = j_1; k = ja \quad (4)$$

Integrating eq. 3 between 0 and t gives

$$kt = \frac{1}{1+k_1/k} \left[\ln \frac{x+k_1/k}{1-x} - \ln \frac{k_1}{k} \right] \quad (5)$$

4. Calculation of the Velocity Constants k and k_1 of Eq. 3.—The conditions for the velocity of oxygen evolution becoming maximum lead to

$$x_m = (1 - k_1/k)/2 \quad (6)$$

In order to get the time corresponding to the maximum velocity of oxygen evolution, t_m , eq. 6 is substituted into eq. 5 giving

$$t_m = [1/(k+k_1)] \times \ln(k/k_1) = [k(1+k_1/k)]^{-1} \times \ln(k/k_1) \quad (7)$$

the maximum velocity of oxygen evolution is obtained by substituting eq. 6 into eq. 3

$$(dx/dt)_m = k[(k+k_1)/2k]^2 = k(1+k_1/k)^2/4 \quad (8)$$

It is useful to conserve the ratio k_1/k in the eq. 7

and 8 above. Rearranging eq. 8 yields

$$k(1+k_1/k) = 4(dx/dt)_m(1+k_1/k)^{-1} \quad (9)$$

and the substitution of eq. 9 into eq. 5 gives finally

$$4t_m(dx/dt)_m = (1+k_1/k) \ln(k/k_1) = L_I \quad (10)$$

Thus from the experimentally found values of maximum reaction velocity $(dx/dt)_m$, and from the corresponding times t_m , we may calculate the ratio k_1/k for the different temperatures by using a graph or a table of the function L_I (eq. 10). Then we compute: (1) the branching chain velocity constant k ; (2) the monomolecular constant k_1 . Ad 1.: eq. 7 gives after rearrangement

$$k = \ln(k/k_1)/[t_m(1+k_1/k)] = 1/(t_m L_{II}) \quad (11)$$

and with eq. 10

$$k = 4(dx/dt)_m(1+k_1/k)^{-2} \quad (12)$$

A graph of the function L_{II} may be helpful in solving eq. 11

$$L_{II} = (1+k_1/k)^{-1} \times \ln(k/k_1) \quad (13)$$

Ad 2.: k_1 is found from k_1/k and from k .

Values for analytical grade $KClO_4$ are contained in Table IV.

TABLE IV

VELOCITY CONSTANTS k AND k_1 (EQ. 3) FOR ANALYTICAL $KClO_4$

Temp., °C.	560	570	580	590	600	610
$10^2 k$	4.14	5.75	5.96	10.2	13.5	15.4
	4.66	8.2	9.6	13.7	16.6	20.3
$10^4 k_1$	7.41	6.44	9.20	21.85	59.8	102.3

PHASE EQUILIBRIA IN THE SYSTEM $LiF-YF_3$

By R. E. THOMA,^{1a} C. F. WEAVER,^{1a} H. A. FRIEDMAN,^{1a} H. INSLEY,^{1a} L. A. HARRIS^{1b} AND H. A. YAKEL, JR.^{1b}

Reactor Chemistry Division and Metallurgy Division
Oak Ridge National Laboratory,² Post Office Box X, Oak Ridge, Tennessee

Received September 19, 1960

The phase equilibrium diagram of the condensed system $LiF-YF_3$ is presented. Data were obtained from thermal analysis of heating and cooling curves and by identifying the phases present in small samples which were quenched after equilibration at high temperatures. Within the system two invariant points occur, the eutectic at 19 mole % YF_3 and 695°, and the peritectic at 49 mole % YF_3 and 819°. The single intermediate compound, $LiF \cdot YF_3$, is formed. It melts incongruently to YF_3 and liquid at 819°, and is tetragonal, $a_0 = 5.26 \pm 0.03$ Å, and $c_0 = 10.94 \pm 0.03$ Å, space group $I4_1/a$. The compound $LiF \cdot YF_3$ is colorless, uniaxial (+), with refractive indices $N_\omega = 1.454$, $N_e = 1.472$. No solid solutions are formed among the equilibrium solids in the system $LiF-YF_3$. The melting point of YF_3 , 1148°, determined by other workers, was corroborated in the present study. A solid state transition in YF_3 was shown to occur at 1052°.

Introduction

Recent investigations at the Oak Ridge National Laboratory of the fused salt mixtures of potential use in the electrolytic reduction of Y^{+++} to yttrium metal have included a review of the phase equilibria in the system $LiF-YF_3$. As a part of a study of the complex fluoride compounds formed from the alkali metal fluorides and Group III metal fluorides, Dergunov³ reported a phase diagram of the system. From that investigation he concluded that LiF and YF_3 form a simple eutectic

system, with the eutectic at 18 mole % YF_3 and at 744°. The absence of intermediate compounds appears anomalous inasmuch as examples of intermediate equilibrium compounds are known⁴ in many systems of $LiF-MF$, $-MF_2$, $-MF_3$, and/or $-MF_4$, where the cation radius of M^+ , M^{2+} , M^{3+} or M^{4+} is as low as 0.30 Å. (Be^{2+}) and as high as 1.67 Å. (Cs^+). Accordingly, an investigation of the phase equilibria in the condensed system $LiF-YF_3$ was made, using the same techniques as have been employed effectively in the determinations of fused salt phase equilibria previously described.⁵

(1) (a) Reactor Chemistry Division. (b) Metallurgy Division

(2) Operated for the U. S. Atomic Energy Commission by the Union Carbide Corporation.

(3) E. P. Dergunov, *Doklady Akad. Nauk S.S.S.R.*, **60**, 1185 (1948).

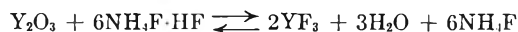
(4) E. M. Levin and H. F. McMurdie, "Phase Diagrams for Ceramists," The American Ceramic Society, Columbus, Ohio, 1959.

(5) C. J. Barton, *et al.*, *J. Am. Ceram. Soc.*, **41**, 63 (1958).

Experimental

Materials.—The mixtures used in these phase equilibrium studies were prepared from commercially available reagent grade lithium fluoride⁶ and from specially purified yttrium fluoride. Pure yttrium fluoride was prepared from the oxide⁷ using ammonium bifluoride as the hydrofluorinating agent.

Establishment of a method for preparing yttrium fluoride of low oxygen content has been a difficult problem for several years. Studies made elsewhere of the conversion of Y_2O_3 to YF_3 by HF ,⁸ $NH_4F \cdot HF$ ⁹ and F_2 ,¹⁰ indicate that the most complete conversion is effected with $NH_4F \cdot HF$. Spedding¹¹ has stated that the conversion method using ammonium bifluoride depends on the reaction



Evidence has been reported that an intermediate hexafluorometallate is formed at 100–150°, and decomposes on heating in the temperature range 400–600°. Freshly purified samples of YF_3 , prepared with the ammonium bifluoride conversion method, contained no greater than 300 p.p.m. oxygen, as determined with the bromine trifluoride method of analysis.¹² Spectroscopic analysis of the yttrium fluoride product indicated that the only impurities present, within the detectable concentration range, consisted of 0.02 Ca, 0.02 Fe and 0.02 Ni (wt. %).

Because YF_3 is hydrolyzed easily at elevated temperatures, it was necessary to remove traces of adsorbed water from the components in the low temperature range as they were heated initially. For this purpose, approximately 10 g. of ammonium bifluoride was added initially to the 50 g. salt mixtures. The presence of this hydrofluorinating agent effectively prevented hydrolysis of the fluorides during heating. To minimize hydrolysis at elevated temperatures, the salt mixtures were heated and cooled in an inert atmosphere.

Water adsorption on YF_3 occurs so rapidly as to require the use of freshly purified samples of YF_3 in elevated temperature phase studies. Phase equilibrium data from the $LiF \cdot YF_3$ quenching experiments were considered to be definitive only if in the quenched samples no evidence of oxygen-containing phases could be detected with the polarized light microscope. X-Ray powder diffraction data do not indicate reliably that YF_3 -containing samples are free of oxide, because a fluoride coating on the very small Y_2O_3 particles can produce all of the X-ray diffraction maxima observable. The differences between the refractive indices of YF_3 and Y_2O_3 and the fact that both YF_3 and Y_2O_3 are transparent to visible light facilitate the determination of the presence of YF_3 coated phases with the polarized light microscope.

The Melting Point and Polymorphism of YF_3 .—An extrapolation of the liquidus curves of the YF_3 -alkali fluoride systems reported by Dergunov³ converges approximately to a YF_3 melting temperature of 1400°. In conjunction with the present $LiF \cdot YF_3$ phase studies the melting point of YF_3 was determined to be $1144 \pm 3^\circ$. This value was determined from the cooling curves obtained on a purified YF_3 sample through which a small current of dried argon gas was passed while the sample was in the liquid state. Cooling rates from 0.7°/min. to 2°/min. were employed. It was determined that the salt remained pure by examining the cooled sample with the polarizing light microscope. Error in this determination is introduced by supercooling,

which routinely occurred as YF_3 crystallized. This value, while probably low, is essentially in agreement with extrapolations of the liquidus curve in the $LiF \cdot YF_3$ phase investigation, and with the values determined by Porter,¹¹ $1148 \pm 3^\circ$, and by Spedding¹² 1152° . Confidence in the 1144° melting temperature rather than the 1400° value was also established by the fact that in melting point experiments a weighted cylinder penetrated a pressed pellet of YF_3 on heating to temperatures above 1160° (measured by optical pyrometry).

Samples of YF_3 were quenched after annealing in the temperature interval 980–1180°. The crystals which appeared in these samples were cryptocrystalline at all temperatures above $1063 \pm 13^\circ$.¹⁶ Below this temperature the crystals were well-formed and had the optical properties reported for YF_3 :¹⁷ colorless, biaxial negative, $2V = 85\text{--}90^\circ$, $N_\alpha = 1.536$, $N_\beta = 1.553$, and $N_\gamma = 1.568$.

Cooling curves of YF_3 also showed evidence of a solid state transition in YF_3 at $1052 \pm 3^\circ$, essentially in agreement with Spedding's value of 1046° for this transition.¹⁶ A moderately large exothermic effect occurs on cooling YF_3 through this transition. The coincidence of the change of crystallinity in quenched samples with an exothermic effect in the YF_3 cooling curve at $1052 \pm 3^\circ$ indicates that YF_3 undergoes a solid state inversion at this temperature and that optical and X-ray properties previously assigned to YF_3 ¹⁸ pertain to the low temperature form of YF_3 . The comparatively large heat effect associated with this transition is considered to be related to the rather small heat of fusion¹⁹ of YF_3 and the inability to derive appreciable thermal effects at the liquidus in the primary phase field of the high temperature form of YF_3 .

Apparatus and Methods.—The techniques used for measurement of the temperatures which define the phase diagrams as well as the methods for identifying phases have been discussed previously.⁵ A variation of the design of the thermal quenching furnace was made to permit a higher maximum temperature of operation than was previously feasible.²⁰ This apparatus was employed only in those experiments which required long annealing periods at temperatures of 850° or higher.

Results and Discussion

The Crystal Structure of $LiF \cdot YF_3$.—Single crystals of $LiF \cdot YF_3$ were mechanically separated from a sample of the compound which had been annealed at 600° for a week in an evacuated nickel capsule. Examination of the product by means of the polarizing microscope and X-ray diffractometer substantiated that this material was entirely single phase $LiF \cdot YF_3$, colorless, uniaxial positive, with refractive indices, $N_\omega = 1.454$, $N_\epsilon = 1.472$.

The X-ray data obtained from the rotation and Weissenberg films ($Cu K\alpha$, $\lambda 1.5418 \text{ \AA}$.) were indexed on the basis of a tetragonal unit cell whose lattice parameters are $c_0 = 5.26 \pm 0.03 \text{ \AA}$. and $a_0 = 10.94 \pm 0.03 \text{ \AA}$. The density was calculated to be 3.77 g./cm.³ with four molecules of $LiF \cdot YF_3$ per unit cell. The space group $I4_1/a$ was chosen on the basis of the systematic extinctions observed on the single-crystal photographs.

Comparisons of formulas, crystal symmetries, lattice dimensions, and ionic radii for $LiF \cdot YF_3$ and $CaO \cdot WO_3$ ²¹ show these compounds to be isostruc-

(6) Lithium fluoride was obtained from the Maywood Chemical Works.

(7) Yttrium oxide was obtained from Iowa State College.

(8) M. Smutz, G. Burnet, J. Walker, R. Tischer and E. Olson, "The Preparation of Low Oxygen Content Yttrium Fluoride," U. S. At. Energy Comm. ISC-1068, 1958.

(9) J. Walker and E. Olson, "Preparation of Yttrium Fluoride Using Ammonium Bifluoride," U. S. At. Energy Comm. IS-2, 1959.

(10) R. L. Tischer and G. Burnet, "Preparation of Yttrium Fluoride Using Fluorine," U. S. At. Energy Comm. IS-8, 1959.

(11) F. H. Spedding, "Semi-Annual Summary Research Report in Chemistry for January–June, 1957," Iowa State College Report ISC-902, 1957, p. 19.

(12) B. J. Sturm, Oak Ridge National Laboratory, to be published.

(13) G. Goldberg, A. S. Meyer, Jr., and J. C. White, *Anal. Chem.*, **32**, 314 (1960).

(14) B. Porter, U. S. Bureau of Mines, Reno, Nevada, personal communication.

(15) F. H. Spedding, ref. 11, p. 20.

(16) The uncertainty in this value indicates the temperature differences between the quenched samples from which the values were obtained.

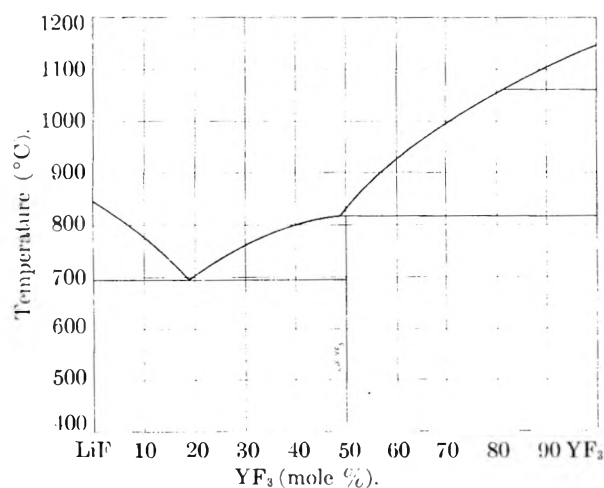
(17) E. Staritzky and L. B. Asprey, *Anal. Chem.*, **29**, 855 (1957).

(18) A. Zalkin and D. H. Templeton, *J. Am. Chem. Soc.*, **75**, 2453 (1958).

(19) A. R. Ubbelohde, *Quart. Revs.*, **4**, 356 (1950).

(20) H. A. Friedman, *J. Am. Ceram. Soc.*, **42**, 284 (1959).

(21) L. Vegard, *Phil. Mag.*, **1**, 1151 (1926).

Fig. 1.—The system LiF-YF₃.

tural. The atoms for LiF·YF₃ were placed in those positions deduced for CaO·WO₃, namely

(Ca) (Y): (b) 0, 0, 1/2, 3/4;

(W) (Li): (a) 0, 0, 0; 0, 1/2, 1/4;

(O) (F): (f) $x, y, z; \bar{x}, \bar{y}, z; x, 1/2 + y, 1/4 - z; \bar{x}, 1/2 - y, 1/4 - z;$
 $\bar{y}, x, \bar{z}; y, \bar{x}, \bar{z}; \bar{y}, 1/2 + x, 1/4 + z; y, 1/2 - x, 1/2 + z;$

where $x = 0.25$, $y = 0.15$, and $z = 0.075$. Table I shows the agreement between calculated intensities and qualitative, visually observed intensities of the first 25 reflections from a Debye-Scherrer photograph (Cu K α radiation, λ 1.5418 Å.) of LiF·YF₃. The former were calculated with the equation

$$I \propto |F|^2 p \frac{1 + \cos^2 2\theta}{\sin^2 \theta \cos \theta}$$

where F is the structure amplitude, and p is the multiplicity factor.

An attempt was made to eliminate the discrepancies observed in Table III by interchanging the metal ion positions in the structure. It is known that the radius ratios Ra:Rx and Rb:Rx embrace a wide range of values in the scheelite structure which allows for either lithium or yttrium atoms in the (a) or (b) positions. However, interchanging the metal ion positions can be shown to affect the intensities of reflections with $2k + l = 4n + 1$ and $2k + l = 4n + 3$ only. Since the observed intensities of these reflections are already in good agreement with calculations based on the given metal ion positions, these positions must be assumed correct and the intensity discrepancies must be ascribed to small variations from the given fluoride ion coordinates.

LiF-YF₃ Phase Equilibria.—The phase equilibrium diagram of the binary system LiF-YF₃ reported here (Fig. 1) represents a synthesis of thermal analysis and thermal gradient quenching data (Tables II and III). Within the system, a single intermediate compound, LiF·YF₃, is formed. No solid solutions have been observed between this compound and either of the components. LiF·YF₃ melts incongruently to the low temperature orthorhombic form of YF₃ and liquid at 815°. The peri-

TABLE I
COMPARISON OF OBSERVED AND CALCULATED INTENSITIES
FOR LiF·YF₃

hkl	$\sin^2 \theta$ obsd.	I obsd.	I calcd.
101	0.0271	VS	9.50
112	.0652	VS	4.36
103	.0688	S	2.38
004	.0825	M	.45
200	.0888	M	.32
202	.1098	VW	.08
211	.1161	S	1.05
114	.1267	S	.55
105	.1508	S	1.38
213	.1574	S	.84
204	.1714	S	1.30
220	.1773	S	.72
222	.1981	VW	0.00
301	.2048	M	.32
116	.2292	S	.59
215	.2397	M	.34
312	.2434	S	1.13
303	.2468	M	.41
224	.2501	M	.43
107	.2756	W	.27
321	.2940	M	.42
314	.3057	VW	.007
008	.3293	W	.02
323	.3351	W	.22
400	.3555	M	.14

tectic invariant point for this reaction occurs at 49 mole % YF₃. The single eutectic in the system is at 19 mole % YF₃ and 695°. The peritectic composition for the YF₃ inversion reaction is at approximately 82 mole % YF₃. No direct determination of this invariant point composition was possible from the observation of quenched samples because of the difficulty of distinguishing the quench growths from primary phase YF₃.

TABLE II
THERMAL EFFECTS OCCURRING DURING THE COOLING OF
LiF-YF₃ MIXTURES

Compn. mole % in liquid	YF ₃	Liquidus temp., °C.	Solidus temp., °C.	Other thermal effects, °C.
90	10	786	690	
80	20	720	690	
70	30	755	697	
60	40	803	697	
50	50	833	825	
40	60	925	829	
35	65	955	830	
15	85		807	1050
0	100	1148		1055

Dergunov³ reported that the system LiF-YF₃ contains a single eutectic, occurring at 744° and at approximately 18 mole % YF₃, and that no complex compounds of LiF and YF₃ are formed. The differences in his results and those reported here probably are related to the fact that in the current investigation (1) the thermal gradient quenching method was used, and that (2) only oxygen-free YF₃ was used.

According to Dergunov, complex compounds are formed only in the alkali fluoride-YF₃ systems,

TABLE III

DATA OBTAINED BY QUENCHING LiF-YF ₃ MIXTURES			
Compn., mole % YF ₃	Phase change temp., °C.	Phases found just above phase change	Phases found just below phase change
3	823 ± 3 ^a	L ^b	LiF + L
3	693 ± 3	LiF + L	LiF + LiF·YF ₃
7	788 ± 3	L	LiF + L
7	693 ± 3	LiF + L	LiF + LiF·YF ₃
11	778 ± 3	L	LiF + L
11	693 ± 3	LiF + L	LiF + LiF·YF ₃
14.3	722 ± 4	L	LiF + L
14.3	684 ± 4	L	LiF + LiF·YF ₃
15	729 ± 2	L	LiF + L
15	698 ± 2	LiF + L	LiF + LiF·YF ₃
17.6	699 ± 3	L	LiF + L
17.6	684 ± 4	LiF + L	LiF + LiF·YF ₃
19	700 ± 2	L	LiF + LiF·YF ₃
21.1	714 ± 4	L	LiF·YF ₃ + L
21.1	684 ± 4	LiF·YF ₃ + L	LiF + LiF·YF ₃
24.8	745 ± 4	L	LiF·YF ₃ + L
24.8	677 ± 4	LiF·YF ₃ + L	LiF + LiF·YF ₃
30	757 ± 5	L	LiF·YF ₃ + L
30	699 ± 4	LiF·YF ₃ + L	LiF + LiF·YF ₃
40	805 ± 4	L	LiF·YF ₃ + L
40	699 ± 4	LiF·YF ₃ + L	LiF + LiF·YF ₃
50	836 ± 3	L	YF ₃ + L
50	830 ± 3	YF ₃ + L	LiF·YF ₃
50	816 ± 3	L	YF ₃ + L
50	807 ± 3	YF ₃ + L	LiF·YF ₃
52	830 ± 5	L	YF ₃ + L
52	821 ± 5	YF ₃ + L	LiF·YF ₃ + YF ₃
66.7	807 ± 3	YF ₃ + L	LiF·YF ₃ + L

^a The uncertainty in temperatures shown in column 2 indicates the temperature differences between the quenched samples from which the values were obtained. ^b The symbol "L" refers to liquid (observed as glass or quench growth).

KF-YF₃, RbF-YF₃ and CsF-YF₃. In these three cases the single compound formed is of the cryolite type, having the generic formula 3MF·YF₃. In the system NaF-YF₃ he found evidence only of solid solution with a pronounced minimum in the liquidus. Preliminary studies of the phase equilibria in the system NaF-YF₃ at this Laboratory have confirmed that the single intermediate compound, reported by Hund²² as NaF·YF₃, occurs within the system and that extensive solid solution is formed between NaF·YF₃ and YF₃.²³ Studies of the miscibility limits of this solution are being investigated. Although the primary phase of the NaF·YF₃-YF₃ solid solution extends to greater than 50 mole % NaF in the system NaF-YF₃, no solid solution is formed between NaF and NaF·YF₃.

Although the single intermediate compound in each of the systems LiF-YF₃ and NaF-YF₃ is of 1:1 ratio, the compounds are not isostructural. The occurrence of a scheelite structure for the compound LiF·YF₃ is unique in the fluoride systems which have been investigated. Because the rare-earth trifluorides of atomic numbers 62-71 (SmF₃ through LuF₃) are isostructural¹⁸ with YF₃, future investigations of the phase equilibria of these fluorides with LiF will probably disclose the occurrence within these systems of 1:1 LiF-MF₃ compounds isostructural with LiF·YF₃.

Acknowledgments.—The authors wish to express their gratitude to W. R. Grimes and J. H. Frye, Jr., for their support and encouragement of the investigations reported here. We are also indebted to S. Cantor and T. S. Carlton for their cooling curve measurements with YF₃.

(22) F. Hund, *Z. anorg. Chem.*, **261**, 106 (1950).

(23) F. Hund, *ibid.*, **263**, 102 (1950).

ANION EXCHANGE AND NON-AQUEOUS STUDIES OF THE ANIONIC NITRATO COMPLEXES OF THE HEXAVALENT ACTINIDES¹

BY J. L. RYAN

Hanford Laboratories Operation, General Electric Company, Richland, Washington

Received September 26, 1960

Spectrophotometric studies in aqueous and non-aqueous systems with miscellaneous supporting data were used to identify the species of the hexavalent actinides which are absorbed by anion-exchange resins from nitrate solutions. The previously unreported tetranitrato complexes, MO₂(NO₃)₄⁻, were identified in solid compounds, in nitromethane solutions, and in anion-exchange resins. The anion-exchange resins were found to absorb predominantly the tetranitrato ions along with a lesser amount of the trinitrato ions MO₂(NO₃)₃⁻. The relative amounts of these two species in the resin phase were found to be dependent on resin phase properties and not detectably dependent on solution phase properties. The formation constant for the reaction UO₂(NO₃)₃⁻ + NO₃⁻ ⇌ UO₂(NO₃)₄⁻ in nitromethane was found to be 4.7 ± 0.2.

Electrical transference data for plutonium(VI) and neptunium(VI) in aqueous solutions has shown that the actinide(VI) ions begin to change from predominantly cationic to anionic species above 10 M HNO₃.² Kaplan, *et al.*,³ have prepared and

identified the uranyl trinitrato complex in ketonic solvents and have shown it to be quite stable in the absence of water. Their work shows no evidence for the existence of a higher nitrato complex of uranyl. They also conclude that formation of the trinitrato complex is only beginning in 16 M HNO₃.

Anion-exchange resins have been shown to absorb uranyl from aluminum nitrate^{4,5} and from other

(1) This paper is based on work performed under Contract No. AT(45-1)-1350 for the U. S. Atomic Energy Commission. Presented before the 138th National Meeting of the American Chemical Society, New York, Sept. 11-16, 1960.

(2) C. K. McLane, J. S. Dixon and J. C. Hindman, "The Transuranium Elements," Division IV, Vol. 14B, Paper 4.3, McGraw-Hill Book Co., Inc., New York, N. Y., 1949, p. 358.

(3) L. Kaplan, R. A. Hildebrandt and M. Ader, *J. Inorg. & Nuclear Chem.*, **2**, 153 (1956).

metal nitrate solutions.⁶ This phenomenon has been attributed, without proof, to the absorption of the $\text{UO}_2(\text{NO}_3)_3^-$ anion.⁶ It was also proposed that the formation of nitrate complexes of uranium-(VI) in various metal nitrate solutions proceeded in the same order as the hydration tendency of the metal ions and that the anion-exchange distributions also increased with increasing tendency of these cations to be hydrated.⁶

It has been proposed that the mechanisms of absorption by anion-exchange resins and extraction by liquid amine extractants are identical and thus the species involved in both processes would be expected to be the same.⁷ In the case of the tetravalent actinide nitrates, this has been shown to be true as the species absorbed by Dowex 1 and extracted by tri-*n*-octylamine in xylene is, in both cases, the $\text{M}(\text{NO}_3)_6^-$ anion.^{8,9} When extended to the hexavalent actinides in nitrate systems, this supposition was not true. Although the uranyl nitrate species extracted by amine solutions was identified as the $\text{UO}_2(\text{NO}_3)_3^-$ ion,⁸ an absorption spectrum of resin loaded from a nitrate solution containing uranyl ion was (surprisingly) unascrivable to the tri-nitrato ion and suggested the presence of at least one other species. The following described work was therefore undertaken to elucidate the nature of the hexavalent actinide species absorbed by anion-exchange resins.

Experimental

Actinide(VI) Nitrates.—Uranyl nitrate solutions were prepared from Mallinckrodt uranyl nitrate hexahydrate. The neptunium was isotopically pure Np^{237} , which was purified, as neptunium(IV), by anion exchange in nitric acid¹⁰ and was found by α -energy analysis¹¹ to contain 0.011 weight % plutonium. Other impurities should be about 100 parts per million parts neptunium. Quantitative conversion to neptunium(VI) occurred during the evaporative concentration of the anion exchange product from 40 g. $\text{Np}/\text{l.}$, 0.6 *M* HNO_3 to 500 g. $\text{Np}/\text{l.}$

The plutonium was a reactor produced isotopic mixture. It was purified as plutonium(IV) by anion exchange in nitric acid^{12,13} and was of comparable purity to the neptunium solution described above. The anion exchange product was converted to Pu(VI) by treatment with electrolytically produced ozone¹⁴ at 80° until no plutonium of lower valence states was detectable spectrophotometrically. By combining the ozone treatment with thermal evaporation very pure Pu(VI) stock solutions of about 800 g. $\text{Pu}/\text{l.}$ were prepared. Plutonium and neptunium stock solution concentrations were determined by controlled potential coulometric titration.^{15,16}

(4) K. A. Kraus and F. Nelson, *Proc. Intern. Conf. Peaceful Uses Atomic Energy, Geneva*, **1955**, **VII**, 119 (1956).

(5) H. E. Ockenden and J. K. Foreman, *Analyst*, **82**, 592 (1957).

(6) J. K. Foreman, I. R. McGowan and T. D. Smith, *J. Chem. Soc.*, **738** (1959).

(7) U. Schindewolf, *Z. Elektrochem.*, **62**, 335 (1958).

(8) W. E. Keder, J. L. Ryan and A. S. Wilson, *J. Inorg. & Nuclear Chem.*, in press.

(9) J. L. Ryan, *J. Phys. Chem.*, **64**, 1375 (1960).

(10) J. L. Ryan, Atomic Energy Commission Research and Development Report, HW-59193 REV. (Hanford Laboratories), Sept. 3, 1959.

(11) F. P. Brauer and R. E. Connally, Atomic Energy Commission Research and Development Report, HW-60974 (Hanford Laboratories), July 10, 1959.

(12) J. L. Ryan and E. J. Wheelwright, Atomic Energy Commission Research and Development Report, HW-55893 (Hanford Laboratories), Jan. 2, 1959.

(13) J. L. Ryan and E. J. Wheelwright, *Ind. Eng. Chem.*, **51**, 60 (1958).

(14) G. L. Putnam, R. W. Moulton, W. W. Fillmore and L. H. Clark, *J. Electrochem. Soc.*, **93**, 211 (1948).

Resins.—Anion-exchange resins were all Dowex 1 of various cross-linkages and in the nitrate form. Dowex 1 is a quaternary ammonium type polystyrene-divinylbenzene copolymer. Two special preparations of low capacity one per cent. crosslinked Dowex 1 were obtained from Dow Chemical Company. These had capacities of 0.39 and 1.2 meq./g. (dry chloride form) versus 4.4 meq./g. for standard resin.

Tetraethylammonium Nitrate.—Tetraethylammonium nitrate was prepared from Eastman tetraethylammonium bromide by anion exchange.⁹ It was dried at 60° and 25 mm. pressure.

Preparation of Actinide(VI) Trinitrato Salts.—Compounds of the general formula $(\text{C}_2\text{H}_5)_4\text{NMO}_2(\text{NO}_3)_3$, analogous to the well known cesium and rubidium salts, were prepared by precipitation of the metal with tetraethylammonium nitrate from concentrated nitric acid solutions. Because of the high solubility of these salts in concentrated nitric acid, concentrated solutions of all reagents were used in their preparation. The uranyl salt was prepared by dissolving stoichiometric ratios of uranyl nitrate hexahydrate and tetraethylammonium nitrate in 15 *M* HNO_3 at 90° and allowing this to cool to 25°. The long needle-like crystals were washed with sufficient 15.7 *M* HNO_3 to dissolve about two-thirds of the product. The compound was either dried over NaOH followed by $\text{Mg}(\text{ClO}_4)_2$ or by heating with a heat lamp until the fumes of nitric acid disappeared. The compound was much less soluble in metal nitrates than in nitric acid and was easily precipitated from calcium, aluminum, or lithium nitrate solution but obviously could not be prepared free of the metal nitrate by this method. Chemical analysis confirmed the composition. Uranium was determined both gravimetrically as U_3O_8 and volumetrically by zinc reduction and ceric titration. The results were identical. Carbon and hydrogen were determined by Schwarzkopf Micro-Analytical Lab., Woodside, New York. Melting point was about 100°.

Anal. Calcd. for $(\text{C}_2\text{H}_5)_4\text{NUO}_2(\text{NO}_3)_3$: U, 40.6; C, 16.39; H, 3.42. Found: U, 40.6; C, 16.43; H, 3.47.

The compound $(\text{C}_2\text{H}_5)_4\text{NNpO}_2(\text{NO}_3)_3$ was prepared by adding a five mole % excess of $(\text{C}_2\text{H}_5)_4\text{NNO}_3$ dissolved in a minimum of concentrated nitric acid to a hot 800 g. $\text{Np}/\text{l.}$ solution 8 *M* in nitric acid. Cooling to 10° resulted in a supersaturated solution from which precipitation of long needles was brought about by drawing air across the surface of the solution. Because of the lower availability of neptunium, washing of the preparation was minimized and the resulting purity probably was somewhat lower than in the case of uranium. The compound was analyzed by determining neptunium by controlled potential coulometric titration in 1 *M* HNO_3 .¹⁶ The melting point was about 100°.

Anal. Calcd. for $(\text{C}_2\text{H}_5)_4\text{NNpO}_2(\text{NO}_3)_3$: Np, 40.5. Found: Np, 40.1.

The compound $(\text{C}_2\text{H}_5)_4\text{NPuO}_2(\text{NO}_3)_3$ was prepared, in the same manner as the neptunium compound, from a plutonium stock solution which had been freshly oxidized with ozone. The solution of the plutonium compound also supersaturated badly and was seeded with a microcrystal of the uranium compound. This compound also precipitated as long needles and melted near 100°. The compound was analyzed for plutonium by controlled potential coulometric titration in 1 *M* HCl solution.¹⁵

Anal. Calcd. for $(\text{C}_2\text{H}_5)_4\text{NPuO}_2(\text{NO}_3)_3$: Pu, 40.7. Found: Pu, 39.2.

Both the neptunium and plutonium salts were unstable, perhaps because of α -radiation induced reduction. For this reason the salts, particularly the Pu salt, had to be used without delay. (After standing several months both the Pu and Np salts were only partially soluble in nitromethane. The soluble plutonium species was determined spectrophotometrically to be only Pu(IV), whereas the soluble neptunium species was completely Np(VI).)

Preparation of Actinide(VI) Tetranitrato Salts.—The compound $[(\text{C}_2\text{H}_5)_4\text{N}]_2\text{UO}_2(\text{NO}_3)_4$ has been reported by

(15) F. A. Scott and R. M. Peekema, *Proc. Second Intern. Conf. Peaceful Uses Atomic Energy, Geneva*, **28**, 573 (1958).

(16) R. W. Stromatt, Atomic Energy Commission Research and Development Report, HW-59447 (Hanford Laboratories), Feb. 2, 1959.

Dieke and Duncan¹⁷ but its composition was not established by analysis. Attempts to prepare it by the method described (slow crystallization at 10° from concentrated HNO₃) resulted in large tabular crystals as described by Dieke and Duncan. When these crystals were dried by blotting and ground in petrolatum, their absorption spectrum was found to be identical with the spectrum of the long (up to 4 cm.) needles of the trinitrato salt obtained at higher temperature. Many preparations were attempted using various uranium, tetraethylammonium and nitric acid concentrations, and crystallization temperatures from -10° to 80°. In every case the crystals obtained had identical visible absorption spectra, when milled in petrolatum, with that of the trinitrato salt described in this work and with the spectrum of the trinitrato ion in ketonic solvents reported by Kaplan, *et al.*³ It seems highly probable, therefore, that the compound reported by Dieke and Duncan was in actuality (C₂H₅)₄NUO₂(NO₃)₃.

The compound K₂UO₂(NO₃)₄ has been reported.¹⁷ Several attempts to prepare this salt by the reported method and variations thereof were carried out, but spectrophotometric examination of each preparation indicated the presence of the UO₂(NO₃)₃⁻ ion. It is possible that the exact conditions of preparation reported were not achieved. The compound (NH₄)₂UO₂(NO₃)₄ has been reported as a "metastable form."¹⁸ Attempts to prepare it by the method described resulted only in crystallization of ammonium nitrate.

The compound [(C₂H₅)₄N]₂UO₂(NO₃)₄ was prepared by fusion of equimolar quantities of (C₂H₅)₄NUO₂(NO₃)₃ and (C₂H₅)₄NNO₃ under an infrared heat lamp. That the product was a new compound rather than a mixture was deduced from the following observations: (1) the yellow color was more intense than that of the trinitrato salt; (2) it fluoresced brilliant yellow whereas the potassium, rubidium, cesium, ammonium and tetraethylammonium trinitrato salts all fluoresced light green; (3) the visible absorption spectrum was entirely different than that of (C₂H₅)₄NUO₂(NO₃)₃ as seen in Fig. 2; (4) fusions of mixtures containing less than one mole (C₂H₅)₄NNO₃ per mole (C₂H₅)₄NUO₂(NO₃)₃ yielded products whose spectra were intermediate between that for a 1:1 fusion and that for the pure trinitrato salt, whereas fusion mixtures containing greater than 1:1 ratio gave the same spectra as a 1:1 material although the 1:1 ratio could not be much exceeded because of the low solubility of (C₂H₅)₄NNO₃ in the fusion mixture; (5) the infrared spectrum of the exactly 1:1 fusion shows only coordinated nitrate with no evidence of ionic nitrate as obtained with (C₂H₅)₄NNO₃¹⁹; (6) the NO₂ and NO stretching frequencies are markedly different from those for (C₂H₅)₄NUO₂(NO₃)₃¹⁹; and (7) the X-ray diffraction pattern is distinctly different than that of (C₂H₅)₄NUO₂(NO₃)₃ and has no line in common with (C₂H₅)₄NUO₂(NO₃)₃.

Both the trinitrato and tetranitrato salts can also be prepared by fusion of (C₂H₅)₄NNO₃ with UO₂(NO₃)₂·6H₂O followed by sufficient heating to drive off the water.

Resin Capacity Measurements.—Dowex 1, X-1 (50 to 100 mesh) (capacity 3.94 meq./g. dry nitrate form) was used in uranium capacity determinations. The resin was dried at 60° and 25 mm. pressure and weighed in the nitrate form. The resin was equilibrated with the aluminum nitrate solutions containing uranyl nitrate with continuous shaking for two to three weeks at 25°. This is considered sufficient time in spite of the poor kinetics of anion exchange in metal nitrate systems in general^{12,13,20} and of the uranyl nitrate system specifically.²¹ The resin was removed from the solution by vacuum filtration on sintered glass and was eluted with 0.1 M HNO₃. The uranium eluted was determined by controlled potential coulometric titration.

(17) G. H. Dieke and A. B. F. Duncan, "Spectroscopic Properties of Uranium Compounds," McGraw-Hill Book Co., Inc., New York, 1949, pp. 139-140 and 149-154.

(18) G. T. Seaborg and J. J. Katz, "The Actinide Elements," McGraw-Hill Book Co., Inc., New York, N. Y., 1954, pp. 830-831.

(19) L. L. Burger, Hanford Laboratories, private communication.

(20) K. A. Kraus and F. Nelson in symposium on Ion Exchange and Chromatography in Analytical Chemistry (1956), Am. Soc. for Testing Materials. Special Technical Publication No. 195, 1958, p. 51.

(21) I. R. Higgins, "The Recovery of Uranium from Calcium Nitrate by Continuous Ion Exchange," Report No. CSC-6003, Chemical Separations Corp., Oak Ridge, Tenn., Sept., 1960.

Uranium in the solution phases was determined by controlled potential coulometric titration or by difference.

Spectrophotometric Measurements.—Spectrophotometric measurements were made with a Cary Model 14 recording spectrophotometer. Solution spectra were obtained using matched 1.00 cm. silica cells.

Acetone used in spectrophotometric studies was c.p. grade and was redistilled. Nitromethane was Eastman spectro grade. Solvents were dried by shaking with either CaO or Drierite (anhydrous CaSO₄) although this step appeared to be unnecessary. Solutions containing mixtures of (C₂H₅)₄NUO₂(NO₃)₃ and (C₂H₅)₄NNO₃ were prepared from stock solutions of each in nitromethane. The stock solutions were prepared from the pure compounds and were not otherwise standardized. Plutonium and neptunium in organic solvents were determined by alpha counting.

Absorption spectra of resins were obtained using 1.00 or 0.50 cm. silica cells and either the visible or infrared source of the Cary Model 14. Attempts to use 0.1 cm. cells with resins having high loading were unsuccessful because of light leakage between the resin beads. Excess liquid was drawn off the resin with a fine tipped pipet to ensure that the resin, which floated on some of the solutions used, was closely packed. The blank was resin treated identically except for the presence of the actinide of interest.

Absorption spectra of solids were obtained from samples prepared by mulling the finely ground compound in petrolatum and using a blank of CaCO₃ in petrolatum or, in the case of low melting compounds, from solid films prepared by melting the salt between fused silica plates. By the latter technique spectra could be obtained over the ultraviolet as well as the visible and infrared ranges of the instrument. Quantitative spectra of the low melting solids were obtained in this way with the silica plates separated by spacers of uniform thickness. The molar extinction coefficient, ϵ , can be obtained without knowing the sample thickness. If a weighed amount of the compound is used and the area that it occupies between the plates is measured the molar extinction coefficient can be calculated from the relation

$$A = \log I_0/I = \epsilon ct = \epsilon \left(\frac{\text{moles}}{\text{l.}} \right) (\text{cm.}) = 1000\epsilon \left(\frac{\text{moles}}{\text{cm.}^3} \right) (\text{cm.})$$

$$\epsilon = 10^{-3} A \left(\frac{\text{cm.}^2}{\text{moles}} \right)$$

The only requirements are that the sample thickness be uniform and continuous. This was checked by measuring the absorption spectra at several points on the sample and as a function of thickness which was varied by as much as a factor of four. The greatest spread between experimentally determined molar extinction coefficients was 3%.

The absorption spectra of Pu(VI) solutions in the range 400-1400 m μ , were obtained at approximately one molar nitrate increments in nitric acid and in various metal nitrate solutions. These solutions all contained identical plutonium concentrations and contained 0.15 M HNO₃ in the case of the metal nitrates. They were all made up and the spectra measured within 32 hours after termination of ozone oxidation of the plutonium stock solutions to minimize the effect of α -reduction of Pu(VI) which occurs at the rate of about 0.6% per day. Nitrate was determined by controlled potential coulometric titration.²²

Results and Discussions

Resin Studies.—Figure 1 shows the absorption spectrum of uranyl loaded on standard capacity Dowex 1, X-1 (50 to 100 mesh) from 2.0 M Al(NO₃)₃. This spectrum does not show the intense fine structure peaks present in the spectrum of the trinitratouranyl ion as published by Kaplan, *et al.*³ (The spectrum of the trinitratouranyl ion is shown in Fig. 2.) The absorption spectrum of uranyl on the resin was found to be essentially identical when the resin was loaded from aluminum, lithium or calcium nitrate. The resin spectrum

(22) L. R. Duncan, Hanford Laboratories, unpublished analytical method.

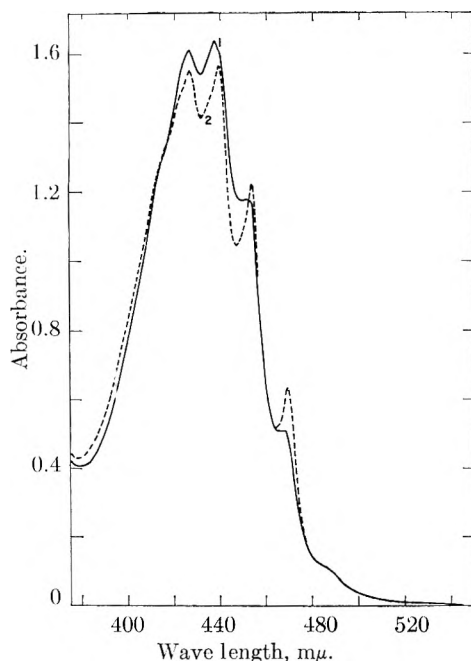


Fig. 1.—Absorption spectra of U(VI) loaded on high and low capacity Dowex 1, X-1 from 2.0 M $\text{Al}(\text{NO}_3)_3$. Resin capacities based on dry chloride form: (1) 4.4 meq./g.; (2) 1.2 meq./g.

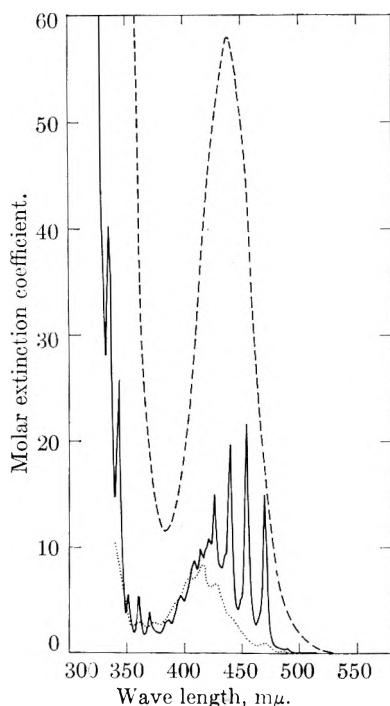


Fig. 2.—Absorption spectra of solid complex U(VI) nitrate salts compared to that of the aqueous uranyl ion: ---, $[(\text{C}_2\text{H}_5)_4\text{N}]_2\text{UO}_2(\text{NO}_3)_4$; —, $(\text{C}_2\text{H}_5)_4\text{NUO}_2(\text{NO}_3)_3$; ····, uranyl nitrate in 0.514 M HNO_3 .

also was found to remain the same over the entire range of nitrate concentration from which sufficient resin loading could be achieved to obtain a resin spectrum. It was also independent of resin cross linkage. It was concluded that either the species absorbed by the resin was not predominantly the trinitrato complex or that the spectrum was vastly perturbed as compared to the spectrum

obtained in ketonic solvents. The former explanation is much more probable in view of previous work which demonstrated that complex anions absorbed on anion resins have absorption spectra almost identical to the spectra of the same complexes in a variety of inert non-aqueous solvents including ketones.⁹ Since the resin spectrum has shoulders or very small peaks at the positions of the four most intense of the vibrational fine structure peaks of the trinitrato uranyl ion, the concept that the resin spectrum might represent a highly distorted trinitrato uranyl spectrum could not be completely dismissed without further evidence. In order to further test the point, absorption spectra of uranyl under a variety of conditions were obtained to see whether conditions existed which could perturb the absorption spectrum of the trinitrato uranyl ion to the extent needed to explain the resin spectrum.

The absorption spectrum of a solid film of $(\text{C}_2\text{H}_5)_4\text{NUO}_2(\text{NO}_3)_3$ was obtained (Fig. 2) and was found to be identical to that of the trinitrato uranyl ion reported by Kaplan, *et al.*, except for a uniform decrease of about 30% in molar extinction coefficient at all wave lengths and a very slight wave length shift (2–3 $\text{m}\mu$) which was constant on an energy basis. The absorption spectrum of a mull of this salt was identical to that of the solid film. Solutions of this compound in acetone or nitromethane gave spectra exactly identical to that reported by Kaplan, *et al.* The salts $\text{CsUO}_2(\text{NO}_3)_3$, $\text{RbUO}_2(\text{NO}_3)_3$, $\text{KUO}_2(\text{NO}_3)_3$ and $\text{NH}_4\text{UO}_2(\text{NO}_3)_3$ (as mulls) gave spectra in which the wave length shift, referred to the non-aqueous solution spectra, was slightly greater than that for the tetrabutylammonium salt and the intense vibrational peaks were broadened slightly. The order of this distortion in the solid compounds was $(\text{C}_2\text{H}_5)_4\text{N} < \text{Cs} < \text{Rb} < \text{K} = \text{NH}_4$. That this distortion in spectrum (which is much less than required to explain the resin spectrum) is due only to lattice perturbations is clear from the fact that the spectra of nitromethane solutions of all of these salts were indistinguishable. Since the perturbation of the spectrum by the completely oriented crystal lattice was less than that required to produce the resin spectrum and since it seems highly improbable that the randomly oriented resin phase would perturb the spectrum as much as the completely oriented crystal lattice, it was concluded that the resin spectrum does not arise from distortion of the trinitrato ion spectrum by the resin. The absorption spectra of resins loaded with plutonium(VI) and neptunium(VI) from aluminum nitrate were compared with the spectra of $(\text{C}_2\text{H}_5)_4\text{NPuO}_2(\text{NO}_3)_3$ and $(\text{C}_2\text{H}_5)_4\text{NNpO}_2(\text{NO}_3)_3$ in nitromethane. In all cases the resin spectra were markedly different from the trinitrato ion spectra and showed a marked diminution in the fine structure associated with the M–O vibrational modes.

To show that difference in water coordination or hydration of the trinitrato ion was not causing the difference in spectra, resin was loaded from non-aqueous media. The resin absorbs uranyl strongly from acetone or nitromethane solutions of $\text{UO}_2(\text{NO}_3)_2 \cdot 6\text{H}_2\text{O}$ or of $\text{UO}_2(\text{NO}_3)_2 \cdot 2\text{H}_2\text{O}$ and from

nitromethane solutions of $(C_2H_5)_4NUO_2(NO_3)_3$. Resins loaded from these solutions all had essentially the same spectra as resins loaded from aqueous metal nitrates. Resin loaded from acetone and dried either by vacuum at 60° or by a heat lamp and suspended in CCl_4 to minimize light reflection from the bead surfaces gave the same absorption spectrum. The fact that the spectra of resins loaded from both aqueous and non-aqueous media were identical eliminates hydration as the factor responsible for the resin spectrum. From the above arguments, it is inferred that the resin spectrum does not arise from the spectrum of the tri-nitrato ion. The alternate hypothesis which suggests itself is that the spectrum is the result of a second species being absorbed.

Uranyl is very strongly absorbed from acetone solution of $UO_2(NO_3)_2 \cdot 2H_2O$ by anion exchange resins and very high loadings can be obtained if finely divided resins of low cross linkage are used. Spectrophotometric study of resin loaded in this manner, although difficult because of the high absorbances involved, showed that the shoulders present at the same wave lengths as the intense trinitrato peaks had become considerably intensified and were now distinct peaks. Since high resin loading would be expected to favor anionic complexes of lower negative charge, it was tentatively concluded that the resin loaded some of the trinitrato complex along with predominantly a higher nitrate complex.

It has been shown that if anionic complexes of different charge are absorbed by a resin, decreased resin capacity will favor the complexes of lower charge.²³ Thus if the trinitrato ion and a higher nitrate complex are both absorbed by the resin, a lower capacity resin should contain a greater proportion of the trinitrato complex. Figure 1 shows the spectrum of uranium on Dowex 1, X-1 of 1.2 meq./g. and compares it to the spectrum of uranium on the standard resin of 4.4 meq./g. Capacities are in terms of grams of dry chloride form resin. Resin of lower capacity (0.39 meq./g.) did not absorb enough uranium(VI) from aluminum nitrate to furnish a spectrum of the resin free of the spectrum of the equilibrium aqueous phase uranium. It is seen from Fig. 1 that the spectrum of the loaded lower capacity resin shows enhanced fine structure as would be expected if it contained more of the trinitrato ion.

As mentioned, high resin loading should also favor anionic complexes of lower negative charge and high uranium loading from aluminum nitrate solutions should enhance the trinitrato peaks in the resin spectrum. Dowex 1, X-1 (standard capacity resin) loaded to about 500 mg. U/g. resin (weight based on dry nitrate form resin) was examined spectrophotometrically. With 5 mm. cells the absorbances were too high to measure. With 1 mm. cells the absorbance at the maximum near $440 m\mu$ was about 1.8, and leakage of light between resin beads badly distorted the spectrum in the high absorbance region. Because of the very poor kinetics of the uranyl absorption from aluminum

nitrate, it is possible, with resins of high crosslinkage, to load the outer surface of the bead without achieving high over-all resin loading. Dowex 1, X-10 (about 100 mesh) was loaded for two minutes at 90° from 50 g./l. uranium (VI) in 2 M $Al(NO_3)_3$ washed with cold 2 M $Al(NO_3)_3$, and mixed with two parts of unloaded resin to one part of loaded resin. The resin spectrum obtained immediately in a 5 mm. cell was very similar to that of the low capacity Dowex 1, X-1 shown in Fig. 1. The resin (still in the cell) was then held at 100° for 45 minutes to cause redistribution of the uranium throughout the resin. By this technique the total uranium in the light beam was held constant, but the actual concentration of uranium in the resin was varied. The spectrum of the resin treated in this way was very similar to that of the high capacity Dowex 1, X-1 shown in Fig. 1, having only shoulders at about 453 and 468 $m\mu$ instead of sharp peaks. But perhaps of greater importance, was the fact that the molar extinction coefficient at 435-440 $m\mu$ had increased by 25%. Since the total uranium in the cell had remained constant the only logical cause for this change in extinction coefficient was a change in the ratio of species absorbed in the resin. A further inference was that the other species in the resin must have a higher molar extinction coefficient at 435-440 $m\mu$ than does the trinitrato complex. The molar extinction coefficients of uranium(VI) in aqueous nitrate solutions (HNO_3 and $Al(NO_3)_3$) are all lower than that of the trinitrato ion at 435 $m\mu$ leading to the conclusion that the other species in the resins is one that is not present to a large extent in aqueous solutions.

Capacity measurements as a function of equilibrium aqueous phase concentration give some insight into the charge of the complex in the resin phase. The stoichiometry is relatively straightforward if only one species is absorbed and is absorbed strongly. If more than one species absorbs, the situation becomes more complex since the species of smaller negative charge are favored by the resin as loading increases. If, however, the more negative complex is absorbed considerably more strongly than the complex or complexes of smaller negative charge, an inflection point in the plot of resin phase *versus* aqueous phase concentrations may occur near the resin capacity for this complex. Figure 3 shows such a plot for uranium(VI) in 2.0 M $Al(NO_3)_3$. The presence of a distinct inflection point near a ratio of 0.5 mole of uranium per equivalent of resin strongly implies that the most strongly absorbed uranium complex has a -2 charge (presumably $UO_2(NO_3)_4^{2-}$). The fact that the resin capacity exceeds the theoretical capacity for this ion may be due to resin invasion. However, the fact that it occurs at relatively low aqueous uranium concentration tends to indicate, although by no means conclusively proves, that a -1 charged anion ($UO_2(NO_3)^-$) also absorbs to some extent.

Figure 2 shows the visible absorption spectrum of $[(C_2H_5)_4N]_2UO_2(NO_3)_4$ obtained from a solid film. The absorption spectrum of the hydrated uranyl ion also is shown in Fig. 2 for comparison.

(23) J. Aveston, D. A. Everest and R. A. Wells, *J. Chem. Soc.*, 231 (1958).

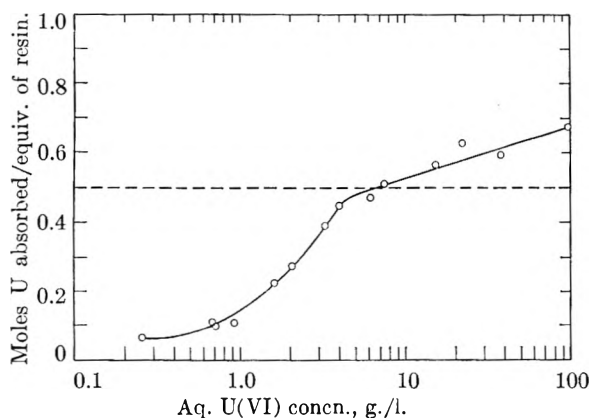


Fig. 3.—Absorption of U(VI) from 2.0 M $\text{Al}(\text{NO}_3)_3$ by Dowex 1, X-1.

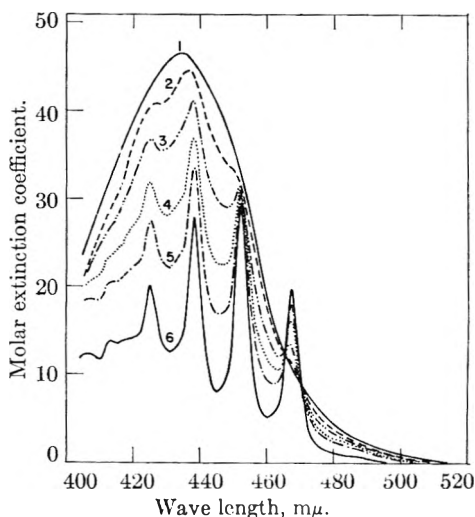


Fig. 4.—Absorption spectra of nitromethane solutions containing 0.0177 M $(\text{C}_2\text{H}_5)_4\text{NUO}_2(\text{NO}_3)_3$ plus tetraethylammonium nitrate: (1) adjusted spectrum of solid $[(\text{C}_2\text{H}_5)_4\text{N}]_2\text{UO}_2(\text{NO}_3)_4$, and (2) 1.58 M, (3) 0.48 M, (4) 0.194 M (5) 0.0972 M, and (6) 0.000 M $(\text{C}_2\text{H}_5)_4\text{NNO}_3$.

The molar extinction coefficient of the tetranitrato salt is much higher than that of the trinitrato salt or aqueous uranyl nitrate solutions. This is in accord with what is required of the higher complex on the resin as previously discussed. The spectrum of this compound was obtained (at 25°) over the range 200–550 $m\mu$, and it is noteworthy that the spectrum showed none of the fine structure commonly attributed to uranium–oxygen vibrations. In contrast, the spectrum of solid $(\text{C}_2\text{H}_5)_4\text{NUO}_2(\text{NO}_3)_3$ contained many intense vibrational peaks throughout the same range. (In the trinitrato salt it appears that there are at least three overlapping series of vibrational peaks which are uniformly separated, on an energy basis, within a given series.) The complete absence of vibrational structure in the spectrum of the tetranitrato salt should be of interest in regard to the nature of the bonds involved. It is possible that vibrational structure might appear at lower temperature.

It appears from Fig. 2 that the resin spectra could result easily from a combination of the trinitrato spectrum and the tetranitrato spectrum. A preparation of $[(\text{C}_2\text{H}_5)_4\text{N}]_2\text{PuO}_2(\text{NO}_3)_4$ was made, and the absorption spectrum of a solid film of it,

though poor in quality, was found to bear considerable likeness to the spectrum of plutonyl absorbed on resin from aluminum nitrate. The spectrum of this compound was found to lack the fine structure present in the spectrum of the plutonyl trinitrato complex. Actual mixtures of the trinitrato and tetranitrato uranyl salts gave spectra very similar to but not exactly like the resin spectra. The reason for the lack of identity was believed due to shifts in wave length and intensity as observed in the case of the solid trinitrato complex when compared to its solution. Experience with other complex salts including some of the actinide chlorides²⁴ indicates that the magnitudes and even the directions of these shifts between solid and solution spectra are not necessarily the same for different complex anions. Thus it is apparent that the resin spectra cannot be reconstructed exactly from solid state spectra. However, since experience has shown that the spectra of complexes in the resin phase can be expected to be very similar to those obtained from non-aqueous solutions,⁹ it became very desirable to obtain the spectrum of the tetranitrato complex in solution.

Non-aqueous Studies.—Kaplan, *et al.*, have stated that addition of excess nitrate to solutions containing the trinitratouranyl ion in ketonic solvents produced essentially no change in spectrum.³ In accord with these findings, it was found that the tetranitrato salt in acetone dissociates to give only the trinitrato ion. Addition of excess tetraethylammonium nitrate produced little if any change. The dielectric constant of acetone is only 20, and it can be expected that the solubility and degree of ionization of tetraethylammonium nitrate might be higher in a solvent such as nitromethane which has a dielectric constant of 38. When relatively large amounts of tetraethylammonium nitrate were added to nitromethane solutions of $(\text{C}_2\text{H}_5)_4\text{NUO}_2(\text{NO}_3)_3$ the spectrum changed markedly. The absorption spectra of a series of solutions made up with constant concentration of $(\text{C}_2\text{H}_5)_4\text{NUO}_2(\text{NO}_3)_3$ and varying concentration of $(\text{C}_2\text{H}_5)_4\text{NNO}_3$ were obtained. Some of these spectra are shown in Fig. 4. Isosbestic points at 465.5 and 470.0 $m\mu$ and a near isosbestic point at 452.0 $m\mu$ indicate that only two uranium species are present in these solutions, that is, only one complex is being formed from the trinitrato ion. It was found that the solutions obeyed the Beer–Lambert law over a fivefold range of uranium concentration.

Calculation of the relative amounts of the trinitrato complex and the higher complex in these nitromethane solutions is complicated by the fact that the absorption spectra continue to change up to the point of saturation of nitromethane with $(\text{C}_2\text{H}_5)_4\text{NNO}_3$ (about 1.7 M), and thus the molar extinction coefficients for the higher complex cannot be determined directly. Certain assumptions are thus necessary with regard to the absorption spectrum of the pure higher complex. These are that the spectrum of the higher complex is identical to that of solid $(\text{C}_2\text{H}_5)_4\text{N}_2\text{UO}_2(\text{NO}_3)_4$ shown in Fig. 2 with two exceptions: (1) the entire spectrum of the solution is shifted uniformly on an energy basis

(24) J. L. Ryan, unpublished results.

relative to that of the solid; and (2) the molar extinction coefficients of the solid and the nitromethane solutions at all wave lengths are related by a constant factor. These assumptions are well founded since these are exactly the changes observed in the spectrum of the trinitrato ion in solid $(C_2H_5)_4N UO_2(NO_3)_3$ when it is dissolved in acetone or nitromethane solution. The molar extinction coefficients of the higher complex in nitromethane are known at the two isosbestic points and can be very closely approximated at the near isosbestic point. Because of the steepness of the solid tetranitrato salt spectrum in this wave length range, only one combination of intensity change and wave length change on the solid will produce the same molar extinction coefficients at all three of these points as measured in solution. The best fit was obtained with molar extinction coefficients of the solid decreased to 80.5% and the wave number increased by 270 cm.^{-1} (wave length decrease of $6.0\text{ m}\mu$ at $474\text{ m}\mu$). The visible absorption spectrum of $[(C_2H_5)_4N]_2UO_2(NO_3)_4$ modified in this way is shown in Fig. 4 with the spectra of the pure trinitrato complex and of mixtures of the trinitrato complex and higher complex in nitromethane.

The amounts of the trinitrato and higher complex in nitromethane were calculated at $460.0\text{ m}\mu$ using the measured molar extinction coefficient of $(C_2H_5)_4N UO_2(NO_3)_3$ in nitromethane and the value for the higher complex calculated in the manner just described. Although essentially the same results are obtained at any wave length where the trinitrato and higher complex have different molar extinction coefficients, $460\text{ m}\mu$ was chosen because it is near the isosbestic points and should give greatest accuracy. At $460\text{ m}\mu$ it was found that the assumptions as to amount of wave length and intensity shift were not critical compared to other wave lengths. For the reaction



a plot of $\log [UO_2(NO_3)_{3+n}^{-(n+1)}] / [UO_2(NO_3)_3^-]$ versus $\log [NO_3^-]$ where brackets indicate concentrations will have a slope, n , if activity coefficients are near unity or cancel. If a very small correction, assuming $n = 1$, is made to the initial nitrate concentrations to account for that used in forming the complex, this plot gives a perfectly straight line of slope 1.04. This is additional evidence that the higher complex is indeed $UO_2(NO_3)_4^-$. The amount of each of the complexes and the formation constant

$$K = \frac{[UO_2(NO_3)_4^-]}{[UO_2(NO_3)_3^-][NO_3^-]}$$

at each nitrate concentration examined are shown in Table I.

Figure 5 compares the absorption spectrum of uranium loaded on standard capacity Dowex 1, X-1 from $2.5\text{ M Al(NO}_3)_3$ with the absorption spectrum of a nitromethane solution containing 80% $UO_2(NO_3)_4^-$ and 20% $UO_2(NO_3)_3^-$. The very close similarity of these two spectra confirm that the principal uranium species in the resin phase is $UO_2(NO_3)_4^-$. Similar nitromethane solutions of $(C_2H_5)_4N NpO_2(NO_3)_3$ and $(C_2H_5)_4N PuO_2(NO_3)_3$ con-

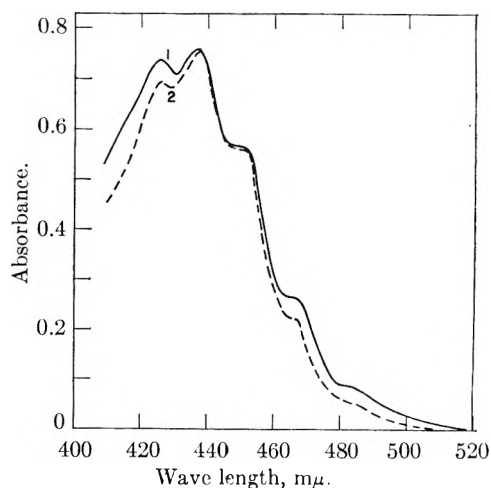


Fig. 5.—Comparison of the spectrum of U(VI) nitrate on anion-exchange resin with that of a nitromethane solution containing a mixture of the trinitrato and tetranitrato uranyl complexes: (1) U(VI) loaded on Dowex 1, X-1 from $2.5\text{ M Al(NO}_3)_3$; (2) mixture of 80% $UO_2(NO_3)_4^-$ and 20% $UO_2(NO_3)_3^-$ in nitromethane.

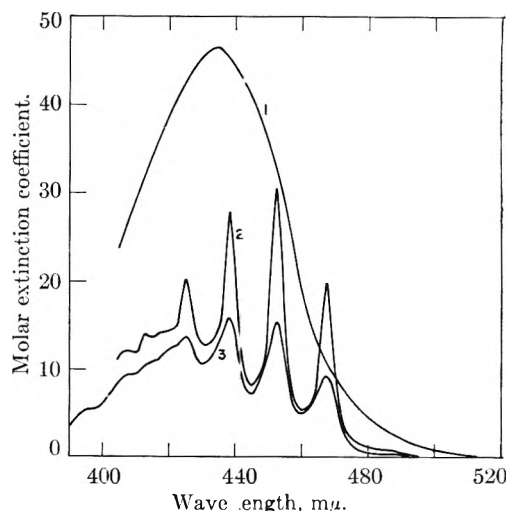


Fig. 6.—Comparison of the spectrum of U(VI) in concentrated nitric acid with the spectra of the anionic nitrate complexes of U(VI): (1) $UO_2(NO_3)_3^-$ from solid $[(C_2H_5)_4N]_2UO_2(NO_3)_4$ and adjusted to nitromethane solution; (2) $UO_2(NO_3)_3^-$ from $(C_2H_5)_4N UO_2(NO_3)_3$ in nitromethane; (3) U(VI) in 20.3 M HNO_3 .

TABLE I
FORMATION OF TETRANITRATOURANYL COMPLEX IN NITROMETHANE

Total uranium constant at 0.0177 M				
Initial molarity $(C_2H_5)_4NNO_3$	Absorbance at $460.0\text{ m}\mu$	% $UO_2(NO_3)_3^-$	% $UO_2(NO_3)_4^-$	K
0.000	0.091	100	0.0	
.0972	.162	71.2	28.8	4.40
.194	.206	53.4	46.6	4.70
.278	.230	43.5	56.5	4.85
.486	.259	31.8	68.2	4.51
.764	.287	20.4	79.6	5.20
1.00	.294	17.5	82.5	4.79
1.58	.308	11.9	88.1	4.71

Av. 4.74 ± 0.17

taining excess nitrate as $(C_2H_5)_4NNO_3$ were found to have absorption spectra very similar to the ab-

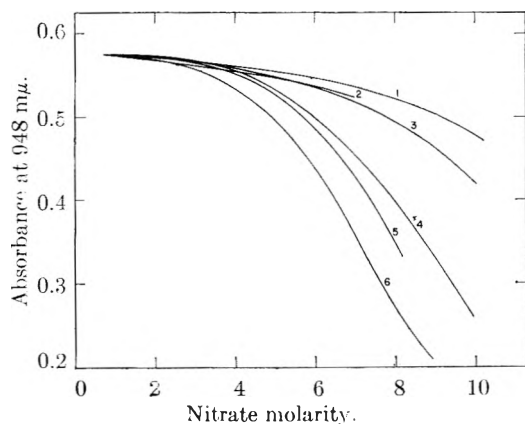


Fig. 7.—The absorbance of Pu(VI) at 948 $m\mu$ as a function of nitrate concentration for several aqueous nitrate salt solutions: (1) $\text{Ca}(\text{NO}_3)_2$; (2) NaNO_3 ; (3) NH_4NO_3 ; (4) LiNO_3 ; (5) $\text{Al}(\text{NO}_3)_3$; (6) HNO_3 .

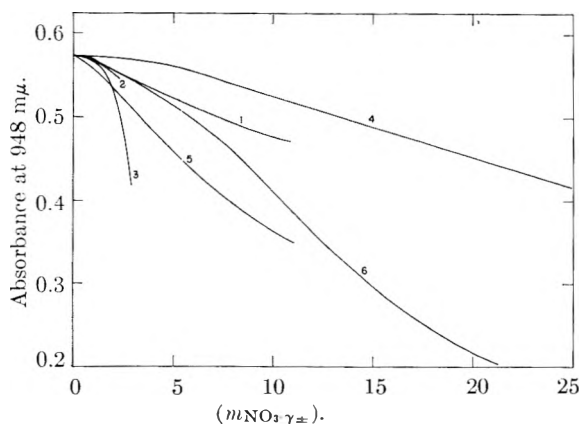


Fig. 8.—The absorbances of Fig. 7 plotted as a function of $(m_{\gamma\pm})$: (1) $\text{Ca}(\text{NO}_3)_2$; (2) NaNO_3 ; (3) NH_4NO_3 ; (4) LiNO_3 ; (5) $\text{Al}(\text{NO}_3)_3$; (6) HNO_3 .

sorption spectra of Np(VI) and Pu(VI) in the resin. These spectra like that of $\text{UO}_2(\text{NO}_3)_4^{=}$ show very little, if any, of the fine structure commonly attributed to the symmetrical metal-oxygen vibrations of the $\text{MO}_2(\text{II})$ entity.

Aqueous Studies.—Kaplan, *et al.*,³ have concluded that in 16 M HNO_3 the predominant complex is $\text{UO}_2(\text{NO}_3)_2(\text{H}_2\text{O})_x$ with some $\text{UO}_2(\text{NO}_3)_3^-$. It is of interest to examine the spectrum of U(VI) in still more highly concentrated nitric acid to see if the tetranitrato complex is detectable in aqueous solutions. Solutions as high as 20.3 M HNO_3 were examined. Ozone was used to remove the yellow color of the fuming nitric acid. Figure 6 compares the absorption spectrum of U(VI) in 20.3 M HNO_3 with that of the pure trinitrato and pure tetranitrato complexes in nitromethane. The relatively low molar extinction coefficients at 440 and 480 $m\mu$ and complete absence of absorption above 493 $m\mu$ indicate that very little if any tetranitratouranil is present in this solution. Figure 6 indicates that less than 50% conversion of the uranium to trinitrato complex has occurred at 20.3 M HNO_3 . Since both Pu(VI) and Np(VI) and presumably also U(VI) become predominantly anionic a little above 10 M HNO_3 ² it must be concluded in agreement with Kaplan, *et al.*, that the other principal species in

concentrated nitric acid solutions is the uncharged complex.

Foreman, *et al.*,⁶ have concluded that the order of resin affinity of U(VI) and order of degree of nitrate complexing in various metal nitrate solutions is $\text{Al}^{+3} > \text{Ca}^{+2} > \text{Li}^+ > \text{NH}_4^+$ and that this is also the order of hydration of these ions. However, their order is based on molar concentrations of the cation rather than on nitrate concentration contributed by the metal nitrate. Their interpretation is further complicated by the use of nitric acid (which suppresses the ion-exchange absorption and renders quantitative interpretation impossible) to keep the nitrate concentration constant at six molar. If their distribution coefficients for solutions containing constant nitrate concentrations and no added acid (or extrapolated to such conditions) are compared, it is found that Li^+ and Al^{+3} are very close together followed by Ca^{+2} which is much poorer in promoting anion exchange and then by NH_4^+ which may be only slightly poorer than Ca^{+2} .

The absorption spectra of Pu(VI) in several aqueous metal nitrate solutions (at constant 0.1 M HNO_3 to prevent hydrolysis) and in nitric acid were obtained in about 1 M increments. The height of the 948 $m\mu$ absorption peak which decreases markedly with nitrate complexing, is shown in Fig. 7. The spectral changes from 400–1400 $m\mu$ were found to be the same for all the nitrates over the range shown in Fig. 7 indicating that the same reactions are involved in each case. Over this range of nitrate concentration no appreciable amount of anionic complexes forms. From Fig. 7 it is apparent that the order of nitrate complexing is $\text{H}^+ > \text{Al}^{+3} > \text{Li}^+ \gg \text{NH}_4^+ > \text{Na}^+ > \text{Ca}^{+2}$. The position of Ca^{+2} indicates that the hydration of the metal cation is by no means the most important factor.

Figure 8 shows the absorbance of the 948 $m\mu$ Pu(VI) peak, the decrease of which is taken as a measure of nitrate complexing, as a function of $(m_{\text{NO}_3-\gamma\pm})$ for several nitrates.²⁵ Aqueous phase mean ionic activity coefficients often have been used in place of the indeterminable single ion activity coefficients and water activity has been neglected in determining formation constants of complexes in concentrated electrolyte solutions from anion-exchange data.^{26–28} If this method of determining formation constants were correct, all the curves of Fig. 8 would be superimposed with the possible exception of nitric acid, in which case formation of the free acid of complex anions might have an effect. Figure 8 points out one of the errors which can occur in the use of anion-exchange data for determination of formation constants in concentrated electrolyte solutions.

(25) Activity data were taken from these sources: (a) NaNO_3 and LiNO_3 : R. A. Robinson and R. H. Stokes, *Trans. Faraday Soc.*, **45**, 612 (1949); (b) $\text{Ca}(\text{NO}_3)_2$: R. H. Stokes and R. A. Robinson, *J. Am. Chem. Soc.*, **70**, 1870 (1948); (c) NH_4NO_3 : B. F. Wishaw and R. H. Stokes, *Trans. Faraday Soc.*, **59**, 27 (1953); (d) HNO_3 and $\text{Al}(\text{NO}_3)_3$: Data reported in Landolt-Bornstein, "Physikalisch-Chemische Tabellen," Julius Springer, Berlin, 1936, Erg. IIIc, pp. 2141 and 2145.

(26) Y. Marcus, *J. Phys. Chem.*, **63**, 1000 (1959).

(27) Y. Marcus, *J. Inorg. & Nuclear Chem.*, **12**, 287 (1960).

(28) J. Danon, *ibid.*, **13**, 64 (1960). (see also reference 9).

Conclusions

This work has shown that anion-exchange resins absorb predominantly the ions $\text{MO}_2(\text{NO}_3)_4^-$ along with some $\text{MO}_2(\text{NO}_3)_3^-$ from aqueous metal nitrate solutions of the hexavalent actinides. It also has shown that the tetranitrato species is a species which does not exist to any appreciable extent in aqueous metal nitrate or nitric acid solutions whereas the trinitrato complex is detected readily in concentrated nitric acid. The relative amounts of these two complexes in the resin phase were found to be, within experimental error, independent of the aqueous phase nitrate concentration but were dependent on properties of the resin phase (degree of resin loading and total resin capacity). Liquid amines have been found to extract only the trinitrato ions of the hexavalent actinides⁸ despite efforts to extract measurable quantities of the tetranitrato complex by varying both amine concentration in hydrocarbon diluent and aqueous phase metal nitrate and nitric acid concentrations.²⁹ This work indicates the fallacy of assuming without direct evidence, as has been done with erroneous

conclusions,^{6,28} what complex is present in the resin phase. There is also some danger in assuming that the same species are extracted by liquid amines as are absorbed by anion-exchange resins. However, in most cases the liquid amines probably do extract the same species as those absorbed by the resins. This is certainly the case with the quadrivalent actinide nitrates where the ions $\text{M}(\text{NO}_3)_6^-$ are extracted by both the liquid amines and the anion-exchange resins.^{8,9}

The recent use of $(m_{\text{NO}_3})_{\gamma \pm}$ to represent ligand anion activity in the calculation of formation constants at high electrolyte concentrations from anion-exchange data²⁶⁻²⁸ has been rendered highly questionable by the Pu(VI) absorption spectra data presented here. Extension of similar spectrophotometric studies of the actinides to chloride media is planned.

Acknowledgment.—The author expresses his appreciation to Robert M. Wheaton of the Dow Chemical Company for his help in obtaining the low capacity anion-exchange resins. The author also thanks the personnel of the Analytical Laboratories Operation who carried out many of the analyses.

(29) W. E. Keder, Hanford Laboratories private communication.

THE MEASUREMENT OF FILM ELASTICITY¹

BY KAROL J. MYSELS, MICHAEL C. COX AND JOHN D. SKEWIS

Chemistry Department, University of Southern California, Los Angeles 7, Calif.

Received October 14, 1960

The elasticity modulus of soap films as defined by Gibbs has been measured for the first time. The method used involves simultaneous determination of the change in the surface tension acting upon a film under observation and of the motion of the interference fringes which this produces. The force acting upon the film is determined as part of the total force acting upon a vertical frame supporting this film in contact with the solution. The changes in surface tension are produced by rapidly withdrawing another film-forming frame from the solution, thus increasing greatly the total surface. The motion of the fringes is recorded photographically and is then translated into the motion of the surface elements on the assumption that the volume of liquid within the film remains constant. Details and limitations of this procedure are discussed. For a number of mobile films the modulus of elasticity is of the order of 10 dynes/cm., while for a rigid film of sodium lauryl sulfate-lauryl alcohol solution it is of the order of 100 dynes/cm. This provides evidence for another factor in the well-known stabilizing effect of lauryl alcohol upon sodium lauryl sulfate foams.

It is well known that only certain liquids are capable of forming foams, bubbles or films of reasonable stability, soap solutions being the classical example of this behavior. It seems to be well accepted² that when such liquids are reduced to thin layers, they develop an increasing resistance to further extension and further thinning. In other materials, particularly in pure liquids or in gases, there is, on the contrary, an increasing tendency to further thinning due to van der Waals forces.³ There is probably a variety of causes for the increasing resistance to thinning shown by film formers. Among these may be cited bulk viscoelastic effects, which may be operative in some polymer solutions; increasing viscosity due to

cooling or evaporation, which accounts for the ease of bubble formation by molten glass⁴; the increase in surface tension due to evaporative cooling which permits sometimes film formation in pure liquids⁵; the repulsion of the two surfaces of the film due to hydration or entropy effects of adsorbed non-ionic surfactants, and especially due to the double layer repulsion of adsorbed ionic surfactants, both of which become operative when the film is thin enough to appear black, *i.e.*, is below about 500 Å.³ A very important reason for the resistance to thinning and one which can operate in films thick enough to show interference colors, in Newtonian liquids and in the absence of cooling or evaporation is surface elasticity.

Surface elasticity is the increase in surface ten-

(1) Presented in part at the Atlantic City Meeting of the American Chemical Society, September, 1959. This work was supported by the Air Force Office of Scientific Research and Development under Contract AF 49(638)-309.

(2) J. A. Kitchener and C. F. Cooper, *Quart. Revs. (London)*, **13**, 71 (1959).

(3) (a) A. J. De Vries, *Rec. trav. chim.*, **77**, 383 (1958); (b) J. Th. G. Overbeek, *J. Phys. Chem.*, **64**, 1178 (1960).

(4) C. V. Boys, "Soap Bubbles, Their Colours and the Forces which Mould Them," (Second Edit on only) Soc. for Promoting Christian Knowledge, London, F. S. Graham, New York, 1912. Reprinted Dover, New York, 1959, pp. 116-117.

(5) G. Van der Mensbrughe, *Mem. Acad. Roy. Sci. Belg.*, **43** (4), (1882); T. H. Hazlehurst and H. A. Neville, *J. Phys. Chem.*, **41**, 1205 (1937).

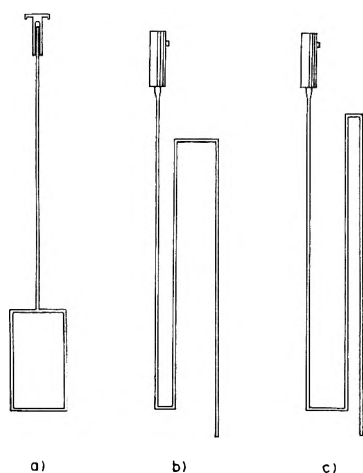


Fig. 1.—Glass frames used in this study.

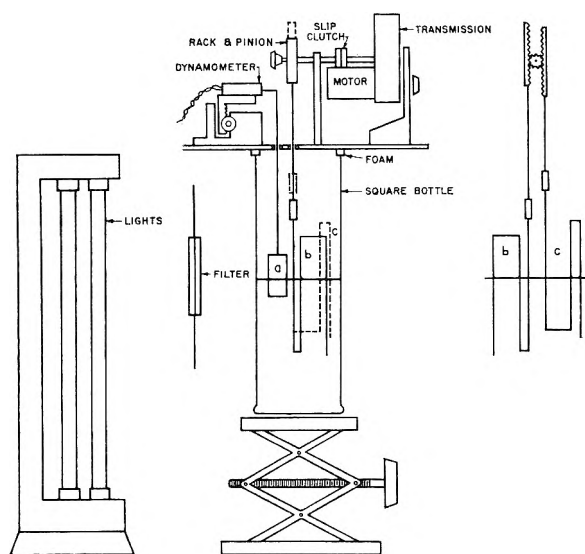


Fig. 2.—Schematic front view of the apparatus for measuring film elasticity. The relative position of frames (b) and (c) is shown on the right.

sion of a film when its area is being extended and, therefore, its thickness decreased. Since the film has two surfaces, this leads to Gibbs'⁶ definition of the modulus of film elasticity, E , as

$$E = 2sd\gamma/ds \quad (1)$$

where s is the surface area and γ is the surface tension. A few years before Gibbs, Marangoni⁷ pointed out in effect that the difference between dynamic and static surface tension provides one reason for surface elasticity. This could be quite effective against sudden disturbances of the film, but in view of the thinness of the film, its relaxation time should be a very small fraction of a second and its effects rather transient. The reason for a smaller but less transient surface elasticity was shown by Gibbs to lie in the depletion of surfactant in the intralamellar solution as it is adsorbed upon the more extended surface. The equilibrium surface concentration thus becomes lower and the sur-

face tension higher. Gibbs also has shown how film elasticity can be calculated in terms of the chemical potential of the surfactant for a pure, two component system. His result is

$$E = 4\Gamma^2 (d\mu/dG) \quad (2)$$

where Γ is the surface density of the solute, μ its chemical potential, and G its total amount present in the film per unit area.

Although the concept of film elasticity is thus quite old and the important role it plays in film stability is well established, little is known about its numerical value. Its theoretical evaluation is difficult because of the uncertainties concerning the chemical potential of surfactants, especially above the critical micelle concentration, and because of the difficulty of realizing a pure, two component system with these materials. Experimentally, no attempt seems to have been made to measure it directly. The present paper describes an experimental approach to measuring film elasticity and presents exploratory results which establish its reality.

Our method is based on qualitative observations reported elsewhere⁸ and consists in simultaneously recording the motion of fringes of a film and the force exerted upon this film. Since fringes are lines of equal thickness and not fixed with respect to the surface of the film, one has to translate their motion into the motion of the surface itself as described below. The force exerted on the film is due to changes in surface tension of the solution in contact with it, and this in turn is changed by the mechanized motion of a large rectangular frame pulling a film in and out of the solution and thus effectively changing the total surface of the system by a considerable fraction.

Experimental

The apparatus is a modification of the one described elsewhere.⁹ It consists essentially of a square bottle 5 × 5 cm. containing the solution and of three frames dipping in the solution and supported from above. The bottle is closed by a heavy brass plate and a foam plastic gasket with connections to the three frames passing through small holes in the plate. One of the frames (a, Fig. 1) bears the film under observation and is supported by a dynamometer measuring the forces acting upon the film. Another frame (b) serves to extend the surface and is operated by a mechanized rack and pinion device mounted above the brass plate. The third frame (c) merely serves to compensate for the buoyancy effect produced by the motion of the second frame and it is moved synchronously but in opposite direction by the same rack and pinion device. Figures 2 and 3 show schematically the arrangement used.

The observation frame (a) was made of very thin glass rod about 1 mm. in diameter and was generally 2 cm. wide, although frames 1 and 2.25 cm. wide were also used. The rod supporting this frame was suspended from the arm of a dynamometer. This suspension was such that the frame could oscillate freely but could not rotate and was fixed at a 45° angle with respect to the incoming light and the direction of observation. The total weight of the frame and suspension was 0.40 g.

The dynamometer was a Statham Instruments, Los Angeles, Calif., transducer model G 10-0.07-2000, which is essentially a lever whose rigidity is due to four sets of wires connected in a bridge network. The changes of resistance of these wires as they contract or expand with the motion of

(6) J. W. Gibbs, "On the Equilibrium of Heterogeneous Substances," *Trans. Connecticut Acad.*, **3**, 108, 343 (1876); "Collected Works," Longmans Green, New York, 1928, 1931, Vol. 1, p. 56.

(7) C. Marangoni, *Nuovo Cimento*, [2] **5**, 6, 239 (1872).

(8) K. J. Mysels, K. Shinoda and S. Frankel, "Soap Films, Studies of Their Thinning and a Bibliography," Pergamon Press, New York, N. Y., 1959, p. 16.

(9) K. J. Mysels and M. C. Cox, *J. Colloid Sci.*, in press.

the lever provide the electric signal. The bridge network is activated by approximately 20 volts d.c. and the strength of the signal is 14 mv. per gram. An external network provides means for zeroing this signal at any desired weight within the range of the instrument, which is ± 2 g. The difference signal was amplified and when desired observed directly on a Hewlett-Packard Model 425A micro-volt-ammeter, whose noise level is of the order of $0.2 \mu\text{v}$. The output of this instrument was generally recorded on a Leeds and Northrup 10 mv. recorder. This arrangement permitted observation of changes of the order of 0.1 dyne acting on the frame which corresponded to about 0.02 dyne/cm. changes in surface tension with a response time of the order of one second. At this sensitivity considerable drift was observed, however, unless the dynamometer was thermally insulated. The dynamometer was calibrated frequently by means of directly suspended weights.

The displacement of the dynamometer arm was about 0.2μ per dyne which is completely negligible.

In early experiments the frame was manually immersed in the solution and then lifted and suspended on the dynamometer; in later experiments the dynamometer bearing the frame was mounted on a dovetail slide manually operated by a rack and pinion. This permitted immersion of the frame and rapid formation of the film without removing the frame from the dynamometer.

The dynamometer was, of course, sensitive not only to the surface tension forces exerted upon the film, but also to those exerted on the frame. In addition, even slight changes in level of the liquid exerted considerable buoyant forces upon the frame. After proper adjustment of the compensating frame (c), these effects did not amount to more than 10% of the total force and were taken into account by blank runs in which the observation frame (a) did not bear a film.

The expansion and compensating frames (b) and (c) were made of the same 1 mm. glass rod to reduce buoyancy effects and were arranged so that the upper horizontal part of frame (b) would just touch the top of the solution and thus assure the formation of a film, while the corresponding part of frame (c) would never touch the solution and thus never bear a film. Both frames were connected to brass rods passing through Teflon bearings in the upper plate and attached to two racks operated by the same pinion so that one frame would move up while the other was moving down. The pinion in turn was operated by a synchronous reversible motor through a multiple speed transmission. A micro-switch operated by adjustable pins on one of the racks permitted automatic reversal of the motion of these frames at any desired point. The maximum speed at which the frames could be operated was 2.15 cm./sec. and this could be reduced by a factor of 2.5, 5, 10, 20, etc.

The width of the film on the extending frame (b) was 2 cm. and a convenient height for its travel was 5.5 cm. Hence, this system permitted an 80% expansion of the surface of the solution in 2.5 seconds and an equally rapid return to the original value.

Recording of Fringes.—The position of the fringes during expansion and contraction was recorded photographically by the method described elsewhere⁹ in which the image of a narrow vertical section of the soap film falls upon a continuously moving photographic film as shown in Fig. 3. This gives a continuous record of the position of each fringe of the soap film. The record was made either on black and white film with monochromatic light or on color film using white light for illumination. A typical record obtained during oscillation of the expanding frame is shown in Fig. 4.

As shown by Fig. 4 there is continuous thinning of the film with time as a result of normal processes such as marginal regeneration. Superimposed on this is the expansion and contraction produced by changes in surface tension. The former must therefore be corrected for and this is done by interpolating, for example, between two crests to get the position that a crest *would* have at the time of the intermediate trough if there had been no expansion.

An alternative procedure was to give the extending frame a single stroke instead of oscillation. In this case the rate of thinning before the stroke was extrapolated to the time when the stroke ended.

In either case the positions of the fringes then permits construction of a profile of the film before and after expansion from the known thickness corresponding to each fringe. In fact, only relative thicknesses are now important. Fig.

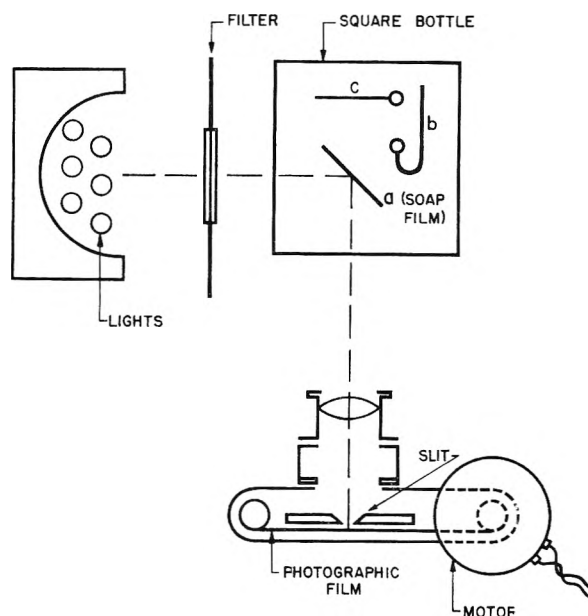


Fig. 3.—Schematic top view of apparatus to measure film elasticity.

ure 5a shows schematically such a pair of profiles. The motion of the fringe, which is a line of equal thickness, is not the same as the motion of the corresponding surface element. The latter can be deduced, however, on the assumption that the amount of liquid in the film from its top to the point of interest remains constant. This amount can be obtained by graphical integration of the profile of Fig. 5a. This integral is shown in Fig. 5b. The difference in height between points of equal volume gives then the expansion of the film at that height, as shown in Fig. 5c. Finally, the slope of this last curve gives the desired relative extension at any point.

A simplified method of calculation which gives the same results for mobile films with the present over-all accuracy of the experimental procedure, is to assume that the motion of the film element is one-half of that of the corresponding fringe corresponding to its initial position. This is based on the approximation of the film profile to a triangle. In this case it is easily seen that the new position of the film element is the harmonic mean of the two positions of the corresponding fringe. For small displacements the harmonic mean may in turn be equated to the arithmetic mean. For rigid films this approximation is too coarse, however. The values reported in Table I were obtained using the more exact procedure of Fig. 5.

Materials.—High purity lauryl alcohol was obtained from Applied Science Laboratories, State College, Pa. Sodium lauryl sulfate was the material prepared by R. J. Otter¹⁰ in this Laboratory. The commercial detergent was liquid Lux which is based on sodium alkyl benzene sulfonates with foam-stabilizing and detergency-aiding additives.

Results

The results of our measurements are summarized in Table I. They show that for several systems giving mobile films, whether "pure" sodium dodecyl sulfate or a commercial detergent, the surface elasticity is of the order of 10 dynes/cm. In contrast, the rigid film of pure sodium dodecyl sulfate and lauryl alcohol has a film elasticity of the order of 100 dynes/cm. A solution of pure sodium lauryl sulfate containing a quantity of lauryl alcohol insufficient to give a rigid film under the conditions of the experiment gave nevertheless a significant increase in surface elasticity to about 26 dynes/cm.

(10) K. J. Mysels and R. J. Otter, *J. Colloid Sci.*, in press.

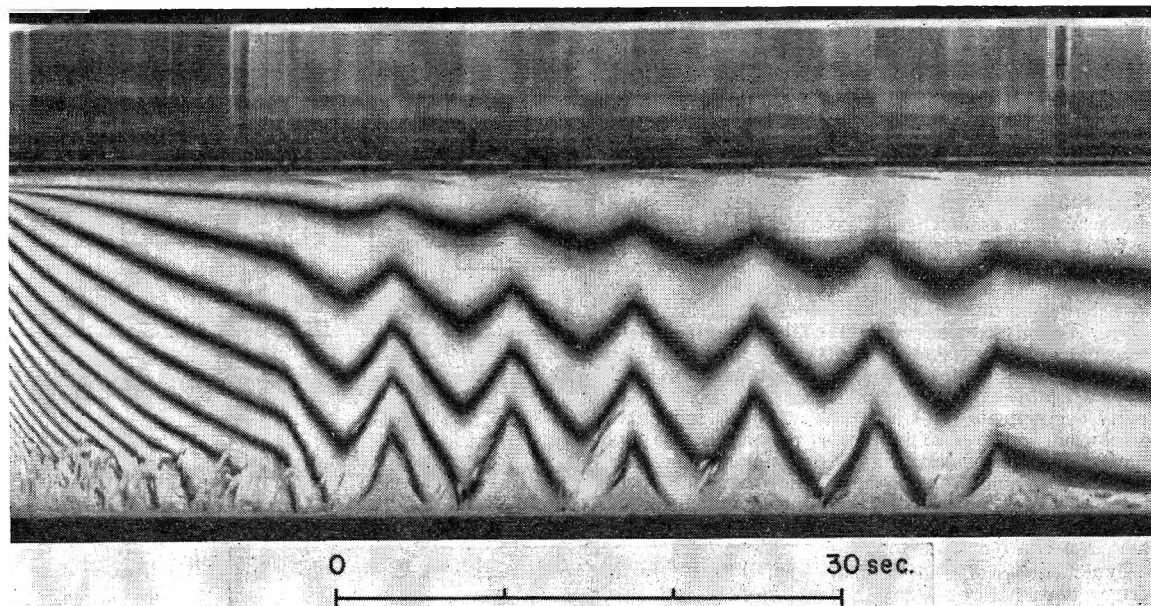


Fig. 4.—Photographic record of the motion of fringes of a soap film as surface tension is alternately increased and decreased.

TABLE I
FILM ELASTICITY MEASUREMENTS

Surfactant	No. of determin.	Range of		Times of elongation, sec.	Film elasticity, $2 d\gamma/(ds/s)$		
		Stresses $d\gamma$, dyne cm.^{-1}	Strains $ds/s \times 10^2$		Median, dyne cm.^{-1}	% Deviation Av.	Max.
Commercial, 1%	21	0.47–0.51	8.2–16	1.96–9.71	9.8	13	29
Same ^a	13	.21–.43	6.9–13	2.5–6.4	6.4	18	52
Same, ^a 37% glycerol	3	.28–.29	10–11	5.8	5.5	3	6
NaLS, 0.29%	29	.27–1.3	4.5–18	0.73–14.3	15	12	43
Same ^a	2	.57–0.85	12–21	5.8	8.8	8	8
NaLS, 0.25% + LOH, 10^{-3} %	23	.52–2.8	4.7–20	.73–14.3	26	14	31
Same diluted 4:5 ^b	13	2.2–5.4	5.2–11	.73–14.3	100	18	35

^a Independent measurements made 6 months earlier. ^b Rigid film (all others are mobile).

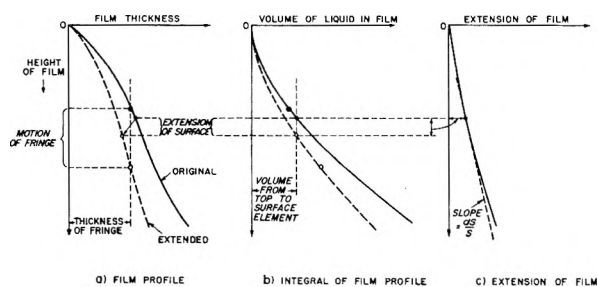


Fig. 5.—Schematic of the graphical translation of movement of fringes into extension of film element.

Discussion

Our assignment of the extension (strain) of the film depends on the assumption that no liquid enters the film during the process along the upper edge of the frame or along its sides. The validity of this assumption is supported by the absence of any marked anomalies in the extension curve (Fig. 5c) and by visual observations as far as the quiescent upper border is concerned. If very large forces are applied to the film, one can see visually that fresh areas are pulled out from the upper border. Being pulled out rapidly, these films are relatively thick according to Frankel's law¹¹ and

may descend as tear drops to their corresponding level in the bulk of the film unless they are promptly resorbed by the border. No significant behavior of this type was observed, however, in our normal determinations. As far as the turbulent side borders are concerned, their effect was found to be negligible by comparing the behavior of films of different widths under the same conditions.

Our procedure is dependent on the change of surface tension which occurs when the bulk solution surface is extended. In principle some change would be expected even for a pure two component system due to the well known difference between dynamic and static surface tension and the finite time required to replenish an expanding surface. However, we find that in our case the recovery time was of the order of 10 seconds or so which makes it very likely that the surface tension changes were largely due to a minor component. It is therefore quite possible that in a pure two component system the method used would not give a sufficient change in surface tension to produce a measurable extension of the film. There are, however, other methods which can be used¹² to lower the surface tension of a solution without affecting

(11) Ref. 8, p. 55; and ref. 9.
(12) Ref. 8, p. 81.

the nature of the observed film, such as dilution or addition of a more active surfactant. Hence, a proper modification of our method could still be used in that case. Furthermore, really pure two component systems of aqueous surfactants are not readily prepared or studied and our procedure should be applicable to almost all normally encountered systems. In fact, our sodium dodecyl sulfate seems extremely pure as far as bulk criteria are concerned.

As mentioned earlier, film elasticity may be either a dynamic effect—the difference between dynamic and static surface tension—or an equilibrium one, the depletion of the intralamellar solution. It is likely, though not completely certain, that our method measures the latter. This conclusion is based on three arguments. First, the same change in surface tension corresponded to almost doubling of the bulk surface but to only 5–20% changes in film area. Hence a different limiting factor, presumably depletion of the intralamellar liquid, must have been effective in the film. Second, an order of magnitude calculation¹³ shows that in a film dynamic effects should last milliseconds and thus could not be observed in our system unless some unsuspected energy barrier is encountered. Third, we could not notice any relaxation of film elasticity either when the bulk surface was extended and kept in the extended state so that bulk surface tension was decaying slowly, or when the bulk surface tension was kept at a constant and higher value by continually extending the surface manually. Both of these experiments were, however, difficult to evaluate and no definiteness can be claimed for them. An argument against this conclusion is that we have not found any strong dependence of film elasticity upon film thickness as would be expected from the depletion theory for a two component system. However, the effect becomes understandable if attributed to a minor third component which is substantially absent from the intralamellar solution and present only in the surface. This would make the behavior of the film dependent on the fact that it is thin but not on how thin it is.

As mentioned earlier, high bulk viscosity as encountered in polymers and glasses, may generate a significant force opposing the extension of the film. For liquids of low viscosity, such as water, and even for glycerol, this effect is, however, negligible, as shown by the following calculation. According to Trouton¹⁴ the rate at which the length L of a cylinder of cross section C and subject to a force F changes with time t is given by

$$\frac{dL}{L dt} = \frac{1}{\lambda} \frac{F}{c}$$

where λ , the coefficient of viscous traction, is given by $\lambda = 3 \eta$ where η is the ordinary coefficient of bulk shear viscosity. For our purposes we can

replace dL/L by ds/s and F/C by γ/δ where δ is the thickness of the film. Hence for a film of 1 μ thickness extending by 20% in one second, which represents rather extreme conditions, the increase in surface tension generated by viscous forces would amount to 10^{-6} dyne/cm. in water of 1 cp. viscosity and to 10^3 times more in pure glycerol, which would still be negligible in our measurements.

That bulk viscosity does not complicate our measurements in other ways either is further indicated by the fact that measurements in a 30% glycerol solution noted in Table I did not show any significant effect upon film elasticity.

The most significant difference in film elasticity is between the rigid film, 100 dyne cm.⁻¹, and the mobile films which are 4 to 20 times more yielding. That this is not an artifact produced by some undetected effect of surface viscosity on our determination is shown by the fact that the mobile films themselves display a fivefold range of elasticities despite their relatively minor differences in surface rheology.

The marked increase in film elasticity upon addition of lauryl alcohol to sodium lauryl sulfate solution indicates also the possibility of another factor explaining the well known increased stability of these mixed films¹⁵ in addition to the generally accepted effect of surface rigidity and the resulting slower rate of drainage.

In the present state of development the precision of the method leaves much to be desired and values reported for a given system are significant only to about $\pm 25\%$. About 5% of this uncertainty is due to the difficulties of measuring the photographic film, of graphic integration, and in general to the interpretation of data, once obtained. A somewhat larger uncertainty is attached to the obtaining of the data themselves, *i.e.*, their reproducibility when the experiment is repeated immediately under the same conditions. A much larger uncertainty is associated, however, with the application of the same conditions at different times. Clearly, there are significant factors in the history and purity of the surface which we have not yet learned to control. This in turn has prevented the study of such factors as the rate of extension or the extent of stretching which seem to have some effect upon the result. However, this uncertainty of some 25%, although very disturbing, is small compared to the 20-fold changes in film elasticity which we have found between the extremes of our systems and we are now able at least to assign approximate values to a quantity whose order of magnitude was previously unknown.

Acknowledgment.—It is a pleasure to acknowledge the stimulating discussions with Professor J. Th. G. Overbeek during the course of this work.

(13) Ref. 8, p. 16.

(14) F. T. Trouton, *Proc. Roy. Soc. (London)*, **A77**, 426 (1906).

(15) *E.g.*, A. G. Brown, W. G. Thuman and J. W. McBain, *J. Colloid Sci.*, **8**, 491 (1953).

ADSORPTION OF NITROGEN AND ARGON ON MINERALOGICAL GRAPHITE AND DIAMOND AT 77 AND 90°K.

BY JUAN DE DIOS LOPEZ-GONZALEZ,¹ FRANK G. CARPENTER² AND VICTOR R. DEITZ

National Bureau of Standards, Washington, D. C.

Received October 31, 1960

Adsorption isotherms were measured in the relative pressure range from 10^{-9} to about 0.5. The samples were outgassed at 450° for 18 hours before each of a series of measurements. Upon the first exposure of the outgassed solid to the gas, a delay occurred in the adsorption. An initial period of low rate of adsorption was followed by a period of much higher rate and finally by attainment of a steady state. The isotherms at the two temperatures based on the steady-state values crossed in the neighborhood of unit coverage (defined by v_m from point B) for both gases and both solids. The isotherms on graphite showed a definite step at relative pressures between 10^{-3} and 10^{-4} . The heats and entropies of adsorption at constant spreading pressure were determined and graphs are presented as a function of coverage. Broad maxima in the heats were observed in the neighborhood of $\theta = 0.1$ to 0.01; the entropy showed minima at $\theta = 1.0$ and increased steadily as the coverage decreased. The systems studied are considered to be examples of interaction with low energy surfaces for which the entropy changes are appreciable, making a significant contribution to the free energy change of the adsorption process.

Introduction

Experimental evidence for the non-uniformity of carbon surfaces, in regard to sites for the physical adsorption of gases, is twofold: (1) the variation of the heat of adsorption with the amount adsorbed, *i.e.*, with surface coverage, and (2) the changes in shape of the adsorption isotherm after controlled heat and/or chemical treatments. There are many examples for the former³ based on either calorimetric data or calculated heats from the adsorption isotherms observed at different temperatures. The work of Polley, Schaeffer and Smith⁴ is a good example of changes observed in the shape of nitrogen adsorption isotherms brought about when carbon blacks were heated at temperatures up to 2700°. These authors attributed the changes to a gradual transition from a heterogeneous to a homogeneous surface as a result of partial graphitization.

Carbon blacks as prepared have a rather diffuse X-ray diffraction structure, but the patterns sharpen up and new bands appear on heating to 3000°. Although the structure attains some similarity to the pattern of graphite, there are striking differences in that *hkl* reflections are absent. In interpreting this behavior as the development of two-dimensional graphite platelets, the question arises as to how fully the adsorption properties of the heat-treated sample of carbon black mimic those of a fully-developed graphite structure.

Adsorption isotherms have been determined for mineralogical graphite and an industrial grade of diamond in the range of relative pressure from 10^{-9} to approximately 0.9 at 77° and to 0.4 at 90°K. There are no recorded adsorption data for mineralogical graphite and, indeed, there are very few measurements on carbon solids in the range of very low pressures (fractional coverage to 0.02). Previous measurements⁶ of nitrogen adsorption with high surface energy carbon adsorbents showed that

the time required to reach a steady state, as well as the level of the steady state, depended upon the outgassing operation preliminary to the measurements. The present work is concerned with what are essentially low surface energy solids and in the present series of measurements each sample was outgassed at 450° for about 18 hours between each series of measurements. The results after other pretreatments will be reported in subsequent communications.

Experimental

The apparatus employed in these measurements has been described.⁶ A vacuum thermocouple gage was added and a recording made of the pressure changes. It proved to be especially valuable in observations of the rates of pressure decrease. This gage was calibrated with a McLeod gage. All final steady-state values of the pressures were determined with either the McLeod gage in the low-pressure range or with a mercury manometer at higher pressures. The reaction vessel was isolated by means of a mercury cutoff. A trap cooled with either liquid oxygen or nitrogen was placed before the reaction vessel to exclude mercury vapors.

The dead space in the reaction vessel holding the diamond sample was 16.3 ml. and that containing the graphite was 8.2 ml. The cold trap had a volume of 13.1 ml. and the room temperature dead space was 61.4 ml. for diamond and 59.0 ml. for graphite. The buret system, connections, and pressure gages had a volume of 160 ml.

Materials.—The graphite was of mineral origin and was sieved to obtain a close fraction of flakes having a cross sectional diameter of 1 mm. The sample was acid-washed repeatedly with boiling hydrochloric acid and then with hydrofluoric acid. The treatment was continued until the thiocyanate spot test for iron was negative. It was washed halogen-free with distilled water. Finally, the graphite was formed into loose cylindrical pellets (1 cm. diameter and 2 cm. high) and heated in a vacuum induction furnace to about 2000° for about 30 minutes. A spectrochemical analysis of the purified graphite revealed the presence of only traces of aluminum, copper, iron, magnesium and silicon in amounts less than 0.001% each. X-Ray and electron scattering showed that the graphite was highly crystalline. The sample (8.01 g.) was sealed into a Pyrex container in which the adsorption measurements were made and then heated for 18 hours at 450° before each series of measurements.

The industrial diamond powder used in this work was in the form of dust (2 to 6 μ in particle size). The sample (28.05 g.) was outgassed in a Vycor adsorption tube for seven days at 600°. After the fourth day of outgassing, the pressure, with the sample at 600° and the vacuum pump in operation, was about 4×10^{-4} mm. When the sample was cooled to room temperature, the pressure was less than 1×10^{-6} mm. and without pumping the pressure rose to about 5×10^{-6} mm. in about one hour.⁷ A spectrographic analysis of the diamond powder after the adsorption experiments showed an appreciable amount of lead and silicon

(1) Chemistry Dept., Universidad de Granada, Granada, Spain.

(2) Research Associate representing the Bone Char Research Project, Inc.

(3) V. R. Deitz, "Bibliography of Solid Adsorbents," Vol. 1, 1900-42, 877 pp., Vol. 2, 1943-53, 1528 pp. N.B.S. Circular 566, Government Printing Office, Washington 25, D. C.

(4) M. H. Polley, W. D. Schaeffer and W. R. Smith, *J. Phys. Chem.*, **57**, 469 (1953).

(5) J. Biscoe and B. E. Warren, *J. Appl. Phys.*, **13**, 364 (1942).

(6) J. de D. Lopez-Gonzalez, F. G. Carpenter and V. R. Deitz, *J. Research Natl. Bur. Standards*, **55**, 11 (1955), RP2600.

which was traced to the "quartz cotton" used to confine the diamond. The X-ray pattern for the diamond showed the crystalline structure of diamond.

The nitrogen from a commercial tank was purified by removing the residual traces of oxygen with hot copper filings and the water vapor with magnesium perchlorate. The argon was analyzed by mass spectrometry and contained 0.06% nitrogen and 0.02% oxygen. The oxygen in the argon was removed with hot copper as above leaving the nitrogen as the maximum impurity in the argon.

Corrections for Thermal Transpiration.—It was necessary to make a correction for thermomolecular flow between the reaction vessel (77.2 or 90.0°K.) and the McLeod gage at room temperature. The equation of Liang,⁸ with the modifications added by Bennett and Tompkins,⁹ was used. The equation and the constants are

$$R = \frac{p_1}{p_2} = \frac{\alpha_{He}(f\Phi_g X)^2 + \beta_{He}(f\Phi_g X) + R_m}{\alpha_{N_2}(f\Phi_g X)^2 + \beta_{N_2}(f\Phi_g X) + 1} \quad (1)$$

where

$$\begin{aligned} p_2 &= \text{obsd. pressure in mm. mercury at } T_2 \\ p_1 &= \text{cor. pressure at bath temp.} \\ \alpha_{He} &= 3.70 [1.70 - 2.6 \times 10^{-3} (T_2 - T_1)]^{-2} \\ \beta_{He} &= 7.88 (1 - R_m) \\ R_m &= (T_1/T_2)^{1/2}; T_1 < T_2, \\ f &= 1, \text{ for the apparatus employed} \\ \Phi_{N_2} &= 3.53 \\ \Phi_A &= 2.70 \\ X &= p_2 d, \text{ and} \\ d &= \text{tubing diameter in mm.} \end{aligned}$$

The equivalent diameter of the connecting tubing was 3.32 mm. when diamond was used and 2.5 mm. for graphite.

Results and Discussion

Sixteen series of adsorption measurements were made with the diamond and eighteen with graphite. The recorded curves for the pressure decrease that followed the first introduction of gas to the freshly outgassed sample showed a marked delay in the rate of adsorption. This was not found for high surface energy carbon adsorbents⁶ where the pressure decreased rapidly at first, and then more slowly until the steady state was obtained. However, in the present work there was a significant delay during which time the pressure decreased very little. This was followed by a period of rapid pressure decrease and then by a gradual decrease until a steady state was reached. The adsorbed volumes were calculated and the fractions of the steady-state value are plotted in Fig. 1 for typical cases. It is significant that no delay in adsorption (curve A, argon on diamond) occurred with the second and further addition of gas. Curve B with delay of about 1 hour was observed for argon on graphite at 77° and a steady-state pressure of 0.077 μ . Curve C was observed for nitrogen on diamond at 90°K. and the steady-state pressure of 27 μ was not attained for about 5 hours.

There may be some uncertainty in the recording of the pressure decrease in the early periods (up to 10 minutes) due to lag in temperature equilibrium following the heat of adsorption and to the diffusion of the gas from the dosing system to the sample compartment. However, there is little doubt that

(7) Subsequent work has demonstrated that this criterion of outgassing is not helpful in so far as being a measure of the reproducibility of the surface of the outgassed solid. A more helpful measurement is the determination of the rate of outgassing of the solid at the elevated temperature.

(8) S. Chu Liang, *J. Appl. Phys.*, **22**, 148 (1951); *J. Phys. Chem.*, **56**, 660 (1952); **57**, 910 (1953).

(9) M. J. Bennett and F. C. Tompkins, *Trans. Faraday Soc.*, **53**, 185 (1957).

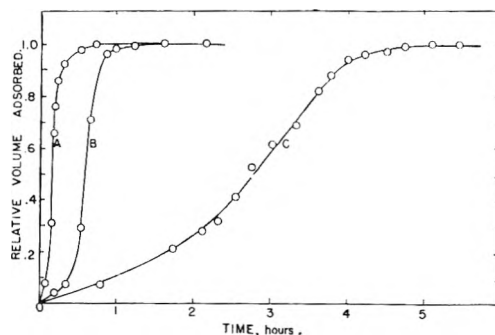


Fig. 1.—Rate of adsorption, calculated as fraction of steady-state values, showing extent of delayed adsorption.

the delay observed for longer periods is real and that the adsorption process is proceeding at radically different rates. There was some correlation between the delay and other variables such as initial and final pressures and the volume adsorbed, or coverage. The delay was observed with both adsorbents, both adsorbates, and at both temperatures. The above phenomenon is obviously quite complex and considerably more work is required for complete understanding.¹⁰

Data at High Relative Pressures.—Ten series of measurements were made at 77.2 and 90.0°K. with nitrogen–diamond, six with argon–diamond, eight with nitrogen–graphite, and ten with argon–graphite. The measurements overlapped and good reproducibility was observed in each series. The volumes of gas adsorbed (ml. at S.T.P.) in the relative pressure ($x = p/p_0$) range from 0.01 to 0.5 are plotted in Fig. 2 as a function of the steady-state pressures. The two isotherms for each system cross over, *i.e.*, there is a relative pressure range in which the adsorption at 90°K. is greater than that at 77.2°K. This was not observed for the corresponding isotherms at relative pressures below 0.01 (see Fig. 3). The isotherms for nitrogen at 90°K. are above those at 77° to a greater degree than for argon for both the graphite and the diamond samples.

A pertinent point to bear in mind is that both isotherms were determined at temperatures above the two-dimensional critical temperature (T_{2c}). The normal critical temperatures of N₂ and Ar are 126.1 and 150.6°K. and the values of T_{2c} are 63 and 75°K., respectively. Consequently, the behavior of the adsorbed layers must be explained in terms of a two-dimensional gas model.

The conventional isosteric heat of adsorption (constant coverage) is calculated from the expression

$$\Delta H_{\text{isosteric}} = R \left[\frac{-\ln(p/p_0)_1 - \ln(p/p_0)_2}{\frac{1}{T_2} - \frac{1}{T_1}} \right] \quad (2)$$

At the crossover point where the values of p/p_0 at the two temperatures are equal, the isosteric heat of adsorption is zero. When $(p/p_0)_{77.2^\circ} < (p/p_0)_{90^\circ}$, the heat is positive and when $(p/p_0)_{77.2^\circ} > (p/p_0)_{90^\circ}$

(10) Many measurements subsequent to those reported in this paper have added experimentally to the understanding of this phenomenon. Procedures have been developed whereby the induction can always be obtained and can be modified at will. A report of this work is given in "Advances in Chemistry" Series, Fall, 1961.

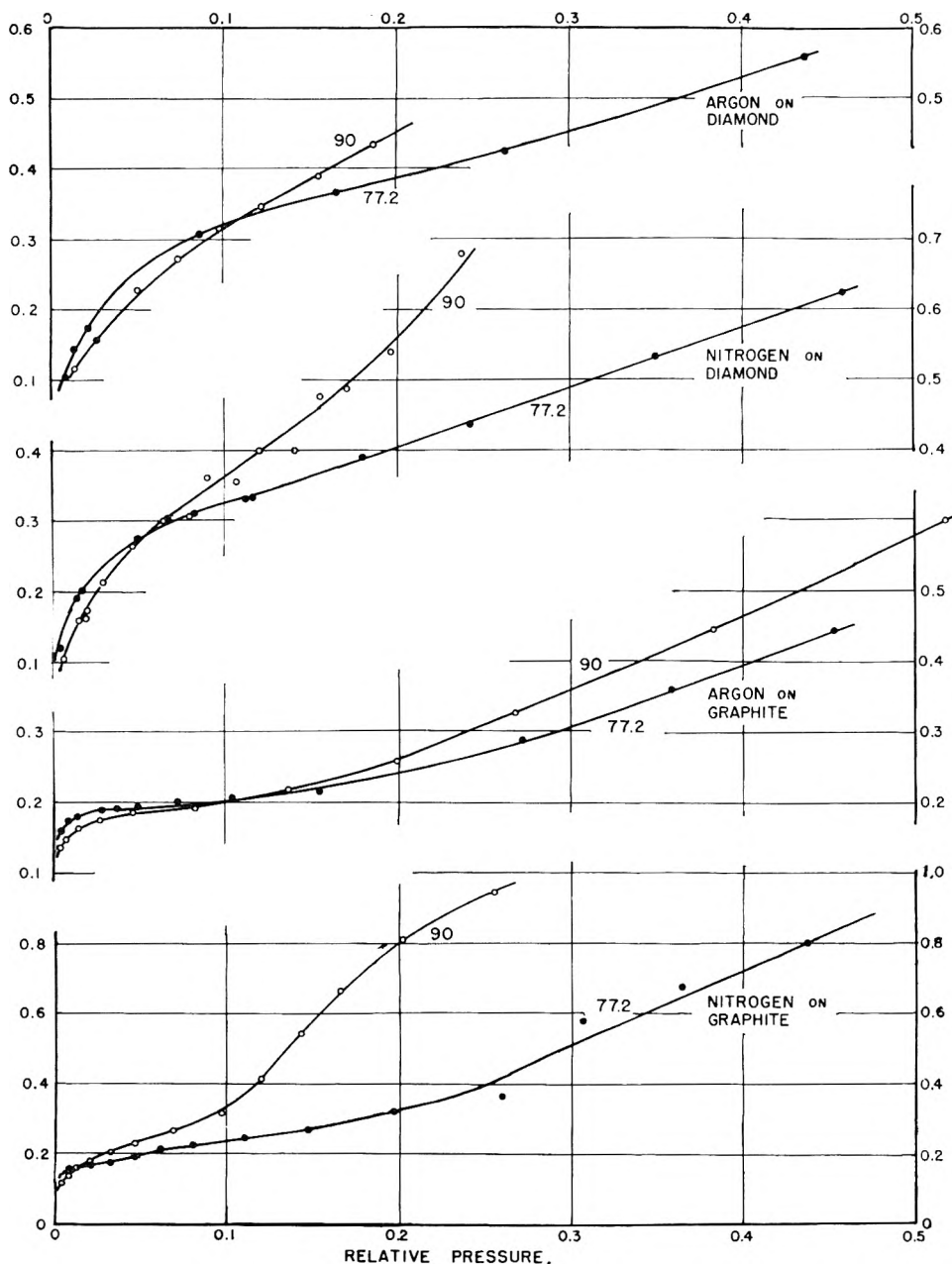


Fig. 2.—Adsorption isotherms at high relative pressures. The coordinate is volume adsorbed, ml. S.T.P.

the heat is negative. Since a reaction must always go in the direction of lowering of the free energy of the system, appropriate entropy changes (involving the ordering of the adsorbed argon and nitrogen molecules) must accompany the interaction in order that the free energy change at 77.2° be greater than that at 90.1°K. It would appear that more than one crossover may take place before saturation pressure is attained. Prenzlou and Halsey¹¹ reported three crossovers (at $p/p_0 = 0.15, 0.4$ and 0.6) and a good indication of a fourth (at $p/p_0 = 0.8$) for adsorption isotherms of argon between 71.1 and 78.5°K. on a bare surface of heat-treated P-33 (2700°). The measurements of Prenzlou and Halsey are believed to be the first

¹¹ C. F. Prenzlou and G. D. Halsey, Jr., *J. Phys. Chem.*, **61**, 1158 (1957).

publication dealing with this aspect of physical adsorption, although isotherms converging at high pressures have been reported by Trapnell¹² for chemisorption systems.

The low-pressure adsorption isotherms are plotted in Fig. 3 on a logarithmic scale in order to cover the considerable range of relative pressure. The numbers denote the particular series of measurements. In some cases the number appears on both isotherms, this being accomplished by change in the refrigerant bath. The smooth curve through all points of the isotherm thus gives a measure of the reproducibility and reversibility of the data. It appears possible to approximate the behavior of each isotherm by a few linear regions, but there is no

¹² B. M. W. Trapnell, "Chemisorption," Chapter 5, Academic Press, Inc., New York, N. Y., 1955, pp. 118-124.

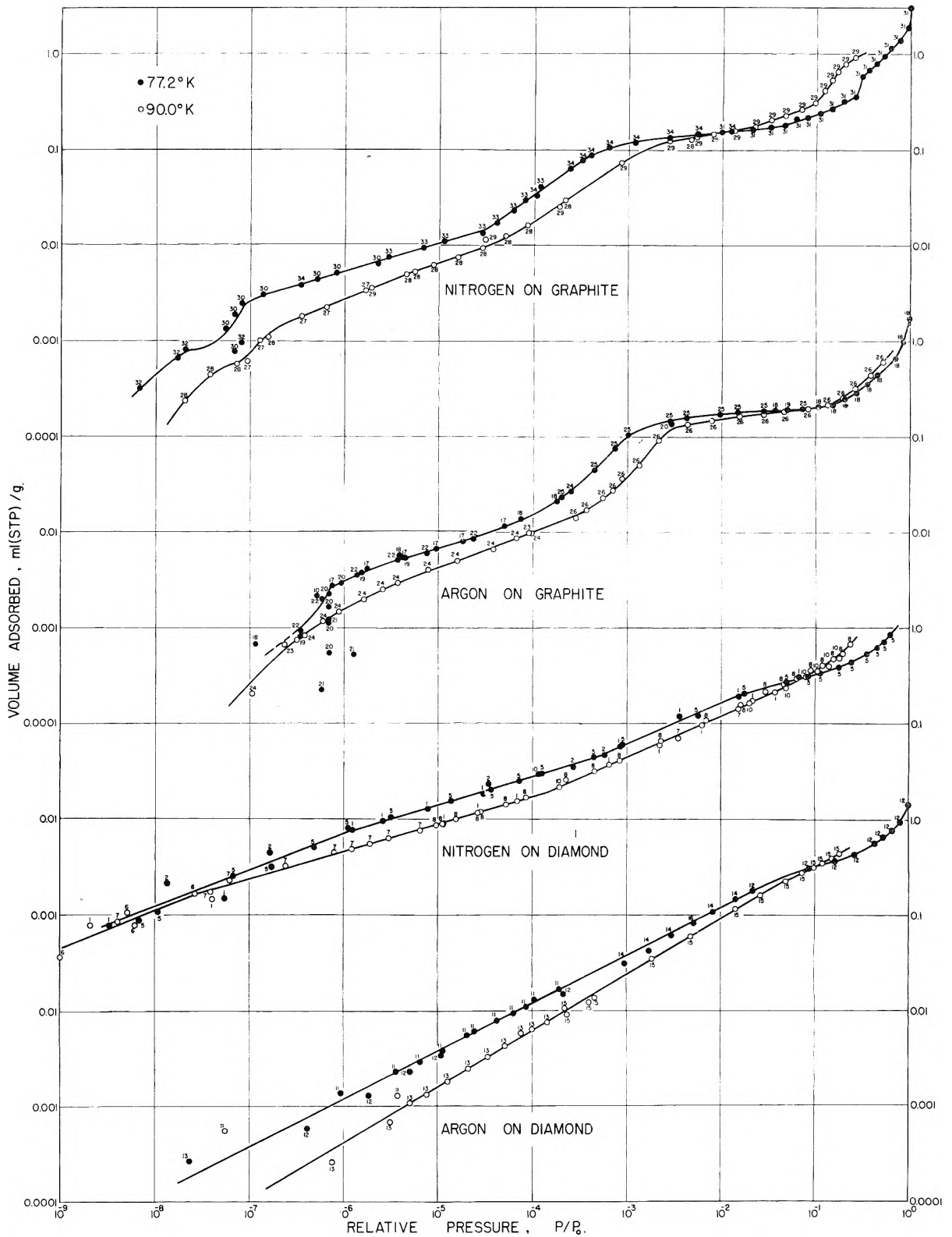


Fig. 3.—Adsorption isotherms at low relative pressures. The ordinate scales are logarithmic in order to cover the range of measurements.

indication that a final Henry's law region was approached in these measurements. The data for this sample of industrial diamond gave a close approximation to a straight line over the entire range of observed pressures in Fig. 3 below about

$p/p_0 = 0.05$ and, therefore, this sample should have a very heterogeneous surface.

The low-pressure isotherms for mineralogical graphite include relatively sharp breaks in slope, even on the logarithmic scale of Fig. 3, which give

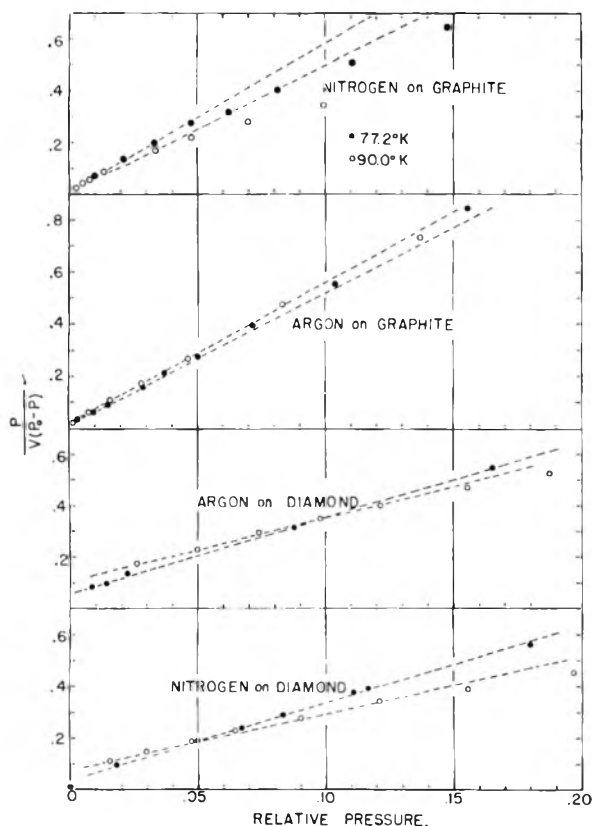


Fig. 4.—B.E.T. plots for the adsorption data (closed circles 77.2°K.; opened circles 90.0°K.). The dotted lines correspond to the value of V_m estimated from point B of the isotherms.

these isotherms a stepwise appearance. The step occurs at a relative pressure between 10^{-3} and 10^{-4} . The scatter in the results below $p/p_0 < 10^{-6}$ make these data of value only in pointing out the general trend of the adsorption isotherms. The step between 10^{-3} and 10^{-4} occurs at far lower values of relative pressure than those originally reported by Polley, Schaeffer, and Smith⁴ and subsequently studied by Singleton, Champion and Halsey¹³ for the case of graphitized carbon blacks. It will be shown that the steps in Fig. 3 correspond to surface coverages much less than 1.

In the isotherm of argon on graphite (see Fig. 3) the slope in the step at about $p/p_0 = 10^{-3}$ is very nearly unity. This particular behavior corresponds to Henry's law, and if data had not been obtained at lower pressures, one might have surmised that a Henry's law region was valid at yet lower pressures, as the simplified models of physical adsorption dictate. While this undoubtedly is true, the region of Henry's law has not as yet been reached in the present work. The step in the isotherm cannot be interpreted as phase changes,¹⁴ since this concept is not plausible at low coverages. Moreover, as already indicated, the isotherms were determined at temperatures above the two-dimensional critical temperature and thus must be inter-

preted in terms of a van der Waal two-dimensional gas.

Estimation of V_m .—The B.E.T. plots for graphite were not linear as shown in Fig. 4. Values of V_m , corresponding to monolayer coverage, were estimated from the point B intercepts and these are listed in Table I. These values correspond to a B.E.T. slope approximated by the dotted lines of Fig. 4 and are listed in Table I together with values corresponding to point B. The B.E.T. plots for the diamond were more linear, but the values derived for V_m differed appreciably from point B. The point B values were used in the following calculations of surface coverage. It may be significant that the crossover points shown in Fig. 2 occur very close to unit coverage as determined by the point B intercept.

TABLE I^a
ESTIMATE OF V_m (ml., S.T.P.)

	Graphite		Diamond	
	Point B	B.E.T. (dotted line Fig. 4)	Point B	B.E.T. (dotted line Fig. 4)
Argon at 77° K.	0.19	0.19	0.30	0.33
Argon at 90° K.	.18	.18	.28	.42
Nitrogen at 77° K.	.21	.17	.30	.35
Nitrogen at 90° K.	.20	.18	.28	.44

^a NOTE: The surface area may be calculated from the following constants derived from the densities of the liquid: argon, 3.66 m.²/ml. at 77.2°K. and 3.86 at 90.0°; nitrogen, 4.37 m.²/ml. at 77.2°K. and 4.62 at 90.0°. The values of p_0 were those of the liquid except argon at 77.2°K. for which the vapor pressure of the solid was used.

Determination of Spreading Pressure.—In order to calculate¹⁵ the heat and entropy quantities at constant spreading pressure, Φ , it is necessary to know the values of Φ as a function of the equilibrium pressure at the two different temperatures. For this purpose, the Gibbs equation was used

$$\Phi = RT \int_0^p \Gamma d \ln p = 0.371 \frac{T}{A} \int_0^x \frac{V}{x} dx \quad (3)$$

where T = absolute temperature, Γ = surface concentration of the adsorbed gas (N_s/A), N_s = number of adsorbed molecules, and A = surface area of the adsorbent. If A is expressed in m.²/g. and V in ml. (S.T.P.)/g., then Φ is given in erg/cm.². The integration was performed graphically for each isotherm down to the lowest experimental point and a suitable extrapolation made to $x = 0$.

The extrapolation to zero pressure was made in all cases from the best line throughout the last few experimental points. The values obtained for Φ at $x = 10^{-6}$ are given in Table II. Because data were available at low pressures, the uncertainty involved in this extrapolation is small. This is illustrated in Table II in which the uncertainty estimated from the upper and lower limits of the scatter of the last few points may be compared with the value of the spreading pressure at $x = 10^{-6}$. The adsorption data for diamond show slightly more scatter at the lower pressures (see Fig. 3) which lead to a slightly higher uncertainty.

(13) J. H. Singleton and G. D. Halsey, Jr., *J. Phys. Chem.*, **58**, 1011 (1954); W. M. Champion and G. D. Halsey, *J. Am. Chem. Soc.*, **76**, 974 (1954).

(14) S. Ross and W. Winkler, *ibid.*, **76**, 2637 (1954).

(15) T. L. Hill, P. H. Emmett and L. G. Joyner, *ibid.*, **73**, 5102 (1951).

TABLE II

ESTIMATE OF THE UNCERTAINTIES IN SPREADING PRESSURE,
(erg/cm.²)

°K.	Φ at $x = 10^{-6}$ Based on the extrapn. of best line through lowest exptl. points	$\Delta\Phi$ Estd. from scatter of data	% of Φ at $x = 10^{-6}$	$\Delta\Phi$ Estd. from dif- ference between Henry and Freundlich extrapn.	% of Φ at $x = 10^{-6}$
Nitrogen and diamond					
77	0.28	0.053	19	0.032	11
90	.27	.062	23	.021	8
Nitrogen and graphite					
77	.46	.023	5	.030	7
90	.22	.009	4	.023	10
Argon and diamond					
77	.057	.018	31	.0059	10
90	.046	.021	45	.0073	16
Argon and graphite					
77	.137	.008	6	.045	33
90	.071	.009	13	.016	23

The difference between a Henry's law and a Freundlich extrapolation to zero pressure was estimated. When $V = kx$ is introduced into equation 3, $\Phi = 0.371(T/A)V$. When $V = kx^{1/n}$, $\Phi = 0.371(T/A)nV$. The difference between the two extrapolations is

$$\Delta\Phi = 0.371 \frac{T}{A} (n - 1)V \quad (4)$$

where V in this instance is the volume adsorbed at the lowest observed point. The results in Table II show that it is small, being of the same order of magnitude as that due to the scatter of the data. The errors in the argon isotherms are larger because these were not obtained at as low relative pressures as nitrogen and the extrapolation was somewhat longer. At higher relative pressures, however, this error in Φ becomes entirely negligible.

Heat and Entropy Quantities.—The heats of adsorption at constant spreading pressure for mineralogical graphite and for the diamond sample were calculated by the method of Hill, Emmett and Joyner.¹⁵ Smooth plots of Φ as a function of relative pressure were drawn on a large scale and the corresponding values of relative pressure at constant Φ at the two temperatures were obtained. The average values for relative pressure, x , and for the temperature, T , were, respectively

$$\ln x = \frac{1}{2} [\ln x_1 + \ln x_2] \text{ and } \frac{1}{T} = \frac{1}{2} \left[\frac{1}{T_1} + \frac{1}{T_2} \right]$$

The isosteric heats and entropies also have been calculated from the isotherms and one of these, the isosteric heat of argon on graphite, is plotted against coverage in Fig. 5. There is a sharp maximum at about $\theta = 0.9$ that is almost identical with the calorimetric behavior reported by Beebe and Young¹⁶ for argon on a Spheron carbon black that had been heated to 2700°. These authors interpreted the maximum as due to lateral interaction on a graphite-like surface, an acceptable explanation in view of the high coverage. The isosteric heat plotted in Fig. 5 increases with decrease in

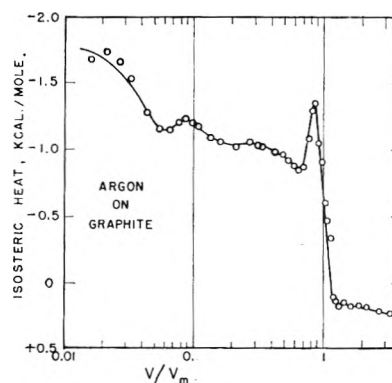


Fig. 5.—Isosteric heats for argon on mineralogical graphite.

coverage, beginning at a coverage of about 0.70 and continuing to about 0.02. Below 0.02 there is an indication that it might drop again, but it is difficult to attribute much certainty to this trend in view of the scatter of the isotherm data at coverages less than 0.02 (*i.e.*, relative pressures less than 10^{-6}).

The heats and entropies at three values of fractional coverage are given in Table III for the different adsorbate-solid systems. At a designated coverage, there are important differences in these quantities, but in the case of argon on diamond, the values at constant spreading pressure agree with those calculated at constant volume adsorbed.

TABLE III

HEAT AND ENTROPY QUANTITIES AT DESIGNATED COVERAGE

Cover- age	Isosteric		Free energy ΔF	Constant spreading pressure	
	ΔH	ΔS		ΔH	ΔS
Nitrogen on diamond ($V_m = 0.29$)					
0.02	-1470	+ 9	-2200	- 100	25
0.1	-1250	+ 1.7	-1400	-1000	6
1.0	- 90	+ 4.2	- 440	- 300	2
Argon on diamond ($V_m = 0.29$)					
0.02	-1200	+ 5.0	-1650	-1200	6
0.1	- 720	+ 5.0	-1150	- 750	5
1.0	- 85	+ 3.9	- 410	- 80	4
Nitrogen on graphite ($V_m = 0.20$)					
0.02	-2200	+ 1	-2300	-1550	9
0.1	- 980	+ 7.0	-1550	- 800	9
1.0	+ 650	+13.8	- 500	0	5
Argon on graphite ($V_m = 0.19$)					
0.02	-1700	+ 5	-2100	-1050	13
0.1	-1200	+ 2.2	-1400	- 850	7
1.0	- 700	- 2	- 580	- 400	2

The variation of the heats of adsorption at constant spreading pressure with coverage is given in Fig. 6. One interesting aspect of these curves is the leveling off at coverages between 0.1 and 1. This is followed in three cases out of four by a steady rise to higher values at lower coverages. The heat of adsorption per molecule might be expected to increase with decrease in coverage, perhaps leveling off at some particular finite value as zero coverage is approached. In the case of nitrogen on diamond, however, there is a pronounced maximum

(16) R. A. Beebe and D. M. Young, *J. Phys. Chem.*, **58**, 93 (1954).

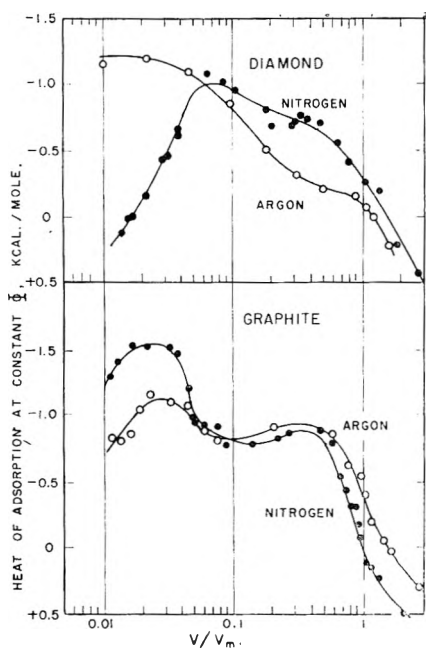


Fig. 6.—Calculated heats at constant spreading pressure (integral heats).

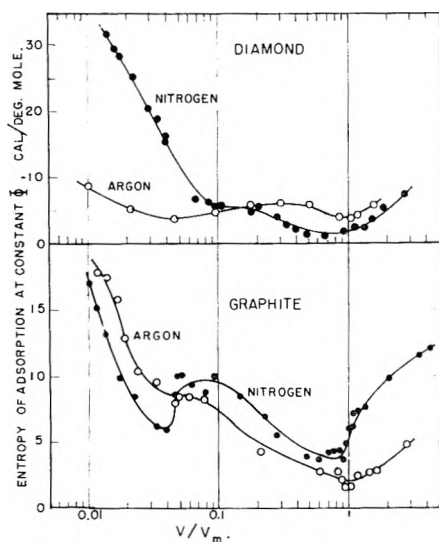


Fig. 7.—Calculated entropies at constant spreading pressure (integral entropies).

at about 7% coverage. Orr¹⁷ made calculations of the differential heats of adsorption from isotherms of argon and nitrogen on potassium chloride and cesium iodide. He reported maxima in the neighborhood of monolayer coverage and explained these in terms of mutual van der Waals attraction of the adsorbed molecules. Drain and Morrison¹⁸ calculated contributions of the dispersive forces to the isosteric heats of adsorption of argon on rutile, but these indicate a similar behavior with the maximum heat in the neighborhood of $\theta = 0.5$. The maxima indicated at still lower coverage in Fig. 6 remain an unexplained but reproducible anomaly.

(17) W. J. C. Orr, "The Adsorption of Non-Polar Gases on Alkali Halide Crystals," *Proc. Roy. Soc.*, **A173**, 349 (1939).

(18) L. E. Drain and J. A. Morrison, *Trans. Faraday Soc.*, **48**, 316, 810 (1952).

The entropies at constant spreading pressure are given in Fig. 7. There are minima in the neighborhood of monolayer coverage in all cases. Graphite shows an additional minimum at about $\theta = 0.03$ for nitrogen and a plateau for argon in the same region. It is interesting to note that there are maxima in the corresponding heat curves of Fig. 6 at about the same values of coverage. It is tempting to suggest that the two minima of the entropy curves on mineralogical graphite are due to the completion of monolayers on two types of sites. At $\theta = 1.0$ the monolayer is completed on the more abundant basal planes and at $\theta = 0.05$ the layer is complete on the prism faces. This is consistent with the estimate that about 5% of the total area is in the prism faces. This behavior of the entropy curves is not seen in diamond because of the difference in crystal structure, the diamond being isotropic.

There is a trend in the molar entropy of the adsorbate to very high values at the lowest coverage. Hill¹⁹ predicted that this must approach $+\infty$ at zero coverage on the basis of the model of statistical mechanics employed to yield the B.E.T. isotherm. The steady increase in entropy is in agreement with the behavior of an adsorbed two-dimensional gas film which must be present under the conditions of these measurements. The entropy of nitrogen on diamond is above that at argon to the lowest coverage, in agreement with the order of the two dimensional critical temperatures (63°K. for nitrogen and 75°K. for argon).

Concluding Remarks

The mounting interest in low energy surfaces brings into a sharp focus the problem of initial sample preparation. The concept of an inert adsorbent surface has been helpful for high energy surfaces in the region of large adsorption. However, it has been shown that the particular topography of the outgassed surface makes a significant contribution and, in fact, it may even make itself felt through several statistical layers of adsorbate as indicated by the work of Singleton and Halsey²⁰ with xenon multilayers.

The location of adsorbed argon atoms or nitrogen molecules on a carbon surface above the critical temperature is indefinite. The use of the van der Waals two-dimensional equation of state attempts to take into account the attractive forces between the adsorbate and the surface atoms. The dimensions of the adsorbate atoms and the separation of the adsorbent surface atoms are generally not commensurable and the interaction results in the formation of clusters, or patches, the sizes of which enlarge with increase in relative pressure. In the formation of the statistical multilayer, the various clusters approach but in all likelihood do not dovetail neatly with each other. This introduces a non-uniformity in the over-all multilayer that can influence the adsorption at individual sites. Some of the peculiarities in the multilayer region might be explicable on such a model. From the point of view of a would-be adsorbate atom or molecule, there are many locations having rather

(19) T. L. Hill, *J. Chem. Phys.*, **17**, 520 (1949).

(20) J. H. Singleton and G. D. Halsey, Jr., *J. Phys. Chem.*, **58**, 330 (1954).

shallow minimum potential energy wells in the region where the clusters merge. In fact it has been suggested²¹ that entropy differences in cluster formation relative to cluster decomposition could possibly account for hysteresis. Although high surface mobility would tend to favor a uniform packing, the residual interaction due to the presence of clusters would tend to counteract this.

There is a possible analogy with the various arrangements realized in packing mono-sized spheres on a macro scale. When spheres are packed experimentally by dumping them into a box, regular packings are never realized. Herdan²² found that upon prolonged vibration the voids are about 39.5% and the corresponding packing essentially orthorhombic. Graton and Frazer²³ concluded that the usual packing of mono-sized spheres consists of colonies of rhombohedral packing with random packing in between. Smith²⁴ measured both porosity and the number of points of contact. For porosities of about 44% there was a maximum at 7 or 8 points of contact, indicating predominantly orthorhombic packing. At porosities of about 37% (achieved by shaking) maxima occurred at both 8

(21) L. F. Gleysteen and V. R. Deitz, *J. Research Natl. Bur. Standards*, **36**, 285 (1945).

(22) G. Herdan, "Small Particle Statistics," Elsevier Publishing Co., Amsterdam, 1953, 520 pp.

(23) L. C. Graton and H. J. Frazer, *J. Geol.*, **43**, 785 (1935).

(24) W. O. Smith, *Phys. Rev.*, **34**, 1271 (1929).

and 12 points of contact, indicating colonies of rhombohedral interspersed with colonies of orthorhombic.

It is likely, therefore, that the arrangement of adsorbate molecules in parts of the monolayer and in the statistical multilayer adsorbed phase can lead to significant entropy changes and, for the case of a low energy surface, these can make a significant contribution to the free energy change of the adsorption process.

It may be concluded that there are many similarities and some differences in the behaviors of mineralogical graphite and heat-treated carbon blacks. The similarity is closest when the carbon black is heated to 2700°. The isosteric heats of adsorption are in close agreement in the neighborhood of monolayer coverage and the partial molar free energies of adsorption at different temperature, *i.e.*, the isotherms, show the same ability to cross-over after monolayer coverage. The behavior at low relative pressures, *i.e.*, the steps in the isotherms, suggests that the surface of graphite may be more homogeneous than a heat-treated carbon black, and the recent work by Ross and Olivier²⁵ provides definite indication that this is more a question of degree than a fundamental difference in the adsorbing surface.

(25) S. Ross and J. P. Olivier, *J. Phys. Chem.*, **65**, 608 (1961).

OPTICAL ROTATORY DISPERSION OF THE β -FORM OF THE POLYPEPTIDE CHAIN

By AKIYOSHI WADA, MASAMICHI TSUBOI¹ AND EMIKO KONISHI

Department of Chemistry, Faculty of Science, Ochanomizu University, Bunkyo-ku, Tokyo, Japan

Received October 31, 1960

The β -form of poly- γ -benzyl-L-glutamate (PBLG) was studied by measurement of the optical rotatory dispersion and infrared absorption spectrum. The fraction x_{β} of this intermolecular hydrogen-bonded configuration of the polypeptide chain increases with the concentration. The relation between x_{β} and the concentration was obtained by comparing the intensities of the 1660 and 1630 cm^{-1} absorption bands. By this relation to analyze the optical dispersion curve, we estimated two unknown constants characteristics of the β -form. It was also confirmed that the hydrogen bond in the β -form and the α -helix of low-molecular weight PBLG is much more labile than that of the α -helix of high-molecular weight PBLG.

Introduction

By physicochemical methods such as X-ray diffraction and infrared absorption spectrum it has been established that the synthetic polypeptide chain exists not only in the α -helix or random coil but also as the β -form in solution.^{2,3} This fact is especially interesting in relation to protein structure since the synthetic polypeptide is a useful model for the study of the chemical and biological properties of the natural protein.

In poly- γ -benzyl-L-glutamate (PBLG), one of the synthetic polypeptides, the stability of the α -helix decreases with the molecular weight even in a solvent which stabilizes the α -helix of high molec-

ular weight PBLG. The critical degree of polymerization for this instability was found to be around ten.⁴ Below this point the polypeptide chain forms an intermolecular rather than an intramolecular hydrogen bond and assumes a pleated sheet configuration which is called the β -form. The extent of intermolecular hydrogen bonding in the β -form depends on the concentration of PBLG in solution.

Yang and Doty⁵ have shown that the optical rotatory dispersion curves also yield useful information for the study of the chain configuration of natural protein and synthetic polypeptides. This method has been used, for instance, to determine the fractions of the α -helix and random coil which coexist in a molecule. Imahori⁶ has extended his

(1) Department of Chemistry, Faculty of Science, Tokyo University, Hongo, Tokyo, Japan.

(2) C. H. Bamford, A. Elliott and W. E. Hanby, "Synthetic Polypeptides," Academic Press, New York, N. Y., 1956.

(3) E. R. Blout and A. Asadourian, *J. Am. Chem. Soc.*, **78**, 955 (1956).

(4) J. C. Mitchell, A. E. Woodward and P. Doty, *ibid.*, **79**, 3955 (1957).

(5) J. T. Yang and P. Doty *ibid.*, **79**, 761 (1957).

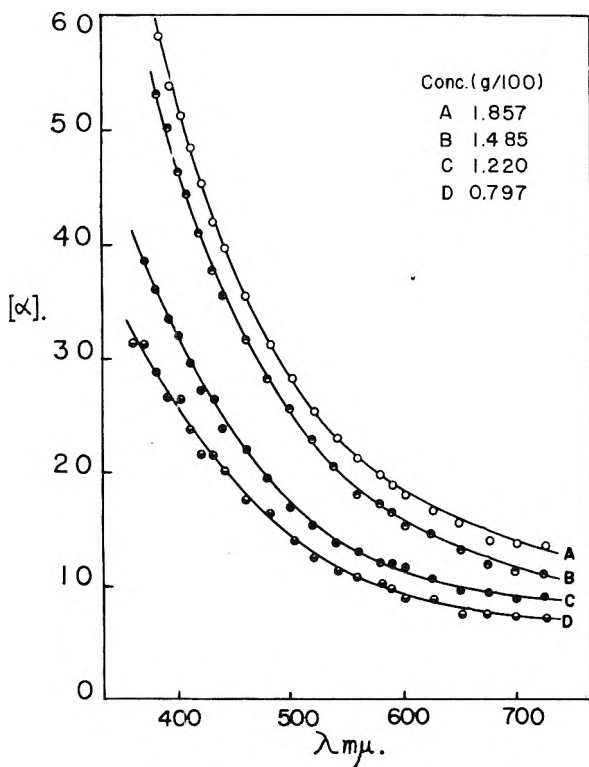


Fig. 1.—Optical rotatory dispersion of PBLG 301-1 in EDC.

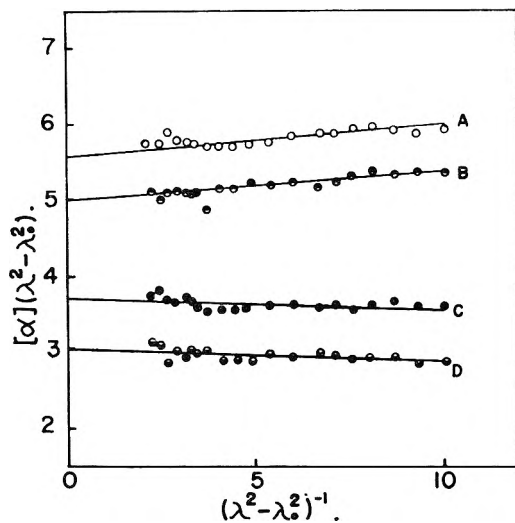


Fig. 2.—Modified plot of the optical rotatory dispersion of PBLG 301-1 in EDC corresponding to Fig. 1; λ_0 is taken as 0.212μ .

work to include the β -form and, on the basis of the theoretical discussion of Moffitt, Fitts and Kirkwood,⁷ developed an empirical equation; the specific optical rotation at the wave length λ can be written in terms of the fraction of α -helix x_H , of β -form x_β , and that of random coil $x_R = (1 - x_H - x_\beta)$ as

$$[\alpha]_\lambda = \frac{100n^2 + 2}{M_0 3} \{a_0^R + a_0^H x_H + a_0^\beta x_\beta\} \frac{\lambda_0^2}{\lambda^2 - \lambda_0^2} + \{b_0^H x_H + b_0^\beta x_\beta\} \frac{\lambda_0^4}{(\lambda^2 - \lambda_0^2)^2} \quad (1)$$

(6) K. Imahori, *Biochem. Biophys. Acta*, **37**, 336 (1960).

(7) W. Moffitt, D. D. Fitts and J. G. Kirkwood, *Proc. Natl. Acad. Sci.*, **43**, 723 (1957).

where M_0 is the residual weight, n is the refractive index of the solvent, and a_0^R is a constant characteristic of each of the amino acid residues. In the case of PBLG, $a_0^R = -540$ was taken as the most reasonable value; a_0^H and b_0^H , the constants for the α -helical configuration, were determined by Doty and Lundberg⁸ as $+680$ and -600 , respectively, for the right-handed α -helix. In spite of the importance of eq. 1 in the study of protein structure, the two constants, a_0^β and b_0^β characteristic of the β -form, have not been determined.

We have studied the β -form of PBLG by optical rotatory dispersion and infrared absorption spectrum measurement. The unknown constants, a_0^β and b_0^β , were determined experimentally.

Experimental

Materials.—For the preparation of the low-molecular weight PBLG, γ -benzyl-N-carboxy-L-glutamate anhydride, synthesized by the Blout-Karlson method⁹ were polymerized in dry dioxane; n -hexylamine was used as an initiator. After completion of the polymerization, the reaction mixture was poured into cold ethyl ether with vigorous stirring. The precipitate was separated by centrifugation and dried *in vacuo*. This product was suspended in formic acid at 20° .^{3,4} After removal of the insoluble portion by centrifugation, the formic acid was vacuum distilled. The distillation residue was washed with ether, dissolved in dioxane, and lyophilized. The purity of this low-molecular weight PBLG was checked by paper chromatography with ethylene dichloride-ethanol-water system. The molecular weights of the samples were estimated from the intrinsic viscosity measured in dichloroacetic acid.⁵ The dioxane was purified according to Fieser's method¹⁰ and fractionally distilled after 24 hours of refluxing with sodium, 101.0° . Ethylene dichloride (EDC) was dried over P_2O_5 and fractionally distilled at 84° .

Measurements. Optical Rotatory Dispersion.—The optical rotation was measured in the wave length range 340–700 $m\mu$ with a Hitachi Photoelectric Polarimeter equipped with a Beckmann-type monochromator and a 10 cm. liquid tube. The concentration range of PBLG was 0.5–5 g./100 ml.; EDC or dioxane was used as the solvent.

Infrared Spectrum.—The infrared spectrum was measured with a Perkin-Elmer 21 Spectrometer equipped with a sodium chloride prism; we used calcium fluoride window-sealed cells of 1, 0.5, 0.2, 0.1 and 0.025 mm. depth.

Results

Optical Rotatory Dispersion.—A typical rotatory dispersion curve of low-molecular weight PBLG is shown in Fig. 1; unlike the curves for the α -helix and the random coil, the $[\alpha]$ values decrease with increasing wave length and tend to increase with the concentration. For convenience in future analysis, these dispersion curves were replotted as shown in Fig. 2. The modified plot, $[\alpha](\lambda^2 - \lambda_0^2)$ vs. $(\lambda^2 - \lambda_0^2)^{-1}$, usually becomes a straight line as shown in the figure, the intercept of which gives $100(n^2 + 2)/3M_0 \{a_0^R + a_0^H x_H + a_0^\beta x_\beta\} \lambda_0^2$ and the slope gives $100(n^2 + 2)/3M_0 \{b_0^H x_H + b_0^\beta x_\beta\} \lambda_0^4$. The intercepts (I) and slopes (S) of two samples at several concentrations are listed in Table I.

Infrared Spectrum.—The fraction of the β -form was estimated from the infrared absorption spectrum. From the spectroscopic studies of Ambrose and Elliott,¹¹ and Bamford, *et al.*,¹² the absorption

(8) P. Doty and R. D. Lundberg, *ibid.*, **43**, 212 (1957).

(9) E. R. Blout and R. H. Karlson, *J. Am. Chem. Soc.*, **78**, 941 (1956).

(10) L. F. Fieser, "Experiments in Organic Chemistry," 2nd Ed., D. C. Heath & Co., Boston, Mass., 1941, p. 361.

(11) E. J. Ambrose and A. Elliott, *Proc. Roy. Soc. (London)*, **205 A** 47 (1957); **A208**, 75 (1951).

band near 1660 cm^{-1} has been assigned to be C=O stretching mode of the α -form, and the band near 1630 cm^{-1} to that of the β -form. Blout and Assadourian³ confirmed these conclusions and in addition found that the absorption intensity at 1630 cm^{-1} , which is proportional to the fraction of the β -form, increases with the concentration of PBLG. Therefore, the absorption intensity at 1630 cm^{-1} can be used as a measure of the fraction of the β -form.

The spectra in the neighborhood of the 1630 and 1660 cm^{-1} bands given by dioxane and EDC solutions at several concentrations are shown in Fig. 3a and Fig. 3b, respectively. For each solution, the optical rotation was measured at the same time as the absorption spectrum. Slight differences in the wave numbers of the absorption maxima were observed for the PBLG solutions in different solvents; maxima were observed at 1629 and 1666 cm^{-1} in dioxane and 1630 and 1665 cm^{-1} in EDC.

We cannot estimate x_β directly from the height of the absorption peak as the residual absorption coefficient of the pure β -form (D_{1630}^0) is not known; furthermore, for analysis of the spectrum the effect due to overlapping by the foot of the neighboring absorption band must be considered. Therefore, we resorted to the following device to estimate the residual absorption coefficient. As mentioned above, the absorption band near 1660 cm^{-1} is supposed to be a contribution from both the α -helix and random coil, and we have assumed for simplicity that the residual absorption coefficient of these two configurations at this wave length is the same. The intensity of the 1660 cm^{-1} band is also assumed to vary linearly with the intensity of the 1630 cm^{-1} band. This assumption is based on the idea that the β -form can be formed only at the expense of the α -helix or random coil, and also that the absorption intensity at these wave number is proportional to the extent of this transformation. We will show later that these assumptions are reasonable and do not seriously effect our conclusions. D_{1660} vs. D_{1630} , the apparent residual absorption coefficient of the 1660 and 1630 cm^{-1} bands, respectively, should give a straight line as shown in Fig. 4. The D_{1630} values must be corrected for the effect of overlapping by the foot of the neighboring absorption band and the corrected absorption coefficients are those indicated by the thin lines (closed circles) which were drawn in such a manner that $D_{1630\text{ cor}}$ is zero at infinite dilution. The intercepts give the values of the residual absorption coefficients: $D_\beta^0 = 630$ (dioxane), 820 (EDC), and $D_{H+R}^0 = 380$ (dioxane), 450 (EDC). Then x_β can be estimated from $x_\beta = D_{1630\text{ cor}}/D_{1630}^0$.

Next, let us reconsider the two assumptions mentioned above. Strictly speaking, the contributions of the α -helix and random coil to the 1660 cm^{-1} band are not equal but depend on the relation¹³

$$D_{1660} = D_{\text{helix}}^0 x_H + D_{\text{coil}}^0 x_R \quad (2)$$

$$(D_{\text{coil}}^0/D_{\text{helix}}^0) = 0.85$$

(12) C. H. Bamford, W. E. Hanby and F. Ilappey, *J. Phys. Chem.*, **A205**, 30 (1951); **A206**, 407 (1951).

(13) K. Imahori, private communication.

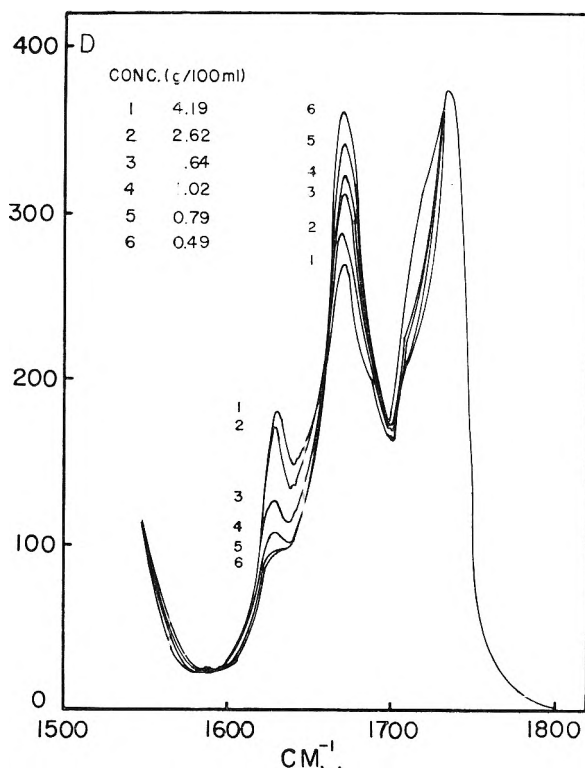


Fig. 3a.—Infrared absorption spectrum of PBLG 701-1 in dioxane (D , apparent residual absorption coefficient).

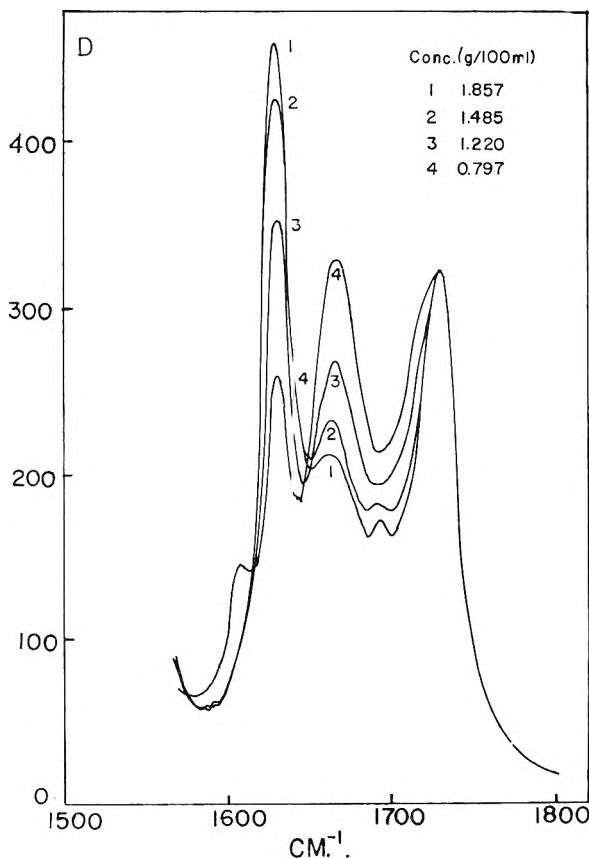


Fig. 3b.—Infrared absorption spectrum of PBLG 701-1 in EDC (D , apparent residual absorption coefficient).

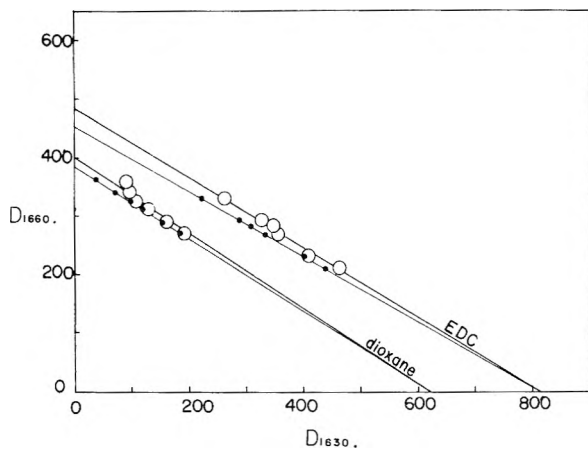


Fig. 4.—Relation between the apparent absorption coefficient of 1630 and 1660 cm^{-1} line (open circle). Closed circles give corrected intensity of the 1630 cm^{-1} absorption band.

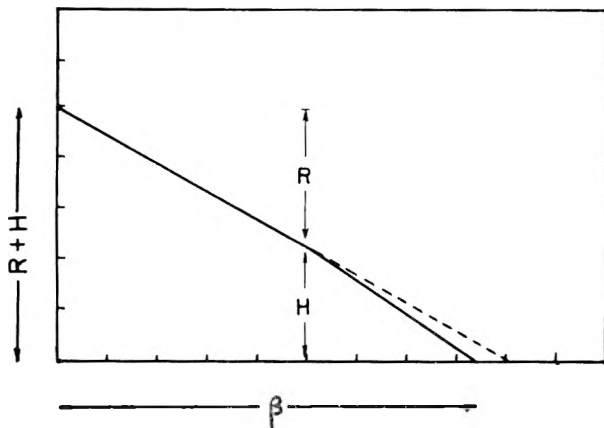


Fig. 5.—Illustration depicting the relation between the intensity of 1630 and 1660 cm^{-1} absorption line under the limiting condition of the transformation.

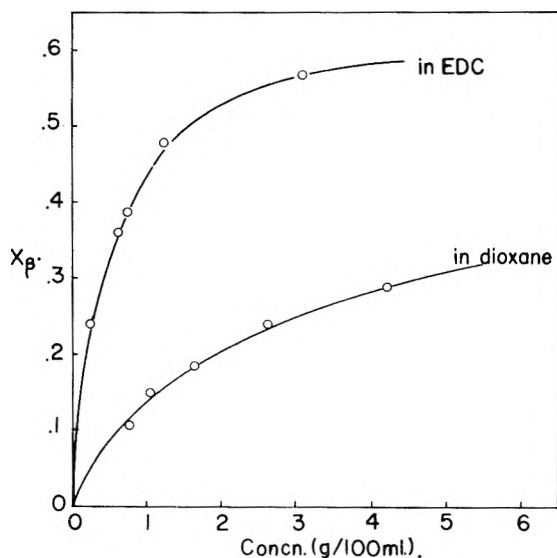


Fig. 6.—Relation between the fraction of β -form and the concentration of low-molecular weight PBLG.

So, if the β -form formation follows a hypothetical limiting process, in which the β -form is first made at the expense of the random coil and next at the

expense of the α -helix, there should be a break in the straight-line relation between D_{1630} and D_{1660} given in Fig. 4. In Fig. 5 we have drawn such a curve for a hypothetical PBLG sample containing the 45% helical form. According to the discussion given above, the D_{1630}^0 required for the estimation of x_β will not be found experimentally. However, the assumption used in Fig. 5, that the 45% helix content in the PBLG is limiting, is a fictitious condition which would not occur in our samples. Thus, such effects can be safely assumed to be negligible, less than 5%, and will not introduce a serious error into our conclusions.

The relation between the fraction of the β -form and concentration is shown in Fig. 6. The fraction of the β -form in EDC is much higher than that in dioxane solution at the same concentration. This finding is in agreement with the results in Table I obtained from the optical rotation data

TABLE I
INTERCEPT AND SLOPE OF MODIFIED OPTICAL DISPERSION CURVE OF PBLG

Sample No.	Solvent	Concn. (g./100 ml.)	I	S
301-1 ^a	EDC	1.857	5.60	0.038
	EDC	1.485	4.97	.038
	EDC	1.220	3.61	-.002
	EDC	0.797	3.03	-.017
701-1 ^b	EDC	1.23	3.60	.015
	EDC	0.74	1.80	-.05
	EDC	0.57	0.60	-.08
	Dioxane	4.19	1.71	.071
	Dioxane	2.62	0.72	.03
	Dioxane	1.64	-0.35	.010
	Dioxane	1.02	-1.64	.000
Dioxane	0.79	-1.85	-.013	

^a Initiator-anhydride ratio; $A/I = 4$, molecular weight = 2200. ^b Initiator-anhydride ratio; $A/I = 4$, molecular weight = 2000.

Discussion

The following method was used to estimate the unknown constants of eq. 1, a_0^β and b_0^β , which are characteristic of the β -form. As frequently mentioned and deduced easily from eq. 1, the intercept I and the slope S of the modified plot are given by equations (3a) and (3b), respectively

$$I = A(a_0^R + a_0^H x_H + a_0^\beta x_\beta) \tag{3a}$$

$$S = B(b_0^H x_H + b_0^\beta x_\beta) \tag{3b}$$

where

$$A = \frac{100}{M^0} \frac{n^2 + 2}{3} \lambda_0^2, \text{ and } B = A \lambda_0^2$$

Eliminating x_H or x_β in eq. 3a and 3b, we have

$$\left(\frac{I}{A} - \frac{S}{B} \times \frac{a_0^H}{b_0^H}\right) = b_0^\beta \left(f - \frac{a_0^H}{b_0^H}\right) x_\beta + a_0^R \tag{4a}$$

$$\left(\frac{I}{A} - \frac{S}{B} \times f\right) = b_0^H \left(\frac{a_0^H}{b_0^H} - f\right) x_H + a_0^R \tag{4b}$$

where $f = a_0^\beta / b_0^\beta$.

When the left side of eq. 4a is plotted against x_β as shown in Fig. 7, the intercept will give a_0^R and the slope $b_0^\beta(f - a_0^H/b_0^H)$, values which are listed in Table II. At this stage we still cannot determine both a_0^β and b_0^β unless one of them is determined by another method. For further analy-

sis, let us plot x_β against x_H , using eq. 4a and 4b, for the several given values of f as a parameter as shown in Fig. 8. If we assume here, as Blout and Assadourian have pointed out, that x_H is constant, in other words, that the β -form formation occur only at the expense of the random coil but not at the expense of the α -helix having a degree of polymerization higher than the critical number, then 2 must be the reasonable value for f , and a_0^β and b_0^β can be determined as listed in the fourth and fifth rows of the Table III.

TABLE II
CONSTANTS OF THE OPTICAL ROTATION OF PBLG IN
DIOXANE AND EDC
 $f = (a_0^\beta/b_0^\beta) = 2$

Solvent	a_0^R	$(f - a_0^H/b_0^H)$	a_0^β	b_0^β	x_H
Dioxane	-250	1300	840	420	0.11
EDC	-500	1300	840	420	0.23

TABLE III
FRACTIONS OF THE HELIX AND β -FORM OF PBLG IN
EDC-DCA SYSTEM

DCA % by vol.	x_β	x_H
0.0	0.45	0.22
0.3	.29	.21
3.0	.08	.00

Although a_0^β and b_0^β can be estimated as described above, there are several points which should be discussed. First, it is believed that a much larger error occurs in the measurement of the slope of the modified plot than of the intercept. To evaluate this source of error a_0^β was estimated also by plotting I against x_β with x_H constant. The values of a_0^β thus obtained were +790 in dioxane and +860 in EDC. These results, obtained without reference to the slope of the modified plot, are quite consistent with those estimated by using both I and S , and indicate that the values listed in Table III are reasonable. The second point to be discussed is the variation of a_0^R in different solvents. Although a_0^R should be a constant for any given amino acid residue, it is known to be changed by the solvation, an effect which will be pronounced in the case of a short polypeptide chain; the difference observed between the EDC and dioxane solutions can be attributed to a solvent effect. The third point is the difference between the meaning of the x_β estimated from the infrared spectrum and that calculated from eq. 1. The former indicates the fraction of the residue which forms an intermolecular hydrogen bond, while the latter is the fraction of the residues having a β -configuration in the backbone chain. The fourth point is that the effect of the chain end is unknown, an effect which may not be negligible especially for such a low-molecular weight sample.

These problems, which should be investigated, may account for the difference in a_0^R values and make the values of x_β somewhat unreliable. However, the fact that the solvent does not affect a_0^β and b_0^β , and that a reasonable value for a_0^β was obtained without recourse to the slope data, indi-

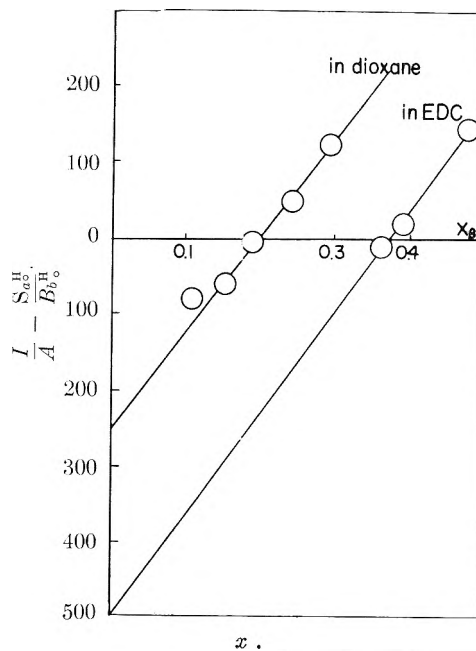


Fig. 7.—Relation between $\frac{I}{A} - \frac{S}{B} \times \frac{a_0^H}{b_0^H}$ and x_β .

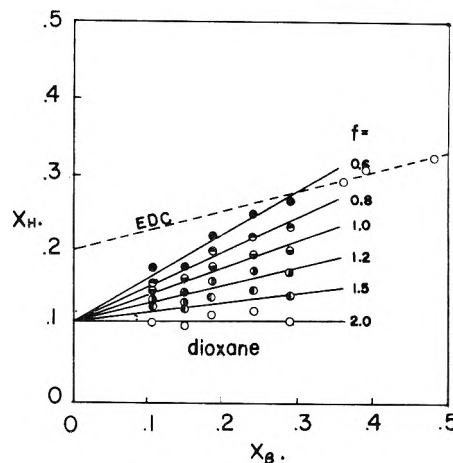


Fig. 8.—Relation between x_β and x_H for different values of the parameter f .

icates that, insofar as the assumption of constant x_H is valid, a_0^β and b_0^β as given in Table II are correct.

With known values for a_0^β and b_0^β , we can study the chain configuration of this low-molecular weight polypeptide. For example, the effect of dichloroacetic acid, which is considered to be a hydrogen bond breaking agent, on x_H and x_β in EDC was measured. As shown in Table III, above a 3% concentration of DCA both x_H and x_β become zero. This means that the hydrogen-bonded-states of such a low molecular weight PBLG are much more labile than that of the α -helix of high-molecular weight polypeptide.

Acknowledgment.—We wish to thank Dr. Kazutomo Imahori for his helpful discussion of this work. We also acknowledge the technical assistance of Miss Sumiko Monoi in the preparative work.

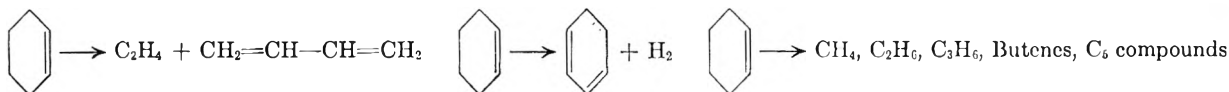
A STUDY OF THE PYROLYSIS OF CYCLOHEXENE¹

BY S. RUVEN SMITH AND ALVIN S. GORDON

Chemistry Division, U. S. Naval Ordnance Test Station, China Lake, California

Received November 17, 1960

The pyrolysis of cyclohexene has been studied over the temperature range 425–535°. There are three concurrent homogeneous decomposition processes.



The first two processes are intramolecular and have been established to be first order with specific rate constants $1.4 \times 10^{17} \exp[-72700/RT \text{ sec.}^{-1}]$, and $1.9 \times 10^{16} \exp[-71200/RT \text{ sec.}^{-1}]$, respectively. The third decomposition path is *via* a free radical mechanism which accounts for 10% or less of the total cyclohexene decomposed. The specific rate constant for the over-all decomposition is $k_0 = 7.7 \times 10^{15} \exp(-67600/RT \text{ sec.}^{-1})$. Mechanisms consistent with the data are proposed. Of especial interest is the interpretation of the data which shows that the energy of activation for the two intramolecular paths is the same within experimental error.

Introduction

Studies of the pyrolysis of cyclohexene to form butadiene and ethylene have been reported by Küchler² to have a first order rate constant and

$$k = 9.0 \times 10^{12} \exp(-57500/RT \text{ sec.}^{-1})$$

more recently by Kraus, Varruska and Bogart,³ who report a homogeneous first order constant of $k = 1.22 \times 10^{12} \exp(-55100/RT \text{ sec.}^{-1})$ in quite good agreement.

Küchler employed a static system and followed the reaction by pressure measurements and analysis of the products. He has identified most of the important products which we identify, with the exception of 1,3-cyclohexadiene. He assumed that all the products except butadiene and ethene resulted from secondary reactions. Kraus, Varruska and Bogart employed a flow system in their work, and report that only butadiene and ethene are the primary products. As will be shown later, our results indicate that there are three concurrent pyrolysis paths.

It was decided to reinvestigate the pyrolysis of cyclohexene. Since the C—C bonds α to the double bond in cyclohexene are at least 15 kcal. weaker than normal C—C bonds, the breaking of one of these bonds should be the first step of the pyrolysis. A six-membered bi-radical would result whose further reactions could be inferred from the products.

Apparatus, Materials and Procedure

Cyclohexene was obtained from the National Bureau of Standards. It was frozen and pumped, then liquefied and refrozen until it was freed of air. Its purity as checked by gas chromatography and mass spectrometry was 99.9%. Deuterium was obtained from the Stuart Oxygen Company. It was freed of any trace of residual air by passage through a charcoal trap at liquid nitrogen temperatures. Mass spectrometer analysis showed it to be 98.9% D₂ with 1.1% HD impurity.

Cylindrical glass reaction vessels of about 50-cc. capacity equipped with a breakseal were sealed to a manifold. A predetermined pressure of cyclohexene was added to the evacuated vessels, each of which was surrounded by liquid nitrogen and removed from the manifold with a torch. For deuterium-cyclohexene mixes the procedure was similar, except that after recording the pressure of cyclohexene at

room temperature the vessel was placed in a liquid nitrogen bath and deuterium was added to a predetermined pressure.

The reaction vessels were preheated in a furnace about 150° below the reaction temperature and then plunged into a salt bath at the desired pyrolysis temperature. A dummy reaction vessel which had a fine wire thermocouple with its junction in the center of the vessel, was cycled through the standard pyrolysis procedure. It showed that the reaction temperature was attained in about 15 seconds. The actual time of immersion was corrected by this interval. After reaction the sample flasks were quenched in an air stream.

The reacted mixture was analyzed by a combination of mass spectrometer and gas chromatography methods. The gas chromatography analyses were carried out by a combination of two columns; a 1.5 squalane on Pelletex column gave complete resolution through the C₃ region, and a 25% 1-methyl-5-(2-methoxyethyl)-tetrazole on C₂₂ brick column separated the C₄-C₇ straight chain, cyclics and aromatic compounds.⁴ Quantitative values from the gas chromatography runs were obtained by measurement of the peak area. The sensitivities of the products (peak area/micromole) were determined under the conditions of column operation. The products of the cyclohexene-deuterium mixtures were separated on the gas chromatograph, trapped, and then analyzed for deuterium content with the mass spectrometer.

Results

Table I shows the products of reaction from the pyrolysis of cyclohexene at a number of tempera-

TABLE I^a
GAS CHROMATOGRAPHIC ANALYSIS OF PRODUCTS OF CYCLOHEXENE PYROLYZED AT VARIOUS TEMPERATURES

Temp., °C.	Products reported in moles $\times 10^7$		
	477	500	535
Time, sec.	916	360	150
Cyclohexene	534.0	528.0	365.3
CH ₄	1.5	2.3	14.7
C ₂ H ₄	45.5	53.8	130.2
C ₂ H ₆	1.0	1.0	7.0
C ₃ H ₆			8.7
1,3-Butadiene	32.8	43.0	111.0
Butanes	1.5	1.0	5.0
Cyclopentane	1.8	0.8	1.3
Methylcyclopentane			
Cyclohexane	5.0	3.7	4.5
Hexene			
1,3-Cyclopentadiene	1.0	1.9	4.7
Hexene			
1,3-Cyclohexadiene	16.4	18.2	24.7
Benzene	2.8	4.1	11.4

^a H₂ is very insensitive in a helium carrier gas and is not listed as a chromatographic product.

(1) Presented before the Cleveland ACS Meeting, 1960.

(2) L. Küchler, *Nach. Ges. Wiss. Göttingen*, **1**, 231 (1939).

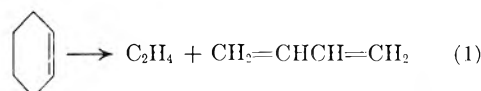
(3) M. Kraus, M. Varruska and V. Bogart, *Chem. Listy*, **50**, 553 (1956).

TABLE II
DEUTERATION OF THE PRODUCTS FROM THE PYROLYSIS OF CYCLOHEXENE
 $T = 500^\circ$, time = 300 sec. $T = 515^\circ$, time = 150 sec. $T = 504^\circ$, time = 183 sec.

	$D_2 = 1/36$				$D_2 = 1/36$				$D_2 = 1/35$			
	d_0	d_1	d_2	d_3	d_0	d_1	d_2	d_3	d_0	d_1	d_2	d_3
Methane	65.7	33.6	0.6	
Ethylene	98.4	0.9	0.4	0.3	98.9	0.8	0.3		99.0	0.9	0.1	
Ethane	60.2	35.4	4.4	
Propylene	71.6	28.6	1.3		71.2	27.3	1.4	0.1	80.3	19.0	0.7	
Propane	75	25			55.2	34.0	9.9	0.8
Isobutene	55.3	36.2	8.5		53.0	38.5	8.5					
cis-Butene-2	28.6	21.6	49.0		48.1	36.0	15.9					
trans-Butene-2	28.9	20.7	50.4		27.9	20.9	50.1	1.0				
1,3-Butadiene	98.5	1.3	0.1	0.1	98.4	1.5	0.1					
Methylcyclopentane	35.0	46.0	19.0					
Cyclohexane	32.3	47.9	19.8		34.0	45.7	20.2					
Hexadiene	58.5	41.5						
Pentadiene	75.3	24.7						
1,3-Cyclopentadiene	97.3	2.7						
Hexadiene	76.7	23.3						
Cyclohexene	98.6	1.3	0.1		99.5	0.4	0.1					
1,3-Cyclohexadiene	99.5	0.5			99.7	0.3						
Benzene	98.6	1.4			98.3	1.7						

tures. The analyses show clearly that ethylene and butadiene appear in about equal amounts (butadiene is so reactive that its value is always somewhat low) and are the major products at all the temperatures.

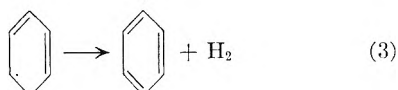
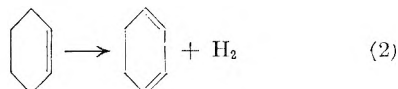
Thus the main decomposition path is an inverse Diels-Alder reaction



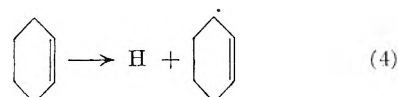
The deuterium marking of the reaction products from the pyrolysis of a $36/1(D_2/\text{Cyclohexene})$ mix is shown in Table II. The ethylene and butadiene products are only very slightly deuterated in agreement with an intramolecular mechanism.

The next most important hydrogen products are 1,3-cyclohexadiene, and benzene. These products are only slightly deuterated in a

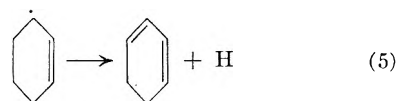
$36/1(D_2/\text{Cyclohexene})$ mix.



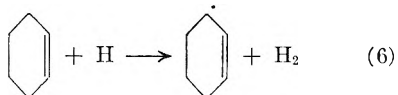
Cyclohexadiene and H_2 could be produced by a free radical mechanism even though the cyclohexadiene is unmarked.



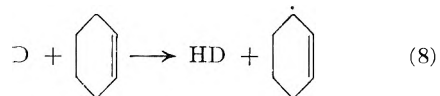
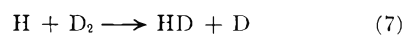
(4) W. G. Finnegan and S. Ruven Smith, *J. Chromatography*, in press.



The H atom would be a chain carrier



If this were the mechanism for the formation of Cyclohexadiene then addition of D_2 to the reacting mixture would provide a competitive reaction path for the atoms

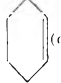
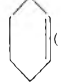
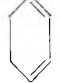

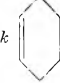


We should observe that the rate of formation of H_2 would decrease, and the decrease in its rate would


TABLE III
PYROLYSIS OF VARIOUS CYCLOHEXENE-DEUTERIUM MIXTURES TO DETERMINE THE EFFECT OF DEUTERIUM ON THE RATE OF H_2 AND HD FORMATION

Partial press. Cyclohexene cm.	$T = 500^\circ$ Partial press. D_2 cm.	Time = 300 sec.	
		Divisions H_2	Divisions HD
4.0	0	19.0	0
4.0	4.0	17.0	3.3
4.0	12.0	16.2	9.1
4.0	20.0	20.1	14.4
4.0	32.0	20.3	16.2
4.0	40.0	20.9	21.3
4.0	48.0	20.6	19.6
4.0	48.0	20.6	26.6
4.0	56.0	20.1	33.5

TABLE IV
KINETIC DATA FOR CYCLOHEXENE DECOMPOSITION
All species are reported as moles $\times 10^7$.

Time, sec. cor.	T, °C.	 (orig.)	 (final)	C ₂ H ₄	 + 	$k_{over-all}$ $\times 10^4$	$k_{C_2H_4}$ $\times 10^4$	k  $\times 10^4$
2485	446	529.2	499.5	19.1	6.0	0.23	0.15	0.046
4985	446	529.2	477.4	35.2	11.2	0.21	.14	.045
285	477	603.0	574.9	14.2	8.9	1.68	.85	.53
588	477	546.4	497.3	34.7	9.5	1.61	1.13	.31
901	477	590.4	520.3	45.5	19.2	1.41	0.91	.39
1225	477	603.0	500.9	49.0	32.4	1.52	0.73	.48
1785	477	603.0	456.5	96.4	34.0	1.56	1.03	.36
1253 ^a	476	494.0	415.7	1.38
525	500	563.3	416.4	87.8	41.1	5.76	3.44	1.61
705	500	563.3	371.5	113.6	48.8	5.90	3.50	1.50
287	500	128.3	108.3	10.5	8.4	5.92	3.08	2.47
588	500	131.0	93.3	21.5	11.2	5.77	3.28	1.71
787	500	122.0	77.3	26.2	13.2	5.80	3.40	1.71
1789	500	125.6	42.0	48.9	21.6	6.13	3.50	1.55
189	500	1388.2	1248.7	99.2	26.3	5.62	4.01	1.06
276 ^a	500	494.0	415.7	4.97
115	517	575.0	484.6	63.8	19.7	14.88	10.45	3.23
195	517	563.3	437.5	93.2	23.3	12.95	9.67	2.42
295	516	539.8	345.5	130.4	41.2	15.13	10.06	3.18
135	535	541.0	352.5	130.2	36.1	31.74	22.01	6.10

^a Glass wool added (~ 100 -fold increase in S/V).

be equal to twice the rate of HD formation. In Table III the effect of various pressures of D₂ on the rate of formation of H₂ and HD from cyclohexene is shown to have no effect on the rate of formation of H₂, but affects that of HD. The observations are consistent with an intramolecular production of H₂ from cyclohexene and a free radical path for the decomposition of cyclohexene, in addition to the two intramolecular paths. The free radicals abstract D from D₂, and the D atom abstracts H from cyclohexene according to reaction 8. As would be expected from this mechanism, the larger the D₂/ ratio, the larger is the rate of production of HD.

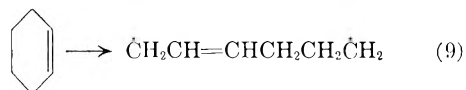
The deuterium marking of the methane, ethane, propane and butene products (Table II) confirms the existence of a free radical path for cyclohexene decomposition.

The surface/volume ratio of the reaction vessel was increased approximately 100-fold by the addition of Pyrex glass wool. As may be seen in Table IV, there is no effect of surface, within experimental error, on the over-all decomposition rate of cyclohexene.

Benzene undoubtedly is produced from 1,3-cyclohexadiene. The calculations of k_2 are made on the basis that the cyclohexadiene formed in reaction 2 is the sum of the cyclohexadiene and the benzene in the products.

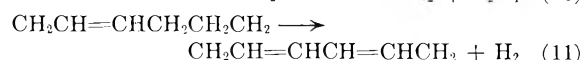
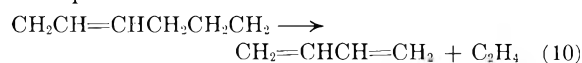
Discussion

As previously noted, the energy of activation for the two intramolecular processes are the same within experimental error. The evidence is consistent with a mechanism where the initial step is the opening of the cyclohexene ring.



If the resonance energy of the allylic radical is 15–20 kcal., then the observed energy of activation could correspond to the C–C bond strength of the bond broken in reaction 9.

The bi-radical could decompose in two competitive paths

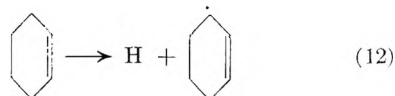


We have shown⁵ previously that hydrocarbon free radicals with a configuration RCHCH₂R¹ where R, R¹ = alkyl group or an H atom, will eliminate a molecule of hydrogen at a rate competitive with the breaking of a C–C bond. The biradical which results from reaction 11 is resonance stabilized at each end. It has a spatial configuration such that the two methylene groups are very close to each other, and they will combine and form 1,3-cyclohexadiene with over 40 kcal./mole of excess vibrational energy. The 1,3-cyclohexadiene has many degrees of freedom, so that the excited 1,3-cyclohexadiene will have a long half-life and a subsequent collision will remove the few kcal. necessary for stabilization. Later collisions will drain off the rest of the excess vibrational energy. If this is the mechanism then the energy of activation of reaction 10 and 11 must be the same within experimental error (about 5 kcal.); otherwise reactions 1 and 2 would not have the same over-all energy of activation.

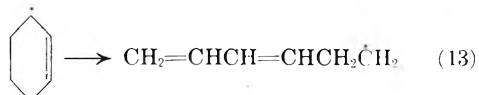
The free radical reaction path is also homo-

(5) A. S. Gordon and S. R. Smith, *J. Chem. Phys.*, in press.

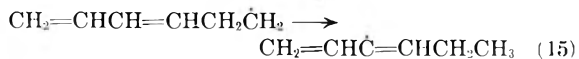
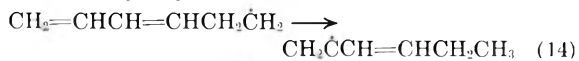
geneous. From the relatively slow rate of this reaction it must have a high energy of activation for the initial process and very short chains. The loss of an H atom



should be endothermic about 75 kcal. The cyclohexenyl radical can open at these temperatures



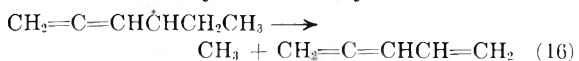
and the resulting linear radical can isomerize itself in two ways by intraradical abstraction



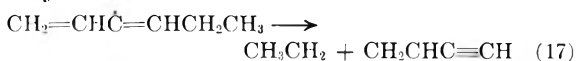
Both the isomerized radicals are resonance stabilized. The other canonical form of the isomerized radical in reaction 14 is



and this form may lose a methyl radical



The radical formed in reaction 15 can split off an ethyl radical



The five-membered tri-ene that results from reaction 16 is isomeric with cyclopentadiene and could be confused with this compound. It is not deuterated (Table II) as would be expected from the proposed mechanism. The mechanism for the production of butenes is complicated by the presence of the reactive 1,3-butadiene which may be its precursor.

The existence of the cyclohexenyl radical is shown by the deuterium marking of the parent cyclohexene (Table II) in the products from the pyrolysis of mixtures of cyclohexene and D_2 .

The H atom formed in reaction 12 would abstract H from its parent to form more cyclohexenyl radical or add to the double bond of its parent to form the cyclohexyl radical. We have studied the reactions of the cyclohexyl radical⁶ and it is the precursor of methyl, ethyl and allyl radical. The allyl radical will form propene at these temperatures by abstraction, and it is seen to be marked d_1 and d_6 (Table II) in harmony with the above mechanism.

The cyclohexane product may be formed by cyclohexyl radical.

Our pre-exponential factor and energy of activation for the over-all rate of cyclohexene pyrolysis are considerably different from previously reported values.^{2,3} We are not able to account for these differences. It is of some interest that Küchler reports an over-all average specific rate constant

(6) A. S. Gordon and S. R. Smith, *J. Phys. Chem.*, in press.

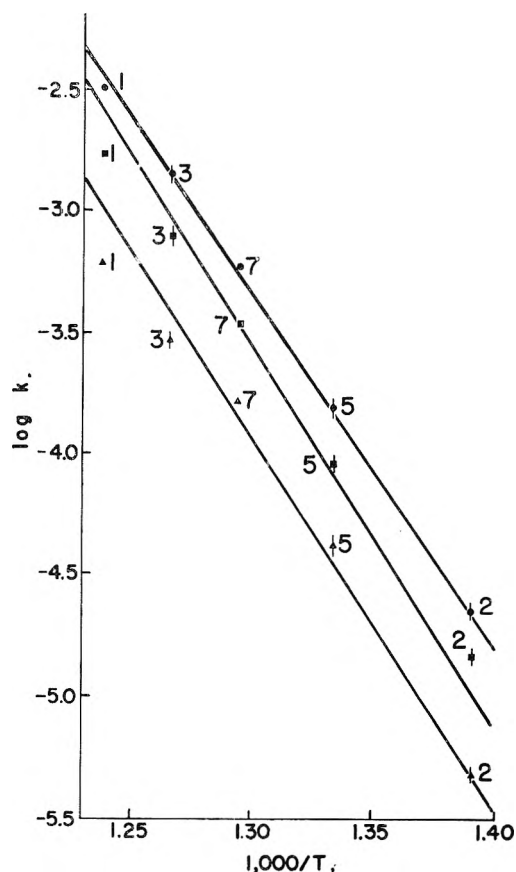
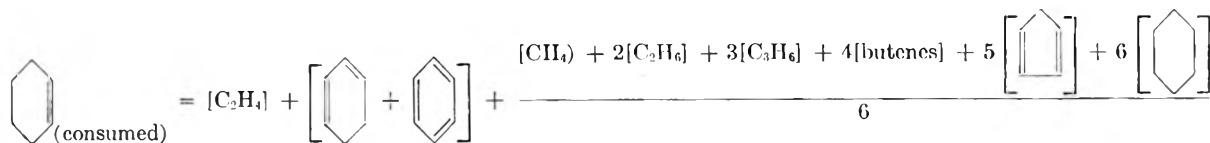


Fig. 1.—Arrhenius plots: ●, over-all rate of decomposition of cyclohexene; ■, rate of formation of ethylene from cyclohexene; ▲, rate of formation of cyclohexadiene from cyclohexene. Numbers indicate the total number of determinations and height of line indicates probable error.


only at 507° of 6.8×10^{-4} , in excellent agreement with our average value of the specific rate constant for the over-all constant of 5.9×10^{-4} at 500°. Our analytical technique involved gas chromatography coupled with mass spectrometry, which has advantages over the analytical techniques used previously. Our data show that even at the lowest percentage decomposition studied (5% or less cyclohexene decomposed), the products of all of the three paths were present, and that the rate constants for each of the paths did not change appreciably with increasing percentage decomposition. The evidence shows clearly that there are three concurrent paths of decomposition, rather than the one path for ethylene and butadiene followed by secondary reactions as the previous workers suggest. Rowley and Steiner⁷ have studied the reverse homogeneous reaction of ethene and butadiene to form cyclohexene. This reaction cannot be of importance in our system; as noted above the specific rate constant for cyclohexene decomposition does not show any trend with increasing percentage decomposition of the cyclohexene.

Determination of the Kinetic Constants of the Two Intramolecular Paths.—The cyclohexene consumed was determined from the amounts of products in the gas chromatography analysis.



(7) D. Rowley and H. Steiner, *Disc. Faraday Soc.*, **10**, 198 (1951).



The amount of cyclohexene originally placed in the pyrolysis flask was determined from the pressure, temperature and volume of the pyrolysis flask. Since the volume of the flasks was not quite constant, the volume of each vessel was determined after its contents had been analyzed. The first-order decomposition constants are shown in Table IV. As may be noted, experiments with different


initial pressures of  show the reaction to be

first order. The effect of added surface is very small. Experiments run for different times of reaction showed that the products had no profound effects on the rate constant. The Arrhenius plot of the rate constants for the rate of disappearance of cyclohexene is shown in Fig. 1. The probable error and the number of observations are also indicated. The slope and intercept are calculated from the least squares fit of the data, and give $k_0 = 7.7 \times 10^{15} \exp(-67600/RT \text{ sec.}^{-1})$. The calculation of the rate constants for the two unimolecular intramolecular reaction paths were calculated from the rate of appearance of ethylene and the sum of

 and . The path producing ethylene, for example, can be formulated.

$$\frac{d(\text{C}_2\text{H}_4)}{dt} = k_1 \left(\begin{array}{c} \text{Cyclohexene} \\ \text{Cyclohexadiene} \end{array} \right) \quad (18)$$

The relation between the amount of cyclohexene present at time t and the original amount of cyclohexene

₀ is given by equation 19

$$\left(\begin{array}{c} \text{Cyclohexene} \\ \text{Cyclohexadiene} \end{array} \right) = \left(\begin{array}{c} \text{Cyclohexene} \\ \text{Cyclohexadiene} \end{array} \right)_0 \exp(-k_0 t) \quad (19)$$

Substituting equation 19 in equation 18 and integrating

$$k_1 = \frac{k_0(\text{C}_2\text{H}_4)}{(1 - \exp(-k_0 t)) \left(\begin{array}{c} \text{Cyclohexene} \\ \text{Cyclohexadiene} \end{array} \right)_0} \quad (20)$$

k_1 may be calculated readily from equation 20 since all the quantities on the right-hand side are determined. The first-order constants for formation of ethylene and of cyclohexadiene are shown in Table IV, and the Arrhenius plots of the rate constants in Fig. 1. The specific first-order rate constants calculated from the least squares best fit of the data are $k_1 = 1.4 \times 10^{17} \exp(-72700/RT) \text{ sec.}^{-1}$, and $k_2 = 1.9 \times 10^{16} \exp(-71200/RT) \text{ sec.}^{-1}$.

Acknowledgments.—We wish to thank Mrs. Helen R. Young and Mr. Joseph H. Johnson for the mass spectrometer analyses and computations.

NUCLEAR MAGNETIC RESONANCE STUDY OF SOME LIQUID-CONTAINING POLY-(HEXAMETHYLENE ADIPAMIDES)

BY R. P. GUPTA¹

Department of Physics, The Pennsylvania State University, University Park, Pa.

Received December 1, 1960

Nuclear magnetic resonance study of poly-(hexamethylene adipamide) containing ethylene glycol, ethyl alcohol, methyl alcohol and acetic acid, has been done with the object to observe the effect of liquid contents on the molecular motion in the polymer. Two main transitions have been observed for the soaked samples: one about at 160°K. and the other at about 270°K. For dry specimen the main transition appears at about 350°K. A shift in the transition temperature, for the soaked sample, has been observed which varies with the samples. The second moment for the dry specimen is lower than the second moment for the soaked samples, below the first transition temperature. The transition at about 260°K. may be attributed to the segmental motion of methylene groups and adjacent non-bonded amide groups. This is due to glass transition for the soaked samples but not for the dry specimen of Nylon 66. Transition at 260°K. may be due to segmental motion of a small number of CH₂ groups in between amide groups, in the amorphous regions. Acetic acid is comparatively more active for this disruption in Nylon than ethylene glycol; it therefore causes a greater shift in transition temperature.

Introduction

Experiments on polyhexamethylene adipamide containing ethylene glycol, ethyl alcohol, methyl alcohol and acetic acid have been done to observe the effect of liquid contents on the molecular motion in the polymer. The results obtained by n.m.r.

experiments have been verified by experiments on dynamic mechanical properties of the same samples, so that the results may be more conclusive.

Experiments on nuclear magnetic resonance with nylon samples have been done by several other workers.²⁻⁴ In the present work a more detailed

(1) Max Planck Institute for Physikalisches Chemie, Goettingen.

(2) R. E. Glick, R. P. Gupta, J. A. Sauer and A. E. Woodward, *J. Polymer Sci.*, **42**, 273 (1960).

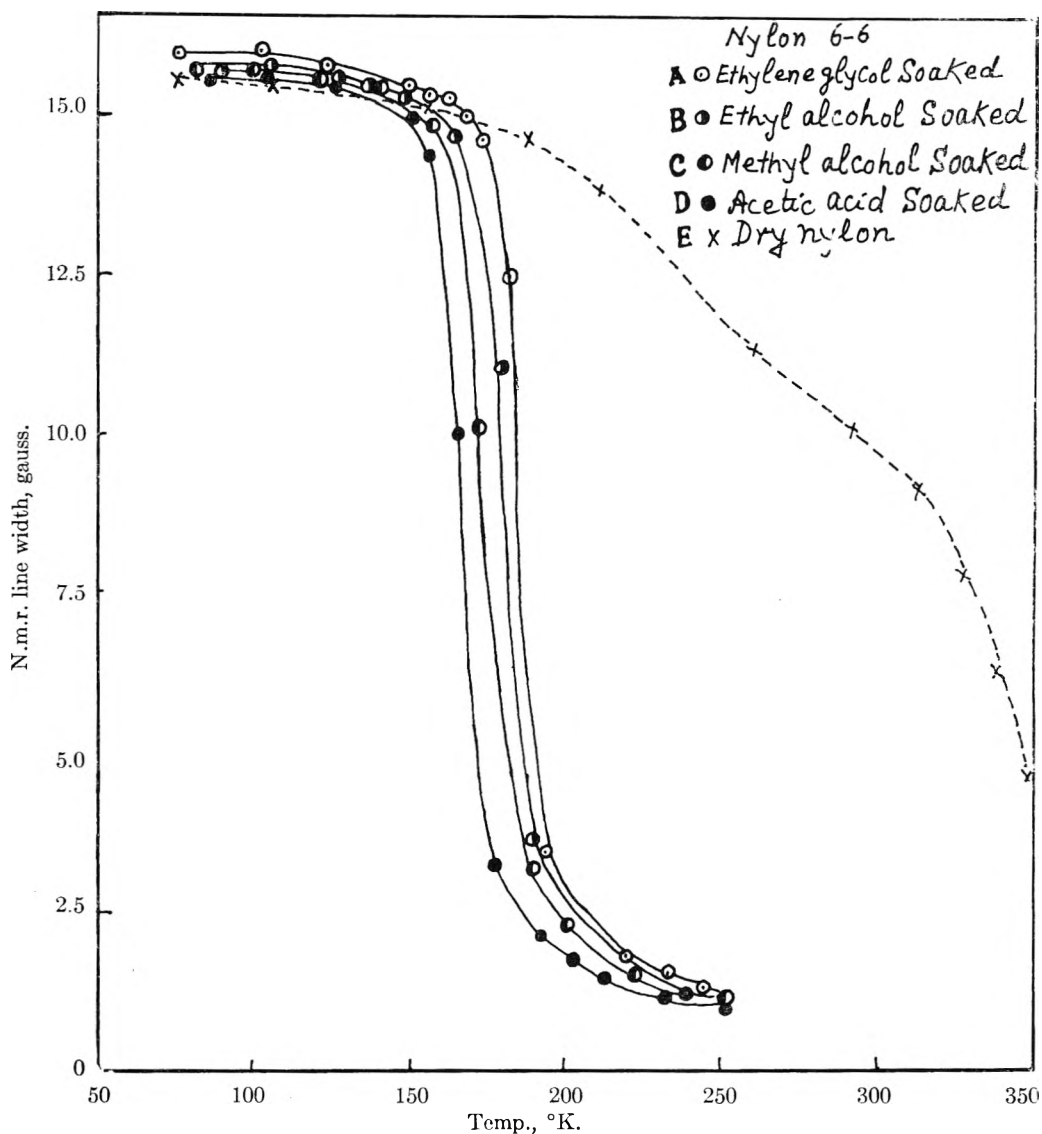


Fig. 1.—Nylon 66 soaked in some organic liquids.

study has been made of the influence of liquid contents on molecular motion in nylon. Some workers⁵⁻⁸ have studied the dynamic mechanical properties of nylons, and with particular interest Woodward⁵ has studied the nylon samples containing water or methyl alcohol. The present work on dynamic mechanical observations with nylon specimens containing several other liquids is an extension of the work done by Woodward. It is stressed that it has proven easier to detect the molecular motions in some cases by the dynamic mechanical method because of the suitability of the frequency range. Comparing dynamic mechanical results with those of n.m.r., one is expected to get a more nearly correct picture of the process re-

sponsible for different transitions connected with various kinds of molecular motions.

Experimental

N.m.r. experiment has been done with a dual purpose Varian model 40 mc. spectrometer, with a 12" electromagnet and a variable temperature probe. To avoid any modulation broadening of the line width the modulation field was monitored from time to time so that the modulation field could be maintained lower than the natural line width of the sample at that temperature. Correction for the increase in second moment due to the modulation field has been done by the method of Andrew.⁹ Line widths and second moments have been determined from the derivative line shape as usual.

To confirm the results and conclusions achieved by n.m.r. experiment, a side by side study of the dynamic mechanical properties of these samples was done. Dynamic mechanical observations were taken on the transverse beam apparatus of Kline,¹⁰ which has been mentioned elsewhere. The sample in the form of a rod was suspended by threads inside a dewar which was covered with a brass plate. Lead balls were kept inside the dewar to maintain a low temperature gradient. It was necessary to keep the temperature of the sample, along its whole length, the same. The flow of

- (3) W. P. Slichter, *J. Appl. Phys.*, **26**, 1099 (1955).
- (4) A. E. Woodward, J. A. Sauer, R. E. Glick and R. P. Gupta, *J. Polymer Sci.*, **45**, 367 (1960).
- (5) A. E. Woodward, J. M. Crissman and J. A. Sauer, *ibid.*, **44**, 23 (1960).
- (6) H. W. Starkweather, Jr., *J. Appl. Polymer Sci.*, **2**, 129 (1959).
- (7) K. Schmieder and K. Wolf, *Kolloid-Z.*, **134**, 149 (1953).
- (8) A. E. Woodward, J. A. Sauer, C. W. Deeley and D. E. Kline, *J. Colloid Sci.*, **12**, 363 (1957).

- (9) E. R. Andrew, *Phys. Rev.*, **91**, 425 (1953).
- (10) D. E. Kline, *J. Polymer Sci.*, **22**, 449 (1956).

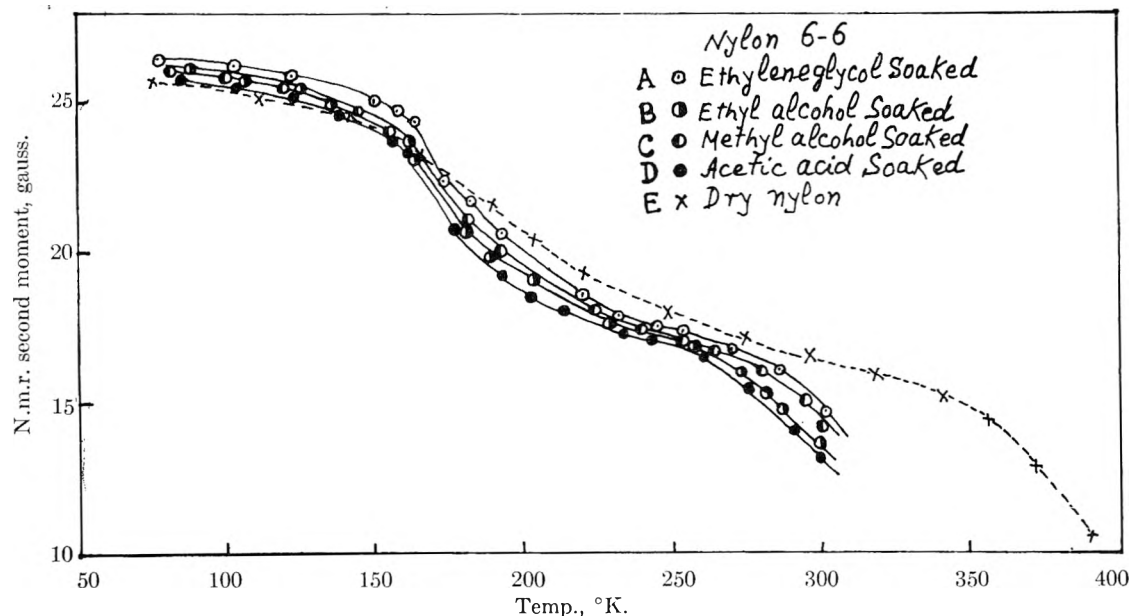


Fig. 2.—Nylon 66 soaked in some organic liquids.

current inside a hot plate, in the dewar, could be monitored to attain a desired temperature. The low temperature runs were made by allowing the temperature to drift up from liquid nitrogen temperature. For high temperature runs as mentioned above current was passed through the plate which heated the lead balls. The radiation of heat from the balls warmed up the surrounding air and, thereby, the sample temperature was raised up.

The sample of Nylon 66 for this experiment was obtained from the Polychemicals Department, du Pont Company. Several pieces of nylon were cut and dried *in vacuo* for several days, until the weight reduced to a constant value. Then they were put in ethylene glycol, ethyl alcohol, methyl alcohol and acetic acid, one piece in each liquid. The nylon sample was allowed to soak in this liquid for about 15 days, at a suitable temperature depending on the chemical activity of that liquid on nylon.

The various samples for this experiment have been: 7.5% ethylene glycol-soaked nylon 66, 8.3% ethyl alcohol-soaked nylon 66, 8% methyl alcohol-soaked nylon 66, 8.1% acetic acid-soaked nylon 66 and dry nylon 66. The weight of the sample has been determined always at room temperature, for which the sample was cooled to room temperature and then the weight was taken. The compositions mentioned above are quoted in weight per cent.

Results and Discussion

In Fig. 1, peak to peak width for n.m.r. narrow line has been plotted against temperature. It is found that the transitions for the soaked specimens appear between 160 and 180°K. There is another transition between 250 and 280°K., which is clear in the second moment plot but it does not appear in the line width plot. The reason for this is that the line width plot is peak to peak for narrow line and at the first transition itself the line becomes extremely narrow. The second transition, which is attributed to motion in crystalline region and does not vary the width for the narrow line, would probably affect the width for a broad line, and a drop in broad line width would occur at that transition temperature. Observations have been taken only up to about room temperature, because heating of the sample would vary the liquid content and the result will not be in the same condition throughout. This could lead to an inconclusive result. The liquids soaked in the polymer will solidify when

cooled, and the line shape attributed to these liquids or solids, as the case may be, may affect the total line-shape. But the contribution to the second moment due to these soaked liquids is little and can be neglected, moreover, this could not cause a shift in the transition temperature. The transition in line width narrowing could be affected due to melting of the liquids, but in our case the transition temperatures do not lie in the region of the melting temperatures of the liquids and therefore we can neglect this effect and conclude that the narrow line transition, observed here, is not due to melting of the liquids in the polymer but to other processes as mentioned later. In Fig. 2a second moment has been shown against temperature. The transition is in the same range as in the case of line width plot, but there is another transition which appears in this plot but not in line width plot as mentioned above. For the dry sample of nylon 66 the main transition appears between 300 and 350°K. In general two transitions have been observed for these samples. The first transition may be attributed due to segmental motion of a small number of CH₂ groups in between amide groups in the amorphous regions. The second transition is presumably on account of segmental motion involving cooperation of methylene groups and adjacent bonded amide groups. The presence of this transition could be due to glass transition, but it is not for dry specimen. The corresponding transition in dry material appears at a higher temperature.

Another feature of these observations is that the value of second moment for the soaked specimen is somewhat higher than the second moment value for the dry specimen, below the first transition temperature. This is because the density of protons is higher for the soaked specimens than for the dry sample. This process has been discussed in detail by Starkweather and Woodward.

It is further observed that there is some shift in

the transition temperature, toward lower temperatures in the order as mentioned here: for ethyl alcohol the transition has shifted for only about 5° toward lower temperature side, with respect to ethylene glycol and for methyl alcohol it has shifted further by about 10° . A further shift of about 10°K . is observed for acetic acid soaked specimen. The content of the liquids in nylon 66 varies a little bit but this may not be the only reason to cause this shift in transition temperature amongst themselves. The shift in transition temperature is due to two reasons: one is that the per cent. content of the liquids varies from sample to sample, though this variation is not much. The other reason is that acetic acid is more chemically active compared with ethylene glycol or ethyl alcohol on a nylon sample; therefore it causes a greater lowering of the transition temperature.

Dynamic mechanical observations show a similar shift in transition temperature for the soaked samples as shown in Fig. 3-5 (the plots for damping *versus* temperature for ethylene glycol soaked sample, ethyl alcohol soaked sample and acetic acid soaked sample). The frequency used for the above measurements has been varied in a range of 2500 to 500 c.p.s. between liquid nitrogen and room temperatures, for these samples. Dynamic mechanical results tally, reasonably, with n.m.r. results. In case of ethyl alcohol soaked sample we get a peak at about 280°K . which is probably due to motion in crystallites and corresponds to the second peak in n.m.r. The corresponding peak for dry material appears at 365°K . For methyl alcohol soaked sample only one peak has been reported by Woodward. Acetic acid soaked nylon sample shows three peaks. The first and second peaks correspond to the peaks detected by n.m.r. The third peak may be due to incomplete saturation of nylon with acetic acid. This could cause the motion in crystallites in two phases and at two different temperatures. The peaks detected by the dynamic mechanical method in the case of the dry sample correspond to n.m.r. peaks. There has been a good agreement between dynamic mechanical and n.m.r. results, but there are some differences which arise mainly because the frequencies used in the two methods are quite different.

To explain the process one may say that the liquids affect the amorphous regions principally, in a partially crystalline polymer and lower the amorphous region transition due to disruption of interchain bonding forces and lead to greater chain rigidity below this transition temperature. The liquid molecules may move between amide and methylene groups and break the hydrogen bonds in the amorphous regions. This tends to keep the hydrocarbon portion of adjacent chains separated and leads to a better packing of these portions. This may be the reason for the higher second moment for soaked specimens than for dry ones, before the first transition temperature. The transition at about 260°K . could be attributed to the segmental motion of methylene groups and adjacent non-bonded amide groups. This is due to glass transition but not for the dry material. For dry material the same transition appears at

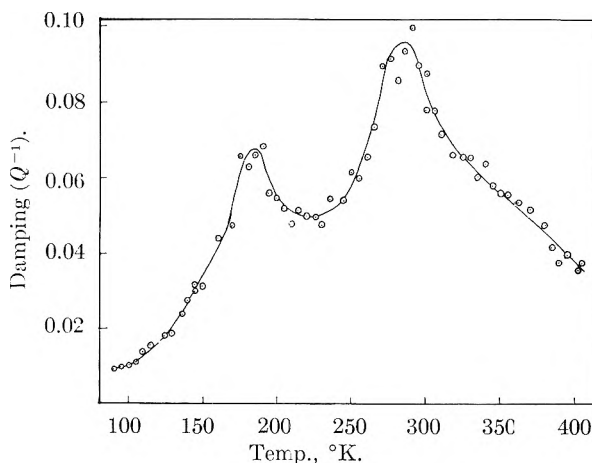


Fig. 3.—Nylon 66 containing ethylene glycol.

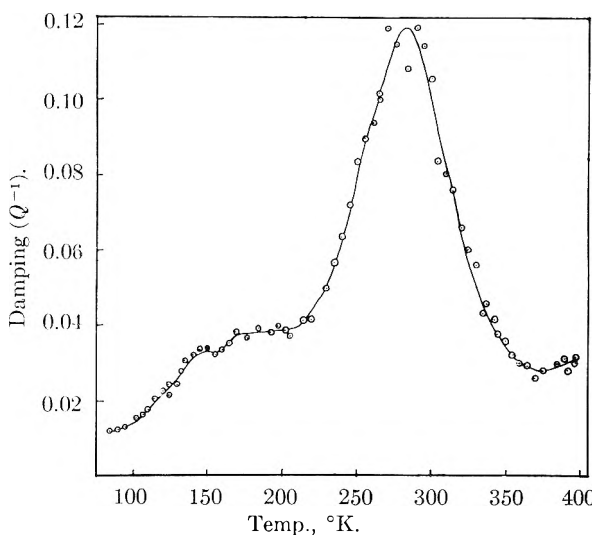


Fig. 4.—Nylon 66 containing ethyl alcohol.

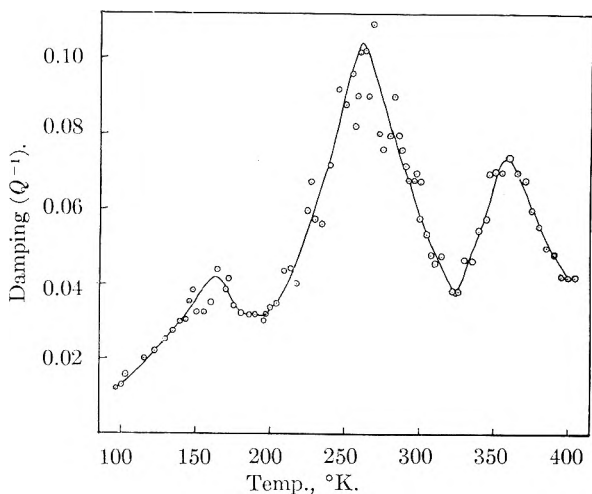


Fig. 5.—Nylon 66 containing acetic acid.

about 350°K . Transition at about 170°K . is due to segmental motion of a small number of CH_2 groups in between amide groups, in the amorphous region. Addition of liquid acts to decrease this CH_2 group motion. It could be due to interference of liquid molecules with moving hydrocarbon segments.

Acetic acid being more active for this disruption in nylon, compared with ethylene glycol, therefore, it causes a greater shift in the transition temperature.

Acknowledgment.—I am very much thankful to Dr. Woodward for suggesting this problem and

taking interest in it. I am grateful, also, to Dr. Sauer for arranging a financial grant from the Atomic Energy Commission to support this work. My thanks are due to Miss K. Fielenbach for her encouragement during the course of this work.

PHOSPHINE OXIDE-HALOGEN COMPLEXES: EFFECT ON P-O AND P-S STRETCHING FREQUENCIES¹

BY RALPH A. ZINGARO AND RICHARD M. HEDGES

Department of Chemistry of the Agricultural and Mechanical College of Texas, College Station, Texas

Received December 12, 1960

The P-O or P-S stretching frequency of a free phosphine oxide or sulfide molecule shifts to a lower frequency on halogen complexing. This shift indicates that such interaction occurs through the oxygen atom. The factors which affect the P-O band are discussed and an empirical correlation relating the steric and polar substituent constants to the location of this band is presented.

Introduction

As part of an over-all study involving molecular complex formation between phosphine oxides, sulfides or selenides and halogens or interhalogens, we have examined the effect of such interaction upon the P-O and P-S stretching frequencies. In these donor molecules, interaction must occur through the oxygen, sulfur or selenium atom, although the possibility of interaction involving aromatic substituents must also be considered in the arylsubstituted compounds. Reported and discussed are the results observed for a series of seven phosphine oxides and four phosphine sulfides. The P-Se stretching frequency is beyond the range of rock salt and the effect of halogen complexing on this vibration is not presently reported. Plans are being made for such investigation.

Although molecular complex formation involving the halogens has been the subject of considerable study during the past decade, to the best of our knowledge, these represent the initial observations involving phosphine oxides as donor molecules. Tsubomura and Kliegman² have carried out an ultraviolet study of the iodine-tri-*n*-butyl phosphate system and have speculated on the donor properties of the P-O groups as compared with the R-O groups in alkyl phosphates. The absence of R-O groups in the phosphine oxides eliminates this difficulty. Sheldon and Tyree³ and Cotton and co-workers⁴ have investigated the effects of metal ion coordination on the P-O stretching frequencies of the trimethyl- and triphenyl- derivatives in the solid state.

Experimental

Phosphine Oxides and Sulfides.—Tri-*n*-octylphosphine oxide (TOPO) of high purity was used and its purification is described elsewhere.⁵ A sample of tri-2-ethylhexylphos-

phine oxide was furnished by the Oak Ridge National Laboratory. Its purification paralleled that for TOPO. The material used had a refractive index of 1.4643 at 20°. All of the other phosphine oxides and phosphine sulfides were prepared in this Laboratory. Every sample was recrystallized to a constant melting point and checked by analysis. The preparative techniques employed and the physical constants of the compounds used are described elsewhere.⁶

Halogens and Interhalogens.—The preparation and/or purification of all of the halogens and halogenoids is described elsewhere.⁷ Solutions of these compounds were prepared by dissolving weighed amounts in appropriate volumes of solvent. The solvents were of spectral grade and were dried and redistilled before use.

Attempts to prepare fairly concentrated (~1 *M*) solutions of either iodine monochloride or iodine monobromide in carbon disulfide led to unexpected results. The solution warmed rapidly and after a few seconds reacted most vigorously, in fact, almost violently, the contents of the flask being very widely scattered. The formation of either sulfuranyl chloride or sulfuranyl bromide, as reaction products, was noted. Inasmuch as iodine monochloride is described in standard reference books as being soluble in carbon disulfide,⁸ it appears that this is true only within certain limits of concentration. Due to the force of the reaction and the toxicity of the reaction products, this observation seemed worthy of note. Consequently it was necessary to prepare solutions of these interhalogens in carbon tetrachloride. While this was undesirable, due to infrared absorption of this solvent, it was nevertheless unavoidable.

Measurement of Spectra.—All measurements were made on a Beckman IR-4 instrument. The instrument was calibrated by means of standard polystyrene sample before each run. Single beam scanning of all solutions was carried out, whenever possible, using comparable slit widths for a given series so that relative intensities could be compared.

A number of experimental difficulties were encountered which made observations impossible in some cases or which reduced the value of some observations. The strong absorption of carbon tetrachloride and chloroform at about 1220 cm^{-1} overlaps the P-O band in the case of triphenylphosphine oxide and the intense absorption of these solvents in the 720–800 cm^{-1} region interfered in the case of measurements of the phosphine sulfides since this is the region of the P-S stretching vibration. In a few cases, the phosphine oxide or sulfide was insoluble in carbon disulfide and similar difficulties were presented due to solvent interference. These

(1) Presented at the Southwest Regional Meeting of the American Chemical Society, Oklahoma City, Oklahoma, December 1, 1960.

(2) H. Tsubomura and J. Kliegman, *J. Am. Chem. Soc.*, **82**, 1314 (1960).

(3) J. C. Sheldon and S. Y. Tyree, *ibid.*, **80**, 4775 (1958).

(4) F. A. Cotton, R. D. Barnes and E. Bannister, *J. Chem. Soc.*, 2199 (1960).

(5) R. A. Zingaro and J. C. White, *J. Inorg. Nucl. Chem.*, **12**, 315 (1960).

(6) C. G. Screttas, Master's Thesis, Agricultural and Mechanical College of Texas, 1960, to be published.

(7) R. A. Zingaro and W. B. Witmer, *J. Phys. Chem.*, **64**, 1705 (1960).

(8) *E.g.*, "Handbook of Chemistry and Physics," Chemical Rubber Publishing Co., Cleveland, Ohio, 1957–1958 edition, p. 537, and other standard reference works.

TABLE I
EFFECT OF HALOGEN COMPLEXING ON P-O AND P-S STRETCHING FREQUENCY IN PHOSPHINE OXIDES AND PHOSPHINE SULFIDES

Derivative	Physical state	Unbonded, $\bar{\nu}$ (cm. ⁻¹)		Bonded, $\bar{\nu}$ (cm. ⁻¹)							
		P-O	P-S	I ₂	- $\Delta\bar{\nu}$	IBr	- $\Delta\bar{\nu}$	ICl	- $\Delta\bar{\nu}$	Br ₂	- $\Delta\bar{\nu}$
1. Tri- <i>n</i> -butyl	Soln., CS ₂	1169		1118	51	1108	61	1104	65	1128	41
2. Tri- <i>n</i> -octyl	Soln., CS ₂	1161		1115 ^b	46					1127 ^b	34
	Soln., CCl ₄	1169				1104 ^b	65	1104 ^b	65		
	Solid	1144									
3. Tri-2-ethylhexyl	Soln., CS ₂	1198 } doublet		1153	54						
		1164 }			11						
	Soln., CS ₂ -CCl ₄	Unchanged				1134 ^b	64	1129 ^b	69	^c	
4. Tricyclohexyl	Soln., CS ₂	1143		1095	48						
	Soln., CS ₂ -CCl ₄	Unchanged				1081 ^d	62	1070 ^d	73	1101 ^d	21
5. Dicyclohexylphenyl	Soln., CS ₂	1176		1139	38					1145	34
	Soln., CS ₂ -CCl ₄	Unchanged				1132	45	1130	46		
6. Diphenylcyclohexyl	Soln., CS ₂	1196		1158	38					1164 ^d	32
	Soln., CS ₂ -CCl ₄	Unchanged				1145	51	1142	54		
7. Triphenyl	Soln., CS ₂	1206		1160 ^e	43						
				Satd. I ₂ { 1160 ^e	43						
				Splits { 1216	-10						
	Soln., CCl ₄	(1217?) ^f		1151	43	1147	47	1142	52	1162	32
	Solid	1193 } doublet									
		1188 }									
8. Dicyclohexylphenyl	Soln., CS ₂		755 ^g	751	4	^c		^c		^c	
			695 ^g	686	9						
9. Tricyclohexyl	Soln., CS ₂		719	713	6	^c		^c		^c	
10. Trimethyl	Soln., CHCl ₃ -CCl ₄		713	698	15	692	21	^c		^h	
	Solid		713								
11. Triphenyl	Soln., CS ₂		712	702	10	698	14	697	15	^h	

^a Halogen/phosphine oxide (sulfide) ratio is unity unless otherwise indicated. ^b Broad band; unless indicated there is little change in the shape of the band. ^c Sepn. of insoluble phase with insufficient concn. of soluble complex remaining in solution to permit measurement. ^d Sepn. of insoluble phase, but sufficient concn. remains to permit measurement. ^e Intensity of band diminished. ^f Uncertain due to solvent absorption. ^g Assignment of P-S band indefinite (see Discussion). ^h Rapid chemical reaction.

difficulties could be largely overcome by the use of double beam observations with pure solvent in the reference beam, or by comparison with the spectrum of the same compound in carbon disulfide or in the solid state. However, band shifts are not strictly comparable under varying solvent environment.

In the case of bromine, rapid chemical reaction took place in some cases, especially with the phosphine sulfides, thus obviating any measurements. Crystalline products which were formed have been isolated and are being studied. The addition of iodine monochloride or iodine monobromide, at relatively high concentrations (*ca.* 1:1 phosphine oxide-halogen molar ratio) sometimes resulted in the separation of a dense, immiscible layer. When this happened, only the more dilute solutions, or the homogeneous less dense bulk liquid phase could be studied.

Thus, it was not possible, in all cases, to make significant comparisons of intensity changes. A clearly defined qualitative study of the band shift was, however, made in all cases.

Results

Although the P-O stretching vibration has been studied in a large number of organophosphorous compounds, the vast majority have been esters in which the organic substituent is linked to the phosphorus *via* an oxygen atom. Gore,⁹ applying Gordy's rule, calculated frequencies in the range of 1100-1300 cm.⁻¹ and 550-750 cm.⁻¹, respectively, as the regions for the location of the P-O and P-S stretching frequencies. Daasch and Smith¹⁰ reported values of 1190 and 1176 cm.⁻¹ for the P-O frequency in triphenyl- and trimethylphosphine oxides, respectively.

(9) R. C. Gore, *Disc. Faraday Soc.*, **9**, 138 (1950).

(10) L. W. Daasch and D. C. Smith, *Anal. Chem.*, **23**, 853 (1951).

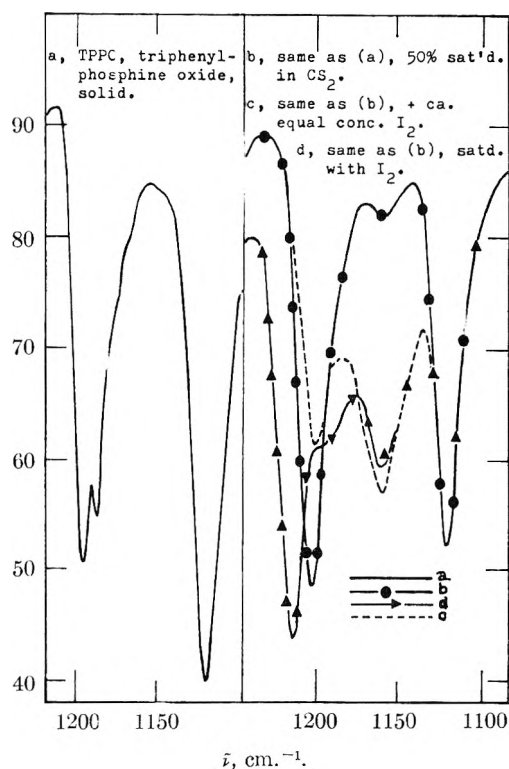


Fig. 1.—P-O stretching frequency of triphenylphosphine oxide: a, TPPO, triphenylphosphine oxide, solid; b, same as (a), 50% satd. in CS₂; c, same as (b), + *ca.* equal concn. I₂; d, same as (b), satd. with I₂.

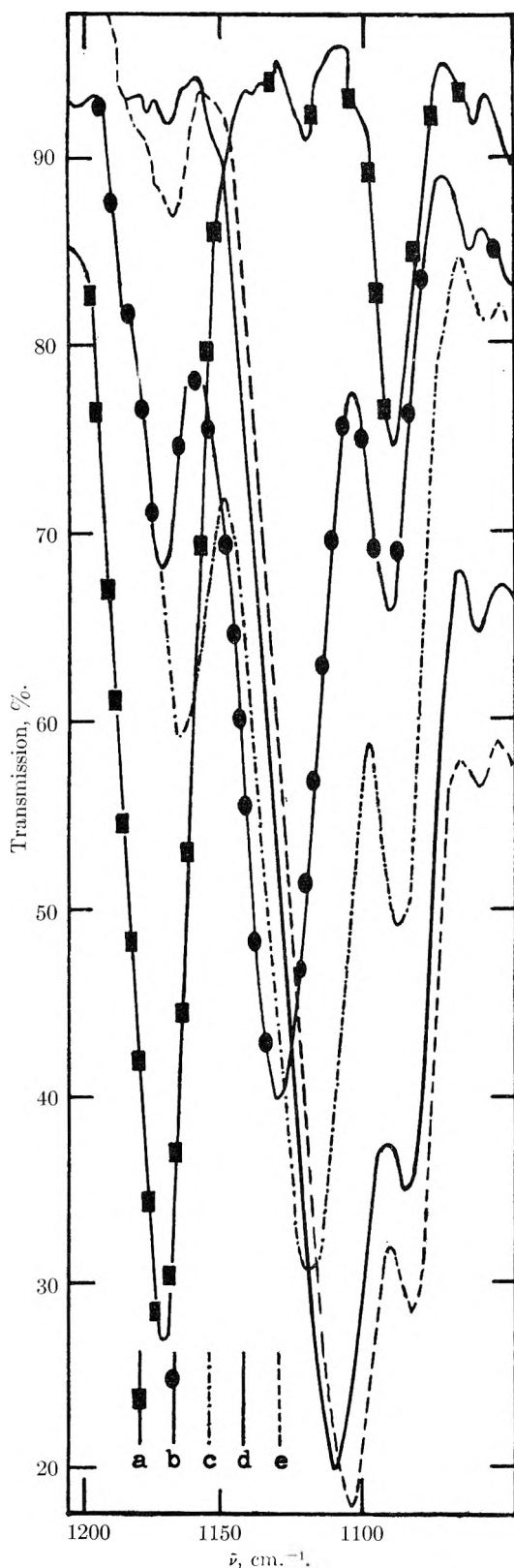


Fig. 2.—a, Tri-*n*-butylphosphine oxide in CS_2 , 0.29 *M*; + equal concentration of: b, Br_2 ; c, I_2 ; d, IBr ; e, ICl .

In Table I are reported the observed P-O and P-S frequencies for the seven phosphine oxides and four phosphine sulfides which were the subject of this investigation. The P-O vibration is located

in the region from 1140–1200 cm^{-1} . There is a change in the location of this band in different solvents and in different physical states, *e.g.*, compounds 2 and 7. The band is clearly resolved into a doublet in the case of the triphenyl- compound, Fig. 1, and is a well defined doublet also in the case of the tris-(2-ethylhexyl) derivative. In all cases the band is strong and easily characterized.

The addition of a halogen, or interhalogen, brings about a shift in the P-O band to a frequency up to 73 cm^{-1} lower than that observed for the free molecule. Invariably (Table I) the change in the P-O frequency is directly related to the polarity of the acceptor molecule being greatest for ICl and following the sequence $\text{ICl} > \text{IBr} > \text{I}_2 > \text{Br}_2$. The interaction with iodine always brings about a greater shift than does that with bromine. In Fig. 2 this trend, observed for all of the compounds investigated, is clearly demonstrated. The removal of iodine by contacting the solution with aqueous thiosulfate resulted in restoration of the original band.

In the case of triphenylphosphine oxide, at high iodine concentrations (Fig. 1 and Table I), the original P-O band is split into two new bands, one corresponding to the shifted band characteristic of the halogen solution and a new, very strong band at a frequency *higher* than that observed for the free molecule. Triphenylphosphine oxide in carbon disulfide is characterized by a P-O band at 1206 cm^{-1} . Upon the addition of an approximately equal concentration of iodine this band is diminished in intensity and a bonded P-O band appears at 1160 cm^{-1} . When this solution is saturated with iodine, in addition to the shifted P-O band there is observed the concurrent appearance of a strong new band at 1216 cm^{-1} . This behavior was observed only for the triphenyl- compound.

In many cases, the addition of Br_2 , IBr , or ICl in equimolecular concentrations brought about the separation of an insoluble liquid phase. The values reported are based on measurements made on the bulk supernatant solution. When this solution was contacted with thiosulfate the original P-O band reappeared, but it was diminished in intensity, indicating that some of the original compound had separated out into the immiscible heavy phase.¹¹

The phosphine sulfide studies were not as informative because of a number of complicating factors. Bromine reacted rapidly and irreversibly with all of the phosphine sulfides investigated. Also, the P-S frequency is weaker and much more poorly characterized than the P-O frequency and it is more difficult to assign because of the presence of other strong bands in this region.

The shift in the P-S band toward lower frequencies upon the addition of iodine is noted in all cases, but it is proportionally not as large as that observed for the P-O band. In the case of triphenylphosphine sulfide the shift for the entire sequence I_2 to IBr to ICl is observed and this follows the same order as is that noted for the oxides.

(11) Some of these oils have been crystallizing and these solids are currently being studied.

Discussion

Bellamy¹² has discussed the frequent occurrence of the P-O band as a doublet and suggested that this doublet character is associated with the P-O vibration itself. The P-O band is clearly resolved as a doublet (Fig. 1) in the case of triphenylphosphine oxide (TPPO) when this compound is examined as a solid and a similar observation is made in the case of the tris-(2-ethylhexyl) compound. The doublet nature of the P-O stretch in TPPO has not been noted in some previous observations,^{4,13} but it has been pointed out by Sheldon and Tyree.³ This doublet character has importance in this work especially in view of the large splitting of this band noted at high iodine:TPPO concentrations. The occurrence of the P-O doublet for at least two of the phosphine oxides clearly indicates that the splitting is associated with the P-O vibration itself and points out the importance of searching out this splitting, especially in the examination of crystalline solids. While this investigation by no means settles the question of the origin of this doublet, a reasonable explanation for the splitting to a higher and lower frequency at high iodine concentration will be given.

The general assignments for the P-C and P-S stretching vibrations in Table I are based upon the following considerations: (1) actual location of the band; (2) comparison with previous observations, *e.g.*, TPPO; (3) the presence or absence of the band in pairs of compounds which would otherwise be identical except for the sulfur or oxygen atom, *e.g.*, TPPO; (4) the reversible shift in the location of the band on the addition of iodine. The last criterion was restricted to iodine interaction since no difficulties were experienced with respect to chemical reactions.

The suggested assignments for the P-O and P-S frequencies, based on the criteria discussed are considered to be quite reliable. There is some question about assignment of the P-S stretching frequency for dicyclohexylphenylphosphine sulfide. In this case (Fig. 3) there occurs a shift in the 755 cm^{-1} band upon the addition of iodine, but the phosphine oxide also absorbs strongly in this region. In the 695-700 cm^{-1} also, both molecules absorb strongly. The sulfide possesses an obvious shoulder superimposed upon the latter band, which may be obscured in the case of the oxides. Addition of iodine brings about an increase in the intensity of the shorter wave length absorption and a much more profound change in the 755 cm^{-1} band. There seems to be no clear-cut evidence for making a definite assignment of the P-S band in this molecule on the basis of these experiments, but the 695 cm^{-1} location is more likely.

A straightforward treatment of the data, using published values¹⁴ for Taft's σ^* and E_s values for

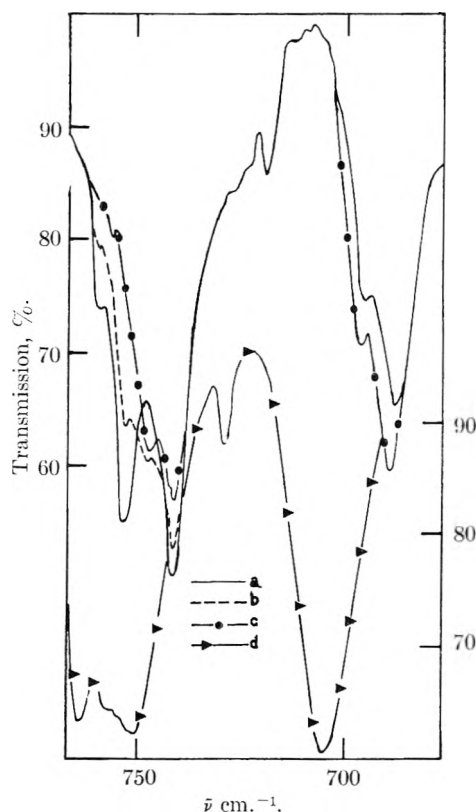


Fig. 3.—a, Dicyclohexylphenylphosphine sulfide, half satd. in CS_2 ; b, $+0.1 M I_2$; c, satd. with I_2 ; d, dicyclohexylphenylphosphine oxide, half satd. The left-hand ordinate corresponds to the transmission of the sulfide and the right to that of the oxide.

the various phosphorus substituents show that the location of the P-O vibration for 10 phosphine oxides in carbon disulfide solution is expressed with a correlation coefficient of 0.993 by the empirical relationship

$$\bar{\nu}_{\text{P-O}} = 1172 + 13.86 \Sigma \sigma^* + 4.11 \Sigma E_s \quad (1)$$

Bell and co-workers¹⁵ developed a linear correlation between the phosphoryl absorption and phosphorus atom substituents which has the form

$$\lambda(\mu)_{\text{P-O}} = \frac{39.96 - \Sigma X}{3.995} \quad (2)$$

The term X is called the "phosphoryl absorption shift constant" and it is directly related to the electronegativity of the substituent group. We have calculated the frequencies for the phosphine oxides which were the subject of this study using equations 1 and 2. In the latter case, Bell's "phosphoryl absorption shift constants" were used,

hexyl; f, dicyclohexylphenyl; g, tricyclohexyl; h, trimethyl; i, tributyl; j, tri-*n*-octyl. The first three values were taken from ref. 10. The E_s values were taken from Table VI of ref. 14 and are for the R group based on the hydrolysis of aliphatic RCOOR' compounds. The polar substituent constants, σ^* , were taken from Table XII of the same source, with the exception of the Cl value which was selected from Table XIb of ref. 14. An E_s value for Cl of 0 was assumed, based on its size relative to that of a methyl group, since tabulated values were not found except for aromatic compounds. The equation 1 was obtained by a least squares treatment of the data. It was found that the use of the single parameter, $\Sigma \sigma^*$ or ΣE_s , or the addition of a third parameter, $\Sigma \sigma^* E_s$ gave equations which demonstrated decidedly poorer correlations.

(15) J. V. Bell, J. Heisler, H. Tannenbaum and J. Goldenson, *J. Am. Chem. Soc.*, **76**, 5185 (1954).

(12) L. J. Bellamy, "The Infrared Spectra of Complex Molecules," John Wiley and Sons, Inc., New York, N. Y., p. 314.

(13) M. Halmann and S. Pinchas, *J. Chem. Soc.*, 3264 (1958).

(14) "Steric Effects in Organic Chemistry," edited by M. S. Newman, John Wiley and Sons, Inc., New York, N. Y., 1956. Equation 1 was based on the following ten phosphine oxides: a, trichloro; b, dichlorophenyl; c, diphenylchloro; d, triphenyl; e, diphenylcyclo-

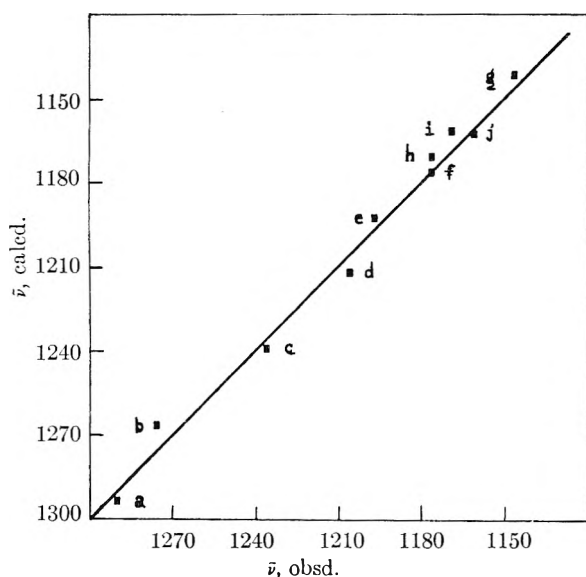
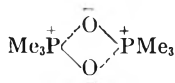


Fig. 4.—Correlation of P—O stretching frequencies calculated by use of eq. 1 with experimentally observed values. The letters correspond to the compounds listed in footnote 14.

but these were available for only four of the compounds. Comparison, on a wave number scale, shows that the average deviation using equation 1 is ± 5 cm^{-1} , with a maximum deviation of 9 cm^{-1} in one case. Equation 2 gives an average deviation of $+50$ cm^{-1} , with absolute deviations of 59 and 96 cm^{-1} in two out of the total of four compounds. In Fig. 4 is shown the correlation between the observed values and those calculated by the use of equation 1. The relatively poor agreement obtained using Bell's constants is not surprising since they are derived from trihalide derivatives for which electronegativity effects appear to be the uniquely determining factors. In the case of the organic substituents, there is a smaller change in the relative electronegativities and it is apparent that the inclusion of a second parameter which allows for steric factors, greatly improves the correlation. This type of correlation will be extended to cover a much larger number of phosphine oxides as soon as more data is compiled.

The existence of stable, modified tetrahedral forms has been suggested¹⁵ as a possible cause of the doublet phosphoryl absorption in the case of triaromatic esters. Recently, Goubeau and Berger¹⁶ have demonstrated the existence of intermolecular association between gaseous trimethylphosphine oxide molecules and have explained the multiplicity of the P—O frequency on the basis of equilibrium among these various intermolecular species. They observed a doublet for the solid (1160 and 1180 cm^{-1}) and suggested molecular interaction of the type



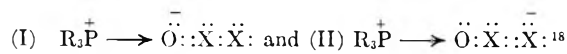
A similar explanation may be offered in the case of solid triphenylphosphine oxide, but due to the

(16) J. Goubeau and W. Berger, *Z. anorg. allgem. Chem.*, **304**, 147 (1960).

electron withdrawing power of the three phenyl groups, structures of the type $\text{X}_3\text{P}=\text{O}$ are probably more important in the triphenyl compound than

would be those of the type $\text{X}_3\text{P}^+ \rightarrow \text{O}^-$. It is suggested, therefore, that intermolecular forces are due to the interaction of the aromatic rings with phosphoryl groups of adjacent molecules rather than as a result of the association of the phosphoryl groups themselves. The donor properties of aromatic systems are well known. The clearly defined doublet observed in the region of the P—O stretch for the tri-(2-ethylhexyl) derivative persists even in solution. That the multiplicity of the P—O bond is due to intermolecular association *via* the P—O groups is quite unlikely due to very large steric effects. Consideration of a Fisher-Taylor-Hirschfelder molecular model shows quite clearly that in order to maintain a stable tetrahedral configuration in this molecule, at least two of the branched ethyl groups will have to be in almost direct contact with the phosphoryl oxygen. Rotation of the 2-ethylhexyl groups in such a manner as to eliminate the P—O interaction results in the mutual interaction of the alkyl groups with each other. This latter effect may give rise to a stable, but distorted tetrahedral geometry, as suggested by Bell, *et al.*¹⁵ The existence of an equilibrium between molecules with a normal tetrahedral configuration (intramolecular P—O bonding) and those with a distorted tetrahedral configuration (unbonded P—O) would give rise to the two P—O frequencies.

The actual shift of the P—O band to lower frequencies on halogen complexing demonstrates that coordination with halogen molecules takes place through the phosphoryl oxygen. The direction of this shift reflects a decrease in P—O bond order. Without making any assumptions concerning the geometry of the phosphine oxide-halogen complexes, and assuming that a 1:1 complex¹⁷ is formed, it is reasonable to assume that the simplest model is represented by a donor-acceptor interaction involving a drift of electrons from the phosphoryl oxygen toward the electronegative halogen. This would result in a net decrease in P—O bond order due to a decrease in oxygen to phosphorus $p\pi_{\text{O}} \rightarrow d\pi_{\text{P}}$ back-bonding. Some of the more important contributing structures are described by the configurations



The degree of $p\pi_{\text{O}} \rightarrow d\pi_{\text{P}}$ back-bonding decreases in the sequence I_2 , IBr , ICl due to the increasing importance of structure (II) with increasing electronegativity of X in the I—X series of interhalogens. This partially explains the observed se-

(17) Based on ultraviolet studies in progress in this Laboratory in connection with equilibria in these solutions. Continuous variation curves show 1:1 complex formation. The results of these studies will be published.

(18) There is no chemical evidence for ionization of the type $(\text{R}_3\text{POX})^+ + \text{X}^-$ as is noted in pyridine-halogen solutions; *cf.* chloroform solutions containing pyridine and a halogen react with silver salts to precipitate silver halide, but no silver halide precipitation was observed under similar conditions when phosphine oxides are substituted for pyridine.

quence in the shift of the P-O band. Although there is noted an increase in band intensity concurrent with the size of the band shift with increasing polarity of the interhalogen, there exists no absolute basis for comparison of intensities since this may be a simple case of equilibrium which results in a higher concentration of the complex and thus a stronger intensity in the shifted band.

The change in the phosphoryl frequency, in every case, is smallest for bromine interaction. The reason for the relatively weak bromine interaction may lie in the weak polarizability of bromine compared with iodine. As a first approximation, using a purely electrostatic approach, the formation of the phosphine oxide-halogen complex involves the interaction of the dipole, $\mu_{\text{P}=\text{O}}$, with the dipole, $\mu_{\text{X}=\text{Y}}$, the latter being induced upon the halogen by the field of the phosphine oxide. The energy of this dipole interaction is proportional to the polarizability of the halogen molecule. Iodine, whose polarizability is considerably greater than that of bromine, thus acquires a much greater induced dipole and the resultant dipole-dipole interaction leads to a lower energy state and a more stable complex. This is an additional factor which must be considered to account for the stronger interaction with the interhalogens.

At high (I₂):(TPPO) ratios, the appearance of a new, intense band at a frequency higher than that observed for unbonded P-O along with the bonded P-O at a lower frequency may be attributed to a secondary equilibrium¹⁹ involving complexing *via* the aromatic substituents. If the aromatic groups act as electron donors toward iodine, there will result additional withdrawal of electrons away from the phosphorus atom. The resultant increase in positive charge on the phosphorus atom enhances $p\pi_{\text{O}} \rightarrow d\pi_{\text{P}}$ back-bonding with increased bond order and an increase in the P-O frequency. Thus, if we consider the equilibrium, K_{a} , involving P-O bonded complexes (decreased P-O frequency) and a secondary equilibrium, K_{b} , involving bonding between the halogen and the phenyl groups (increased P-O frequency); if $K_{\text{a}} \gg K_{\text{b}}$, the secondary equilibrium will become important at high molar ratios.²⁰

There is no question that a given phosphine sulfide forms a more stable complex²¹ than the cor-

responding oxide. The observed shift in the P-S frequency on halogen complexing is smaller, $\Delta\bar{\nu}_{\text{max}} = 21 \text{ cm.}^{-1}$ (Table I), compared with that observed for the phosphine oxide, $\Delta\bar{\nu}_{\text{max}} > 70 \text{ cm.}^{-1}$. This indicates that there is a net decrease in $p\pi_{\text{S}} \rightarrow d\pi_{\text{P}}$ back-bonding, which results in decreased P-S bond order, and a lowering of the frequency. This must be overcome by other effects which operate to bring about an increase in the frequency so that the net decrease is not as large as that observed for the phosphine oxides.

A knowledge of the effect of the coupling of the two oscillators P-O (or P-S) and O-I (or S-I) on the P-O (or P-S) frequencies is highly pertinent to this discussion. By the use of the equation²² for a linear X-Y-Z triatomic molecule which makes use of the frequencies and the force constants of the two free oscillators, X-Y and Y-Z, it is possible to make some calculations on the effect of such coupling. Using a value of $k_{\text{PO}} = 8.73 \text{ md./\AA.}^4$ and $k_{\text{OI}} = 0.5-2.5 \text{ md./\AA.}$ we calculate that such coupling results in an increase in this frequency of from 10-100 cm.^{-1} . Similarly, using a value of $k_{\text{PS}} = 5.24 \text{ md./\AA.}^9$ we calculate that S-I coupling increases the P-S frequency by 5-50 cm.^{-1} for the range $k_{\text{SI}} = 0.5-2.5 \text{ md./\AA.}$ Making use of the experimentally observed values, we calculate $k_{\text{PO}} = 5.83-7.19$ and $6.66-8.03 \text{ md./\AA.}$ at $\bar{\nu}_{\text{PO}} = 1100$ and 1160 cm.^{-1} , respectively, for the halogen bonded P-O frequencies and for the same range of k_{OI} previously used. Likewise, for the halogen bonded P-S frequencies, $k_{\text{PS}} = 5.72-6.83 \text{ md./\AA.}$ at $\bar{\nu}_{\text{PS}} = 700 \text{ cm.}^{-1}$. These calculations demonstrate that k_{PO} is effectively lowered on halogen complexing with a concurrent decrease in P-O bond order. The extremely small P-S shift indicates that there is actually a small increase in k_{PS} on halogen bonding with a negligible change in P-S bond order and that it may, in fact, be slightly increased.

The most reasonable conclusion we can draw from these observations and calculations is that the back donation of $p\pi$ halogen electrons to the $3d\pi$ orbitals of sulfur contributes to a very large degree to the stability of these complexes. Concurrent $p\pi_{\text{X}} \rightarrow d\pi_{\text{S}}$ and $p\pi_{\text{S}} \rightarrow d\pi_{\text{P}}$ back-bonding leads to contributing structures of the type $\text{R}_3\text{P}=\ddot{\text{S}}=\ddot{\text{X}}-\ddot{\text{X}}:$ and $\text{R}_3\text{P}=\overset{-}{\ddot{\text{S}}}-\overset{+}{\ddot{\text{X}}}-\overset{+}{\ddot{\text{X}}}:$. These structures, impossible in phosphine oxides because of the non-availability of $3d$ orbitals in oxygen are most reasonable in view of the equal electronegativity of sulfur and iodine. Such structures increase the P-S bond order and, as the calculations indicate, more than compensate for the decrease in the P-S bond order which would otherwise result from halogen complexing. This also furnishes a partial explanation of the greater stability of the phosphine sulfide complexes.

(21) Ultraviolet studies¹⁷ show that the formation constants for a pair of corresponding molecules is about 10^2 greater for the sulfide than for the oxide.

(22) G. Herzberg, "Infrared and Raman Spectra," D. Van Nostrand Co., Inc., New York, N. Y., 1945, p. 173.

(19) This is corroborated by ultraviolet studies.^{11,17} The usual "blue shift" is noted with the uncomplexed iodine band at $510 \text{ m}\mu$ shifted to $363 \text{ m}\mu$. As the TPPO:(I₂) ratio is increased, the $363 \text{ m}\mu$ also disappears and the solution eventually shows an ultraviolet cut-off at $285 \text{ m}\mu$ and no remaining visible or ultraviolet peaks.

(20) One of the reviewers wondered about the occurrence of a similar effect in the dicyclohexylphenyl and cyclohexyldiphenyl compounds. The present studies indicate only that a secondary equilibrium involving bonding *via* the phenyl groups is not observed for these compounds in the range of concentrations studied. This by no means implies that such interaction does not, or may not occur. It does suggest that the presence of one, or two, cyclohexyl groups on the phosphorus atom neutralizes the electron withdrawing effect of the phenyl groups to such a degree that the donor capabilities of the phosphoryl group are not greatly impaired. This suggests that $K_{\text{a}}/K_{\text{b}}$ (*vide supra*) is much larger for the cyclohexyl containing compounds than for the triphenyl derivative. The existence of a secondary equilibrium may, indeed, take place with the other compounds, but such an equilibrium would have to be observed at much higher halogen/donor molar ratios than those used in this study.

Acknowledgment.—We should like to express our appreciation to the United States Atomic Energy Commission for financial support under Contract AT-(40-1)-2733.

THE DETERMINATION OF DENSITY DISTRIBUTIONS AND DENSITY GRADIENTS IN BINARY SOLUTIONS AT EQUILIBRIUM IN THE ULTRACENTRIFUGE¹

BY JAMES B. IFFT,² DONALD H. VOET³ AND JEROME VINOGRAD

Gates and Crellin Laboratories of Chemistry,⁴ California Institute of Technology, Pasadena, California

Received December 14, 1960

The calculation of density gradients and density distributions in binary solutions at sedimentation equilibrium in an ultracentrifuge is presented. The differential equation describing sedimentation equilibrium is $\beta(\rho)d\rho = \omega^2 r dr$ where β is a function of the temperature and the activity, molecular weight, and partial specific volume of the solute at a density ρ . Values of β have been calculated from published data for density and activity over the entire concentration range for CsCl, KBr, RbBr, RbCl, LiBr and sucrose at 25.0°. For each binary system $\beta(\rho)$ has been expressed as a cubic polynomial in ρ . The integral form of the above equation was then solved for the integration constants using a digital computer for the first four salts mentioned above. The integration constant is the radial distance at which the initial density of the solution occurs. This is the isocorcentration position. Experimental confirmation of the density gradient and of a density distribution for CsCl are presented.

Introduction

The analysis of results obtained with the recently developed procedures for sedimentation equilibrium of macromolecules in a density gradient in the ultracentrifuge⁵ requires a knowledge of the density and the gradient of density in the liquid column. For a single dilute species, the apparent molecular weight⁶ of the macromolecule is given by the relation

$$M_{\text{app}} = \frac{RT\rho_0}{\sigma^2(d\rho/dr)_0\omega^2 r_0} \quad (1)$$

where ρ_0 is the buoyant density of the solvated species of molecular weight, M_{app} , σ is the standard deviation of the Gaussian concentration distribution of the macromolecule, $(d\rho/dr)_0$ is the density gradient at the position r_0 , the center of the Gaussian band, and ω is the angular velocity.

In previous work, the buoyant density has been evaluated by asserting that the isocorcentration distance, r_c , and the corresponding original density, ρ_c , are to be found at the radial center of the liquid column. For bands near the center of the liquid column, to a good approximation

$$\rho_0 = \rho_c + (d\rho/dr)_c \Delta r \quad (2)$$

where Δr is the displacement of the mode from the center of the liquid column.

The density gradient is evaluated by one of two alternative methods.⁷ The optical method makes use of the relation

$$\frac{d\rho}{dr} = \frac{dn}{dr} \times \frac{d\rho}{dn} \quad (3)$$

where dn/dr is the measured refractive index gradient in the schlieren optical system and $d\rho/dn$ is obtained experimentally by refractometry of solutions of known composition. In the physical chemical method, the density gradient is calculated from the relation for sedimentation equilibrium in a two-component system

$$\frac{d\rho}{dr} = \frac{d\rho}{d \ln a} (1 - \bar{v}\rho) \frac{M\omega^2 r}{RT} \quad (4)$$

where M , a and \bar{v} are the molecular weight, activity and partial specific volume of the solute species.

In this paper a method is presented for evaluating r_c . The method is based upon integrating a form of equation 4, using the conservation condition to obtain the integration constant. As a part of the procedure, it has been necessary to tabulate the values of the $d\rho/dr$ as a function of ρ and to express these as polynomials. The results for a series of solutes in water are first presented. The results of the integrations are given in the latter portion with some experimental confirmation of the results.

Results and Discussion

The Calculation of the Density Gradient.—For any binary solution, equation 4 may be written

$$\beta(\rho) \frac{d\rho}{dr} = \omega^2 r \quad (5)$$

where

$$\beta(\rho) = \frac{d \ln a}{d\rho} \frac{RT}{(1 - \bar{v}\rho)M}$$

The quantity β was evaluated by graphical methods from published data of densities^{8,9} and activity coefficients.¹⁰ The partial specific volume, \bar{v} , was

(8) "International Critical Tables," Vol. 3, McGraw-Hill Book Co., New York, N. Y., 1928.

(9) F. Bates and Associates, "Polarimetry, Saccharimetry and the Sugars," Circular 440, National Bureau of Standards, Washington, D. C., 1942, p. 626.

(10) R. A. Robinson and R. H. Stokes, "Electrolyte Solutions," Butterworths, London, England, 1955.

(1) (a) This investigation was supported in part by Research Grant H-3394 from the National Institutes of Health, U. S. Public Health Service; (b) this work was presented in part before the 33rd National Colloid Symposium, Division of Colloid Chemistry, American Chemical Society, Minneapolis, Minnesota, June 18 to 20, 1959.

(2) U. S. Public Health Service Research Fellow of the National Cancer Institute, 1959-1960; Division of General Medical Sciences, 1960-1961.

(3) Supported for one summer by the National Science Foundation Undergraduate Research Participation Program, N.S.F.-G7954.

(4) Contribution No. 2653.

(5) M. Meselson, F. W. Stahl and J. Vinograd, *Proc. Natl. Acad. Sci.*, **43**, 581 (1957).

(6) R. L. Baldwin, *ibid.*, **45**, 939 (1959).

(7) M. Meselson, Ph.D. Dissertation, California Institute of Technology, 1957.

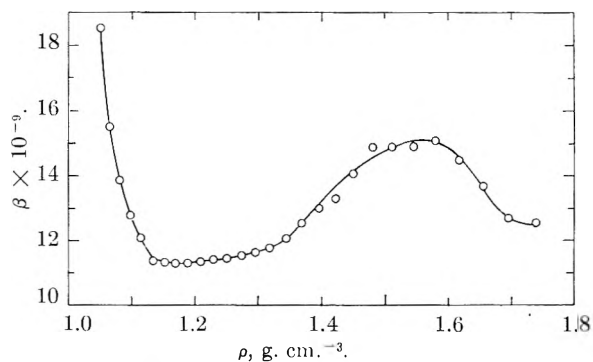
evaluated by the chord method on a large scale plot of $1/\rho$ vs. Z_2 , the weight fraction of the solute. Thus a graph of \bar{v} vs. ρ was obtained. Activities were calculated from data relating mean ion activity coefficient and molality. Corresponding density data were derived from the almost linear weight fraction vs. density plot. The variation of $d\rho/d \ln a$ with ρ was evaluated graphically by determining tangents to the ρ vs. $\ln a$ curve. The values of $d\rho/d \ln a$ and \bar{v} at corresponding densities were tabulated and $\beta(\rho)$ calculated. The results for CsCl,^{10a} RbBr, RbCl, KBr and sucrose are given in Table I. The data for LiBr are given separately in Fig. 1. These results may be used directly to evaluate the density gradient in a phase of density ρ at equilibrium in the ultracentrifuge.

TABLE I

ρ	VARIATION OF β WITH SOLUTION DENSITY				
	Sucrose	KBr	RbBr	RbCl	CsCl
1.02	8.091				
1.03	6.789				
1.04	5.605				
1.05	4.643		6.729	9.817	
1.06	4.019				
1.075		7.496			
1.08	3.449				
1.10	3.237	6.121	3.643	5.532	
1.12	3.121				
1.125		5.229			
1.14	3.091				
1.15		4.594	2.536	4.109	2.491
1.175		4.151			
1.20		3.848	2.122	3.445	1.984
1.225		3.637			
1.250		3.469	1.772	3.172	1.715
1.275		3.330			
1.30		3.213	1.635	3.083	1.546
1.325		3.112			
1.35			1.528	2.777	1.430
1.40			1.434	2.334	1.346
1.45			1.372		1.286
1.50					1.245
1.55					1.216
1.60					1.197
1.65					1.190
1.70					1.190
1.75					1.199
1.80					1.215
1.85					1.236

In this treatment, the effects of pressure have been neglected. Neglecting these effects is equivalent to stating that the solution is incompressible and that $\beta(\rho)$ is the same at atmospheric pressure and at the pressures in the rotating liquid column. The solution, however, is not incompressible. The compression gradient at density ρ is $K\rho^2\omega^2r$, where K is the compressibility coefficient. At the center of the sectorial cell for CsCl solutions, this compression gradient is of the order of 10% of the density gradient due to salt redistribution. The effects of pressure in density gradient systems are to be presented in a future publication.

(10a) The reciprocals of $\beta(\rho)$ for CsCl have been calculated by R. Trautman, *Arch. Biochem. Biophys.*, **87**, 289 (1960), by a somewhat different procedure. The data for CsCl in Table I have been compared with Trautman's data and differ by less than 1%.

Fig. 1.—Variation of β with solution density, LiBr.

The latter statement regarding the effect of pressure on $\beta(\rho)$ appears to be valid, as is demonstrated in the experimental section, at the center of a 1.287 g. cm.⁻³ CsCl solution (2.57 molal) in a sector cell at 56,100 r.p.m. The density gradient calculated from equation 5 agrees with the gradient determined by schlieren optical methods to within 0.7%. In this experiment, the density gradient due to the redistribution of CsCl and H₂O at equilibrium is evaluated by subtracting the schlieren elevation photographed just after reaching full speed from the elevation obtained at equilibrium. This procedure substantially eliminates the effects of pressure on the liquid, the cell windows and the centerpiece.

The density distributions in CsCl and RbBr solutions and in KBr and RbCl solutions should be similar in the density region, 1.15 to 1.30. In addition, the former two salts produce higher density gradients than the latter two in their common density regions.

The Construction of the Polynomials $\beta(\rho)$.—In order to use the tabulated values of $\beta(\rho)$ most effectively, a polynomial $\text{ave}(y_i) = \sum_{j=0}^k a_j \xi_{ji}$ was fitted to each set of data by the method of least squares. The polynomials were constructed by orthogonalizing the linearly independent functions $1, x, x^2, \dots, x^k$ by the Gram-Schmidt orthogonalization procedure. This method of curve fitting is described in Bennett and Franklin.¹¹ Tables of the numerical values of the ξ 's are given by Fisher and Yates.¹² Thus, polynomials of the form

$$\beta(\rho) = \beta_0 + \beta_1\rho + \beta_2\rho^2 + \dots + \beta_k\rho^k \quad (6)$$

were obtained for the solutes previously mentioned. The values of the first four β coefficients are given in Table II.

The accuracy with which the polynomial $\beta(\rho)$ gives the curve represented by the original β vs. ρ data depends upon k , the degree of the polynomial and upon n , the number of points used to calculate the polynomial. In this work, third degree polynomials were used. In the case of CsCl, a fifth degree polynomial reduced the maximum deviation of the β values calculated from the polynomial equation from the β values originally derived from

(11) C. A. Bennett and N. L. Franklin, "Statistical Analysis in Chemistry and the Chemical Industry," John Wiley and Sons, New York, N. Y., 1954, pp. 255-264.

(12) R. A. Fisher and F. Yates, "Statistical Tables," Oliver and Boyd, London, 1957, pp. 90-100.

TABLE II

Salt	Density range	POLYNOMIAL COEFFICIENTS ^a			
		$\beta_0 \times 10^{-9}$	$\beta_1 \times 10^{-9}$	$\beta_2 \times 10^{-9}$	$\beta_3 \times 10^{-9}$
CsCl	1.15-1.85	47.9726	-85.3724	51.7764	-10.4312
RbBr	1.05-1.45	620.9619	-1,416.8024	1,079.2080	-273.7280
RbCl	1.05-1.40	1,222.1450	-2,878.2225	2,264.0729	-593.3408
KBr	1.075-1.325	966.7593	-2,280.4334	1,802.8082	-475.9704
Sucrose	1.02-1.14	860.6168	-2,320.1077	2,085.6993	-625.0000

^a See text for polynomial equation.

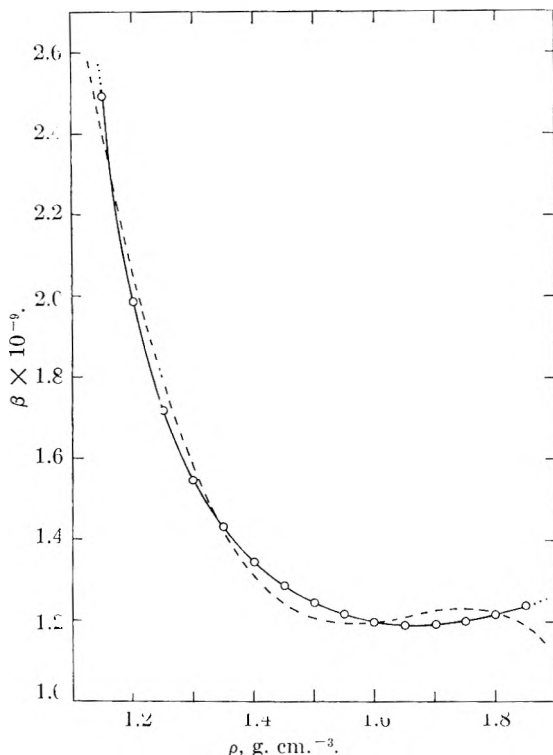


Fig. 2.—Comparison of polynomial $\beta(\rho)$ curve and original $\beta(\rho)$ curve, CsCl. Solid line, original $\beta(\rho)$ curve; dashed line, polynomial $\beta(\rho)$ curve.

activity and density data from 3% in β to 1%. The third degree polynomial was adequate to give the values of the isoconcentration points, r_e , to within 0.1%, except for RbBr. The value of n used depended on the shape of the $\beta(\rho)$ curve and varied from 15 to 21.

The maximum deviation of the β values calculated from the third degree polynomial from the corresponding original β values was $\pm 1\%$ for KBr, $\pm 3\%$ for CsCl and sucrose, $\pm 6\%$ for RbCl and $\pm 12\%$ for RbBr. The agreement between the derived relations and the original data is illustrated in Fig. 2 for CsCl.

Integration of the Polynomial Expansion of the Sedimentation Equilibrium Equation.—Equation 5 represented as a third degree polynomial may be integrated to give a fourth degree polynomial.

$$\alpha_4(\rho^4 - \rho_e^4) + \alpha_3(\rho^3 - \rho_e^3) + \alpha_2(\rho^2 - \rho_e^2) + \alpha_1(\rho - \rho_e) + \omega^2(r_e^2 - r^2)/2 = 0 \quad (7)$$

where the α 's are constants. The integration constant, r_e , was evaluated using the outside condition of conservation of mass of the solute

$$c_e = \frac{\int_0^V c \, dv}{V} \quad (8)$$

where c is the concentration at $v(r)$, c_e the initial concentration, and V is the total liquid volume in the cell. Since these concentrations are in units of mass/volume

$$c = Z_2 \rho \quad (9)$$

Examination of the relation between Z_2 and $1/\rho$ shows that these quantities are linearly related over the maximum density increments of 0.1 to 0.2 g. cm.⁻³ encountered in a gradient column. Combining this linear relation

$$Z_2 = k_1(1/\rho) + k_2 \quad (10)$$

where k_1 and k_2 are constants, with equation 9 and with the conservation relation 8, we obtain

$$\rho_c = \frac{\int_0^V \rho \, dv}{V} \quad (11)$$

For sector and cylindrical cells, equation 11 takes the forms

$$\rho_c = \frac{2 \int_{r_a}^{r_b} \rho r \, dr}{(r_b^2 - r_a^2)} \quad (11a)$$

and

$$\rho_c = \frac{\int_{r_a}^{r_b} \rho \, dr}{(r_b - r_a)} \quad (11b)$$

respectively, where r_a and r_b are the radii at the top and bottom of the cell.

The solution of equation 7 incorporating the conservation conditions 11a or 11b was performed with a Burroughs 205 digital computer. Input data for the computer are the constants $\alpha_1, \alpha_2, \alpha_3, \alpha_4, \rho_e, \omega, r_a, r_b, n$, the number of evenly spaced intervals in the liquid column, either 4 or 6, and $R_e(1)$ and $R_e(2)$, two bracketing estimates for r_e .

Equation 7 rewritten for a specific ρ_i and r_i is

$$\alpha_4 \rho_i^4 + \alpha_3 \rho_i^3 + \alpha_2 \rho_i^2 + \alpha_1 \rho_i = \frac{\omega^2}{2} (r_i^2 - r_e^2) + \alpha_4 \rho_e^4 + \alpha_3 \rho_e^3 + \alpha_2 \rho_e^2 + \alpha_1 \rho_e = -\alpha_0$$

The constant, α_0 , is computed using $R_e(1)$ and one of the values of r_i . Then the quartic polynomial is solved for the corresponding ρ_i . Each of the $n + 1$ points (r_i, ρ_i) is computed similarly and Simpson's rule used to compute the integral $I_1 = \int \rho r \, dr$, in the case of the sector. The procedure is repeated for $R_e(2)$. A linear interpolation is used to find $R_e(3)$. I_3 is calculated and compared with $I_0 = \rho_e(r_b^2 - r_a^2)/2$. The procedure is continued with parabolic interpolations until satisfactory agreement is reached between I_m and I_0 , whereupon the last set of values of ρ_i and r_i and the final value of r_e are printed out.

The program was operated for aqueous solutions

of CsCl, RbCl, RbBr and KBr for both sector cells and cylindrical cells containing 2, 3 and 5 ml. of solution over a range of solution densities and for several angular velocities. The limiting radii were chosen to correspond to a 0.70-ml. liquid volume in a 12-mm. 4° sector in the analytical ultracentrifuge or to the above volumes in 5 ml. plastic tubes in the SW-39 swinging bucket rotor in the preparative ultracentrifuge.

Representative density distribution data are given as follows: Fig. 3 presents the data for CsCl in cylinders of varying length and initial density. The distributions are as expected in that they become more linear as the cell lengths decrease and they are steeper for the higher ρ_e 's reflecting the higher gradients. The maximum density difference which can be obtained for CsCl is seen to be about 0.4 g. cm.⁻³.

Figure 4 gives the distributions for the four salts in 3-ml. cylinders at varying angular velocities. The slope of the curves increases with increasing velocity as required by the density gradient expression. The isoconcentration point is not invariant with changes in ω as is suggested by the small scale plots, Fig. 4, but varies as shown in Figs. 6 and 7.

The numerical values for the CsCl density distribution in sectors are given in Table III.

TABLE III
DENSITY DISTRIBUTIONS
CsCl Sector

ρ	ω , r.p.m.	Density at				
		$r_a = 6.0$	$r = 6.3$	$r = 6.6$	$r = 6.9$	$r_b = 7.2$
1.2	56,100	1.137	1.164	1.195	1.231	1.273
1.3	56,100	1.217	1.252	1.293	1.340	1.394
1.45	56,100	1.343	1.390	1.443	1.502	1.564
1.6	56,100	1.484	1.538	1.595	1.654	1.715
1.7	56,100	1.585	1.639	1.695	1.753	1.814
1.2	44,770	1.160	1.177	1.197	1.219	1.244
1.45	44,770	1.382	1.413	1.446	1.482	1.521
1.7	44,770	1.629	1.662	1.697	1.733	1.771
1.7	33,450	1.660	1.679	1.698	1.719	1.740

The remainder of the density data can be calculated from the isoconcentration point data given below. This data provides ρ_c and r_c in equation 7 which can then be solved for the density distribution noting that $\alpha_n = \beta_{n-1}/n$. Also, a stepwise integration can be performed using the isoconcentration point and $\beta(\rho)$ data. Alternatively, approximate density distributions for intermediate values of the parameters can be evaluated by interpolation.

The order of magnitude of the errors in the above distributions can be evaluated by considering the areas between the polynomial and actual $\beta(\rho)$ curves. To a good approximation, the point ρ_c, r_c is the same for both the polynomial calculation and for the actual distribution. This will be demonstrated in a later section. We then can use equation 5 to estimate the deviations at other points in the distribution.

The area under the polynomial curve between ρ_e and ρ is equal to $\int_{\rho_e}^{\rho} \beta(\rho) d\rho$. A similar integral can be written for the area under the real curve.

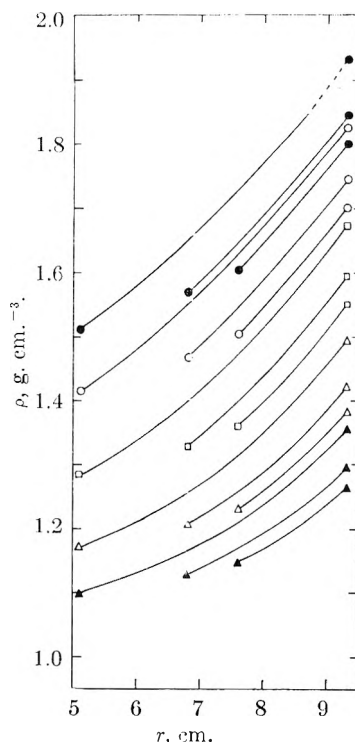


Fig. 3.—Density distributions in cylinders: CsCl; 39,000 r.p.m. ●, $\rho_e = 1.7$; ○, $\rho_e = 1.6$; □, $\rho_e = 1.45$; △, $\rho_e = 1.3$; ▲, $\rho_e = 1.2$.

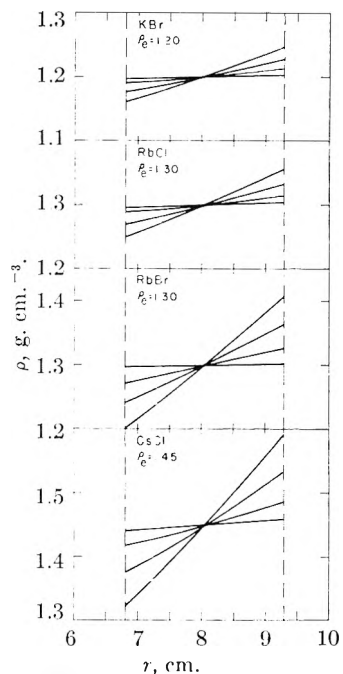


Fig. 4.—Density distributions for four salts in 3 ml. cylinders at varying speeds. In the order of increasing slope, the curves are for 10,000, 20,000, 30,000 and 33,000 r.p.m.

The area between the two curves from ρ_e to ρ is given by

$$\int_{\rho_e}^{\rho} \beta(\rho)_r d\rho - \int_{\rho_e}^{\rho} \beta(\rho) d\rho = \frac{\omega^2}{2} (r_p^2 - r_c^2)$$

From a measurement of this area, the real value of r at ρ, r_r , can be calculated. The value for ρ as given by the polynomial is obtained from the

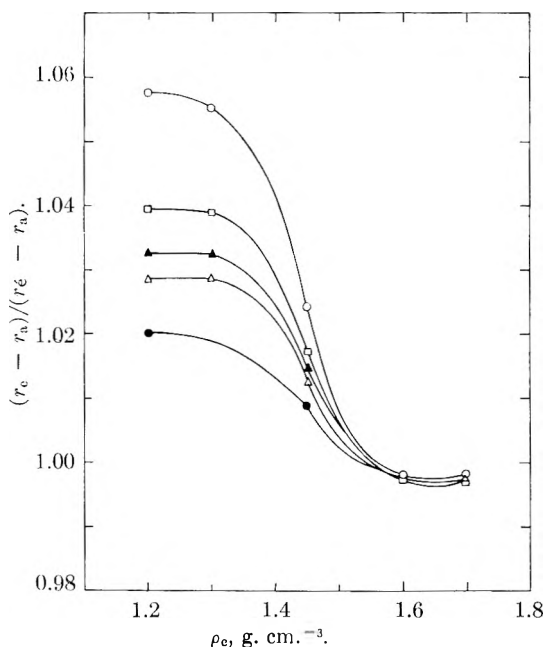


Fig. 5.—Variation of normalized isoconcentration point with original solution density, CsCl: ○, 5-ml. cylinder, 39,000 r.p.m.; □, 3-ml. cylinder, 39,000 r.p.m.; △, 2-ml. cylinder, 39,000 r.p.m.; ▲, sector, 56,100 r.p.m.; ●, sector, 44,770 r.p.m.

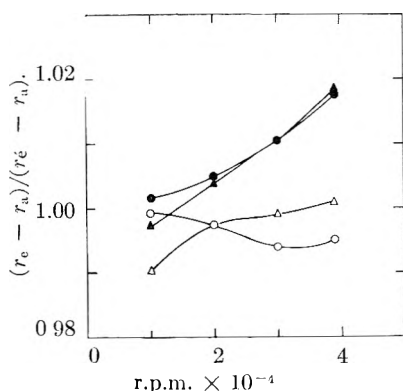


Fig. 6.—Variation of normalized isoconcentration point with angular velocity, 3-ml. cylinders: ●, CsCl, $\rho_c = 1.45$; ○, RbBr, $\rho_c = 1.3$; ▲, KBr, $\rho_c = 1.2$; △, RbCl, $\rho_c = 1.3$.

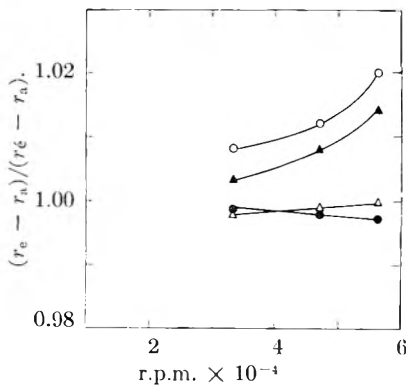


Fig. 7.—Variation of normalized isoconcentration point with angular velocity, sectors: ●, CsCl, $\rho_c = 1.7$; ○, RbBr, $\rho_c = 1.3$; ▲, KBr, $\rho_c = 1.3$; △, RbCl, $\rho_c = 1.3$.

density distribution plots. For the case of CsCl of $\rho_c = 1.7$ and 56,100 r.p.m. in a sector integration from r_e to the cell bottom showed that the

difference in r for which both distributions had a density of 1.81 was 0.012 cm. This corresponds to a density difference of 0.002 g. cm.⁻³ The differences in ρ are successively less as the distances from r_e decrease. The density differences between the real and computer distributions will be approximately the same in the cylindrical cases since the area in the example discussed was nearly maximal. Also the values of r in the cylindrical case are larger and hence, for a given area between the curves, the difference in r_p and r_r will be smaller. Thus the maximum deviation which can be attached to each of the densities in the CsCl distributions reported is 0.002 g. cm.⁻³ Inspection of the areas between the curves for the other salts indicates that the maximum deviations in density for KBr will be smaller than 0.002 g. cm.⁻³ and for RbCl and RbBr will be less than the accuracy with which Fig. 4 can be read.

To be of greatest use, the isoconcentration points obtained in the above program were normalized in two ways. Since the actual values obtained for r_e depend on the r_a and r_b used in the program, they were first normalized by dividing the difference between r_e and r_a by the length of the liquid column to yield $(r_e - r_a)/(r_b - r_a)$. The isoconcentration positions were further normalized by dividing this fraction by another fraction, $(r_e' - r_a)/(r_b - r_a)$, where r_e' is a limiting value for r_e , to give $(r_e - r_a)/(r_e' - r_a)$.

Under the assumption that $\beta(\rho)$ is constant, the integrated form of equation 5 and the conservation equations 11 may be combined to give values for the limiting isoconcentration points in sectors, equation 12a, and in cylinders 12b

$$r_e' = \sqrt{\frac{r_b^2 + r_a^2}{2}} \quad (12a)$$

$$r_e' = \sqrt{\frac{r_b^2 + r_a r_b + r_a^2}{3}} \quad (12b)$$

Equation 12a was derived earlier by Rinde¹³ under the assumption that $M(1 - \bar{v}\rho)\omega^2(r_b^2 - r_a^2)/2RT \ll 1$. We will now expect that the actual values of r_e in a real situation will converge on r_e' when β approaches a constant value. This is the case, for example, for CsCl solutions in the density range 1.65 to 1.75 g. cm.⁻³. Within this range are the buoyant densities for cesium deoxyribonucleates. For any system, of course, the change in β from the top to the bottom of the liquid column becomes smaller as the angular velocity or the length of the liquid column is decreased.

The normalized isoconcentration points are presented in Figs. 5–7 and in Table IV. In the density range 1.6–1.7, the β curve for CsCl, Fig. 2, goes through a broad minimum. Thus it would be expected that the value of the normalized isoconcentration point should approach 1.000 in this region which it does as shown in Fig. 5. Also to be noted is the increasing divergence of r_e from r_e' as either the cell length or the angular velocity increases. As previously discussed, this is to be expected since either variation reduces the constancy of β . In Figs. 6 and 7, it is seen that r_e does vary slightly with angular velocity and, as

(13) H. Rinde, Dissertation, Uppsala, 1928.

expected, tends toward r_c' as ω is reduced to zero.

TABLE IV

NORMALIZED ISOCONCENTRATION POINTS

	ω , r.p.m.	Volume, ml.	ρ_c	RbBr	RbCl	KBr
A. Sectors	56,100	0.7	1.1	1.049	1.033	1.025
	56,100	0.7	1.2	1.036	1.016	1.015
	44,770	0.7	1.1	1.032	1.021	1.016
	44,770	0.7	1.2	1.024	...	1.009
B. Cylinders	39,000	5	1.1	1.093	1.059	1.044
	39,000	5	1.2	1.084	1.027	1.026
	39,000	5	1.3	...	1.006	...
	39,000	3	1.1	1.063	1.040	1.030
	39,000	3	1.2	1.064	1.019	1.018
	39,000	3	1.3	0.995	1.001	1.018

The graphs may be viewed as describing the errors which arise when the readily available limiting values of r_c are employed. The error in r_c , if r_c' is used, is given adequately by the approximate expression $(r_c - r_c')/r_c = \delta \cdot (r_b - r_a)/(r_b + r_a)$ where δ is the variation from 1.000 in the $(r_c - r_a)/(r_c' - r_a)$ plot. The error in ρ_0 encountered on using r_c' for r_c may be found approximately by multiplying $\delta \cdot (r_b - r_a)/2$ by the density gradient. In general, ρ_0 is desired to within 0.001 g. cm.⁻³, which in the case of a 0.15 g. cm.⁻⁴ gradient corresponds to specifying the band position to 67 μ . Under these conditions, r_c' may be used in place of r_c for any sector run in CsCl where $\delta < 0.011$ or equivalently, for $\rho_c > 1.5$. The maximum δ allowable, if the same accuracy in determining ρ_0 is to be achieved in cylinders, decreases with increasing length to a value of 0.003 for a 5-ml. CsCl cylinder.

Generally, the practice to date has been to use the radial center of the cell for r_c . For CsCl of $\rho_c = 1.7$ in a 12 mm. cell where $r_m = (r_b + r_a)/2 = 6.60$, multiplication of $d\rho/dr$ at r_c by $(r_c - r_m)$ yields the following errors in computing ρ_0 : 0.005 at 56,100 r.p.m., 0.003 at 44,770 r.p.m., and 0.002 at 33,450 r.p.m. Thus depending on the conditions of the experiment, rather serious errors may occur in determining ρ_0 if the center of the cell is used for r_c .

Comparison of Figs. 2 and 5 indicates that there is a close correlation between the slope of the $\beta(\rho)$ curve and the value of r_c obtained. It was further noted that a straight line represents the $\beta(\rho)$ curve better than the polynomial over short regions of the curve pertinent to an experiment. Thus an expression for r_c in closed form was sought by solving equation 5 in linear form using the conservation condition, equation 11, as before.

Using $\beta = \beta_0 + \beta_1\rho$, equation 5 was integrated and solved for $(\rho - \rho_c)$. This variable was substituted into $\int_{r_a}^{r_b} (\rho - \rho_c)r dr = 0$, which is another form of the conservation equation 11a for sectors. This equation was integrated to give an expression for r_c using two approximations. The first involved a good expansion in powers of $(r_c')^2 - (r_c)^2$. The second expansion is accurate to within $\pm 1\%$ in $(r_c')^2 - (r_c)^2$ if $D = \beta_1\omega^2/\beta^2$ is less than 0.05, which is the case for the maximum centrifuge velocities attainable except for the lowest density regions of

each salt. The expression obtained is

$$(r_c')^2 - (r_c)^2 = D(r_b^2 - r_a^2)/48 \quad (13)$$

Using this equation, values of r_c were computed for three points on each of the $\beta(\rho)$ curves. These points in general corresponded to portions of the curves where either the slope of the polynomial had a different sign than the actual curve, the deviation between the curves was a maximum, or the slopes were large. In all cases examined, the use of the slope of the tangent to the polynomial curve yielded values within 0.004 cm. of the computer value. This demonstrates not only the validity of this equation but also the fact that a tangential line yields satisfactory values compared with the computer value which is the exact solution for the polynomial curve. This is important because, under the restriction noted, the isoconcentration points can be obtained by the tangent method given above and thus without recourse to a computer. The same results were obtained through the use of the straight line through the points corresponding to the densities at the cell ends as given by the computer.

Typical values for r_c were calculated for each of the salts using the tangents to the actual β curve. In all cases, except under conditions where the expansion is poor, the agreement of this value with the computer r_c for CsCl, RbCl and KBr was within 0.005 cm. This corresponds, for a large gradient, to the acceptable error of 0.001 d.u. The numbers for RbBr differ by as much as 0.016 cm. This is due primarily to the large error noted previously in the polynomial fit. The isoconcentration points for RbBr given in Figs. 6 and 7 and Table IV were obtained by the use of equation 13.

An expression for r_c in closed form in the cylindrical case using a linear β equation as above could not be obtained. Thus, all of the isoconcentration point data for cylinders are those obtained by the computer. By analogy, we assume that the values for RbCl, CsCl and KBr are accurate; the RbBr data probably are good only on the average to 0.01 cm.

The Resolving Power of the Density Gradient Method for Macromolecules of Different Buoyant Densities.—With the availability of information regarding the density gradient formation for various salt solutions, it is of interest to consider the effect of the selection of the salt on the resolution obtainable between substances separated in the gradient column.

We will define resolution, Λ , for two homogeneous macromolecular species in a density gradient as

$$\Lambda = \frac{\Delta r}{(\sigma_1 + \sigma_2)} \quad (14)$$

the distance between the modes, Δr , divided by the sum of the standard deviations of the bands. For small distances, equation 5 is $\Delta r = \Delta\rho(\beta/\omega^2r)$. Substituting this expression and equation 1 for σ into equation 14 under the simplifying assumptions of a constant density gradient and $\Delta\rho \ll \rho_0$ and $\Delta r \ll \bar{r}_0$, the resolution equation becomes

$$\Lambda = \Delta\rho \left(\frac{1}{RT}\right)^{1/2} \left[\frac{(M_1M_2)^{1/2}}{[(M_1)^{1/2} + (M_2)^{1/2}]} \right] \left(\frac{\beta}{\rho}\right)_{r_0}^{1/2} \quad (15a)$$

where $\Delta\rho$ is the difference in buoyant densities

of the macromolecular solutes of molecular weights M_1 and M_2 and both β and ρ are evaluated at the mean banding position \bar{r}_0 . For two solutes of nearly the same molecular weight M , but different buoyant densities, the resolution equation becomes

$$\Lambda = \frac{\Delta\rho}{2} \left[\left(\frac{M}{RT} \right)^{1/2} \right] \left(\frac{\beta}{\rho} \right)_{\bar{r}_0}^{1/2} \quad (15b)$$

This equation is further simplified by recalling that β , cf. equation 5, is proportional to RT . Introducing $\beta' = \beta/RT$, equation 15b can be written

$$\Lambda = \frac{\Delta\rho}{2} \left(\frac{M\beta'}{\rho} \right)_{\bar{r}_0}^{1/2} \quad (15c)$$

Thus Λ does not depend as strongly on temperature as is indicated in equations 15a and 15b. It is independent of T except for the small effects of temperature on the activity coefficients.

For a given pair of macromolecules in a given salt gradient, the resolution is independent of angular acceleration. This is to be expected since both Δr , for a given $\Delta\rho$, and σ are proportional to $(\omega^2 r)^{-1}$. As the bands become narrower, they approach each other. Resolution is therefore not affected by changes in velocity.

On the other hand, resolution is improved by carrying out experiments in solvents having the largest β values. For the aqueous salt solutions previously discussed, these are the solutions containing salts of low molecular weights. At a density of 1.3, potassium bromide and rubidium chloride solutions resolve better than cesium chloride solutions by factors of 1.45 and 1.41, respectively, even though the gradients achieved at a particular angular velocity are smaller.

A value of $\Lambda = 1$ will lead to such overlap that only one maximum will be evident in the concentration profile. At $\Lambda = 2$, concentration profiles will intersect such that 5% of the material will be intermixed. At $\Lambda = 3$, almost complete separation is achieved.

Alternately, the resolution can be measured by the elevation midway between the modes. On a plot normalized by dividing c by c_0 , this elevation is given by $y = 2e^{-\Lambda^2/2}$ if the initial concentrations and σ 's are identical. If the initial concentrations are unequal, both the degree of mixing and the elevation y will be increased.

An experimental test of the resolution equation has been afforded in the experiments of Meselson and Stahl.¹⁴ They observed a density separation of 0.014 density unit for the DNA's containing ¹⁴N and ¹⁵N isotopes. Using their molecular weight and buoyant densities to calculate Δr and the standard deviations, a Λ of 3.6 is obtained. Substitution in equation 15b yields the same density separation as observed indicating the internal consistency of the resolution equation. The elevation of the trough between the concentration distributions presented in this paper appears to be considerably higher than would be the case for two Gaussian distributions having a $\Lambda = 3.6$. This is due in part to the unequal initial concentrations and possibly due to not having reached equilibrium or to the presence of a small amount of impurity.

(14) M. Meselson and F. W. Stahl, *Proc. Natl. Acad. Sci.*, **44**, 671 (1953).

For proteins of $M = 10^5$ and $\rho = 1.3$, $\Lambda = 35 \Delta\rho$ for CsCl solutions and $50 \Delta\rho$ for KBr solutions. Therefore to obtain a resolution of 2, $\Delta\rho$ must be 0.058 and 0.040 in CsCl and KBr, respectively. Thus appropriate macromolecules in the size range of proteins may be segregated in a single density gradient column. Such a segregation recently has been reported by Bock¹⁵ for β -galactosidase and ¹⁵N-D- β -galactosidase.

Experimental

Preparation of Solutions.—The CsCl solutions were prepared from CsCl obtained from the Maywood Chemical Co., Maywood, N. J. Solution densities were determined with a Zeiss refractometer utilizing the linear relation¹⁶ between ρ and n , $\rho^{25.0} = 10.8601n^{25.0D} - 13.4974$. The N-43 fluorochemical was supplied by the Minnesota Mining and Manufacturing Co., Fluorochemical Department.

A. Measurement of $d\rho/dr$.—A CsCl solution of $\rho_0 = 1.287$ was centrifuged to equilibrium at 56,100 r.p.m. in a Spinco Model E analytical ultracentrifuge and schlieren photographs made.

The density gradient was determined experimentally from equation 3. The refractive index gradient was measured from the relation $dn/dr = y \tan \theta/LTm$ where y is the vertical distance on the schlieren curve between the baseline, photographed immediately at velocity, and the equilibrium curve, θ is the diaphragm angle, L the optical lever arm, T the cell thickness, and m the cylindrical lens magnification. The value of dn/dr was determined at the isoconcentration point and, after correction for dispersion,¹⁷ found to be 0.0136. Multiplication by the slope of the ρ vs. n relation given above yields $d\rho/dr = 0.147$. The value for the gradient derived theoretically from the β curve is 0.146. The 0.7% discrepancy can be accounted for in the uncertainties both in the experimental parameters and in the accuracy of β .

B. Measurement of the Density Distribution in a CsCl Solution in a Preparative Centrifuge Cell.—Fluorocarbon (0.33 ml.) was used to place the false bottom 0.5 cm. from the bottom of the plastic cell. Two ml. of CsCl solution of $\rho_0 = 1.700$ was added, and then a layer of mineral oil to prevent evaporation and cell collapse. The SW-39 rotor then was spun 24 hr. to equilibrium at 39,000 r.p.m. in a Spinco Model L preparative centrifuge. After braking to a halt, the cell was immediately sampled dropwise into previously weighed vials. This was done by making a small hole in the bottom of the tube with a pin and controlling the drop rate with a syringe attached to the tube. The vials then were reweighed and the refractive index of each sample measured.

From these data, calculations yielded a plot of ρ vs. r which is presented in Fig. 8 together with the theoretical distribution. The experimental curve, representative of a number of such runs, differs significantly from the theoretical distribution. Identical runs made with no braking and runs of 48 hr. yielded similar results, indicating that these differences were not due to rapid braking or failure to attain equilibrium.

The small but consistent elevation of the experimental curve suggests that some evaporation occurred during sampling and analysis. The significant departure of the curve at the ends of the cell could be due to back diffusion, which therefore was further investigated.

(15) Private communication from R. M. Bock.

(16) This relationship is the least squares line through data abstracted from "International Critical Tables" and confirming data obtained in this Laboratory.

(17) The schlieren photographs were made with light from an AH-6 mercury lamp filtered through an Eastman number 16 wratten filter and registered on Eastman metallographic plates. The effective wave length in these photographs is a pressure-broadened 5460 Å. Hg line. Since $(dn/dr) = (dn/dc)(dc/dr)$, the dispersion factor desired is $(dn/dr)_{5460}/(dn/dr)_{5460} = (dn/dc)_{5460}/(dn/dc)_{5460}$. Data for the calculation of the latter ratio are given by A. Heydewiller, *Physik. Z.*, **26**, 526 (1925). Several reasonable interpolations lead to a value of 0.999 for the dispersion factor for solutions of CsCl in the range 2 to 4 molar. The measured elevation is multiplied by the dispersion factor to give $(dn/dr)_{5460}$.

C. Measurement of the Rate of Back Diffusion.—An analytical centrifuge cell was filled with CsCl of $\rho_0 = 1.700$ and the cell brought to 39,460 r.p.m. at maximum acceleration. Using a pulse counter as a guide, baseline photographs were obtained at 9,945 r.p.m. and just at full speed. After equilibrium was achieved, as determined by a series of schlieren patterns, the angular velocity was reduced to 9,945 r.p.m. in 6 minutes. Schlieren photographs then were made at suitable intervals to determine the rate of back diffusion.

At various radii, the distances y_i between the curves and their corresponding baselines were measured on enlarged tracings of the photographic plates. The resulting plots were integrated numerically using the meniscus as the origin. The integrals evaluated up to two points, r_1 and r_2 , 0.26 and 0.56 mm. from the top and bottom of the liquid column, respectively, were combined with the densities at these positions, as determined from the computer data, to give the following relation between ρ and the summations

$$\rho_r = \alpha \left(\sum_{r_a}^r y_i - \sum_{r_b}^{r_2} y_i \right) + \rho_{r_2}$$

where

$$\alpha = \frac{\rho_{r_1} - \rho_{r_2}}{\left(\sum_{r_a}^{r_1} y_i - \sum_{r_b}^{r_2} y_i \right)}$$

It is thus unnecessary to know either $d\rho/dn$ or the machine constant in the relation between the measured elevations and the refractive index gradient. Only the exptl. distribution curve at 39,460 r.p.m. is shown in Fig. 9 since it agrees so closely with the computer distribution. The distributions are superimposed at the cell ends as required by this treatment. The exptl. distribution deviates slightly downward in the central region to a maximum difference of 0.0005 g. cm.⁻³.

The schlieren data obtained after reduction of speed were converted to density distributions by essentially the procedure described above with the additional assumption that the position of the isoconcentration point did not change in the expt. This assumption is justified as indicated in Fig. 7. The value of r_e changes only very slightly if the curve is extrapolated to an ordinate of 1.000 at zero speed.

As is to be expected, the first effect observed on lowering the speed is the Archibald effect. That is, the concentration profile remains approximately the same throughout the center portion of the liquid column but changes very abruptly at the ends. Thus even at 12 min. after reduction of speed, there are significant deviations at the top and the bottom about 2 mm. in from the ends, but no deviation in the middle portion. At 29 min., there are deviations of 0.015 and 0.021 g. cm.⁻³ at the top and bottom of the cell, respectively. The deviations from the theoretical curve noted on sampling a 1.7 cm. preparative cell at 30 min. after braking are correspondingly 0.034 and 0.023 g. cm.⁻³. The deviations at the bottom are expected to be in closer agreement since the sampling procedure examines this portion of the liquid column first. The deviations in the preparative cell are necessarily larger since the cell is longer and also since the analytical centrifuge expt. could not be performed at rest. We conclude that the major portion of the deviations noted at the ends of the liquid column in the preparative run is due to back diffusion.

NOTE ADDED IN PROOF.—In subsequent publications (Hearst and Vinograd and Hearst, Ifft and Vinograd, *Proc. Natl. Acad. Sci.*, July (1961)), it is shown that the effective density gradient which must be used in dealing with buoyant

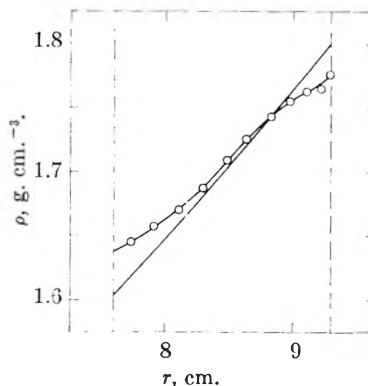


Fig. 8.—Density distributions in the preparative centrifuge; 2 ml. cylinder; CsCl; 39,000 r.p.m.: solid line, theoretical distribution; O, exptl. distribution.

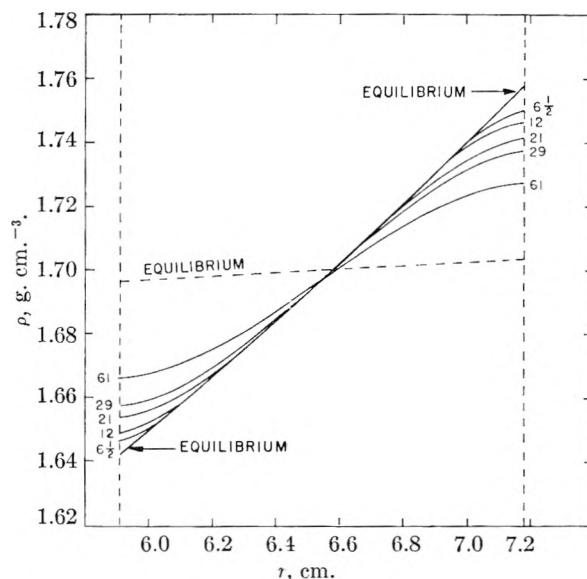


Fig. 9.—Exptl. density distributions in the analytical ultracentrifuge at equilibrium at 39,460 r.p.m. and after reducing velocity to 9945 r.p.m.: dashed line, theoretical distribution at 9945.

macromolecules, is the sum of the composition density gradient and density gradient terms associated with the effects of pressure and solvation. In this paper, the term density gradient is used to describe only the composition gradient. The density gradient employed in equations 1 and 15 should properly be the effective density gradient.

Acknowledgment.—The authors wish to thank Mr. Eugene Robkin and Prof. Matthew Meselson for their contributions in the early stages of this work; and Mr. John E. Hearst for many helpful and illuminating discussions. We also wish to thank Mr. Arthur Robison who calculated the LiBr data.

DEALKYLATION OF *t*-BUTYLBENZENE BY CRACKING CATALYSTS

BY MARVIN F. L. JOHNSON AND JOHN S. MELIK

Sinclair Research, Inc., Harvey, Illinois

Received December 17, 1960

A low-conversion flow reactor system is used to measure rates of dealkylation of *t*-butylbenzene over a variety of catalysts, as a function of temperature and of added water vapor, in an attempt to classify catalysts according to Brønsted acid activity. With but one exception, activation energies are the same for all catalysts studied. Differences in activity between catalysts are believed due to differences in the number of sites capable of catalyzing this reaction. The addition of water vapor with the hydrocarbon has little effect, up to a point, upon the activity of silica-alumina, kaolinite-based catalyst, mixed base catalyst, or silica-alumina-zirconia. Water is harmful to borica-alumina or fluoride-alumina, by causing volatilization of the promoter. Water enhances the activity of silica-magnesia or montmorillonite-based catalyst.

I. Introduction

The catalytic acidity of cracking catalysts has been the subject of much work in recent years. In attempting to measure what one terms catalyst acidity the concepts of number of acid sites and of the strengths of these sites must be considered. Techniques such as the non-aqueous titration with *n*-butylamine¹ or quinoline adsorption,² among others, give a measure of the number of such sites. Benesi³ has extended the butylamine titration to permit estimation of relative acid strengths, by using a series of indicators of varying *pK*. These techniques, while they serve a definite purpose in characterizing catalysts, suffer from the fact that they may not represent the actual interactions involved in a catalytic reaction.

Another aspect of the characterization of acidic properties of catalysts is the question of whether the sites are Lewis or Brønsted acids. Tamele⁴ has suggested that silica-alumina is a Lewis acid in the absence of water, Brønsted acid in the presence of water. On the other hand, Milliken, *et al.*,⁵ postulate the presence only of potential Lewis acids, until the approach of a base (*e.g.*, a hydrocarbon) causes a shift to the Lewis acid form. This picture completely eliminates the possibility of Brønsted acids. Hansford⁶ has given a rebuttal to this theory, pointing out that there is a considerable body of evidence that protons can and do exist on cracking catalysts at elevated temperatures, and that it is difficult to see how the polarizing ability of any but the most polar molecules (*e.g.*, water) could exert the postulated effect on catalyst structure. Mapes and Eischens⁷ reported infrared spectral evidence for both Lewis and Brønsted acids (or hydrated Lewis acids) in silica-alumina, with the Lewis acids predominating. Haldeman and Emmett,⁸ in a study of the water content of silica-alumina, found that there are not enough protons present to furnish one for each Al³⁺, hence at least some of the sites must be the Lewis type. Trambouze, *et al.*,⁹ made measurements of

Lewis and Brønsted acid concentrations by room temperature titrations; they found an increase in the former upon heating to successively higher temperatures, the sum of the two types remaining constant.

It appears most likely that in actuality silica-alumina contains, at least potentially, both Lewis and Brønsted acid sites, the actual amounts of the two types depending upon the degree of hydration. That there is an effect of water on the activity of silica-alumina is well-known.¹⁰⁻¹³ The possibility exists that a similar effect may be observed with other types of acidic oxide catalysts. The work reported here is an attempt to classify catalysts according to Brønsted acid activity as defined by the rate of a catalytic reaction which is believed to be catalyzable only by Brønsted acids, *e.g.*, the dealkylation of aromatics. A classification of Lewis acid activity by a catalytic reaction would be more difficult; a paraffin, for example, can be converted to a carbonium ion by hydride abstraction by a Lewis acid, or by proton donation from a Brønsted acid to a small amount of olefin produced by thermal cracking.

II. The Aromatic Dealkylation Reaction

Not only is the catalytic dealkylation of cumene a very rapid reaction, but it is highly selective; furthermore, the rate does not decrease with time due to coke formation.^{14,15} It is therefore well suited for a test reaction. One of the drawbacks to the use of cumene is, however, the fact that hydroperoxides can form fairly easily, and serve as inhibitors.¹⁵ For this reason, and because its rate of reaction is much higher (*ca.* 10 \times), we have chosen to use *t*-butylbenzene (TBB).

It is generally believed, although without direct evidence, that this reaction is catalyzed by a Brønsted acid, so that the rate of reaction can serve as a measure of Brønsted acid activity. A mechanism not involving proton transfer does not appear reasonable in view of the effect of hydrocarbon substituent on dealkylation rate¹⁶ and in view

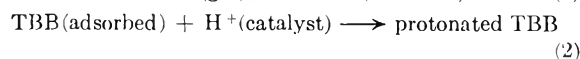
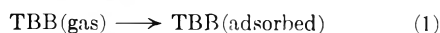
(1) O. Johnson, *J. Phys. Chem.*, **59**, 827 (1955).
 (2) G. A. Mills, E. R. Boedeker and A. G. Oblad, *J. Am. Chem. Soc.*, **72**, 1554 (1950).
 (3) H. A. Benesi, *J. Phys. Chem.*, **61**, 970 (1957).
 (4) M. W. Tamele, *Disc. Faraday Soc.*, **8**, 270 (1950).
 (5) T. H. Milliken, *ibid.*, **8**, 279 (1950).
 (6) R. C. Hansford, *Advances in Catalysis*, **IV**, 1 (1952).
 (7) J. E. Mapes and R. P. Eischens, *J. Phys. Chem.*, **58**, 1059 (1954).
 (8) R. G. Haldeman and P. H. Emmett, *J. Am. Chem. Soc.*, **78**, 2917 (1956).
 (9) Y. Trambouze, L. DeMourges and M. Perrin, *J. chim. phys.*, **51**, 723 (1954).

(10) R. G. Haldeman and P. H. Emmett, *J. Am. Chem. Soc.*, **78**, 2922 (1956).
 (11) R. C. Hansford, *Ind. Eng. Chem.*, **39**, 849 (1947).
 (12) R. C. Hansford, P. G. Waldo, L. C. Drake and R. E. Honig, *ibid.*, **44**, 1108 (1952).
 (13) S. C. Hindin, G. A. Mills and A. G. Oblad, *J. Am. Chem. Soc.*, **73**, 278 (1951).
 (14) R. W. Maatman, R. M. Lago and C. D. Prater, *Advances in Catalysis*, **IX**, 531 (1957).
 (15) C. J. Plank and D. M. Nace, *Ind. Eng. Chem.*, **47**, 2374 (1955).
 (16) B. S. Greensfelder, H. H. Voge and G. N. Good, *ibid.*, **37**, 1168 (1945).

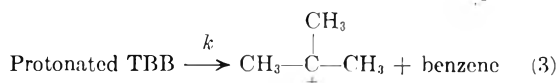
of the effect of aromatic substitutions on the cracking of unsymmetrical diarylethanes.¹⁷ In addition, our own observations of the effect of added water in certain cases support the viewpoint of proton transfer.

The kinetics of cumene dealkylation over silica-alumina catalyst have been discussed by Prater and Lago.¹⁸

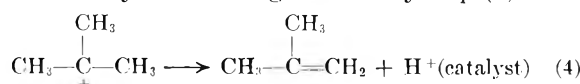
The following scheme is believed to represent the steps involved in dealkylation; this essentially follows Prater and Lago, except that the first step of adsorption of reactant is included here



The protonated TBB ultimately decomposes, perhaps by way of π and σ complexes; regardless of the details, the over-all reaction in this step will be



The catalyst acid is regenerated by step (4)



Step (2), that of proton transfer to the hydrocarbon, is the important one as far as the catalyst acid is concerned if we can assume equilibrium in the adsorption steps. The equilibrium constant of this step, K , is a measure of the strength of the acid, when working with a given base (hydrocarbon). K will have a temperature-dependency of the form

$$K = Fe^{-H/RT} \quad (5)$$

where F is a constant containing the entropy of interaction, H is the heat of reaction. Since entropies of interaction between a given base and a series of acids tend to be constant, the heat of interaction is a measure of acid strength.

In carbonium ion chemistry the formation of the catalyst complex has never been found to be the rate-determining step. The rate-determining reaction will then be steps (3), with the rate given by

$$\text{Rate} = k(\text{protonated TBB}) \quad (6)$$

Since

$$K = \frac{(\text{Protonated TBB})}{B_0} \quad (7)$$

Then

$$\text{Rate} = kB_0K \quad (8)$$

where B_0 = number of sites. This is essentially the equation proposed by Prater and Lago except that the interaction-equilibrium constant, K , has replaced their adsorption-equilibrium expression. Since

$$k = De^{-E/RT} \quad (9)$$

where D contains the entropy of activation and E is the energy of activation

(17) D. R. Mey, K. W. Saunders, E. L. Kropa and J. K. Dixon, *Disc. Faraday Soc.*, **8**, 290 (1950).

(18) C. D. Prater and R. M. Lago, *Advances in Catalysis*, **VIII**, 293 (1956).

$$\text{Rate} = B_0DFe^{-(E+H)/RT} \quad (10)$$

The observed activation energy, E_a , will then be $E+H$. E_a is obtained from the slopes of log rate vs. $1/T$ plots, log A from the intercepts, where A is the pre-exponential factor, B_0DF . If it can be assumed that the entropy factors are constant, then variations in A are due only to B_0 , the number of acid sites. Since E will probably be the same for all catalysts, differences in E_a will represent differences in H , or acid strength of the surface sites.

III. Experimental and Data Analysis

A. Equipment and Procedure.—The measurements are obtained in a differential reactor, that is, at low conversions and high space velocities. The advantage of a differential reactor system is that kinetic data can be obtained with a single run, since conversions are so low that composition of the vapor is relatively unchanged; in an integral reactor, composition changes through the bed, so that runs at several space velocities must be made to obtain kinetic data.

In a differential reactor system one measures the rate of formation of product, not the degree of conversion. The observed rates equal the rate constants of the reaction. The present equipment is suitable for a reaction which produces a gaseous product from a liquid; the rate of gas production is measured. Whereas it was desired to hold conversions at the 1% level, in actuality some catalysts (e.g., silica-alumina) were so active that even with 50 mg. of catalyst and TBB flow rates of 5 ml./min. conversions approaching 10% were obtained. However, this level does not markedly affect the results.

The apparatus as depicted in Fig. 1. 50–500 mg. of catalyst, ground to pass 250 mesh, are placed in the reactor at the tip of the thermowell, supported by a small quantity of glass wool. Tubular alumina is placed above the catalyst, to serve as preheat; no reaction is observed over tubular alumina in the absence of catalyst, below 500°. The reactor is surrounded by a fluidized sand-bath, to minimize temperature gradients, the whole being placed in a 2" Hoskins furnace, controlled by a Gardsman temperature controller. Catalyst samples are prepared for testing by drying the ground and sieved catalyst in flowing dry air, 3 hours at 565°; they are then stored in a desiccator until ready for use.

After charging the system with catalyst, the latter is dried *in situ* with flowing dry N_2 , either 1 hour at 482° or 12 hours at 565°; no differences in activity resulted from the two types of drying, as the data plots demonstrate. The nitrogen also serves the purpose of flushing air from the system before starting hydrocarbon flow.

The catalyst is then cooled to the appropriate temperature, N_2 flow stopped, and TBB flow started, normally at 5.0 ml. liquid/min.; some runs at 4.0 ml./min. were made. A Corson-Cervený bellows pump is used to feed the TBB. A 5–10° drop in temperature will be observed, due to vaporization, before the temperature is lined out. The reactor effluent passes through a helical cooler held at 190–200° by means of an external winding, thence to the U-tube used for the liquid-gas separation. The latter is held at, or close to, the boiling point of TBB (179°), to minimize solution of isobutylene in the liquid; control of this temperature is very critical to precision of the data, since too low a temperature will permit isobutylene to remain in the liquid, while at too high a temperature the constant-level liquid seal will not be maintained. Liquid overflowing the U-tube drains off in one direction, to be re-purified later, while the gas passes in the other direction through a condenser to remove benzene, thence to the buret where it is collected over water. Rate measurements are made using a stopwatch to time the evolution of a measured volume of gas. Gas volumes are corrected to standard conditions, and the rates expressed as cc.(STP)/g./min. It is assumed that the gas is 100% isobutylene. Periodic mass spectrographic analyses show its concentration always to be greater than 96–97%, a difference less than other experimental errors.

As shown in the drawing, provision is made for the addition of water at very low flow rates, by means of an Aminco Compensator. This consists of a motor-driven ground-glass

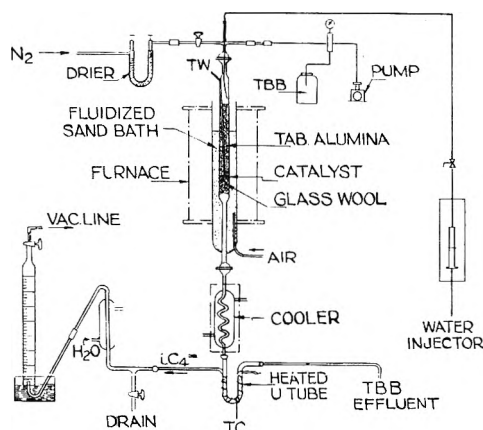


Fig. 1.—Differential reactor system for *t*-butylbenzene dealkylation.

syringe, with graduations, connected to the reactor by means of hypodermic tubing which passes through a rubber stopper into the top of the reactor; the end of this tubing contacts the wall of the reactor, to avoid surges due to drop formation at the tip. Water rates from 0.8–12.1 ml./hr. are obtained, by varying the size of the syringe and the gear ratio of the motor. To avoid excess ebullition in the U-tube when using water, excess water is removed periodically through the drain stopcock.

Normally, rate measurements on the same charge of catalyst, at the same temperature, are made with varying water rates; some runs were made starting dry, then going to different water rates, while for others the reverse procedure was used. It cannot be stated for certain whether the previous water history has an effect on the rate at a given water level. In practice, all data for a given catalyst at a given water level are grouped.

The dealkylation reaction is unique among cracking reactions in that activity usually does not decline with time due to coke; this has been discussed earlier. After an initial period of high activity the rate becomes constant for at least an hour or so. Our practice has been to take four to six rate measurements over a period of 30–60 min., and average the results. This serves the purpose of checking on constancy. Certain catalysts will rapidly lose activity when run in the absence of added water, as will be discussed later.

As a simple means of obtaining data as a function of temperature, it was first thought to make rate measurements at successively higher temperatures with a single catalyst charge. However, not only was the reproducibility very poor, but rates at the higher temperatures were lower than for a series in which separate charges of catalyst were used for each temperature. All data reported here were obtained by using fresh catalyst for each run at a single temperature. Temperature was varied from 260 to 500°, with most data in the 300–450° range.

TBB is obtained as the Pure Grade from Phillips, and is further purified by refluxing with liquid sodium, and distilling at atmospheric pressure, discarding 5% at either end; just prior to use it is passed through a column of F-20 alumina. Reactor effluent, containing perhaps 5% benzene, is recovered for further use by distillation at sub-atmospheric pressure in a 2" Stedman column, at 21/1 reflux ratio; this also is passed through an alumina column just prior to use. Chromatographic analyses of the purified materials indicate a purity of at least 99.95%.

B. Treatment of Data and Error Analysis.—The errors in these measurements are such that it is difficult to distinguish small differences between catalysts or between water vapor levels by comparing single runs, but even relatively small changes in activity due to changing water levels can be observed in a single run. The chief source of error is probably the liquid-gas separation; 0.1 mole % isobutylene in the effluent leads to an error of 15 to 150 cc. (STP)/g./min., depending on catalyst weight. At one time, small differences in the state of hydration were felt to be responsible; this was ruled out by the observation that wide variations in the severity of the *in situ* pretreat seem to have no effect.

The data for each water level and each catalyst were fitted to an Arrhenius equation ($\log \text{rate vs. } 1/T$) by least squares. This calculation provides values for E_a , $\log A$, and for the standard deviations of E_a , $\log A$ and of $\log \text{rate}$. (The standard deviation of the observed rates from the least squares line has no meaning, since rates in a given set vary over a 50-fold range.) The standard deviations correspond to variations in the rates which average about 35%.

C. Catalysts.—A listing of the catalysts used for this work may be found in Table I, together with some of their properties. Surface areas and pore volumes were obtained from nitrogen adsorption-desorption isotherms; by application of a modified Barrett-Joyner-Halenda calculation¹⁹ the desorption isotherms were converted to pore volume distributions, from which the positions of the peaks were taken as the most probable pore radii. One may note the fairly good agreement between this value and that of the average calculated from area and pore volume.

TABLE I
CATALYST PROPERTIES

Catalyst	Area (m. ² /g.)	Pore volume (cc./g.)	Pore radius, A. Av. ^a	Most Probable ^b	<i>n</i> -Butylamine titration ^c (meq./g.)
Nalcat Si-Al:HA	385	0.87	45	52	0.45
Nalcat Si-Al:LA	637	.80	25	25	.30
Aerocat Si-Al:LA	67644
Nalcat 0783-mixed base	266	.72	54	60	.265
Clay-K	134	.30	45	(Broad)	.16
Boria-alumina	39474
Silica-magnesia, XDA-30	599	.535	18	22	.69
Silica-alumina-zirconia	442	.73	33	33	.25
Clay-M	330	.41	25	(Broad)	.175

^a Calculated as $2 \times (\text{pore volume/area}) \times 10^4$. ^b Corresponding to peak position in pore volume distribution. ^c Cf. ref. 3.

Also shown are the values obtained by *n*-butylamine titration following the technique of Benesi.³ For the silica-aluminas, silica-zirconia-alumina, and boria-alumina, the titer was nearly independent of indicator *pK*; for the rest, the titer listed was that corresponding to the most basic indicator, that of *pK* = 4.0.

Most of the catalysts are commercially available, as indicated in Tables I and II. HA refers to high-alumina (nominally 25%), LA to low-alumina (12–13%). Clay-K and Clay-M are kaolinite- and montmorillonite-based catalysts, respectively, received from the Filtrol Corporation.

The boria-alumina was prepared by precipitating sodium borate with aluminum sulfate, washing, drying, calcining at 560°; it contains 10% B₂O₃. Silica-alumina-zirconia was prepared from a silica hydrogel, by adding a solution of zirconyl nitrate and aluminum chloride, then ammonium hydroxide, washing free of chloride, drying, calcining at 560°. It contains 7.25% ZrO₂ and 3.35% Al₂O₃. Fluoride-aluminas were prepared from calcined aluminas prepared by precipitation from the chloride by impregnation with ammonium fluoride solutions and subsequent calcination.

IV. Results

The complete data for HA silica-alumina (Si-Al) and for silica-magnesia (Si-Mg) are shown in Figs. 2 and 3, respectively, as typical examples; similar plots were used for the other catalysts. The same results are obtained whether the *in situ* pretreatments were carried out at 482° or at 565°. Table II summarizes the results of the least-squares analyses of all the data, including rates at the arbitrarily chosen temperature of 455°.

(19) A. Wheeler, "Catalysis," Vol. II, ed. by P. H. Emmett, Reinhold Publ. Corp., New York, N. Y., 1955, p. 105.

TABLE II

Catalyst	Mole % H ₂ O	No. of exptl. points	Reaction rate ^a		Pre-exp term, log A		Activation energy ^b	
			L.S. Value at 455°	Std. dev. log rate	Value	Std. dev.	Value	Std. dev.
Nalcat Si-Al-HA	0	18	1550	0.099	7.40	0.24	14.0	0.7
Nalcat Si-Al-HA	6	12	2060	.079	7.87	0.27	15.2	0.8
Nalcat Si-Al-HA	15	4	1980	(.09)	8.2	(0.5)	16.2	(1.5)
Nalcat Si-Al-HA	18	3	990	(.17)	8.7	(1.4)	19.0	(4.0)
Nalcat Ai-Al-LA	0	6	1600	.20	8.72	0.99	18.4	2.9
Nalcat Si-Al-LA	6	6	1700	.17	8.49	.82	17.5	2.4
Nalcat Si-Al-LA	15	6	1800	.11	8.26	.54	16.7	1.6
Aerocat Si-Al-LA	0	9	1750	.17	7.61	.65	14.6	1.9
Nalcat #0783—mixed base	0	4	740	(.052)	6.6	(.48)	12.3	(1.5)
Nalcat #0783—mixed base	6	6	760	.13	7.98	.65	17.0	2.0
Nalcat #0783—mixed base	15	6	760	.098	8.14	.49	17.4	1.5
Clay-K	0	12	440	.17	7.17	.49	15.1	1.4
Clay-K	6	10	410	.17	6.77	.64	13.8	1.9
Clay-K	15	11	490	.18	7.53	.53	16.1	1.5
Boria-alumina	0	5	216	.093	7.18	.55	16.1	1.7
Silica-magnesia	0	20	67	.16	5.84	.33	13.4	1.0
Silica-magnesia	2	5	90	.072	5.62	.59	12.2	1.9
Silica-magnesia	6	10	127	.11	6.62	.31	15.0	0.9
Silica-magnesia	15	5	175	.067	6.98	.31	15.8	0.9
Silica-magnesia	18	4	87	(.05)	7.2	(.4)	17.5	(1.3)
Silica-alumina-zirconia	0	6	171	.071	6.54	.34	14.4	1.0
Silica-alumina-zirconia	6	6	148	.048	6.59	.23	14.7	0.7
Silica-alumina-zirconia	15	6	172	.060	7.15	.29	16.4	0.9
Clay-M	0	18	74	.13	5.02	.27	10.5	0.8
Clay-M	6	17	96	.15	5.15	.36	10.5	1.1
Clay-M	15	15	107	.15	5.60	.40	11.9	1.2
Clay-M	26	5	100	.080	4.96	.39	9.8	1.2

^a Cc. (STP)/g./min. ^b Kcal./mole.

With the exception of that for Clay-M, the activation energies are approximately the same for all catalysts; this is particularly apparent when comparisons are made a constant water level, such as 15%. There appears to be a tendency for the activation energy to increase slightly with increasing moisture; at the same time, log *A* increases. For any given catalyst, a plot of E_a vs. log *A* is approximately linear, an example of the so-called "compensation effect."²⁰

Reaction rates themselves provide a better means of rating catalysts in this case than considerations of the kinetic factors, since small changes in *E* or log *A* may markedly affect the rates. On this basis the order of decreasing activity is: silica-alumina, mixed-base, Clay-K, boria-alumina, silica-aluminum-zirconia, silica-magnesia, Clay-M. This agrees with the ratings observed by cumene dealkylation for some of these by Swegler, *et al.*²¹ Water has little effect on silica-alumina activity until the 15% level is reached, beyond which further water lowers activity. No effect is apparent for Clay-K, mixed base, or silica-alumina-zirconia, although experiments beyond 15% water were not carried out. There is apparently a definite although small effect of water on the activity of Clay-M which increases with increasing water to a constant level. The effect is much more pronounced with silica-magnesia for which a twofold increase in

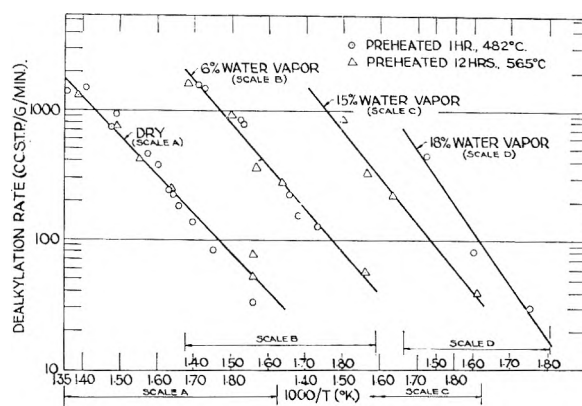


Fig. 2.—*t*-Butylbenzene dealkylation NALCAT HA, Si-Al, 25% Al₂O₃.

activity was observed on going from 0 to 15% water; again, at the 18% level there was a definite decrease. For both of these catalysts the increase in activity on going from no water to a given water level was more apparent during a given run than is the comparison of the correlated data from a number of runs. This is because in any given run the variations in rates during the run were less than the variations between runs. Not shown is the effect of water on boria-alumina, since a marked decrease in activity, due to boria removal, was observed.

Another effect of water should be mentioned which is not apparent from the data as presented. That is, for the two catalysts for which water is

(20) E. Creiner, *Advances in Catalysis*, VII, 75 (1955).

(21) F. W. Swegler, R. L. Golden, R. M. Lago, C. D. Prater and P. B. Weisz, A.C.S. Meeting, Petroleum Division, April, 1956.

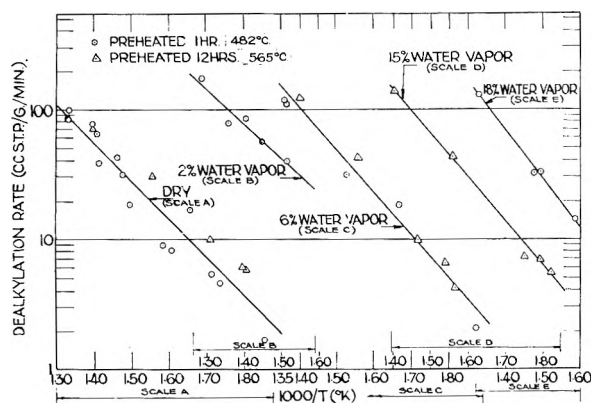


Fig. 3.—*t*-Butylbenzene dialkylation XDA-30 Si-Mg.

found to promote the reaction, namely, silica-magnesia and Clay-M, it was frequently observed when running in the absence of water that the activity was falling, to a much greater extent than with the other catalysts. This effect was not observed in the presence of water. It is possible, therefore, that gradual dehydration of the catalysts during processing is responsible for activity loss.

Alumina is at best only slightly active for dealkylation. In the presence of water, transient rates as high as 10 cc.(STP)/g./min. at 455° were obtained using a pure alumina prepared by precipitation from aluminum chloride. Another alumina, prepared by aluminum isopropoxide hydrolysis, produced similar results.

Just as addition of silica or boria to alumina produces catalytic acidity, so does the addition of fluoride ion, although for different reasons. Dealkylation activity increases approximately in proportion to the amount of fluoride added. However, this activity declines quite rapidly, in contrast to the constancy observed for the other catalysts, hence the data are not shown. The addition of water accelerates the decline in activity, by removal of fluoride; a similar situation was observed in the boria-alumina system.

V. Discussion

It seems perfectly clear from the fact that these catalysts possess dealkylation activity that Brønsted acids of some sort must exist on the surfaces of each. If the severity of drying prior to each run were to be increased markedly to drive off firmly bound water no doubt the activity would decrease. The fact that in most cases the prior treatment with reasonably dry nitrogen failed to reduce activity indicates that these sites are quite stable. If one accepts the Tamele view of silica-alumina that Brønsted acids are hydrated Lewis acids, then the

water of hydration is very firmly bound; this is not too surprising. Additional evidence for this strong binding may perhaps be the observation that high partial pressures of water failed to increase dealkylation activity of silica-alumina or Clay-K; otherwise less strongly bound hydrates would have to be postulated.

The differences in activity among the various catalysts may be ascribed to differences in the pre-exponential factor and not to the activation energy, except for Clay-M. Hence, it is most probable that B_0 , the number of sites per gram, is the factor responsible for the different activities. Prater and Lago¹⁸ have as a matter of fact calculated a value of B_0 from cumene dealkylation data, using absolute reaction rate theory, which is in agreement with values obtained by quinoline adsorption.

Clay-M is known to require water during catalytic cracking for best performance. Silica-magnesia is known to be a material which is readily dehydrated and hydrated. Hence it is not too unexpected that one should observe an effect of moisture on the Brønsted acid activity of these catalysts. It is not necessary to postulate, however, that Lewis acids are formed upon dehydration unless demonstrated by actual experiment, such as has been done for silica-alumina⁹; rather, one can only say at this point that Brønsted acid sites are lost upon dehydration. The water of hydration in silica-magnesia is less firmly bound than in silica-alumina.

An alternative way of expressing the effect of water is to consider that the rates observed are the results of both the $\log A$ and the E_a terms. Since both of these tend to increase somewhat with increasing water concentrations, whether or not a change in reaction rate occurs depends upon how well these opposing effects balance. Thus, they balance very well in the case of silica-alumina until an excess degree of hydration is reached, but not as well with silica-magnesia for which an increased activity is observed, again until overhydration occurs. According to this picture, the presence of water vapor will cause the creation of more sites upon adsorption, but these sites will be weaker than the majority of sites already present.

It should be noted that there is no correlation among the various types of catalyst between dealkylation activity and *n*-butylamine titer. Hence these techniques measure different aspects of catalyst surfaces.

Acknowledgments.—The authors are grateful to Dr. M. L. Bender, Dr. O. H. Thomas and Dr. S. H. Bauer for helpful discussions, to Mr. R. D. Duncan for preparation of the figures, and to Sinclair Research, Inc., for permission to publish this paper.

SOME ASPECTS OF MOLECULAR EFFUSION

BY E. W. BALSON

*Department of Chemistry, University of Southampton, Southampton, England**Received December 17, 1960*

Methods used originally by Clausing to compute the chance of outflow at low pressure through cylindrical outlets have been extended and generalized in order to deal with the chance of outflow through a conical orifice, the question of molecular flow through a sharp pipe bend, and the over-all chance that a molecule shall effuse in a typical set-up for measuring vapor pressures by the Knudsen effusion-weight loss method. Values of the chance of outflow in some typical instances are listed.

Although the Knudsen effusion method for measuring low vapor pressures has been much used in the past, it is only comparatively recently that particular attention has been focussed on the consistent errors with which it is always associated. Under ideal conditions, the saturated vapor in an enclosure effuses out through a perfect hole into a space where the pressure of vapor is zero, the vapor pressure then being calculated from the area of the effusion outlet and the rate of weight loss.

In practice, the effusion outlet usually takes the form of a short cylinder, though occasionally outlets of conical form have been employed. Values for the chance of outflow for cylindrical holes of various length to radius ratios have been computed by Clausing,¹ but the case of the conical outlet does not appear to have been treated.

This paper describes a generalization of the methods used by Clausing which can be used to deal completely with the problem of effusion from a cylindrical container with a small axial effusion hole, a matter which has received attention recently from Whitman,² who describes an approximate treatment of the problem which is most likely to be in error as the area of the effusion hole is made smaller, relatively, and the vapor within approaches saturation. A somewhat similar treatment has been described by Motzfeldt,³ which includes a practical solution to the problem.

It has proved possible to deal not only with the above problem, but also to treat the problem of molecular flow through a conical outlet, and to examine the flow through a sharp pipe bend.

Matters will be dealt with in the reverse order to that given above, the question of the pipe bend being discussed initially, since in this instance the operations can be dealt with in a concise way.

Preliminary Discussion.—As in the treatment of Clausing, the function $WSS(x)$ is defined as the chance that a molecule passes through a circular disc of radius R and enters another similar disc at distance x , without collision with other molecules or surfaces.

Figure 1 shows the coaxial discs S enclosed by the spherical surface $ABCDEF$. The chance $WSS(x)$ is given directly by the ratio of the spherical surface ABC to that of $ABCDEF$ provided that the cosine law for emission of molecules applies, for when this is so, molecules emitted through the plane ED from surface DEF land evenly over the remainder of the spherical surface.

In terms of the dimensions x , and R

$$WSS(x) = 1 + x^2/2R^2 - (x/2R^2)(x^2 + 4R^2)^{1/2}$$

The chance of direct motion from a disc S on to a ring of width dx and radius R distant x from S , is $WSR(x)$, and is given by

$$WSR(x) = -\frac{d}{dx} [WSS(x)]$$

and is related to the chance of motion in the opposite direction, $WRS(x)$, by

$$R^2 WSR(x) = 2R WRS(x) dx$$

since in a closed system the rate of passage from ring to disc must equal that from disc to ring.

Finally, the chance of direct motion from one ring of radius R and width dx , to a similar ring at distance x , $WRR(x)$, is given by

$$WRR(x) = -\frac{d}{dx} [WRS(x)]$$

Molecular Flow through a Sharp Pipe Bend.—

The relation for $WSS(x)$ in terms of x and R will apply equally well if the surfaces S are not coaxial, and they might well be disposed as in Fig. 2, where they meet at an angle θ , such that $\tan \theta/2 = x/2R$.

Hence, in terms of θ

$$WSS(\theta) = \tan^2(\pi - \theta)/4 \quad (1)$$

Also

$$WSR(\theta) = -\frac{d}{d\theta} WSS(\theta) = \frac{1}{2} [\tan(\pi - \theta)/4 + \tan^3(\pi - \theta)/4] \quad (2)$$

Since the molecules which arrive at a ring defined by an angular increase $d\theta$, land on an area given by $2\pi R^2 d\theta$, then

$$2WRS(\theta)d\theta = WSR(\theta) \quad (3)$$

Figure 3 shows a sharp pipe bend of total angle θ , with one ring formed by the increment $d\psi$ at angle ψ from the exit, and two other rings which make angles of λ and μ with that at ψ .

If n is the rate at which molecules arrive per unit area at the entrance to the bend, then the rate of exit of those molecules which never collide with the walls is

$$\pi R^2 n WSS(\theta)$$

and, if n_ψ is the rate at which molecules leave unit area of a ring at ψ as shown in Fig. 3, then the rate at which they emerge from the exit is

$$2\pi R^2 n_\psi WRS(\psi) d\psi$$

and the total efflux from the pipe walls will be

$$\int_0^\theta 2\pi R^2 WRS(\psi) n_\psi d\psi = \pi R^2 \int_0^\theta n_\psi WSR(\psi) d\psi$$

(from eq. 3)

Since the ideal outflow rate would be $\pi R^2 n$ molecules sec^{-1} , then the over-all chance of outflow W_θ is given by

(1) P. Clausing, *Ann. Physik*, **12**, 961 (1932).

(2) C. I. Whitman, *J. Chem. Phys.*, **20**, 161 (1952).

(3) K. Motzfeldt, *J. Phys. Chem.*, **59**, 139 (1955).

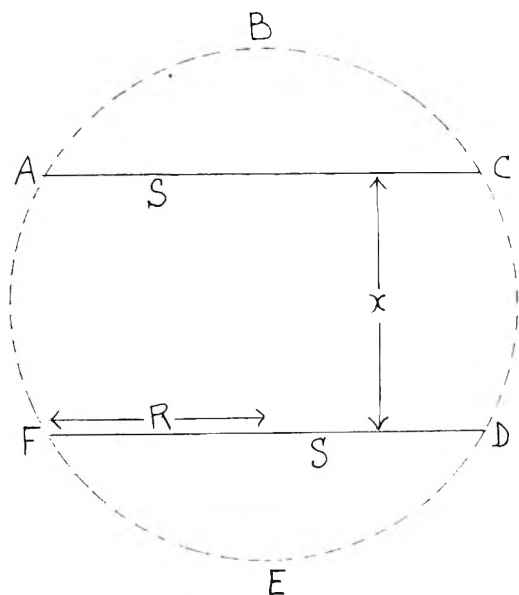


Fig. 1.

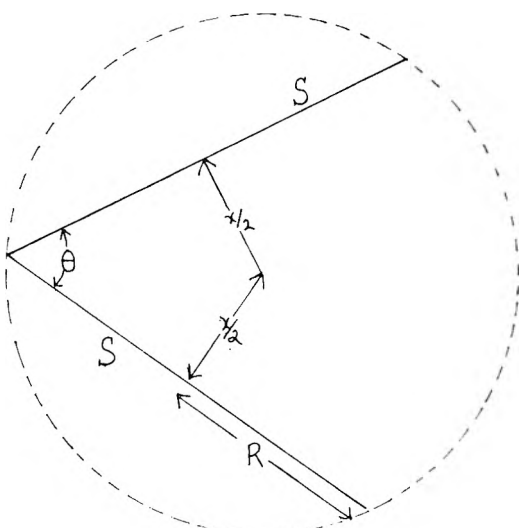


Fig. 2.

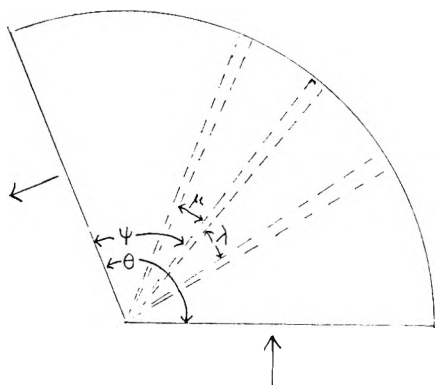


Fig. 3.

$$W_\theta = WSS(\theta) + \int_0^\theta (n_\psi/n) WSR(\psi) d\psi \quad (4)$$

so the problem reduces to finding the manner in which n_ψ/n varies along the bend.

Initially, a linear variation of n_ψ/n is tried, with the added proviso that the value of n_ψ/n at $1/2\theta$ is exactly 0.5, for it is clear from the symmetry of the problem that in a completely closed system the arrival rates at a central ring will be equal from both sides, not only for those molecules which arrive directly from the ends; with one end open, the arrival rate is then halved.

For this reason, the tentative relation

$$n_\psi/n = 1/2 - 1/2b + b(\psi/\theta) \quad (5)$$

is assumed, and its validity then is checked as shown below.

The rate at which molecules arrive at a ring of area $2\pi R^2 d\psi$ at angle ψ , is composed of four terms

$$\begin{aligned} &\pi R^2 n WSR(\theta - \psi) && \text{from below} \\ &\int_0^\psi 2\pi R^2 n_{\psi-\mu} WRR(\mu) d\mu && \text{from rings between 0 and } \psi \\ &\int_0^{\theta-\psi} 2\pi R^2 n_{\psi+\lambda} WRR(\lambda) d\lambda && \text{from rings between } \psi \text{ and } \theta \end{aligned}$$

This combined arrival rate must equal that of emission, $2\pi R^2 n_\psi d\psi$, so that

$$n_\psi/n = WRS(\theta - \psi) + \int_0^\psi (n_{\psi-\mu}/n) WRR(\mu) d\mu + \int_0^{\theta-\psi} (n_{\psi+\lambda}/n) WRR(\lambda) d\lambda \quad (6)$$

After inserting the value of n_ψ/n from (5) into (6) and integrating, it is found that the right-hand side exceeds n_ψ/n by E_ψ , where

$$2E_\psi = WRS(\theta - \psi) - WRS(\psi) + b\{WRS(\psi) - WRS(\theta - \psi) + (1/\theta)\{WSS(\psi) - WSS(\theta - \psi)\}\} \quad (7)$$

Inspection of (7) shows that E_ψ always vanishes when $\psi = 1/2\theta$ and the values of the coefficients in (7) are also symmetrical about this point.

For this reason some five values of ψ are chosen in the interval up to $1/2\theta$ and the coefficients of the terms on the right-hand side of (7) computed, to give five equations, for which a value of b which minimizes E_ψ is found by the method of least squares.

Table I below shows the results for such an operation for a right angle bend.

TABLE I

TEST OF INTEGRAL EQUATION 6: VALIDITY OF EQUATION 5
Bend angle, 90°; $b = 0.41519$ (eq. 7)

ψ (degrees)	0	10	20	30	40
n_ψ/n	0.2924	0.3385	0.3846	0.4307	0.4769
E_ψ	-0.0012	+0.0005	+0.0011	+0.0009	+0.0003

The table shows that the tentative relation (5) expressing the variation of n_ψ/n is quite adequate, for the values of E_ψ never exceed about 0.3% of n_ψ/n at any point.

By insertion of the value of b , computed from equation 7, into (5), which in turn is combined with (4) gives by integration

$$W_\theta = 1/2(1 - b)\sec^2(\pi - \theta)/4 + (4b/\theta)[1 - \tan(\pi - \theta)/4] - b \quad (8)$$

Table II lists values of W_θ obtained in this way, together with values of W for straight tubes obtained by graphical interpolation from the values given by Clausius, assuming that the bend has been

straightened out to give a tube of length to radius ratio of θ .

TABLE II

CHANCE OF OUTFLOW FROM A TUBE BEND

Bend angle (θ , deg.)	30	60	90	120	150	180
W_θ (eq. 8)	0.7919	0.6497	0.5467	0.4688	0.4089	0.3629
W (Claus- ing)	0.792	0.651	0.570	0.502	0.451	0.410

The values listed support broadly the contention that the insertion of a bend into a low pressure line has little effect on the resistance to pumping, for it is seen that for bends up to 90° , replacement of the bend by its equivalent straightened length scarcely alters the chance of outflow, though for bends of a larger angle there appears to be a comparatively small increase in resistance to flow, as compared to a straight length.

Effusion from a Conical Outlet.—An approximate solution to the problem of effusion from a conical outlet can be derived simply by using the chance function $WSS(x)$ mentioned at the outset. Figure 4 shows an arrangement where the conical outlet of semi-angle β , entrance radius r , exit radius R , and length L , drawn in full line, is enveloped by the spherical surface drawn in broken line, the latter being then divided into three zones of areas A , B and C , respectively.

The approximate solution is then derived by replacing the conical outlet by the portion B of the spherical surface which it closely resembles, particularly when the outlet is short.

The whole chance of emergence is composed of two portions, for a molecule may emerge after collision with the wall, or may emerge as part of a beam, without wall collision. The latter chance W_b is given directly by

$$W_b = C/(B + C)$$

and the former, W_w , by

$$W_w = \frac{B}{(B + C)} \frac{C}{(A + C)}$$

where the first term in the product is the chance of landing on the wall, and the second, the chance that a molecule on the wall shall emerge through C . The whole chance of emergence W_Δ , is then given by

$$W_\Delta = W_b + W_w = \frac{C}{B + C} \times \frac{A + B + C}{A + C} \quad (9)$$

W_Δ is best represented in terms of the two angles θ and ψ shown in Fig. 4 and is then given by

$$W_\Delta = \frac{(1 + \cos \theta)}{(1 + \cos \psi)(2 - \cos \psi + \cos \theta)} \quad (10)$$

where

$$\cot \psi = \tan \beta + (L/2r)(1 + \tan^2 \beta) = (R^2 + L^2 - r^2)/2rL$$

$$\tan \theta = \frac{1 + (L/r) \tan \beta}{\tan \beta + (L/2r)(\tan^2 \beta - 1)} = 2LR/(R^2 - L^2 - r^2)$$

It remains to discover the limits of applicability of the approximate equations 9 and 10, and for this reason a more thorough analysis of the position has been undertaken using methods similar to those described in the previous section, for the case where the semi-angle of the cone is 45° , since here a considerable simplification of the mathematics is possi-

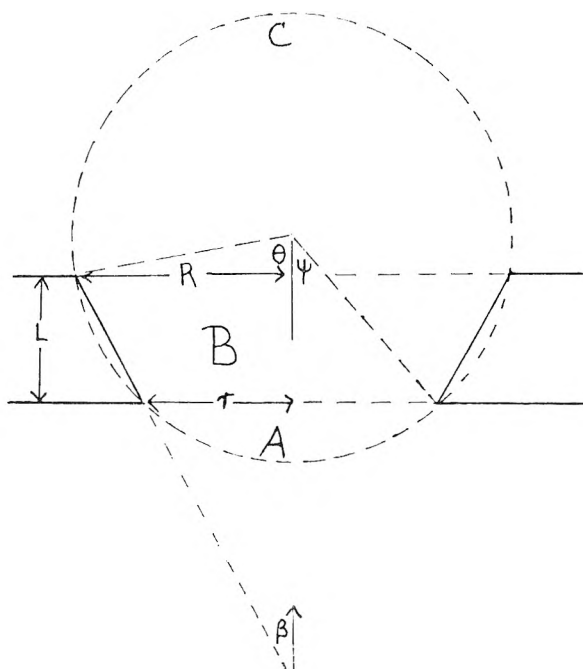


Fig. 4.

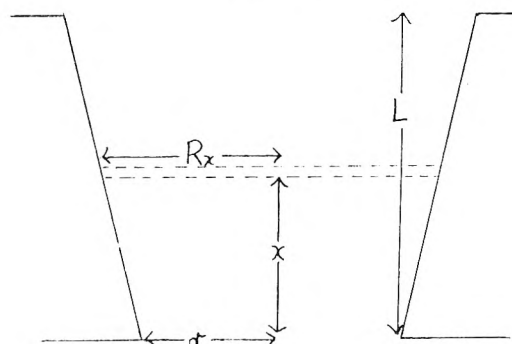


Fig. 5.

ble; a semi-angle of 45° is assumed in the discussion which follows.

The function $WSS(x)$ already noted can be modified to the form $WSS_s(x)$ the chance of direct motion downwards from the larger disc S of radius R , to the smaller coaxial disc s of radius r , at distance x , as shown in Fig. 5

In terms of R , r and x

$$WSS_s(x) = \frac{(R^2 + r^2 + x^2)/2R^2 - (1/2R^2)[(R^2 - x^2 - r^2)^2 + 4x^2R^2]^{1/2}}{(11)}$$

In the case of the outlet with the 45° cone

$$R = r + x$$

and as before

$$-\frac{d}{dx} WsS(x) = WsR(x)$$

but the molecules landing on the ring defined by the increment in axial distance dx , in fact land on an area of $2\sqrt{2}\pi(r+x)dx$, so that

$$r^2 WsR(x) = 2\sqrt{2}(r+x)WR_{xs}(x)dx$$

where R_x is the cone radius at distance x .

By a procedure analogous to that used in deriving equation 4 it is found that the over-all chance of

downward motion through the convergent cone W_{\triangleright} , as in Fig. 5, is given by

$$W_{\triangleright} = WSs(L) +$$

$$(1/R_L^2) \int_0^L 2\sqrt{2}(r+x)WR_{xs}(x)(n_x/n)dx$$

i.e.

$$W_{\triangleright} = (r^2/R_L^2)[1 - \int_0^L WSr_x(x)(1 - n_x/n)dx] \quad (12)$$

Since the value of the emission rate per unit area n_x , at distance x along the wall of the outlet cannot be much less than the corresponding value n , at the entrance to the cone, then the final integral in (12) is quite small and can be evaluated graphically without serious error.

From Fig. 5 it is seen that the arrival rate of $2\sqrt{2}\pi(r+x)n_x dx$ molecules sec.⁻¹ at the ring at distance x , is composed of arrivals from the upper entrance, from the series of rings y , between 0 and x and the series z , between x and L . Consequently,

$$n_x/n = W_{rx}S_L(L-x) + \int_0^x WR_x r_{x-y}(y)(n_{x-y}/n)dy + \int_0^{L-x} W_{rx}R_{x+z}(z)(n_{x+z}/n)dz$$

and assuming the relation

$$n_x/n = a + bx + cx^2 \quad (13)$$

for the variation of n_x/n along the outlet walls, inserting into the integral equation above, and rearranging, it is found that the right hand side exceeds n_x/n by the amount E_x , where

$$E_x = W_{rx}S_L(L-x) - a \left[1 - \int_0^x WR_x r_{x-y}(y)dy - \int_0^{L-x} W_{rx}R_{x+z}(z)dz \right] - b \left[x - \int_0^x WR_x r_{x-y}(y)(x-y)dy - \int_0^{L-x} W_{rx}R_{x+z}(z)(x+z)dz \right] - c \left[x^2 - \int_0^x WR_x r_{x-y}(y)(x-y)^2dy - \int_0^{L-x} W_{rx}R_{x+z}(z)(x+z)^2dz \right]$$

which may be put into the form

$$E_x = K_x + aA_x + bB_x + cC_x \quad (14)$$

After graphical integration of the terms in the equation above at from four to six points along the cone, values of a , b , and c are computed to minimize E_x in equation 14 above.

When $L = 0.8$, and with five points along the outlet for which $x = 0.0, 0.2, 0.4, 0.6$ and 0.8 unit, respectively, the values of E_x are $-0.0007, +0.0052, -0.0002, +0.0022$ and -0.0009 unit, respectively, thus showing that equation 13 for n_x/n affords quite an accurate estimation of the position. The values of the constants a , b and c , in this case are $0.8388, 0.3755$ and -0.2814 , respectively.

Recalling that the chance of downward motion through the convergent cone W_{\triangleright} and the chance of upward motion W_{\triangleleft} are connected by

$$r^2 W_{\triangleleft} = R L^2 W_{\triangleright}$$

and with the help of equations 12 and 13, it is found that

$$W_{\triangleleft} = 1 - \int_0^L WSr_x(1 - a - bx - cx^2)dx \quad (15)$$

Table III shows values of W_{\triangleleft} computed from the more exact equation 15, and from the approximate equation 10, together with those listed by Clausing (W), which refer to a cone angle of zero.

TABLE III
CHANCE OF EMERGENCE W_{\triangleleft} FROM A DIVERGENT CONICAL OUTLET

L/r	W_{\triangleleft} (eq. 10)	W_{\triangleleft} (eq. 15)	W (Clausing)
0.2	0.9910	0.9902	0.9092
.4	.9865	.9862	.8341
.6	.9845	.9840	.7711
.8	.9838	.9828	.7177
1.0	.9838	.9783	.6720
2.0	.9866	.9720	.5136
3.0	.9913	.9662	.4205
4.0	.9937	.9609	.3589

It will be noted that the values of W_{\triangleleft} remain quite high even at comparatively large values of L/r , particularly when compared with those for cylindrical outlets.

It is concluded that the simple approximate procedure for the computation of W_{\triangleleft} using equation 10 is quite adequate when the cone angle is 45° or greater, and the length to radius ratio no greater than unity, for the approximation becomes more exact as the cone angle is increased.

Although conical effusion outlets have been used in several instances, it is rare to find their dimensions quoted, as is the case with a determination of the vapor pressure of rhenium silicides by Searcy and McNees,⁴ who used one cylindrical and three conical outlets having the dimensions shown in Table IV.

TABLE IV
DIMENSIONS OF EFFUSION OUTLETS
(Searcy and McNees), (Dimensions in mm.)

L	1.85	1.10	2.00	3.71
r	0.94	1.635	2.36	2.125
R	3.39	2.855	4.59	2.125
β (deg.)	53	48	48	0
L/r	1.97	0.67	0.85	1.74
W_{\triangleleft}	0.995	0.987	0.987	...
W	0.510	0.752	0.706	0.546

In the table, L is the length of the outlet, r , the (smaller) entrance radius, and R the outlet radius.

Values of W_{\triangleleft} are computed from equation 10, while those for W are interpolated from values listed by Clausing for cylindrical tubes with the values of L/r shown.

With $ReSi_2$ all three conical holes were used and were assumed perfect ($W_{\triangleleft} = 1$) by the authors; all gave results showing very little scatter indeed when the usual plot of $\log p$ against $1/T$ was made, indicating that the values of W_{\triangleleft} for all three were very similar despite the range both in hole areas and in L/r . Results for both Re_3Si and $ReSi$ showed a fair measure of scatter; for the former, two conical outlets were used, and for the latter two conical outlets and the cylindrical outlet were employed. In

(4) A. W. Searcy and R. A. McNees, *J. Am. Chem. Soc.*, **75**, 1578 (1953).

the latter instance although some of the results obtained using the cylindrical outlet (duly corrected for W) lay within the scatter of those found for the conical forms, which amounted to about $\pm 10\%$, others were higher, particularly at the higher temperatures. They appeared less consistent among themselves, and seemed to lie on a line of slightly different slope from those obtained with the cone outlets. As a result, no critical assessment of the relative values of $W_{\bar{S}}$ and W can be made, though the high values of $W_{\bar{S}}$ for the conical outlets are to some extent confirmed.

Effusion from a Cylindrical Effusion Vessel with Small Axial Effusion Outlet.—Figure 6 shows a small perfect outlet s of radius r , at the center of the annular surface \bar{S} , at the right hand end of the cylinder of length L and radius R . A ring of width dx , at distance x from the exit hole at s , is shown. If the entry rate of molecules into S from the left is n molecules $\text{sec.}^{-1} \text{cm.}^{-2}$, and the emission rate per cm.^2 at the ring dx , at x , is n_x then the chance of outflow W_0 is given by

$$W_0 = (R^2/r^2)WSs(L) + (2R/r^2) \int_0^L (n_x/n) WRS(x)dx \quad (16)$$

for equation 11 applies here, and both r and R are constants, while

$$R^2WSs(x) = r^2WsS(x)$$

and

$$-\frac{d}{dx} [WSs(x)] = WSR(x); \quad -\frac{d}{dx} [WsS(x)] = WsR(x)$$

$$R^2WSR(x) = 2rWsR(x)dx; \quad r^2WsR(x) = 2RWRS(x)dx$$

Consequently, equation 16 can be written

$$W_0 = WsS(L) + \int_0^L WsR(x)(n_x/n)dx \quad (17)$$

If, as is usual, $S \gg s$, then n_x/n cannot be much less than unity along the entire length L , with a minimum value when x is a little smaller than $1/2L$, since $WSR(x)$ decreases quite rapidly as x increases, and \bar{S} is a little smaller than S .

The tentative relation

$$n_x/n = a + b(x/L) + c(x/L)^2 \quad (18)$$

is assumed for the variation of n_x/n along the length L , and is then checked as in the previous instance.

Before proceeding further, it will be helpful to list other chance functions and their interconnecting equations, for there are now three surfaces, S , \bar{S} and s to be considered.

$$WRS(x) = WR\bar{S}(x) + WRS(x); \quad WSS(x) = WSS(\bar{r}) + WSS(x)$$

$$R^2WSR(x) = (R^2 - r^2)W\bar{S}R(x) + r^2WsR(x)$$

$$R^2WSS(x) = (R^2 - r^2)W\bar{S}S(x) + r^2WsS(x)$$

The rate Z at which molecules arrive at \bar{S} is given by

$$Z = \pi R^2 n [WSS(L) - WsS(L)] + \int_0^L \pi n_x [R^2 WSR(x) - r^2 WsR(x)] dx$$

As a result, the ring at x receives

$$\int_0^x 2\pi R WRR(y)n_{x-y} dy$$

molecules from rings between 0 and x ,

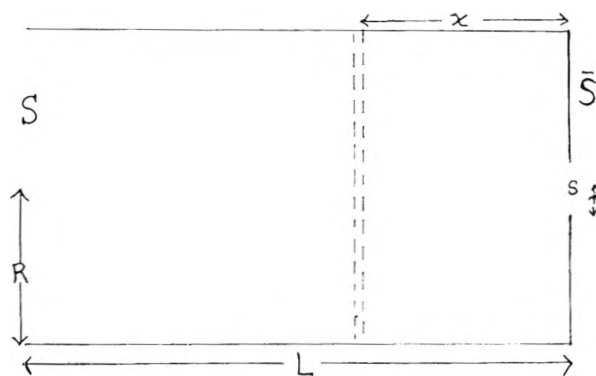


Fig. 6.

$$\int_0^{L-x} 2\pi R WRR(z)n_{x+z} dz$$

molecules from rings between x and L

$Z.W\bar{S}R(x)$ and $\pi R^2 n WSR(L-x)$ molecules from \bar{S} and S , respectively, and emits $2\pi R n_x dx$ molecules sec.^{-1} . Consequently

$$n_x/n = \int_0^x WRR(y)(n_{x-y}/n)dy + \int_0^{L-x} WRR(z)(n_{x+z}/n)dz + WRS(L-x) - [R^2/(R^2 - r^2)]\Delta WRS(x)[\Delta WSS(L) + (2/R) \int_0^L (n_x/n)WRS(x)dx] \quad (19)$$

where $\Delta WSS(L) = WSS(L) - WsS(L)$, etc.

The tentative solution for n_x/n of equation 18 can now be tested by insertion in (19) above, and integrating. Most of the terms can be integrated by parts, though a few have to be dealt with graphically.

The error equation of the form

$$E_x = K_x + aA_x + bB_x + cC_x \quad (20)$$

then results, where E_x is the amount by which the right-hand side of (19) exceeds n_x/n , as given by (18).

Values of the coefficients K_x , A_x , B_x and C_x have been computed at each of eleven points equally spaced along a cylinder of length 2 and radius 1 unit, with axial effusion holes of radii 0.1, 0.2, 0.3, 0.4, 0.5 and 1 unit, respectively.

Solution of the eleven equations, by the method of least squares, for each hole size, leads to the values of a , b and c , shown in Table V, and the values of these constants, when inserted into equation 20, lead to the individual deviations D_x , and to the probable deviation D , shown in the table.

TABLE V
CONSTANTS OF EQUATION 18, FOR CYLINDER WITH $R = 1$; $L = 2$

Effusion hole (radius r)	a	Constants b	c	Probable deviation (D)
0.1	0.99562	-0.00979	0.01094	0.00126
.2	.96426	-.03244	.05233	.00167
.3	.92108	-.06804	.11250	.00378
.4	.86396	-.11030	.18816	.00661
.5	.79506	-.14500	.26465	.01029
1.0	.23851	.52914	-.01212	.00270

By combination of equation 18 with 17, it is found that

$$W_0 = a + (1 - a - b - c)WsS(L) + \int_0^L (b/L + 2cx/L^2)WsS(x)dx \quad (21)$$

The final integral in equation 21 is quite small when $R \gg r$ and can be evaluated graphically. For example, when $r/R = 0.2$, the three terms in (21) are 0.96426, 0.00315, and 0.00299, respectively.

Table VI shows values of the over-all chance W_0 computed in this way, together with those calculated from the relation developed by Whitman; the procedure of Motzfeldt leads to the same result.

TABLE VI

THE OVER-ALL CHANCE OF OUTFLOW W_0 FROM A CYLINDRICAL EFFUSION VESSEL ($R = 1$; $L = 2$) WITH SMALL AXIAL EFFUSION HOLE (r)

Hole radius (r)	0.1	0.2	0.3	0.4	0.5	1.0
W_0 (EWB)	0.96530	0.97040	0.93480	0.88906	0.83546	0.51348
W_0 (W. M)	0.99606	0.9635	0.9215	0.8685	0.8083	...

It is considered that the uncertainty in the computed values of W_0 is somewhat less than the probable deviation shown in Table V, since the constant a is the major contributor to W_0 when $R \gg r$.

The case when $R = r = 1$ corresponds to the open tube discussed by Clausing, who reports a value of 0.5136 for W_0 , in close agreement with that given above. Furthermore, the theory shows that in this instance the ratio n_x/n at half distance along the cylinder should be exactly 0.5 (cf. the pipe bend mentioned earlier).

The values of a , b and c listed in Table V give a value of 0.50004 for n_x/n at half distance.

The Outflow through a Short Cylindrical Effusion Hole.—The extension of the computations to the case when effusion takes place through a short cylindrical outlet can be made with some certainty if the molecules which enter this outlet do so uniformly over the whole of the entrance area. This is very nearly the case when $r/R = 0.1$, for here the minimum value of n_x/n along the container is 0.9934, so that conditions within are virtually those which obtain when the effusion vessel is part of a completely closed system and, when this is so, the nature and amount of flow from left to right is the same as that in the opposite direction.

The resultant chance for an effusion vessel with such an outlet will be W_0W_{1r} to a first approximation, where W_{1r} is the chance of outflow for the outlet of length l and radius r . This is, however, an underestimate, for some of the molecules which collide with the walls of the outlet return to the walls of the container and so augment the arrival rate n_x .

With a short outlet, this increase will be small and leads to a further term $W_0(1 - W_{1r})WRS(x)$ on the right-hand side of equation 19. Revised constants a' , b' and c' then lead to a more exact value for W_0' .

When this cyclic approximation is applied to the case when $R = 1$, $L = 2$, with $r = 0.1$ and $l/r = 0.5$ (a value greater than would normally be used in practice), for which W_{1r} is 0.8013, and $W_0 = 0.99530$, it is found that $W_0' = 0.99673$, and $W_0'' = 0.99670$, for two cycles. The successive values

of W_0 thus differ by little more than 0.1% even with the comparatively large value of l/r chosen, so that with this and shorter outlets the resultant chance is quite adequately represented by W_0W_{1r} .

The Influence of the Evaporation Coefficient.—Consider a plane surface of evaporating material placed across the entrance to the containing cylinder (Fig. 6), from which surface the emission rate is n molecules sec.⁻¹ cm.⁻² and the outflow rate through the ideal hole is $\pi r^2 n W_0$ molecules sec.⁻¹.

If the maximum evaporation rate is n_0 molecules sec.⁻¹ cm.⁻², and the evaporation coefficient is α , the emission rate of $\pi R^2 n$ from S is composed of $\pi R^2 n_0 \alpha$ molecules actually evaporating, together with those which arrive from the walls and from \bar{S} and fail to condense.

The arrival rate at S is

$$\int_0^L 2\pi R n_x WRS(L-x)dx + W\bar{S}(L) \left[\int_0^L 2\pi R WR\bar{S}(x)n_x dx + \pi R^2 n W\bar{S}(L) \right] = \pi R^2 n \left[\int_0^L (n_x/n) WSR(L-x)dx + W\bar{S}(L) \left\{ (W\bar{S}(L) + \int_0^L (2/R)(n_x/n) WRS(x)dx \right\} \right]$$

This we write as $\pi R^2 n G$, for brevity, where G can be computed from the relative dimensions and the calculated values of n_x/n .

The outflow rate is now

$$\frac{W_0 \pi r^2 n_0 \alpha}{1 - G(1 - \alpha)}$$

and leads to the over-all chance of outflow $W_{0,\alpha}$, where $W_{0,\alpha}/W_0$ is given by

$$W_{0,\alpha}/W_0 = \frac{\alpha}{1 - G(1 - \alpha)}$$

Now $W_{0,\alpha} \rightarrow W_0$ as $G \rightarrow 1$ and so becomes independent of α . For example, when $r/R = 0.1$, the value of α has little influence on $W_{0,\alpha}$.

In this instance n_x/n is almost unity along the entire length of the container, so that it is convenient to work in terms of $(1 - n_x/n)$ in the relation for G , which then becomes

$$G = 1 - W\bar{S}(L) - \int_0^L (1 - n_x/n) WSR(L-x)dx - \frac{R^2}{L^2 - r^2} \Delta W\bar{S}(L) \int_0^L (2/R) \times (1 - n_x/n) \Delta WRS(x)dx \quad (23)$$

The last two terms in (23) are comparatively small and can be evaluated graphically, when it is found that when r/R is 0.1, G is 0.9968, and has fallen to 0.9531 when r/R has risen to 0.2.

Table VII shows the influence of the value of α the evaporation coefficient on the ratio $W_{0,\alpha}/W_0$ in these two instances.

The table shows the slight influence of the value of the evaporation coefficient on the over-all effusion rate; reduction of α from unity to 0.5 reduces the over-all rate by only 0.3% when r/R is 0.1, and by only 3% when α is as low as 0.1. When r/R is raised to 0.2, the influence of the magnitude of α is much more pronounced. The expression deduced by Motzfeldt to cover the influence of α on the chance of outflow has been used to compute values of $W_{0,\alpha}/W_0$ shown in columns (M), for comparison.

TABLE VII

THE INFLUENCE OF THE EVAPORATION COEFFICIENT ON THE EFFUSION RATE FROM A CYLINDRICAL CONTAINER WITH SMALL EFFUSION HOLE

(Container: $R = 1, L = 2$)

Evaporation coefficient (α)	$W_0, \alpha/W_0$ $\tau/R = 0.1$		$W_0, \alpha/W_0$ $\tau/R = 0.2$	
	(EWB)	(M)	(EWB)	(M)
0.9	0.9996	0.9990	0.9948	0.9960
.8	.9992	.9975	.9884	.9905
.7	.9986	.9955	.9803	.9840
.6	.9979	.9933	.9697	.9750
.5	.9968	.9900	.9552	.9625
.4	.9952	.9850	.9342	.9460
.3	.9926	.9770	.9013	.9180
.2	.9874	.9615	.8420	.8660
.1	.9720	.9095	.7031	.7425
.01	.7463	.5050	.1767	.2076

When considering the influence of the evaporation coefficient it must be borne in mind that the evaporating surface, if that of a solid, will seldom approximate to a plane surface, and will usually consist of a layer of small crystals, loosely packed, with small irregular spaces between them. Conditions within these "irregular effusion vessels" may well be similar to those already discussed, so that the effective rate of evaporation from the "surface" will be greater than that indicated by the evaporation coefficient.

At the same time it is clear that the practice of filling the effusion vessel full of chips, crystals, or turnings, etc., in an effort to assist the saturation of the vapor within, may in some circumstances have the opposite effect to that desired, for in the limiting case, with the effusion vessel filled completely up to the effusion hole, the value of $W_0, \alpha/W_0 = \alpha$ for G is then zero, and the evaporation coefficient is exerting its maximum effect. This effect has been noted by Stern and Gregory,⁵ who report a marked diminution in the effusion rate for iodine when the effusion vessel was filled to within about 1 mm. or less from the top; substantially constant effusion rates were recorded when less iodine was used, provided that there was sufficient to cover the base of the cylindrical effusion vessel.

The Vapor Path to the Cold Trap.—It remains finally to estimate the chance that a molecule shall reach the cold trap having emerged from the effusion hole.

Since the effusion rate from the cylindrical vessel in Fig. 6 is $\pi r^2 n W_0$ molecules sec.^{-1} , while that of entry is $\pi R^2 n$, then the chance W_{LR} that a molecule travels right through from left to right is given by

$$W_{LR} = (\tau/R)^2 W_0$$

Furthermore, if the cylinder shown is part of a closed system, equal numbers of molecules must travel in the opposite direction, *i.e.*

$$R^2 W_{LR} = \tau^2 W_{RL}$$

so

$$W_0 = W_{RL}$$

where W_{RL} is the chance of motion from right to left.

(5) J. H. Stern and N. W. Gregory, *J. Phys. Chem.*, **61**, 1226 (1957).

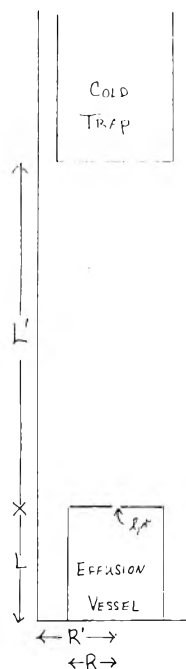


Fig. 7.

Consequently, for the experimental arrangement depicted schematically in Fig. 7, the chance that an emergent molecule shall reach the cold trap is $W_{L'R'}$ and the over-all chance W for the whole system is given by

$$W = W_0 W_{R'L'} W_{rl} \quad (24)$$

where W_0 refers to the effusion vessel, $W_{R'L'}$ to the path to the cold trap, and W_{rl} to the effusion outlet.

Of the three terms in equation 24, W_{rl} is likely to be the smallest, for with $\tau = 0.1$, $R = 1$, and $L = 2$, then l , the length of the outlet, will not be much smaller than 0.01, so that W_{rl} will be about 0.95, while $W_0 = 0.9953$, and $W_{R'L'}$ will be about 0.99 with a compact experimental arrangement.

It is not always possible to ascertain the value of $W_{R'L'}$ for in many cases the path from outlet hole to cold trap is less direct than that shown, and it is desirable that it should be so in order that there is no direct path between the cold surface and the effusion vessel; radiation of heat from vessel to trap is then prevented. However, a value for $W_{R'L'}$ can be inferred from the ratio of the straightened length of the outlet path to that of its radius, for in this section it was shown that the introduction of a bend into the path has little effect on the over-all chance of outflow.

In such cases an extrapolation method similar to that used by the author,⁶ in the case of spherical effusion vessels where the effusion recoil force was measured, could be used. In this, a value of the vapor pressure, at a constant temperature, duly corrected for the imperfection of the effusion hole, is found for each of a series of effusion vessels with outlets of varying size, in an apparatus where all of the geometry save that of the outlets is kept constant; the plot of this corrected pressure against the

(6) E. W. Balson, "Surface Phenomena in Chemistry and Biology," Pergamon Press, New York, N. Y., 1958, pp. 117-132.

area of the effusion hole, is approximately linear, for both W_0 and $W_{R'L'}$ are approximately linear functions of the hole area when the latter is small, and the intercept at zero area gives the saturation vapor pressure.

For an effusion vessel with $R = 1$ and $L = 2$, and with $R' = 2$ and $L' = 4$, then when $r = 0.1$, $W_0 = 0.9953$, while $W_{R'L'}$ will be even closer to unity, at ca. 0.999, so the combined probability will be a little more than 0.994, provided that the evaporation coefficient is not far from unity. When r is raised to 0.2, the combined probability has fallen to about 0.942, indicating that results for this orifice should lie about 5% lower than those for the former, but should the evaporation coefficient fall seriously short of unity, the difference is even greater. An extreme case has been reported by Stern and Gregory (ref. 5), who find a very low value for the evap-

oration coefficient of iodine. Several effusion vessels were used with values of r/R between 0.01 and 0.1. Despite these low values, values for the effusion rate per unit area of hole were about twice as large using the smaller holes as with the larger.

It may be concluded that an effusion cell with dimensions near to $R = 1$, $L = 2$, and $r = 0.1$, should be most satisfactory, for all of the correction terms, save perhaps that for the path to the cold trap, differ but little from unity. The use of much smaller holes is of doubtful advantage, since it is then difficult to keep the ratio of length to radius small, and to be certain of a truly cylindrical profile; the use of divergent conical holes would seem to offer some advantage here, since the value of W_0 remains high even when the length to entrance radius ratio is quite large, and the outlet need not be formed in very thin material.

HYDROGENATION OF 3,3-DIMETHYL-1,4-PENTADIENE ON NICKEL CATALYSTS. A TEST OF THE DEGREE OF DIFFUSIONAL CONTROL IN CATALYTIC HYDROGENATIONS¹

BY REMOLO CIOLA AND ROBERT L. BURWELL, JR.²

Department of Chemistry, Northwestern University, Evanston, Illinois

Received December 19, 1960

On nickel wire and on nickel-silica catalysts in the vapor phase and on nickel-silica in the liquid phase, the two double bonds of 3,3-dimethyl-1,4-pentadiene appear to hydrogenate independently. In the absence of diffusional control, 3,3-dimethylpentene is the only initial product. If substantial concentration gradients in the catalyst pores lead to diffusional control, 3,3-dimethylpentane appears as an apparent initial product and its initial ratio to dimethylpentene constitutes a measure of the degree of diffusional control introduced by hydrocarbon concentration gradients. Under the conditions employed in the vapor phase reaction, such gradients were small or negligible for oxidized nickel wire, large on 40-60 mesh nickel-silica and still larger on 20-40 mesh nickel-silica. In the liquid phase at room temperatures on 100-200 mesh nickel-silica, the concentration gradients of olefin were small but those of hydrogen appeared to introduce a serious degree of diffusional limitation. In the liquid phase, the ratio of the rate constants of hydrogenation of the diene and of the mono-ene was about 9 and the ratio of 3,3-dimethylbutene and 3,3-dimethylpentene was 1.6. On the assumption that the kinetic forms for the rates of hydrogenation of diene and mono-ene are identical, a kinetic treatment of the course of hydrogenation is derived as a function of the initial ratio of mono-ene to alkane.

In any heterogeneous catalytic reaction, reactants must diffuse to the catalyst surface and products must diffuse from it. With usual porous catalysts, two stages of diffusion may be characterized: diffusion between the bulk fluid phase of the reactant stream and the exterior surface of the catalyst particle; diffusion between the exterior surface and the interior surface through the pore structure of the catalyst particle. In gas phase reactions, the first type of diffusion is usually rapid but the second type frequently will affect over-all rates and kinetics.³

In practice, two methods of assessing the degree of diffusional control have been most commonly employed. In one, one compares reaction rates obtained with equal weights of different particle sizes of the same catalyst. The degree to which reaction rate increases with decreasing size of

catalyst particles measures the degree of diffusional control. The other involves a theoretical treatment of diffusional control often *via* the dimensionless parameter, h , of Wheeler which is a function of catalyst particle geometry, the pore volume and surface area of the catalyst, diffusion coefficients and the rate constant of the reaction.^{3a}

Quantitative application of either method requires a knowledge of the exact kinetics of the reaction. The first method is applicable only to catalysts in reproducible steady state conditions. The second method always involves some degree of uncertainty in its quantitative application because of the simplifying assumptions about pore geometry made in its derivation.

The question of the presence or absence of diffusional control continually befogs attempts at mechanistic interpretation of studies of heterogeneous catalytic reactions. It would be useful to have a simple experimental means of assessing the degree of diffusional control which was independent of particular assumptions about the nature of pore structure and which did not require determination of exact kinetics. The present

(1) This work was supported by the Air Force Office of Scientific Research and Development. Presented at the New York meeting of the American Chemical Society, September 14, 1960.

(2) To whom inquiries about this paper should be sent.

(3) For reviews of this subject see: (a) A. Wheeler, "Catalysis," edited by P. H. Emmett, Vol. 11., Chap. 2, Reinhold Publ. Corp., New York, N. Y., 1955; (b) A. Wheeler, *Advances in Catalysis*, **3**, 250 (1950); (c) E. Wicke, *Z. Elektrochem.*, **60**, 774 (1956);

paper presents a partial approach to such a procedure.

Consider a molecule A-A which contains two *identical and non-interacting* A-groups which convert catalytically to B-groups. Suppose that concentration gradients in the pores are small (diffusion is fast relative to reaction rates). At low conversions, the only apparent initial product will be A-B. If, however, concentration gradients are large (diffusion slow), a molecule of A-B formed in a pore will have a finite probability of reacting further to B-B before it escapes into the reactant stream. Thus, B-B as well as A-B will appear to be an initial product. The initial ratio of B-B to A-B diagnoses the degree of diffusional control.

This procedure is implicit in previous discussion of the effect of diffusional control upon selectivity in a reaction sequence $A \rightarrow B \rightarrow C$,^{3a,b} and one might, in principle, use any pair of successive reactions in this way. However, in our specific application, the kinetic forms of both steps are necessarily the same and, as will appear in the derivation of equation 4, one consequently evades knowing the exact nature of the kinetic forms. This is the key to the present procedure.

This procedure has been applied to isotopic exchange between deuterium and alkanes on metallic catalysts⁴ and on chromium oxide gel.⁵ On metallic catalysts, isotopic exchange between deuterium and a molecule such as heptane leads initially to the formation of polydeuterated alkane much of which is perdeuterioalkane. One might propose that each period of adsorption of a molecule of heptane leads to the exchange of one and only one hydrogen atom but that diffusion is slow. Thus, a molecule which had once penetrated into a pore might suffer several exchanges before it escaped into the reactant stream. However, the initial product of exchange of 3,3-dimethylpentane contains no species more exchanged than $C_7H_{11}D_5$. If diffusional control were involved as proposed, one should observe $C_7H_{16}D_{10}$ at least. Clearly then, perdeuterioheptane results from one period of adsorption and multiple deuteration is the consequence of alternation among a variety of adsorbed species. The *gem* dimethyl group of 3,3-dimethylpentane blocks the propagation of the exchange process and confines exchange to one ethyl side chain. Here then, A represents C_2H_5 ,

B represents C_2D_5 and the group CH_3CCH_3 repre-

sents the insulating hyphen. Identity of rate constants and kinetics is adequately established and the reaction constitutes an example of the proposed test of diffusional control. However, the reaction was slow in the temperature range studied and one would not expect to have observed diffusional control. At temperatures high enough to observe diffusional control, the reaction might be complicated by hydrogenolysis of the alkane.

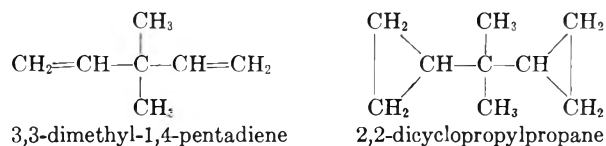
Similar isotopic exchange on chromium oxide gel forms monodeuterioalkane as the initial product;

(4) H. C. Rowlinson, R. L. Burwell, Jr., and R. H. Tuxworth, *J. Phys. Chem.*, **59**, 225 (1955).

(5) R. L. Burwell, Jr., A. B. Littlewood, M. H. Cardew, G. Pass and C. T. H. Stoddart, *J. Am. Chem. Soc.*, **82**, 6272 (1960).

with ethane, for example, only C_2H_5D is formed initially. Here also diffusional control is absent since its presence must lead to the appearance of di- and tri-deuterioalkanes.

If one attempts to extend these results to the use of much more rapid reactions, one inevitably considers the two molecules



Both have the insulating group which was effective in isotopic exchange with 3,3-dimethylpentane. In the first case one studies the successive addition of hydrogen to the two double bonds, in the second, the successive hydrogenolyses of the cyclopropyl rings. A subsequent paper will report the results of the hydrogenolytic reaction on the somewhat simpler compound dicyclopropylmethane. The present paper reports an exploratory investigation of the hydrogenation of the pentadiene on nickel wire and on nickel-silica in the vapor phase and on nickel-silica in the liquid phase.

Experimental

Materials.—The preparations of 3,3-dimethyl-1,4-pentadiene and 3,3-dimethylpentane have been described.⁶ 3,3-Dimethylbutene was kindly provided by Prof. H. Pines. Nickel wire was 30 gauge Nickel 651 of the Haskins Manufacturing Co. of Detroit. Nickel-silica was Harshaw nickel-kieselguhr.

Analysis.—Analyses of product compositions were performed by gas chromatography on a 9 foot column of mineral oil on firebrick at 70°.

Vapor Phase Hydrogenation.—This was studied in a flow reactor. Gaseous mixtures of hydrogen and pentadiene were prepared by saturation of hydrogen with the diolefin at a suitable temperature. Hydrogen was passed through a capillary flow meter and then into a bubbler containing the diolefin. The bubbler was maintained 5–10° above the desired saturation temperature. The gas stream then passed through a condenser held at the desired saturation temperature. The catalyst chamber for nickel-silica consisted of a tube whose inside diameter was 1.8 mm. In the experiments with nickel wire, 3.4 g. of wire was wound into helices of 1.5 mm. outside diameter each weighing about 0.67 g. and having a calculated gross surface area of 12 cm.². These were packed in a tube which had a diameter several times the helix diameter. The spaces between the helices were largely filled with thin glass rods.

The effluent from the catalyst chamber passed into a trap cooled by Dry Ice. The condensed hydrocarbon was removed for gas chromatographic analysis.

In our first experiments, the hydrogenation of the pentadiene on nickel wire, severe poisoning of the catalyst was observed. Accordingly, two traps were inserted in the hydrogen line just before the unit which saturated the hydrogen with olefin. The first trap contained reduced nickel-silica catalyst; the second contained charcoal cooled with liquid nitrogen. In addition, all subsequent samples of olefin were stored over reduced nickel-silica for several days before use. This treatment had no effect upon the gas chromatograms of the samples. As the result of the traps and the sample treatment, equivalent conversions were obtained at temperatures more than 100° lower than first necessary. Since reaction rates still fell with time although very much less than before, poisoning probably had not been completely eliminated.

Liquid Phase Hydrogenation.—This was studied in a batch reactor at a constant pressure of one atmosphere. The apparatus employed a gas buret with mercury as the confining fluid. The buret was filled with tank electrolytic hydrogen which was passed through a Deoxo unit and a trap

(6) R. Ciola and R. L. Burwell, Jr., *J. Org. Chem.*, **23**, 1063 (1958).

containing activated charcoal cooled with liquid nitrogen. The buret was connected to the hydrogenation flask by flexible Tygon tubing. A liquid nitrogen trap was inserted between the buret and the Tygon tubing. The hydrogenation flask was shaken in a water thermostat at 25.5° by a motor-driven eccentric. For rate runs, the flask was a simple tube with a small bulb at the end. The bottom of the bulb was flattened. For runs in which it was desired to follow composition changes, the flask was provided with a small side tube terminated with a flat piece of silicone rubber which was squeezed against the end of the side tube by a mechanical fitting. Samples of the hydrogenating mixture could be removed by a hypodermic syringe.

An arrangement was provided in which the nickel-silica catalyst was reduced in a stream of hydrogen, withdrawn from the furnace zone and dumped into the hydrogenation flask without being exposed to air. In most experiments we employed about 50 mg. of catalyst and about 4 mmoles of olefin.

The rate of hydrogenation was determined by measurement of hydrogen absorption. Composition change with time then was determined in a subsequent experiment under the same operating conditions. One had to interrupt the agitation of the hydrogenation flask during sample removal. Hydrogen absorption ceased immediately and started immediately upon restarting the agitation.

Results and Discussion

Vapor Phase Hydrogenation.—Results for nickel wire are given in Table I. The hydrogen/diolefin mole ratio was 5.0. The sample of nickel wire was first oxidized at 550° in air for 16 hours, reduced at 350° for 2.5 hours, reoxidized for two hours and re-reduced for two hours. Seven runs then were made at 150° at space velocities (expressed as g. of diolefin per g. of catalyst per hour) increasing from 0.042 to 0.36. All led to complete hydrogenation. During experiments 1 to 5 which then followed, activity steadily declined. The catalyst then was exposed to four cycles of oxidation and reduction. Each oxidation lasted three hours as did each reduction. Activity was restored but fell again during 9 to 13.

TABLE I

HYDROGENATION OF 3,3-DIMETHYL-1,4-PENTADIENE ON NICKEL WIRE

Run no.	HMSV ^a	Temp., °C.	Mole fraction		
			C ₇ H ₁₂	C ₇ H ₁₄	C ₇ H ₁₆
1	0.370	53	0.852	0.112	0.036
2	.425	53	.952	.048	.000
4	.137	53	.918	.082	.000
5	.0125	53	.932	.064	.006
9	.110	65	.420	.210	.370
10	.260	65	.749	.142	.109
11	.210	65	.965	.020	.015
12	.045	65	.980	.020	.000
13	.011	65	.928	.042	.030

^a Space velocity in g. of diolefin per g. of catalyst per hour.

Results for nickel-silica are presented in Table II. The 40 to 60 mesh catalyst was first reduced at 550° for 17 hours. In runs 20 to 23, catalytic activity declined drastically either from poisoning or from reaction of the diolefin to produce some kind of surface complex. Subsequent runs were all preceded by reduction for one hour at 450°. This process led to substantial restoration of activity.

The 20-40 mesh catalyst was reduced for 16 hours at 450°. Its much increased activity which presumably resulted from the lower temperature of reduction made it difficult to obtain adequately low

TABLE II

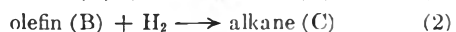
HYDROGENATION OF 3,3-DIMETHYL-1,4-PENTADIENE ON NICKEL-SILICA AT 92°

Run no.	HMSV	nH/nD ^a	Mole fraction		
			C ₇ H ₁₂	C ₇ H ₁₄	C ₇ H ₁₆
40-60 mesh nickel-silica					
20	158	2.6	0.265	0.176	0.560
21	136	2.5	.671	.115	.214
22	94	2.6	.870	.078	.053
23	38	2.5	.860	.084	.056
24	135	3.2	.675	.087	.238
25	132	5.2	.752	.074	.175
26	169	5.0	.860	.048	.093
27	193	5.0	.959	.019	.021
28	198	4.9	.959	.021	.019
29	143	5.0	.954	.029	.016
20-40 mesh nickel-silica					
30	215	5.0	0.315	0.050	0.635
31	135	5.0	.211	.056	.724
32	248	5.0	.177	.094	.728
33	415	5.0	.263	.148	.587
40 ^b	417	5.0	.502	.077	.422
41	810	5.0	.714	.059	.228
42	1200	5.0	.785	.045	.170
43	2500	5.0	.791	.064	.144

^a Mole ratio of hydrogen to diolefin is feed. ^b New batch of catalyst.

conversions. To keep consumption of the diolefin within reasonable bounds, runs were but five minutes long and followed one another in succession without intervening treatment of the catalyst. Accordingly, values for space velocity are rather uncertain and we cannot be sure that saturation of the hydrogen with diolefin was maintained.

The reactions of interest are



It will be assumed that the reaction 3 appears only as a result of slow diffusion and that the same kinetic form applies to all three reactions. The rate of any reaction is given by

$$r_i = k_i \phi (P, X_A, X_B, X_{H_2})$$

where X_A is the mole fraction of diene, etc. Then

$$-L dA = k_1 (1 - \alpha) \phi' \frac{A}{A+B} dV + k_1 \alpha \phi' \frac{A}{A+B} dV$$

$$-L dB = k_2 \phi' \frac{B}{A+B} dV - k_1 (1 - \alpha) \phi' \frac{A}{A+B} dV$$

where L is the flow rate, k_1 is the rate constant for hydrogenation of diene, the fraction, $1 - \alpha$, going to olefin, the fraction, α , going to alkane. A represents the fraction of diene in total hydrocarbon, k_2 is the rate constant for hydrogenation of monoolefin and dV represents an infinitesimal layer of catalyst perpendicular to the direction of flow. Dividing the two equations to obtain dB/dA eliminates L , ϕ' , V , and the terms $(A+B)$. Integration then gives

$$B = \frac{k_1(1-\alpha)}{k_1 - k_2} [A^{k_2/k_1} - A] \quad (4)$$

This equation has been reported for certain specialized kinetic forms by de Boer and van der Borg.⁷

It is assumed that ϕ' contains a term depending upon $(A + B)$ and that the rate of reaction 1 is given by $k_1\phi'$ multiplied by the fraction of the total olefin which is diene, $A/(A + B)$. This must be correct for a reaction which is first order in A and it would be correct for a reaction which obeys the Langmuir-Hinshelwood approximation. Consider a case in which α is zero.

$$-L dA = k_1\theta_A\theta_{H_2}dV = k_1 \frac{b_A p_A}{1 + \sum f_i(b_i p_i)} \theta_{H_2} dV$$

All terms would have this form and division of $L dB$ by $L dA$ would lead to the same result as in equation 4 although k_1 and k_2 would contain adsorption coefficients.

The curved lines in Fig. 1 represent equation 4 with $k_1/k_2 = 2$ and with α equal 0.0, 0.2, 0.5, 0.667 and 0.8 in the sequence from the upper to the lower curve. The curves also are shown in the magnified portion covering the range of A from 1.0 to 0.8. In this region almost any theory of diffusion control must give curves of the type shown, *i.e.*, a set of lines which start from $A = 1.00$ with a constant slope which subsequently decreases gradually. Only small errors can result from our assumptions that reaction 3 has the same kinetic form as reactions 1 and 2 and that the value of α is independent of conversion. Therefore, the present test of diffusion control best utilizes data in this region and the degree of diffusion control may be expressed by either $(C/B)_{\text{initial}}$ or by α since $(C/B)_{\text{in}} = \alpha/(1 - \alpha)$.

As may be seen from the magnified portion of Fig. 1 $(C/B)_{\text{in}}$ parallels the expected degree of diffusion control. On nickel wire the ratio was low or zero in runs 1-5. Following further oxidation and reduction (runs 9-13), the ratio was about 0.8 if one excepts run 12. The oxidation-reduction sequence increased the thickness of the porous surface layer of nickel and the wire had a distinctly matte appearance at this point. On 40-60 mesh catalyst (runs 20-29), the ratio averaged a little larger than with runs 9-13. The even larger ratio on 20-40 mesh catalyst (runs 30-43) is consistent with its larger particle size and greater catalytic activity.

Equation 4 becomes increasingly speculative in the region, $A = 0.8$ to 0.0. Nevertheless, the plots in this region are useful for correlative purposes and the data indicate some form rather like equation 4 must be valid.

Rather substantial deactivation accompanied all sets of runs except those on 20-40 mesh nickel-silica. As the over-all reaction rate falls, one might expect that diffusional control would decrease in importance and that the experimental points would move toward lines of lower values of α . This is observed in the sequences, runs 1-5, 21-23 and 26-29. There are, however, certain anomalies. Thus, the flow rates and the fractions of diene reacted are nearly the same in runs 21 and 24 yet α is distinctly larger in run 24. The values of α are smaller in 33 than in 30 and in 43 than in 42 although there is no corresponding decline in activity.

(7) J. H. de Boer and R. J. A. M. van der Borg, Second International Congress on Catalysis, Paris, July 4-9, 1960, paper 40, equation 12. See also W. M. Hamilton and R. L. Burwell, Jr., *ibid.*, paper 44, for the techniques of this derivation.

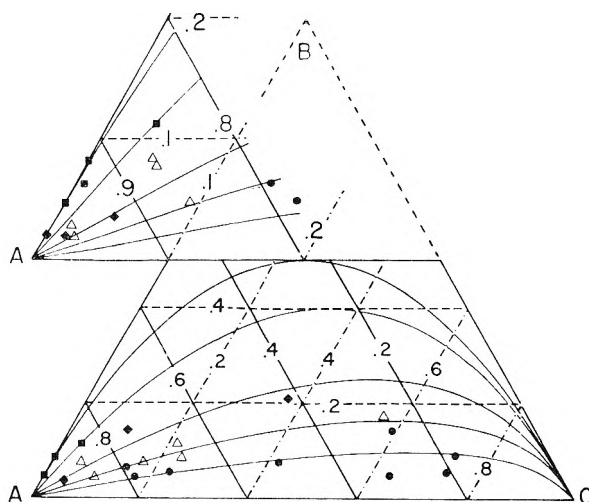


Fig. 1.—Vapor phase hydrogenation of 3,3-dimethylpentadiene; A is the diene, B is 3,3-dimethylpentene, C is 3,3-dimethylpentane; ■, runs 1-5 on nickel wire; ◆, runs 9-13 on nickel wire; △, runs 20-29 on 40-60 mesh nickel-silica; ●, runs 30-43 on 20-40 mesh nickel-silica. The curves represent equation 4 with $k_1/k_2 = 2.0$ and, from the uppermost to the lowest, with $\alpha = 0.0, 0.2, 0.5, 0.667$ and 0.8.

Our assumption that diene cannot react to form alkane during one period of residence on the surface is reasonably well established for nickel wire but the extension of this conclusion to nickel-silica while plausible cannot be rigorously established.

The value of k_1/k_2 influences any detailed consideration of α and of the maximum yield of mono-olefin. If a double bond in the diene has the same chance of hydrogenation as one in the mono-olefin $k_1/k_2 = 2$. The present data do not establish the exact value of k_1/k_2 but 2.0 is probably a lower limit since, as will appear, the ratio is about 9 in liquid phase hydrogenations.

For $k_1/k_2 = 2$, the maximum yield of mono-olefin, 50%, occurs at $\alpha = 0$ (see Fig. 1). In Wheeler's treatment of the system, $A \rightarrow B \rightarrow C$,³ the maximum yield would sink to about one-half of this value (25%) as the degree of diffusional control increased. Similarly, $(C/B)_{\text{in}}$ increases from zero to $\sqrt{k_2/k_1}$ with increasing diffusional control. $(C/B)_{\text{in}}$ cannot, then, exceed 0.7 if $k_1/k_2 = 2$. An increase in k_1/k_2 would increase the maximum yield and decrease the value of $(C/B)_{\text{in}}$. Yet on the 20-40 mesh catalyst, the maximum yield is only 10% and $(C/B)_{\text{in}}$ is about 3.

In Wheeler's model the reactions are first order in A and B. Perhaps a treatment using the true kinetics of the present reactions would give values closer to those observed. Or, lower values of maximum yields and larger values of $(C/B)_{\text{in}}$ might result from poisoned pore mouths.^{3a,b} However, the high activity and short length of runs is something of an argument against this in the case of the 20-40 mesh catalyst.

The present treatment does not, of course, interpret the experimental data in terms of any particular model of diffusional limitation. It merely represents the degree of diffusional limitation in terms of $(C/B)_{\text{in}}$ or of α . Any type of concentration gradient might lead to an apparent positive

value of α . For example, if there was channeling in the flow paths through a catalyst bed, one stream would react to a higher conversion than the remainder. When the streams remix, $(C/B)_{in}$ would be larger than in an experiment which proceeded to the same conversion in the absence of channeling. However, at low conversions, channeling must be rather severe for this effect to be serious.

Liquid Phase Hydrogenation.—Rates of hydrogenation of 3,3-dimethyl-1,4-pentadiene, 3,3-dimethyl-1-pentene and 3,3-dimethyl-1-butene were measured at 25.5° using 100–200 mesh catalyst which had been reduced at 350° for 16 hr. All runs were substantially zero order in olefin. The rate of hydrogen consumption was constant at least to 80% conversion. Beyond this point there was sometimes a slight decline in rate. The rate constants for the three hydrocarbons expressed in millimoles of hydrogen absorbed per second per mg. of catalyst were: pentadiene, 5.4×10^{-5} ; pentene, 5.0×10^{-5} ; butene, 5.8×10^{-5} .

The dependence of rate of hydrogenation upon amount of catalyst was tested with 3,3-dimethylpentene. The rate constants expressed in millimoles of hydrogen adsorbed per second per mg. of catalyst were 5.0×10^{-5} , 4.9×10^{-5} and 5.0×10^{-5} in experiments with 54 mg. of catalyst and 3.13 mmoles of olefin; 116 mg. and 4.10 mmoles; 49 mg. and 4.33 mmoles. Thus, it appears that the rates of hydrogenation are essentially proportional to the amount of catalyst in the range which we have employed.

Hydrogenation of the pentadiene was also run with 20–40 mesh pellets. During the run, the agitation led to the disintegration of most of the pellets to form much finer material. The rate of hydrogenation started at about 1/20th that of 100–200 mesh catalyst and steadily increased throughout the course of the reaction. The terminal value of the rate was nearly 1/3rd that with 100–200 mesh catalyst.

The rapid increase in rate attendant upon disintegration of the 20–40 mesh pellets suggests the existence of serious concentration gradients within the catalyst pore structure. This rate increase and the observation that rates were proportional to amount of catalyst indicates that hydrogen transfer between gas and liquid phase was not rate limiting.⁸ Rate of diffusion of olefin is unlikely to be rate limiting since the reaction is zero order in olefin. Thus, it appears probable that the diffusional limitation results from the diffusion of hydrogen within the pores of the catalyst. This is a plausible consequence of the low value of the concentration of hydrogen in a hydrocarbon when the dissolved hydrogen is in equilibrium with gas at about one atmosphere.⁹ It would be interesting to extend this study to high hydrogen pressures under which condition the relative importance of diffusional limitations might shift from hydrogen to olefin. Our conclusions with regard to the type of diffusional limitations present in our system are

very similar to those of Freund and Hulburt¹⁰ for the hydrogenation of styrene by Raney nickel. (Other authors^{9,11} have proposed the existence of rate limiting hydrogen concentration gradients at other locations during hydrogenations in liquid phases.)

Mixtures of the butene with the pentadiene and with the pentene were also hydrogenated. If

$$dM/dN = mM/nN$$

where m involves the adsorption coefficient and perhaps a rate constant for reaction of M , then

$$\log(M^0/M) = (m/n) \log(N^0/N)$$

where M is the mole fraction of M in the hydrocarbon mixture and M^0 is the initial value of the mole fraction.

The competitive hydrogenation of 3,3-dimethylpentene and 3,3-dimethylbutene gave an excellent fit to this equation with $n/m = 1.6$ (more rapid hydrogenation of the butene). The fit for the hydrogenation of the mixture of pentadiene and butene was less good but the value of n/m was about 5.5 in favor of pentadiene.

In the liquid phase hydrogenation, the relative reactivity of two olefins results from competition between the two for the surface and from the relative reactivity of the adsorbed olefins. In the Langmuir–Hinshelwood approximation¹²

$$\theta_A = \frac{aA}{1 + aA + bB} \quad (5)$$

The rate of reaction of A is $r_A = k_A \theta_A \phi(\theta_{H_2})$. Thus, the relative reactivity is given by

$$\frac{dB}{dA} = \frac{k_B b B}{k_A a A} \quad (6)$$

However, a small amount of diffusional involvement of olefin could occur without clearly detectable departure of kinetics from zero order in olefin. As in the derivation of equation 4, one may say that the fraction, $1 - \alpha$, of A reacts to form B . Because of slow diffusion, a fraction, α , appears in the liquid phase directly as C . Further, since the term, $k_B b$, cannot be resolved into two terms by our experiments, we can use b to represent the product. Thus, as before

$$\frac{dB}{dA} = \frac{bB}{aA} - (1 - \alpha)$$

This integrates to

$$B = \frac{1 - \alpha}{1 - (b/a)} [A^{b/a} - A] \quad (7)$$

which is equivalent to equation 4 with b/a replacing k_2/k_1 .

As shown in Fig. 2 the maximum yield of pentene during the hydrogenation of 3,3-dimethylpentadiene on 100–200 mesh nickel-silica (filled circles) is 69%, a value much larger than any found in vapor phase hydrogenations. The value of a/b must exceed 2.0 for which no yield in excess of 50% is possible as shown in Fig. 1. The best fit of equation 7 to these data results from $a/b = 9$ and $\alpha = 0.088$. One could estimate a/b from the selectivity

(8) H.-C. Yao and P. H. Emmett, *J. Am. Chem. Soc.*, **81**, 4125 (1959).

(9) R. H. Price and D. B. Schiewetz, *Ind. Eng. Chem.*, **49**, 807 (1957).

(10) T. Freund and H. M. Hulburt, *J. Phys. Chem.*, **61**, 909 (1957).

(11) G. W. Watt and M. T. Walling, Jr., *ibid.*, **59**, 7 (1955).

(12) J. C. Jungers, "Cinétique Chimique Appliquée," Société des Éditions Techniq., Paris, 1958, p. 409 *et seq.*

ties obtained in hydrogenating mixtures of 3,3-dimethylbutene with pentadiene and with pentene, $a/b = 5.5 \times 1.6 = 8.8$. The check is well within the experimental errors.

Although the fit of equation 7 is fairly good, possible errors in analysis preclude a really critical test. The equation does seem less exact at very low values of diolefin. For example, one point showed: diene 0.001; monoene, 0.613; and alkane, 0.386. Equation 7 would give 0.01 for diene. The discrepancy might result from failure of a main simplifying assumption of the Langmuir-Hinshelwood model, that a/b is independent of the concentrations of A and B.

Data from the competitive hydrogenation of diene and butene (triangles) and from the hydrogenation of pentadiene with 20-40 mesh catalyst (squares) are also shown in Fig. 2. In principle, presence of dimethylbutene should not change a/b since it affects θ_A and θ_B only by adding a term to the denominator of equation 5 which cancels in proceeding to equation 6. However, selectivity to monoolefins is greater in the hydrogenation of the mixture as measured both by initial yield of alkane and by maximum yield of monoolefin. The increased selectivity results mainly from a reduced value of α , 0.028 against 0.088. We do not know whether such variation is within the ordinary limits of reproducibility. The experiment with the larger particle catalyst exhibits lowered selectivity as one would expect but the comment of the previous sentence applies here also.

There are plausible but not absolute arguments that diene cannot react to alkane in one surface step as we have noted. The initial yields of alkane in our liquid phase hydrogenations, although small, were too large for α to be zero. Thus, it appears probable that the liquid phase hydrogenations were attended by degrees of diffusional limitation which were small for olefin but large for hydrogen.

The value of a/b is distinctly larger than a possibly expected value of 2.0. Although only one double-bond of the diene can chemisorb in a form leading to hydrogenation, it appears that the van der Waals interaction of a vinyl group with the surface is larger than that of an ethyl group. The departure of a/b from 2.0 is unfortunate since it suggests that this ratio may vary from metal to metal and even from support to support. This would not affect the validity of equation 4 at low conversions but it will complicate any detailed interpretation of the empirical quantity α .

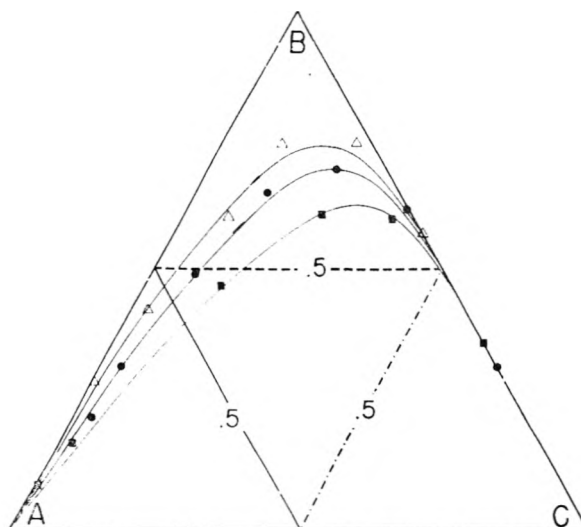


Fig. 2.—Liquid phase hydrogenation of 3,3-dimethylpentadiene; A, B, and C are the diene, 3,3-dimethylpentene and 3,3-dimethylpentane, respectively: ●, hydrogenation with 100-200 mesh nickel-silica; ■, hydrogenation with an initially 20-40 mesh nickel-silica; Δ, hydrogenation of mixture of 3,3-dimethylpentadiene and 3,3-dimethylbutene. Composition data are given only for the pentadiene and its reaction products. The curves represent equation 7 with $a/b = 9.0$ and with $\alpha = 0.028, 0.088$ and 0.178 for the upper middle and lower curves, respectively.

Nevertheless, we believe that hydrogenation of 3,3-dimethylpentadiene can provide a useful degree of information about diffusional limitation for other reactions on metallic catalysts. Given a reaction which proceeds at a certain rate on a particular catalyst at a particular temperature. One would study the hydrogenation of pentadiene at such a temperature that the gross rate of production of product was the same as in the reaction under question and at a flow rate such that conversions of diene were less than 20%. The value of $(C/B)_{in}$ gives some indication as to the degree of diffusion control. Where possible, it would probably be preferable to adjust the temperature so that

$$\text{rate}_1/D_1 = \text{rate}_2/D_2$$

where subscript 1 refers to the reaction in question and subscript 2 to that of dimethylpentadiene. The D 's are the corresponding diffusion coefficients which are evaluated readily for Knudsen diffusion (vapor phase reactions at low pressures). In appropriate hydrogenation reactions, it would be possible merely to add the pentadiene to the compound being hydrogenated provided the total product can be suitably analyzed.

VALIDITY OF THE STEADY-STATE APPROXIMATION IN UNIMOLECULAR REACTIONS

BY HYUNG KYU SHIN AND J. CALVIN GIDDINGS

Department of Chemistry, University of Utah, Salt Lake City 12, Utah

Received December 20, 1960

The departure from steady-state conditions for reactions following the Lindemann mechanism is formulated quantitatively. Two approximate methods, both yielding linear equations, are used. One of the methods accounts for transients that may be found in the system. This method, the more complicated of the two, yields the departure term, ϵ , in terms of exponential integrals for both first-order and second-order cases. The departure terms obtained by the second method are relatively simple functions of reaction rate constants. The results of these derivations are compared with older criteria for validity of the steady state. Application is made to very fast reactions where the departure from steady-state conditions may be significant.

The Lindemann mechanism¹⁻⁴ for unimolecular reactions, along with recent modifications,⁵ has led to a successful interpretation of unimolecular phenomena. One of the basic postulates of the Lindemann mechanism, the assumption of steady-state conditions, has received little attention although related problems involving unimolecular reactions have been treated extensively.⁶⁻⁸ The justification of the steady state by intuitive arguments is not sufficiently quantitative to indicate the extent of steady-state deviations and limitations. Particularly with fast reactions, where the steady-state approximation is sometimes questionable, a method is needed for estimating the departure from steady state. Such a method is proposed here.

The departure from steady-state conditions can be expressed in terms of the departure term,⁹ ϵ , defined by $(B) = (B)^*(1 + \epsilon)$, where (B) and $(B)^*$ are the actual and steady-state concentrations of intermediate, respectively. Differentiation of the above leads to an equation¹⁰ for ϵ

$$(B)^* \frac{d\epsilon}{dt} + (1 + \epsilon) \frac{d(B)^*}{dt} = r_B \quad (1)$$

where r_B is the rate of formation of B, $d(B)/dt$, and is a function of ϵ . This equation is highly involved for unimolecular reactions, even in the high pressure range. A satisfactory approximation to ϵ (involving an error in the order of ϵ^2) can be obtained by replacing the reactant concentration (A) by the value, $(A)^*$, obtained by assuming steady-state conditions, and by neglecting second and higher order terms in ϵ . This approximate method¹⁰ (method 1) renders equation 1 linear, and the approximate departure term, ϵ_1 , can be easily obtained.

(1) F. A. Lindemann, *Trans. Faraday Soc.*, **17**, 599 (1922).

(2) C. N. Hinshelwood, "The Kinetics of Chemical Change in Gaseous Systems," 3rd ed., Clarendon Press, Oxford, 1933.

(3) O. K. Rice and H. C. Ramsperger, *J. Am. Chem. Soc.*, **49**, 1617 (1927); **50**, 617 (1928).

(4) L. S. Kassel, "Kinetics of Homogeneous Gas Reactions," Chemical Catalog Co., New York, N. Y., 1932.

(5) N. B. Slater, "Theory of Unimolecular Reactions," Cornell Univ. Press, Ithaca, N. Y., 1959.

(6) B. J. Zwolinski and H. Eyring, *J. Am. Chem. Soc.*, **69**, 2702 (1947).

(7) E. W. Montroll and K. E. Shuler, "Advances in Chemical Physics," Vol. I, Interscience Publishers, Inc., New York, N. Y., 1958, p. 361.

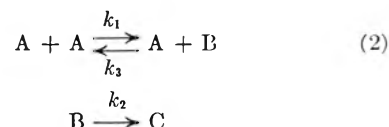
(8) F. P. Buff and D. J. Wilson, *J. Chem. Phys.*, **32**, 677 (1960).

(9) J. C. Giddings and J. O. Hirschfelder, *J. Phys. Chem.*, **61**, 738 (1957).

(10) J. C. Giddings and H. K. Shin, *Trans. Faraday Soc.*, **57**, 468 (1961).

A somewhat simpler approximation which is valid beyond a short, initial transient period is obtained by setting $d(B)^*/dt = r_B$. It may be necessary using this method (method 2) to replace (A) by $(A)^*$ and neglect ϵ^2 , etc. The departure term obtained is shown as ϵ_2 .

The mechanism employed for this analysis is



It is assumed that the product is continually removed from the system such that activation occurs only by collision between A's. There is nothing which would prevent obtaining ϵ as a function of the energy of B; however, any deviations from steady-state kinetics would depend only on the over-all ϵ obtained here.

The quantity $d(B)^*/dt$, needed for the evaluation of ϵ , is found to be

$$\frac{d(B)^*}{dt} = \frac{k_1(A)[2k_2 + k_3(A)]}{[k_2 + k_3(A)]^2} \frac{d(A)}{dt} \quad (3)$$

Formulating $d(A)/dt$ from (2), and substituting $(B)^*(1 + \epsilon)$ for (B), we obtain

$$\frac{d(B)^*}{dt} = \frac{k_1^2(A)^2[2k_2 + k_3(A)][-k_2 + k_3(A)\epsilon]}{[k_3(A) + k_2]^3} \quad (4)$$

The quantity $r_B = d(B)/dt$ can be similarly obtained as

$$r_B = -k_1(A)^2\epsilon \quad (5)$$

While results for the pressure range intermediate between first-order and second-order cases can be obtained numerically,¹⁰ it is much simpler to treat the two cases individually.

In the high-pressure unimolecular case, where $k_3(A) \gg k_2$, we have $(B)^* = k_1(A)/k_2$ and $d(B)^*/dt = k_1^2(A)[-k_2 + k_3(A)\epsilon]/k_3^2$. Employing method 1 we obtain

$$\frac{d\epsilon}{dt} + [(k_1 + k_3)(A)_0 e^{-kt} - k]\epsilon = k \quad (6)$$

where k is the apparent rate constant, $k_1 k_2 / k_3$, and $(A)_0$ is the initial value of (A). The last term in brackets is negligible as long as $k_1/k_3 = (B)^*/(A) \leq 1$ by virtue of the condition $k_3(A) \gg k_2$. Thus

$$\frac{d\epsilon}{dt} + (k_1 + k_3)(A)_0 e^{-kt} \epsilon = k \quad (7)$$

The solution of this equation appears in terms of

exponential integrals, $-E_i(-x) = \int_x^\infty (e^{-v}/v)dv$

$$\epsilon_1 = e^{\alpha e^{-kt}} [Ei(-\alpha) - Ei(-\alpha e^{-kt})] - e^{\alpha(e^{-kt}-1)} \quad (8)$$

where $\alpha = (k_1 + k_3)k_3(A)_0/k_1k_2$. The initial condition, $\epsilon = -1$ at $t = 0$, has been employed to illustrate the nature of initial transients. While the equations are not intended to evaluate ϵ when it is as large as unity, the transients obtained have been quite satisfactory when compared to exact values.

Equation 8 can be simplified somewhat by considering the magnitude of the arguments of the exponential integrals. The term $\alpha e^{-kt} = [k_3(A)^*/k_2] (1 + k_3/k_1) \gg 1$ because of the first-order assumption. The term α is even larger. For large x we may write $-Ei(-x) \cong e^{-x}/(x+1) \cong e^{-x}/x$. When we use this approximation, ϵ_1 becomes

$$\epsilon_1 = \frac{1}{\alpha} [-(\alpha+1)e^{\alpha(e^{-kt}-1)} + e^{kt}] \quad (9)$$

The first term in the brackets is the transient term which rapidly becomes negligible. The time constant for the transient is the order of $1/(k_1 + k_3)(A)_0$. Thereafter the second term in the brackets is the only one of importance.

The use of method 2 leads to the departure

$$\epsilon_2 = \frac{e^{kt}}{\alpha} \quad (10)$$

This value is identical with ϵ_1 from equation 9 after passage of the transient.

In the low-pressure second-order case, $k_2 \gg k_3(A)$, $(B)^* = k_1(A)^2/k_2$, and $d(B)^*/dt = -2k_1^2(A)^3/k_2$. The value of (A) obtained from steady-state considerations is $(A)^* = (A)_0/[1 + k_1(A)_0t]$. Method 1 leads to the equation

$$\frac{d\epsilon}{dt} + \left[k_2 - \frac{2k_1(A)_0}{1 + (A)_0k_1t} \right] \epsilon = \frac{2k_1(A)_0}{1 + (A)_0k_1t} \quad (11)$$

This has the solution

$$\epsilon_1 = - \left\{ 1 + \lambda^2 e^{-\gamma\lambda} \left[\frac{e^{\gamma\lambda}}{\lambda^2} (1 + \gamma\lambda) - e^{\gamma} (1 + \gamma) - \gamma^2 (Ei(\gamma\lambda) - Ei(\lambda)) \right] \right\} \quad (12)$$

where $\gamma = k_2/k_1(A)_0$ and $\lambda = 1 + k_1(A)_0t$.

Method 2 gives the following result for the bimolecular case

$$\epsilon_2 = \frac{2}{\gamma\lambda} = \frac{2(B)^*}{(A)^*} \quad (13)$$

Considerations slightly different from the above will apply if collisions other than those between two A molecules lead to activation. The collision of A with C, if the product is not removed, or with inert molecules will lead to the formation of B. The departure term, ϵ , will depend on the species and rate constants involved. One of the simplest alternative mechanisms to (2) is the assumption that the collective sum of all molecules leads to a constant rate of activation per unit concentration of A; $A + M \rightleftharpoons M + B$ where M is constant in time, and may be absorbed into the rate constants. This mechanism is not as difficult to treat as (2), and both exact and approximate departure term have been obtained.¹⁰

The importance of the transient may be gauged in terms of the relaxation time of B, defined by¹¹

$$t_B = \frac{-(B)^*\epsilon}{d(B)/dt} \quad (14)$$

In fact the entire phenomenon of departure from the steady state may be considered¹¹ in terms of the relaxation of the concentration, (B), toward the constantly changing steady-state value, $(B)^*$. The value of (B) lags behind $(B)^*$ by the time t_B as may be seen by rewriting equation 14 as $(B)^* - (B) = [d(B)/dt]t_B$.

The relaxation time of B found in mechanism (2) by applying equation 14 is

$$t_B = \frac{1}{k_2 + k_3(A)} \quad (15)$$

This becomes $1/k_3(A)$ in the unimolecular case, and $1/k_2$ in the bimolecular case. It was concluded also that the time constant for the transient in the unimolecular case was $1/(k_1 + k_3)(A)_0$. In the majority of cases where $(B)^*/(A) \ll 1$, this becomes $1/k_3(A)_0$, the initial relaxation time of B. If $(B)^*/(A)$ is not much less than unity, the relaxation time itself can be redefined to bring it into agreement with the transient time constant. This is probably not necessary because the primary use of the relaxation time is only semi-quantitative in nature.

The above concepts can be used¹⁰ to explain the reason for the increase of ϵ with time as shown by equations 9 and 10 for the unimolecular case. The relaxation time, $1/k_3(A)$, becomes larger as the reaction proceeds and (A) diminishes. Thus (B) is no longer able to adjust rapidly to changes in $(B)^*$, and the divergence from steady-state conditions increases.

The steady-state approximation often has been assumed valid for those mechanisms in which the (intermediate/reactant) concentration ratio, or $(B)/(A)$, is small compared to unity. It is very often true, as illustrated by equation 13, that ϵ is equal or nearly equal to this ratio, thus justifying the assumption. In other cases, however, ϵ differs from this ratio by a substantial factor. The ϵ_2 of equation 10 can be written approximately as $[k_2/k_3(A)^*][(B)^*/(A)]$, where $k_2/k_3(A) \ll 1$. In general, the smallness of $(B)^*/(A)$ can be considered neither as a necessary nor as a sufficient condition for the smallness of ϵ .

Calculations and Conclusions

The magnitude of the rate constants, needed to obtain ϵ , have been discussed by many people, including Hinshelwood,² Rice and Ramsperger,³ Kassel,⁴ and more recently by Slater.⁵ These constants may be estimated by use of the equations

$$k_1 = \frac{Z}{(s-1)!} \left[\frac{E^0}{RT} \right]^{s-1} e^{-E^0/RT} \quad (16)$$

$$k_3 = Z \quad (17)$$

$$k_2 = kk_3/k_1 \quad (18)$$

where Z is the collisional frequency, s the number of normal modes of vibration, and E^0 the minimum energy required for reaction. Since k is often obtained by means of direct experiment, it is em-

(11) J. C. Giddings, *J. Chem. Phys.*, **26**, 1210 (1957).

ployed in the expression for k_2 . The experimental activation energy obtained by assuming the Arrhenius law $k = \nu e^{-E_{\text{exp}}/RT}$, is given by $E^0 - (s - 3/2)RT$. Equation 16 is the first term in a series which adequately represents k_1 only if $E^0 \gg (s - 1)RT$. This condition also implies that $k_1/k_3 \ll 1$.

If these expressions are employed in the first-order range, equation 10, we obtain

$$\epsilon_2 = \frac{k}{Z(A)^*} \quad (19)$$

whereas the second-order case, equation 13, yields

$$\epsilon_2 = \frac{2k_1^2(A)^*}{kZ} \quad (20)$$

It is apparent from these expressions that the steady-state approximation is excellent under most conditions. Assuming $k = 1 \text{ sec.}^{-1}$, $Z = 10^{14} \text{ cc. mole}^{-1} \text{ sec.}^{-1}$ and $(A) = 10^{-5} \text{ mole cc.}^{-1}$ for the first-order reaction, we obtain $\epsilon_2 = 10^{-9}$. The relaxation time of B is also found to be 10^{-9} sec. , and thus the initial transient does not influence the course of the reaction. These values will increase somewhat as (A) is decreased, but beyond a certain limit the reaction becomes second order. In this case, either equation 20 or equation 13 can be used. Equation 13 shows ϵ_2 to be small for the majority of systems in which the energetic species, B, exists at a low concentration level. As an example, the activation energy of ozone has been found by Benson and Axworthy¹² to be 24,000 cal. Assuming $\nu = 10^{13} \text{ sec.}^{-1}$ we find that $\epsilon_2 = 2.2 \times 10^{-13}$ at 400°K. and 5.6×10^{-8} at 800°K. The relaxation time of B at these two temperatures

(12) S. W. Benson and A. E. Axworthy, Jr., *J. Chem. Phys.*, **26**, 1718 (1957).

is 1.1×10^{-11} and $3.0 \times 10^{-12} \text{ sec.}$, respectively. The half-life of the reaction, $1/k_1(A)$, is approximately 100 sec. in the first case and $1.1 \times 10^{-4} \text{ sec.}$ in the second.

Only in the case of some very fast reactions does the steady-state approximation need to be considered with suspicion. These reactions, observed when temperatures are high or activation energies low, are associated with large values of k and k_1 . Employing the same values of Z , (A) and ν as above, equation 19 shows that for first-order reactions $\epsilon_2 = 0.061$ when $E_{\text{exp}}/RT = 12$ and $\epsilon_2 = 0.45$ when $E_{\text{exp}}/RT = 10$. (Because of errors incurred when ϵ_2 is large, the latter value is not entirely accurate, but does indicate the order of departure.) The reaction half-lives are very short; $6.1 \times 10^{-7} \text{ sec.}$ and $4.5 \times 10^{-8} \text{ sec.}$, respectively. The value of s must be >24 in the former case and >53 in the latter if first-order conditions are to be maintained. We see that extreme conditions such as these can lead to very serious departures from the steady state.

Second-order processes do not lead to such large departures under similar circumstances. Thus at 2000°K., E_{exp}/RT for ozone is approximately 6 and $\epsilon_2 = 2 \times 10^{-5}$. The decomposition time is $6.4 \times 10^{-8} \text{ sec.}$ Each case, of course, is individual and must be treated separately. In many cases at high temperatures (or with low-activation energies) the conditions $E^0 \gg (s - 1)RT$ and $k_1/k_3 \ll 1$ are no longer valid and the previous equations must be expanded to allow for this.

Acknowledgment.—This investigation was supported by a research grant, NSF-G9498, from the National Science Foundation.

TRIFLUOROBOROXINE: PREPARATION, INFRARED SPECTRUM AND STRUCTURE¹

By H. D. FISHER, W. J. LEHMANN AND I. SHAPIRO

Chemistry Department, Hughes Tool Company—Aircraft Division, Culver City, California

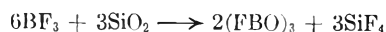
Received December 20, 1960

The reaction of boron trifluoride with various oxygen-containing compounds leads to the formation of a compound with the empirical formula of $(\text{BOF})_3$. Ruff and co-workers² envisioned a coordination complex between BF_3 and B_2O_3 ; however, Baumgarten and Bruns^{3,4} and Goubeau and Keller⁵ have presented experimental evidence for the formation of trifluoroboroxine. On the basis of the present spectroscopic work, we confirm the ring structure.

Experimental

Boron trifluoride was purified by complexing with acetyl chloride⁶ followed by fractionation through a -155° bath prior to each experiment. No impurities could be detected by infrared analysis. The infrared cell was similar to that described by Becker and Pimentel.⁷ The copper block

and sodium chloride plate were maintained at the desired temperatures by means of precooled nitrogen. Boron trifluoride of known isotopic content was passed over quartz heated to 500° , where the reaction occurred



The gas stream then was cooled rapidly on the NaCl plate, which was maintained at -150° . At this temperature the trifluoroboroxine condensed on the NaCl window, while the unreacted boron trifluoride and silicon tetrafluoride were removed by pumping. The samples were cooled to -196° , and their spectra were recorded on a Beckman IR-4 infrared spectrophotometer equipped with NaCl optics.

Goubeau and Keller⁵ reported that trifluoroboroxine is stable only above 250° ; it is possible, however, to isolate and maintain this compound at temperatures below -135° , at which temperature the rate of disproportionation becomes negligible. When trifluoroboroxine is allowed to

(1) Presented in part at the 138th Meeting of the American Chemical Society, New York, N. Y., September, 1960.

(2) O. Ruff, A. Braida, O. Bretschneider, W. Menzel and H. Plaut, *Z. anorg. allgem. Chem.*, **206**, 59 (1932).

(3) P. Baumgarten and W. Bruns, *Ber.*, **72B**, 1753 (1939).

(4) P. Baumgarten and W. Bruns, *ibid.*, **74B**, 1232 (1941).

(5) J. Goubeau and H. Keller, *Z. anorg. allgem. Chem.*, **267**, 1 (1951).

(6) H. C. Brown, E. I. Schlesinger and A. B. Burg, *J. Am. Chem. Soc.*, **61**, 673 (1939).

(7) E. D. Becker and G. C. Pimentel, *J. Chem. Phys.*, **25**, 224 (1956).

TABLE I

INFRARED SPECTRA OF TRIFLUOROBOROXINE AND ASSIGNMENTS COMPARED WITH MESITYLENE AND TRIMETHYLBOROXINE (CM.⁻¹)

Assignment for F ₃ B ₃ O ₃	F ₂ B ₃ ¹⁰ O ₃ ^a	F ₃ B ₃ ¹⁰ O ₃	Mesitylene	Me ₃ B ₃ ¹⁰ O ₃	Me ₃ B ₃ ¹⁰ O ₃
Ring puckering (out of plane, ν_2'')	714s ^b	733	ν_4 690	784	786
B-F stretching (out of phase, e')	966m ^c	968	ν_{20} 930	918	942
Ring stretching (e')	1381s ^b	1431	ν_{19} 1385	1227	1260
Ring stretching (e')	1450s ^b	1477	ν_8 1610	1384	1430
(Unassigned)	1233w	1260
(Unassigned)	1280w	1290

^a s, strong; m, medium; w = weak. ^b Broad. ^c Sharp.

warm to temperatures above -135° , it disproportionates rapidly into boron trifluoride and boric oxide in a 1:1 ratio, as indicated by chemical analysis. The course of the disproportionation was followed by alternately warming the sample in the infrared cell to predetermined temperatures and quenching in liquid nitrogen, pumping off the evolved boron trifluoride, and examining spectra of the residue. The disproportionation proceeds through isolatable unstable intermediates and is essentially complete (>99%) within one hour at room temperature.

Boron trifluoride reacts much faster with silica than with boric oxide. When B¹⁰-enriched boron trifluoride was passed rapidly through a heated quartz tube coated with isotopically normal boric oxide and the resulting trifluoroboroxine was subsequently decomposed, the evolved BF₃ had the same isotopic content as the initial BF₃, thus indicating no reaction with B₂O₃. However, with longer contact time, B¹¹-enrichment in the product BF₃ showed that some reaction with B₂O₃ had occurred.

Discussion of Spectra

The infrared absorption frequencies of both isotopically normal and B¹⁰-enriched (ca. 95% B¹⁰) trifluoroboroxines are listed in Table I.

Planar trifluoroboroxine belongs to symmetry point group⁸ D_{3h}. The 14 internal vibrations are of the following species with the indicated Raman and infrared activity⁸: 3A₁' (R) + 2A₂' (inactive) + 2A₂" (I) + 5E' (RI) + 2E" (R). From analogy with mesitylene (1,3,5-trimethylbenzene),⁹ one would expect only four vibrations to have infrared bands in the sodium chloride range (above 650 cm.⁻¹). By no coincidence, four principal bands have been observed and are assigned as shown in Table I. These assignments are discussed below in greater detail.

Of special interest is the band at 966 cm.⁻¹, which is assigned to the doubly degenerate out-of-phase stretching mode of the three B-F groups. Its small B¹⁰-isotope shift of ca. 2 cm.⁻¹ confirms the ring structure. Any other reasonable structure would exhibit a much larger isotope effect. For example, the minimum shift for an F-B=O monomer is 8 cm.⁻¹ [calculated by treating the molecule as diatomic F-(BO)]. The FBO monomer also is eliminated on the basis of the Average

(8) G. Herzberg, "Infrared and Raman Spectra of Polyatomic Molecules," D. Van Nostrand Co., Inc., Princeton, N. J., 1945, pp. 12, 138, 252.

(9) K. S. Pitzer and D. W. Scott, *J. Am. Chem. Soc.*, **65**, 803 (1943).

(10) W. J. Lehmann, *Spectroscopia Mol.*, **9**, 62 (1960); also see *J. Mol. Spectroscopy*, submitted 1960.

(11) The weighted average of the BF₃ frequencies (1454 and 888 cm.⁻¹)^{12,13} is 1265 cm.⁻¹. From force-constant comparisons it has been determined that the BF bond in BF₃ has one-third double-bond character,^{14,15} thus leading to 1096 cm.⁻¹ for a B-F single-bond.

(12) J. Vanderyn, *J. Chem. Phys.*, **30**, 331 (1959).

(13) L. P. Lindeman and M. K. Wilson, *ibid.*, **24**, 242 (1956).

(14) J. Goubeau, W. Bues and F. W. Kampmann, *Z. anorg. allgem. Chem.*, **283**, 123 (1956).

(15) J. Goubeau, *Angew. Chem.*, **69**, 77 (1957).

Rule,¹⁰ which predicts a frequency of ca. 1096 cm.⁻¹ for the B-F single-bond in FBO¹¹; nothing is observed in that vicinity.

The absorption at 966 cm.⁻¹ is a logical assignment for the doubly degenerate B-F stretching frequency of a boroxine derivative. From this assignment and the above-mentioned average of 1096 cm.⁻¹, the Raman-active (infrared-inactive) in-phase frequency is calculated to be 1356 cm.⁻¹ (1377 cm.⁻¹, if root-mean-squares are used in the calculation), which falls into line with corresponding frequencies in other boroxines¹⁶: 1286, 1147 and 1155 cm.⁻¹, respectively, for B-O, B-N and B-C. The validity of this correlation is supported by analogy with trimethylborane¹⁷ and trimethylboroxine.^{10a,16,18} The various frequencies and their averages are summarized in Table II. The present assignment supports the belief of Goubeau¹⁴ and Becher¹⁹ that there is no double bonding in B-F₁ groups. When more data are available, it will be worthwhile to attempt a normal-coordinate calculation of the type performed by Watanabe *et al.*,²⁰ for borazine derivatives.

TABLE II

B-C AND B-F STRETCHING FREQUENCIES OF BX₃ AND X₃B₃O₃ COMPOUNDS (CM.⁻¹)

Compound	Out-of-phase stretching ^a	In-phase stretching ^b	Weighted average
B(CH ₃) ₃	1156	675	996
(CH ₃) ₃ B ₃ O ₃	918	1155	997
BF ₃	1454	888	1265
B-F single-bonded	1096
F ₃ B ₃ O ₃	966	1356 ^c	1096

^a Infrared active. ^b Raman active. ^c Calculated.

To date, little evidence has been presented regarding possible resonance stabilization of the boroxine ring, although this type of stabilization repeatedly has been demonstrated for borazine rings (X₃B₃N₃Y₃, also known as borazoles). Mass spectral studies indicate that trimethylboroxine²¹ exhibits some aromaticity. In view of the in-

(16) J. Goubeau and H. Keller, *Z. anorg. allgem. Chem.*, **272**, 303 (1953).

(17) W. J. Lehmann, C. O. Wilson, Jr., and I. Shapiro, *J. Chem. Phys.*, **31**, 1071 (1959).

(18) We disagree with Goubeau and Hummel [*Z. physik. Chem. (Frankfurt)*, **20**, 15 (1959)], who assign 783 cm.⁻¹ to the out-of-phase B-C stretching vibration of trimethylboroxine, rather than 918 cm.⁻¹.

(19) H. J. Becher, *Z. anorg. allgem. Chem.*, **291**, 151 (1957).

(20) H. Watanabe, M. Narisada, T. Nakagawa and M. Kubo, *Spectrochim. Acta*, **16**, 78 (1960).

(21) W. J. Lehmann, C. O. Wilson, Jr., and I. Shapiro, *J. Inorg. and Nuclear Chem.*, in press (1961).

creased electronegativity of fluorine over methyl substituents, one would predict trifluoroboroxine to exhibit greater aromaticity than trimethylboroxine. This prediction is supported by the increase in the ring-stretching frequencies of tri-

fluoroboroxine over trimethylboroxine (see Table I). Further, the relative magnitudes of the boron-isotope shifts of the B-X stretching mode in the two boroxine derivatives indicate that the ring is more rigidly bonded in trifluoroboroxine.

FLUORINE BOMB CALORIMETRY. I. THE HEAT OF FORMATION OF ZIRCONIUM TETRAFLUORIDE^{1,2}

BY ELLIOTT GREENBERG, JACK L. SETTLE, HAROLD M. FEDER AND WARD N. HUBBARD

Chemical Engineering Division, Argonne National Laboratory, Argonne, Illinois

Received December 21, 1958

The heat of formation of zirconium tetrafluoride was measured by direct combination of the elements in a bomb calorimeter. ΔH_f° at 25° was found to be -456.80 ± 0.25 kcal. mole⁻¹. The experimental techniques are presented in detail. Because of the reactivity of fluorine, combustion calorimetry with fluorine promises to become a widely useful thermochemical procedure and should prove especially valuable in providing a means of obtaining thermochemical data for refractory compounds.

Introduction

Fluorine is an extremely reactive gas which can be made to react quantitatively with a large variety of substances. In the classical period of thermochemistry Berthelot and Moissan³ made a pioneering calorimetric study of fluorine reactions. In the 1920's and 1930's von Wartenberg and Ruff contributed a notable series of papers⁴ on the same subject. Their experimental difficulties with fluorine, however, make some of their results suspect. For example, the direct reaction of fluorine with charcoal^{4c} led to a value for the heat of formation of tetrafluoromethane of -162 kcal. mole⁻¹, whereas a value of -218 kcal. mole⁻¹^{5,6} undoubtedly is more nearly correct. Since the war, techniques for preparing and handling fluorine have improved and new materials have become available; consequently, interest in fluorine reaction calorimetry has been stimulated. Gaseous fluorine has been used successfully as a reactant in both flow calorimeters^{5,7,8} and constant-volume, glass calorimeters.⁹ In this Laboratory the techniques and materials of oxygen bomb calorimetry have been modified for use with fluorine in order to provide an additional source of thermochemical data which will meet modern standards of precision and accuracy.

(1) This work was performed under the auspices of the U. S. Atomic Energy Commission.

(2) Presented in part at the 138th meeting of the American Chemical Society in New York, September, 1960.

(3) M. Berthelot and H. Moissan, *Ann. chim. et phys.*, [6] **23**, 570 (1891).

(4) (a) H. v. Wartenberg and O. Fitzner, *Z. anorg. allgem. Chem.*, **161**, 313 (1926); (b) H. v. Wartenberg and G. Klinkott, *ibid.*, **193**, 409 (1930); (c) O. Ruff and H. Wallauer, *ibid.*, **196**, 421 (1931); (d) O. Ruff and W. Menzel, *ibid.*, **198**, 375 (1931); (e) H. v. Wartenberg, *ibid.*, **200**, 235 (1931); (f) H. v. Wartenberg and H. Schütza, *ibid.*, **206**, 65 (1932); (g) H. v. Wartenberg and R. Schutte, *ibid.*, **211**, 222 (1933); (h) H. v. Wartenberg, *ibid.*, **242**, 406 (1939).

(5) D. W. Scott, W. D. Good and G. Waddington, *J. Am. Chem. Soc.*, **77**, 245 (1955).

(6) (a) R. S. Jessup, R. E. McCoskey and R. A. Nelson, *ibid.*, **77**, 244 (1955); (b) C. A. Neugebauer and J. L. Margrave, *J. Phys. Chem.*, **60**, 1318 (1956).

(7) R. S. Jessup, F. G. Brickwedde and M. T. Wechsler, *J. Research Natl. Bur. Standards*, **44**, 457 (1950).

(8) E.g., G. T. Armstrong and R. S. Jessup, *ibid.*, **64A**, 49 (1960).

(9) P. Gross, C. Hayman and D. L. Levi, *XVIIth Intern. Congr. Pure and Appl. Chem., Abstracts*, **1**, 90 (1959).

One obvious application of fluorine bomb calorimetry is the determination of the heats of formation of the elemental fluorides. For a few elemental fluorides ΔH_f° values have been determined¹⁰ with acceptable accuracy; for the remainder the values are only estimates¹¹ from heats of solution, solubility products and ionic entropies, and other summation methods. In fluorine bomb calorimetry the heat of formation of an elemental fluoride may be determined by direct synthesis from the elements in a bomb so that almost the entire measured energy arises from the formation of the compound. This report is concerned with the heat of formation of zirconium tetrafluoride, previously known only as an estimate of -445 ± 30 kcal. mole⁻¹¹¹ at 298°K. Because this is a first report concerning new techniques, the experimental procedures are presented in some detail.

Experimental

Fluorine Handling Manifold.—All apparatus for handling fluorine was enclosed in a well-ventilated hood.¹² High pressure fluorine supply tanks were placed in protective metal enclosures. The installation of double valves¹³ and a ballast tank between the high pressure source and the manifold facilitated the smooth reduction of pressure. The manifold was constructed mainly from Teflon-packed stainless steel valves (Autoclave Engineers Series 30 VM) and the quick-coupling fittings supplied for use with these valves. Stainless steel ferrule-type tubing fittings were used for frequently disconnected joints. Silver solder (American Platinum Works No. 355) was used only for making special joints or adapters. Where massive valves were undesirable (e.g., gas sample bulbs, infrared spectrophotometer cells) Hoke type 1103 or 413-A or a specially fabricated valve was used. Pressure measurements were made with welded Monel Bourdon tube gauges.

The corrosion resistance of nickel and most other construction metals to fluorine depends on the formation of a

(10) "Selected Values of Chemical Thermodynamic Properties," National Bureau of Standards Circular 500, U. S. Government Printing Office, Washington, D. C., 1952.

(11) E.g., L. Brewer, L. A. Bromley, P. W. Gilles and N. L. Lofgren, Paper 6, "The Chemistry and Metallurgy of Miscellaneous Materials: Thermodynamics," L. L. Quill, Editor, McGraw-Hill Book Co., Inc., New York, 1950, pp. 76-192.

(12) Safety Note: It is desirable for the operator to wear a leather coat, leather gloves, and a plastic face shield while manipulating the more fragile parts of the equipment.

(13) J. Gordon and F. L. Holloway, *Ind. Eng. Chem.*, **52**, No. 5, 63A (1960).

protective film. Before being placed into service, all equipment was thoroughly cleansed of foreign matter and pre-fluorinated by cautious, stepwise addition of fluorine until conditions of pressure and temperature were reached which were more severe than those subsequently encountered.

Fluorine.—The fluorine used in the calorimetric combustion experiments was prepared by fractional distillation of high purity (99–99.5%) tank fluorine. The still¹⁴ and its auxiliary equipment are shown in Fig. 1. The stainless-steel still pot J is equipped with liquid nitrogen jacket H and auxiliary heater I. The fractionating section of the stainless-steel column is packed with 1/8-inch diameter nickel helices and is surrounded by radiation shield G. The reflux condenser section of the column is cooled by liquid nitrogen jacket C. The entire still is encased in an evacuated brass cylinder to reduce heat leakage.

Approximately 250 g. of fluorine was fractionated per distillation. The operation of the still was relatively uncomplicated and only the following points need be mentioned. (1) During introduction of the fluorine the reflux condenser was maintained colder than the still pot jacket in order to condense fluorine at the top of the column to wet the packing. (2) The still was operated under total reflux for about one hour. (3) Forecuts, some containing as much as 10% impurity, were discarded *via* a chemical trap; condensation in the receiver was begun when less than 0.2% impurity was detected in the overhead vapors. Distillation of the main fraction required about five hours.

The quantity of impurity in the fluorine was determined by the mercury titration method.⁸ Mass spectrometric analysis of the residual gas from the titration indicated that the impurities in the fractionally distilled fluorine consisted of about 0.04% oxygen, 0.01% nitrogen, and traces of argon and helium. The distilled fluorine was transparent in the infrared.

Helium.—U. S. Bureau of Mines, Grade A, helium (99.995%) was used.

Zirconium.—Iodide-deposited, hafnium-free (<1000 p.p.m.), Grade I crystal bar, supplied by Westinghouse Electric Corp., Pittsburgh, Pa., was arc-melted, cast, and rolled to 0.1 × 0.1 inch rods and 0.005 inch foil. Table I is a summary of the impurities found in the zirconium sample. No other metallic impurities were detected. The sample was thus about 99.95% zirconium. The chemical state of the impurities was unknown. High-purity zirconium wire (0.010 inch diameter), used as fuse material, was obtained from The Carborundum Co., Akron, N. Y. The composition of the zirconium fuse is not reported here because of its negligible effect.

TABLE I
IMPURITIES IN ZIRCONIUM SAMPLE

Element	P.p.m.	Element	P.p.m.
Spectrochemical analysis			
Zn	150	Pb	7
Si	70	Na	7
Cu	70	Mn	3
Fe	40	Ag	3
Al	30	Mg	2
Ni	15	B	0.3
Chemical analysis			
C	56	H	27
O	28	N	<10

Combustion Technique.—Preliminary combustions were performed in a glass bomb¹⁵ in order to observe the ignition and burning characteristics of zirconium. Zirconium wire and foil were readily ignited electrically; they, in turn, could be used to ignite more massive pieces. Zirconium, when burned in pure fluorine, melted and dropped onto the support assembly. By appropriate dilution of the fluorine with helium the burning temperature was sufficiently lowered to prevent melting, and upright rods underwent smooth, flameless combustion. Most of the combustion product sublimed to the cooler parts of the bomb.

(14) This still was patterned after a smaller version constructed by L. Stein of this Laboratory.

(15) R. L. Nuttall, M. A. Frisch and W. N. Hubbard, *Rev. Sci. Instr.*, **31**, 461 (1960).

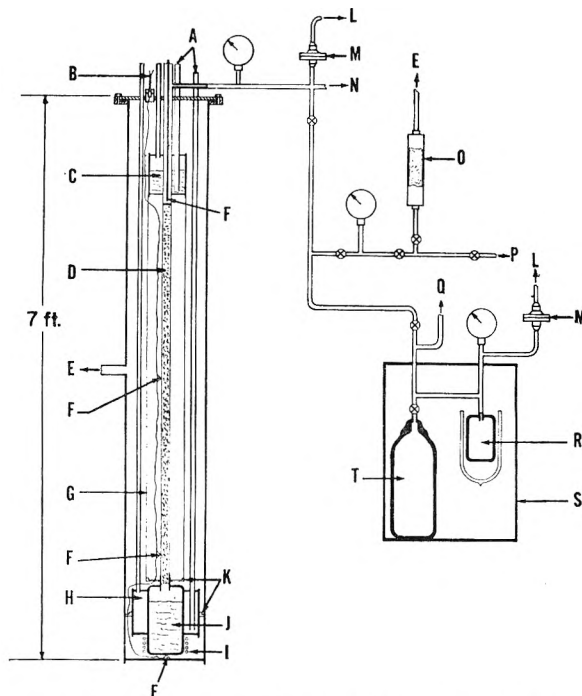


Fig. 1.—Fluorine still: A, coolant filling tubes; B, electrical leads; C, reflux condenser; D, packing, nickel helices; E, connection to vacuum; F, thermocouple; G, radiation shield; H, still pot jacket; I, resistance heater; J, 400-ml. still pot; K, Lucite spacers; L, connection to surge tank; M, rupture disc; N, connection to commercial fluorine supply; O, activated alumina trap; P, connection to gas sample bulb; Q, connection to bomb charging manifold; R, purified fluorine condenser; S, metal enclosure; T, purified fluorine storage cylinder.

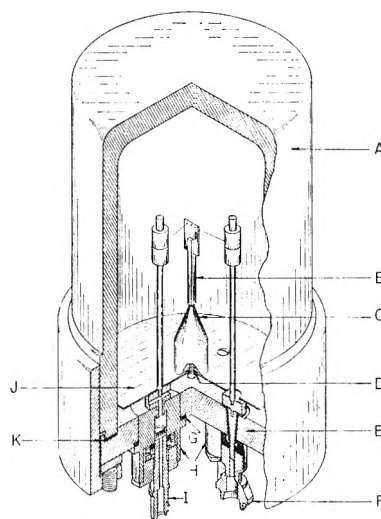


Fig. 2.—Combustion bomb and sample arrangement: A, body (nickel); B, sample (zirconium); C, sample stand (nickel); D, electrical insulation (Teflon); E, cap (nickel); F, insulated electrode terminal (stainless steel); G, gasket (lead); H, valve housings (nickel); I, valve stem (hard Monel); J, protective disc (nickel); K, gasket (gold).

The sample arrangement which evolved from these preliminary experiments is shown in Fig. 2. The top of the sample rod B was slotted to accommodate a small piece of 0.005 inch foil which was crimped in place. The fuse wire was threaded through three small holes in the foil. The lower end of the rod was turned down to a 0.035 inch pin and inserted into a relatively massive nickel sample stand C. The stand provided an effective heat sink so that the burn-

ing of the rod was extinguished after about 75% was consumed. This arrangement obviated the necessity for providing an inert support for the burning zirconium which was, in effect, always supported by unburned zirconium. The contact area between the sample rod and the sample stand remained relatively cool and no evidence of reaction between zirconium and nickel was observed.

Reaction Products.—Chrétien and Gaudreau¹⁶ observed only β -ZrF₄ to be formed by the combustion of zirconium in fluorine. In the present investigation, this observation was confirmed by X-ray diffraction analysis of the products of several calorimetric combustions. With the exception of a few very faint lines all of the diffraction lines observed could be assigned to the pattern for the beta variety of zirconium tetrafluoride.^{17,18}

After each of several calorimetric runs a portion of the gas remaining in the bomb was discharged into an infrared cell equipped with silver chloride windows. The observed absorption bands could be attributed to CF₄, SiF₄ and a trace of HF. Another portion of the bomb gas was allowed to react with mercury for removal of fluorine, and the residual gas then was subjected to mass spectrometric analysis. The bomb atmosphere after combustion was thus shown to contain about 0.1% N₂ and 0.2% O₂. All of the gaseous impurities could be qualitatively accounted for as arising from contaminants in the zirconium sample and in the fluorine charge.

Determination of the Amount of Reaction.—After the completion of each calorimetric measurement the bomb gases were discharged and the unburned zirconium was recovered and weighed. The parts which were weighed included the unburned portion of the sample rod, the unconsumed ends of the fuse wire, and two small beads, each weighing less than one milligram, which had apparently fused, ripped from the ends of the fuse wire, and solidified rapidly. These parts were soaked in water to loosen adherent zirconium tetrafluoride, scrubbed with Nylon tweezers, and scraped clean with a razor blade.

Calorimetric System.—The calorimetric system, which consisted of the bomb (Ni-T), the calorimeter (ANL-R1), the isothermal jacket and the temperature measuring equipment, was a rotating bomb system.^{19,20} The operational procedure was conventional¹⁹ except that the bomb was not rotated in these experiments. The combustion bomb (Fig. 2) had an internal volume of 0.358 l. The body A and cap E were fabricated of commercial nickel (Grade A) and were sealed together with a 0.06 inch thick, soft gold gasket K. Two nickel valve housings H were screwed into the cap and sealed with lead gaskets G. The valve packing gland parts were made of nickel; the packing was a Teflon washer. A Teflon disc was recessed in the end of the threaded, hard-Monel valve stem I; closure was effected by seating the disc against the port of the valve. Teflon tubing was used as a gasket between the insulated electrode and the cap. A nickel disc J served to shield the cap and its fittings. The electrode parts were made of nickel. Thin Teflon discs D were used for electrical insulation. The external parts of the bomb which were not in contact with fluorine were made of stainless steel.

System Calibration.—The energy equivalent of the calorimetric system, $\epsilon(\text{calor.})$, was determined by combustion of benzoic acid (N.B.S. Standard Sample No. 39g). The heat of combustion of this sample was given as $26,433.8 \pm 2.6$ absolute joules ($6,317.83 \pm 0.62$ defined calories) per gram mass under certificate conditions. Ignition energy was measured with a current integrating circuit similar to one already described.²¹ Thirteen satisfactory benzoic acid calibration combustions were completed, some preceding and some following the zirconium combustions. Both one-half and one gram samples of benzoic acid were used. The temperature rises for these samples bracketed the temperature rises obtained in the zirconium combustions.

(16) A. Chrétien and B. Gaudreau, *Compt. rend.*, **248**, 2878 (1959).

(17) R. D. Burbank and F. N. Bensey, Jr., U. S. Atomic Energy Commission Report K-1280 (1956).

(18) A. Chrétien and B. Gaudreau, *Compt. rend.*, **246**, 2266 (1958).

(19) W. N. Hubbard, C. Katz and G. Waddington, *J. Phys. Chem.*, **58**, 142 (1954).

(20) W. D. Good, D. W. Scott and G. Waddington, *ibid.*, **60**, 1080 (1956).

(21) G. Pilcher and L. E. Sutton, *Phil. Trans. Roy. Soc. London*, **A248**, 23 (1955).

The average value for $\epsilon(\text{calor.})$ was 3567.0 cal. deg.⁻¹, with a standard deviation of the mean of 0.3 cal. deg.⁻¹, or 0.01%.

Bomb Charging Procedure.—The assembled bomb was connected to a manifold, evacuated, purged three times with 9 atmospheres of helium and once with one atmosphere of fluorine. The bomb then was charged with a gas mixture which, at 25°, consisted of 2000 mm. pressure of pure fluorine and sufficient helium to raise the total pressure to 12.0 atm. If no leaks²² were detected by discoloration of moist strips of starch-iodide paper or by the odor of fluorine, the bomb was placed in the calorimeter and the calorimetric measurements were made in the usual manner.^{19,23}

To test for the absence of reaction between zirconium and fluorine before intentional ignition, the bomb was charged, allowed to stand, and discharged. No significant change in weight of the zirconium sample was observed.

Results

Experimental Results.—Table II is a summary of the results of seven combustion experiments, expressed in terms of the defined calorie equal to (exactly) 4.184 absolute joules. The corrections to standard states²⁴ were applied with suitable modification²⁵ for fluorine bomb calorimetry. The entries in Table II are: (1) the mass *in vacuo* of the zirconium reacted; (2) the observed increase in the calorimeter temperature, corrected for heat exchanged between the calorimeter and its surroundings; (3) the energy equivalent of the calorimetric system, multiplied by the corrected temperature increase; (4) the energy absorbed by the contents of the bomb during the hypothetical isothermal process at 25°; (5) the measured energy input for ignition of the fuse; (6) the correction for the hypothetical compression and decompression of the bomb gases; (7) the net correction for impurities in the zirconium sample; and (8) the energy change per gram of zirconium for the reaction



with the reactants and products in their standard states at 25°.

For calculation of item 4 the following values were assumed: Heat capacities at constant pressure of 0.1058, 0.28, 0.0659 and 0.148 cal. deg.⁻¹ g.⁻¹ for Ni,¹⁰ Teflon,²⁰ Zr²⁶ and ZrF₄,²⁷ respectively; heat capacities at constant volume of 5.50 and 2.981 cal. deg.⁻¹ mole⁻¹ for F₂²⁸ and He,¹⁰ respectively. The coefficients $(\partial E/\partial P)_T$, and μ (in the equation $PV = nRT(1 - \mu P)$) which are required for calculation of item 6, were estimated by the method of Hirschfelder, *et al.*,²⁹ from the force constants for F₂³⁰ and

(22) Leakage of fluorine into the calorimeter water-bath was a potential hazard. It was found that as much as 500 ml. per min. of fluorine could be introduced into water through a small opening without the occurrence of a violent reaction.

(23) J. Coops, R. S. Jessup and K. van Nes, Chapter 3, "Experimental Thermochemistry," F. D. Rossini, Editor, Interscience Publishers, Inc., New York, N. Y., 1956, pp. 27-58.

(24) W. N. Hubbard, D. W. Scott and G. Waddington, Chapter 5, "Experimental Thermochemistry," F. D. Rossini, Editor, Interscience Publishers, Inc., New York, N. Y., 1956, pp. 75-128.

(25) W. N. Hubbard, Chapter 5, Vol. II, "Experimental Thermochemistry," H. A. Skinner, Editor, Interscience Publishers, Inc., New York, N. Y., to be published.

(26) G. B. Skinner and H. L. Johnston, *J. Am. Chem. Soc.*, **73**, 4549 (1951).

(27) E. F. Westrum, Jr., and D. H. Terwilliger, to be published.

(28) W. H. Evans, T. R. Munson and D. D. Wagman, *J. Research Natl. Bur. Standards*, **55**, 147 (1955).

(29) J. O. Hirschfelder, C. F. Curtiss and R. B. Bird, "Molecular Theory of Gases and Liquids," John Wiley and Sons, New York, N. Y., 1954.

TABLE II
 RESULTS OF COMBUSTION EXPERIMENTS^c

1. m , g.	0.99354	1.01707	1.00775	1.0370 ^b	1.03397	1.03119	1.03902
2. Δt_c , deg.	1.38883	1.42021	1.40831	1.45052	1.44617	1.44187	1.45247
3. ϵ (calor.)($-\Delta t_c$), cal.	-4954.68 ^c	-5066.63 ^c	-5024.17 ^c	-5173.96	-5159.52	-5143.11	-5180.92
4. $\Delta E_{\text{contents}}$, cal. ^d	-10.65	-10.89	-10.80	-11.13	-11.10	-11.06	-11.14
5. $\Delta E_{\text{ignition}}$, cal.	1.98	1.90	2.00	2.19	1.79	1.91	1.17
6. ΔE_{gas} , cal. ^e	-0.23	-0.23	-0.23	-0.24	-0.24	-0.24	-0.24
7. $\Delta E_{\text{impurities}}$, cal.	1.12	1.15	1.14	1.17	1.17	1.17	1.17
8. $\Delta Ec^\circ/M$, cal. g. ⁻¹	-4994.72	-4989.53	-4993.37	-4997.08	-4998.11	-4995.52	-4995.05

Av. $\Delta Ec^\circ/M = -4994.8$ cal. g.⁻¹

Std. dev. of mean = ± 1.1 cal. g.⁻¹

^a The symbols employed are explained in ref. 24. ^b The mass of one of the fused beads from the fuse wire had to be estimated. ^c Because of parts replacements, ϵ (calor.) for these experiments was $3567.5 \text{ cal. deg.}^{-1}$. ^d $\Delta E_{\text{contents}} = \epsilon(\text{cont.})(t_i - 25) + \epsilon(\text{cont.})(25 - t_i + \Delta t_{\text{corr.}})$ in which t_i was 23.481° . ^e $\Delta E_{\text{gas}} = \Delta E^f(\text{gas.})]_0^{P^i(\text{gas.})} + \Delta E^f(\text{gas.})]_0^{P^f(\text{gas.})}$.

He.²⁹ The coefficients, as functions of composition, at 25° were

$$\mu = 0.000801(1 - 3.61x + 2.03x^2)\text{atm.}^{-1} \quad (2)$$

$$(\partial E/\partial P)_T = -1.780(1 - 1.767x + 0.7635x^2) \text{ cal. atm.}^{-1} \text{ mole}^{-1} \quad (3)$$

where x represents the mole fraction of helium in the mixture. For estimating the internal volume of the bomb these densities were assumed: 8.90, 2.24, 6.50 and 4.43 g. cc.⁻¹ for Ni, Teflon,²⁰ Zr and ZrF₄, respectively.

Hydrogen, oxygen and carbon were assumed to be present in the sample as ZrH₂, ZrO₂ and ZrC, respectively. The gaseous combustion products of these impurities were assumed to be HF, O₂ and CF₄, respectively. The remaining impurities were assumed to be present in the sample as elements, and to form their most stable fluorides during combustion. The requisite heats of formation were taken from reference 10 except for ZrH₂³¹ and CF₄.⁵ The corrections to the measured heat for the known impurities were: H, +0.018%; Si, +0.010%; C, +0.009%; O, -0.008%; Zn, -0.007%; Al, +0.004%; Cu, -0.004%; all others (including hafnium) negligible. The net correction for all impurities (item 7) was $(+0.02 \pm 0.02)\%$ of the measured heat. The large uncertainty attached to the impurity correction arises in part from analytical uncertainties and in part from the possibility that the elements existed in states of combination other than those assumed.

The remaining corrections to standard states were all negligible. $\Delta Ec^\circ/M$ is just the sum of items 3 through 7 divided by the mass of zirconium reacted.

Observation of the preliminary combustions in a transparent bomb permitted an estimate to be made of the time-temperature conditions which might prevail in the calorimetric bomb during combustion. By combining this information with data³² on the kinetics of the nickel-fluorine reaction the maximum heat effect due to formation of nickel fluoride was estimated to be a quarter of a calorie per experiment.

Derived Data.—The following data were de-

rived for the formation of β -zirconium tetrafluoride at 25°

Energy of formation, $\Delta Ef^\circ = \Delta Ec^\circ = -455.62 \pm 0.25$ kcal. mole⁻¹

Heat of formation, $\Delta Hf^\circ = -456.80 \pm 0.25$ kcal. mole⁻¹

Entropy of formation, $\Delta Sf^\circ = -81.16$ cal. deg.⁻¹ mole⁻¹

(Gibbs) free energy of formation, $\Delta Ff^\circ = -432.69 \pm 0.25$ kcal. mole⁻¹

The atomic weight of zirconium³³ was taken as 91.22 g. (g.-atom)⁻¹. The entropies, S° , at 25° , of Zr(c),²⁴ F₂(g)²⁶ and ZrF₄(c)²⁵ were taken as 9.29, 48.45 and 25.03 cal. deg.⁻¹ mole⁻¹, respectively. The estimated uncertainties given are uncertainty intervals³¹ equal to twice the combined standard deviations arising from known sources.

Discussion

The standard heat of formation of zirconium tetrafluoride has been determined to be -456.80 ± 0.25 kcal. mole⁻¹ by direct combination of the elements in a bomb calorimeter. This value should replace a previous estimate¹¹ of -445 ± 30 kcal. mole⁻¹.

The precision of the present results appears to be comparable with that obtained by oxygen bomb calorimetry. Important sources of systematic errors, such as impure materials and extraneous reactions with support materials and glass, which confronted earlier workers in fluorine reaction calorimetry, were largely overcome in this research. The applicability of fluorine bomb calorimetry appears greatly enhanced by the evidence that no significant reaction occurred between the fluorine and the nickel borab.

In addition to the determination of the heats of formation of elemental fluorides, fluorine combustion calorimetry may be applicable to a variety of stable, inert substances. Examples of substances which we hope to study by this new technique are BN, SiC, MoSi₂, or, in general, the refractory compounds resulting from the combinations of boron, carbon, nitrogen and silicon with each other, and with metallic elements. Heat of formation determinations for these substances often are lacking because of the inapplicability of standard methods such as oxygen bomb or solution calorimetry.

(30) D. White, J. H. Hu and H. L. Johnston, *J. Chem. Phys.*, **21**, 1149 (1953).

(31) A. Sieverts, A. Gotta and S. Halberstadt, *Z. anorg. allgem. Chem.*, **187**, 155 (1930).

(32) E. J. Barber and H. A. Bernhardt, U. S. Atomic Energy Commission Report K-1421 (1959).

(33) E. Wichers, *J. Am. Chem. Soc.*, **80**, 4121 (1958).

(34) F. D. Rossini, Chapter 14, "Experimental Thermochemistry," F. D. Rossini, Editor, Interscience Publishers, Inc., New York, N. Y., 1956, pp. 297-320.

The accumulation of the missing data will be useful to the growing field of high temperature chemistry.

Acknowledgment.—The assistance of Messrs. R. W. Bane, B. D. Holt, J. A. Goleb and R. V.

Schablaske in performing special analyses is greatly appreciated. We also wish to thank F. J. Karasek for fabricating the zirconium rod and foil for these experiments.

THERMOLUMINESCENCE IN ARAGONITE AND MAGNESITE

BY W. L. MEDLIN

Socony Mobil Oil Company, Inc., Field Research Laboratory, Dallas, Texas

Received December 25, 1960

The important features of thermoluminescence in aragonite and magnesite have been studied by investigating the properties of synthetic samples. The synthetic aragonite samples were prepared by precipitation at 80–90° and the magnesite samples were precipitated by hydrothermal techniques. The results of adding all of the impurities which may occur in natural samples and which are likely to produce thermoluminescence have been investigated by coprecipitating each of them in synthetic samples. The effects of vacancy defects have also been considered. The results show that all of the thermoluminescence in natural samples is due to the presence of divalent manganese. It was also found that Co^{++} and Ni^{++} quench the Mn^{++} luminescence in both minerals whereas Fe^{++} is a quencher in aragonite only. Quantitative results have been compiled for the luminescent efficiency of each of the Mn^{++} glow peaks in aragonite and magnesite as a function of impurity concentration. Quantitative results have also been included to illustrate the relative quenching effects of Fe^{++} , Co^{++} and Ni^{++} . The impurity concentrations in the synthetic samples were determined by colorimetric methods. Measurements of isothermal decay curves were made for each of the prominent glow peaks in aragonite and magnesite and the effect of varying the temperature and the excitation time was investigated. The activation energies associated with the traps for most of the glow peaks also were determined. Glow curves for natural samples are compared with the curves for synthetic samples and the results interpreted on the basis of impurity concentrations in the natural samples. Practical applications of the results are discussed.

I. Introduction

All of the common naturally occurring carbonate minerals including calcite, dolomite, aragonite and magnesite are thermoluminescent to some extent. The properties of calcite and dolomite have been investigated^{1,2} and it has been shown that the prominent glow peaks found in natural samples are due to the presence of divalent manganese. This paper describes an investigation of the thermoluminescent properties of aragonite and magnesite which are closely related in crystal structure to calcite and dolomite.

The general procedure followed here is the same one used for the calcite and dolomite investigations. High purity samples containing one or more added impurities were prepared by coprecipitation methods and the thermoluminescent properties of the synthetic samples were compared with the characteristics of natural samples. The effects of certain lattice defects such as ion vacancies were also studied.

In determining the concentrations of the various impurities in the synthetic samples, the colorimetric methods used for the calcite and dolomite investigations were applicable with only minor changes in procedure. Analyses of natural samples were made spectrographically. The glow curve apparatus used here has been described in a previous article.³ The samples were heated at a constant rate of 0.5 deg./sec. The departure from linearity of the heating rate was less than 5% above 100°K. and the temperature variation over the surface of the sample was less than 5°K. All samples were excited by 35 K.V. X-rays from a Mo tube operated at 20 ma. plate current. For most of the glow curves a 5 minute excitation period was used

which provided an exposure of about 500 roentgens.

The results of this investigation satisfactorily explain all of the important thermoluminescent properties of natural samples of aragonite and magnesite.

II. Experimental Procedure and Results

The direct precipitation of aragonite by the mixing of calcium and carbonate ions in solution is hindered by the formation of calcite which is the most stable polymorph of CaCO_3 under normal conditions (a third form, vaterite is less stable than aragonite). However, at elevated temperatures the relative stability of aragonite increases and between 80 and 100° it is possible to obtain nearly pure aragonite by initially seeding the solution.

A more convenient method which takes advantage of the differences in crystal structure between aragonite and calcite was used here. It was found that the presence of trace amounts of such impurities as Sr^{++} or Hg^{++} in the original solution favors the precipitation of aragonite because of similarities in coordination numbers and ionic radii. The theoretical coordination number of the Ca^{++} ion in calcite is only 6 whereas it is 8 in aragonite; furthermore, the ionic radius of Ca^{++} is slightly larger in aragonite. It follows that impurity ions such as Hg^{++} and Sr^{++} which exhibit an 8 coordination only and have about the right ionic radii should enhance the precipitation of aragonite. In practice, Sr^{++} was found to be better for this purpose than Hg^{++} and the optimum concentration was about 1000 p.p.m.

Improved results were obtained by controlling both the concentrations of the Ca^{++} and CO_3^{--} solutions and the rate of addition of the Ca^{++} solution. It was found that 0.05 *M* solutions of $\text{Ca}(\text{NO}_3)_2$ and Na_2CO_3 solutions provided the best results when the Ca^{++} solution was added at a rate of 20 ml./min. The temperatures of both solutions were maintained at $90 \pm 5^\circ$ and the rate of addition was controlled by adding the Ca^{++} solution dropwise from a heated separatory funnel. The carbonate solution was stirred during the precipitation to maintain reasonably homogeneous distributions of the various ions. The impurities added to the aragonite samples were included in the calcium ion solution since their carbonates usually were insoluble.

The $\text{Ca}(\text{NO}_3)_2$ solution was prepared by dissolving high purity CaCO_3 (provided by Johnson-Mathey Company of England) in HNO_3 . The carbonate solution was prepared with high purity Na_2CO_3 (also available from Johnson-Mathey Company).

(1) W. L. Medlin, *J. Chem. Phys.*, **30**, 451 (1959).

(2) W. L. Medlin, *J. Chem. Phys.*, **34**, 672 (1961).

(3) W. L. Medlin, *Phys. Chem. Solids*, **18**, 238 (1961).

The precipitation of magnesite presents a special problem because the stable forms of $MgCO_3$ under normal conditions are the hydrates, $Mg_2(OH)_2CO_3 \cdot 3H_2O$ and $5MgO \cdot 4CO_2 \cdot 5H_2O$. At elevated temperatures nesquehonite, $MgCO_3 \cdot 3H_2O$ can be precipitated and magnesite can be obtained by heating this precipitate to temperatures high enough to remove the water of hydration. However, this method is not acceptable for the present application because the removal of the water molecules ruptures the crystal lattice badly enough to prevent the formation of sufficiently large crystallites of magnesite.

A satisfactory method of precipitating well crystallized samples of magnesite at elevated temperatures and CO_2 pressures has been developed by Jantsch and Zemek.⁴ A modified version of their procedure has been used here. The method consists of raising the temperature of an acid solution of $MgCl_2$ and urea under a CO_2 pressure of several atmospheres. At elevated temperatures, the urea decomposes to form NH_3 and CO_2 which raises the pH of the solution sufficiently to precipitate magnesite, the stable form of $MgCO_3$ under these conditions. The precipitation of the hydrated forms at lower temperatures is prevented by the acidity of the solution. The impurity ions to be included in the magnesite lattice were coprecipitated by adding them, in appropriate concentrations, to the $MgCl_2$ solutions.

The samples were precipitated at 220° under 60 atmospheres of CO_2 pressure in a 1 liter autoclave. It was possible to include five samples in the autoclave chamber by using 35 ml. Pyrex test-tubes filled to about 70% of their volume with the $MgCl_2$ -urea solution. In order to obtain sufficient quantities of sample under these conditions it was necessary to use concentrations of 0.018 g./ml. Mg^{++} , 0.013 g./ml. urea, and 0.7% HCl. The solutions were protected from contamination by loose-fitting glass covers on the sample tubes. The autoclave was filled to about 30% of its volume with water to provide thermal contact with the walls. At 220° the 30% fill was not enough to raise the water level above the tops of the sample tubes so that there was no danger of contamination from this source.

Under these conditions the complete precipitation required 10 to 12 hours. The precipitation is more rapid at higher temperatures but above 220° the solubility of the Pyrex sample tubes is high enough to contaminate the samples with silicon and other glass constituents.

It is reasonable to assume that most of the trapping sites and luminescent centers which produce thermoluminescence in aragonite and magnesite are due to the presence of impurity ions. In order to explain the glow peaks in naturally occurring samples of these minerals it is possible to eliminate a number of impurities either because they are not likely to serve as activators or because they are not normally found in natural samples. All impurity ions with only one possible valence state are eliminated for the first reason⁵ and all of the rare earth elements can be disregarded for the second reason. On this basis the following impurities have been investigated: Pb^{++} , Zn^{++} , Cd^{++} , Sb^{+++} , Co^{++} , Ni^{++} , Fe^{++} , Sn^{++} , Bi^{+++} , Cu^+ , Li^+ , Al^{+++} , Ag^+ and Mn^{++} . Each of these ions was included in the lattice of synthetic aragonite and magnesite samples by the coprecipitation methods described earlier. The inclusion of anion impurities was not considered since they appear to be unimportant in the carbonate minerals.

The effects of cation and anion vacancies were investigated by adding Sn^{4+} and $P_2O_4^{4-}$ ions, respectively. It is reasonable to assume that these tetravalent ions introduce cation and anion vacancies to compensate for the charge differences involved but there is no direct evidence that either ion is included in the aragonite or magnesite lattice. The addition of these ions did not affect the thermoluminescence of either aragonite or magnesite.

Of the impurities mentioned above, Mn^{++} was the only ion found to be an activator of thermoluminescence in either aragonite or magnesite. Figure 1 shows the glow curves for some synthetic aragonite samples containing various concentrations of Mn^{++} and in Fig. 2 the results for magnesite are illustrated. In aragonite the Mn^{++} activator accounts for two prominent glow peaks at 180 and $250^\circ K$. All of the thermoluminescence is confined to temperatures below $300^\circ K$, which is not surprising since aragonite is converted to calcite (at a temperature dependent rate) above $400^\circ K$.

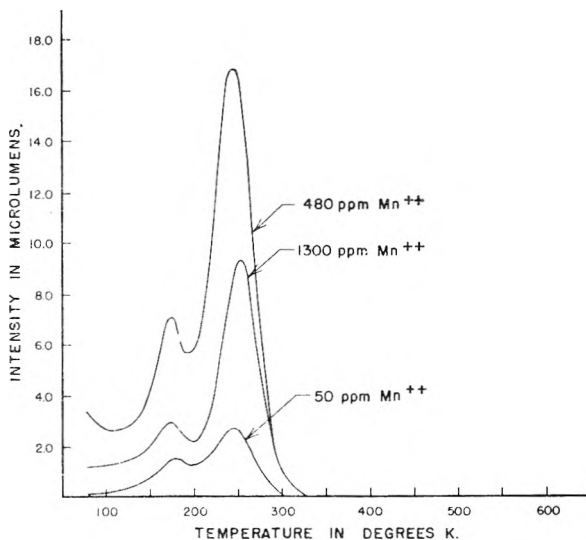


Fig. 1.—Glow curves for some synthetic aragonite samples containing various concentrations of Mn^{++} .

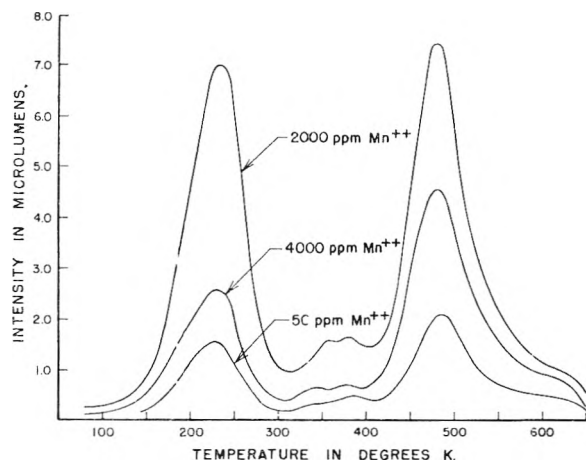


Fig. 2.—Glow curves for some synthetic magnesite samples containing various concentrations of Mn^{++} .

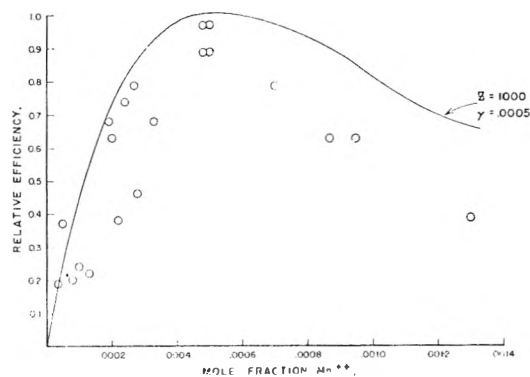


Fig. 3.—Efficiency of thermoluminescence for the $180^\circ K$ glow peak due to Mn^{++} in aragonite. The theoretical curve was computed from equation 1 for $z = 1000$ and $\gamma = 0.0005$.

The two prominent glow peaks are preceded at lower temperatures by a more or less continuous level of emission which is roughly proportional in intensity to the peak heights.

The effects of annealing at elevated temperatures have also been investigated. The glow curves for natural samples of aragonite and magnesite were unaffected by this treatment but it was found that the glow peaks were measurably en-

(4) G. Jantsch and F. Zemek, *Radex Rundschau*, **3**, 110 (1949).

(5) R. Ward, *J. Phys. Chem.*, **57**, 773 (1953).

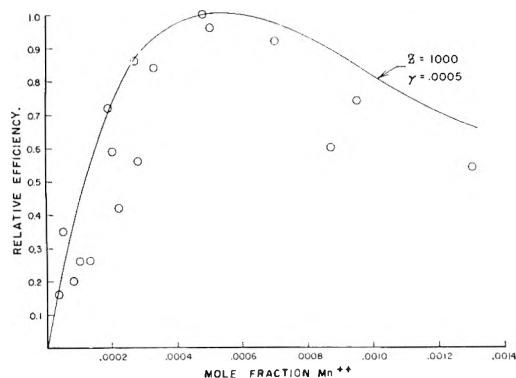


Fig. 4.—Efficiency of thermoluminescence for the 250°K. glow peak due to Mn^{++} in aragonite. The theoretical curve was computed from equation 1 for $z = 1000$ and $\gamma = 0.0005$.

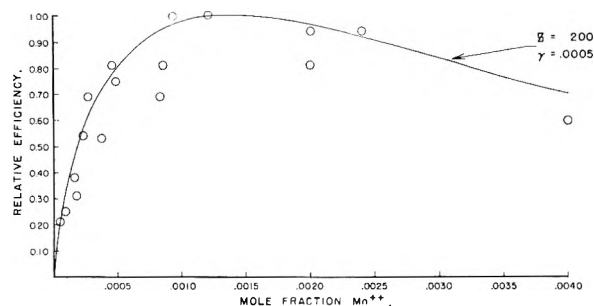


Fig. 5.—Efficiency of thermoluminescence for the 230°K. glow peak due to Mn^{++} in magnesite. The theoretical curve was computed from equation 1 for $z = 200$ and $\gamma = 0.0005$.

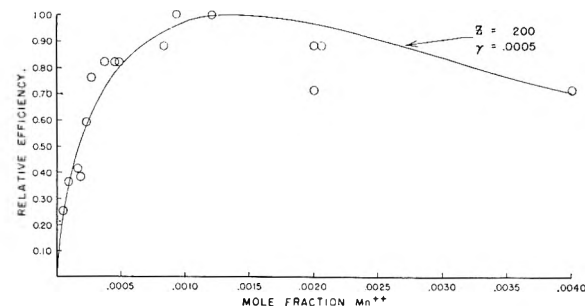


Fig. 6.—Efficiency of thermoluminescence for the 480°K. glow peak due to Mn^{++} in magnesite. The theoretical curve was computed from equation 1 for $z = 200$ and $\gamma = 0.0005$.

hanced in the synthetic aragonite samples. There was no effect in the synthetic magnesite samples. The aragonite samples were annealed for several hours at 110–120° which is about the maximum allowable to avoid conversion to calcite. The magnesite samples were annealed for several hours at 450° which is just below the range of decomposition to MgO.

The results of annealing at elevated temperatures are in accordance with those observed for calcite and dolomite, which have been interpreted on the basis of localized distortions removed by heating. The effect is presumably not observed in the magnesite samples prepared at elevated temperatures and pressures because distortions of this type are removed during growth.⁶ Since natural samples are unaffected by annealing it appears that the distortions have been removed in this case at the ambient temperature of the earth's crust over geologic times.

The two glow peaks due to Mn^{++} in aragonite are sufficiently separated to determine the relative efficiency of thermoluminescence for each of them as a function of impurity concentration. These results are plotted in Fig. 3 and

4 and the accompanying theoretical curves were computed from the expression for an isolated activator ion

$$\eta = \frac{c(1-c)^z}{c + \gamma(1-c)} \quad (1)$$

where η is the efficiency of thermoluminescence, c is the molar concentration and z and γ are parameters characteristic of the spacing between impurity ions and the cross sections for trapping and recombination.⁷

In magnesite the presence of Mn^{++} accounts for two prominent glow peaks at 230 and 480°K. and at least three minor peaks at 340, 380 and 620°K. In general the glow peaks in magnesite are broader than those in any of the other carbonates, probably because the electron traps are spread over a range of energies in this case. The efficiency of luminescence for the two prominent glow peaks in magnesite is plotted in Fig. 5 and 6 along with the theoretical curves.

The quenching properties of Fe, Co and Ni have been well established in both calcite and dolomite and similar effects are to be expected in aragonite and magnesite. The effects of these impurities as well as Cu^{++} , Al^{+++} and Be^{++} which sometimes act as quenchers have been investigated by adding increasing concentrations of each along with a constant amount of Mn^{++} . The manganese concentrations were chosen to correspond approximately to the optimum levels (500 p.p.m. for aragonite and 1500 p.p.m. for magnesite) so that small fluctuations would not affect the glow peak intensities appreciably. The largest variations in Mn^{++} content for all of the samples was less than 100 p.p.m. Fe was added in both the 2+ and 3+ states but it was impossible to add the divalent ion without including some of the trivalent ion also.

The results showed that in aragonite, Fe^{++} , Co^{++} and Ni^{++} inhibited the Mn^{++} luminescence whereas in magnesite only Co^{++} and Ni^{++} acted as quenchers. It should be noted that for very low concentrations Co^{++} enhances the Mn^{++} luminescence in magnesite. In both cases Fe^{+++} , Al^{+++} , Cu^{++} and Be^{++} had no effects on the glow peaks due to Mn^{++} . Some representative results are shown in Fig. 7 and 8 for aragonite and Fig. 9 for magnesite. The results are plotted as relative efficiency of thermoluminescence as a function of the quenching-ion concentration for the 250°K. glow peak in aragonite and the 230°K. peak in magnesite. Similar results were obtained for the glow peak at 180°K. in aragonite and at 480°K. in magnesite.

All of the impurity concentrations for the activator and quencher ions in synthetic samples were determined by colorimetric methods. This technique offers several advantages in this case. All of the impurities to be determined (Mn, Fe, Co and Ni) are transition elements which form strong color complexes and since both aragonite and magnesite are very soluble in acid solutions it is possible to determine concentrations of only a few p.p.m. with good accuracy. Furthermore, the difficulty of interference from other impurities is eliminated because the samples were of high purity except for the added activator or quencher ions. The procedures for all of the ions involved here already have been developed for calcite¹ and dolomite.²

The decay of phosphorescence measured at constant temperatures near a glow peak provides information about the electronic transitions involved in the trap emptying and recombination processes. The decay curves for all of the principal glow peaks due to Mn^{++} in aragonite and magnesite have been measured and found to be of the form

$$I = I_0 \left(\frac{b}{b+t} \right)^m \quad (2)$$

where b and m are constants. This form of decay has been observed for calcite, dolomite and anhydrite³ and can be interpreted as being characteristic of a second-order mechanism.³ A first-order process would result in an exponential decay but it can be shown that a proper combination of first-order decay curves would result in a decay having the form of equation 2.⁹ Therefore the decay curves could possibly be interpreted as indicating a first-order decay process from a distribution of trapping levels.

Some measured values for the parameters b and m are given in Table I for the 250°K. peak due to Mn^{++} in

(7) P. D. Johnson and F. E. Williams, *ibid.*, **18**, 1477 (1950).

(8) J. Saddy, *J. Phys. Rad.*, **20**, 890 (1959).

(9) E. I. Adirovitch, *ibid.*, **17**, 705 (1956).

(6) W. L. Medlin, *J. Chem. Phys.*, **31**, 943 (1960).

aragonite and the 230 and 480°K. peaks due to Mn⁺⁺ in magnesite. The results show that *b* increases with excitation time whereas *m* remains approximately constant. The effect of temperature cannot be determined over any appreciable ranges because of interference between neighboring glow peaks (cf. Fig. 1 and 2) except for the region above the 250°K. Mn⁺⁺ peak in aragonite.

TABLE I

VALUES OF THE PARAMETERS *b* AND *m* FOR ISOTHERMAL DECAY IN ARAGONITE AND MAGNESITE

Sample	Impurity, p.p.m.	Glow peak (°K.)	Excitation time (sec.)	Temp. (°K.)	<i>b</i>	<i>m</i>
Aragonite	80 Mn ⁺⁺	250	45	245	15	1.1
Aragonite	80 Mn ⁺⁺	250	45	273	20	1.5
Aragonite	80 Mn ⁺⁺	250	300	273	30	1.3
Aragonite	80 Mn ⁺⁺	250	45	300	25	2.1
Aragonite	80 Mn ⁺⁺	250	300	300	25	1.7
Magnesite	260 Mn ⁺⁺	230	45	250	5	1.2
Magnesite	260 Mn ⁺⁺	230	300	250	5	1.3
Magnesite	260 Mn ⁺⁺	480	45	480	5	1.1
Magnesite	260 Mn ⁺⁺	480	300	480	30	0.93

The depth of the electron trap associated with each peak in the glow curve usually can be determined graphically from the initial rise in emission due to the peak. It can be shown¹⁰ that the intensity of emission in this region is approximately proportional to $\exp(-E/kT)$, where *k* is Boltzmann's constant, *T* is the temperature, and *E* is the trap depth or the activation energy required to remove an electron from the trap.

In Table II, the trap depths measured by this method are given for the 250°K. glow peak due to Mn⁺⁺ in aragonite and for the 230°K. and 480°K. glow peaks due to Mn⁺⁺ in magnesite. The activation energy associated with the 180°K. peak due to Mn⁺⁺ in aragonite was not measurable by this method because of interference from the more or less constant emission at temperatures below the peak. The traps responsible for this emission can be emptied by warming the sample to the 160–180°K. range. However, many of these traps are refilled (at the expense of the filled traps associated with the 250°K. glow peak) when the temperature is again lowered to 77°K. by immersion in liquid nitrogen. Phenomena similar to this have been observed in calcite and dolomite as well as anhydrite and a mechanism for explaining it already has been proposed.³ Incidentally, the traps associated with the 180°K. glow peak are not refilled by this procedure. A similar phenomenon occurs in magnesite for the emission in the 77–150°K. range. The traps associated with this emission can be emptied and refilled at the expense of the filled traps responsible for the 230°K. glow peak. However, the interference is much smaller in this case and does not prevent a reasonably accurate determination of the trap depth for the 230°K. peak.

TABLE II

VALUES OF THE ACTIVATION ENERGY *E* AND FREQUENCY FACTOR *ν* FOR SOME OF THE TRAPPING CENTERS DUE TO Mn⁺⁺ IN ARAGONITE AND MAGNESITE

Sample	Impurity, p.p.m.	Glow peak (°K.)	<i>E</i> (e.v.)	<i>ν</i> (sec. ⁻¹)
Aragonite	80 Mn ⁺⁺	250	0.36	10 ⁶
Aragonite	490 Mn ⁺⁺	250	.39	3 × 10 ⁶
Magnesite	930 Mn ⁺⁺	230	.17	10 ²
Magnesite	930 Mn ⁺⁺	480	1.0	7 × 10 ⁸
Magnesite	50 Mn ⁺⁺	230	0.16	10 ²
Magnesite	50 Mn ⁺⁺	480	1.2	10 ⁹

Table II also contains values for the frequency factor *ν* associated with each of the trapping levels and computed from the relation¹⁰

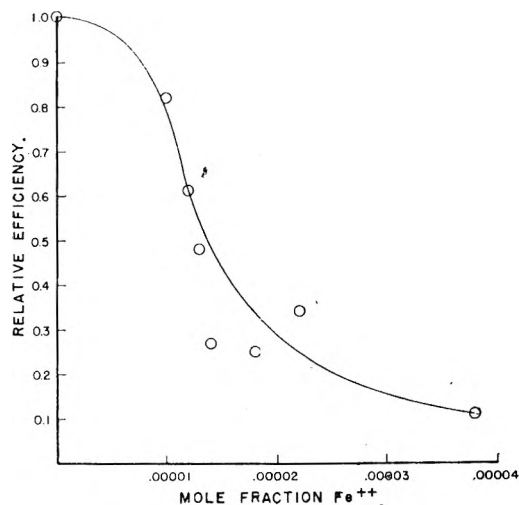


Fig. 7.—Quenching effect of Fe⁺⁺ in the presence of Mn⁺⁺ in aragonite.

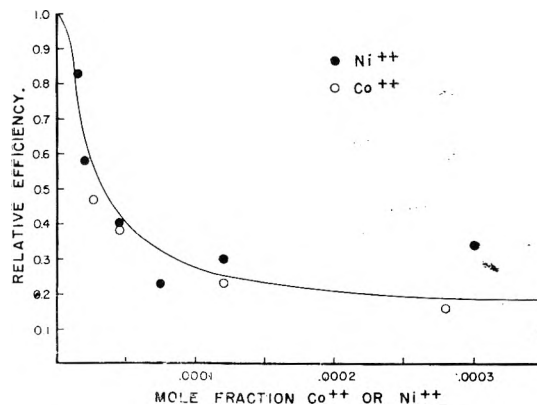


Fig. 8.—Quenching effect of Co⁺⁺ or Ni⁺⁺ in the presence of Mn⁺⁺ in aragonite.

$$\nu = \frac{\beta E}{kT_G^2} e^{E/kT_G} \quad (3)$$

where β is the heating rate (0.50°/sec. in this case) and *T_G* is the temperature of the glow peak.

In order to verify the results predicted for natural samples of aragonite and magnesite by the thermoluminescent properties of the synthetic samples, glow curves were produced for a number of natural specimens of both minerals. In Fig. 10 some representative glow curves for a group of aragonite shell samples collected from various locations are illustrated. The striking similarities between these curves and those of Fig. 1 demonstrate that Mn⁺⁺ accounts for all of the thermoluminescence in most natural aragonite. It is significant that the general level of emission of all of the aragonite samples collected was quite low. Spectrographic analyses revealed that this effect resulted from the quenching effect of Fe (found in concentrations ranging from 10 to 50 p.p.m.) and to the small amounts of manganese present (less than 5 p.p.m. in most samples).

In all of the samples of natural magnesite collected the thermoluminescence was negligible. In a few samples there was evidence of the Mn⁺⁺ glow peaks at 230 and 480°K. (cf. Fig. 2) but in most cases the only measurable thermoluminescence was attributed to small amounts of calcite or dolomite present in the samples. These results indicate a more or less complete exclusion of manganese in natural magnesite and this was verified by spectrographic analyses which showed undetectable amounts (<2 p.p.m.) of this impurity.

III. Discussion of Results

The results of this investigation have shown that the thermoluminescent properties of naturally

(10) J. T. Randall and M. H. F. Wilkins, *Proc. Roy. Soc. (London)*, **184A**, 347 (1945).

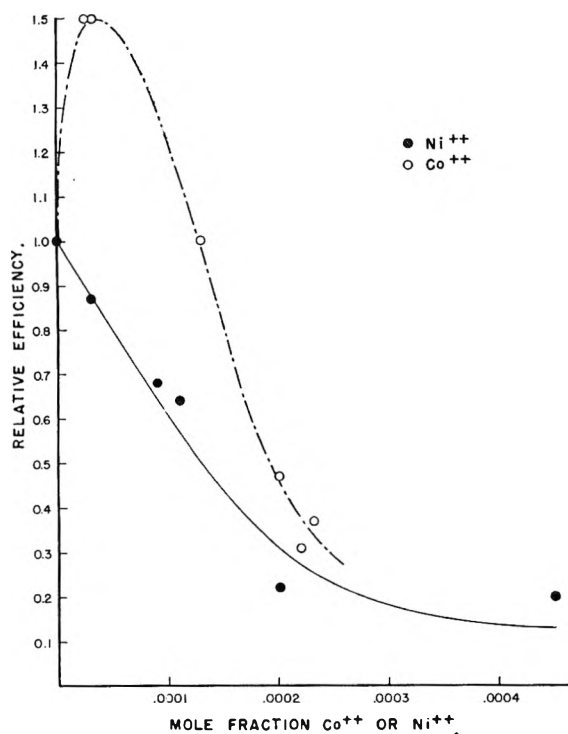


Fig. 9.—Quenching effect of Co^{++} or Ni^{++} in the presence of Mn^{++} in magnesite.

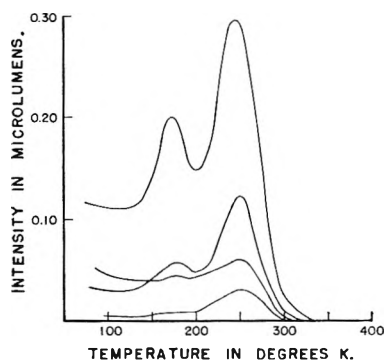


Fig. 10.—Glow curves for some natural aragonite samples.

occurring aragonite and magnesite are subject to simple interpretations. In both cases the thermoluminescence appears to be due solely to the presence of divalent manganese. Lattice defects such as ion vacancies evidently are not important in either crystal.

At optimum manganese concentrations (500 p.p.m. in aragonite and 1500 p.p.m. in magnesite) the respective levels of thermoluminescent intensity are of about the same order of magnitude for aragonite and magnesite (*cf.* Fig. 1 and 2). This level is about one order of magnitude lower than the thermoluminescence due to the optimum Mn^{++} concentrations in calcite or dolomite. In natural samples of these minerals, however, the calcite and dolomite luminescence is several orders of magnitude greater in general than the emission from aragonite and the thermoluminescence in natural magnesite is usually negligible. These results are mostly due to the effective exclusion of manganese from aragonite and magnesite, a result which is not surprising in view of the fact that Mn^{++} has the

wrong coordination number to be included readily in the aragonite lattice and is too large to fit into the magnesite structure very well.

The results of the efficiency *vs.* concentration curves of Fig. 3–6 indicate that the effects of concentration quenching are considerably different in aragonite and magnesite. The parameter, z , determined empirically from equation 1 for each of the glow peaks due to Mn^{++} is a measure of this effect. Its value is equal to the number of nearest neighbor cation sites surrounding a Mn^{++} center which cannot be occupied by another manganese ion without quenching the luminescence.⁷ Therefore, a z of 1000 for the aragonite glow peaks indicates that the thermoluminescent transitions due to a Mn^{++} center generally are quenched when another manganese ion is located as close as 5 or 6 nearest neighbor distances. Similarly, the z of 200 for the magnesite peaks indicates a quenching radius of 2 or 3 nearest neighbor distances. Thus the distortions produced in the crystal field by the substitution of a Mn^{++} ion extend over a larger region in aragonite than in magnesite.

The isothermal decay curves for aragonite and magnesite have the same form as those observed for calcite, dolomite and anhydrite. The form given by equation 2 is characteristic of a second-order process but the behavior of the parameter b as a function of excitation time is in disagreement with the behavior predicted by this model. As shown in Table I, b generally increased with excitation time whereas the inverse relation is to be expected.⁹

The values reported in Table II for the frequency factor ν deserve some comment. Since ν is essentially the frequency with which an electron attempts to escape from a trapping site its value cannot exceed the frequency of atomic vibration (10^{13} sec.⁻¹). In most crystals for which values have been reported, ν falls in the range 10^6 – 10^{10} sec.⁻¹¹¹ and most of the values reported here are within this range. However, the value of 10^2 obtained for the 230°K. peak in magnesite is unreasonably low and it is doubtful that this result is valid. Since the values for ν are calculated from the graphically determined values of E , it appears that the method for determining E is not valid in this case. Incidentally, the determination of E is only possible by this technique when the glow peaks are isolated and are due to a single discrete trapping level. Because of the complexity of the magnesite glow curve (*cf.* Fig. 2) it is quite possible that either of these conditions is violated.

IV. Conclusions

All of the important thermoluminescent properties of aragonite and magnesite are due to divalent manganese. The presence of Mn^{++} results in glow peaks at 180 and 250°K. in aragonite and at 230 and 480°K. in magnesite. The presence of Co^{++} or Ni^{++} quenches the Mn^{++} luminescence in both minerals. In aragonite, Fe^{++} quenches the Mn^{++} luminescence more effectively than Co^{++}

(11) G. F. J. Garlick and A. F. Gibson, *Proc. Phys. Soc. (London)*, **60A**, 574 (1948).

or Ni^{++} but in magnesite it has no appreciable effect.

Because of the differences in ionic radii and coordination numbers, Mn^{++} is not easily substituted into either the aragonite or the magnesite lattice. Therefore, its concentration in natural samples of these minerals is exceedingly small, particularly in magnesite where it is generally undetectable. As a result of this, the intensity of thermoluminescence is generally very low in aragonite and usually negligible in magnesite. The presence of iron in most aragonite samples is a further cause of reduced emission. The thermoluminescence found in most natural magnesite samples generally is due to the presence of some calcite or dolomite. Consequently, magnesite is of little interest in interpreting the thermoluminescence of rock samples except as its presence reduces the intensity of emission from other minerals by acting as a more or less inert material. Aragonite is not very important either although the Mn^{++} glow peaks usually are measurable in this case.

Since most natural magnesite samples contain negligible concentrations of Mn^{++} and since all of the aragonite thermoluminescence is confined to temperatures below 350°K ., neither of these minerals is useful in age measuring applications.

The isothermal decay of phosphorescence has the same form for all of the glow peaks in aragonite and magnesite as for anhydrite, calcite and dolomite. The form of the decay curve can be explained on the basis of a second-order process involving transitions through the conduction band of the crystal. Furthermore, a discrepancy in the predicted behavior of one of the decay parameters which was reported for the other minerals also has been observed in aragonite and magnesite.

The activation energy, E , and frequency factor, ν , for the traps associated with the various glow peaks are about the right order of magnitude except for the 230°K peak in magnesite. For this peak, the value of ν is several orders of magnitude smaller than any values previously reported.

ELECTRON IMPACT SPECTROSCOPY OF ETHYLENE SULFIDE AND ETHYLENIMINE¹

BY EMILIO GALLEGOS AND ROBERT W. KISER

Department of Chemistry, Kansas State University, Manhattan, Kansas

Received January 3, 1961

The appearance potentials and relative abundances determined with a time-of-flight mass spectrometer are reported for the principal positive ions in the mass spectra of ethylene sulfide and ethylenimine. The probable ionization and dissociation processes consistent with the computed energetics are given. Molecular ionization potentials are calculated using the equivalent orbital method and are compared to the observed ionization potentials of 9.94 ± 0.15 e.v. for ethylenimine and 8.87 ± 0.15 e.v. for ethylene sulfide. A comparison of the fragmentation patterns and dissociation processes is given for ethylene oxide, ethylene sulfide and ethylenimine.

Introduction

We have determined the mass spectral cracking patterns and the appearance potentials of the principal ions from ethylenimine and ethylene sulfide, and compared these with the information reported previously for ethylene oxide.² Consistent with the probable ionization and dissociation processes and with the ionization and appearance potentials obtained, the heats of formation of the various principal ions of ethylene sulfide and ethylenimine have been determined. The mass spectral cracking pattern of ethylene sulfide and ethylenimine are reported; that for ethylenimine compares favorably with that listed in the A.P.I. tables of mass spectra.³ The appearance potential data of ethylenimine and ethylene sulfide and the mass spectral cracking pattern of ethylene sulfide are newly reported.

Experimental

The general features of the Bendix model 12-100 time-of-flight (TOF) instrument used in this study have been described.² The resolving power of this instrument is $(M/\Delta M) \cong 140$, as determined from the "5% peak width," $\Delta H/H = 0.1$, $\Delta h/h = 0.001$ and $1/\Gamma^{1/2}$.⁴

The sample of ethylenimine was obtained from Matheson, Coleman and Bell, and was used as received. It was stated to have a minimum purity of 98%. Dr. R. P. Ciula of these laboratories provided the samples of ethylene sulfide; these were synthesized from ethylene carbonate and potassium thiocyanate at $115-120^\circ$ and the samples were distilled over at 52° . The ethylene sulfide was used immediately after preparation to avoid any polymer formation in the sample. No significant impurities were observed in the mass spectra of either ethylenimine or ethylene sulfide. Gas-liquid partition chromatographic analysis of ethylene sulfide on tri-*n*-tolyl phosphate revealed no impurity peaks; therefore, it was estimated that the ethylene sulfide had a purity >99.5 mole %.

Mass spectra were obtained for nominal electron energies of 70 e.v. The voltage scale was calibrated by using mixtures of krypton or xenon with the compound being investigated, and by subsequent comparison of the observed ionization potential of the rare gases with their known spectroscopic values.⁵ The extrapolated difference method of obtaining ionization and appearance potentials has been described.² Ionization potentials also were determined

(1) This work was supported in part by the U. S. Atomic Energy Commission, under Contract No. AT(11-1)-751 with Kansas State University. Portion of a dissertation to be presented by E. J. Gallegos to the Graduate School of Kansas State University in partial fulfillment for the degree of Doctor of Philosophy in Chemistry. Presented at the 139th Meeting of the American Chemical Society, St. Louis, Mo., March 21-30, 1961.

(2) E. J. Gallegos and R. W. Kiser, *J. Am. Chem. Soc.*, **83**, 773 (1961).

(3) "Mass Spectral Data," American Petroleum Institute Research Project 44, National Bureau of Standards, Washington, D. C.

(4) J. H. Beynon, "Mass Spectrometry and its Applications to Organic Chemistry," Elsevier Publishing Co., Amsterdam, 1960, pp. 51-54.

(5) C. E. Moore "Atomic Energy Levels," Natl. Bur. Standards Circ. 467, Vol. 3, 1958.

TABLE I

MASS SPECTRUM AND APPEARANCE POTENTIALS OF PRINCIPAL IONS OF ETHYLENIMINE

<i>m/e</i>	Relative abundance, %	A.P., e.v.	Process	ΔH_f^\dagger , kcal./mole
12	1.9			
13	3.8			
14	10.4	19.7 \pm 0.3	$C_2H_5N \rightarrow CH_2^+ + HCN + 2H$	345
			$\rightarrow N^+ + C_2H_5$	458
15	35.3	15.5 \pm 0.3	$\rightarrow CH_3^+ + HCN + H$	300
16	1.7			
17	1.2			
18	0.5			
20.5	0.1			
21	1.4			
21.5	0.14			
24	0.4			
25	2.1			
26	7.6	16.4 \pm 0.4	$\rightarrow C_2H_2^+ + NH + H_2$	323
27	12.3	16.9 \pm 0.3	$\rightarrow C_2H_3^+ + NH + H$	283
28	79.8	13.3 \pm 0.2	$\rightarrow C_2H_4^+ + NH$	252
29	2.6	12.8 \pm 0.2	$\rightarrow CH_3N^+ + CH_2$	253
			$\rightarrow C_2H_5^+ + N$	210
30	0.9			
38	5.4	23.0 \pm 0.4	$\rightarrow C_2N^+ + H_2 + 3H$	400
39	7.4	18.1 \pm 0.6	$\rightarrow C_2HN^+ + H_2 + 2H$	340
40	18.1	17.0 \pm 0.2	$\rightarrow C_2H_2N^+ + 3H$	262
41	26.1	15.2 \pm 0.3	$\rightarrow C_2H_3N^+ + 2H$	273
42	100.0	12.2 \pm 0.1	$\rightarrow C_2H_4N^+ + H$	255
43	59.9	9.94 \pm 0.15	$\rightarrow C_2H_5N^+$	255
44	2.4			

TABLE II

MASS SPECTRUM AND APPEARANCE POTENTIALS OF THE PRINCIPAL IONS OF ETHYLENE SULFIDE

<i>m/e</i>	Relative abundance, %	A.P., e.v.	Process	ΔH_f^\dagger , kcal./mole
12	1.0			
13	1.7			
14	4.9	(20.4 \pm 0.5) (?)	$C_2H_1S \rightarrow CH_2^+ + CS + 2H$ (?)	330
15	1.6			
24	0.3			
25	2.8			
26	19.1	17.9 \pm 0.5	$\rightarrow C_2H_2^+ + SH + H$	347
27	44.6	14.6 \pm 0.2	$\rightarrow C_2H_3^+ + SH$	323
28	7.8			
29	2.8			
32	7.9	(13.1 \pm 0.2) (?)	$\rightarrow S^+ + C_2H_4$	309
33	3.8			
34	12.1	13.4 \pm 0.1	$\rightarrow H_2S^+ + C_2H_2$	274
35	0.2			
36	0.2			
44	2.7			
45	100.0	12.3 \pm 0.2	$\rightarrow CHS^+ + CH_2$	271
46	2.8	12.7 \pm 0.2	$\rightarrow CH_2S^+ + CH_2$	245
47	3.6			
56	0.8			
57	8.0			
58	20.2	15.0 \pm 0.2	$\rightarrow C_2H_2S^+ + 2H$	261
59	69.0	11.4 \pm 0.2	$\rightarrow C_2H_3S^+ + H$	230
60	75.8	8.87 \pm 0.15	$\rightarrow C_2H_4S^+$	224
61	5.9			
62	2.5			

using the technique of Lossing, Tickner and Bryce⁶ and Honig's critical slope method.⁷ Typical plots of the ioniza-

tion efficiency curves for the parent ions from ethylenimine and ethylene sulfide are shown in Fig. 1.

Results

The results of the mass spectral cracking pattern determinations and the appearance potential meas-

(6) F. P. Lossing, A. W. Tickner and W. A. Bryce, *J. Chem. Phys.*, **19**, 1254 (1951).

(7) R. E. Honig, *ibid.*, **16**, 105 (1948).

urements for these compounds are summarized in Tables I and II. In the first two columns are given the principal ions formed by 70 e.v. electrons from each compound and their relative abundances. No isotope correction has been made in either spectrum. In columns 3 and 4 are given the appearance potentials measured for the observed ions from the parent molecule and the probable processes by which they are formed, as calculated from the various appearance potentials. ΔH_f^+ indicates the heat of formation of the ion, e.g., $\Delta H_f^+(\text{C}_2\text{H}_4)$; in this way we distinguish it from the heat of formation of the molecule or radical, e.g., $\Delta H_f(\text{C}_2\text{H}_4)$.

The N.B.S. values⁸ for heats of formation of the various molecules were used in the thermochemical calculations, and values for heats of formation of the different ions were taken from Field and Franklin.⁹ The heats of formation for ethylenimine (g)¹⁰ and ethylene sulfide (g)¹¹ were taken to be 26.0 and 19.29 kcal./mole, respectively. The heat of formation used for SH (g) was 33 kcal./mole, obtained from $\Delta H_f(\text{H}) = 52.1$ kcal./mole,⁸ $D(\text{HS}-\text{H}) = 90$ kcal./mole¹² and $\Delta H_f(\text{H}_2\text{S}) = -4.8$ kcal./mole.⁸ In the same manner $\Delta H_f(\text{HCN}) = 31.2$ and $\Delta H_f(\text{NH}_3) = -11.04$ kcal./mole⁸ were used with $D(\text{H}_2\text{N}-\text{H}) = 102$ and $D(\text{H}-\text{CN}) = 114$ kcal./mole¹² to obtain $\Delta H_f(\text{NH}_2) = 39$ and $\Delta H_f(\text{CN}) = 93$ kcal./mole. $\Delta H_f(\text{N})$ was taken to be 111 kcal./mole and $\Delta H_f(\text{NH})$ was taken to be 81 kcal./mole.¹³

Mass Spectra.—The 70 e.v. mass spectrum of ethylenimine obtained with the TOF mass spectrometer is in agreement with that given in the A.P.I. tables of mass spectral data, serial no. 763.³ Similar results were obtained for ethylene oxide and propylene oxide.² The 70 e.v. spectrum for ethylene sulfide, as reported in Table II, is new. Figure 2 indicates the manner in which the abundance of the principal ions from these three compounds varies with the electron energy.

Ionization Potentials.—The electron impact ionization potentials measured for ethylenimine and ethylene sulfide are vertical transitions according to the Franck-Condon principle. Calculation of the ionization potentials for these molecules using the equivalent orbital treatment^{14,15} leads to some interesting results. Table III presents these calculations, based on the parameters given by Franklin¹⁵ for amines, and on parameters calculated by us for the sulfides and thiols. The disagreement

TABLE III
MOLECULAR IONIZATION POTENTIALS OF SOME SULFUR AND NITROGEN-CONTAINING COMPOUNDS

Molecule	Ionization potential (e.v.)		Ref.
	Calcd.	Measd.	
a	13.31 ^a		
b	1.55 ^a		
f	10.46		
c	1.99		
CH ₃ SH	(9.44)	9.440	b
CH ₃ CH ₂ SH	9.30	9.29	b,c
CH ₃ CH ₂ CH ₂ SH	9.28	9.195	b
(CH ₃) ₂ S	8.73	8.684, 8.73	b,c
CH ₂ -S-CH ₂ CH ₃	8.65	8.55	b
(CH ₃ CH ₂) ₂ S	8.58	8.43, 8.48	b,c
CH ₂ CH ₂ S	9.08	8.87	d
CH ₂ CH ₂ CH ₂ S	8.43	8.64	c
CH ₂ (CH ₂) ₂ CH ₂ S	8.62	8.48	c
CH ₂ (CH ₂) ₃ CH ₂ S	8.54	8.36	c
e	13.31 ^a		
b	1.55 ^a		
f	10.52 ^a		
c	2.08 ^a		
CH ₂ CH ₂ NH	9.04	9.94	d
CH ₂ CH ₂ CH ₂ NH	3.35		
CH ₂ (CH ₂) ₂ CH ₂ NH	8.55	9.2	e,f
CH ₂ (CH ₂) ₃ CH ₂ NH	8.47	9.2	e,f

^a These parameters are by Franklin.¹⁵ ^b See ref. 21. ^c See ref. 22. ^d Data reported in this work. ^e J. Hissel, *Bull. soc. roy. sci. Liege*, 21, 457 (1952). ^f See ref. 18.

of the calculated and experimental results for ethylenimine is to be noted. Ionization potentials obtained by electron impact methods for amines¹⁶⁻¹⁸ are significantly greater than those obtained by the photoionization method.⁹⁻²² It appears from this work that this is also true of the cyclic imines, and that the adiabatic ionization potential for ethylenimine will be closer to 9.1 e.v.

The calculations of the ionization potentials for the sulfur-containing compounds shown in Table III were carried out in the same manner as done by Franklin.¹⁵ A number of alkyl-sulfur compounds have been included here to test the applicability of the parameter *c*, calculated from the ionization potential of methanethiol. The agreement throughout is considered good, although there is a tendency for the calculated values to be slightly higher

(16) J. D. Morrison and A. J. C. Nicholson, *ibid.*, 20, 1021 (1952).

(17) I. Omura, K. Higasi and H. Baba, *Bull. Chem. Soc. Japan*, 29, 501, 504 (1956).

(18) J. Collin, *Bull. soc. chim. Belges*, 62, 411 (1953); *Bull. soc. roy. sci. Liege*, 23, 395 (1954), 25, 441 (1956); *Can. J. Chem.*, 37, 1053 (1959).

(19) K. Watanabe, *J. Chem. Phys.*, 26, 542 (1957).

(20) K. Watanabe and J. R. Mottl, *ibid.*, 26, 1773 (1957).

(21) K. Watanabe, T. Nakayama and J. Mottl, "Final Report on Ionization Potential of Molecules by a Photoionization Method," December, 1959. Dept. Army #5B99-01-004 ORD-#TB2-001-OOR-#1624. Contract No. DA-04-200-ORD 480 and 737.

(22) L. D. Isaacs, W. C. Price and R. G. Ridley, "Vacuum Ultraviolet Spectra and Molecular Ionization Potentials," in "The Threshold of Space," edited by M. Zelikoff, Pergamon Press, Ltd., London, 1957, pp. 143-151.

(8) F. D. Rossini, D. D. Wagman, W. H. Evans, S. Levine and I. Jaffe, "Selected Values of Chemical Thermodynamic Properties," National Bureau of Standards Circular 500, U. S. Government Printing Office, Washington, D. C., 1952.

(9) F. H. Field and J. L. Franklin, "Electron Impact Phenomena and the Properties of Gaseous Ions," Academic Press, New York, N. Y., 1957.

(10) R. A. Nelson and R. S. Jessup, *J. Research Natl. Bur. Standards*, 48, 206 (1952).

(11) G. B. Guthrie, D. W. Scott and G. Waddington, *J. Am. Chem. Soc.*, 74, 2795 (1952).

(12) T. L. Cottrell, "The Strengths of Chemical Bonds," 2nd Edition, Butterworths Scientific Publications, London, 1958, pp. 184, 187, 188 and 271.

(13) J. L. Franklin, V. H. Dibeler, R. M. Reese and M. Krauss, *J. Am. Chem. Soc.*, 80, 298 (1958).

(14) G. G. Hall, *Trans. Faraday Soc.*, 49, 113 (1953); 50, 319 (1954).

(15) J. L. Franklin, *J. Chem. Phys.*, 22, 1304 (1954).

than the values determined experimentally. The ionization potential of 8.87 ± 0.15 e.v. reported here for ethylene sulfide is new, and is in agreement with the calculated value. Unfortunately, the ionization potentials of neither of the two heterocyclic compounds investigated here were calculated by Streitwieser using the ω -technique,²³ but his theoretical calculations for some of the amines give rather high values, often in better agreement with electron impact results than with photoionization results, as is the case with the calculations made by Franklin.¹⁵

Ethylenimine

m/e 14.—The ion observed with this *m/e* value might be either CH_2^+ or N^+ . If it is CH_2^+ , the neutral products would be $\text{HCN} + 2\text{H}$, and if it is N^+ , the neutral products would be C_2H_5 . Field and Franklin⁹ give $\Delta H_f^+(\text{CH}_2) = 333$ kcal./mole and $\Delta H_f^+(\text{N}) = 448$ kcal./mole. Beynon's high resolution technique²⁴ would certainly be helpful in deciding the nature of this ion.

m/e 15.—From the energetics for the formation of this ion, it appears that the ion is CH_3^+ and that the neutral fragments are $\text{HCN} + \text{H}$ rather than CH_2N . $\Delta H_f^+(\text{CH}_3)$ obtained from the thermochemistry is about 35 kcal./mole greater than that given by Field and Franklin.⁹ However, energetic considerations clearly rule out the possibility that this ion is NH^+ . It would appear from the curves of Fig. 2 that this ion may actually occur *via* decomposition of $\text{C}_2\text{H}_4\text{N}^+$ while still in the ion source.

m/e 26.—This ion apparently is C_2H_2^+ , but the neutral fragments might be either $\text{NH}_2 + \text{H}$, in which case nearly perfect agreement is reached for $\Delta H_f^+(\text{C}_2\text{H}_2)$ with Field and Franklin's⁹ values, or $\text{NH} + \text{H}_2$, in which case the value of $\Delta H_f^+(\text{C}_2\text{H}_2)$ is a little high, but still in range of values listed.⁹ The tendency for results to be slightly high suggests that the process to form *m/e* 26 is as given in Table I.

m/e 27.—This ion is C_2H_3^+ , and the neutral products formed with it are, on the basis of observed appearance potential, $\text{NH} + \text{H}$. Energetics rule out that this ion is HCN^+ , although at 70 e.v. there may be a contribution from HCN^+ ; this could be observed with the high resolution technique²⁴ if it were so.

m/e 28.—The energetics indicate that the products are C_2H_4^+ and NH . The calculated heat of formation of C_2H_4^+ is 252 kcal./mole which agrees reasonably well with $\Delta H_f^+(\text{C}_2\text{H}_4) = 255$.⁹ However, the very large peak corresponding to the (parent-15 amu) in the mass spectra of ethylene oxide, ethylenimine and ethylene sulfide suggests that at 70 e.v. this ion is due to the loss of a methyl group. If the process is $\text{C}_2\text{H}_5\text{N} \rightarrow \text{CH}_2\text{N}^+ + \text{CH}_3$, $\Delta H_f^+(\text{CH}_2\text{N}) = 300$ kcal./mole. The small *m/e* 28 peak in the ethylene sulfide and ethylene oxide spectra indicates that loss of the hetero atom or group in these molecules is small. Isotopically labelled ethylenimine or high resolution mass

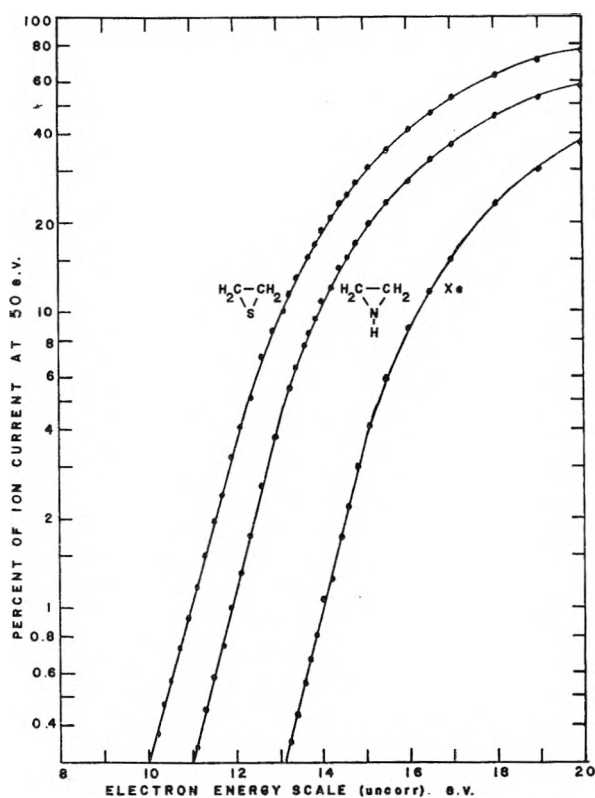


Fig. 1.—Lower energy of typical ionization efficiency curves for ethylene sulfide, ethylenimine and the xenon standard.

spectroscopy would help to establish this ion with greater certainty.

m/e 29.—Energetics appear to favor the formation of $\text{CH}_3\text{N}^+ + \text{CH}_2$. The value calculated for $\Delta H_f^+(\text{C}_2\text{H}_5)$ is 210 kcal./mole for the reaction $\text{C}_2\text{H}_5\text{N} \rightarrow \text{C}_2\text{H}_5^+ + \text{N}$. Tabulated values⁹ for $\Delta H_f^+(\text{C}_2\text{H}_5)$ are 224–240 kcal./mole. $\Delta H_f^+(\text{H}_3\text{CN}^+)$ is calculated to be 253 kcal./mole if CH_2 is the neutral fragment. The literature⁹ gives $\Delta H_f^+(\text{CH}_3\text{N}) = 246$ to 264 kcal./mole.

m/e 38.—The appearance potential of this ion is 23.0 ± 0.4 e.v. This ion could only be C_2N^+ , and the neutral products must be some combination of hydrogen atoms and molecules. If 5H are the neutral products, $\Delta H_f^+(\text{C}_2\text{N}) = 296$ kcal./mole; if $\text{H}_2 + 3\text{H}$ are products, $\Delta H_f^+(\text{C}_2\text{N}) = 400$ kcal./mole; and if the products are $2\text{H}_2 + \text{H}$, $\Delta H_f^+(\text{C}_2\text{N}) = 504$ kcal./mole. Field and Franklin⁹ give $\Delta H_f^+(\text{C}_2\text{HN}) = 369$ kcal./mole, suggesting $\Delta H_f^+(\text{C}_2\text{N}) \geq 400$ kcal./mole; on this basis the most reasonable neutral products would be $\text{H}_2 + 3\text{H}$. Results of a mass spectrometric study of cyanogen and cyanoacetylenes by Dibeler, Reese and Franklin²⁵ indicate $\Delta H_f^+(\text{C}_2\text{N}) = 419$ kcal./mole. This is in approximate agreement with our results and substantiates the choice of this dissociation process. Tate, *et al.*,²⁶ give A.P. (C_2N^+) from $\text{C}_2\text{N}_2 = 19.9$ e.v., and list N as the neutral fragment; from this datum and the heats of formation of

(23) A. Streitwieser, Jr., *J. Am. Chem. Soc.*, **82**, 4123 (1960).

(24) J. H. Beynon, "High Resolution Mass Spectrometry of Organic Materials," in "Advances in Mass Spectrometry," edited by J. D. Waldron, Pergamon Press, London, 1959, pp. 328–354.

(25) V. H. Dibeler, R. M. Reese and J. L. Franklin, *J. Am. Chem. Soc.*, **83**, 1813 (1961).

(26) J. T. Tate, P. T. Smith and A. L. Vaughn, *Phys. Rev.*, **48**, 525 (1935).

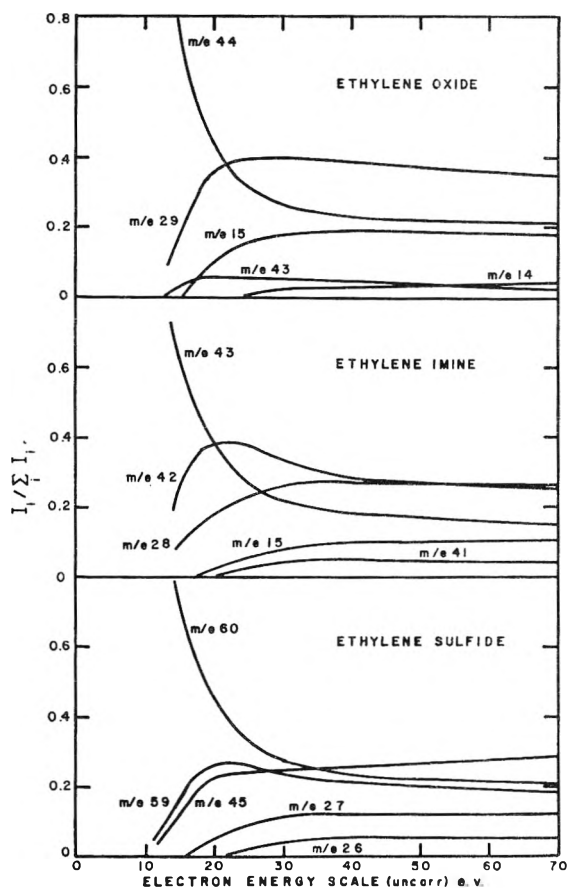


Fig. 2.—Variation of the principal ions in the mass spectra of ethylene oxide, ethylenimine and ethylene sulfide with the energy of the impacting electrons.

cyanogen and atomic nitrogen, $\Delta H_f^+(\text{C}_2\text{N}) = 447$ kcal./mole.

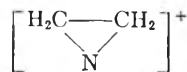
m/e 39.—This ion could only be C_2NH^+ . The only process which has a value for $\Delta H_f^+(\text{C}_2\text{HN})$ close to the value of ~ 369 given by Field and Franklin⁹ is $\text{C}_2\text{H}_5\text{N} \rightarrow \text{C}_2\text{HN}^+ + \text{H}_2 + 2\text{H}$. The appearance potential of 18.1 ± 0.6 e.v. gives $\Delta H_f^+(\text{C}_2\text{HN}) = 340$ kcal./mole.

m/e 40.—The two possible neutral products accompanying $m/e 40$ are 3H , with a calculated $\Delta H_f^+(\text{C}_2\text{H}_2\text{N}) = 262$ kcal./mole, and $\text{H}_2 + \text{H}$, with a calculated $\Delta H_f^+(\text{C}_2\text{H}_2\text{N}) = 365$ kcal./mole. Tabulated values for the heats of formation of various ions list $\Delta H_f^+(\text{C}_2\text{H}_2\text{N}) = 299$ kcal./mole.⁹

m/e 41.—This ion, $\text{C}_2\text{H}_3\text{N}^+$, may have accompanying neutral fragments of either H_2 or 2H . The value of $\Delta H_f^+(\text{C}_2\text{H}_3\text{N})$ calculated for the former case is 377 kcal./mole and for the latter case is 273 kcal./mole. It is suggested that this ion still may have a cyclic nature and that $\Delta H_f^+(\text{C}_2\text{H}_3\text{N}) = 273$ kcal./mole. Field and Franklin⁹ indicate $\Delta H_f^+(\text{C}_2\text{H}_3\text{N}) = 309$ kcal./mole from studies of CH_3CN .

m/e 42.—It is possible that a cyclic structure is retained for this ion, $\text{C}_2\text{H}_4\text{N}^+$. The only possible neutral fragment is H and this leads to a $\Delta H_f^+(\text{C}_2\text{H}_4\text{N}) = 255$ kcal./mole in fair agreement with results reported by Dibeler, Franklin and Reese.²⁷

The prominence of this ion in the spectrum (see Table I) indicates the parent molecule ion loses H quite readily, more so than either ethylene sulfide or ethylene oxide.² This suggests the H atom lost comes from the imine group, giving a cyclic structure for this ion.



m/e 43.—The ionization potential of ethylenimine, determined from the ionization efficiency curve of the ion of $m/e = 43$, is 9.94 ± 0.15 e.v. Thus, $\Delta H_f^+(\text{C}_2\text{H}_5\text{N})$ is calculated to be 255 kcal./mole.

Ethylene Sulfide

m/e 14.—This ion could only be CH_2^+ . The neutral fragments produced with CH_2^+ are believed to be $\text{CS} + 2\text{H}$ on the basis of the following considerations. Smyth and Blewett²⁸ give the ionization potential of CS as 10.6 ± 0.3 e.v. and Field and Franklin⁹ give $\Delta H_f^+(\text{CS}) = 300$ kcal./mole. This leads to $\Delta H_f^+(\text{CS}) = 55$ kcal./mole. Using this value, $\Delta H_f^+(\text{CH}_2)$ for the above process is calculated to be 330 kcal./mole in close agreement with the value of 333 kcal./mole listed by Field and Franklin.⁹

m/e 26.—The only ion which can result from electron bombardment of ethylene sulfide to give $m/e = 26$ is C_2H_2^+ , and $\Delta H_f^+(\text{C}_2\text{H}_2)$ is calculated to be 347 kcal./mole, from the process shown in Table II. This value is high in comparison to the value given in the literature⁹ where $\Delta H_f^+(\text{C}_2\text{H}_2) = 317$ kcal./mole. The data shown in Fig. 2 suggest that $m/e 26$ is the result of the fragmentation of $m/e 59$ while still in the ion source, and thus the process of yielding the neutral fragments $\text{SH} + \text{H}$ is enhanced.

m/e 27.—The appearance potential of 14.6 ± 0.2 e.v. for $m/e 27$, C_2H_3^+ , from ethylene sulfide leads to a value of $\Delta H_f^+(\text{C}_2\text{H}_3) = 323$ kcal./mole using the suggested process. The reaction to produce $\text{C}_2\text{H}_3^+ + \text{H} + \text{S}$ leads to a low value for $\Delta H_f^+(\text{C}_2\text{H}_3)$. The literature⁹ value is $\Delta H_f^+(\text{C}_2\text{H}_3) = 280$ kcal./mole.

m/e 32.—This ion could only be S^+ . The accompanying neutral product is C_2H_4 , giving $\Delta H_f^+(\text{S}) = 309$ kcal./mole in good agreement with the value of 304 kcal./mole listed by Field and Franklin.⁹ The medium sized $m/e 32$ peak observed at 70 e.v. for ethylene sulfide indicates that the C-S bonds in this heterocyclic are weaker than the corresponding C-N and C-O bonds in the other heterocyclics. The other heterocyclics show almost no evidence of the elimination of the hetero atom or group as an ion upon electron impact.

m/e 34.— H_2S^+ , the ion of $m/e = 34$, must be formed as a result of rearrangement, and therefore $\Delta H_f^+(\text{H}_2\text{S})$ calculated from the measured appearance potential is expected to be somewhat greater than that derived from the ionization potential of H_2S . The only reasonable neutral fragment here is C_2H_2 , and this gives $\Delta H_f^+(\text{H}_2\text{S}) = 274$ kcal./mole, substantially greater than the value of 236 kcal./mole given by Field and Franklin.⁹

(27) V. H. Dibeler, J. L. Franklin and R. M. Reese, *J. Am. Chem. Soc.*, **81**, 68 (1959).

(28) H. D. Smyth and J. P. Blewett, *Phys. Rev.*, **46**, 276 (1934).

m/e 45.—This ion is the result of the formation of CHS^+ and neutral fragments of either CH_3 or $\text{CH}_2 + \text{H}$. Considering the reaction to be $\text{C}_2\text{H}_4\text{S} \rightarrow \text{CHS}^+ + \text{CH}_3$, a value of $\Delta H_f^+(\text{CHS}) = 271$ kcal./mole is calculated. This is a reasonable value in relation to the value of $\Delta H_f^+(\text{CS}) = 300$ kcal./mole.⁹ A value of 178 kcal./mole is calculated for $\Delta H_f^+(\text{CHS})$ taking the neutral products to be $\text{CH}_2 + \text{H}$. This latter value appears too low in relation to the value for $\Delta H_f^+(\text{CS})$ and the value of $\Delta H_f^+(\text{CH}_3\text{S}) = 222$ kcal./mole.⁹

m/e 46.—A value of 245 kcal./mole is calculated for $\Delta H_f^+(\text{CH}_2\text{S})$ assuming the neutral fragment to be CH_2 . $\Delta H_f^+(\text{CH}_2\text{S})$ has not previously been determined, but our value appears reasonable in comparing it with $\Delta H_f^+(\text{CHS}) = 271$ kcal./mole, determined above, and $\Delta H_f^+(\text{CH}_3\text{S}) = 222$ kcal./mole.⁹

m/e 58.—Energetics indicate that the ion and neutral fragments responsible for $m/e = 58$ are $\text{C}_2\text{H}_2\text{S}^+$ and 2H , respectively. The calculated $\Delta H_f^+(\text{C}_2\text{H}_2\text{S})$ is 261 kcal./mole, in agreement with the value of 265 kcal./mole given by Field and Franklin.⁹

m/e 59.—This ion could only result from the

ionization and dissociation of the parent molecule $\text{C}_2\text{H}_4\text{S}$ to give $\text{C}_2\text{H}_3\text{S}^+ + \text{H}$. The calculated $\Delta H_f^+(\text{C}_2\text{H}_3\text{S})$ for this process is 230 kcal./mole. The relatively large (parent minus hydrogen) peak at $m/e 59$ for 70 e.v. electrons provides additional evidence for the weakened bonds in ethylene sulfide compared to those in ethylene oxide and ethylenimine.

m/e 60.—This is the parent molecule-ion, $\text{C}_2\text{H}_4\text{S}^+$. Using the observed ionization potential and the heat of formation of the parent compound, a value of $\Delta H_f^+(\text{C}_2\text{H}_4\text{S}) = 224$ kcal./mole is calculated. It seems reasonable to assume that this ion retains its cyclic structure.

Further theoretical considerations of the construction of the mass spectra of these three-membered heterocyclics will be given in more detail in a future publication.

Acknowledgment.—The authors wish to thank Dr. R. P. Ciula for providing the samples of ethylene sulfide. It is a pleasure to acknowledge the aid and comments of Dr. J. L. Franklin, and we wish to thank him for making available some of his data prior to publication.

STUDY OF THE HYDROGENATION OF ETHYLENE OVER HOMOGENIZED COPPER-NICKEL ALLOY FILMS

BY M. K. GHARPUREY¹ AND P. H. EMMETT

The Johns Hopkins University, Baltimore, Md.

Received January 6, 1961

Heating thin films of copper on nickel or nickel on copper at 300° in hydrogen overnight produced homogeneous films having the same color and the same activity for ethylene hydrogenation regardless of the order in which the metals were deposited. The relative reaction rates for ethylene hydrogenation per unit area at 0° were 9.3, 13.9, 8.3, 8.8, 9.7 and 6.6 for pure Ni, and alloys containing 87.4, 74.2, 67.0, 63.0 and 18.3% nickel, respectively.

Introduction

The activity of Cu-Ni alloy catalysts for the hydrogenation of ethylene was reported by Best and Russell² to be several orders higher than that of a pure Ni catalyst. Hall and Emmett³ later reported a dependence of the activity for this reaction on the pretreatment, for a series of alloy catalysts. When the catalysts, after reduction, were flushed with helium at reduction temperature and then cooled in helium, the activity decreased with an increase in copper content of the catalyst. On the other hand, if the catalysts were cooled in hydrogen, the activity related to alloy composition showed two maxima (see Fig. 1), and the initial additions of Cu to the Ni increased the activity to nearly twice that of pure Ni. Hydrogen thus was shown to have a promoting effect on the activity of the alloy catalysts and a poisoning effect on the activity of the pure Ni catalyst. These results were confirmed in substance by Pass⁴ who studied a series of alloys in the range 0-24% Cu.

Hall, Cheselske and Lutinski⁵ recently have shown that Cu-Ni alloys cooled in hydrogen take up an amount of this gas many times as large as would be required for a monolayer, whereas pure nickel catalysts take up a monolayer or less. This large take-up of hydrogen has further been shown by them to be associated with the small amount of oxygen left in the alloys by incomplete reduction. The question arises as to whether the promoting effect of hydrogen on the alloy catalysts is indirectly related to the presence of small amounts of oxygen within the catalyst. One approach to answering this question appeared to be the study of ethylene hydrogenation on alloy catalysts prepared as homogeneous evaporated Cu-Ni films and hence substantially free of oxygen.

Almost all the work on evaporated film catalysts has been on pure metal films, since homogeneous alloy films are difficult to prepare. Recently, Foss and Eyring⁶ reported that sintered Ni films for the ethylene hydrogenation reaction could be reacti-

(1) National Chemical Laboratory, Poona, India.

(2) R. J. Best and W. W. Russell, *J. Am. Chem. Soc.*, **76**, 838 (1954).

(3) W. K. Hall and P. H. Emmett, *J. Phys. Chem.*, **63**, 1102 (1959).

(4) G. Pass, unpublished results.

(5) W. K. Hall, F. J. Cheselske and F. E. Lutinski, International Conference on Catalysis, Paris, 1960.

(6) J. G. Foss and H. Eyring, *J. Phys. Chem.*, **62**, 103 (1958); J. G. Foss, Ph.D., Thesis, Univ. of Utah, 1956.

vated by baking them in hydrogen for half an hour at a temperature of about 250-300°. This suggested the possibility of preparing Cu-Ni alloy films by homogenizing in hydrogen at 300° composite films made by depositing copper on nickel or nickel on copper.

Experimental

An apparatus similar to that of Foss and Eyring was set up. The reaction chamber was a 500-ml. Pyrex balloon flask and the electrical connections were made through a press seal. Ni was evaporated from a Driver & Harris A Grade Ni wire (0.02" dia.) which was weighed before and after the experiment. Two equal pieces of Cu wire (0.01" dia.) were placed on a W-wire loop at some distance (~1 cm.) from each other, the plane of the W-wire loop being normal to that of the Ni wire loop. The Ni and W wires were fastened tightly to the Ni-leads with short pieces of fine gauge Ni wire. Desiccants, followed by Na-K alloy bubblers were used for both ethylene (Research Grade) and hydrogen, the latter being initially passed through a palladium deoxo catalyst.

The evacuation procedure also was similar to that of Foss and Eyring. After evacuation to about 1 μ , the reaction chamber was filled to a pressure of 5 cm. with H₂. The two filaments were in turn kept at dull red heat for 10 min. each to reduce the oxide layer. Then the chamber was heated to 500° for one hour. At the end of this period, it was evacuated and left pumping out at this high temperature overnight after the two filaments were degassed by being heated to a dull red heat. From this stage onwards, the reaction chamber before cooling was protected from the rest of the apparatus by a Dry Ice trap.

The required quantity of Ni was evaporated by passing constant current (~6.0 amp.) through the wire for certain lengths of time. The whole quantity of Cu was evaporated off the W-wire. The Ni and the Cu were evaporated one after the other to obtain possible extremes in surface composition. On completion of the evaporation, the composite film was baked at 300° in 5 cm. of H₂ overnight.

After a dose of 50:50 mixture of ethylene and hydrogen (total pressure ~1.5 mm.), was admitted, the course of the reaction was followed with a silicone oil manometer and a travelling microscope. The activity of the films was normally measured successively at 0, -15, +15 and 0°. Reactivation of the film between runs was carried out by pumping it for ten minutes, baking it at about 250-300° in 5 cm. of hydrogen for 40 minutes, cooling it to reaction temperature, and pumping it for 10 minutes. The fourth run, at 0°, always showed the same activity as the first run.

The surface area of the films was measured by the B.E.T. method with ethane (area assumed per ethane molecule = 20.5 A.²) at liquid oxygen temperature. Pretreatment of the film with ethane was made at room temperature. The accuracy of the surface area measurement was estimated to be about 10%.

Results

Two experiments were performed initially: 1. The activity of a 12.5 mg. of Ni film was determined at a series of temperatures. 2.05 mg. of Cu then was evaporated on top of the reactivated film. The activity of this composite film was measured after a half hour bake-out in 5 cm. of hydrogen at about 300° and was found to be nearly double that of the pure Ni film. 2. 12.5 mg. of Ni was evaporated on top of a 2.05 mg. of Cu film. The activity of this film after a similar bake-out in hydrogen⁷ was found to be equal to that of the composite film in the first experiment where Cu was evaporated on top of the Ni.

The above runs indicated that a half hour treatment at 300° was enough to homogenize the films.

(7) The homogenization here observed is not unreasonable when compared to that for 1000 Å. Ni-Cu films recently reported by Belsler [*J. Appl. Physics*, **31**, 362 (1960)] *in vacuo* at 400°. The present films had an average thickness of 300 to 500 Å.

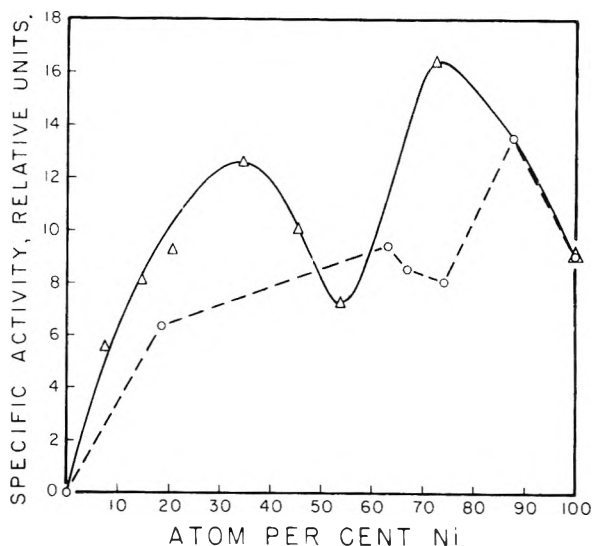


Fig. 1.—Hydrogenation of ethylene over Ni-Cu alloy films: \odot , present data (temp. 0°); \triangle , data of Hall and Emmett (temp. 200°K.). The activity units for the two sets of data have been made to coincide for nickel.

In the later experiments, however, the films were left overnight in 5 cm. of hydrogen at 300° before measuring the activities. (It was found that Cu-rich films took slightly longer for homogenization.) The results of these later experiments are summarized in Table I and Fig. 1. The following points may be noted: (a) The specific activity at 0° of a Cu-topped 87.4% Ni film is decidedly higher (~1.5 \times) than that of pure Ni film. (b) The specific activities of Ni-topped 63% Ni film and Cu-topped 67% Ni film lie in the same range within experimental error of surface area measurement. (c) The activity of the Cu-topped 81.7% Cu film is higher than that of pure Cu by at least two orders, and comparable to that of the pure Ni film. (d) The initial coppery appearance (on the outside) of the Ni-topped films would disappear in a short time when they were baked at 300°, thus indicating substantial homogenization in this short time. (e) The above results are consistent with a good homogenization of the films throughout their thickness. Variation in the composition of the film over the surface is expected due to directional non-uniformity of deposition leading to variation in the relative layer thickness of the individual metals. Such variations can of course be minimized with proper geometry, etc., of the evaporation set-up. (f) The above results follow similar trends to those of Hall and Emmett on hydrogen-cooled catalysts (Fig. 1). (g) From the activity determinations at only three temperatures, it is not correct to determine the exact value of the activation energies. However, the activation energy appeared to lie in the range 6-8 kcal./mole with no systematic variation with composition. This also is in approximate agreement with the results of Hall and Emmett, though they found the activation energy to be more nearly 4 kcal./mole. (h) The reaction was found to be zero order in ethylene and about 0.4 order in hydrogen over both pure Cu and 74.2% nickel films.

TABLE I

Mass evapd. mg.	Atom % Ni	Metal deposited on top	Activity at 0° (arbitrary units) k^a	Surface area, cm. ²	Specific activity at 0°, $k_0 = k/A$
11.77	100	Ni	4521	549	9.3
15.7	87.4	Cu	5815	418	13.9
15.7	74.2	Cu	4563	550	8.3
12.55	67.0	Cu	4452	509	8.8
11.3	63.0	Ni	6582	680	9.7
15.15	18.3	Cu	4563	695	6.6
15.8	0	Cu	8.314	≅300	≅.028

^a The k as here specified = $10^6 k'$ where k' is defined by $-dP/dt = k' P_{H_2} = k'(2P - P_0)/2$. P is the total pressure at time t , and P_0 is the initial pressure. t is in seconds.

Summary

The above experiments show a simple means of obtaining homogeneous alloy films for catalytic work. The results are in approximate agreement

with those of Hall and Emmett both as regards the variation of activity with alloy composition and the near constancy of the activation energy. They suggest that the presence of unreduced oxide in the bulk catalyst does not appear to be essential to the rather high activities (compared to that of pure Ni) of some of the Cu-Ni alloy catalysts observed for the ethylene hydrogenation reaction.

Acknowledgments.—Thanks are due to Dr. Colin T. H. Stoddart for many helpful discussions. The appointment of M. K. Gharpurey was supported by the International Coöperation Administration under the Visiting Research Scientists Program administered by The National Academy of Sciences of the USA. Experiments and materials were supported through the Air Force Office of Scientific Research of the Air Research and Development Command under contract No. AF 18(603)-129.

THE HEAT CAPACITY OF ALUMINUM OXIDE FROM 1000 TO 2000° AND OF THORIUM DIOXIDE FROM 1000 TO 2500°¹

By MICHAEL HOCH² AND HERRICK L. JOHNSTON

The Department of Chemistry, Ohio State University, Columbus, Ohio

Received January 6, 1961

The enthalpy (referred to 0°) of aluminum oxide (corundum) and of thorium dioxide has been determined in the range 1000–2000 and 1000–2500°, respectively, by the drop method.

Introduction

Al₂O₃ was proposed by the Calorimetry Conference in 1949 as a high temperature standard for heat capacity measurements. Its heat content has been determined by various authors from room temperature to 1500°. This work extends the range up to 2000°, just below the melting point.

ThO₂ is another oxide which would be suitable for a high temperature heat capacity standard. It does not absorb water or carbon dioxide.

Experimental Procedure

Samples.—The aluminum oxide was synthetic sapphire, obtained from the National Bureau of Standards, which prepared it for the Calorimetry Conference, March, 1949. The weight of the sample was 3.9335 g.

The thorium dioxide was obtained from the Maywood Chemical Company and was the same material as that used for vapor pressure measurements by the authors.³ The weight of the sample was 9.188 g.

Apparatus.—The apparatus was described in a previous paper.⁴ As Al₂O₃ reacts with tantalum, the sample holder was made of molybdenum. The ThO₂ was contained in a tantalum holder. Only a very slight reaction was observed between ThO₂ and the tantalum holder. Only two sets of runs were taken with each substance, one with the empty cell and one with the filled cell.

Results

Twenty runs were made on each empty cell. This made it possible to interpolate linearly be-

tween two empty runs for the temperature of the run with the sample. The interpolation interval was always less than 50°. This procedure was necessary because the same setting of the oscillator did not always give exactly the same temperature.

Table I gives the data for Al₂O₃. Table II gives those for ThO₂. Column 1 gives the order in which the points were taken; column 2 gives the temperature; column 3 gives the mass of mercury corresponding to Al₂O₃ or ThO₂; and column 4 gives the enthalpy in calories per gram of substance (1 g. Hg = 64.638 cal.).

$$\text{for Al}_2\text{O}_3: H_0^t = 0.2584 \times t + 1.375 \times 10^{-5}t^2$$

$$\text{for ThO}_2: H_0^t = 0.06269 \times t + 4.70 \times 10^{-6}t^2$$

with a standard deviation of 0.6 and 0.8%, respectively.

TABLE I
HEAT CONTENT OF ALUMINUM OXIDE

Run no.	Temp., °C.	Mass of mercury, ^a g.	Enthalpy H_0^t , cal./g.
6	1282	21.24	349.0
1	1315	22.26	365.8
2	1463	24.94	409.8
3	1598	27.45	451.1
4	1706	29.23	480.3
5	1713	29.41	483.3
7	1912	33.02	542.6
8	1930	33.41	549.0
9	2005	34.87	573.0

^a Weight of Al₂O₃ was 3.9335 g.

(1) This work was supported in part by the Office of Naval Research under contract with the Ohio State University Research Foundation.

(2) Department of Metallurgical Engineering, University of Cincinnati, Cincinnati 21, Ohio.

(3) M. Hoch and H. L. Johnston, *J. Am. Chem. Soc.*, **76**, 4833 (1954).

(4) M. Hoch and H. L. Johnston, *J. Phys. Chem.*, **65**, 855 (1961).

TABLE II
HEAT CONTENT OF THORIUM DIOXIDE

Run no.	Temp., °C.	Mass of mercury, ^a g.	Enthalpy H_0^t , cal./g.
1	1183	11.35	79.85
6	1185	11.44	80.48
3	1461	14.59	102.64
4	1610	16.25	114.32
8	1780	18.16	127.76
5	2053	21.05	148.09
2	2184	22.43	157.80
9	2215	22.81	160.47
7	2380	25.00	175.88
10	2480	26.32	185.16

^a Weight of ThO_2 was 9.188 g.

The heat content of the sample plus container was 3 times as large as that of the Al_2O_3 sample itself and 3.5 times as large as that of the ThO_2 sample. The error in a single determination of the amount of Hg will be the same as previously, 0.08%.⁴ Combining two determinations, and remembering that the value being calculated is 1/3.5 as large as the measured value, the maximum error in the Hg determination will be $2 \times 0.08 \times 3.5 = 0.56\%$. The precision, using the same errors for the weight of the sample and temperature as in the previous paper,⁴ will be $\sqrt{0.56^2 + 0.29^2 + 0.05^2} = 0.63\%$.

Using the limits for any systematic errors as determined before,⁴ 0.35%, and the maximum uncertainty in the temperature scale,⁴ 0.3%, an accuracy for H_0^t of within 1.3% of the true values is obtained.

The errors involved are the same as described previously,⁴ with the exception of the error in the determination of the amount of Hg, because in this case the enthalpy is the difference of two large numbers.

Comparison with Earlier Data.—Figures 1 and 2 show the plot of the mean specific heat, $c_p = H_0^t/t$, from the different sources. The authors' data on Al_2O_3 agree well (within 1%) with those of Gronow and Schwiete⁵ and of Shomate and Naylor.⁶ The agreement between the authors'

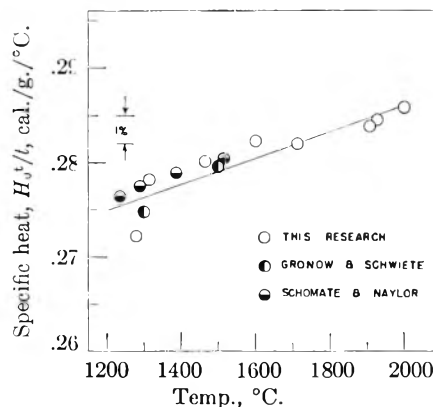


Fig. 1.—Specific heat of Al_2O_3 .

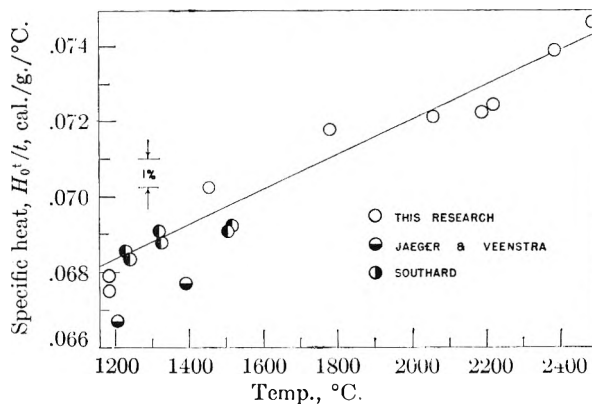


Fig. 2.—Specific heat of ThO_2 .

data on ThO_2 and the data of Jaeger and Veenstra⁷ and of Southard⁸ is also good (within 1%).

Acknowledgment.—We wish to thank J. B. Zink, A. J. Lamantia and R. W. Mattox, who helped us with the experimental work.

(5) H. E. Gronow and H. E. Schwiete, *Z. anorg. Chem.*, **216**, 185 (1933).

(6) C. H. Shomate and B. F. Naylor, *J. Am. Chem. Soc.*, **67**, 72 (1945).

(7) F. M. Jaeger and W. A. Veenstra, *Proc. Acad. Sci. Amsterdam*, **37**, 327 (1939).

(8) T. C. Southard, *J. Am. Chem. Soc.*, **63**, 3142 (1941).

THE SYSTEM POTASSIUM BROMIDE-CADMIUM CHLORIDE.

I. SURFACE TENSION¹BY R. B. ELLIS, J. E. SMITH, W. S. WILCOX AND E. H. CROOK²*Southern Research Institute, Birmingham, Alabama**John Harrison Laboratory of Chemistry, University of Pennsylvania, Philadelphia, Pennsylvania**Received January 9, 1961*

Studies of the surface tension of the fused-salt system CdCl_2 -KBr at temperatures from near the melting point up to 900° show that mixtures of these salts are decidedly non-ideal. Deviations from ideality reach maxima at 40 to 60 mole % KBr in the stated temperature range. Also there is a pronounced maximum in the "surface heat of mixing" at about 60 mole % KBr, which may be taken as an indication of the formation of complex ions. Observations of Raman spectra of melts at 67 and 40 mole % KBr show evidence of complex ion formation. The observed Raman bands may be attributed to the species CdCl_4^{2-} and CdBr_4^{2-} .

Introduction

Our work on the surface tension of fused salts³ has led us into a study of the KBr- CdCl_2 system, a system in which the formation of ionic aggregates or complex ions is to be expected. The Gibbs absorption rule leads one to expect the surface tension of a solution to be quite sensitive to small changes in solute species. Surface tension measurements should, therefore, give some indication of changes in the ionic constitution of liquids. We have measured the surface tension of the KBr- CdCl_2 system at 10 compositions ranging from 0 to 100 mole % KBr, and we have found this system to be far from ideal.

The existence of complex ions in fused salt systems has been the subject of much investigation and discussion, and a large part of this attention has been directed toward systems involving cadmium halides. Several reviews have covered the subject.⁴⁻⁸ The cadmium halide complexes are of the type $\text{CdX}_n^{-(n-2)}$, where $n = 3, 4$ or 6 , as discussed by Barton and Bloom.⁹ The tetra-halo complex, CdX_4^{2-} , appears to be the most likely one in most cases; see, for example, Bredig and Van Artsdalen.¹⁰ Most of the work has been done on chloride systems; none has been reported in which more than one halogen was involved.

Boardman, Palmer and Heymann¹¹ have reported surface tension measurements on a number of binary salt mixtures containing three ions, that is, two cations with the same anion or two anions with the same cation. They found that the sur-

face tension of mixtures showed negative deviations from simple additivity that increased with the difference in size of the replacing ions. In some systems the deviations were of sufficient magnitude to imply the presence of complex ions, one of these systems being KCl- CdCl_2 . However they did not consider a case in which there were two cations and two anions.

Experimental

A. Surface Tension. Method.—Measurements were made by the maximum bubble pressure method and surface tensions were calculated from the data by means of the Schrödinger equation.¹²

Apparatus.—The surface tension apparatus was a conventional maximum-bubble-pressure apparatus¹³ set up in a specially designed dry box. The capillary consisted of a short length of 19-gauge hypodermic tubing, made of 89% platinum-11% ruthenium alloy, swaged into a heavy platinum-rhodium shank 12 in. long. The precious metal shank was in turn welded to a nickel extension tube which gave an over-all length of 24 in. The capillary bore was measured across eight diameters, 45° apart, by means of a microscope fitted with a filar micrometer. Measurements were made to ± 0.0001 cm., and corrections were applied for thermal expansion. Bubbles were formed with helium, and a helium atmosphere was provided within the dry box. Sample temperatures were determined by use of a calibrated platinum-platinum-10% rhodium thermocouple, encased in a platinum-rhodium sheath and immersed in the salt mixture.

Chemicals.—In all cases, Baker and Adamson reagent grade salts were used. KBr and CdCl_2 were oven dried at 200°, mixed in the proper proportions, and ground in a ball mill. Drying of the mixtures was then completed by heating *in vacuo* at 400°. If possible, they were filtered through a Pyrex frit before use. The melting points of mixtures containing more than 0.6 mole fraction KBr prevented their filtration in a Pyrex apparatus. These KBr-rich mixtures were fused in Vycor and reground before use. In all cases, the mixtures were handled in an inert atmosphere after the drying *in vacuo*.

Procedure.—For a typical run, three samples of a given mixture, contained in platinum crucibles within sealed jars, were placed in the dry box of the surface tension apparatus, the box was thoroughly purged, and measurements were made on each sample, over the desired temperature range, on succeeding days. Bubble pressures were measured with a dibutyl phthalate manometer, read with a cathetometer. Immersion of the capillary to a known depth and bubble formation were accomplished by accepted techniques.¹³ The density of the mixture, needed for surface tension calculations, was determined in a separate apparatus by the buoyancy method. Sample compositions were determined by analysis after the run—cadmium by direct EDTA titra-

(1) This work was supported in part by the Atomic Energy Commission under Contract No. AT-(40-1)-2073 and in part by Southern Research Institute.

(2) Rohm and Haas Research Laboratories, Bristol, Pa.

(3) R. B. Ellis, J. E. Smith, and E. B. Baker, *J. Phys. Chem.*, **62**, 766 (1958).

(4) H. Bloom and J. O'M. Bockris, in "Modern Aspects of Electrochemistry No. 2," Ed. by J. O'M. Bockris, Academic Press, New York, N. Y., 1959, Ch. 3.

(5) G. J. Janz, C. Solomons and H. J. Gardner, *Chem. Revs.*, **58**, 461 (1958).

(6) E. R. Van Artsdalen, *J. Phys. Chem.*, **60**, 172 (1956).

(7) E. R. Van Artsdalen, in "The Structure of Electrolytic Solutions," Ed. by W. J. Hamer, John Wiley & Sons, Inc., New York, N. Y., 1959.

(8) G. E. Blomgren and E. R. Van Artsdalen, in "Annual Review of Physical Chemistry" Vol. 11, Ed. by H. Eyring, Annual Reviews, Inc., Palo Alto, Calif., 1960.

(9) J. L. Barton and H. Bloom, *Trans. Faraday Soc.*, **55**, 1792 (1959).

(10) M. A. Bredig and E. R. Van Artsdalen, *J. Chem. Phys.*, **24**, 478 (1956).

(11) N. K. Boardman, A. R. Palmer and E. Heymann, *Trans. Faraday Soc.*, **51**, 277 (1955).

(12) E. Schroedinger, *Ann. Physik*, **46**, 413 (1917).

(13) See for example: F. M. Jaeger, *Z. anorg. allgem. Chem.*, **101**, 1 (1917); and "Optical Activity and High Temperature Measurements," McGraw-Hill Book Co., New York, N. Y., 1930; and J. L. Dahl and F. R. Duke, *J. Phys. Chem.*, **62**, 1498 (1958).

TABLE I
SURFACE TENSION OF KBr-CdCl₂ MIXTURES
 $\gamma = a - bt$ (γ in dynes/cm. and t in degrees centigrade)

Mole % KBr	a	b	Standard dev.	No. of individual points involved	Temp. range, °C.	$H_{s/a}$ dynes/cm.	$(H_{s/a})_{m^n} -$ $(H_{s/a})_m$ dynes/cm.
0	101.4	0.0280	0.6	14	580-921	109	0
7.8	101.0	.0288	.7	26	569-769	109	-4
30.0	113.5	.0484	.3	30	479-736	127	+3
40.4	117	.056	1.6	51	484-702	132	+3
49.9	116.4	.0516	0.9	25	466-642	130	-3
60.4	110	.042	1.2	31	479-684	121	-8
70.1	124.1	.0590	0.7	22	571-812	140	-3
80.3	127.9	.0579	.8	31	622-926	144	-4
90.3	130.9	.0581	.8	25	688-912	147	-6
100	139.6	.0668	.8	11	803-972	158	0

tion, bromide and chloride by potentiometric titration with AgNO₃, and potassium by difference.

B. Raman Spectra. Apparatus.—A Cary Model 81 recording Raman spectrometer was used with the modification that a resistance wire was wrapped around the sample tube and cooling water was circulated through the container for the filter solution. The mercury blue line at 4358 Å. was used for excitation.

Procedure.—A filled sample tube was heated in a flame to melt down the sample and then was placed in the instrument where the resistance winding was used to maintain the desired temperature. Exposures next were made by the normal procedure for this instrument.

Results

A. Surface Tension.—The coefficients of linear equations derived by the method of least squares from the surface tension data obtained on the KBr-CdCl₂ system are listed in Table I. Surface tension-composition isotherms, calculated from these equations at three temperatures, are shown in Fig. 1. Our data for KBr are 2% higher than those reported by Bloom, Davis and James,¹⁴ and our CdCl₂ data are 2% higher than the values given by Boardman.¹¹ The difference in the CdCl₂ data is not surprising since Boardman determined the surface tension of this salt relative to tap water and our measurements were made by an absolute technique. The details of Bloom's work are not available to us at the present time and hence no comparison between our data and his is justified. It should be noted, however, that the KBr and CdCl₂ data presented in this paper have about the same temperature coefficients as the data given by the other investigators. The precision of the points plotted in Fig. 1 is about ± 0.5 dyne/cm. in surface tension and ± 0.5 mole % in composition. Although the experimental errors are of the same order of magnitude as the difference between the points from 0 to 60 mole % KBr, in the 600° isotherm, the points were connected as shown in order to emphasize the minima at 40 and 60 mole %, since the subsequent discussion supports the reality of these minima.

B. Raman Spectra.—Spectra on samples of two compositions, 40 and 67 mole % KBr, were obtained at temperatures varying from 300 to 500°. In each case two peaks were seen, at 251-252 and 168-169 cm.⁻¹. An estimate of line intensities was not made, since the experimental techniques

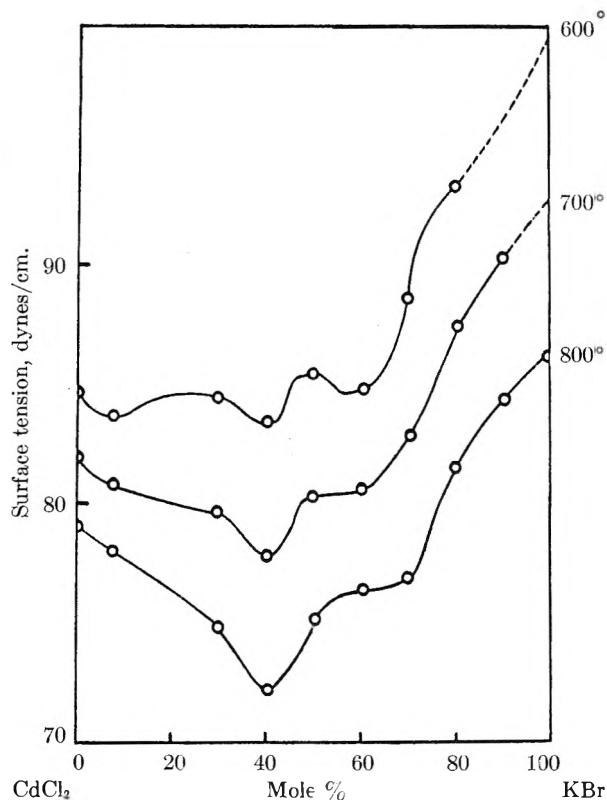


Fig. 1.—Surface tension-composition isotherms in KBr-CdCl₂ system.

for obtaining the spectra were designed to give only qualitative results.

Discussion

Our measurements on the KBr-CdCl₂ system indicate an extreme deviation from additivity at 40 mole % KBr and a secondary deviation at 60 mole % KBr. The temperature dependence of the magnitude of the deviation is of particular interest. At 40 mole % KBr the deviation from additivity increases with increasing temperature while at 60 mole % KBr the reverse is true. The same types of variations appear in Boardman's KCl-CdCl₂ data. Noteworthy is the fact that, in both sets of data, the composition of the extreme deviation shifts from 60 to 40% with increasing temperature.

Bloom¹⁴ has suggested that the surface heat content per unit area, $H_{s/a} = \gamma - T(d\gamma/dT)$, be

(14) H. Bloom, F. G. Davis and D. W. James, *Trans. Faraday Soc.*, **56**, 1179 (1960).

used to compare different salts. The quantity $H_{s/a}$ is a constant, independent of temperature, for a molten salt. In the case of an ideal mixture, surface heat contents should be additive

$$(H_{s/a})_m^0 = X_1(H_{s/a})_1 + X_2(H_{s/a})_2$$

where X is the mole fraction of the component indicated by the subscript. The difference between the actual value of $(H_{s/a})_m$ and the ideal value, $(H_{s/a})_m^0$, is, therefore, a measure of the departure of a system from ideal behavior. $H_{s/a}$ for non-polar liquids is about 50 dyne cm.⁻¹ and for highly ionic molten salts 150–200 dyne cm.⁻¹. Furthermore, as the degree of association of a molten salt increases, $H_{s/a}$ decreases; e.g., the value for MgCl₂ is 77 dyne cm.⁻¹ (Bloom¹⁴).

The values of $H_{s/a}$ and of $(H_{s/a})_m^0 - (H_{s/a})_m$, calculated from our data, are given in Table I. Except for the value at 60 mole % KBr, the deviations from additivity are not significant. The extremum at 60 mole % KBr may be taken as evidence for the existence of a complex on the basis of Bloom's argument. It should be emphasized that the composition at the extremum is not necessarily the composition of the complex.

The variation of surface entropy with composition, indicated by the temperature coefficients in Table I, has some significance. There is a negative deviation from additivity at 60 mole % KBr, which is consistent with the existence of a complex, since a complex would introduce more order into the distribution of ions in the surface. On the other hand, there is a positive deviation near 40 mole % KBr, indicating an increase in disorder, which may be explained in terms of mixing several ionic and molecular species of different sizes.

Mlle. Delwaille¹⁵ has reported an intense Raman line for the CdBr₄²⁻ complex at 163 cm.⁻¹ and one for CdCl₄²⁻ at 250 cm.⁻¹, in aqueous and alcoholic solutions. Bues¹⁶ found a line at 259 cm.⁻¹ in fused mixtures in the KCl–CdCl₂ system. He originally assigned the formula CdCl₃⁻ to the chloro-complex, but it is now generally accepted that the formula should be CdCl₄²⁻.¹⁰ Crook¹⁷ also has observed the line at 258–259 cm.⁻¹ in fused KCl–CdCl₂ mixtures and one at 166–167 cm.⁻¹ in fused KBr–CdBr₂ mixtures. Therefore the spectra of our KBr–CdCl₂ mixtures may be taken as evidence for the existence of both CdBr₄²⁻ and CdCl₄²⁻ complexes in these mixtures.

Conclusions

It is not possible to describe accurately the na-

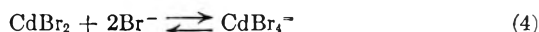
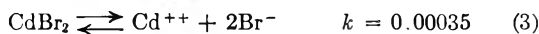
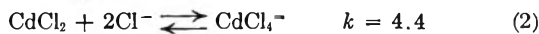
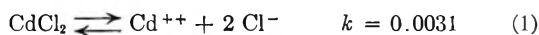
(15) M. L. Delwaille, *Bull. soc. chim. France*, 1294 (1955).

(16) W. Bues, *Z. anorg. allgem. Chem.*, **279**, 104 (1955).

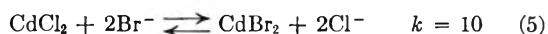
(17) E. H. Crook and J. O'M. Bockris, to be published.

ture of the surface of fused mixtures of KBr and CdCl₂, but there are some assumptions that are reasonable and consistent with existing data.

1. The species present will be principally determined by these equilibria, assuming that KBr is completely ionized



The equilibrium constants were determined at 300° by Van Artsdalen.⁶ It is reasonable to assume that the equilibrium constant for (4) will be somewhat higher than that for (2). It is evident that there will be very little free Cd⁺⁺. From the relative magnitudes of the k 's, Br⁻ will tend to displace Cl⁻



and the concentration of free Br⁻ will be low except for mixtures rich in KBr (>75 mole %). Therefore the species present in major proportions will be K⁺, CdCl₂, CdBr₂, CdCl₄²⁻, CdBr₄²⁻ and Cl⁻.

2. The un-ionized molecules, CdCl₂ and CdBr₂, and the complex ions, CdCl₄²⁻ and CdBr₄²⁻, will tend to lower the surface tension of the mixtures and therefore will tend to concentrate in the surface.

3. The large negative deviations in surface tension from additivity, reaching an extremum at 40 mole % KBr, are due to the presence in the surface of the several species. The fact that the deviations become more pronounced with increasing temperature may be explained on the basis of the disorder arising from the variety of species of different sizes.

4. The secondary minimum in the surface tension–composition isotherms at 60 mole % KBr may be associated with a maximum total concentration of complexes, CdCl₄²⁻ and CdBr₄²⁻.

Acknowledgments.—The authors wish to acknowledge the assistance of Mr. A. C. Freeman and Mr. Bobby C. Park in performing the laboratory work. Also we thank Dr. J. O'M. Bockris for permission to use the Raman spectrometer in his laboratory and for helpful discussions. Furthermore we express our appreciation to Dr. Bloom for making his paper¹⁴ available to us in advance of publication.

THE KINETICS OF THE REACTIONS OF AROMATIC HYDROCARBONS IN SULFURIC ACID. III. MESITYLENE

BY MARTIN KILPATRICK, MAX W. MEYER AND MARY L. KILPATRICK

Department of Chemistry, Illinois Institute of Technology, Chicago, Ill.

Received January 11, 1961

Mesitylene undergoes sulfonation to the mono-sulfonic acid, and simultaneously mesitylenesulfonic acid desulfonates, in an excess of 12–13.5 molar sulfuric acid at 12.3°. Upon resolution of the observed first-order velocity constant into k_S and k_D it is found that k_D increases with sulfuric acid concentration less rapidly than the k_D 's for the sulfonic acids of penta-methylbenzene, isodurene and durene. To interpret the results, use is made of the kinetic law found valid for sulfonation, and of the data of Feilchenfeld on the solubility of sulfonic acids in aqueous sulfuric acid.

Unlike benzene and the mono-, the di-, and the other trimethylbenzenes^{1,2} when mesitylene (1,3,5-methylbenzene) is dissolved in 12–13.5 *M* H₂SO₄ at 12.3°, sulfonation does not go to completion. When mesitylenesulfonic acid is dissolved in sulfuric acid of the same range of concentration, both mesitylene and mesitylenesulfonic acid are present at the end of the reaction. In both cases the appearance or disappearance of mesitylene-sulfonic acid is of the first order in the substrate in the constant medium of excess sulfuric acid and water. This is illustrated in Fig. 1. The initial concentration of mesitylene or its sulfonic acid was approximately 7×10^{-5} *M*.

A graph of the logarithm of the observed first-order velocity constant *vs.* the molarity of sulfuric acid is given in Fig. 2. The results of experiments starting with mesitylene are not as reproducible as with benzene, due to the slowness and difficulty of dissolving mesitylene. The procedure finally adopted was to make up a stock solution of one drop of mesitylene in 200 ml. of 10 *M* H₂SO₄ (at 5°), then to a portion of this add concentrated sulfuric acid, with cooling, to give the desired molarity. Two samples of mesitylene were used, one from the Aldrich Chemical Company, one from the National Bureau of Standards; no difference in rate was found between them. For the experiments starting with mesitylene

$$\log(k_{\text{obs}} \times 10^6) = -7.045 + 0.7954[\text{H}_2\text{SO}_4]_{\text{st}} \quad (1)$$

as found by the method of least squares; for the experiments starting with the sulfonic acid

$$\log(k_{\text{obs}} \times 10^6) = -5.670 + 0.6946[\text{H}_2\text{SO}_4]_{\text{st}} \quad (2)$$

over the range 12.5–13.7 *M* H₂SO₄. For all the experiments the least-squares equation is

$$\log(k_{\text{obs}} \times 10^6) = -6.281 + 0.7400[\text{H}_2\text{SO}_4]_{\text{st}} \quad (3)$$

All first-order constants were calculated using decadic logarithms and are 0.4343 times the true constant; the unit of time is the minute, and [H₂SO₄]_{st} is the stoichiometric concentration of sulfuric acid in moles per liter.

Since the first-order constants (k_{obs}) are about the same starting with mesitylene and with its sulfonic acid, and since the spectra of the final solutions were identical, it is presumed that

$$k_{\text{obs}} = k_S + k_D \quad (4)$$

where k_S is the velocity constant for sulfonation

(1) M. Kilpatrick, M. W. Meyer and M. L. Kilpatrick, *J. Phys. Chem.*, **64**, 1433 (1960).

(2) M. Kilpatrick and M. W. Meyer, *ibid.*, **65**, 530 (1961).

and k_D that for desulfonation in the same constant medium containing an excess of sulfuric acid and water. Although the equilibrium constant for the reversible sulfonation cannot be calculated due to insufficient information about the species concentrations, it is still possible to calculate k_S and k_D for an individual experiment since the medium is constant. The experiments starting with the sulfonic acid were utilized for this purpose, and the resolution into k_S and k_D was made as follows.

A weighed amount (approximately 2 mg.) of the sodium salt of mesitylenesulfonic acid was shaken with 100 ml. of standardized sulfuric acid (cooled to 5°) for three minutes, then filtered through a fritted glass filter (Corning C). The 10-cm. absorption cell was filled with the solution, placed in the thermostated compartment of the Cary spectrophotometer, and the recorder started immediately scanning from 290 to 270 *mμ*, the peak being at 283 *mμ*. The process of preparing the solution and filling the cell took approximately ten minutes. In order to determine the initial concentration of sulfonic acid, the material left on the filter was dissolved in 100 ml. of water and the weight of the sulfonate determined from the optical density. The optical density of the reacting solution at the time of mixing, OD₀, was obtained by a short extrapolation, and OD_∞ was obtained from the final reading (after 9 to 10 half-lives) by making a small correction for the absorption of the mesitylene present at equilibrium. The sodium salt of mesitylenesulfonic acid used in the kinetic runs were prepared from mesitylene according to the directions of Gibson³; it was purified by repeated recrystallization from water, and its spectrum showed no disulfonate. Letting *F* be the fraction of sulfonic acid reacted, the ratio of sulfonic acid to hydrocarbon at equilibrium, *R*, is given by

$$R = \frac{1 - F}{F} = \frac{\text{OD}_\infty}{\text{OD}_0 - \text{OD}_\infty} = \frac{k_S}{k_D} \quad (5)$$

The velocity coefficients k_S and k_D calculated from (4) and (5) for each experiment are given in the sixth and seventh columns of Table I. A similar resolution of k_{obs} is theoretically possible for the reaction starting with mesitylene, but mesitylene's slowness to dissolve and its low molar extinction make the determination of the initial hydrocarbon concentration impractical.

Log k_S , log k_D and log k_{obs} for these runs are shown in Fig. 3 plotted *vs.* [H₂SO₄]_{st}, the least-

(3) C. S. Gibson, *J. Chem. Soc.*, **117**, 948 (1920).

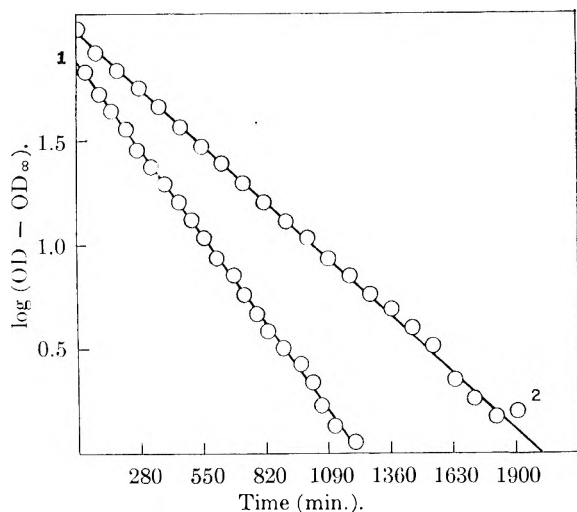


Fig. 1.—Mesitylene—typical first-order plots: (1) sulfonation of mesitylene in 12.90 M H_2SO_4 at 12.3° , $k_{\text{obs}} = 15.6 \times 10^{-4} \text{ min.}^{-1}$, $t_{1/2} = 193 \text{ min.}$ (2) Desulfonation of mesitylenesulfonic acid in 12.49 M H_2SO_4 at 12.3° , $k_{\text{obs}} = 10.0 \times 10^{-4} \text{ min.}^{-1}$, $t_{1/2} = 301 \text{ min.}$

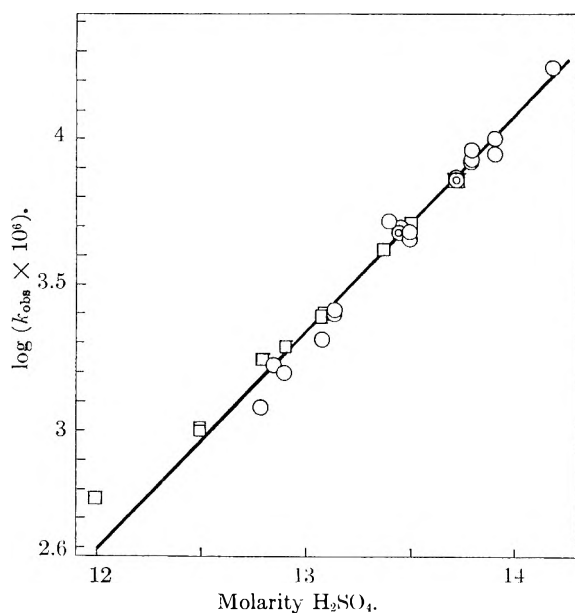


Fig. 2.—Sulfonation of mesitylene and desulfonation of mesitylenesulfonic acid in H_2SO_4 at 12.3° : O, $\log(k_{\text{obs}} \times 10^6)$ for sulfonation; □, $\log(k_{\text{obs}} \times 10^6)$ for desulfonation.

TABLE I

THE DESULFONATION OF MESITYLENESULFONIC ACID AND THE CALCULATION OF k_s AND k_D FROM k_{obs} AT 12.3°

H_2SO_4 , moles/l.	$k_{\text{obs}} \times 10^4$, min.^{-1}	OD_0	OD_∞	R	$k_s \times 10^4$, min.^{-1}	$k_D \times 10^4$, min.^{-1}
13.50	51.7	0.766	0.571	2.93	38.5	13.2
13.37	41.6	.855	.573	2.03	27.8	13.7
13.07	24.7	.800	.439	1.22	13.6	11.1
12.90	19.3	.815	.418	1.05	9.92	9.42
12.49	10.0	1.594	.443	0.385	2.78	7.22
12.49	10.2	1.152	.308	.365	2.72	7.45
11.99	5.87	1.158	.183	.188	0.93	4.94

squares lines for the two former being given by the equations

$$\log(k_s \times 10^6) = -11.255 + 1.1000[\text{H}_2\text{SO}_4]_{\text{st}} \quad (6)$$

and

$$\log(k_D \times 10^6) = -0.816 + 0.2941[\text{H}_2\text{SO}_4]_{\text{st}} \quad (7)$$

It will be noted that below 12.5 molar the curve for $\log k_{\text{obs}}$ in Fig. 3 (and also in Fig. 1) departs from linearity, its slope approaching that of the $\log k_D$ line as sulfonation becomes very slow. If $\log k_D$ is plotted vs. $-H_0$, a slope of 0.59 is found; this is considerably less than the slope of 0.90 reported by Long and Paul⁴ for the kinetic data of Crafts⁵ on the desulfonation of mesitylenesulfonic acid in 0.55 to 6 M H_2SO_4 at 100° . It is also considerably less than the slopes vs. $-H_0$ found by Kilpatrick and Meyer⁶ for the sulfonic acid of pentamethylbenzene (0.94), of isodurene (0.85), and of durene (1.00) at 12.3° .

It was shown in the first and second papers of this series^{1,2} that the rates of sulfonation obtained in vitriol support the kinetic equation

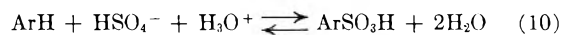
$$\frac{-d[\text{ArH}]}{dt} = \frac{d[\Sigma \text{ArSO}_3\text{H}]}{dt} = k \times \frac{[\text{H}_2\text{SO}_4]_{\text{st}}^2 [\text{ArH}]}{a_{\text{H}_2\text{O}}} \times F \quad (8)$$

where F is an activity coefficient ratio which over the limited range of $[\text{H}_2\text{SO}_4]_{\text{st}}$ where convenient rates are obtained for a particular hydrocarbon, would not be expected to undergo great change. If under the experimental conditions employed sulfonation proceeds by a single path, and if only one of the partial reactions which comprise the net reaction is rate-determining, and if the stoichiometric number of this partial reaction is unity⁷ the rate of the back reaction (desulfonation) may be obtained from that of the forward (sulfonation) and the equilibrium constant of the net reaction by means of the equation

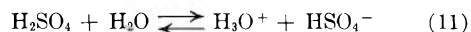
$$v_D = v_S(Q/K) \quad (9)$$

where Q is the activity ratio (products/educts) and K the equilibrium constant of the net reaction.

Although mesitylene functions as a base in a solvent of high proton availability, the ratio $[\text{ArH}\cdot\text{H}^+]/[\text{ArH}]$ in 12–13.5 M H_2SO_4 would be less than 0.01, as calculated from the pK_a value reported by Kilpatrick and Hyman,⁸ and mesitylene may be taken to be present largely as the neutral molecule. If mesitylenesulfonic acid is present largely as the neutral molecule, the net reaction is



since in this range molecular sulfuric acid is not present at concentrations sufficiently high to have been estimated by Raman spectral measurements. Taking K_{10} as the equilibrium constant of reaction 10, and K_{11} as that of the reaction



it follows from (8) and (9) that if the assumptions above are met

$$v_D = \frac{k}{K_{10}K_{11}^2} \times \frac{[\text{H}_3\text{O}^+][\text{HSO}_4^-][\text{ArSO}_3\text{H}]}{a_{\text{H}_2\text{O}}} \times F' \quad (12)$$

(4) F. A. Long and M. A. Paul, *Chem. Revs.*, **57**, 935 (1957).

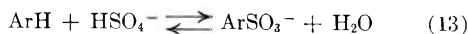
(5) J. M. Crafts, *Bull. soc. chim. France*, [4] **1**, 917 (1907).

(6) M. Kilpatrick and M. W. Meyer, to be published.

(7) J. Horiuti, *J. Res. Inst. Catalysis, Hokkaido University*, **1**, 8 (1948); J. Horiuti and T. Nakamura, *Z. physik. Chem. (Frankfurt)*, **11**, 358 (1957).

(8) M. Kilpatrick and H. Hyman, *J. Am. Chem. Soc.*, **80**, 77 (1958).

where F' is a new activity coefficient ratio. On the other hand, if the sulfonic acid is present largely as anion, the net reaction would be



and

$$v_D = \frac{k}{K_{11}^2 K_{13}} \times \frac{[\text{H}_3\text{O}^+]^2 [\text{HSO}_4^-] [\text{ArSO}_3^-]}{a_{\text{H}_2\text{O}}^2} \times F'' \quad (14)$$

Thus if (12) applies, one expects k_D to increase with increasing sulfuric acid concentration about as rapidly as $[\text{H}_3\text{O}^+][\text{HSO}_4^-]/a_{\text{H}_2\text{O}}$, and if (14) applies, about as rapidly as $[\text{H}_3\text{O}^+]^2 [\text{HSO}_4^-]/a_{\text{H}_2\text{O}}^2$. However, taking $[\text{H}_3\text{O}^+]$ as $2[\text{SO}_4^{2-}] + [\text{HSO}_4^-]$, and using for $[\text{SO}_4^{2-}]$ and $[\text{HSO}_4^-]$ values taken from the curves given by Young⁹ and Walrafen, at 25°, and for $a_{\text{H}_2\text{O}}$ the values of Giauque,¹⁰ k_D was found to increase with $[\text{H}_2\text{SO}_4]_{\text{st}}$ less rapidly than called for by either (12) or (14), the decrease in $k_D/([\text{H}_3\text{O}^+][\text{HSO}_4^-]/a_{\text{H}_2\text{O}})$ amounting to ca. 40%, and that in $k_D/([\text{H}_3\text{O}^+]^2 [\text{HSO}_4^-]/a_{\text{H}_2\text{O}}^2)$ to ca. 80% over the measured range. For the other sulfonic acids, the rates of increase of k_D with $[\text{H}_2\text{SO}_4]_{\text{st}}$ were found to lie between that expected from (12) and that expected from (14), the rate of increase in the case of isodurenesulfonic being close to that expected from (12).

It was proposed by Lantz¹¹ that the rate of desulfonation was governed by the reaction between the anion of the sulfonic acid and the molecular H_2SO_4 (or other undissociated strong acid). In accordance with this view, Cowdrey and Davies¹² showed that, in 40–70% H_2SO_4 , the first-order velocity constants of Pinnow¹³ for the desulfonation of quinolsulfonic acid, at 100°, and of Lantz¹⁴ for that of naphthalene- α -sulfonic acid, could be represented roughly by the equation

$$k_D = k' [\text{H}_3\text{O}^+] [\text{HSO}_4^-] / [\text{H}_2\text{O}] \quad (15)$$

if $[\text{H}_3\text{O}^+]$ and $[\text{HSO}_4^-]$ were taken as equal to $[\text{H}_2\text{SO}_4]_{\text{st}}$ and $[\text{H}_2\text{O}]$ as equal to the stoichiometric concentration of water minus $[\text{H}_2\text{SO}_4]_{\text{st}}$. A decrease in k_D with increase in the concentration of strong acid Lantz attributed to a decrease in the proportion of substrate present as anion. It may be mentioned that Pinnow found simultaneous sulfonation of quinol and desulfonation of its sulfonic acid to occur over the range 7.8 to 9.8 M H_2SO_4 , and that for his data $\log k_D$ plotted *vs.* $-\log a_{\text{H}_2\text{O}}$ gives a line with slope close to 0.6.

A different mechanism of desulfonation was proposed by Spryskov and Ovsyankina,¹⁵ *viz.*, formation of a complex between ArSO_3H and H_3O^+ in a pre-equilibrium, followed by the rate-determining reaction of the complex with any available bases (Cl^- , HSO_4^- , ArSO_3^-) to yield the hydrocarbon, H_2SO_4 , and the secondary acid product. Leitman and Pevzner¹⁶ studied the desulfonation of the sulfonic

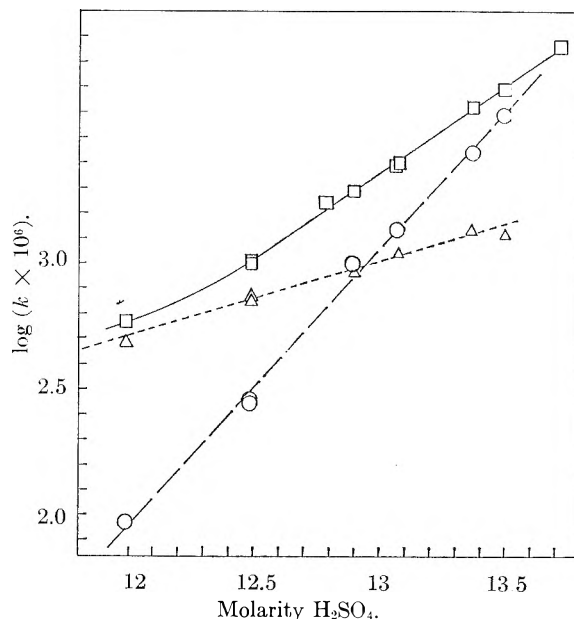


Fig. 3.—Desulfonation of mesitylenesulfonic acid at 12.3°C: □, $\log(k_{\text{obs}} \times 10^6) = \log[(k_s + k_D) \times 10^6]$; ○, $\log(k_s \times 10^6)$; △, $\log(k_D \times 10^6)$.

acids of the xylene isomers and ethylbenzene in an excess of 50–75% sulfuric acid at 90–145°, and considered their findings to support Spryskov's mechanism. Their systems were homogeneous at the start, but at the higher temperatures and sulfuric acid concentrations a hydrocarbon phase appeared as the reaction progressed in some cases. The first-order constant, which was calculated from the formula for an irreversible reaction, was found to rise to a maximum in the range 60–70% sulfuric acid; the subsequent decrease was attributed to the occurrence of sulfonation. The location of the maximum at ca. 65% sulfuric acid Leitman and Pevzner regarded as strong evidence for the Spryskov mechanism, since Feilchenfeld¹⁷ had shown that in the systems *p*-toluenesulfonic acid– H_2SO_4 – H_2O and *p*-xylenesulfonic acid– H_2SO_4 – H_2O maximum separation of the phase $\text{ArSO}_3\text{H} \cdot \text{H}_2\text{O}$ occurred at a spent acid composition of ca. 65% H_2SO_4 and had interpreted the increase in solubility of the sulfonic acid at higher concentrations of sulfuric acid as due to the formation of the cation $\text{ArSO}_3\text{H}_2^+$.

It seems desirable to examine Feilchenfeld's results in more detail. Upon adding sulfuric acid to a saturated solution of ArSO_3H in water at 30°, the solubility of the sulfonic acid decreases, then remains at a fairly constant low value, and finally increases. His interpretation is that in the region of initial decrease in solubility the ArSO_3^- is reacting with H_3O^+ to form the molecular acid; in the region of fairly constant low solubility (ca. 55–80% H_2SO_4 for *p*-toluenesulfonic, 50–75% H_2SO_4 for *p*-xylenesulfonic acid) the sulfonic acid is present predominantly as molecular acid; in the region of final marked increase in solubility $[\text{H}_3\text{O}^+]/[\text{H}_2\text{O}]$ is large and the reaction

(9) T. F. Young and G. E. Walrafen, *Trans. Faraday Soc.*, **57**, (34) (1961).

(10) W. F. Giauque, E. W. Hornung, J. E. Kunzler and T. R. Rubin, *J. Am. Chem. Soc.*, **82**, 62 (1960).

(11) R. Lantz, *Bull. soc. chim. France*, [5] **12**, 1004 (1945).

(12) W. A. Cowdrey and D. S. Davies, *J. Chem. Soc.*, 1871 (1949).

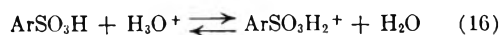
(13) J. Pinnow, *Z. Elektrochem.*, **21**, 380 (1915); **23**, 243 (1917).

(14) R. Lantz, *Bull. soc. chim. France* [5], **2**, 2092 (1935).

(15) A. A. Spryskov and N. A. Ovsyankina, *Sbornik. Statei Obshchei Khim.*, **2**, 878 (1953).

(16) Y. I. Leitman and M. S. Pevzner, *J. Applied Chem., U.S.S.R.*, **32**, 2830 (1959).

(17) H. Feilchenfeld, *Ind. Eng. Chem.*, **48**, 1935 (1956).



is pulled to the right. The ion $\text{ArSO}_3\text{H}_2^+$ had previously been suggested to explain the results of cryoscopic studies¹⁸ in sulfuric acid.

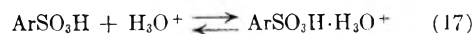
The mechanism of desulfonation proposed by Spryskov, with $\text{ArSO}_3\text{H}\cdot\text{H}_3\text{O}^+$ as an Arrhenius intermediate, and its reaction with HSO_4^- (in vitriol) as the rate-determining step, requires the transition state to be constructed from ArSO_3H , H_3O^+ and HSO_4^- ; if the reversible desulfonation-sulfonation proceeds by a single path with a single rate-determining step, the same transition state is involved in sulfonation. For sulfonation, however, we found the transition state to be constructed from ArH and $\text{H}_2\text{S}_2\text{O}_7$ (or its equivalent).^{1,2} The solubility study of Feilchenfeld suggests that above 65% sulfuric acid there is probably a new species of sulfonic acid present in increasing and appreciable quantity. The species $\text{ArSO}_3\text{H}\cdot\text{H}_3\text{O}^+$ appears more probable than the unhydrated $\text{ArSO}_3\text{H}_2^+$ deduced from cryoscopic measurements with 100% sulfuric acid; cf. the species H_5SO_5^+ (or $\text{H}_3\text{O}^+\cdot(\text{H}_2\text{SO}_4)$) which is believed to exist in 80–100% sulfuric acid,^{19,9} while the species H_3SO_4^+ becomes important only above 98%.

Returning to the question of desulfonation in vitriol, let us examine the consequences of assuming the sulfonic acid to be present partly as ArSO_3H and partly as $\text{ArSO}_3\text{H}\cdot\text{H}_3\text{O}^+$, and of taking the latter to be unreactive. It also will be assumed that simultaneous sulfonation occurs at a rate given by (8), and that there is in the reaction

(18) R. J. Gillespie and J. A. Leisten, *Quart. Rev. (London)*, **8**, 40 (1954).

(19) P. A. H. Wyatt, *Trans. Faraday Soc.*, **56**, 490 (1960).

scheme a single rate-determining step. Then if the average value of the classical equilibrium constant for the reaction



over the range of $[\text{H}_2\text{SO}_4]_{\text{st}}$ used is $(K_{17})_c$

$$[\text{ArSO}_3\text{H}] = [\text{ArSO}_3\text{H}]_{\text{st}} / \{1 + (K_{17})_c[\text{H}_3\text{O}^+]\}$$

where $[\text{ArSO}_3\text{H}]_{\text{st}}$ is the stoichiometric concentration of sulfonic acid, and from (12)

$$v_D = \frac{k}{K_{10}K_{11}^2} \times \frac{[\text{H}_3\text{O}^+][\text{HSO}_4^-][\text{ArSO}_3\text{H}]_{\text{st}}}{a_{\text{H}_2\text{O}}\{1 + (K_{17})_c[\text{H}_3\text{O}^+]\}} \times F' \quad (18)$$

If this applies, to explain the results obtained it is necessary for mesitylenesulfonic acid to have a greater tendency to form the cation $\text{ArSO}_3\text{H}\cdot\text{H}_3\text{O}^+$ than the other sulfonic acids. In particular, in the case of mesitylene and isodurene, which in anhydrous hydrofluoric acid undergo the reaction $\text{ArH} + \text{HF} \rightleftharpoons \text{ArH}\cdot\text{H}^+ + \text{F}^-$ to about the same extent,²⁰ and whose sulfonic acids desulfonate at comparable rates in 12–13.5 *M* sulfuric acid, the slopes obtained on plotting $\log k_D$ vs. $-H_0$ are 0.59 and 0.85, respectively. Thus, although the hydrocarbons show about the same tendency to attach a proton, their sulfonic acids may show rather different tendencies to attach the bulkier H_3O^+ , and one might expect the attachment to be easier for the more symmetrical mesitylenesulfonic acid.

Acknowledgment.—This research was supported in part by a grant from the Petroleum Research Fund administered by the American Chemical Society. Grateful acknowledgment is hereby made to the donors. Thanks are also due to the Simoniz Company for yearly grants to the department.

(20) M. Kilpatrick and F. E. Luborsky, *J. Am. Chem. Soc.*, **75**, 577 (1953).

SUB-SOLIDUS EQUILIBRIA IN THE SYSTEM Nb_2O_5 – Ta_2O_5 ¹

BY F. HOLTZBERG AND A. REISMAN

Research Center of International Business Machines, Yorktown Heights, N. Y.

Received January 12, 1961

Phase equilibria in the system Nb_2O_5 – Ta_2O_5 have been reinvestigated using thermal analysis and X-ray techniques. The results are not in agreement with Schäfer, Durkop and Jori's proposed diagram, which shows a continuous series of homogeneous solid solutions. A compound formed above 1450°, having the composition $2\text{Nb}_2\text{O}_5\cdot\text{Ta}_2\text{O}_5$, has been indexed on the basis of a body centered cubic unit cell with $a_0 = 15.76$ Å. Below 1450°, the compound decomposes sluggishly to form a two phase region extending from 25–51 mole % Ta_2O_5 . An explanation is offered to account for the apparent reversibility of Nb_2O_5 phases reported by Schäfer, *et al.*

Introduction

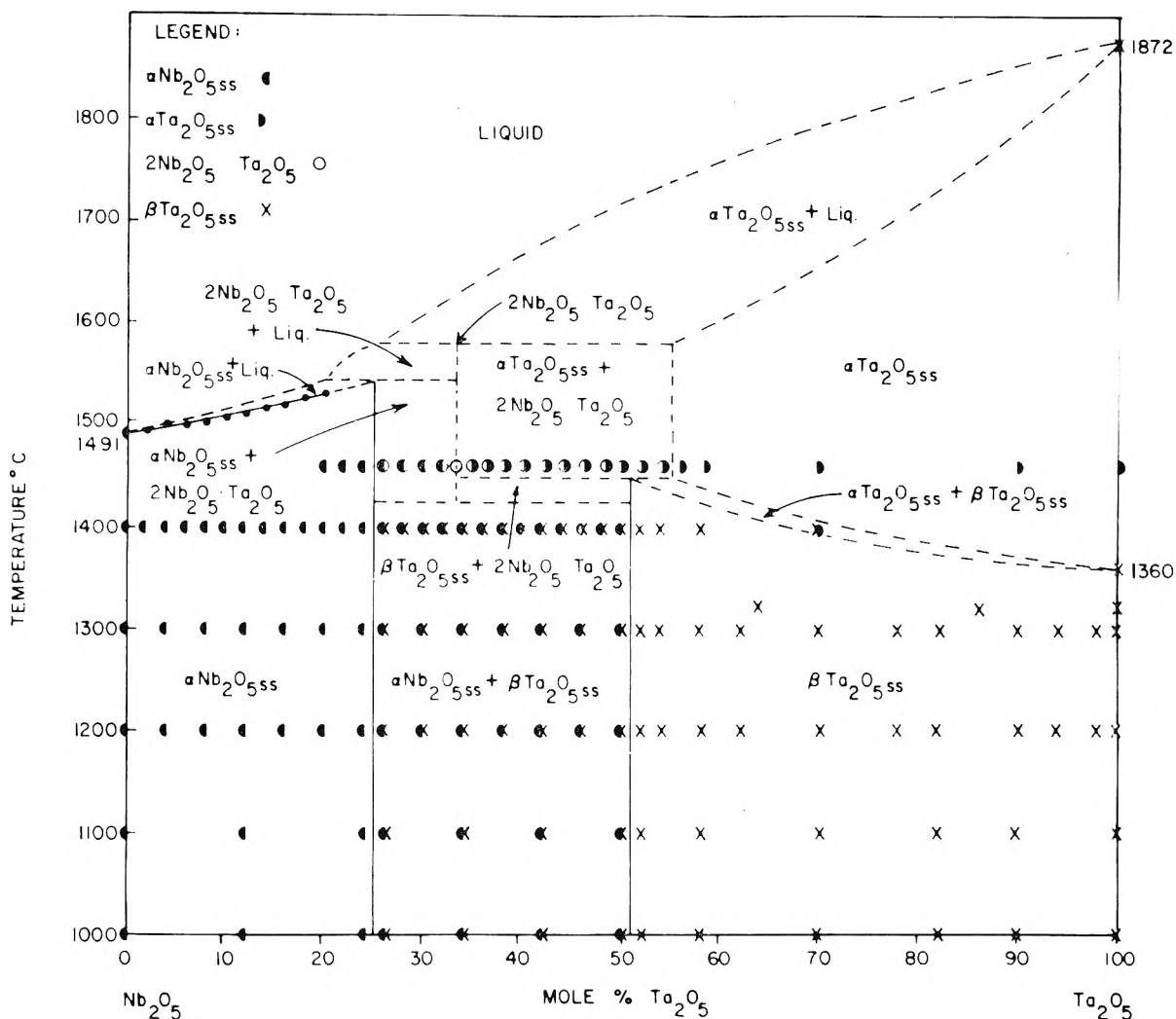
Studies of the systems alkali oxide with Ta_2O_5 indicate that there is no one-to-one correspondence with compounds formed in analogous niobate systems.² This is somewhat surprising since their analytical chemistry is in general similar. Furthermore, their cations coordinate oxygen octahedrally and have essentially the same ionic radii, leading one to suspect that the oxides are also structurally similar.

(1) This paper was presented in part at the 136th ACS Meeting in September 1959.

(2) A. Reisman and F. Holtzberg, *J. Am. Chem. Soc.*, **80**, 6503 (1958).

In 1954, Schäfer, Durkop and Jori³ published the results of a partial X-ray study of the interaction of niobium and tantalum pentoxides. The X-ray data were interpreted as being indicative of the formation of a continuous series of solid solutions between the end members. It was suggested that if a region of heterogeneity exists in the mixed oxide system, it does so in a narrow composition interval. The authors, however, were unable to detect its presence. Their interpretation is based primarily on the belief that their experiments showed Nb_2O_5 to be dimorphic. It is significant that the proof of

(3) H. Schäfer, A. Durkop and M. Jori, *Z. anorg. allgem. Chem.*, **275**, 19 (1954).

Fig. 1.—Phase diagram of the system $\text{Nb}_2\text{O}_5\text{-Ta}_2\text{O}_5$.

reversibility of the Nb_2O_5 phase transformation required the addition of Ta_2O_5 to Nb_2O_5 rich samples, and Nb_2O_5 to Ta_2O_5 rich samples under isothermal conditions. The apparent reversibility observed in such experiments was extrapolated to pure Nb_2O_5 for which reversibility could not be established on the basis of thermal cycling.

While Nb_2O_5 , depending on method of preparation and thermal history, has been reported to exist in a variety of crystallographic forms, it has been demonstrated^{4,5} that only one of the modifications is stable under standard pressures. Ta_2O_5 , on the other hand, is clearly dimorphic with a reversible phase transformation at 1360° ,⁶ neither of the phases being isomorphic with the stable Nb_2O_5 phase. Consequently, one would not expect to observe the formation of a continuous series of homogeneous solid solutions in the equilibrium oxide-oxide interaction. These considerations have led to a reinvestigation of the system $\text{Nb}_2\text{O}_5\text{-Ta}_2\text{O}_5$.

(4) F. Holtzberg, A. Reisman, M. Berry and M. Berkenblit, *J. Am. Chem. Soc.*, **79**, 2039 (1957).

(5) A. Reisman and F. Holtzberg, *ibid.*, **81**, 3182 (1959).

(6) A. Reisman, F. Holtzberg, M. Berkenblit and M. Berry, *ibid.*, **78**, 4514 (1956).

Experimental Procedure

A. Sample Preparation.—Samples of high purity Nb_2O_5 and Ta_2O_5 powder obtained from the Fansteel Metallurgical Company were dried at 1000° for 24 hours and then weighed, mixed in a rotating vial and fired at 1460° . The reaction mixtures were then ground and examined with X-rays. The procedure was repeated until no further change was observed in X-ray patterns, and generally required a 4-day cycling.

B. X-Ray.—325 mesh powder samples were examined with a Philips Diffractometer and Debye-Scherrer camera using Ni filtered Cu radiation.

C. D.T.A.—The differential thermal analysis apparatus previously described⁷ was used to establish the solidus curve in the region 0 to 20 mole % Ta_2O_5 .

D. Strip Furnace.—A rhodium strip furnace was employed in conjunction with a Leeds and Northrup optical pyrometer to analyze general trends in liquidus behavior beyond the 20 mole % Ta_2O_5 composition.

Discussion

Since transformations in $\text{Nb}_2\text{O}_5\text{-Ta}_2\text{O}_5$ solid solutions are sluggish, the system lent itself to the application of quenching techniques. Samples which had initially been equilibrated at 1460° were divided into two fractions. One fraction was heated at 1000° over a six-month period, and then incrementally equilibrated to 1460° with intervening

(7) A. Reisman and F. Holtzberg, *J. Phys. Chem.*, **64**, 748 (1960).

TABLE I
 HEAT TREATMENT DATA

T_i , °C. Mole % Nb	Nb = Nb ₂ O ₅ Ta = Ta ₂ O ₅		Nb _{ss} = Nb ₂ O _{5,ss} Ta _{ss} = Ta ₂ O _{5,ss}		2:1 = 2Nb ₂ O ₅ .Ta ₂ O ₅			
	1460	1400	1360	1320	1300	1200	1100	1000
100		α -Nb			α -Nb	α -Nb	α -Nb	α -Nb
98		α -Nb _{ss}						
96		α -Nb _{ss}			α -Nb _{ss}	α -Nb _{ss}		
94		α -Nb _{ss}						
92		α -Nb _{ss}			α -Nb _{ss}	α -Nb _{ss}		
90		α -Nb _{ss}						
88		α -Nb _{ss}			α -Nb _{ss}	α -Nb _{ss}	α -Nb _{ss}	α -Nb _{ss}
86		α -Nb _{ss}						
84		α -Nb _{ss}			α -Nb _{ss}	α -Nb _{ss}		
82		α -Nb _{ss}						
80	α -Nb _{ss}	α -Nb _{ss}			α -Nb _{ss}	α -Nb _{ss}		
78	α -Nb _{ss}	α -Nb _{ss}						
76	α -Nb _{ss}	α -Nb _{ss}			α -Nb _{ss}	α -Nb _{ss}	α -Nb _{ss}	α -Nb _{ss}
74	α -Nb _{ss} , 2:1	α -Nb _{ss} , β -Ta _{ss}			α -Nb _{ss} , β -Ta _{ss}	α -Nb _{ss} , β -Ta _{ss}	α -Nb _{ss} , β -Ta _{ss}	α -Nb _{ss} , β -Ta _{ss}
72	α -Nb _{ss} , 2:1	α -Nb _{ss} , β -Ta _{ss}						
70	α -Nb _{ss} , 2:1	α -Nb _{ss} , β -Ta _{ss}			α -Nb _{ss} , β -Ta _{ss}	α -Nb _{ss} , β -Ta _{ss}		
68	α -Nb _{ss} , 2:1	α -Nb _{ss} , β -Ta _{ss}						
67	2:1							
66	α -Ta _{ss} , 2:1	α -Nb _{ss} , β -Ta _{ss}			α -Nb _{ss} , β -Ta _{ss}	α -Nb _{ss} , β -Ta _{ss}	α -Nb _{ss} , β -Ta _{ss}	α -Nb _{ss} , β -Ta _{ss}
64	α -Ta _{ss} , 2:1	α -Nb _{ss} , β -Ta _{ss}						
62	α -Ta _{ss} , 2:1	α -Nb _{ss} , β -Ta _{ss}			α -Nb _{ss} , β -Ta _{ss}	α -Nb _{ss} , β -Ta _{ss}		
60	α -Ta _{ss} , 2:1	α -Nb _{ss} , β -Ta _{ss}						
58	α -Ta _{ss} , 2:1	α -Nb _{ss} , β -Ta _{ss}			α -Nb _{ss} , β -Ta _{ss}	α -Nb _{ss} , β -Ta _{ss}	α -Nb _{ss} , β -Ta _{ss}	α -Nb _{ss} , β -Ta _{ss}
56	α -Ta _{ss} , 2:1	α -Nb _{ss} , β -Ta _{ss}						
54	α -Ta _{ss} , 2:1	α -Nb _{ss} , β -Ta _{ss}			α -Nb _{ss} , β -Ta _{ss}	α -Nb _{ss} , β -Ta _{ss}		
52	α -Ta _{ss} , 2:1	α -Nb _{ss} , β -Ta _{ss}						
50	α -Ta _{ss} , 2:1	α -Nb _{ss} , β -Ta _{ss}			α -Nb _{ss} , β -Ta _{ss}	α -Nb _{ss} , β -Ta _{ss}	α -Nb _{ss} , β -Ta _{ss}	α -Nb _{ss} , β -Ta _{ss}
48	α -Ta _{ss} , 2:1	β -Ta _{ss}			β -Ta _{ss}	β -Ta _{ss}	β -Ta _{ss}	β -Ta _{ss}
46	α -Ta _{ss} , 2:1	β -Ta _{ss}			β -Ta _{ss}	β -Ta _{ss}		
44	α -Ta _{ss}							
42	α -Ta _{ss}	β -Ta _{ss}			β -Ta _{ss}	β -Ta _{ss}	β -Ta _{ss}	β -Ta _{ss}
38					β -Ta _{ss}	β -Ta _{ss}		
36				β -Ta _{ss}				
30	α -Ta _{ss}	α -Ta _{ss} , β -Ta _{ss}			β -Ta _{ss}	β -Ta _{ss}	β -Ta _{ss}	β -Ta _{ss}
22					β -Ta _{ss}	β -Ta _{ss}		
18					β -Ta _{ss}	β -Ta _{ss}	β -Ta _{ss}	β -Ta _{ss}
14				β -Ta _{ss}				
10	α -Ta _{ss}				β -Ta _{ss}	β -Ta _{ss}	β -Ta _{ss}	β -Ta _{ss}
6					β -Ta _{ss}	β -Ta _{ss}		
2					β -Ta _{ss}	β -Ta _{ss}		
0	α -Ta		α -Ta \rightarrow β -Ta	β -Ta	β -Ta	β -Ta	β -Ta	β -Ta

X-ray characterization after quenching from given isotherms. The high temperature fraction was correspondingly treated to the lower temperature

limit in order to compare the results obtained in approaching equilibrium from two directions. Because of apparently lower diffusion rates at the

lower temperatures, the samples required anywhere from three weeks to six-months of heat treatment before X-ray patterns showed reproducibility.

In the course of thermal treatment, it was found that the samples acted as "getters" for the trace quantities of silica and alumina present in the furnace atmosphere. The absorption of silica and alumina during lengthy heat treatment required to achieve equilibrium was sufficient to alter markedly the structural characteristics of the niobiantantalum mixed phases. Although no attempt was made to partially elucidate the systems Nb_2O_5 or Ta_2O_5 with SiO_2 , Al_2O_3 or both, test samples of the pentoxides prepared with the suspected contaminants gave X-ray patterns identical with those exhibited by the samples believed to be contaminated. The contamination was minimized by using closed platinum crucibles and large (50-100 g.) quantities of reactants. Since the pure pentoxides were found to be extremely sensitive to such contamination, they were used as controls in all heat treatments. Under these conditions no discernible change was detected in X-ray patterns of the end members or in the freezing point of Nb_2O_5 . It is suggested that some of the uncorroborated Nb_2O_5 phases, heretofore reported in the literature, may be the result of such contamination.

Sub-solidus Equilibria of the System $\text{Nb}_2\text{O}_5\text{-Ta}_2\text{O}_5$.—The proposed equilibrium phase diagram based on the results shown in Tables I and II is illustrated in Fig. 1.

TABLE II

THERMAL DATA FOR THE SYSTEM $\text{Nb}_2\text{O}_5\text{-Ta}_2\text{O}_5$		
Nb_2O_5 , mole, %	Ta_2O_5 , mole, %	Solidus transition, °C.
100	0	1491
98	2	1494
96	4	1498
94	6	1500
92	8	1502
90	10	1506
88	12	1510
86	14	1514
84	16	1520
82	18	1525
80	20	1531

A. The 1460° Isotherm.—Figure 1 shows a homogeneous region $\alpha\text{-Nb}_2\text{O}_{5ss}$ extending from 0 to 25 mole % Ta_2O_5 . The system then enters a two phase region bounded by 25 and 33 mole % Ta_2O_5 . In addition to the $\alpha\text{-Nb}_2\text{O}_{5ss}$ diffraction pattern, a new pattern, not characteristic of any of the known stable or metastable phases of the end members, is obtained. The new pattern increases in intensity from 25-33 mole % Ta_2O_5 with an attendant decrease of intensity of $\alpha\text{-Nb}_2\text{O}_{5ss}$ lines. The pattern of the pure phase was observed at 33 mole % Ta_2O_5 , with the nearest small whole number ratio being $2\text{Nb}_2\text{O}_5\text{-Ta}_2\text{O}_5$. The compound was indexed on the basis of a body centered cubic unit cell with $a = 15.76 \text{ \AA}$. The solid solubility of either Nb_2O_5 or Ta_2O_5 in the 2:1 compound is extremely small, since no homogeneous region was observed for this phase at either higher or lower Ta_2O_5 composition, within the limits of the experiment.

The question of whether the compound melts congruently or incongruently could not be resolved by means of X-rays alone, even though an extensive $\alpha\text{-Nb}_2\text{O}_{5ss}$ region might be indicative of a peritectic type liquidus behavior. Examination of the liquidus between 0 and 20 mole % Ta_2O_5 with differential thermal analysis, and from 20 to 40 mole % Ta_2O_5 with strip furnace techniques, showed that the liquidus and solidus curves increased monotonically with increasing Ta_2O_5 concentration, confirming that the system is peritectic.

From 34-45 mole % Ta_2O_5 there is a two phase region of $2\text{Nb}_2\text{O}_5\text{-Ta}_2\text{O}_5$ with $\alpha\text{-Ta}_2\text{O}_{5ss}$, showing analogous X-ray intensity variation as described above. The high temperature polymorphic structure of $\alpha\text{-Ta}_2\text{O}_5$ persists from 46-100 mole % Ta_2O_5 .

It is interesting to note that the lattice constants of neither the $\alpha\text{-Nb}_2\text{O}_{5ss}$ nor $\alpha\text{-Ta}_2\text{O}_{5ss}$ varied as a function of composition in their respective extensive regions. This probably is a consequence of the similarity of ionic radii of the two elements.

The Diagram below 1450°.—The temperature of the $\alpha \rightarrow \beta\text{-Ta}_2\text{O}_5$ transformation is elevated by the addition of Nb_2O_5 , intersecting the $\alpha\text{-Ta}_2\text{O}_{5ss}\text{-}2\text{Nb}_2\text{O}_5\text{-Ta}_2\text{O}_5$ miscibility gap between 1400 and 1450°.

$2\text{Nb}_2\text{O}_5\text{-Ta}_2\text{O}_5$ is unstable below 1450° and in the range 25-51 mole % Ta_2O_5 the compound decomposes to form the two phases $\alpha\text{-Nb}_2\text{O}_{5ss}$ and $\beta\text{-Ta}_2\text{O}_{5ss}$. The $\beta\text{-Ta}_2\text{O}_{5ss}$ extends from 51-100 mole % Ta_2O_5 .

The liquidus curves have been sketched into the diagram as they might appear, being consistent with the small range of DTA data obtained, the melting point of the end members, and the sub-solidus diagram.

From an examination of Fig. 1 it is apparent that the region 25 to 51 mole % Ta_2O_5 would give the most experimental difficulty. In other regions where simple solid solution exists, the observation of a single phase was taken as an indication that reaction was complete. While attempting to define the phase boundaries in the region 25 to 51 mole % Ta_2O_5 , several false equilibria were encountered. For samples originally fired at 1460° it was found that $2\text{Nb}_2\text{O}_5\text{-Ta}_2\text{O}_5$ persisted down to the 1000° isotherm and the boundaries varied with each experiment in the initial series of experiments where equilibration was assumed complete in 3 to 4 days. The transition $2\text{Nb}_2\text{O}_5\text{-Ta}_2\text{O}_5$ to $\alpha\text{-Nb}_2\text{O}_{5ss}$ and $\beta\text{-Ta}_2\text{O}_{5ss}$ requires a significant reconstruction and equilibrium was only achieved when samples were treated at the appropriate temperatures for periods extending from three weeks to six months. The outline of the $2\text{Nb}_2\text{O}_5\text{-Ta}_2\text{O}_5$ to $\alpha\text{-Nb}_2\text{O}_{5ss}$ plus $\beta\text{-Ta}_2\text{O}_{5ss}$ boundary has been shown as a dotted line since within the limits of experiments performed, it is not possible to state the actual transformation temperature. No attempt was made to establish the temperature of transformation to better than the 50° interval suggested by the diagram.

Schäfer's diagram indicates a continuous series of solid solutions interrupted only by a single phase transformation line. Unfortunately, his interpretation indicating homogeneous solid solution is

not validated by his own data. Whereas he assumed he was moving across a simple crystallographic phase transformation line, he actually was moving across miscibility gap boundaries. Superimposing Schäfer's phase transformation line on the present diagram one observes the following interesting consequence of varying Nb_2O_5 and Ta_2O_5 concentrations to either induce or verify reversibility of transformations. Starting with $\alpha\text{-Nb}_2\text{O}_5$, an addition of sufficient $\beta\text{-Ta}_2\text{O}_5$ will result in a sample having a composition in the $\beta\text{-Ta}_2\text{O}_5$ field.

If one adds more $\alpha\text{-Nb}_2\text{O}_5$, the displacement in composition can now carry into the $\alpha\text{-Nb}_2\text{O}_5$ field. Since metastable $\gamma\text{-Nb}_2\text{O}_5$ ^{4,5} is crystallographically indistinguishable from stable $\beta\text{-Ta}_2\text{O}_5$, the impression created is that reversibility has been achieved and that a thermodynamic phase transformation does exist.

Acknowledgment.—The authors wish to thank Miss B. Agule for sample preparation and Mrs. C. Pfister and Mrs. M. Witzen for collection of X-ray data.

ULTRAVIOLET SPECTRA OF $-\text{N}=\overset{\text{I}}{\text{C}}-\overset{\text{I}}{\text{C}}=\text{N}-$ COMPOUNDS¹

BY ROBERT H. LINNELL AND A. KACZMARCZYK²

Department of Chemistry, University of Vermont, Burlington, Vt.

Received January 13, 1961

Ultraviolet spectra in buffered aqueous and sulfuric acid solutions for 2,2'-bipyridine, *o*-phenanthroline, 2,2'-biquinoline and pyrazine are reported. pK_{BH^+} and $pK_{\text{BH}_2^{++}}$ values are determined from the spectra and correlated with the structures of the several compounds.

Compounds containing the $-\text{N}=\overset{\text{I}}{\text{C}}-\overset{\text{I}}{\text{C}}=\text{N}-$ structure have been widely used as chelating agents. Ionization constants have been reported for several of these compounds, and the previous literature results as well as those reported here are summarized in Table I. Two of our compounds (2,2'-bipyridine and 2,2'-biquinoline) could exist in *cis* or *trans* form or in some intermediate non-

planar form involving twisting about the $=\overset{\text{I}}{\text{C}}-\overset{\text{I}}{\text{C}}=$ bond. The other two (*o*-phenanthroline and pyrazine) are planar and must remain so whether existing as B, BH^+ or BH_2^{++} forms.³ Nakamoto⁴ has reported recently the ultraviolet spectra of 2,2'-bipyridine and 2,2',2''-tripyrindine in aqueous solutions of various pH; for the former, bands at 279 and 232 $m\mu$ in basic solution and organic solvent are considered to indicate *trans* form, and bands at 301 and 240 $m\mu$ in acidic solution similar to bands for $\text{Ni}(\text{bipy})_3\text{Cl}_2$ indicate *cis* form (favored by electrostatic considerations). M. Kasha⁵ has suggested that H_2SO_4 could be used to tie up both non-bonding electrons in diazines. Hammett⁶ has earlier used spectrophotometric methods for determining pK_a values of very weak bases using H_2SO_4 , and recent work by Brand⁷ and co-workers has yielded pK_a values for aromatic nitro-compounds by this technique. We were interested in $pK_{\text{BH}_2^{++}}$ values for the four $-\text{N}=\overset{\text{I}}{\text{C}}-\overset{\text{I}}{\text{C}}=\text{N}-$

compounds reported here to obtain information on the configurations in solution and data of value in studies with metal chelates of these compounds in acidic solutions.

Experimental

Materials.—2,2'-Bipyridine was obtained from Eastman Organic Chemicals, Rochester, New York. Purified pyrazine was kindly supplied by Dr. R. C. Ellingson, Mead Johnson and Company. *o*-Phenanthroline was Fisher Certified Reagent, A.C.S. 2,2'-Biquinoline was from the British Drug House. Organic solvents were of spectroscopic grade, and all other reagents were Analytical Reagent grade.

Spectral Measurements.—All ultraviolet spectra were measured on a Beckman Model DU quartz instrument with H_2 source and 1.00 cm. silica cells corrected for mis-match. Ambient temperature, $23 \pm 2^\circ$ prevailed. Merck concentrated C.P. H_2SO_4 used titrated 16.75 *M*. Except at high acidities an ionic strength of 0.02 was used with HCl, NaOAc-HOAc, NH_4OAc and Na_2HPO_4 buffers covering pH 1.31 to 9.05. All solutions yielded spectra stable with time over a several-weeks period.

Determination of pK Values in H_2SO_4 .—We have plotted molar extinction coefficients of the maximum for each absorption band *vs.* pH and read off the pH at the mid-point of the inflection where C_B/C_{BH^+} (or $C_{\text{BH}^+}/C_{\text{BH}_2^{++}}$) is unity. The values for the aqueous solutions have been corrected by Debye-Hückel theory. The pH scale used for H_2SO_4 was obtained by graphical interpolation of the data of Paul⁸ using $H_0 \equiv \text{pH}$. Although this method is empirical it yields useful comparison values. This is the technique originally developed by Hammett^{6,9} and co-workers.

Results

I. 2,2'-Bipyridine.—The ultraviolet spectra of 2,2'-bipyridine are shown in Fig. 1. The bands at 281 and 233 $m\mu$ for B, and 301 and 241 for BH^+ , agree with literature values.^{4,10} In concentrated H_2SO_4 only one band at 289 $m\mu$ is found (reported as 290 $m\mu$ by Westheimer¹¹), with the indication of another band with a maximum somewhat below

(1) The experimental part of this work was performed in the Chemistry Laboratories, American University of Beirut, Beirut, Lebanon.

(2) Department of Chemistry, Harvard University, Cambridge, Mass.

(3) Throughout this paper we use B to represent the free base, BH^+ to represent the mono-cation, and BH_2^{++} to represent the dication.

(4) K. Nakamoto, *J. Phys. Chem.*, **64**, 1420 (1960).

(5) F. Halverson and R. C. Hirt, *J. Chem. Phys.*, **19**, 717 (1951).

(6) L. P. Hammett and A. J. Deyrup, *J. Am. Chem. Soc.*, **54**, 2721 (1932).

(7) J. C. D. Brand, W. C. Horning and M. B. Thornley, *J. Chem. Soc.*, 1374 (1952).

(8) M. A. Paul and F. A. Long, *Chem. Revs.*, **57**, 15 (1957).

(9) L. P. Hammett and M. A. Paul, *J. Am. Chem. Soc.*, **56**, 827 (1934); L. A. Flexser, L. P. Hammett and A. Dingwall, *ibid.*, **57**, 2103 (1935).

(10) P. Krumbholz, *ibid.*, **73**, 3487 (1951).

(11) F. H. Westheimer and O. T. Benfey, *ibid.*, **78**, 5309 (1956).

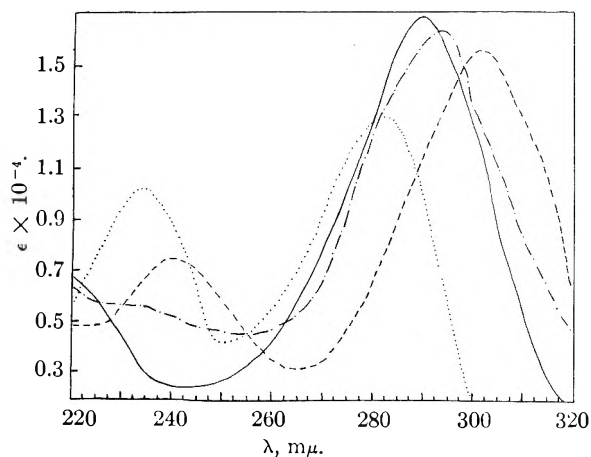


Fig. 1.—2,2'-Bipyridine:, B form; ----, BH^+ form; —, BH_2^{++} form; - · - ·, 15% (wt.) H_2SO_4 .

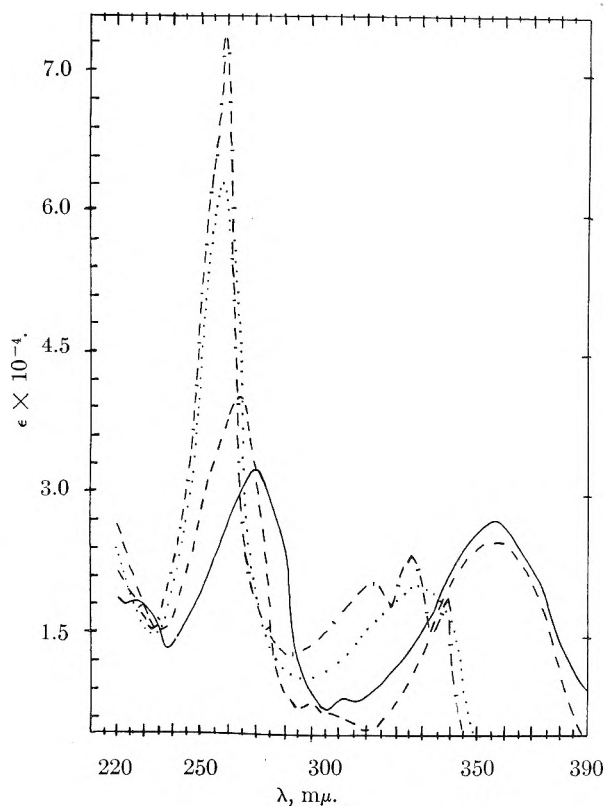


Fig. 2.—2,2'-Biquinoline:, B form; ----, BH^+ form; —, BH_2^{++} form; - · - ·, cyclohexane.

220 $m\mu$. We attribute this to the BH_2^{++} form. Krumholz¹² mentions a shift of the 2,2'-bipyridine spectrum to shorter wave lengths in 2.2 M HCl (but gives no data) and assumes BH_2^{++} is formed (which agrees with our results reported here), and calculates $K_{BH_2^{++}} = 1.4 \pm 0.3$ ($pK = -0.15$) (in 2.2 M mixtures of HCl + LiCl) from spectral data, or $K_{BH_2^{++}} = 1.67$ ($pK = -0.22$) from Fe (II) complex-ion studies. We find $pK_{BH^+} = 4.25$ and $pK_{BH_2^{++}} = -0.2$ (which compares with Westheimer's¹¹ value of -0.52).

II. 2,2'-Biquinoline.—The ultraviolet spectra of 2,2'-biquinoline are shown in Figs. 2–4. In cyclohexane there is structure in the long wave length

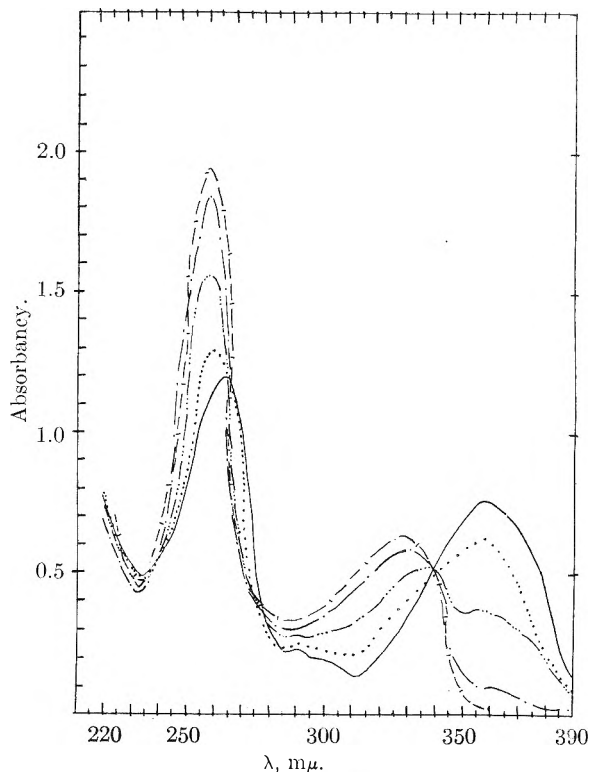


Fig. 3.———, pH 1.32;, pH 2.17; - · - ·, pH 2.84; - · - ·, pH 3.71; - · - ·, pH 6.14; 2,2'-biquinoline, 3.07×10^{-5} molar.

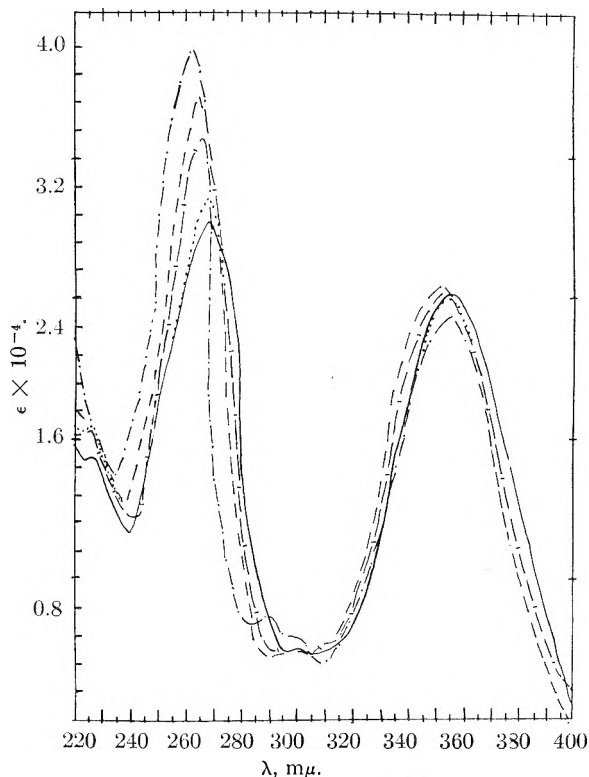


Fig. 4.—2,2'-Biquinoline; $BH_2^{++} \rightleftharpoons BH^+ + H^+$: —, 94% (wt.) H_2SO_4 ;, 80% H_2SO_4 ; - · - ·, 52% H_2SO_4 ; —, 31% H_2SO_4 ; - · - ·, 1.5% H_2SO_4 .

band (λ_{max} 334, 326 and 313 $m\mu$) and a short wave length maximum at 259 $m\mu$. This compound is not sufficiently soluble in water to make measure-

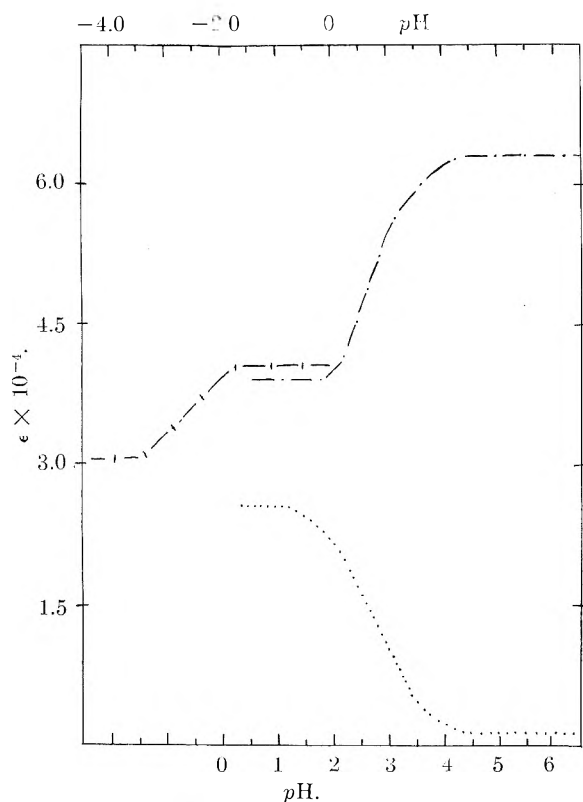


Fig. 5.—2,2'-Biquinoline: —, λ 258–264 $m\mu$ (lower pH scale); — — —, λ 264–270 $m\mu$ (upper pH scale); ·····, λ 357 $m\mu$ (lower pH scale).

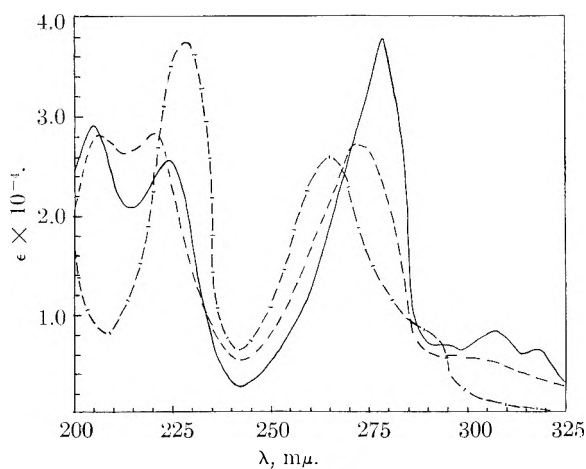


Fig. 6.—*o*-Phenanthroline: —, B form; — — —, BH^+ form; ·····, BH_2^{++} form.

ments; hence ϵ 40% EtOH–60% H_2O (volume %) solvent was used. In the H_2SO_4 solutions, formation of BH^+ and BH_2^{++} gave solubility without EtOH. In the EtOH solvent, pH 4.47–6.38 we find λ_{max} at 328 and 258 $m\mu$ which is characteristic of the free B form. Figure 3 shows the spectral shift in acid solutions pH 6.15 to 1.32 due to the equilibrium $BH^+ \rightleftharpoons B + H^+$ with an isosbestic point at 340 $m\mu$ showing that only the B and BH^+ are involved. Maxima at 357 and 264 $m\mu$ are characteristic of BH^+ . Plots of λ_{357} vs. pH and $\lambda_{258-264}$ vs. pH show breaks with mid-points at pH 2.68 which is therefore pK_{BH^+} for 2,2'-biquinoline. In the H_2SO_4 solutions the long wave length band

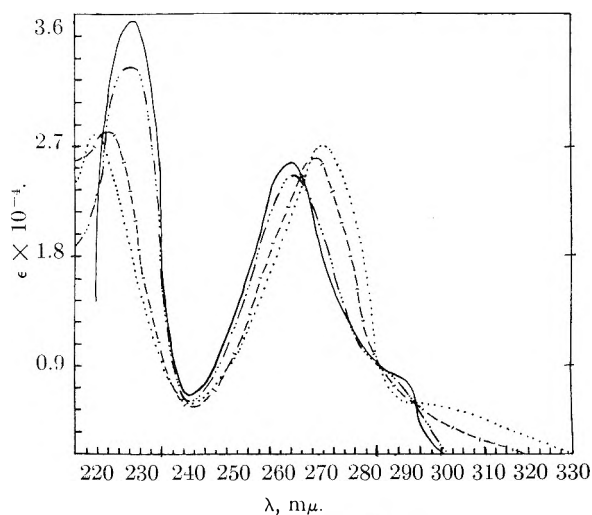


Fig. 7.—*o*-Phenanthroline, $BH^+ \rightleftharpoons B + H^+$: —, pH 14; ·····, pH 8.90; — — —, pH 4.00; — · — ·, pH 1.66.

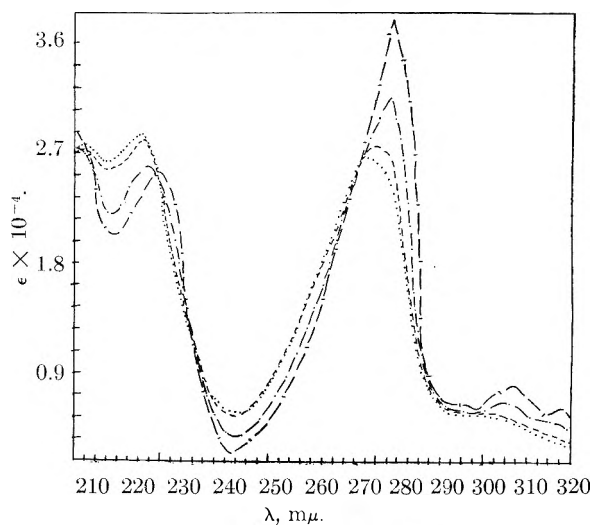


Fig. 8.—*o*-Phenanthroline: $BH_2^{++} \rightleftharpoons BH^+ + H^+$: ·····, H_2SO_4 , pH 0.14; — — —, 18% H_2SO_4 ; — · — ·, 31% H_2SO_4 ; —, 68% H_2SO_4 .

changes little from the BH^+ value of 357 $m\mu$, but a small increase in intensity may be noted probably due to changed dielectric constant. Figure 4 shows the spectral shift in H_2SO_4 solutions for the equilibrium $BH_2^{++} \rightleftharpoons BH^+ + H^+$. The short wave length band shifts from λ_{max} 264 to 270 $m\mu$ with decreased intensity on converting from BH^+ to BH_2^{++} . A plot of $\lambda_{264-270}$ vs. our pH scale for H_2SO_4 yields a mid-point at pH –3.0 which is therefore $pK_{BH_2^{++}}$ for 2,2'-biquinoline.

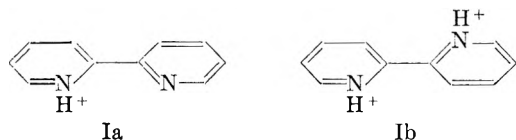
III. *o*-Phenanthroline.—The ultraviolet spectra of *o*-phenanthroline are shown in Figs. 6–8. The free base B is characterized by λ_{max} at 265 and 229 $m\mu$. The λ_{max} values of the B form vary with solvent, and for cyclohexane, absolute EtOH, and pH 11–14 aqueous NaOH they are: 265 $m\mu$, 2.70, 2.76 and 2.60; 229 $m\mu$, 5.07, 40.6 and 3.73 (all $\times 10^4$). A small shoulder at 290 $m\mu$ is seen in the high pH aqueous solutions. In Fig. 7 is shown the shift from B to BH^+ form, characterized by disappearance of the 290 $m\mu$ shoulder, shift of λ_{max} 265 to 272 $m\mu$, and shift of λ_{max} 229 to 220

$m\mu$ with a new band at $206 m\mu$.¹³ In H_2SO_4 solutions (Fig. 8) the long wave length band shifts to $279 m\mu$ while the short wave length band shifts to $224 m\mu$ with a new band at $205 m\mu$ ¹³ and two new weak bands at 307 and $318 m\mu$. The plot of $\lambda_{265-272-279}$ vs. pH shows anomalous behavior but the $\lambda_{229-220-224}$ vs. pH plot (Fig. 9) yields $pK_{BH^+} = 5.46$ (literature 4.27 at 20° in 50% EtOH,¹⁴ 4.77 in H_2O at 25° at zero ionic strength¹⁵) and both λ vs. pH plots give $pK_{BH_2^{++}} = -1.6$.

IV. Pyrazine.—The ultraviolet spectra of pyrazine are shown in Fig. 10. Pyrazine has a weak band at $320 m\mu$ (with structure) in cyclohexane, shifting to $300 m\mu$ in aqueous solution above $pH 2$ (the free B form). A strong band at $260 m\mu$ in cyclohexane and in aqueous solutions above $pH 2$ is also characteristic of the free B form. The weak long wave length band disappears and the strong $260 m\mu$ band increases in intensity and shifts to $282 m\mu$ as the H_2SO_4 concentration is increased. A new band with a maximum below $220 m\mu$ is in evidence in the concentrated H_2SO_4 spectrum. These results are in agreement with published spectra of pyrazine.¹⁶ Figure 9 clearly shows two breaks in the plot of $\lambda_{260-284}$ vs. pH with $pK_{BH^+} = 0.4$ (literature 0.6 ¹⁵) and $pK_{BH_2^{++}} = -6.8$.

Discussion

As pointed out by Nakamoto,⁴ the BH^+ form of 2,2'-bipyridine has a spectrum similar to the metal chelate form and is therefore the *cis* form Ia. The BH_2^{++} form would be expected to have nearly planar *trans* form Ib due to electrostatic



repulsion and slight twisting from repulsion due to two orthohydrogens. The ratio of $K_{BH^+}/K_{BH_2^{++}}$ is about 3.5×10^{-5} showing electrostatic repulsion from the twisted *trans* structure.¹² The existence of one band only in the BH_2^{++} form indicates large twist⁴ but we are somewhat doubtful of this point since the evidence given here indicates a second band just below $220 m\mu$. Nakamoto⁴ has explained the shift $301-290$ on changing from BH^+ to BH_2^{++} forms as due mainly to conversion from *cis* form (Ia) to *trans* form (Ib). For the 2,2'-biquinoline we find $K_{BH^+}/K_{BH_2^{++}}$ is about 2.1×10^{-6} . We expect the BH_2^{++} form of the biquinoline to have a slightly twisted *trans* structure similar to the bipyridine case and hence to have a similar K ratio. If one compares the *trans* forms of 2,2'-bipyridine with 2,2'-biquinoline (using Fisher-Hirschfelder-Taylor models), there is found to be more steric repulsion in the 2,2'-biquinoline case; thus greater twisting is expected which will increase electrostatic repulsion. Our smaller K ratio confirms this expected effect.

(13) Instrument slit opening near maximum and some uncertainty about this band.

(14) A. Albert, R. Goldacre and J. Phillips, *J. Chem. Soc.*, 2240 (1948).

(15) T. S. Lee, I. M. Kolthoff and D. L. Leussing, *J. Am. Chem. Soc.*, 70, 2348 (1948).

(16) F. Halverson and R. C. Hirt, *J. Chem. Phys.*, 19, 711 (1951).

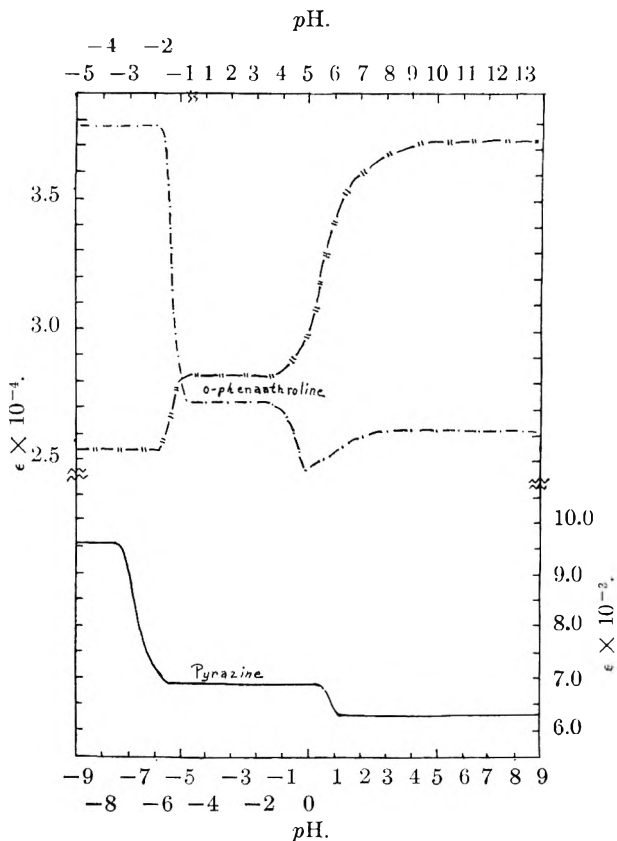


Fig. 9.—*o*-Phenanthroline: — — —, $229-220-224 m\mu$ (upper pH scale); — · —, $265-272-279 m\mu$ (upper pH scale); Pyrazine: — — —, $260-284 m\mu$ (lower pH scale).

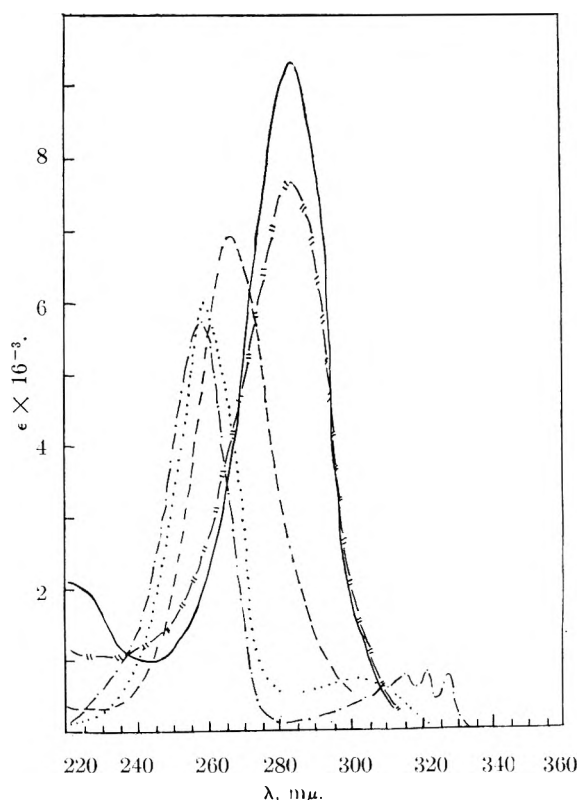


Fig. 10.—Pyrazine: — — —, B form; — — —, BH^+ form; — · —, BH_2^{++} form; — — —, cyclohexane; — — —, 79.5% H_2SO_4 .

TABLE I

Compound	DISSOCIATION CONSTANTS FOR $\begin{array}{c} \\ -N=C-C=N- \\ \end{array}$ BASES		$K_{BH^+}/K_{BH^{2+}}$
	$BH^+ \rightleftharpoons B + H^+ \quad pK_{BH^+} = \log [BH^+]/[B][H^+]$	$BH_2^{2+} \rightleftharpoons BH^+ + H^+ \quad pK_{BH_2^{2+}} = \log [BH_2^{2+}]/[BH^+][H^+]$	
Pyridine	5.23 (20°) ¹⁴
Quinoline	4.94 (20°) ¹⁴
2,2'-Bipyridine	4.25 (4.34, 25°) ^b	-0.2 (-0.52 ¹¹) (-0.15 or -0.22 ¹²)	3.5×10^{-5}
<i>o</i> -Phenanthroline	5.46 (4.77, 25°) ¹⁶	-1.6	8.7×10^{-8}
2,2'-Biquinoline	2.68 (40% EtOH)	-3.0	2.1×10^{-6}
Pyrazine	0.4 ^a (0.6) ¹⁵	-6.8	4.0×10^{-6}
Anabasine ^d	11.1	3.21	1.3×10^{-10}
2,2',2''-Tripyridine ^e	4.33	2.64	2.0×10^{-2}

Experimental measurements this work $23 \pm 2^\circ$.

^a These values are not true thermodynamic constants since no activity coefficients have been taken into account. ^b Thermodynamic value, $K_a = 4.6 \times 10^{-6}$. P. Krumholz, *J. Am. Chem. Soc.*, **71**, 3654 (1949). ^c If we correct pK_{BH^+} to water solvent, yielding 3.5, the K ratio then becomes 3.2×10^{-7} . ^d This is 2-(3'-pyridyl)-piperidine. Thermodynamic values. R. H. Linnell, *J. Am. Chem. Soc.*, **76**, 1391 (1954). ^e Thermodynamic values. R. Bruce Martin and Jo Ann Lissfelt, *ibid.*, **78**, 938 (1956). We looked in the present work for $pK_{BH_2^{2+}}$ and found it more negative than 7. Using -7, we find $K_{BH^+}/K_{BH_2^{2+}} = 4.7 \times 10^{-12}$ and $K_{BH_2^{2+}}/K_{BH_3^{3+}} = 2.3 \times 10^{-10}$.

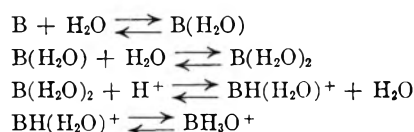
Both *o*-phenanthroline and pyrazine will have greater electrostatic repulsion forces influencing $pK_{BH_2^{2+}}$ because of planar structures with shorter N...N distances. The fused ring system of *o*-phenanthroline can accommodate more change, and the data show pyrazine having the predicted more pronounced electrostatic repulsion.

We have included data on anabasine whose K ratio is even smaller than that for pyrazine. Models indicate H-repulsion will allow only highly twisted forms of the BH_2^{2+} form; thus we expect strong electrostatic repulsion. The loss of one aromatic ring will mean less change accommodation so we explain the exceptionally low K ratio as due to these two factors.

For 2,2',2''-tripyrindine, Nakamoto⁴ has concluded that the BH_2^{2+} form is *cis-cis* with protons on opposite nitrogens. The much greater N...N distance compared to the other compounds reported here gives a vastly reduced electrostatic repulsion and hence a much larger K ratio. We have only estimated $pK_{BH_2^{2+}}$ but the result shows the expected large electrostatic effect.

We note an anomalous behavior in *o*-phenanthroline in the long wave length band (λ 260-272 $m\mu$) when ϵ_{max} values are plotted *vs.* pH (see Fig. 9) but only for the $BH^+ \rightleftharpoons B + H^+$ equilibrium.

Tentatively we suggest that *o*-phenanthroline is hydrated in aqueous solution and that several equilibria exist



where ϵ_{max} values at 265-272 $m\mu$ vary according to $\epsilon_{BH(H_2O)^+} < \epsilon_{B(H_2O)_2} < \epsilon_{BH_3O^+}$. It has been suggested recently¹⁷ that pyridazine forms a special H-bonded species in aqueous solution with one H_2O bonded to the two nitrogens. The monohydrate of *o*-phenanthroline is well known and it has a dissociation heat of 7.25 kcal. per H-bond.¹⁸ Our pK_{BH^+} value for *o*-phenanthroline is higher than literature values, and some unusual influence is suggested.

Acknowledgment.—The authors greatly appreciate financial support from Research Corporation. Thanks are due to Dr. R. Bruce Martin for guidance of this work while the senior author was on a leave of absence.

(17) R. H. Linnell, *J. Chem. Phys.*, **34**, 698 (1961).

(18) J. S. Fritz, R. W. Cable and G. F. Smith, *J. Am. Chem. Soc.*, **71**, 2480 (1949).

ELECTRICAL DOUBLE LAYER CAPACITY OF PASSIVE IRON AND STAINLESS STEEL ELECTRODES¹

BY PRANJIVAN V. POPAT AND NORMAN HACKERMAN

Department of Chemistry, The University of Texas, Austin, Texas

Received January 19, 1961

These measurements were made in sulfate solutions as a function of pH . The method of charging curves, utilizing square wave input signals was used, and the metals were polarized over the range between oxygen and hydrogen evolution potentials. At potentials slightly less anodic than that for oxygen evolution the e.d.l. capacity for all three metals in neutral solution was about the same, *viz.*, $18 \mu f./cm.^2$. For all three metals this is a minimum value which increased with increased acidity. The capacity-potential behavior of stainless steel was similar to that of platinum over the whole range. If there is no bulk oxide on the platinum under these conditions it can be postulated that the passivity of stainless steel is not caused by bulk oxide; certainly the behavior differs from that of aluminum and tantalum. There is a hump in the capacity value for both with increasing cathodic potential. With increasing pH the position of the maximum is more cathodic and the height is greater. With iron, it is not possible to distinguish between the metal dissolution region and the hydrogen evolution region by capacity values alone. However, there is a region where the iron potential changes suddenly from active to passive and this is paralleled by a capacity decrease. The non-oxide argument for stainless steel (above) is equally valid here. Even while recognizing the problems imposed by polycrystalline, solid metals in interpreting these measurements in terms of differential capacity, it is suggested that comparison of the three metals in these terms is valid.

Two principal schools of thought on the cause of electrochemical passivity of metals suggest (i) formation of a stoichiometric three dimensional oxide film on the metal surface, or (ii) some suitable sorbed oxygen-containing species. There is evidence for each of these views. A postulate reconciling both views has been proposed.²

It suggests a sequence of events, the most important of which is the rapid sorption of up to a monolayer of some oxygen-containing species. This accounts for the rapid potential changes and the periodic phenomena associated with the onset and loss of passivity of iron. Passivity, then, is caused by a thin, insoluble, disordered film of oxygen-containing ions and metal ions. It is suggested that the film is formed by migration of the metal ions into the array displayed by the sorbed species.

The controversy certainly has not been resolved. Measurement of the electrical double layer (e.d.l.) capacity, at the metal-solution interface before, during, and after electrochemical passivation appears to us to be pertinent. The measured capacity of a metal electrode with a continuous oxide film should be lower in a given electrolyte than for the same metal without such a film. This is illustrated by the experimental results of Ershler, *et al.*,³ for a nickel electrode in 1 *N* NaOH before and after chemical oxidation, *i.e.*, 22 to 27 and $7 \mu f./cm.^2$ respectively.

No fully satisfactory analog circuit is available for such an oxide-bearing electrode. However, lower capacity in the presence of an oxide film can be explained by assuming that its presence should lower the surface charge density, increase the thickness of the double layer, and thereby decrease the capacity. Alternatively, the oxide film may be considered as forming a capacitor in series with the e.d.l. capacity. Then since the capacity of the oxide film (lower dielectric constant) is small

compared to that of the e.d.l. the measured capacity should be low.

Work is in progress in this Laboratory on the e.d.l. capacity of several solid metals. Some results for iron and 18-8 stainless steel electrodes under passive and active conditions in solutions of various pH are reported here. The results are compared with published values for other metals.

Experimental

The method of charging curves based on the application of a square-wave signal was used for the double layer capacity measurements.⁴ This method is suitable for solid metal electrodes having geometrical areas as large as 2 to 3 $cm.^2$. The frequency of the square-wave signal in all the experiments reported here was 500 c.p.s. unless otherwise stated. The standard resistance through which the input square-wave signal passed before entering the cell was 15,000 ohms.

The Pyrex cell used in these experiments was similar to that already described.^{5a} A large area, platinized platinum, cylindrical wire gauze was used as a non-polarizable auxiliary electrode. All potential measurements were made against a saturated calomel electrode (SCE).

Triple-distilled conductivity water was used for preparing all solutions. Analytical reagent grade chemicals were further purified by recrystallization from conductivity water. In some cases, the solutions were first filtered through activated charcoal to remove traces of organic impurities. Contamination by grease or other organic materials was carefully avoided. Bureau of Mines Grade A helium, reported as 99.997% pure and containing less than $10^{-6}\%$ O_2 was bubbled through the experimental cell throughout the measurements. The helium was pre-saturated by passing it through conductivity water at the temperature of the experimental solution. The gas passed out through a similar trap to prevent back diffusion of air.

Reagent grade iron wire (0.009" dia.) supplied by Baker Chemical Co. (Phillipsburg, N.J.) and reported as better than 99.8% pure (0.02% C) was used. Stainless steel electrodes were made from AISI 302 wire (dia. 0.015") supplied by Alloy Metal Wire Division (Moore Station-Prospect Park, Pa.). Test pieces of the metal wire under investigation were sealed in 6 mm. soft glass tubing. The length of the test electrodes was such that a projected area of 1.0 $cm.^2$ was exposed to the electrolyte in each case. The glass tube holding the electrode was sealed to a ground glass holder which fitted the experimental cell. Electrical contact between the test electrode and the rest of the circuit was made by a column of mercury.

Each electrode was polished with 4/0 emery paper, rinsed with acetone, washed thoroughly with distilled water, treated with 2 *N* H_2SO_4 for about a minute (till H_2 evolution was

(1) Presented at the symposium in commemoration of David C. Grahame, sponsored by the Divisions of Colloid Chemistry and Physical Chemistry, at the 138th meeting of the American Chemical Soc., New York, Sept. 13, 1960.

(2) N. Hackerman, *Z. Elektrochem.*, **62**, 632 (1958).

(3) A. Rakov, T. Borisova and B. Ershler, *Zhur. Fiz. Khim.*, **22**, 1390 (1948).

(4) (a) R. J. Brodd and N. Hackerman, *J. Electrochem. Soc.*, **104**, 704 (1957); (b) J. J. McMullen and N. Hackerman, *ibid.* **106**, 341 (1959).

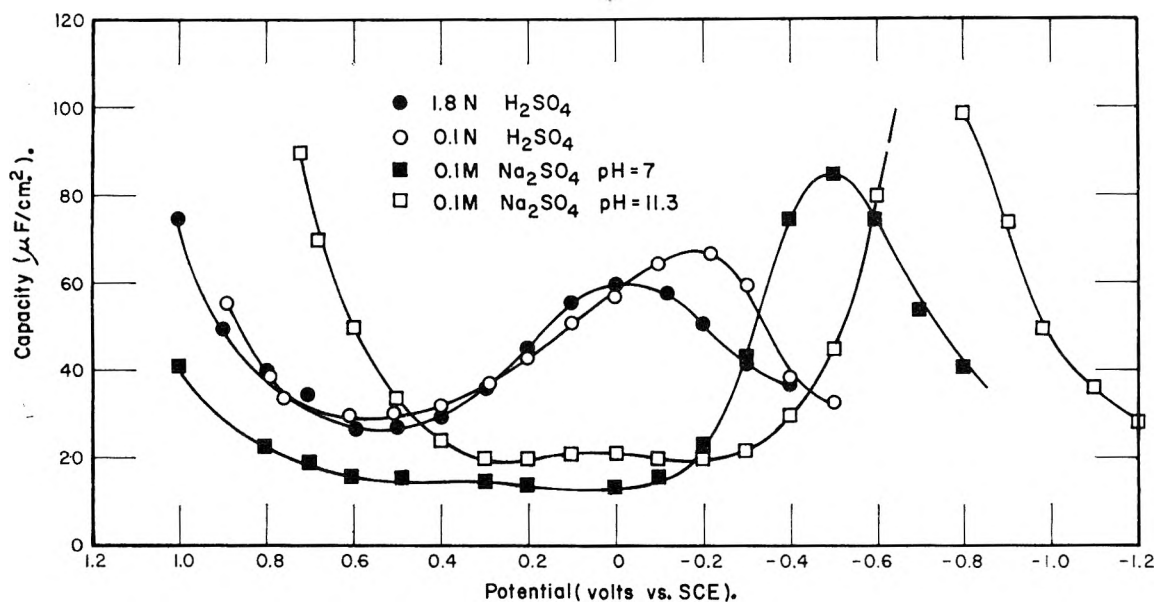


Fig. 1.—Differential capacity-potential curves for stainless steel. Anodic (oxidizing) potential to the left.

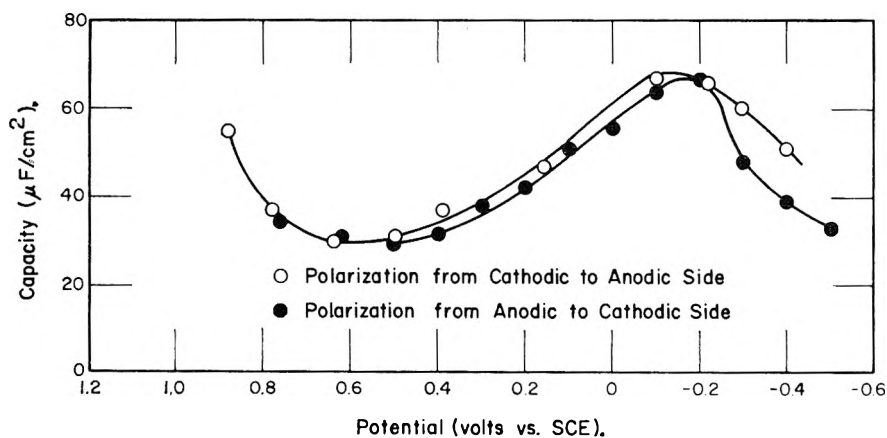


Fig. 2.—As for Fig. 1 with 0.1 N H₂SO₄, and showing the absence of hysteresis.

visible in the case of iron), and washed again with conductivity water. Finally, the electrode was rinsed with the test solution before introducing it into the cell containing the test electrolyte. Each electrode was used only once.

For the oxygen evolution and passivation of the stainless steel electrode, a polarizing potentiometer with an upper limit of 1.5 v. was sufficient. For iron, however, it was necessary to use a high voltage (or high current) d.c. source to cause oxygen evolution. The current required for the oxygen evolution was generally determined by measuring the potential drop across a standard resistor of 50 ohms in series with the polarizing circuit. Oxygen evolution on an iron electrode in a sulfate solution at a pH of about 3 required no more than about 10 ma./cm.². Once started, it was still visible at 0.1 ma./cm.². For neutral and alkaline solutions, the anodic current density required for oxygen evolution and passivation for iron electrodes was considerably less. In some cases the electrode was first cathodically polarized to hydrogen evolution, and the potential then was gradually changed to more anodic values.

All experiments were carried out at room temperature. Before taking data at each potential of the test electrode, sufficient time was allowed for the capacity values to become constant. This normally required 10 minutes or less.

Experimental Results and Discussion

Stainless Steel Electrodes.—Figure 1 represents the differential e.d.l. capacity of 18-8 stainless steel electrodes as a function of electrode potential in sulfate solutions. The data of each of the curves

of Fig. 1, except that for 0.1 N H₂SO₄, is an average of three independent experiments made with fresh solutions and new electrodes in each case. The agreement between individual runs for each pH was better than 5%.

The data for 0.1 N H₂SO₄ is an average of two runs made with the same electrode and the same solution in the following way. Initially, this electrode was made sufficiently cathodic for hydrogen to evolve. The potential was then gradually changed to more anodic values until the O₂ evolution potential was reached. In the other run, the direction of the applied potential was reversed so that the electrode potential gradually changed from that for O₂ evolution to that for H₂ evolution. The agreement between the two runs was very good, as shown by the data of Fig. 2.

The curves for 1.8 N H₂SO₄ and 0.1 N H₂SO₄ are similar in shape to one reported by Kolotykin for 1.0 N H₂SO₄⁵ and are in fair agreement quantitatively.

The steep branch at the extreme left for each curve of Fig. 1 comes at potentials probably suf-

(5) Y. M. Kolotykin, *Z. Elektrochem.*, **62**, 664 (1958).

ficient for oxygen evolution with little or no overvoltage. The more or less shallow minimum in each curve at potentials slightly less anodic than this represents the passive region. The value of the minimum capacity in this region is about $30 \mu\text{f./cm.}^2$ for 0.1 and 1.8 N H_2SO_4 , about $20 \mu\text{f./cm.}^2$ for 1 N NaOH and 12 to 13 $\mu\text{f./cm.}^2$ for 0.1 N Na_2SO_4 . Bockris and Potter⁶ observed a similar effect of $p\text{H}$ on Ni electrodes. They reported $28 \mu\text{f./cm.}^2$ for 0.01 N HCl , $37 \mu\text{f./cm.}^2$ for 0.1 N HCl , $41 \mu\text{f./cm.}^2$ for 1.0 N HCl , $22 \mu\text{f./cm.}^2$ for 0.006 N NaOH , and $27 \mu\text{f./cm.}^2$ for 0.12 N NaOH . A similar effect of $p\text{H}$ on capacity was seen with platinum.⁷ Figure 1 shows that stainless steel passivity can be maintained at more and more cathodic potentials as the $p\text{H}$ of the solution is increased.

Comparison of Stainless Steel and Platinum Electrodes.—The capacity-potential curves (C vs. E) of Fig. 1 are qualitatively similar to those for platinum.⁸ The presence of the peaks in the curves for both metals, and the not greatly different minimum capacity values in the anodic region (left of peak), is notable. Also, the C vs. E behavior of stainless steel in the anodic region was similar to that for platinum. In neither case was there a discontinuity in the curve on changing the potential gradually from oxygen to hydrogen evolution. Moreover, within experimental error, no hysteresis was observed in either case in going from anodic to cathodic potentials and reverse, within the potential range used.

The general similarity of the C vs. E curves for platinum and mercury in the corresponding potential range, *i.e.*, no electrochemical reaction taking place, has been established.⁸ The e.d.l. capacity for clean dropping mercury in neutral fluoride solution⁹ is about $20 \mu\text{f./cm.}^2$ on the anodic side of the potential of zero charge (ZPC) for mercury. This is close to the values reported here for stainless steel and for platinum⁸ under similar conditions. A rough estimate of the thickness of the compact double layer at anodically polarized mercury can be obtained if it is assumed that the double layer structure is analogous to a parallel plate capacitor with the distance between the two plates replaced by the thickness of the double layer. Then the capacity per unit area of the electrode, $C = \epsilon/4\pi d$, where d is the thickness of the double layer and ϵ is the dielectric constant of the medium within it. However, a difficulty arises in selecting the latter value. Presumably it lies between unity (corresponding to a vacuum) and ϵ for the bulk solvent (about 80 for water at room temperature). Assuming a value 10, the thickness of the compact layer having a capacity of $20 \mu\text{f./cm.}^2$ is 4.5 Å. Using the same value of ϵ with platinum and stainless steel, the thickness of the compact double layer at the minimum capacity on the anodic side is of the order of 5 Å. Because of the uncertainty in ϵ it is perhaps more meaningful to think in terms of ϵ/d rather than of d alone.

(6) J. O'M. Bockris and E. C. Potter, *J. Chem. Phys.*, **20**, 614 (1952).

(7) P. V. Popat and N. Hackerman, unpublished results.

(8) P. V. Popat and N. Hackerman, *J. Phys. Chem.*, **62**, 1198 (1958).

(9) S. Minc and J. Jastrzebska, *J. Electrochem. Soc.*, **107**, 135 (1960).

A clean dropping mercury electrode near the ZPC is not likely to have an oxide film on it. However, there is still some question whether oxygen evolution on platinum occurs on bulk oxide or on some oxygen-containing chemisorbed species. Unfortunately, most published results can be explained on either basis. Giner's work¹⁰ on the behavior of platinum electrodes in 1 N H_2SO_4 indicates that the behavior is determined by chemisorbed oxygen and not by specific oxides. Laitinen and Enke¹¹ working on the anodic behavior of platinum in perchloric acid solution, reported that there is a film about one atomic layer thick (one oxygen atom per surface platinum atom), as determined by the chronopotentiometric method. The minimum capacity before oxygen evolution was about $20 \mu\text{f./cm.}^2$ but the capacity increased to $60 \mu\text{f./cm.}^2$ on further anodization. They observed that, although the formation of the oxide is energetically favorable at potentials lower than that required for oxygen evolution, the oxide formation reaction is immeasurably slow at these potentials. They postulated the formation of a polar "oxygen evolution intermediate which is absorbed on the electrode surface" as the first step in the oxygen evolution reaction.

Kolotykin⁵ considers the absence of oxide on platinum electrodes in the potential region ordinarily encountered, (including oxygen evolution), as a well-established fact. Trapnell¹² indicated that oxygen chemisorption takes place with the formation of oxide ions at the surface following electron donation from the s and p bands of the metals.

Capacity-potential data for platinum generally support the proposition that bulk oxide is not involved in the processes occurring prior to and during oxygen evolution.

The minimum capacity on the anodic side before oxygen evolution on platinum in Na_2SO_4 solution is the same as for Cl_2 (or Br_2) evolution on platinum from Cl^- or Br^- .⁸ Thus, there does not appear to be any fundamental difference in the nature of the metallic surface of the electrodes in the two cases. It is unlikely that Cl_2 evolution takes place on a chloride covered surface, because of solubility.

The close similarity of the C vs. E behavior for stainless steel and platinum on the anodic side suggests that bulk oxide is not involved during electrochemical passivation and oxygen evolution on stainless steel. This view is further supported by the absence of hysteresis with stainless steel (Fig. 2). It is unlikely that hydrogen evolves on oxide covered stainless steel. Note that C vs. E for platinum and for stainless steel were essentially independent of the frequency of the square-wave signal, within experimental error. Enke¹³ reported similar behavior for platinum in HClO_4 solution.

The behavior just discussed should be contrasted

(10) J. Giner, *Z. Elektrochem.*, **63**, 386 (1959).

(11) H. A. Laitinen and C. G. Enke, *J. Electrochem. Soc.*, **107**, 773 (1960).

(12) B. M. W. Trapnell, *Proc. Roy. Soc. (London)*, **218A**, 566 (1953).

(13) E. G. Enke, *Dissertation Abstr.*, **20**, 3088 (1960).

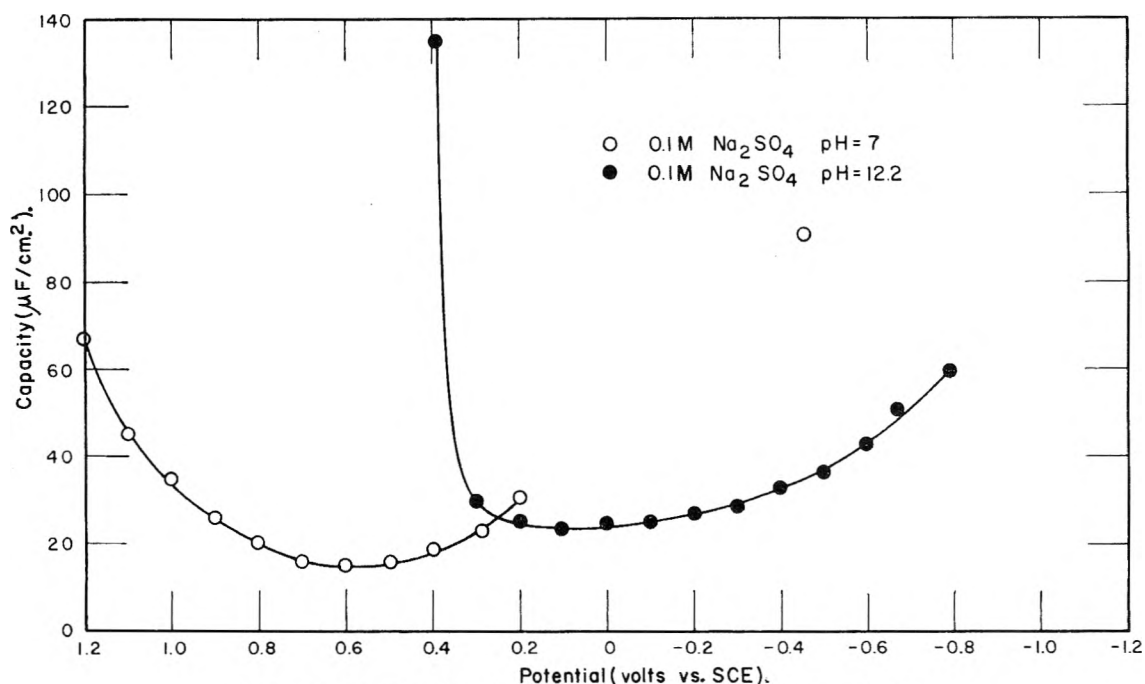


Fig. 3.—As for Fig. 1 but for iron first passivated to oxygen evolution.

with that of metals like aluminum and tantalum which have appreciable bulk oxides on them. For instance, capacity values of about $8 \mu\text{f./cm.}^2$ for aluminum and about $3 \mu\text{f./cm.}^2$ for tantalum in $1.0 N \text{Na}_2\text{SO}_4$ have been reported.^{4b} The effective double layer thickness, using the same assumptions used above, are 20 and 8 Å., respectively.

Determination of the effective film thickness on an electrochemically passivated surface does not appear to be a decisive method of differentiating between a chemisorbed film and a three-dimensional oxide film. The effective film thickness on metals such as Hg, Pt or stainless steel (about 5 Å.) is not significantly different from that of oxide bearing metals like Al or Ta. Also, it must be recalled that a wide range of values can be obtained depending on the value of the dielectric constant used. It is therefore necessary to weigh carefully the supporting evidence before firm conclusions can be made concerning the nature of the films. Thus it is more significant that the stainless steel electrode does not show hysteresis, whereas aluminum and tantalum do.^{4b} Also, the capacity values for the latter two are essentially independent of the potential over a wide range but not for platinum and stainless steel, an impressive fact.

On the basis of these observations, it may be concluded that there is a fundamental difference in the mechanism of electrochemical passivation of platinum and stainless steel electrodes on the one hand and in the anodic oxidation of aluminum and tantalum electrodes on the other.

The significance of the peak in the capacity potential curves for the stainless steel electrode and the effect of the solution pH on the position and the magnitude of the peaks is less clear. Based on an interpretation advanced earlier for similar peaks for platinum in the presence of various anions, it is suggested that adsorption-desorption processes

involving OH^- and/or H^+ are responsible. At the minimum on the anodic side of the peak, anions populate the compact double layer, at the minimum on the cathodic side, cations do so. In going from anodic to cathodic side anions are desorbed. During this process the ratio dq/dE changes rapidly giving rise to the peaks. The ratio ϵ/d changes also, and the peaks can be interpreted in terms of these changes as well.

There is some difference in the C vs. E behavior of platinum and stainless steel on the cathodic side of the peak. Whereas the e.d.l. capacity for platinum rises at high cathodic potentials, due to hydrogen evolution, it does not with stainless steel within the potential range investigated. This indicates higher hydrogen overvoltage, but the region was not investigated to any great extent during this study.

Iron Electrodes.—Figures 3 and 4 give the C vs. E curves for iron during electrochemical passivation and activation in $1 N \text{Na}_2\text{SO}_4$ of different pH values. The data of the curves of Fig. 3 are averages of three, separate runs reproducible to within 5%. Figure 4 represents the behavior in an unbuffered acidic solution at about pH 3. This behavior was reproduced in several runs.

With iron in neutral solution (Fig. 3), at potentials slightly more anodic than 0.76 v., the capacity value was about $50 \mu\text{f./cm.}^2$. The potential-time trace (not shown) exhibited curvature, suggesting some charge transfer. At about 0.76 v., however, the trace abruptly became linear and the capacity dropped from 50 to $18 \mu\text{f./cm.}^2$. This phenomenon was quite reversible and reproducible within the narrow potential range in which it occurred. Thus, at a slightly more anodic potential C rose to $50 \mu\text{f./cm.}^2$, with some curvature in the time-potential trace. At slightly more cathodic potentials, the trace was linear, giving $18 \mu\text{f./cm.}^2$ irrespective of the direction of the potential change.

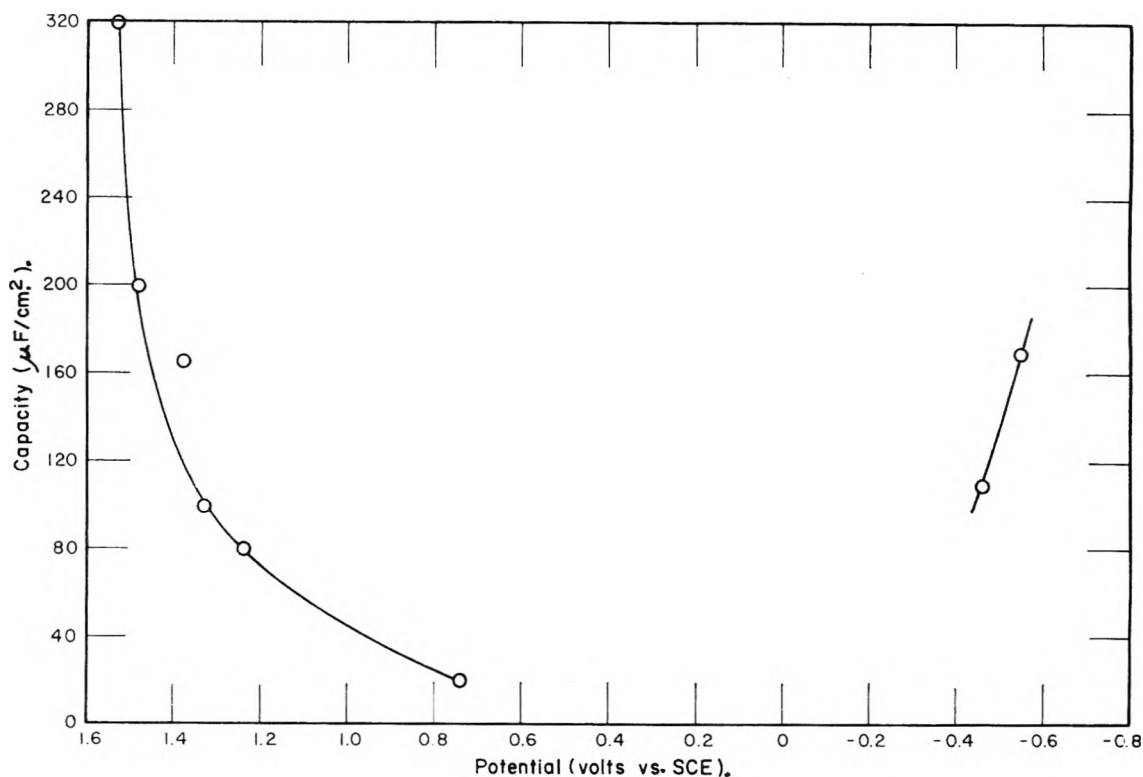


Fig. 4.—As for Fig. 3, except in 0.1 N Na_2SO_4 at $pH \sim 3$.

The potential value around which this happened depended on the pH of the solution. There was no induction period involved in this transition.

Between about 0.76 and 0.2 v. at pH 7, the electrode potential responded normally to changes in polarizing potentials. In this range the electrode is believed to be still passive. When the electrode potential was set slightly more cathodic than 0.2 v., it rapidly and irreversibly changed to -0.45 v. The capacity rose at the same time from about 20 to about 90 $\mu f./cm.^2$. This behavior was typical in neutral sulfate solution. No such abrupt changes were noticed for the alkaline system. In the presence of F^- or ClO_4^- , it was not possible to measure any difference in capacity as a function of applied potential. At all polarizing potentials it was immeasurably large, indicating an electrode reaction was taking place. Considerable iron was found in the solution in these cases.

It was not possible to maintain passivity with the polarizing potentiometer. After passivating iron in pH 3 solution at about 10 $ma./cm.^2$, the electrode potential suddenly went from 0.74 to -0.47 v., and the capacity rose from 20 to above 90 $\mu f./cm.^2$, indicating decay of the passive layer. If the electrode potential was initially made highly cathodic, and then changed to more anodic values, the capacities always remained above 90 $\mu f./cm.^2$. It was not possible, therefore, to distinguish be-

tween the hydrogen evolution stage and the metal dissolution stage by the present method. Nor was it possible to passivate the iron on approaching it from the cathodic side, contrary to the case for stainless steel. Evidently the processes involved in the passivation and activation of iron are somewhat different from those for stainless steel. It will be necessary to study the behavior in greater detail using a potentiostat before definite conclusions can be made concerning the nature of this passive film.

The only notable similarity between iron and stainless steel or platinum is the value of the minimum capacity in the passive region. For iron this is about 18 $\mu f./cm.^2$ in neutral and 20 $\mu f./cm.^2$ in acid and alkaline solution, much like those for platinum and stainless steel. The contrast with aluminum and tantalum electrode is also apparent. On the basis of the C vs. E behavior the metals studied so far can be put into the not unusual classifications: (a) noble metals like Pt and some alloys like stainless steel; (b) oxide-forming metals like Al and Ta; and (c) active metals like iron and copper.

Acknowledgment.—The authors are pleased to note that this work had the financial support of the Robert A. Welch Foundation of Houston, and of the Office of Naval Research (Contract Nonr 375(02)).

THE RADIOLYSIS OF *n*-PROPYL BROMIDE^{1,2}

BY RICHARD J. NEDDENRIEP AND JOHN E. WILLARD

Department of Chemistry of the University of Wisconsin, Madison, Wis.

Received January 23, 1961

The radiolysis of degassed liquid *n*-propyl bromide by Co⁶⁰ γ -rays produces no elemental bromine, but yields HBr with initial *G*-values of 0.06, 0.12, 2.9 and 10.5 at -78 , 0 , 25 and 50° , respectively. At 25 and 50° *G*(HBr) decreases to zero with increased time of irradiation, the steady-state concentration at 50° being three times as great as at 25° . A brownish non-volatile "telomer" is formed with an estimated *G*, for C₃H₆ groups incorporated, of 0.09, 0.6 and 4.3 at 0 , 25 and 50° , respectively. Added Br₂ increases *G*(HBr), decreases *G*(C₃H₆) and eliminates telomer formation. Added C₃H₆ increases telomer production. In the presence of 1 mole % or greater of added HBr or with an O₂ concentration of 0.06 mole % or higher, elemental bromine is produced. These and related data on hydrogen, hydrocarbon and organic bromide production reveal the existence of a number of competing elementary reactions some of which are temperature dependent.

Introduction

The radiation chemistry of the alkyl iodides³ has been investigated extensively but only a few exploratory experiments have been reported on the radiolysis of alkyl bromides.⁴ Reasons for expecting differences between the two systems include the following: (1) the carbon-iodine bond is weaker than the carbon-bromine bond; (2) in an alkyl halide molecule the electron fraction of the halogen atom is greater with iodine than it is with bromine; (3) the activation energy for the abstraction of hydrogen from C-H bonds by iodine atoms is too high for the reaction to occur as a thermal reaction at room temperature whereas bromine atoms can cause such an abstraction; (4) the absolute and relative activation energies for reaction of free radicals with HX and X₂ would be expected to be different when X is iodine than when it is bromine.

In the present work the radiolysis of *n*-propyl bromide has been studied and much briefer investigations have been made of the radiolysis of isopropyl bromide and *n*-propyl chloride. The *G*-values for the production of hydrogen bromide, hydrocarbons, and alkyl bromides have been determined as a function of radiation dose, temperature and the concentrations of additives and have been considered in seeking evidence on the elementary steps.

Experimental¹

γ -Irradiations.—Samples for irradiation were contained in annular glass vessels which fit closely around a 400 curie cobalt-60 source of the design described earlier,⁵ or in 6 mm. o.d. tubes which could be reproducibly positioned next to the source. The volume of liquid in the annular vessels was 5 ml. and that in the tubes (which were used for gas chromatographic analysis) was 0.3 ml.

The dose rate for both the samples in the tubes and those in the annular vessels during the period of this work was approximately 1×10^{20} e.v./g.-hr. (2×10^6 r./hr.). The exact values were determined by ferrous sulfate dosimetry using 15.6 as the number of ferric ions formed per 100

e.v. absorbed and 2240 as the molar absorptivity index of Fe⁺⁺⁺ at 3050 Å. and 27° . From the ferrous sulfate determinations the dose rates in the propyl halides were calculated by applying corrections for electron density and for the small contribution of absorption by the photoelectric effect in propyl bromide.²

Irradiation temperatures of 0 and -78° were maintained by ice-water and acetone-Dry Ice mixtures contained in a two liter Dewar into which the Co⁶⁰ source was lowered. Irradiations at 50° were carried out in a thermostatically controlled mineral oil-bath; the " 25° " irradiations were conducted in air at room temperature.

Sample Preparation.—Eastman propyl bromide was stirred for 48 hours with three successive portions of concentrated sulfuric acid, washed with 1 *M* sodium bicarbonate and with water, and dried over anhydrous magnesium sulfate, and fractionally distilled. Gas chromatographic analysis of purified samples showed 0.08% *i*-C₃H₇Br to be the only impurity.

The annular vessels were filled under vacuum with each sample undergoing 5 degassing cycles of freezing, evacuation and thawing before being sealed. When bromine, HBr, oxygen or propene was added to a sample, the additive was metered on the vacuum line by *PVT* measurements. Experiments done in the course of this work showed that at 25° or below,² over 95% of the HBr metered into the irradiation vessels was dissolved in the *n*-C₃H₇Br. In those experiments where oxygen was added the concentration of dissolved oxygen was estimated on the assumption that its solubility in *n*-C₃H₇Br is the same as its solubility in C₂H₅I, *i.e.*, 0.8×10^{-9} mole per ml. per mm. pressure.^{3a}

Analysis for HBr.—Irradiation vessels from which HBr was to be measured were constructed with a break-off tip. After irradiation the tip was broken under a measured volume of water doubly distilled from alkaline permanganate and the HBr was extracted from the organic layer. Vigorous agitation of the two layers was required for complete extraction. An aliquot of this acidic solution was then mixed with an equal volume of 2 *N* KI to which some solid KIO₃ had been added. The triiodide produced by the reactions $6\text{H}^+ + 5\text{I}^- + \text{IO}_3^- \rightarrow 3\text{H}_2\text{O} + 3\text{I}_2$ and $\text{I}^- + \text{I}_2 \rightleftharpoons \text{I}_3^-$ was determined by measuring the triiodide absorbance at 3500 Å. with a Beckman DU spectrophotometer. A value of 2.77×10^4 determined with standard HCl solutions, was used as the triiodide molar absorptivity index in 1 *N* KI at this wave length. When bromine was present after irradiation, successive extractions with CCl₄ were used to remove the Br₂ from the aqueous layer before the KI-KIO₃ was added.

Analyses for Br₂.—A square Pyrex cell attached by 6 mm. tubing to the annular irradiation vessel permitted spectrometric analyses to be performed without breaking open the vessel. Bromine analyses were conducted at 4060 Å. on a Beckman DU Spectrophotometer. Absorbances as high as 5.0 could be determined with the aid of a photomultiplier attachment, a filter to cut out scattered light, and a reference cell of known bromine concentration. The molar absorptivity index of bromine in *n*-C₃H₇Br was determined to be 207 l. mole⁻¹ cm.⁻¹ at 4060 Å.

Analysis for H₂ and CH₄.—Samples which were to be used for methane and hydrogen measurements were contained in irradiation vessels fitted with break-seals which could be attached to a modified Saunders-Taylor apparatus⁶ follow-

(1) Presented before the International Congress of Radiation Research, Burlington, Vermont, August, 1958.

(2) Additional details of this work are given in the Ph.D. thesis of Richard J. Neddenriep, University of Wisconsin, 1957, available from University Microfilms, Ann Arbor, Michigan.

(3) See for examples and references: (a) E. O. Hornig and J. E. Willard, *J. Am. Chem. Soc.*, **79**, 2429 (1957); (b) R. J. Hanrahan and J. E. Willard, *ibid.*, **79**, 2434 (1957); (c) R. F. Pottier, W. H. Hamill and R. R. Williams, *ibid.*, **80**, 4224 (1958).

(4) (a) R. H. Schuler and W. H. Hamill, *ibid.*, **74**, 6171 (1952); (b) J. C. Chien and J. E. Willard, *ibid.*, **77**, 3441 (1955); (c) W. S. Wilcox, *Radiation Research*, **10**, 112 (1959).

(5) R. F. Firestone and J. E. Willard, *Rev. Sci. Instr.*, **24**, 904 (1953).

(6) K. W. Saunders and H. A. Taylor, *J. Chem. Phys.*, **9**, 616 (1941).

ing irradiation. With the aid of this apparatus *PVT* measurements were made on the non-condensable gases and they were then pumped into a mass spectrometer sample bulb. We are indebted to Prof. Irving Shain and Mr. Kenneth Martin for assistance with the mass spectrometric analyses, which were made on a Consolidated Model 21-620 mass spectrometer.

Analysis for Propane.—A 12 foot long 6 mm. i.d. spiral glass column packed with 30-60 mesh alumina was used for the gas chromatographic determination of propane. The chromatography equipment was calibrated with known amounts of propane. Effective separation of a synthetic propane-propene mixture was achieved when the column was held at 115°, but no propene (less than 25% of the propane) was found when irradiated samples of *n*-C₃H₇Br were tested. Traces of propene, ethene and ethane (1.4, 0.08 and 0.15% of the propane) were detected when a column of silicone oil firebrick at 25° was used in tandem with a firebrick column coated with propylene glycol saturated with AgNO₃. It is possible that propene was converted to propyl bromide by reaction with HBr on the alumina column. A short pre-column of powdered KOH used in conjunction with the alumina column did not remove the HBr completely but did spread out the HBr peak so that it blended into the background and did not interfere with the propane peak.

The small glass sample tubes were broken in the gas stream at the entrance to the column and little tailing was experienced when the helium carrier gas was passed through a preheater. A commercial Gow-Mac thermal conductivity unit served as the detecting device, the output being fed to a Speedomax type G recorder with a full scale sensitivity variable from 1-20 mv.

Analysis for Organic Bromides.—Radioactive organic bromides produced by irradiating *n*-C₃H₇Br in the presence of radiobromine were separated with a 12 foot spiral column of 40-60 mesh firebrick coated with GE-S F-96 (40) silicone oil. Elemental bromine and HBr were removed from the irradiated bromides by extraction with sulfite solution, following which the organic layer was injected onto the separation column through a rubber serum bottle cap.

The column temperature could be raised from 50 to 200° while the sample was passing through. The most satisfactory results were obtained with a temperature rise of 5° per minute and a carrier gas flow rate of 40 ml./min., using a 0.1 ml. sample. The outlet tube of the column had in it a U-type trap which fit into the well of a NaI(Tl) scintillation crystal. The outputs of the scintillation detector and of a thermocouple recording the column temperature were fed to a two pen Brown chart recorder. The yield of each bromide was obtained from the product: (g. atoms of Br₂ added initially) × (fraction of activity in organic phase after irradiation) × (fraction of organic activity represented by the chart recorded peak for the particular compound). To identify the recorded radioactivity peaks small amounts of known bromides were added to the irradiated samples in some runs and the effluent gas from the column was subjected to thermal conductivity detection as well as radioactivity detection. When a thermal conductivity peak superimposed on a radioactivity peak the latter was considered to be identified.

The organic bromides formed in experiments without added radiobromine were determined in much the same way as the radioactive bromides except that the column was held at constant temperature. Two analyses, one at 95° and one at 150° were made on each irradiated solution in order to obtain good resolution of all the products. The sensitivity of the detector cell to the bromides was calibrated by running 1% solutions of various bromides in *n*-C₃H₇Br through the apparatus.

Results

Hydrogen Bromide Production.—The radiolysis of the propyl bromides without additives at room temperature differs from that of the alkyl iodides³ in that no free halogen is produced, and in that the net rate of production of hydrogen halide decreases to zero with increasing dose, rather than remaining constant. The production of HBr as a function of radiation dose is shown in Fig. 1 for *n*-propyl bromide at 50, 25, 0 and -78°. The initial values

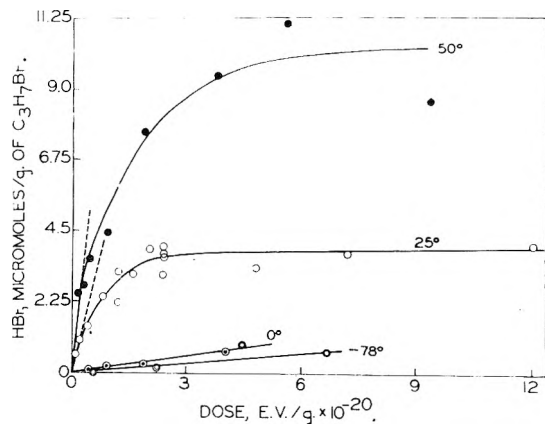


Fig. 1.—Production of HBr as a function of radiation dose and temperature during the radiolysis of initially pure *n*-C₃H₇Br.

of *G*(HBr) estimated from the initial slopes of the curves of Fig. 1 are 11.5, 2.9, 0.12 and 0.06, respectively. The plateaus of the curves for 25 and 50° indicate that at these temperatures there is a reaction which consumes HBr more and more rapidly as the concentration increases, until the rate of consumption is equal to the rate of production. The effect of temperature indicates that one or more of the elementary steps involved in producing this effect has an appreciable activation energy. The data for the initial slopes are not sufficiently accurate to allow an exact evaluation of the over-all activation energy but it appears to be between 15 and 22 kcal./mole.

Under the conditions of these experiments, where the ratio of liquid volume to gas volume in the irradiation cell was about one, more than 95% of the HBr was in solution at 25° and below, and it was estimated that 85% was in solution at 50°.

To explore the competitive reactions indicated by Fig. 1, the production of HBr was measured in runs with added Br₂, HBr and O₂. Added Br₂ greatly increases the initial *G*(HBr) (from 2.9 to about 12 at 25° and from 0.06 to 1.5 at -78°) and also increases the HBr concentration at which the incremental values of *G*(HBr) approach zero. Although there is too much scatter in the data of Fig. 2 to allow a conclusive comparison, it appears that the initial values of *G*(HBr) with 1 and 5 mole % added Br₂ are the same. If this is the case it establishes the fact that the increase in *G*(HBr) caused by the added Br₂ is not caused solely by the fact that a greater fraction of the radiation energy dissipated in the system is absorbed by Br₂ rather than by C₃H₇Br. This conclusion is further supported by the fact that if all of the energy absorbed directly by the Br₂ in the 1% solutions were utilized to cause the formation of Br atoms by Br₂ → 2Br, at the rate of 1 bond rupture per 2 e.v. absorbed, and if each atom abstracted a hydrogen atom from C₃H₇Br to form HBr, the contribution to *G*(HBr) by this sequence would be only 1.2. It appears probable that the increase of *G*(HBr) with added bromine results from competition of reactions of the type R + Br₂ → RBr + Br, (I), with reactions of the type R + HBr → RH + Br, (II). The concentration of Br₂ is sufficiently high so that

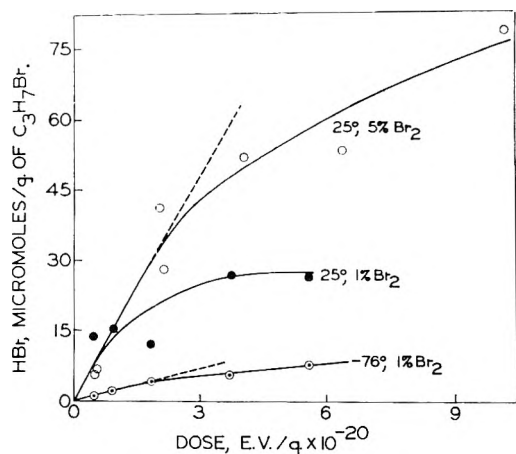


Fig. 2.—Production of HBr as a function of radiation dose and temperature during the radiolysis of $n\text{-C}_3\text{H}_7\text{Br}$ containing added Br_2 .

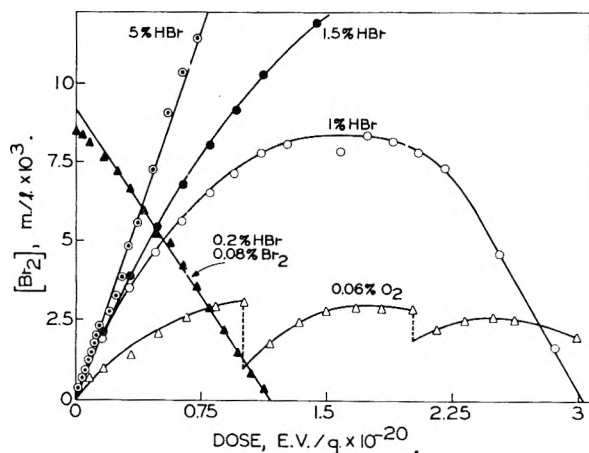


Fig. 3.— Br_2 concentration as a function of radiation dose during radiolysis of $n\text{-C}_3\text{H}_7\text{Br}$ containing added O_2 , HBr or Br_2 .

the competition may be, in part, with intraspur reactions.

Production of Br_2 in Presence of Added HBr or O_2 .—Although no bromine is produced by the radiolysis of n -propyl bromide without additives, bromine is formed when concentrated solutions of HBr in n -propyl bromide or more dilute solutions of oxygen in n -propyl bromide are irradiated. The steady-state concentrations of HBr indicated by the plateaus at 25 and 50° in Fig. 1 fall at about 0.05 and 0.13 mole % of dissolved HBr, respectively. No observable bromine was formed either under such conditions, or by the radiolysis of a 0.5 mole % solution of HBr in n -propyl bromide at 25°. However when solutions of 1, 1.5 or 5 mole % HBr were irradiated, an initial G -value for bromine production of about 7 was obtained in each case as indicated by the curves of Fig. 3. As with the effect of added bromine, the effects of added HBr cannot be explained on the basis of increased primary energy absorption by the HBr itself.

Since oxygen is known to act as a scavenger for free radicals and might thereby prevent their reaction with other species in the propyl bromide system, two irradiations were made in the presence of oxygen. It was found that 0.006 mole %

dissolved oxygen did not lead to the production of bromine but that, as shown in Fig. 3, 0.06% dissolved oxygen did. This effect of oxygen may possibly be to prevent radicals from reacting with very small amounts of Br_2 in the system to reform organic bromides, or it may be that peroxy radicals formed liberate bromine by reaction with HBr. It is notable that the concentration of oxygen required to result in bromine production is at least tenfold lower than the lowest HBr concentration that yields bromine. The vertical dotted lines in Fig. 3 shows a decrease in bromine concentration when the sample was allowed to stand overnight without irradiation, following a period of irradiation. This effect occurred only in solutions which contained oxygen.

Figure 3 shows that at concentrations of HBr or O_2 sufficiently high to lead to bromine production $G(\text{Br}_2)$ decreases with increasing radiation dosage, and in some cases becomes negative, so that the bromine concentration goes through a maximum. This presumably results from the ability of the Br_2 to compete with the HBr or O_2 for some reaction intermediate, and from the fact that when the HBr or O_2 reacts it is permanently consumed. At the peak of the 1 mole % HBr curve of Fig. 3 the ratio of HBr to Br_2 is about 13, while at the peak of the oxygen curves the O_2 to Br_2 ratio is only about 1 suggesting that oxygen is a more effective radical scavenger than HBr.

Consumption of Added Br_2 .—From the fact that bromine produced by irradiation of $n\text{-C}_3\text{H}_7\text{Br}$ in the presence of added HBr or O_2 is consumed on prolonged irradiation (Fig. 3), it would be expected that initially added Br_2 would also be consumed. This was confirmed in three experiments, starting with 0.19, 0.13 and 0.08 mole % Br_2 in which the Br_2 concentration was followed as a function of radiation dose. In the third of these experiments (for which the data are plotted in Fig. 3) HBr was initially present at a concentration of 0.18 mole %. In each case the G for disappearance of Br_2 was constant with increasing dosage down to a Br_2 concentration of 0.03 mole % or below. The presence of the added HBr did not alter the reaction. The average $G(-\text{Br}_2)$ for the three experiments was 3.5.

Telomer Formation.—Radiolysis of pure degassed $n\text{-C}_3\text{H}_7\text{Br}$ produced a brown material which could not be extracted with aqueous sulfite solution and which remained as a non-volatile brown film when the propyl bromide was removed by evaporation under vacuum. The spectrum of this material in solution showed a smooth continuous increase in absorbance from 5500 to 2200 Å. Concentrations of Br_2 as small as 0.05 mole % completely prevented its formation, as did 0.06 mole % of dissolved oxygen. Apparently HBr is not as effective in this respect since the "telomer" formation was observed in the presence of 0.05 mole % HBr, the plateau concentration of HBr attained (Fig. 1) when $n\text{-C}_3\text{H}_7\text{Br}$ is irradiated for prolonged periods at 25°. Formation of the brown compound was, however, prevented by 0.5 mole % HBr.

Figure 4 shows the telomer absorbance at 3750 Å.

as a function of radiation dose received by degassed $n\text{-C}_3\text{H}_7\text{Br}$ at three temperatures. There appears to be an induction period at 0 and at 25, but not at 50°. A plot of the log of the G -values (arbitrarily calculated as C_3H_6 groups incorporated in telomer per 100 e.v. absorbed, assuming it is composed only of C_3H_6 groups) vs. $1/T$ gives three points on a straight line with a slope which corresponds to an activation energy of 14 kcal./mole. For this purpose the G -values after the induction period were used for 0 and 25° while the initial G -value was used for 50°.

The non-volatile nature of the brown compound requires that it have a high molecular weight compared to the other products observed in this work. Since propene is a plausible product of $n\text{-C}_3\text{H}_7\text{Br}$ radiolysis and might be expected to react with free radicals in chain lengthening steps, a 5 mole % solution of propene in $n\text{-C}_3\text{H}_7\text{Br}$ was irradiated. After a short induction period this resulted in a constant G of 4 for production of the brown material, a value 6.5 times greater than that with no added propene. This result is consistent with the conclusion that propene formed in the radiolysis is an intermediate in the formation of the brown compound. The induction period in this experiment with added propene indicates that necessity for buildup of propene concentration cannot be the sole reason for the apparent induction period of the 25° curve in Fig. 4. The 5 mole % concentration of C_3H_6 completely prevented HBr production. In corollary experiments in which both HBr and C_3H_6 were dissolved in $\text{C}_3\text{H}_7\text{Br}$, the concentration of HBr decreased in irradiated samples but not in unirradiated samples kept in the dark.

In most of the radiolysis experiments at 25° and below the amounts of the brown product formed were too small for satisfactory weighing. An 8 hour irradiation at 50° produced 5.9 mg. however, and 42.7 mg. was obtained from a 10-hour irradiation at 25° of 5 ml. of a 5 mole % solution of propene in $n\text{-C}_3\text{H}_7\text{Br}$. These gave values of 1.5 and 2.1 mg. per ml. per absorbancy unit at 3750 Å., respectively. Possibly the telomer formed with added propene may have more colorless units in it than the other, accounting for the higher weight per absorbance unit. The value of 1.5 mg./abs. unit obtained from the 50° irradiation was used for the calculation of the G -values of Fig. 4. In this calculation the arbitrary assumptions were made that the product at 50° is the same as at other temperatures and that the telomer is made up only of C_3H_6 units.

Hydrogen and Hydrocarbon Production.—Hydrogen, methane and propane were all produced linearly with radiation dose up to about 10^{21} e.v./g.; this was true both in pure $n\text{-C}_3\text{H}_7\text{Br}$ and in $n\text{-C}_3\text{H}_7\text{Br}$ with 5 mole % HBr or 5 mole % Br_2 added. These G -values, calculated for 25° from the slopes of the curves, are given in Table I. Since these products are not completely eliminated by 5 mole % bromine, they must be formed in part by hot reactions. Methane and H_2 may be formed only in this way since 5 mole % of additive is sufficient to interfere with reactions within the spurs. The changes in $G(\text{H}_2)$ and $G(\text{CH}_4)$ with 5% HBr and

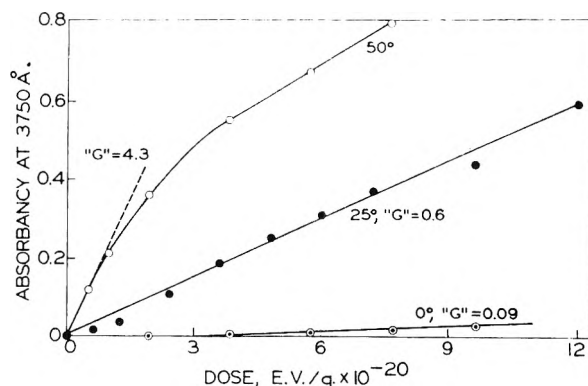


Fig. 4.—Telomer production during radiolysis of $n\text{-C}_3\text{H}_7\text{Br}$, as indicated by absorbancy at 3750 Å. The " G " values indicate C_3H_6 groups incorporated in telomer per 100 e.v. absorbed, assuming that it is composed only of C_3H_6 groups.

5% Br_2 probably are due to HBr and Br_2 interference with hot reactions. If all of the energy absorbed directly by the HBr were used to split HBr bonds (3.5 ev.), giving hydrogen atoms which yielded H_2 by abstraction from the substrate, the $G(\text{H}_2)$ from this source alone would be 0.5, or somewhat less than the increase observed.

The increase in $G(\text{C}_3\text{H}_8)$ in the presence of 5 mole % HBr suggests a competition of HBr with addition to olefin molecules or recombination reactions in the spurs. Some of the decrease in $G(\text{C}_3\text{H}_8)$ with 5 mole % Br_2 probably also results from interference with spur reactions, but the fractional decrease in $G(\text{C}_3\text{H}_8)$ is much larger than that of $G(\text{H}_2)$ or $G(\text{CH}_4)$. The eleven-fold decrease in $G(\text{C}_3\text{H}_8)$ suggests that in the pure bromide some C_3H_8 is formed by C_3H_7 radicals which abstract hydrogen from HBr or $\text{C}_3\text{H}_7\text{Br}$ at some distance from their parent spurs.

No propene was found by gas chromatographic analysis using an alumina column but when the propylene glycol column was used 3.5 μ moles was found after a 2 hour irradiation and 5 μ moles after a 10 hour irradiation of a 5-ml. sample. The $\text{C}_3\text{H}_8/\text{C}_3\text{H}_6$ ratio in the latter case was 66/1. The non-linearity of C_3H_6 production suggested by these two experiments is qualitatively as would be expected if this compound is consumed by telomer formation and HBr addition.

Just a trace of C_2 hydrocarbons was observed in the chromatogram from the 10 hr., 10^{21} e.v./g. irradiation. The $\text{C}_3\text{H}_8/\text{C}_2$ ratio was about 1000, indicating that very little $\text{C}_2\text{H}_5\text{-CH}_2\text{Br}$ bond rupture occurs. There was also no evidence of C_6H_{14} .

TABLE I

G-VALUES FOR PROPANE, HYDROGEN AND METHANE	G-VALUES FOR PROPANE, HYDROGEN AND METHANE		
	Pure bromide	5 mole % HBr	5 mole % Br_2
C_3H_8	3.5	4.5	0.3
CH_4	0.06	0.1	.03
H_2	0.5	1.3	.4

Organic Bromide Production.—Gas chromatographic analyses of samples of pure $n\text{-C}_3\text{H}_7\text{Br}$ which had received irradiations of 2×10^{20} to 9×10^{20} e.v./g. indicate that CH_3Br , $\text{C}_2\text{H}_5\text{Br}$, $i\text{-C}_3\text{H}_7\text{Br}$, $1,2\text{-C}_3\text{H}_6\text{Br}_2$ and $1,3\text{-C}_3\text{H}_6\text{Br}_2$ (and/or $n\text{-C}_6\text{H}_{13}\text{Br}$ which was not distinguishable from $1,3\text{-C}_3\text{H}_6\text{Br}_2$ by

the method used) are each produced at a constant rate, independent of dosage in this range. The slopes of these curves yielded G -values for the five bromides of 0.04, 0.1, 2.1, 1.7 and 1.3, respectively. When Br_2 was added following irradiation after exposure to air but prior to determination of the dibromides, no marked change was observed in the bromide yields, indicating that the irradiated $n\text{-C}_3\text{H}_7\text{Br}$ did not contain large amounts of the olefins C_3H_6 and $\text{C}_3\text{H}_5\text{Br}$. The analyses in these tests showed more experimental fluctuations than usual, so that the conclusions as to linearity of production rate, G -values and the effect of added Br_2 must be considered as qualitative. In another experiment, radiobromine was added under vacuum to $n\text{-C}_3\text{H}_7\text{Br}$ which had received a γ -ray dose of 5×10^{19} e.v./g., and allowed to stand in the dark before analysis. Equal amounts of tagged 1,2- $\text{C}_3\text{H}_6\text{Br}_2$ and 1,2,3- $\text{C}_3\text{H}_5\text{Br}_3$ were found, and the 10^{-3} mole/l. C_3H_6 concentration deduced from the yield agreed with that determined by other means.

Irradiations of 5×10^{19} e.v./g. in the presence of radiobromine at a bromine mole fraction of 9×10^{-3} produced eight radioactive organic bromides which were identified as $i\text{-C}_3\text{H}_7\text{Br}$, $n\text{-C}_3\text{H}_7\text{Br}$, 1,2- $\text{C}_2\text{H}_4\text{Br}_2$, 1,2- $\text{C}_3\text{H}_6\text{Br}_2$, 1,3- $\text{C}_3\text{H}_6\text{Br}_2$, 1,1,2- $\text{C}_2\text{H}_3\text{Br}_3$, 1,1,2- $\text{C}_3\text{H}_5\text{Br}_3$ and 1,2,3- $\text{C}_3\text{H}_5\text{Br}_3$. The G -values for these eight bromides, each based upon Br^{82} uptake during the half hour irradiation, were 0.4, 3.5, 0.2, 6.7 (or 3.3)⁷, 0.15, 0.01, 0.08 and 0.17, respectively. These products were derived from the reaction of free radicals, ions, or olefins with Br_2 and hence are indicative of the primary reactive chemical species formed by the absorption of radiation. The concentration of Br_2 (nearly 1 mole %) was sufficient to prevent most interspur reactions of radicals by competing effectively with $n\text{-C}_3\text{H}_7\text{Br}$ or HBr for the reactive intermediates. As might be expected, the yields show little or no temperature dependence in the range from 25 to -78° (a factor of 2 or less in every case) and little or no change in product distribution with bromine concentration in the range of 10^{-4} to 10^{-2} mole fraction. This is the concentration range in which the Br_2 acts primarily as a radical scavenger. However, when the Br_2 mole fraction is increased from 10^{-2} to 0.1 and 0.5, the percentage of the organic activity in $n\text{-C}_3\text{H}_7\text{Br}$ drops from 34 to 17 to 9% while that as 1,2- $\text{C}_3\text{H}_6\text{Br}_2$ increases from 58 to 76 to 92%. At the same concentrations the percentages of the total bromine which entered organic combination with a dose of 5×10^{19} e.v./g., were 11, 1.3 and 0.2%.

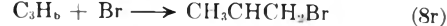
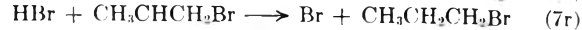
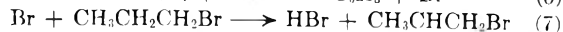
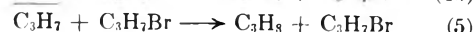
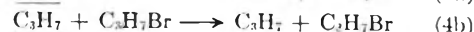
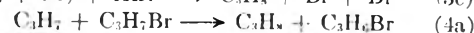
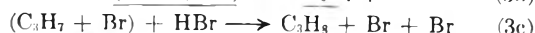
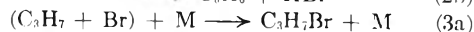
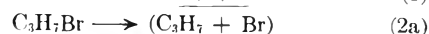
Radiolysis of Isopropyl Bromide.—A few experiments in which isopropyl bromide was irradiated indicated an initial $G(\text{HBr})$ at 25° of about 0.5, as contrasted to 2.9 for $n\text{-C}_3\text{H}_7\text{Br}$, and the steady-state plateau concentration of HBr was about one-fifth that found at the same dosage rate with $n\text{-C}_3\text{H}_7\text{Br}$. The telomer color produced in i -

$\text{C}_3\text{H}_7\text{Br}$ was only one third as intense as with $n\text{-C}_3\text{H}_7\text{Br}$ and the $G(\text{H}_2)$ of 0.4 and $G(\text{CH}_4)$ of 0.04 were both slightly lower than with $n\text{-C}_3\text{H}_7\text{Br}$. In a 5×10^{19} e.v. irradiation in the presence of 0.9 mole % radiobromine, $i\text{-C}_3\text{H}_7\text{Br}$ gave the following G -values for labeled bromide production: $i\text{-C}_3\text{H}_7\text{Br}$, 7.8; $n\text{-C}_3\text{H}_7\text{Br}$, 0; 1,2- $\text{C}_2\text{H}_4\text{Br}_2$, 0.9; 1,2- $\text{C}_3\text{H}_6\text{Br}_2$, 6.0; 1,3- $\text{C}_3\text{H}_6\text{Br}_2$, 0; 1,1,2- $\text{C}_2\text{H}_3\text{Br}_3$, 0; 1,1,2- $\text{C}_3\text{H}_5\text{Br}_3$, 0; 1,2,2- $\text{C}_3\text{H}_5\text{Br}_3$, 0.07; and 1,2,3- $\text{C}_3\text{H}_5\text{Br}_3$, 0.1. In arriving at these values it was again assumed that one bromine in each of the di- and tri-bromides was from the parent molecule and so did not contribute to the radioactive labeling. The G of 7.8 for incorporation of labeled bromine in $i\text{-PrBr}$ indicates a distinctly higher probability of absorbed energy being channeled into C-Br bond rupture in $i\text{-PrBr}$ than in the irradiation of $n\text{-PrBr}$ where G for incorporation of radiobromine as $n\text{-PrBr}$ is 3.5. This may be related to the central position of the Br atom or to the relative weakness of the C-Br bond.

Radiolysis of n -Propyl Chloride.—Exploratory experiments on the radiolysis of liquid $n\text{-C}_3\text{H}_7\text{Cl}$ at 25° indicate that HCl , H_2 and CH_4 are formed linearly with dose up to at least 7×10^{20} e.v./g. with G -values of about 5, 1.1 and 0.15, respectively. These values are in approximate agreement with more recent work on the radiolysis of $n\text{-C}_3\text{H}_7\text{Cl}$,^{8,9} but the $G(\text{HCl})$ is significantly higher than reported for the butyl chlorides.¹⁰ The linear production of HCl is in contrast to the decrease in G with dose observed for HBr from $n\text{-C}_3\text{H}_7\text{Br}$.

Discussion

It seems probable that reactions 1 to 11 below are important in determining the characteristics of the radiolysis of $n\text{-C}_3\text{H}_7\text{Br}$ reported above. Additional steps which may be involved in the formation of minor products will also be discussed. The underlined species are those which still possess energy in excess of thermal energy, and the species enclosed in parentheses are those which have not escaped the possibility of diffusive recombination. Although they may be important, ion molecule reactions do not seem to be required to explain the observations.

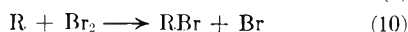


(7) In calculating the G -values, it was assumed that each tribromide molecule had incorporated two Br atoms from the radiobromine in solution but that each dibromide and monobromide molecule had incorporated only one. Consequently if 1,2- $\text{C}_3\text{H}_6\text{Br}_2$ was actually formed by $\text{C}_3\text{H}_6 + \text{Br}_2 \rightarrow \text{C}_3\text{H}_6\text{Br}_2$ rather than by $\text{R} + \text{C}_3\text{H}_6\text{Br} \rightarrow \text{RH} + \text{C}_3\text{H}_6\text{Br}$ followed by $\text{C}_3\text{H}_6\text{Br} + \text{Br}_2 \rightarrow \text{C}_3\text{H}_6\text{Br}_2$, its G -value should be given as 3.3 rather than 6.7.

(8) H. Benson and J. E. Willard, unpublished.

(9) R. E. Johnson and C. E. Miller, Jr., *J. Phys. Chem.*, **63**, 641 (1959).

(10) E. B. Dismukes and W. S. Wilcox, *Radiation Res.*, **11**, 754 (1959).



Primary Reaction Steps.—Extensive work on the pyrolysis of ethyl bromide and the propyl bromides has been reported in the literature.¹¹ In these researches, conducted at higher temperatures in the gas phase, both steps 2a and step 2b have been suggested by different workers as the initial step in the thermal decomposition process. The major primary step in the radiolysis of liquid *n*-C₃H₇Br at 25° appears to be rupture of the C–Br bond and escape of the C₃H₇ radical and Br atom from each other (2a, 3b). This is indicated by the fact (Table I) that $G(\text{C}_3\text{H}_8)$ is 3.5 in the absence of added bromine and drops to 0.3 in the presence of bromine, while G for incorporation of radiobromine in *n*-C₃H₇Br is about 3.5 in irradiations with 0.9 mole % labeled bromine present. The effect of 5 mole % HBr in raising $G(\text{C}_3\text{H}_8)$ to 4.5 suggests that at 25°, in the absence of added HBr, some C₃H₇ radicals are consumed by a reaction such as addition to propene¹¹ or recombination with their parent partner (3a) rather than by hydrogen abstraction (3c, 4a, 5, 6). The effects of Br₂ and HBr at 5 mole % may both include some competition (*e.g.*, 3c) with recombination reactions such as (3a) and hot reactions in the spurs (*e.g.*, 4a) as well as reaction with thermal radicals (6, 10). The results show that there are no C₁ or C₂ hydrocarbons or alkyl bromides formed with G greater than 0.2. This means that rupture of carbon–carbon bonds must occur less than 10% as frequently as bond ruptures of Br or H atoms attached to the C₃ chain. Essentially all of the C–C bond rupture that does occur takes place at the C–C bond furthest removed from the bromine atom.

In the irradiation of *n*-C₃H₇Br containing 9×10^{-3} mole fraction of radiobromine a G of 6.7 was found for the production of labeled 1,2-C₃H₆Br₂, assuming that only one of the bromine atoms could come from the labeled Br₂ while the other was that from the parent molecule. This assumption is valid if the dibromide is formed by reaction of Br₂ with C₃H₆Br radicals produced by either primary rupture of a C–H bond (C₃H₇Br → C₃H₆Br + H) or by abstraction of hydrogen (C₃H₇Br + Br → C₃H₆Br + HBr). Our data do not exclude either of these processes but strongly suggest that the hydrogen abstraction reaction 7 may be important in determining the temperature sensitivity of the system. The third avenue for dibromide production is Br₂ + C₃H₆ → C₃H₆Br₂. If the dibromide were formed by this mechanism the G -value would be half that calculated from the other mechanisms since either Br atom could be tagged. C₃H₆ can be formed either by reactions 7 and 8, which are temperature dependent, or by primary radiolytic decomposition, reaction 2b. As discussed later, the

G for reaction 2b cannot be greater than 1.5 and is probably much less.

From the data of Table I it appears that G (H atoms from C–H bond rupture) must be at least 0.9 (*i.e.*, 1.3 minus 0.4). It may be higher if H atoms are used up predominantly by the reaction H + C₃H₇Br → C₃H₇ + HBr or if the yield of H₂ in the presence of 5 mole % Br₂ ($G = 0.4$) is the result of H abstraction by hot H atoms rather than the result of unimolecular splitting out of molecular H₂. The yield of tagged C₃H₅Er₃ ($G = 0.3$) in the presence of added bromine suggests strongly that the yield of molecular hydrogen is at least 0.3.

HBr Production.—It is apparent from the observed effects of temperature and additives on the radiolysis of *n*-C₃H₇Br that, except for the minor contribution of hot reactions not affected by 5 mole % of Br₂ or HBr, the net yields of stable products are dependent on the relative rates of competing temperature-sensitive elementary reaction steps. This is illustrated by the values of initial $G(\text{HBr})$ of 0.06, 0.12, 2.9 and 10.5 at –78, 0, 25 and 50°; by the increase in $G(\text{HBr})$ from 0.06 to 1.5 at –78° and from 2.9 to 12 at 25° when Br₂ is added; by the elimination of telomer by added HBr and Br₂; and by the pronounced reduction of propane production by added bromine.

The $G(\text{HBr})$ of 1.5 in the presence of 1 mole % Br₂ at –78° sets an upper limit on the primary formation of HBr by the concerted elimination step C₃H₇Br → C₃H₆ + HBr (2b) for all temperatures unless this step is sensitive to “caging” effects which are temperature dependent. The 1.5 value must represent the total production of HBr at this temperature since all free radicals and olefins which might consume HBr would be removed by the bromine. It is the sum of HBr produced by the HBr elimination process and by abstraction processes involving hot Br atoms since abstraction of H by thermal Br atoms would be negligible at this temperature.

The increase in $G(\text{HBr})$ with increase in temperature must be due in part at least to the increasing rate constant for reaction 7 and it seems probable that this reaction plays a dominant role as a step in chain processes for radical production at 25° and above. Because the secondary hydrogen bonds of *n*-C₃H₇Br are probably several kcal./mole weaker than the primary bonds reaction 7 is expected to form the CH₃CHCH₂Br radical. Preferential abstraction of the secondary hydrogen is indicated by the small amount of 1,3-C₃H₆Br₂ formed with 1 mole % Br₂ in comparison to the G of 6.7 for 1,2-C₃H₆Br₂.

It is interesting to note the qualitative agreement at 25° among the values of G (organic incorporation of radiobromine) = 12, $G(\text{HBr})$ in the presence of added Br₂ = 12, and $G(1/2\text{Br}_2)$ in the presence of added HBr = 14. Each of these may be taken as a measure of the concentration of radicals which are scavengeable at the additive concentrations employed. It is consistent with the observed results to ascribe the decrease in $G(\text{HBr})$ with increasing dose in the absence of additives to HBr addition to C₃H₆, *via*, perhaps, reactions 8r and 7r, as the concentrations of both compounds

(11) (a) A. Blades and G. W. Murphy, *J. Am. Chem. Soc.*, **74**, 6219 (1952); (b) J. B. Peri and F. Daniels, *ibid.*, **72**, 424 (1950); (c) P. Aguis and A. Maccoll, *J. Chem. Phys.*, **18**, 158 (1950); (d) A. Maccoll and P. J. Thomas, *ibid.*, **19**, 977 (1951); (e) J. H. S. Green, G. D. Harden, A. Maccoll and P. J. Thomas, *ibid.*, **21**, 178 (1953); (f) A. Maccoll and P. J. Thomas, *ibid.*, **23**, 1722 (1955); (g) A. E. Goldberg and F. Daniels, *J. Am. Chem. Soc.*, **79**, 1314 (1957).

increase. In a $n\text{-C}_3\text{H}_7\text{Br}$ solution containing 2×10^{-2} mole/l. each of added C_3H_6 and HBr , a dose of 2.4×10^{19} e.v./g. was sufficient to decrease the HBr concentration tenfold, the final HBr concentration being lower than the normal steady state reached upon prolonged irradiation of pure bromide. No addition occurred in the dark. The limited propene data obtained from radiolyzed solutions indicate that it reaches a steady-state concentration of about 10^{-3} mole/l. while the corresponding HBr concentration is 5×10^{-3} mole/l. The fact that telomer production is prevented by added HBr (or Br_2), but is enhanced by added propene, suggests that HBr competes with other species for reaction with propene or radicals involved in telomer formation.

$G(\text{C}_3\text{H}_6)$ and $G(\text{HBr})$ would be equal if the two compounds are formed by reactions 3b, 7 and 8, or by reaction 2b and did not enter subsequent reactions. The fact that $G(\text{HBr})$ and $G(\text{telomer})$ both increase with temperature may be attributed to increasing rate constants for reaction 7 and 8, the propene formed *via* 8 reacting with radicals in chain lengthening steps to form the telomer. The consumption of C_3H_6 to form telomer reduces its net G -value far below that of HBr . For the 25° steady-state condition shown in Fig. 1 the hypothesis suggested is that HBr and propene are reacting with each other at a rate equal to that of their formation. Disturbing of this steady state with scavenger additions changes completely the spectrum of the radiation products. Thus HBr addition eliminates telomer production and results in bromine formation while 5% propene addition enhances the telomer rate but eliminates net HBr production. These effects presumably are due to reactions of the type $\text{R} \cdot + \text{HBr} \rightarrow \text{RH} + 1/2 \text{Br}_2$, which may be able to compete with $\text{C}_3\text{H}_6\text{Br}$ decomposition *via* reaction 8, or to reaction of HBr with other chain initiating or carrying intermediates. Within the framework of the reaction hypothesis, such a competition would be required to yield the observed G of 7 for Br_2 production.

Mary Benedict¹² in our laboratory has found that when solutions of tritium bromide of 9×10^{-3} mole/l., about twice the 25° plateau level in Fig. 1, are irradiated, appreciable tritium enters combination as $n\text{-C}_3\text{H}_7\text{Br}$. This observation seems to require the reaction $\text{C}_3\text{H}_6\text{Br} + \text{TBr} \rightarrow \text{C}_3\text{H}_6\text{TBr} + \text{Br}$. In this same work the tritiated propane yield was negligible even after applying a maximum correction factor for the isotope effect. This indicates that essentially all of the C_3H_8 must be produced *via* reactions 4a and 5 rather than by hydrogen abstraction from HBr . Propyl radicals which react with solvent remove the opportunity for $\text{C}_3\text{H}_7\text{T}$ formation *via* reaction with TBr , whereas $\text{C}_3\text{H}_6\text{Br}$ radicals which react with the solvent are replaced by an identical radical, thus favoring eventual reaction with TBr to form $\text{C}_3\text{H}_6\text{TBr}$.

Bromine Production.—No visible amounts of bromine were produced in any irradiations of propyl bromide without additives, but it is possible that visually undetectable amounts were present. Since the activation energy for H atom abstrac-

tion from the substrate by Br atoms is probably appreciably lower than for the corresponding Br atom abstraction, and is sufficiently low to compete effectively with $\text{Br} + \text{Br} \rightarrow \text{Br}_2$ at the Br atom concentrations of these solutions, the only Br_2 formed would seem to be that formed by hot reactions. Any such bromine would react with any propene present even in the absence of radiation and would also compete with HBr for radicals formed during radiolysis.

If for the purpose of a rough estimate it is assumed that the reactions of radicals with Br_2 and with HBr have equal frequency factors and that the activation energy for reaction with HBr is 3 kcal./mole and for reaction with Br_2 is 1 kcal./mole, values of $k_{\text{HBr}}/k_{\text{Br}_2}$ of 0.04 at 25° and 0.007 at -78° are obtained. At the maximum of the curve of Fig. 3, for the experiment starting with 1 mole % HBr , the HBr/Br_2 ratio is about 13. Since the rates of reaction of radicals with Br_2 and with HBr are presumably equal at this point, the data indicate that $k_{\text{HBr}}/k_{\text{Br}_2} = 0.08$. If these estimates of $k_{\text{HBr}}/k_{\text{Br}_2}$ are approximately correct, in experiments under the conditions of the plateau of the 25° curve of Fig. 1, the steady-state concentration of Br_2 was less than about 10^{-4} mole/l., which is at about the limit of visual detection in the reaction cells used.

Organic Bromides.—Among the conclusions suggested by the data on the production of bromides in the absence of additives and on the production of labeled bromides in the presence of radiobromine are the following.

(1) Since CH_3Br and CH_4 are observed as products of the irradiation of pure $n\text{-C}_3\text{H}_7\text{Br}$ but no $\text{CH}_3\text{Br}^{82}$ was found for irradiations in the presence of radiobromine at 9×10^{-3} mole fraction, formation of a hot methyl radical *via* $\text{C}_3\text{H}_7\text{Br} \rightarrow \text{CH}_3 + \text{C}_2\text{H}_4\text{Br}$ is indicated. A G of 0.1 is indicated for $\text{CH}_3\text{-C}_2\text{H}_4\text{Br}$ bond rupture. The hot CH_3 radicals may then form either CH_3Br or CH_4 by abstracting either Br or H atoms from the substrate. This reaction must take place very shortly after CH_3 formation. The $\text{C}_2\text{H}_4\text{Br}$ fragment appears to react *via* a thermal reaction to yield $\text{C}_2\text{H}_5\text{Br}$ or, in the presence of Br_2 , or give $\text{C}_2\text{H}_4\text{Br}_2$, as observed with radiobromine.

(2) The G of 6.7 for $1,2\text{-C}_3\text{H}_6\text{Br}_2$ in the experiments with radiobromine suggests a G of 6.7 for $\text{C}_3\text{H}_7\text{Br} + \text{Br} \rightarrow \text{C}_3\text{H}_6\text{Br} + \text{HBr}$ under the conditions of the experiment if $\text{C}_3\text{H}_6\text{Br}$ reacts with bromine to form $\text{C}_3\text{H}_6\text{Br}_2$. If $\text{C}_3\text{H}_6\text{Br}$ decomposes before reaction with bromine, giving Br and C_3H_6 , followed by addition of Br_2 to C_3H_6 , the G -value is 3.3. In view of other evidence cited for reaction of the $\text{C}_3\text{H}_6\text{Br}$ radical with added HBr or Br_2 before decomposition (including material balances for G -values of HBr and Br_2 production in the excess of the other as additive, and for the scavenging of radicals by radioactive bromine) the 6.7 value appears to be the more nearly correct.

(3) The fact that $i\text{-C}_3\text{H}_7\text{Br}$ is formed with a G of 2.1 in the irradiation of pure $n\text{-C}_3\text{H}_7\text{Br}$ while the G of the radioactive $i\text{-C}_3\text{H}_7\text{Br}$ formed in the presence of 1% radiobromine is only 0.4 indicates either that Br_2 inhibits the formation of $i\text{-C}_3\text{H}_7\text{Br}$ or that

(12) M. Benedict, M. S. Thesis, University of Wisconsin, 1959.

it is formed by an intramolecular isomerization which does not involve a thermal free radical. In the analogous alkyl chloride system it has been found⁸ that $n\text{-C}_3\text{H}_7\text{Cl}$ is isomerized to $i\text{-C}_3\text{H}_7\text{Cl}$ by radiation in a chain reaction catalyzed by HCl, G -values in excess of 100 being observed. This chain is eliminated by low concentration of I_2 . The isomerization appears to occur by the sequence $\text{Cl} + n\text{-C}_3\text{H}_7\text{Cl} \rightarrow \text{CH}_3\text{CHCH}_2\text{Cl} + \text{HCl}$; $\text{CH}_3\text{CHCH}_2\text{Cl} \rightleftharpoons \text{CH}_3\text{CHClCH}_2$; $\text{CH}_3\text{CHClCH}_2 + \text{HCl} \rightarrow i\text{-C}_3\text{H}_7\text{Cl} + \text{Cl}$, $\text{Cl} + n\text{-C}_3\text{H}_7\text{Cl} \rightarrow \text{CH}_3\text{-}$

$\text{CHCH}_2\text{Cl} + \text{HCl}$, etc. It may be that $\text{CH}_3\text{CH-CH}_2\text{Br}$ radicals occasionally isomerize and are stabilized by a similar mechanism. Such a possibility is consistent with our data and could account for the effect of added Br_2 on $G(i\text{-C}_3\text{H}_7\text{Br})$.

Acknowledgment.—This work was supported in part by the United States Atomic Energy Commission and in part by the University Research Committee with funds made available by the Wisconsin Alumni Research Foundation.

EFFECT OF CHLORIDE ON THE KINETICS OF ELECTROOXIDATION OF CHROMIUM(II) IN ACIDIC PERCHLORATE MEDIUM¹

BY DAVID A. AIKENS² AND JAMES W. ROSS, JR.

Department of Chemistry and Laboratory for Nuclear Science of the Massachusetts Institute of Technology, Cambridge, Mass.

Received January 26, 1961

The effect of chloride on the kinetics of the electrooxidation of chromium(II) in acidic 1 *M* sodium perchlorate solution has been studied by the potentiostatic technique at the hanging mercury drop electrode. A convenient method of *in situ* generation of chromium(II) for electrode kinetic studies has been devised by a simple modification of the direct potentiostatic technique. At constant applied potential, the oxidation of chromium(II) is enhanced by chloride, the reaction following two parallel paths. The first is independent of chloride, yielding hexaaquachromium(III), and the second is first order in chloride at chloride concentrations up to 50 millimolar, yielding chloropentaaquachromium(III). The ability of the halides to enhance the reaction increases from fluoride to chloride to iodide, indicating that tendency of the halides toward specific adsorption at the electrode surface determines their relative efficiencies in enhancing the reaction.

Introduction

In contrast to numerous studies of the electroreduction of chromium(III) species, few studies have been concerned with the electrooxidation of chromium(II). Pecsok and Lingane³ studied the anodic polarography of chromium(II) in a wide variety of aqueous media. They observed that the $E_{1/2}$ of the irreversible chromium(II) oxidation shifted from -0.34 v. to -0.40 v. vs. the SCE as the supporting electrolyte was changed from 0.1 *M* potassium chloride to 1.0 *M* potassium chloride, and that the $E_{1/2}$ was -0.43 v. vs. the SCE in 0.1 *M* tetramethylammonium bromide. Abubacker and Malik⁴ have also made a qualitative study of the electrooxidation of chromium(II) and conclude that the reaction is accelerated by chloride ion. It is plain that chloride and bromide both facilitate the oxidation of chromium(II) and that the latter is the more effective. However, the $E_{1/2}$ of an irreversible polarographic wave is often quite sensitive to the total salt concentration as well as to the concentrations of ions which are directly involved in the electrode reaction.⁵ The concentration and type of salt are important as they determine the structure of the electrical double layer

in which the electrode reaction occurs. Because of such "non-specific salt effects" only qualitative significance can be attached to the above data.

The purpose of the present investigation is to determine quantitatively the effect of chloride ion on the kinetics of the electrooxidation of chromium(II) at a mercury electrode in acidic perchlorate solution and to elucidate the role of chloride in the reaction. Chloride is of interest as typical of the halide ions, which, because of their simple structure, are of importance in theories of the mechanism of electron transfer.

Rate constants of slow electrochemical reactions can be deduced from polarographic data.⁶ However, the potentiostatic technique using a hanging drop electrode offers significant advantages and has been employed in this study. Slow electrode reactions ($k < 10^{-2}$ cm./sec.) can be studied with relatively simple apparatus. The rate constant of the electrode reaction can be evaluated by a simple extrapolation of current-time data.

As in polarographic studies, non-specific salt effects are operative and will be reflected as variations in rate constants with double layer structure. In this work variation due to non-specific salt effects is negligible since the total electrolyte concentration is maintained constant and the composition nearly constant, varying from 1.0 *M* sodium perchlorate to 0.95 *M* sodium perchlorate-0.05 *M* sodium chloride. The observed variation in rate with composition is thus indicative of the stoichiometry of the electrode reaction.

Considerable difficulty was experienced in main-

(1) Taken in part from the Ph.D. Thesis of David A. Aikens, Massachusetts Institute of Technology, June, 1960. This work was supported in part by the U. S. Atomic Energy Commission under Contract AT(30-1)905.

(2) E. I. du Pont Teaching Fellow, 1958-1959; National Science Foundation Regular Fellow, 1959-1960.

(3) R. L. Pecsok and J. J. Lingane, *J. Am. Chem. Soc.*, **72**, 189 (1950).

(4) K. M. Abubacker and W. U. Malik, *J. Indian Chem. Soc.*, **36**, 463 (1959).

(5) (a) M. Breiter, M. Kleinerman and P. Delahay, *J. Am. Chem. Soc.*, **80**, 5111 (1958); (b) W. H. Reinmuth, L. B. Rogers and L. E. I. Hummelstedt, *ibid.*, **81**, 2947 (1959).

(6) (a) J. Koutecky, *Coll. Czechoslov. Chem. Commun.*, **18**, 597 (1953); (b) P. Delahay, "New Instrumental Methods in Electrochemistry," Interscience Publ., New York, N. Y., 1954.

taining polarographic concentrations of chromium(II) in perchlorate medium. In spite of precautions to exclude oxygen and to remove potential oxidants from the solution by pre-electrolysis, it was found that chromium(II) was oxidized within 45 minutes of addition of an aliquot to the perchlorate supporting electrolyte.

The generation of chromium(II) at the electrode surface by a modification of the direct potentiostatic method has been found to be a convenient solution to this problem. A solution containing a known concentration of chromium(III) was electrolyzed at -1.10 v. *vs.* the SCE for 15 seconds. The potential was sufficiently cathodic that the concentration of chromium(III) at the electrode surface is zero, and a layer of chromium(II) is generated in the vicinity of the electrode. Shifting the potential to a value at which the oxidation of chromium(II) occurs results in a current-time curve for the oxidation which approximates that which would result if the solution initially contained chromium(II) at the same concentration as the chromium(III) in the actual experiment. The validity of the approximation depends upon two factors: the equality of the diffusion coefficients of chromium(II) and chromium(III) and the generation time being long compared to the interval in which the reoxidation is observed. The first requirement is met as can be seen from published values of I , the diffusion current constant for these species. Lingane and Pecsok⁷ report that the I for aquachromium(III) in 0.25 *M* potassium chloride is 1.50 and Abubacker and Malik⁴ report that for aquachromium(II) to be 1.54 in 0.1 to 1.0 *M* potassium chloride. The second requirement is met by limiting the observation of the reoxidation to 1 second and extrapolating the experimental current to zero time.

Experimental

Recorder and Switching Network.—Current-time curves were recorded with a Sanborn Model 151 Recording Galvanometer fed by a Sanborn Model 150-1800 d.c. amplifier. The full scale deflection was 5 mv. and the full scale response time was 0.01 sec. All curves were recorded at a chart speed of 100 mm./sec.

In order to standardize the operations involved in recording current-time curves a switching network activated by a synchronous timer was employed. The network applied the appropriate potentials to the cell for the generation step and the subsequent reoxidation and connected the recorder for the observation of the latter. The potentials were derived from 50 ohm Helipot potentiometers fed by three 4 FH Burgess 1.5 volt cells in parallel and were adjusted to ± 0.25 mv. with a potentiometer. Clare mercury wetted relays were used throughout. A delay of 0.02 second between the application of the second potential to the cell and the connection of the recorder was introduced to prevent serious overloading of the latter by the large charging current pulse associated with the sudden change in applied potential.

Cell.—The cell was constructed of glass and Teflon and was of conventional design. A large saturated calomel electrode served as a working reference electrode, connection to the cell being made with a fritted disc salt bridge filled with saturated sodium nitrate solution. The over-all cell resistance was 350 ohms. The working electrode was a hanging mercury drop electrode,⁸ a fresh drop being employed for each current-time curve. The drop area was calculated by collecting and weighing 50 drops. The system was thermo-

stated at $25 \pm 0.1^\circ$. Solutions were deaerated with pre-purified nitrogen for 30 minutes before a series of measurements and the nitrogen stream was passed over the surface of the solution during the measurements.

Reagents.—All materials were analytical grade reagents. Solutions were prepared with laboratory supply distilled water which had been redistilled from basic permanganate and dilute sulfuric acid, successively, to destroy traces of surface-active organic matter.

Chromium(III) perchlorate was prepared by reduction of sodium dichromate with hydrogen peroxide in perchloric acid followed by boiling to destroy excess peroxide. The salt was recrystallized and dissolved in 0.1 *M* perchloric acid.

Sodium perchlorate served as the basic constituent of the supporting electrolyte, the ionic strength of which was 1.0 in all cases. Halides were added as the sodium salts. The sodium perchlorate solution was prepared by reaction of the appropriate amount of sodium carbonate with a slight excess of perchloric acid (*pH* 2) followed by boiling to remove carbon dioxide. The *pH* of the final electrolyte solution was 2.0.

The concentration of chromium in the solutions used in the potentiostatic studies was determined spectrophotometrically as chromate, as described by Haupt.⁹ A Beckman DU spectrophotometer was used and calibrated with solutions prepared from potassium dichromate.

The bound chloride content of chromium(III) species was determined by reaction with excess standard silver nitrate at 100° as described by Elving and Zemel.¹⁰ Free chloride had been removed previously by potentiometric titration with silver nitrate at 0° . The absorption spectrum of chloropentaaquachromium(III) was determined from a solution prepared by the method of Elving and Zemel.¹⁰

Rate constants were evaluated from plots of current *vs.* the square root of time. Ross¹¹ has shown that for the case of uniform initial concentration of reactant, the plot becomes linear at short values of time at a spherical electrode allowing an accurate extrapolation to zero time. The residual current was subtracted whenever its contribution to the total current was greater than 2%. At zero time the relation between current and rate constant for a first-order electrode reaction is given by

$$i = knAFC$$

where i is the current in amp., n is the number of electrons involved in the reaction, A is the electrode area in square cm., F is the value of the faraday, C is the concentration of reactant in moles/cc., and k is the rate constant of the electrochemical reaction in cm./sec. Correction was made for iR drop in the cell as calculated from the initial current and the cell resistance. Because of increasing curvature of the plots with increasing values of k , the largest value of k which could be determined satisfactorily with this apparatus was about 10^{-2} cm./sec.

Results

The effect of 0 to 5×10^{-2} *M* chloride on the kinetics of the electrooxidation of chromium(II) is shown in Fig. 1. The rate constant data are presented as apparent first-order rate constants based on the chromium(II) concentration. In the absence of chloride, the reaction is first order in chromium(II) from 0.5 to 7.0×10^{-3} *M* in chromium(II). At a fixed chloride concentration the rate constant varies approximately exponentially with potential, reflecting both the variation of the non-specific salt effect with potential and the exponential dependence of rate on potential predicted by the Eyring treatment of electrode kinetics.¹²

At a fixed potential the increase in rate constant with chloride concentration is proportional to the chloride concentration. The rate law for the ox-

(9) G. W. Haupt, *J. Research Natl. Bur. Standards*, **48**, 414 (1952).

(10) P. J. Elving and B. Zemel, *J. Am. Chem. Soc.*, **79**, 1281 (1957).

(11) J. W. Ross, Jr., Ph.D. Thesis, University of Wisconsin, 1957.

(12) S. Glasstone, K. Laidler and H. Eyring, "The Theory of Rate Processes," McGraw-Hill Book Co., New York, N. Y., 1941.

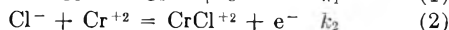
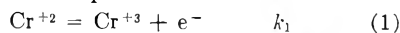
(7) J. J. Lingane and R. L. Pecsok, *J. Am. Chem. Soc.*, **71**, 425 (1949).

(8) H. G. Gerrischer, *Z. physik. Chem. (Leipzig)*, **202**, 302 (1953).

dation of chromium(II) takes the form

$$k = k_1 + k_2(\text{Cl}^-)$$

where k is the observed apparent first-order rate constant, k_1 is the first-order rate constant for the oxidation of chromium(II) in the absence of chloride at the potential in question and k_2 is a second-order rate constant. Values of $k_1 \times 10^5$ in cm./sec. at 50 mv. intervals from -0.500 v. vs. the SCE to -0.300 v. vs. the SCE are 6.7, 13.8, 28, 57 and 119, while the corresponding values of k_2 in cm.⁴/mole sec. are 6.3, 20, 60, 172 and 380. The kinetic data correspond to the parallel reactions



The product of reaction 2 has been identified by analysis of the products of a large scale electrolytic oxidation of chromium(II) at a mercury pool under such conditions that virtually all of the chromium(II) should follow path 2. The chromium(II) solution was prepared by reducing a solution of 0.01 M chromium(III) in 0.85 M sodium perchlorate, 0.10 M sodium chloride, 0.05 M perchloric acid in a Jones reductor, introducing the effluent directly into the electrolysis cell under an atmosphere of prepurified nitrogen. The oxidation was carried out at -0.10 v. vs. the SCE by manually varying the potential applied between the pool and an external platinum electrode. The electrolysis was stopped after 4 hours and it is estimated from the decay of the current that approximately 90–95% of the chromium(II) had been oxidized.

The ratio of bound chloride to chromium(III) in the product mixture was 0.85 as determined by titration. The low result probably is due to air oxidation of the chromium(II) during or after the electrolysis. This was confirmed by comparing the absorption spectra of the products of the electrolysis, pure chloropentaquachromium(III), and the air oxidation product of chromium(II) obtained under the experimental conditions.

The enhancement of the electrooxidation of chromium(II) by halide ion decreases in the order I^- , Cl^- , F^- , as shown in Fig. 2. Comparison of the halides was made at an ionic halide concentration of $5.0 \times 10^{-3} M$. The case of fluoride is complicated by the low dissociation constant of hydrofluoric acid, which must be taken into account to ensure the same concentration of halide ion in each case. The fluoride ion concentration was adjusted using the stoichiometric hydrogen ion concentration of the solution, $5.1 \times 10^{-3} M$, and Ahrlund and Larsson's¹³ value for the dissociation constant of hydrofluoric acid in this medium of 1.15×10^{-3} .

Discussion

No evidence was found for a reaction higher than first order in chloride over the range of variables investigated. Such a reaction may become important at high chloride concentrations, but the rate of the electrode reaction places study of its kinetics beyond the capabilities of the present apparatus. Furthermore, proof of the path of the reaction by identification of the product is precluded by the rapid reaction

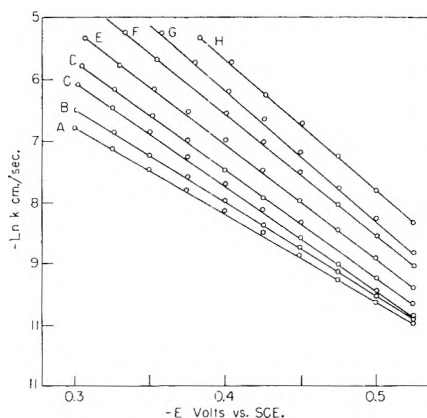


Fig. 1.—Apparent first-order rate constant for oxidation of chromium(II) in sodium perchlorate-sodium chloride medium: A, $\text{Cl}^- = 0.000 M$; B, $\text{Cl}^- = 0.001 M$; C, $\text{Cl}^- = 0.003 M$; D, $\text{Cl}^- = 0.005 M$; E, $\text{Cl}^- = 0.010 M$; F, $\text{Cl}^- = 0.020 M$; G, $\text{Cl}^- = 0.030 M$; H, $\text{Cl}^- = 0.050 M$.

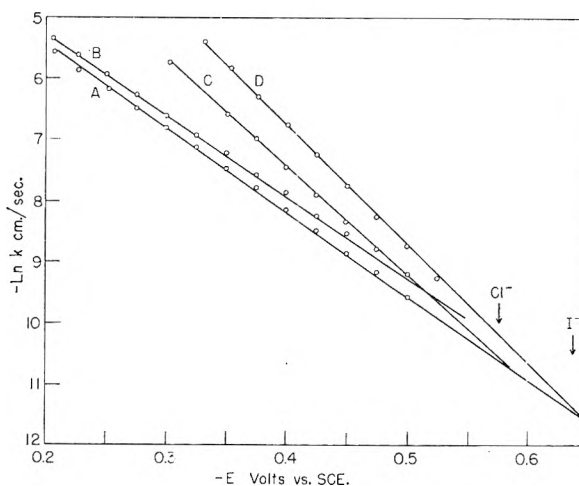


Fig. 2.—Effect of 0.005 M halide ions on apparent first-order rate constant for oxidation of chromium(II): A, no halide present; B fluoride; C, chloride; D, iodide. Arrows indicate e.c.m. potentials of chloride and iodide-containing solutions.



Taube and Myers¹⁴ found the second-order rate constant for this reaction to be 10^4 l./mole min. at 0° . Thus dichlorochromium(III) species would be converted rapidly into the monochloro species as long as chromium(II) were present, obscuring the results of the electrode reaction.

The kinetic data describe the effect of chloride quantitatively but do not indicate the manner in which it enhances the reaction rate. Two immediate possibilities arise. First, halide specifically adsorbed on the mercury surface may act as an efficient bridge for electron transfer as proposed by Heyrovský¹⁵ to explain the increased ease of reduction of indium ion in the presence of halides. The second possibility, which would be kinetically identical with the first, is the oxidation of a monochlorochromium(II) complex formed in the bulk of the solution.

The relatively large effect of chloride on the rate suggests the former possibility as does the fact that

(14) H. Taube and E. Myers, *J. Am. Chem. Soc.*, **76**, 2103 (1954).

(15) J. Heyrovský, *Disc. Faraday Soc.*, **1**, 212 (1947).

(13) S. Ahrlund and R. Larsson, *Acta Chem. Scand.*, **8**, 354 (1954).

the contribution of the chloride path increases rapidly as the potential is made more positive. Although the ratio k_2/k_1 is not meaningful *per se*, the variation of this ratio with potential is. The ratio increases from 9.4×10^4 at -0.500 v. vs. the SCE to 3.2×10^5 at -0.300 v. vs. the SCE. At a chloride concentration of $0.01 M$, 48% of the reaction would proceed *via* the chloride path at -0.500 v. vs. the SCE, while at -0.300 v. vs. the SCE, 76% of the reaction would follow this path. An interpretation based upon such evidence alone is conjectural at best, however.

Comparison of the relative enhancement caused by a series of halides is a much better test of the two hypotheses since the tendencies of the halides toward specific adsorption on mercury is opposite to their tendencies to coordinate with chromium(II). The specific adsorption of iodide is greater than that of chloride, while fluoride shows no tendency toward specific adsorption according to Grahame.¹⁵ Although no direct evidence is available on the relative stabilities of chromium(II)-halide complexes, indirect evidence indicates that the stability should decrease sharply from fluoride to iodide. The measured stability constants of the monochloro- and the monofluorochromium(III) species as quoted by Bjerrum,

(16) D. C. Grahame, *Chem. Revs.*, **41**, 441 (1947).

et al.,¹⁷ are 4 and 10^{-5} at zero ionic strength, and the stabilities of the chromium(II) species would be expected to follow the same order. Further, Ahrland, *et al.*,¹⁸ in a detailed survey of the complex formation tendencies of metal ions conclude that the stability of chromium(II) halide complexes should decrease from fluoride to iodide.

The results presented in Fig. 2 strongly support the halide adsorption hypothesis. The effectiveness of the halides in facilitating the chromium(II) oxidation increases from fluoride to iodide, paralleling the extent of adsorption. The effect of chloride and iodide is the greatest at the more positive potentials where the adsorption is the greatest. The potentials at which they become ineffective are slightly negative of the electrocapillary maxima of the respective solutions, which in turn are slightly positive of the potentials at which adsorbed anions are completely desorbed. The effect of fluoride in contrast is nearly independent of potential. Since fluoride is not specifically adsorbed, the difference between its behavior and that of chloride and iodide offers additional support for the adsorption mechanism.

(17) J. Bjerrum, G. Schwarzenbach and L. Sillén, "Stability Constants of Metal-Ion Complexes," Part II, The Chemical Society, London, 1958.

(18) S. Ahrland, J. Chatt and N. R. Davies, *Quart. Revs. (London)*, **12**, 265 (1958).

THE FLUORIDE COMPLEXES OF SILVER AND STANNOUS IONS IN AQUEOUS SOLUTION

BY ROBERT E. CONNICK AND ARMINE D. PAUL

Department of Chemistry and Lawrence Radiation Laboratory, University of California, Berkeley, Calif.

Received January 28, 1961

Leden and Marthen's work on the fluoride complexing of argentous ion has been repeated at an ionic strength of $0.5 M$ and as a function of temperature to yield values for the equilibrium constant, heat and entropy of formation of the first fluoride complex. A value for the first fluoride complex of stannous ion was measured at 25° using both an e.m.f. method and a spectrophotometric method. The former made use of the tin amalgam-stannous ion couple while the latter depended on uranyl ion as a spectrophotometric indicator for fluoride ion. Although the results of the two methods are in substantial agreement with each other, the values of the equilibrium quotient as a function of stannous ion and hydrogen ion concentrations are not constant. No explanation has been found for this discrepancy.

In a continuation of the study of the stability of fluoride complexes of +2 ions in aqueous solution^{1,2} the complexing constants for the first fluoride complexes of Ag^+ and Sn^{++} were determined. Leden and Marthen³ previously had measured the complexing of silver ion at an ionic strength of 1.0 and at 25° . Their work was extended to other temperatures but at an ionic strength of $0.50 M$. Schaap, Davis and Nebergall⁴ had reported a very high value for the stability constant for the stannous fluoride complex containing three fluorides, but apparently no quantitative data were available for the lower complexes.

The measurements were made potentiometrically on the silver-silver ion couple and the tin amalgam-

stannous ion couple. Additional experiments on tin were done using a spectrophotometric measurement of the competition between uranyl ion and stannous ion for fluoride ion.

Experimental

Silver.—Two half cells were connected by means of a $1.6 M$ sodium perchlorate-agar agar salt bridge in order to minimize junction potentials, and an atmosphere of nitrogen was maintained. Each half cell initially contained solutions of silver perchlorate, sodium perchlorate and perchloric acid. The solutions were stirred continuously. The cells and measuring apparatus were the same as described elsewhere.^{5,6} The cells and caps were painted black to prevent action of light on the silver.

The silver-silver ion electrodes were prepared by rapidly electrolyzing onto platinum a $0.1 M$ silver nitrate solution slightly acidified with nitric acid. The more rapid the electrolysis, the more rapid, reversible, and reproducible were the electrodes. In the limit, however, the silver deposit was so

(1) R. E. Connick and Maak-Sang Tsao, *J. Am. Chem. Soc.*, **76**, 5311 (1954).

(2) R. E. Connick and A. D. Paul, *ibid.*, **80**, 2069 (1958).

(3) I. Leden and L. Marthen, *Acta Chem. Scand.*, **6**, 1125 (1952).

(4) W. B. Schaap, J. A. Davis and W. B. Nebergall, *J. Am. Chem. Soc.*, **76**, 5226 (1954).

(5) H. W. Dodgen and G. K. Rollefson, *ibid.*, **71**, 2600 (1949).

(6) L. G. Hepler, J. W. Kury and Z. Z. Hugus, Jr., *J. Phys. Chem.*, **58**, 26 (1954).

spongy that it would not adhere well to the platinum. In practice, the electrodes usually were electrolyzed at a current of about 30 milliamp. for 5 or 10 min. or until the surface of the platinum was entirely covered with silver. Before the plating, the electrodes were cleaned by dipping for a second in warm aqua regia. Electrodes prepared under these conditions usually agreed within 0.2–0.3 mv. and came to equilibrium within 5 minutes.

One hundred-ml. aliquots of stock solution containing the desired concentrations of silver perchlorate, perchloric acid and sodium perchlorate at an ionic strength of 0.5 *M* were pipetted into each half cell. After the initial zero potential had become constant, known quantities of sodium fluoride were added to half cell A and the same quantity of sodium perchlorate added to half cell B and the difference in potential from the initial zero potential measured after each addition.

Stannous Ion.—Each half cell initially contained solutions of stannous perchlorate, perchloric acid and sodium perchlorate. At low acidities, the cells were connected by means of a sodium perchlorate–agar agar salt bridge. Since the agar agar is not stable in perchloric acid solutions whose concentration is greater than 1 *M*, for such solutions a bridge was used with tiny ground glass stoppers at each end and filled with a perchloric acid–sodium perchlorate solution whose concentration was equal to that in the cells.

The cells and measuring apparatus were the same as used for the silver experiments. The electrodes were J-shaped pieces of glass tubing, the short arm consisting of a small cup with a sealed-in platinum wire connecting to a short column of mercury for electrical contact in the long arm. The cup was filled with tin amalgam. For most experiments a saturated tin amalgam⁷ was prepared by warming about 1.2 g. of metallic tin in 10 cc. of triply distilled mercury. The electrodes responded rapidly, were reversible and reproducible, and came to equilibrium almost instantly.

The cells were flushed out with nitrogen for 15 minutes before use. Known volumes of sodium perchlorate, perchloric acid, boiled conductivity water and freshly prepared stannous perchlorate were added to each half cell. The stannous perchlorate was prepared not more than an hour before use. The initial ionic strength was either 0.50 or 2.00 *M*. The cells were stirred constantly and an atmosphere of nitrogen was maintained. The nitrogen was purified by passing it through solutions of vanadyl sulfate according to the method of Meites and Meites.⁸ Under these conditions not more than one per cent. of the total tin was oxidized to stannic at the end of an experiment as shown by an iodine titration. The presence of this quantity of stannic ion was shown not to affect the behavior of the tin amalgam–stannous ion electrode.

After the initial small zero potential (0.1 mv. or less for the last three expts. of Table IV) had become constant, known quantities of sodium fluoride were added to half cell A and the same quantity of sodium perchlorate added to half cell B and the potential measured after each addition.

Solutions.—The source and purity of water, perchloric acid, sodium perchlorate and sodium fluoride have been given elsewhere.⁶

Mallinckrodt Analytical Reagent Ag₂O was dissolved in perchloric acid to give a silver perchlorate solution. Silver was determined by titration with sodium chloride according to Mohr's method and the acidity was found by titration with sodium hydroxide after precipitation of silver chloride with sodium chloride.

Solutions of Sn(ClO₄)₂·HClO₄ were prepared by passing a solution of cupric perchlorate through a column containing metallic tin according to the method of Noyes and Toabe.⁹ The column and flask in which the stannous perchlorate was collected were filled with nitrogen at all times to prevent oxidation. Stannous ion was determined by titration with standard iodine under an atmosphere of nitrogen, and the acidity determined by titration with standard sodium hydroxide. The stannous ion concentration and acidity determined by this method agreed sufficiently well with the copper concentration and acidity of the initial cupric perchlorate solution, so that in later experiments the iodine titration was eliminated and the stannous ion concentration

taken to be equal to the copper concentration and the acidity taken to be equal to the acidity of the cupric perchlorate solution.

A uranyl perchlorate solution was prepared by dissolving UO₂ in excess perchloric acid. The concentration of uranyl ion was determined by evaporating to dryness and igniting at 900° to U₃O₈. The acidity was determined by precipitating the uranium as UO₄·xH₂O with hydrogen peroxide and titrating with standard NaOH to the phenolphthalein endpoint.¹⁰

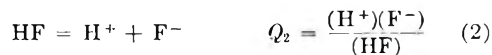
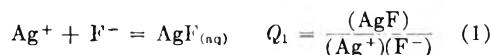
Results and Discussion

Silver.—The initial conditions and highest stoichiometric fluoride concentration for each experiment are summarized in Table I. At each temperature the initial acidity was varied over twenty-fold and the silver ion concentration five-fold. In Table II are given half of the data for a representative experiment. The *E* values are for the cell potential, corrected for the small initial potential with no added fluoride. The complete experimental data may be found elsewhere.¹¹

TABLE I
INITIAL CONDITIONS FOR SILVER EXPERIMENTS AT AN IONIC STRENGTH OF 0.50 *M*

Temp., °C.	HClO ₄ , <i>M</i> × 10 ³	AgClO ₄ , <i>M</i> × 10 ²	NaClO ₄ , <i>M</i>	Highest (ΣF ⁻), <i>M</i>
15, 35	21.45	4.190	0.4368	0.13
15, 35	4.849	21.00	.2851	.19
15, 35	0.9675	4.190	.4571	.13
25	41.26	10.53	.3534	.12
25	4.862	21.06	.2846	.13
25	0.9704	4.203	.4571	.12

The equilibria which must be considered are



where *Q* is the equilibrium quotient expressed in concentration units of moles per liter. Values for *Q*₂ for μ (ionic strength) = 0.50 *M* are in the literature.¹² Brøene and DeVries' value for *Q*₃ at μ = 0 was used at all temperatures¹³; the correction was always small.

The voltage of the cell can be expressed as

$$E = -\frac{RT}{F} \ln \frac{(\text{Ag}^+)_A}{(\text{Ag}^+)_B} \quad (4)$$

assuming the activity coefficients of silver ion to be equal. Since the silver ion in B is not complexed and the initial silver concentrations were equal in half cells A and B

$$(\text{Ag}^+)_B = (\text{Ag}^+)_i \frac{V_i}{V} \quad (5)$$

where the subscript *i* refers to the initial condition. Substitution of (5) into (4) gives

(10) R. E. Connick, "Chemistry of Uranium," J. J. Katz and E. Rabinowitch, editors, U. S. Atomic Energy Commission, Technical Information Service Extension, Oak Ridge, Tenn., 1958, p. 173.

(11) Armine D. Paul, Thesis, University of California, Berkeley, April 1955; unclassified University of California Radiation Laboratory Report UCFL-2926, April 1955.

(12) R. E. Connick, L. G. Hepler, Z. Z. Hugus, Jr., J. W. Kury, W. M. Latimer and M.-S. Tsao, *J. Am. Chem. Soc.*, **78**, 1827 (1956).

(13) H. H. Brøene and T. DeVries, *ibid.*, **69**, 1644 (1947).

(7) M. M. Haring and J. C. White, *Trans. Electrochem. Soc.*, **73**, 211 (1938).

(8) L. Meites and T. Meites, *Anal. Chem.*, **20**, 984 (1948).

(9) A. A. Noyes and K. Toabe, *J. Am. Chem. Soc.*, **39**, 1537 (1917).

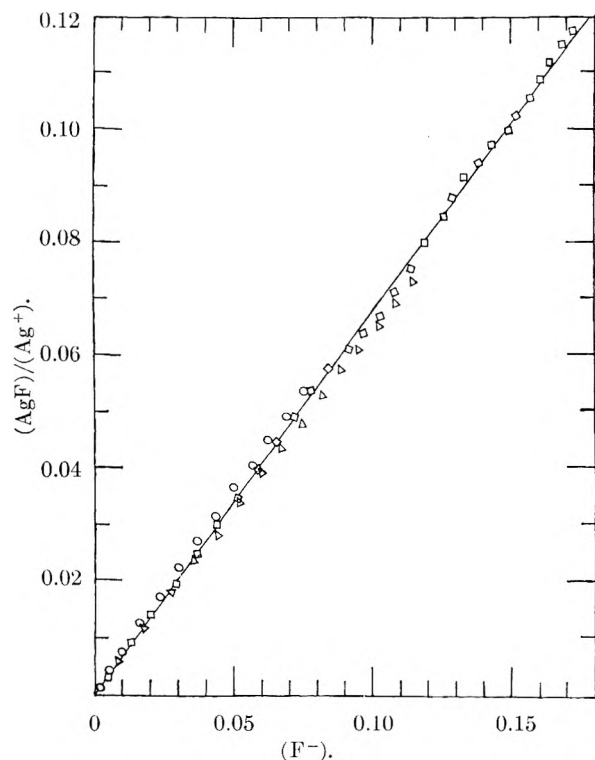


Fig. 1.—Plot of $(\text{AgF})/(\text{Ag}^+)$ values vs. (F^-) for the experiments at 25° in Table I: \circ , first experiment; \square , second experiment; \triangle , third experiment.

TABLE II

TYPICAL EXPERIMENTAL DATA FOR COMPLEXING OF Ag^+ BY FLUORIDE ION: SECOND EXPERIMENT AT 25° OF TABLE I

Initial concn.		Ionic strength 0.500 M			
$\text{HClO}_4 = 0.004862 M$		Temp. $25.00 \pm 0.01^\circ$			
$\text{AgClO}_4 = 0.21056 M$		Initial volume 99.95 ml.			
$\text{NaClO}_4 = 0.2845 M$		0.5004 M NaF added			
NaF added, ml.	E , mv.	NaF added, ml.	E , mv.	NaF added, ml.	E , mv.
2.040	0.08	22.440	1.34	42.840	2.25
4.080	.23	24.480	1.44	44.880	2.31
6.120	.36	26.520	1.52	46.920	2.38
8.160	.49	28.560	1.58	48.960	2.44
10.200	.63	30.600	1.66	51.000	2.50
12.240	.76	32.640	1.76	53.040	2.58
14.280	.87	34.680	1.87	55.080	2.65
16.320	1.00	36.720	1.97	57.120	2.72
18.360	1.12	38.760	2.08	59.160	2.79
20.400	1.23	40.800	2.16	61.200	2.85

$$(\text{Ag}^+)_A = (\text{Ag}^+)_i \frac{V_i}{V} e^{-EF/RT}$$

The concentration of silver complexed is then obtained

$$(\text{AgF}) = (\Sigma \text{Ag}^+)_A - (\text{Ag}^+)_A \quad (6)$$

where $(\Sigma \text{Ag}^+)_A$ is the total stoichiometric silver concentration. The concentrations of H^+ , F^- , HF and HF_2^- were obtained by solving equations 2 and 3 and allowing for the fluoride complexed by silver. A plot of the values of $(\text{AgF})/(\text{Ag}^+)$ vs. (F^-) is shown in Fig. 1 for all of the 25° experiments. It is seen that the data are fitted well assuming only the first complex to be important—a reasonable result since only a small fraction of the silver was ever complexed.

The equilibrium quotients found at the three temperatures are given in Table III along with an estimate of the true equilibrium constant at 25° , made using the activity coefficient of silver nitrate. From the temperature dependence data the values of ΔH_{298} and ΔS_{298} for reaction 1 at an ionic strength of 0.50 are -2.8 ± 1.0 kcal. and -10 ± 4 e.u., respectively. The uncertainties were estimated by assuming an error of 0.1 mv. in the potential.

TABLE III

EQUILIBRIUM QUOTIENT FOR THE FLUORIDE COMPLEXING OF SILVER ION

Temp., $^\circ\text{C}$.	15	25	35
$Q_1 (\mu = 0.50 M)$	0.77	0.68	0.56
$K_1 (\mu = 0)$		2.4	

Leden and Marthen³ studied the same reaction using silver-silver chloride electrodes at an ionic strength of 1.0 and 25° . Correcting their value of 0.48 to an ionic strength of 0.50 by means of the activity coefficient of silver nitrate yields a value of 0.75 which is in fair agreement with the present value of 0.68.

Stannous Ion. E.M.F. Measurements.—The initial conditions of 8 of 14 e.m.f. titration experiments are shown in Table IV along with the highest stoichiometric fluoride concentration. All but one of the other experiments were of lower acidity. The complete data are given elsewhere.¹¹

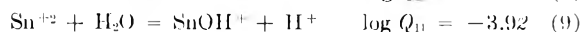
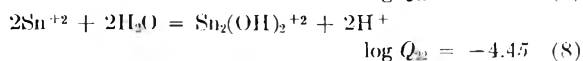
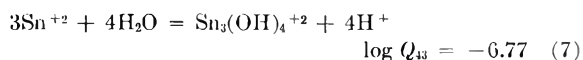
TABLE IV

Expt.	INITIAL CONDITIONS FOR TIN EXPERIMENTS					
	HClO_4 , M	$\text{Sn}(\text{ClO}_4)_2$, M	NaClO_4 , M	Highest (ΣF^-)	μ	Q_{10}
4	0.1605	0.03947	0.2214	0.14	0.50	18.8
5	.1633	.09541	.0506	.13	.50	13.8
7	.08965	.06849	.2047	.14	.50	8.8
8	.4225	.01580	.00	.12	.50	25.0
9	.3998	.03359	.00	.12	.50	18.2
11	1.6936	.01603	.2584	.16	2.00	10.6
12	1.6723	.1044	.0210	.21	2.00	8.0
14	1.7085	.003995	.2794	.16	2.00	11.2

The behavior of the cell can be described by an equation analogous to that of the silver experiments

$$(\text{Sn}^{++})_A = (\text{Sn}^{++})_i e^{-EF/2RT}$$

In applying this equation it is necessary to correct for any hydrolysis of stannous ion. Tobias¹⁴ has discussed the literature and reported his own results for a 3 M NaClO_4 solution at 25°



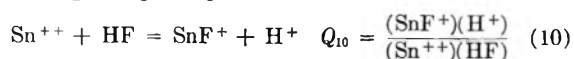
At 0.1 M H^+ and 0.1 M Sn^{++} one calculates that there would be only 0.2% of the tin hydrolyzed at $\mu = 3 M$. It seems likely that at $\mu = 0.5 M$ the hydrolysis would still be small.

Because the above data were not available when the present work was done, a side experiment was performed in which the stannous ion activity was measured using the tin amalgam electrode coupled with hydrogen reference electrode. The acidity

(14) R. S. Tobias, *Acta Chem. Scand.*, **12**, 198 (1958).

was kept constant while the stannous concentration was varied. Two sets of experiments were performed, one set at 1 *M* HClO₄ and the other at 0.1 *M* HClO₄ plus 0.9 *M* NaClO₄. In both cases, a plot of e.m.f. vs. log (Sn⁺⁺) revealed a straight line with the correct theoretical slope from 0.1 to 0.001 *M* Sn⁺⁺. Thus, there was no evidence of the presence of any polymeric tin species. Comparison between the experiments gave no indication of hydrolysis. Deviations from the straight line occurred below 0.001 *M* Sn⁺⁺, but these could be explained by oxidation of some of the tin to Sn(IV).

An attempt was made to interpret the high acid data of Table IV, *i.e.*, expts. 11, 12 and 14, by plotting the quantity (complexed stannous ion)/(uncomplexed stannous ion) vs. (HF)/(H⁺), assuming the principal reaction to be



A straight line through the origin of slope Q_{10} should be obtained if reaction 10 is the only important equilibrium. The experimental curves showed a small, relatively sharp curvature (concave upwards) near the origin that might have been due to a small amount of Sn(IV) being complexed preferentially by fluoride ion. As (HF)/(H⁺) increased the curves were fairly straight but deviated upwards, as expected if higher complexes were becoming important. From the slope at relatively low (HF)/(H⁺), the values of Q_{10} indicated in the last column of Table IV were estimated.

At lower acidity somewhat higher and more variable values of Q_{10} were found. In addition the data of experiments 5 and 7, when interpreted as above, indicated that more than one stannous ion was used per fluoride ion at low fluoride concentrations, suggesting the existence of polymers such as Sn₂F⁺³.

It is obvious from Table 4 that Q_{10} is not constant. Several interesting features were noted from the variation of Q_{10} with acidity and stannous concentration. For a given μ , the highest values of Q_{10} are obtained when the acidity is high and the total stannous concentration low (Experiments 8 and 14). For a given total stannous ion concentration, Q_{10} does not vary much with acidity (Experiments 4 and 9, 5 and 12, 8 and 11). At constant acidity and varying stannous concentration, Q_{10} varies widely (Experiments 4 and 5, 11 and 12, 8 and 9). This effect was greater at the lower acidities.

The cause of these discrepancies is not apparent. If one attempts to interpret the data assuming the principal reaction to be $2\text{Sn}^{++} + \text{HF} = \text{Sn}_2\text{F}^{+3} + \text{H}^+$, the discrepancies are even worse, since one essentially divides the Q_{10} values in Table IV by (Sn⁺⁺). Interpretation assuming the reaction to be $\text{SnOH}^+ + \text{HF} = \text{SnF}^+ + \text{H}_2\text{O}$ likewise proved futile. More than one equilibrium should probably be considered at the low acidities, but such calculations are extremely difficult. At high acid, however, it seems that no combination of equilibria would account for the discrepancies.

The reproducibility of the experiments was shown by repeating expts. 4 and 12 under identical condi-

tions. Each e.m.f. reading of the repeat experiments agreed with the original result to within 0.05 mv. A third experiment was repeated using dilute tin amalgam instead of saturated amalgam in the electrode and again the two sets of results checked to within 0.05 mv.

Tin or tin amalgam electrodes have been used by Vanderzee,¹⁵ Prytz¹⁶ and Duke and Courtney¹⁷ to study the chloride complexing of stannous ion. All of these investigators worked at stannous ion concentrations less than 0.01 *M*, and all except Prytz worked at acidities of 2 or 3 *M*. The fact that the equilibrium constants of all these workers are self-consistent, and the fact that the constants are the same order of magnitude as those obtained by conductivity,¹⁸ light absorption¹⁹ and kinetics,²⁰ seems to indicate that the electrodes were behaving properly, at least in solutions whose stannous ion concentration was less than 0.01 *M*.

It was suggested that perhaps the stannic fluoride complexes were stable enough to cause a disproportionation reaction such as $2\text{Sn}^{++} + \text{F}^- = \text{SnF}^{+3} + \text{Sn}$ to occur. This postulate was tested by titrating solutions of Sn⁺⁺, H⁺, F⁻ and ClO₄⁻ with triiodide solution. The stannous concentrations were 0.01 or 0.1 *M*, and the fluoride concentration in each case varied from 0 to about 0.1 *M*. Within experimental error the amount of triiodide required for the titrations was the same as that required for a solution with no added fluoride. Further, no precipitate of metallic tin was visible in any of the solutions.

Spectrophotometric Measurements.—The complexing was studied further by measuring the (HF)/(H⁺) concentration by an entirely different method. This was done spectrophotometrically by studying the competition between uranyl ion and stannous ion for fluoride ion. The measurements were made with a Beckman Model DU spectrophotometer at 4750 Å. where the percentage difference in optical density between uranyl perchlorate solutions and uranyl perchlorate solutions containing sodium fluoride was greatest. There was the disadvantage, however, that the extinction coefficient of uranyl ion in this region is so low ($\epsilon = 0.27$) that it was necessary to work at rather high (0.04 *M*) uranyl concentrations. This made the calculations difficult, since one did not know the (HF)/(H⁺) ratio with any certainty. It was not possible to work in the ultraviolet region where uranyl ion has a high extinction coefficient because of the intense absorption of stannous ion in this region.

A series (No. 1) of solutions was prepared with $\Sigma\text{UO}_2^{++} = 0.0387$ *M*, (H⁺) = 0.5 *M*, and $\Sigma\text{F}^- = 0-0.2$ *M*. A second series (No. 2) was prepared with the same uranyl and fluoride concentrations, but with (H⁺) = 0.09 *M*. The ionic strength

(15) C. E. Vanderzee and D. E. Rhodes, *J. Am. Chem. Soc.*, **74**, 3552 (1952).

(16) M. Prytz, *Z. anorg. allgem. Chem.*, **172**, 147 (1928).

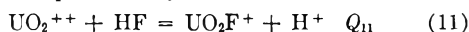
(17) F. R. Duke and W. G. Courtney, *Iowa State Coll., J. Sci.*, **24**, 397 (1950).

(18) S. W. Young, *J. Am. Chem. Soc.*, **23**, 20 (1909).

(19) H. Fromherz and H. J. Wells, *Z. physik. Chem.*, **A178**, 29 (1936).

(20) F. R. Duke and R. C. Pinkerton, *J. Am. Chem. Soc.*, **73**, 3045 (1951).

was ca. 0.65 M in both cases. From these data an equilibrium quotient Q_{11} for the reaction



was calculated. The calculations were performed by first assuming a value of Q_{11} from which $(\text{HF})/(\text{H}^+)$ was calculated. Knowing $(\text{HF})/(\text{H}^+)$ the extinction coefficient of (UO_2F^+) could be determined. This quantity was calculated for various values of Q_{11} , and the value of Q_{11} which gave the most constant $\epsilon_{\text{UO}_2\text{F}^+}$ was taken to be the true value. The value of Q_{11} was found to be 15, which agrees reasonably well with the value at 25° and $\mu = 0.5$ of 25 reported by Day and Powers²¹ from extraction studies with TTA. The value of $\epsilon_{\text{UO}_2\text{F}^+}$ was found to be 1.43. At total fluoride ion concentrations greater than 0.01 M , the species UO_2F_2 begins to become important. No calculations were made of equilibria involving this species.

Series 1 and 2 described in the preceding paragraph were again prepared, this time containing 0.01669 M Sn^{++} and 0.06674 M Sn^{++} , respectively. These conditions were such as to resemble very closely the conditions for e.m.f. experiments 8 and 7. Titration with triiodide after the optical density measurements were made indicated that less than 1% of the total tin was oxidized to $\text{Sn}(\text{IV})$.

The optical density D of uranyl fluoride solutions under conditions where the principal species is UO_2F^+ is given by the equation

$$\frac{D}{(\Sigma\text{UO}_2^{++})(l)} = \frac{\epsilon_0 + Q_{11} \epsilon_1 \frac{(\text{HF})}{(\text{H}^+)}}{1 + Q_{11} \frac{(\text{HF})}{(\text{H}^+)}}$$

where l is the cell length in cm., ϵ_0 the extinction coefficient of UO_2^{++} , and ϵ_1 the extinction coefficient of UO_2F^+ . The $(\text{HF})/(\text{H}^+)$ ratio for uranyl solutions containing stannous ion can be calcu-

(21) R. A. Day and R. M. Powers, *ibid.*, **76**, 3895 (1954).

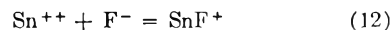
lated from this equation. Knowing $(\text{HF})/(\text{H}^+)$, the SnF^+ concentration can be calculated from the equations

$$\begin{aligned} (\Sigma\text{UO}_2^{++}) &= (\text{UO}_2^{++}) + (\text{UO}_2\text{F}^+) \\ (\Sigma\text{F}^-) &= (\text{HF}) + (\text{F}^-) + (\text{UO}_2\text{F}^+) + (\text{SnF}^+) \end{aligned}$$

Values of Q_{10} were calculated for series 1 and 2. In the case of series 1, Q_{10} was found to be a constant with a value of 24, which agrees exceptionally well with the value of 25 obtained in experiment 8 of the e.m.f. measurements. For series 2, Q_{10} was found to vary from 5 to 12, increasing regularly with increasing fluoride concentration. This is of the same order of magnitude as was found in experiment 7 of the e.m.f. measurements, *i.e.*, 8.0.

Although the spectrophotometric method is not nearly so accurate as the e.m.f. method, yet it does confirm the e.m.f. measurements and indicates that the tin amalgam-stannous ion electrode was functioning properly. Consequently the cause of the variability of Q_{10} remains unknown. Clearly this system needs further study.

Due to the variation with stannous concentration, it is impossible to quote a precise value for Q_{10} . However, from e.m.f. experiments 11 and 14 at high acid, it would seem that the best value of Q_{10} at $\mu = 2.00$ is about 11. It should be noted that this value does not appear to hold for stannous ion concentrations greater than 0.01 M . For the reaction in terms of F^-



Q_{12} is about 10^4 at $\mu = 2.00$ and estimated to be about 7×10^4 at $\mu = 0$. These results are in qualitative agreement with the polarographic work of Schaap, *et al.*,⁴ on the stability of SnF_3^- , if one assumes that the stability of the successive fluoride complexes decreases by a factor of 10; they reported $Q = 8 \times 10^9$ for the reaction $\text{Sn}^{++} + 3\text{F}^- = \text{SnF}_3^-$ at $\mu = 0.8 M$.

THE ELECTRICAL CONDUCTIVITY OF SOLUTIONS OF METALS IN THEIR MOLTEN HALIDES. II. SODIUM-SODIUM IODIDE, POTASSIUM-POTASSIUM IODIDE, AND POTASSIUM-POTASSIUM FLUORIDE¹

BY H. R. BRONSTEIN AND M. A. BREDIG

Chemistry Division, Oak Ridge National Laboratory, Oak Ridge, Tennessee

Received January 30, 1961

The study of the alkali metal-halide systems was extended to NaI-Na , KI-K and KF-K . The results confirm the striking difference in the behavior of the sodium and potassium solutions at the particular test temperatures. The equivalent conductance of the dissolved metal rises monotonically toward that of the pure metal in the case of potassium, but goes through a deep minimum in the case of sodium. In the latter case, electrons are thought to be trapped in the covalent bonds of Na_2 molecules. The enhancing effect of the polarizability of the anion upon the equivalent conductance of the metal in dilute solutions, Λ_M^∞ , is again demonstrated: *e.g.*, at 900°, Λ_M^∞ in KF-K is 800, but in KI-K is 8100 $\text{ohm}^{-1} \text{cm}^2 \text{equiv}^{-1}$. The difference in the power of the cations Na^+ and K^+ to polarize the large I^- anion, and thus to lower the potential barrier for electron movement, is seen reflected in the difference of Λ_M^∞ , 16,000 $\text{ohm}^{-1} \text{cm}^2 \text{equiv}^{-1}$ for NaI-Na as against 8100 for KI-K .

Introduction

In an attempt to elucidate the nature of solutions of metals in their molten halides, a study of the

electrical conductance appeared to have particular merits as it was likely to give some direct information on the state of the electron carried by the metal atom into the salt solution. Thus, the first paper²

(1) Work performed for the U. S. Atomic Energy Commission at the Oak Ridge National Laboratory operated by the Union Carbide Corporation, Oak Ridge, Tennessee.

(2) H. R. Bronstein and M. A. Bredig, *J. Am. Chem. Soc.*, **80**, 2077 (1958).

dealing with the conductivity in the alkali metal-halide systems demonstrated a large contribution by the dissolved metal to the electrical conductance, proving the presence of mobile electrons. This is in distinction from findings in other systems ($\text{CdCl}_2\text{-Cd}$,³ $\text{BiCl}_3\text{-Bi}$ ⁴ and $\text{CaCl}_2\text{-Ca}$ ⁵) where conductivity decreased on addition of metal. The following is a report on an extension of the earlier measurements² to a number of additional alkali metal-halide systems, namely, NaI-Na , KI-K and KF-K , intended to illustrate still more clearly some of the previous conclusions. The pair of iodide systems was chosen to verify the effect, discussed earlier,² of the different polarization of a highly polarizable anion such as I^- by the two cations Na^+ and K^+ , differing considerably in size and, therefore, in polarizing power. The potassium fluoride system was investigated because anion polarization by the cation is here at a minimum among the alkali halide systems studied, and thus a relatively low conductivity of the dissolved metal, in dilute solutions, was expected.

Experimental

The apparatus and procedure for the electrical conductance measurements on these solutions has been fully described in the first paper.² Since magnesium oxide is inert to molten potassium fluoride, a cell fabricated from a single crystal was used in the KF-K solutions. For the other solutions, a cell of single crystal aluminum oxide was used as in the previous work.

Commencing with approximately 14 mole % potassium in potassium iodide, the resistance of the solutions (cell constant 265 cm^{-1}) rapidly decreased with increasing concentration of potassium to below 10 ohms. As a check on the accuracy of the resistance measurements in this range, the resistance of the solutions was measured both by the Jones bridge and a modified transformer bridge.⁶ This bridge was designed originally for use with a four terminal type conductivity cell, two current carrying electrodes and two potential probe electrodes. This arrangement was easily modified for use with only two electrodes by simply connecting a current-carrying lead and potential-probe lead together at each of the two electrodes. The same lead resistance correction of 0.15 ohm was thus applicable to both types of measurements. By the use of this bridge, it was possible to continue the measurements to approximately 42 mole % potassium in potassium iodide. In the range of 10 to 1.0 ohm, the agreement between the Jones bridge and the transformer bridge was 0.2%. Below 1.0 ohm, the lack of sensitivity of the Jones bridge led to variations of from 0.5 to 3.0% between the two; therefore, the transformer bridge value was taken as nearer the correct value.

Sodium iodide and potassium iodide were of reagent grade and were dried at 180° for several days before use. Anhydrous reagent grade potassium fluoride was loaded directly into the apparatus. Each salt was further dehydrated in the apparatus by vacuum drying at temperatures up to 50° below their melting points until a pressure of approximately 20 μ of Hg was obtained. At this point, the system was pressurized with argon to 45 p.s.i. absolute and the salt melted. Samples of salt treated in this manner never showed alkalinity from hydrolysis. The conductivity of pure sodium iodide agreed with the value obtained by Van Artsdalen and Yaffe⁷ to 0.2%. A plot of the specific conductivity of KI vs. temperature differed in curvature from that of Yaffe and Van Artsdalen⁸ with a maximum negative

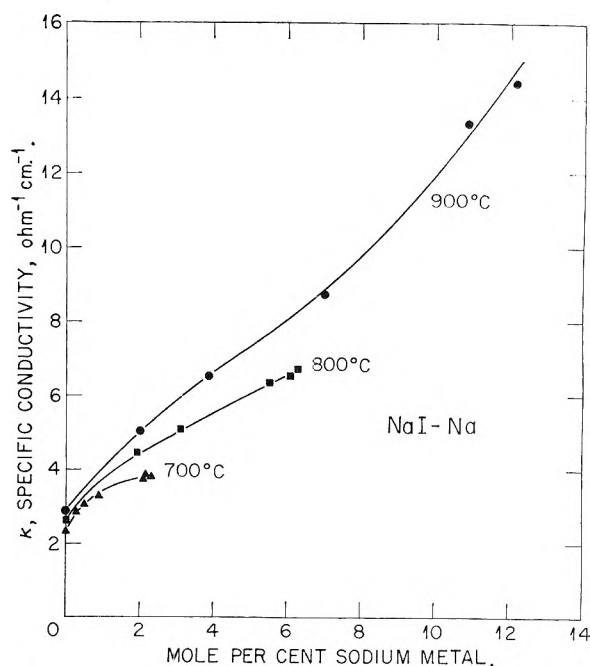


Fig. 1.—Specific conductance vs. metal concentration for solutions of Na in NaI.

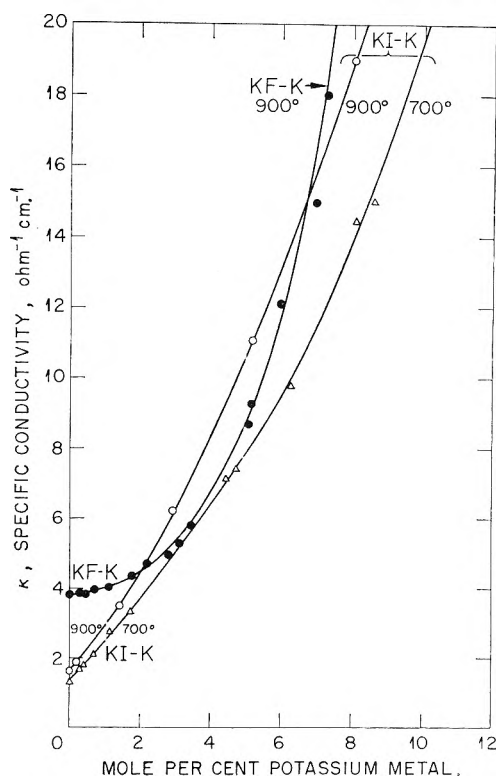


Fig. 2.—Specific conductance vs. metal concentration for solutions of K in KF and KI.

deviation of 5% at 780°. The specific conductivity of potassium fluoride agreed within 1.0% with the values of Yim and Feinleib⁹ over the temperature range 875 to 945°, but dis-

above the melting point to the melting point of potassium iodide, an effect not observed with the other alkali halides. Our data gave a slight temperature dependence of the apparent heat of activation for conductance quite similar to the other alkali halides.

(9) E. W. Yim and M. Feinleib, *J. Electrochem. Soc.*, **104**, 626 (1957).

(3) A. H. W. Aten, *Z. physik. Chem.*, **73**, 578 (1910).

(4) A. H. W. Aten, *ibid.*, **66**, 641 (1909).

(5) D. D. Cubicciotti, MDDC-1058 (1946-1949).

(6) E. Fairstein, "An A.C. Bridge for Measuring Low Resistances," in Oak Ridge National Laboratory Instrumentation and Controls Division Semiannual Progress Report, ORNL-1997, 9 (July 31, 1955).

(7) E. R. Van Artsdalen and I. S. Yaffe, *J. Phys. Chem.*, **59**, 118 (1955); **60**, 1125 (1956).

(8) Yaffe and Van Artsdalen's plot of the apparent heat of activation, ΔH^* , for conductance vs. $(t - t_m)^9$ shows a rapid rise from 60°

TABLE I
 CONDUCTIVITY OF SOLUTIONS OF ALKALI IN THEIR MOLTEN HALIDES

Temp., °C.	Mole % metal	Soln. sp. cond., ohm ⁻¹ cm. ⁻¹	Metal equiv. cond., × 10 ⁻³ , ohm ⁻¹ cm. ² equiv. ⁻¹	Temp., °C.	Mole % metal	Soln. sp. cond., ohm ⁻¹ cm. ⁻¹	Metal equiv. cond., × 10 ⁻³ , ohm ⁻¹ cm. ² equiv. ⁻¹
Sodium-sodium iodide				Potassium-potassium fluoride			
704	0.00	2.38	(16.0) ^a	902	0.00	3.80	(0.80) ^a
704	.30	2.85	8.8	901	0.32	3.86	1.13
712	.54	3.10	7.2	892	0.45	3.86	1.03
704	.92	3.31	5.6	908	0.45	3.84	0.45
706	2.09	3.76	3.7	911	0.73	3.98	0.92
696	2.35	3.80	3.4	900	1.16	4.05	0.97
702	2.15	3.86	3.9	906	1.78	4.40	1.48
				909	2.20	4.67	1.47
800	0.00	2.66	(>12.0)	897	2.82	4.99	1.61
801	1.95	4.46	5.3	893	3.17	5.34	1.85
799	3.12	5.13	4.6	916	3.44	5.81	2.12
798	5.47	6.37	3.9	916	5.09	8.64	3.51
803	6.32	6.75	3.7	911	5.16	9.24	3.66
797	6.08	6.59	3.7	905	6.07	12.10	4.80
				911	7.04	15.10	5.58
900	0.00	2.92	(>12.0)	912	7.27	18.10	6.77
899	2.01	5.05	6.3	908	8.96	30.60	10.36
894	3.89	6.57	5.6	909	9.10	31.20	10.43
899	7.01	8.75	4.9	910	9.19	34.80	11.67
899	10.93	13.40	5.5	910	11.04	57.50	17.00
897	12.15	14.40	5.4	912	12.68	80.00	21.25
Potassium-potassium iodide							
708	0.00	1.33	(8.2) ^a	801	12.1	33.3	18.4
707	0.29	1.69	8.7	801	14.0	46.9	22.6
708	0.31	1.70	8.3	799	16.8	64.8	26.2
710	0.37	1.75	8.1	798	18.2	78.0	29.2
704	0.46	1.89	8.6	796	22.2	118.0	36.0
710	0.64	2.07	8.0	798	22.9	131.0	38.8
705	1.20	2.80	8.5	801	24.1	139.0	39.0
703	1.75	3.29	7.8	794	25.7	161.0	42.5
699	4.44	7.11	9.2	795	27.9	197.0	47.8
708	4.77	7.40	8.7	800	30.5	251.0	55.6
703	5.15	9.79	9.4	800	32.8	302.0	61.0
706	8.12	14.4	11.0	804	33.0	312.0	63.5
697	8.61	15.0	10.8	802	35.0	350.0	67.2
706	11.6	26.1	14.5	803	36.8	409.0	74.4
695	11.8	27.5	14.9	804	38.4	443.0	76.9
709	13.9	37.6	17.5	799	40.3	566.0	93.4
701	15.6	50.0	20.9	805	42.2	602.0	94.7
708	16.4	58.5	23.3				
700	18.5	75.7	26.7	896	0.00	1.64	(8.1) ^a
705	20.5	94.7	30.3	895	0.21	1.86	7.9
706	22.7	114.0	33.0	899	1.43	3.46	9.5
706	22.8	119.0	34.4	899	2.94	6.20	11.6
705	23.3	120.0	33.7	898	5.19	11.0	13.4
730	24.5	139.0	37.4	896	8.02	19.0	15.9
735	36.9	408.0	72.1	897	9.32	24.1	18.0
				897	11.2	31.7	19.6
806	0.00	1.51	(8.0) ^a	892	12.3	39.6	22.6
799	0.35	1.88	7.9	893	14.2	48.5	24.0
800	0.60	2.20	8.5	901	15.7	62.9	28.3
799	2.51	4.78	9.4	892	16.8	68.3	28.6
803	5.41	10.50	11.8	898	18.2	83.1	32.3
802	6.46	13.60	13.3	894	23.6	137.3	41.0
806	7.84	16.5	13.6	899	26.1	168.8	45.6
801	8.67	19.8	14.9	899	32.6	303.6	65.1
800	10.8	27.2	16.8				

^a Extrapolated value.

agreed considerably (e.g., + 4.5% at 900°) with those of Winterhager and Werner.¹⁰ The latter authors employed a frequency of 40 K.c.p.s. which undoubtedly produced an inductive effect with a resulting increase in apparent resistance.

Results and Discussion

Table I contains the results for the following solutions: Sodium dissolved in molten sodium iodide, potassium in potassium fluoride, and potassium in potassium iodide. Maximum concentration limits in the case of the sodium iodide solutions were imposed by the solubility of sodium metal in the molten iodide.¹¹ In the measurements on the KI-K system, the limitation was imposed by the questionable accuracy of the measurement of small resistances, at higher metal concentrations. The higher vapor pressure of potassium in the less ideal system KF-K prevented measurements above 13 mole % K. At this concentration, the conductivity of the solution was more than 20 times the conductivity of the pure salt. However, the specific conductivity of the solutions of K in KI was followed to a value as high as 400 times that of the pure salt. The equivalent conductance of the dissolved metal, Λ_M , was calculated according to the equation in the same manner as previously.²

$$\Lambda_M = [\Lambda_{\text{soln.}} - (1 - X_M)\Lambda_{\text{salt}}]/X_M$$

Figures 1 and 2 are plots of the *specific* conductance vs. concentration expressed in mole % metal. The *specific* conductivity rises monotonically with metal concentration as in the four systems studied previously. Figure 3 is a plot of the *equivalent* conductance of the metal vs. concentration. Here again is demonstrated the remarkable difference between sodium and potassium at the test temperatures: The equivalent conductance of the metal rises monotonically in the KF-K and KI-K systems, e.g., at 900° from 8,100 and 8,100 $\text{ohm}^{-1}\text{cm}^2\text{equiv.}^{-1}$, respectively, at "infinite dilution." It was found to drop sharply in the NaI-Na system, namely from more than 12,000 $\text{ohm}^{-1}\text{cm}^2\text{equiv.}^{-1}$ to a minimum of 4,800 $\text{ohm}^{-1}\text{cm}^2\text{equiv.}^{-1}$ at 7.5 mole % Na. At 800 and 700°, the minima occurring at slightly lower metal concentrations are 3,600 and 2,100 $\text{ohm}^{-1}\text{cm}^2\text{equiv.}^{-1}$, as estimated by extrapolation of the conductivity vs. metal concentration curves beyond the solubility limits. The occurrence of similar minima in the NaCl-Na and NaBr-Na systems in combination with the observed positive deviation from Raoult's law¹¹ was interpreted² in terms of the formation of diatomic molecules, Na_2 . The large drop from 16,000 to 2,100 $\text{ohm}^{-1}\text{cm}^2\text{equiv.}^{-1}$ at 700° in the NaI-Na system is particularly noteworthy. It shows that it is not just the total number of metal particles, monomers and dimers, present per metal equivalent that determines the equivalent conductance of the metal, but that the "trapping" of the electrons in the lower energy state of the covalent bonds of the diatomic molecules inhibits their participation in the conduction process. As explained previously,² the indicated increase in the equivalent conductance

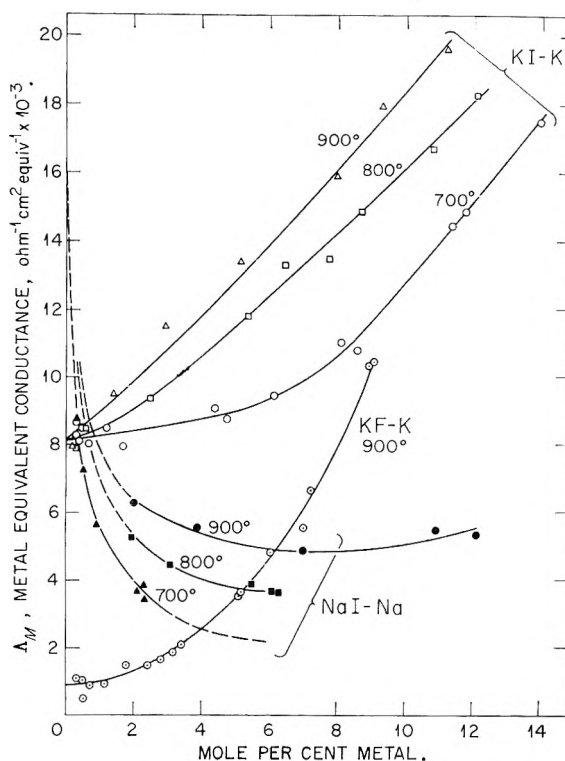


Fig. 3.—Equivalent conductance of metal, Λ_M , vs. metal concentration for NaI-Na, KI-K and KF-K systems. (KF-K curve not fully shown to avoid interference with KI-K.)

beyond the minima in the sodium systems is interpreted as being due to the gradual establishment of the metallic conduction band by overlap of the orbitals of the diatomic metal molecules in the salt melt.

The relatively greater lowering of the equivalent conductance to the minimum, in going from the chloride to the iodide system, may indicate that the association constant is largest in the iodide system. This may be due to the more effective shielding of the Na^+ ions by the larger iodide ions; or, in other words, the solvation of sodium atoms by sodium ions competes less effectively in going from chloride to iodide.

It appears that, as expected, the connection of the equivalent conductance with the state of association of the metal is also reflected in the KI-K system, although to a much lesser degree than in the NaI-Na solutions. Especially between 3 and 12 mole % K (Fig. 3), the temperature coefficient of the equivalent conductance of the potassium metal is much larger in the temperature interval between 700 and 800°, below and near the consolute temperature of 717° than between 800 and 900° where the metal solution is more nearly ideal, or monodispersed. Measurements at the highest metal concentrations reached thus far, ca. 40 mole % potassium, indicate that the temperature coefficient all but vanishes in that region. At still higher metal concentrations, the temperature coefficient is expected to become negative as the conduction process would more closely resemble that of the pure metal.

In the previous paper,² a strong dependence of

(10) H. Winterhager and L. Werner, *Forschungsber. Wirtschafts-u. Verkehrsministeriums Nordrhein-Westfalen*, 438 (1957).

(11) M. A. Bredig and H. R. Bronstein, *J. Phys. Chem.*, **64**, 64 (1960), and earlier papers in that series.

the equivalent conductance at "infinite dilution" of the alkali metal dissolved in its alkali halide on the nature of both the anion and the cation of the salt was noted. On this basis, it was expected that Λ_M^∞ of K metal dissolved in KF would reach a value lower than any in the alkali metal-halide systems (except Cs or Rb in their fluorides) and that Λ_M^∞ of K in KI should have a value higher than that in the bromide. Also, Λ_M^∞ for Na in NaI should lie above that of the bromide and represent a maximum among these systems (except possibly for LiI). This has been verified in the present investigation (Table II). As proposed earlier,² the anion effect

is believed to be connected with the polarizability of the anion: electron transfer between two oxidation states of a metallic element is known to be greatly facilitated by greater polarizability of the anion.^{12,13} The polarizability of the fluoride ion (0.99 Å.³) is very low compared with that of the chloride, bromide or iodide ion (3.05, 4.17, 6.28 Å.³, respectively). The greater Λ_M^∞ in the sodium systems as compared with the potassium systems containing the same anion is not fully understood at present. Possibly a lowering of the negative charge on the anion by a slightly more strongly polarizing cation such as Na⁺ might facilitate electron transfer by lowering the potential barrier to electron motion, which the anions represent.

Acknowledgment.—Helpful discussions with Professor William T. Smith, Jr., University of Tennessee, Chemistry Department, are gratefully acknowledged.

- (12) H. Taube and H. Myers, *J. Am. Chem. Soc.*, **76**, 2103 (1954).
 (13) C. Zener, *Phys. Rev.*, **82**, 403 (1951).

TABLE II
EQUIVALENT CONDUCTANCE OF METAL IN ALKALI METAL-HALIDE SYSTEMS AT INFINITE DILUTION (900°)

Metal	Λ_M^∞ (ohm ⁻¹ cm. ² equiv. ⁻¹)			
	F	Cl	Br	I
Na		6000	13,000	16,000
K	800	2800 (820°)	6,500 (870°)	8,100

THERMOCHEMICAL STUDIES. V.¹ HEATS OF STEPWISE NEUTRALIZATION OF ETHYLENEDIAMINE AND DIETHYLENETRIAMINE

BY MARIO CIAMPOLINI AND PIERO PAOLETTI

Istituto di Chimica Generale e Inorganica dell'Università di Firenze, Florence, Italy

Received January 30, 1961

The results of a calorimetric investigation of the stepwise heat of neutralization for ethylenediamine in *M* KCl and for diethylenetriamine in 0.1 *M* KCl are presented.

Introduction

In the course of calorimetric investigations on the heat of formation of metal complexes with ethylenediamine (en)² and diethylenetriamine (den),¹ it was necessary to know the accurate values of the stepwise heats of neutralization for these polyamines. Heats of neutralization of ethylenediamine determined both calorimetrically and potentiometrically are reported in the literature,^{3,4} whereas only potentiometric values are known for diethylenetriamine.^{4,5} All these values, however, are referred to ionic media different from those used by us and often disagree one with the other. Hence it seemed worthwhile to determine, by direct calorimetric measurement, the heat changes for the successive stages of neutralization of these two amines in the same ionic medium used for the metal systems. A *M* KCl solution for ethylenediamine and a 0.1 *M* solution for diethylenetriamine were employed.

The results of these investigations are discussed below.

- (1) Part IV, M. Ciampolini, P. Paoletti and L. Sacconi, *J. Chem. Soc.*, in press.
 (2) M. Ciampolini, P. Paoletti and L. Sacconi, *ibid.*, 4553 (1960).
 (3) T. Davies, S. S. Singer and L. A. K. Staveley, *ibid.*, 2304 (1954).
 (4) G. H. McIntyre, Jr., B. P. Block and W. C. Fernelius, *J. Am. Chem. Soc.*, **81**, 529 (1959).
 (5) H. B. Jonassen, R. B. LeBlanc, A. W. Meibohm and R. M. Rogun, *ibid.*, **72**, 2430 (1950).

Experimental

Materials.—Anhydrous ethylenediamine and diethylenetriamine were put twice through a Todd fractionating column. The cuts of these two bases used in the experiments were analyzed by potentiometric titration against hydrochloric acid and found to be 99.9 and 99.6% pure, respectively. Approximately *M* solutions of these amines were made up with carbon dioxide-free potassium chloride solutions of the same ionic strength used in the measurements. The concentrations of these solutions were determined by potentiometric titration against ca. 1.5 *N* hydrochloric acid which had been standardized gravimetrically as silver chloride. This same hydrochloric acid was used in the measurements of the heat of neutralization.

Calorimetric Measurements.—The calorimeter, described in a previous paper,⁶ was placed in a thermostatic bath at 25.000 ± 0.005°. Its capabilities have been tested by measurements of the heat of solution of potassium chloride in water, in the molar ratio 1:167 at 25°. The mean of eight determinations was 4194 ± 5 cal./mole. The values reported in the literature, corrected for this dilution, are: 4184 ± 8,³ 4187.⁷ For each run the bottle was filled with a weighed amount of the amine stock solution. Hydrochloric acid was placed in the dewar flask and the volume made up by adding carbon dioxide-free potassium chloride solution of the desired ionic strength. The final volumes (Table I) were evaluated from the known weights of the reactants and the final density of the calorimetric liquid. The heats of dilution of the hydrochloric acid were measured by diluting a weighed sample of it in the same volume of the ionic medium as with the experiments with

- (6) L. Sacconi, P. Paoletti and M. Ciampolini, *Ricerca Sci.*, **29**, 2412 (1959); *J. Am. Chem. Soc.*, **82**, 3828 (1960).
 (7) K. P. Mischenko and Yu. Ya. Kaganovich, *J. Appl. Chem., U. S. S. R.*, **22**, 1078 (1949).

amines. In every case the heat of dilution of the amine solution by the water contained in the hydrochloric acid solution was found to be negligible.

Results

In order to determine the over-all and stepwise heats of neutralization it is necessary to measure the heats evolved for different hydrochloric acid-amine ratios and to calculate the exact amount of the protonated forms of the polyamines before and after the reaction. The basicity constants employed were those of Edwards⁸ in *M* KCl at 25° for ethylenediamine and those of Prue and Schwarzenbach⁹ in 0.1 *M* KCl at 20° for the diethylenetriamine. The latter constants were corrected to 25° by using approximate ΔH values. The experimental results are shown in Table I. To check the reproducibility of these measurements, three independent sets of six runs were carried out for ethylenediamine but not all of these are reported here. The heat evolved, corrected for the heat of dilution of hydrochloric acid, is reported in the third column. Allowance must also be made for the heat effect due to the neutralization of hydroxyl ions which arise from the basic dissociation of the amine. This correction is recorded in the last column. The heats of stepwise neutralization were obtained by combining the results of runs carried out for different hydrochloric acid-amine ratios and solving the set of simultaneous equations

$$Q - Q_{\text{corr}} = b [(\alpha_{1\text{after}} - \alpha_{1\text{before}})\Delta H_1 + (\alpha_{2\text{after}} - \alpha_{2\text{before}})\Delta H_{1-2} + \dots]$$

where $\alpha_1, \alpha_2, \dots$, are the degrees of formation of the monoammonium, diammonium, etc., ions and b are the moles of amine used in each experiment.

TABLE I

CALORIMETRIC DATA FOR THE SYSTEMS POLYAMINE + HCl

Base	Base (10 ⁻⁶ mole)	HCl (10 ⁻⁶ mole)	Q (cal.)	Q _{corr} (cal.)
en (V 887 ml.) (M KCl)	3004	3000	367.0	27.2
	2994	3004	368.5	27.0
	2629	3356	402.0	25.4
	2672	3355	401.8	25.4
	1473	2984	339.2	18.8
	1470	2993	337.7	18.8
den (V 928 ml.)	3030	3038	348.0	17.0
	3034	3037	347.4	16.7
	3021	3025	346.2	16.6
	1511	3027	352.1	12.0
	1510	3038	353.3	12.0
	1509	3027	351.2	12.0
	975	3037	295.7	9.6
	991	3113	299.9	9.7
	1004	3102	303.7	9.7

Table II reports the values for the thermodynamic functions ΔF , ΔH and ΔS relative to the successive neutralization steps. The relative accuracies of the heats of stepwise and over-all neutralization are not the same. In fact, for each polyamine, measurements were carried out with such an excess of hydrochloric acid that practically only the fully protonated cation was present. Therefore, the accuracy of the over-all heat of

neutralization is of the same order of magnitude as the reproducibility of the calorimetric measurements, *viz.*, better than $\pm 0.2\%$. The heat changes for the successive stages of neutralization are, on the contrary, less accurate because of their critical dependence on the values of the basicity constants.

TABLE II

THERMODYNAMIC FUNCTIONS FOR THE SUCCESSIVE NEUTRALIZATION STAGES OF POLYAMINES AT 25°

	$-\Delta F$ (kcal./ mole)	$-\Delta H$ (kcal./ mole)	ΔS (e. u.)
en + H ⁺ → enH ⁺	13.90	12.20	5.7
enH ⁺ + H ⁺ → enH ₂ ²⁺	10.15	10.60	-1.5
den + H ⁺ → denH ⁺	3.35	11.20	7.2
denH ⁺ + H ⁺ → denH ₂ ²⁺	12.25	11.95	1.0
denH ₂ ²⁺ + H ⁺ → denH ₃ ³⁺	5.80	7.20	-4.7

Discussion

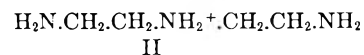
The ionic strength markedly affects the heats of neutralization of ethylenediamine, as is found by comparing our values in *M* KCl with those of Davies, Singer and Staveley in 0.1 *M* KCl.³ In fact, while the $-\Delta H_1$ increases with the ionic strength, the opposite is true for the $-\Delta H_2$; the over-all ΔH_{1-2} thus being nearly constant. It must be noted that the ionization constant values for ethylenediammonium ions *vs.* temperature over the 0.0-0.3 ionic strength range investigated by Everett and Pinsent,¹⁰ confirms such a trend for the heats of neutralization.

The heat change for the second neutralization stage is lower than for the first stage by *ca.* 1.6 kcal./mole. This can be accounted for, at least in part, in terms of the electrostatic repulsion of the two adjacent positive charges.

In contrast to ethylenediamine, diethylenetriamine may produce two tautomeric structures on linking a proton⁹



I



II

If by *A*(I) and *A*(II) we denote the amount of the isomers (I) and (II) and by k_a (I) and k_a (II) their acid dissociation constants, respectively, then

$$A(\text{I})/A(\text{II}) = k_a(\text{II})/k_a(\text{I})$$

Unfortunately, only the sum $k_a(\text{I}) + k_a(\text{II}) = k_{a3}$ has been measured whereas the individual values are unknown. Very likely, however, these two constants are of the same order of magnitude since the dissociation constant of ethylenediamine (a primary diamine, $pK_{a2}(15^\circ) = 10.25^{10}$) is nearly equal to that of piperazine (a secondary diamine, $pK_{a2}(15^\circ) = 9.95^{11}$). If such is the case, the two tautomers (I) and (II) will be present in comparable amounts.

The heat actually measured for the first neutralization stage is 11.20 kcal./mole, *i.e.*, 0.70 kcal./mole lower than that of the ethylenediamine in the same ionic medium. This may lead one to believe that the heat of neutralization of the diethylenetriamine secondary nitrogen is lower than that of the

(8) L. J. Edwards, *Diss.*, Univ. Michigan, 1950.

(9) J. Prue and G. Schwarzenbach, *Helv. Chim. Acta*, **33**, 985 (1950).

(10) D. H. Everett and B. R. W. Pinsent, *Proc. Roy. Soc. (London)*, **A215**, 416 (1960).

(11) I. M. Kolthoff, *Biochem. Z.*, **162**, 289 (1925).

primary nitrogen although the unknown influence of both the inductive effect of these chains as well as of hydration make this conclusion somewhat uncertain.

On the contrary only one form of the denH_2^{2+} ion probably exists. Prue and Schwarzenbach have hypothesized that the two protons are being tied to the two terminal nitrogens in such a way that the mutual electrostatic repulsion between positive charges is reduced. The enthalpy data are in agreement with this hypothesis. The value of the $-\Delta H_{1-2}$ for the denH_2^{2+} ion formation is higher than that for the enH_2^{2+} ion thus indicating that the repulsions in the first ion are actually smaller than in the second one. The heat change for the second neutralization stage is higher than that for the first stage by *ca.* 0.75 kcal./mole. This is in accordance with the hypothesis of a lower heat of neutralization for the secondary nitrogen and of the presence of two tautomeric forms in the first stage. In such a case the passage of the hydrogen ion from the secondary to the primary nitrogen, which takes place in the second stage, is accompanied by evolution of heat.

The neutralization of the third amine group of the diethylenetriamine is less exothermic than that of the first two. This is due to the repulsive action of the two adjacent electric charges, and, probably, to the fact that we are dealing with a secondary nitrogen.

For the first neutralization stage the entropy values are positive. This is in agreement with the hypothesis presented earlier for the heterocyclic

(12) L. Sacconi, P. Paoletti and M. Ciampolini, *J. Am. Chem. Soc.*, **82**, 3831 (1960).

bases containing nitrogen,¹² according to which the neutralization of the nitrogen atom is always accompanied by the release of a considerable number of water molecules and consequent increase of translational entropy. The successive entropies of neutralization decrease until they become negative, as it was found for other stepwise reactions between polyamines and ions of transition metals.^{1,2}

A decrease of successive neutralization entropy changes is expected as a consequence of statistical factors, but for ethylenediamine the decrease calculated on this basis^{10,13} ($R \ln 4 = 2.8$ e.u.) is much smaller than that found experimentally (7.2 e.u.). For the diethylenetriamine the calculation is not so straightforward due to the non-equivalence of the various nitrogen atoms, but it is unlikely that the statistical effect may be so pronounced to account completely for the decrease found. In addition to this there are other effects which contribute to the successive ΔS decreases, as for instance the chain stiffening due to the repulsion of hydrocarbon chain by the ammonium group, the former representing a region of low dielectric constant.¹⁰ This effect will increase in the di- and tri-ammonium ions on account of the repulsion between the positive charges.

Acknowledgments.—The authors are indebted to Prof. L. Sacconi for helpful suggestions and criticism. Acknowledgment is made to the Italian "Consiglio Nazionale delle Ricerche" for the support of this research.

(13) E. Q. Adams, *ibid.*, **38**, 1503 (1916); J. Bjerrum, "Metal Amine Formation in Aqueous Solution," Haase & Son, Copenhagen, 1957, p. 24.

CRITICAL PHENOMENA IN THIN FILMS USING THE BRAGG-WILLIAMS APPROXIMATION

BY K. NISHIKAWA, D. PATTERSON AND G. DELMAS

University of Montreal, Montreal, Canada

Received February 1, 1961

The critical properties of thin films of binary regular solutions are treated using the Bragg-Williams approximation. The lowering of the critical solution temperature is discussed as a function of film thickness, surface tension of the pure components and adsorption properties of a supporting solid substrate. The possibility of the existence of more than one critical point is considered.

Introduction

Some theoretical and experimental importance is attached to the effect of size and of the surface on the bulk properties of a system. These may be the melting temperature, critical solution point, heat capacity, etc. Saraga and Prigogine,¹ for instance, conclude that a surface layer of molecular thickness on a binary regular solution will have a critical temperature different from that exhibited by the bulk of the solution, and that, under certain conditions, an independent phase separation should be observable in the surface layer. We have considered the critical properties of films of a binary regular solution and the effect on the film thickness

and surface properties, including the role of adsorption on a supporting substrate. The results obtained are somewhat different from those of Saraga and Prigogine except for a particular case. The lattice model with the Bragg-Williams approximation has been employed, as originally introduced and used in the study of surface properties of solutions.²⁻⁴

Although fluctuations in the composition will be important near the critical point, the treatment should be adequate to give its position. After presenting the model, we treat the special and

(2) E. A. Guggenheim, "Mixtures," Oxford University Press, 1952, Chapter IX.

(3) I. Prigogine and R. Defay, *Trans. Faraday Soc.*, **46**, 199 (1956).

(4) F. Murakami, S. Ono, M. Tamura and M. Kurata, *J. Phys. Soc. Japan*, **6**, 309 (1951).

(1) L. Saraga and I. Prigogine, *C. R. 2e Réunion soc. chim. Phys., Paris*, 458 (1952).

relatively simple case when there is no surface tension difference between the two pure components, A and B, and if the film is supported by adsorption on a substrate, then the interactions between the substrate and the two molecular species are taken to be the same.

A single value of T_c is found and is a function of film thickness. Next we discuss the effect on T_c of small values of the surface tension difference and of the difference in the interaction with the supporting substrate. The perturbation method used is checked by numerical calculations. Some general considerations are made and the possibility of the existence of more than one critical temperature is discussed.

The Model.—We consider a thin film of a regular mixture of molecular species A and B containing M molecular layers with N molecules and lattice sites in each layer. The number concentration of the B species in the M layers is written in the vectorial form

$$X \equiv \{x_1, x_2, \dots, x_M\} \quad (1)$$

The grand partition function of the system at activities λ^A and λ^B , and temperature T is given by

$$\Omega = \sum_X \Xi(X, \lambda^A, \lambda^B, T) \quad (2)$$

where

$$\Xi = \left[\prod_{j=1}^M \frac{N!}{N x_j! N(1-x_j)!} (\lambda^A q_j^A)^{N(1-x_j)} (\lambda^B q_j^B)^{N x_j} \right] e^{-\frac{Nw}{kT} V(X)} \quad (3)$$

Here the q_j are partition functions of molecules in the pure components. For $2 \leq j \leq M-1$ we put as a reasonable approximation

$$q_j = q$$

At the surface of the film, however, q_1 and q_M comprise terms dealing with the surface free energy of the film. If, for instance, layer 1 is in contact with a supporting substrate, q_1 will also entail energies (or free energies) of interaction with the substrate. Then,³ we have

$$\begin{aligned} \ln \frac{q_1^A}{q_1^B} / \frac{q_1^B}{q_1^B} &= \frac{a\Delta\gamma - \Delta E}{kT} \\ \ln \frac{q_M^A}{q_M^B} / \frac{q_M^B}{q_M^B} &= \frac{a\Delta\gamma}{kT} \end{aligned} \quad (4)$$

where a is the molecular area and $\Delta\gamma = \gamma^A - \gamma^B$ the difference between the surface tensions of the pure components, and $\Delta E = E^A - E^B$ the difference in energies of adsorption of the molecular species on the substrate. The exponential term in (3) is a partition function for mixing the two species and in the Bragg-Williams approximation is

$$V(X) = l \sum_{j=1}^M x_j(1-x_j) + m \sum_{j=2}^M x_{j-1}(1-x_j) + x_j(1-x_{j-1}) \quad (5)$$

where l is the fraction of the nearest neighbors in the same lattice layer and m is that in each adjoining layer, satisfying the relation

$$+ 2m = 1$$

w is a measure of the interchange free energy² in mixing the two components, and may contain a term due to a change of vibrational frequency of a molecule due to a change of neighbors. (Such a change will be particularly great for a particle-hole system treated as a binary solution.) The condition that the summand in (3) be a maximum gives the equilibrium concentration in each layer through

$$\lambda \equiv \ln \frac{\lambda^B q^B}{\lambda^A q^A} = \ln \frac{x_j}{1-x_j} + \frac{w}{kT} \{ (1-2x_j) + 2m(2x_j - x_{j+1} - x_{j-1}) \} \quad (6)$$

where x_0 and x_{M+1} are defined by

$$\begin{aligned} x_0 &= \frac{1}{2} + \frac{RT}{2mw} \ln \frac{q_1^A q^B}{q_1^B q^A} \\ x_{M+1} &= \frac{1}{2} + \frac{kT}{2mw} \ln \frac{q_M^A q^B}{q_M^B q^A} \end{aligned} \quad (7)$$

The critical conditions⁶ are given by

$$\delta\lambda = 0, \delta^2\lambda = 0 \quad (8)$$

for an infinitesimal displacement of X , or written explicitly

$$u_j \delta x_j + \delta x_{j+1} + \delta x_{j-1} = -\frac{kT}{2mw} \delta\lambda = 0 \quad (9)$$

$$\begin{aligned} u_j \delta^2 x_j + \delta^2 x_{j+1} + \delta^2 x_{j-1} &= v_j (\delta x_j)^2 \\ \text{for } j &= 1, 2, \dots, M \end{aligned} \quad (10)$$

with the boundary conditions

$$\delta x_0 = \delta x_{M+1} = \delta^2 x_0 = \delta^2 x_{M+1} = 0 \quad (11)$$

where

$$u_j = \frac{1}{m} \left\{ l - \frac{\tau_c}{4} \frac{1}{x_j(1-x_j)} \right\} \quad (12)$$

$$v_j = \frac{\tau_c}{4m} \frac{2x_j - 1}{x_j^2(1-x_j)^2} \left(\frac{\delta x_j}{\delta x_1} \right)^2 \quad (13)$$

$$\tau_c = \frac{2kT_c}{w} \quad (14)$$

From (9) and (10), we get

$$\Delta_{1M}(u) \equiv \begin{vmatrix} u_1 & 1 & & & \\ 1 & u_2 & & & \\ & & \ddots & & \\ & & & 1 & u_M \end{vmatrix} \quad (15)$$

$$\Delta_{1M}(u) \equiv 0 \quad (15')$$

$$D_k(u, \tau) \equiv \begin{vmatrix} u_1 & 1 & & & v_1 & & & & \\ 1 & u_2 & & & v_2 & & & & \\ & & \ddots & & \vdots & & & & \\ & & & 1 & v_{K-1} & & & & \\ & & & & u_{K-1} & & & & \\ & & & & 1 & & & & \\ & & & & & v_K & & & \\ & & & & & \vdots & & & \\ & & & & & v_{K+1} & & & \\ & & & & & & 1 & & \\ & & & & & & & & u_M \end{vmatrix} \quad (16)$$

$$D_k(u, v) \equiv 0 \quad (16')$$

for $k = 1, 2, \dots, M$

The conditions may be written in a different form as follows (see appendix I for proof)

$$F_M(u) = 0 \quad (17)$$

$$\sum_{j=1}^M \frac{2x_j - 1}{x_j^2(1-x_j)^2} \{F_{j-1}(u)\}^3 = 0 \quad (18)$$

where we define

(5) B. B. Fisher and W. G. McMillan, *J. Chem. Phys.*, **28**, 555 (1960).
 (6) I. Prigogine and R. Defay, "Chemical Thermodynamics," Longmans, Green & Co., New York, N. Y., 1954, p. 240.

$$F_K(u) = -u_K F_{K-1}(u) - F_{K-2}(u)$$

$$F_1(u) = 1; F_{-1}(u) = 0 \tag{19}$$

Effect of Film Thickness on T_c when $\Delta\gamma = \Delta E = 0$.—In this special case

$$x_0 = x_{M+1} = 1/2$$

and the second critical condition (18), together with eq. 6 determines the composition at the critical point

$$X = \left\{ \frac{1}{2}, \frac{1}{2}, \dots, \frac{1}{2} \right\} \tag{20}$$

Here all u_j become identical, and putting

$$u_j = \frac{1}{m} (l - \tau_c) = -2 \cos \theta \tag{21}$$

we can easily find the solution of the difference eq. 19 as

$$F_K(u) = \frac{\sin (K+1)\theta}{\sin \theta} \tag{22}$$

The critical condition (17) then gives

$$\theta = \frac{n\pi}{M+1} \quad n = 1, 2, \dots, M \tag{23}$$

We thus see that formally there are M solutions of the critical temperature associated with the M values of n . However, all except the highest critical temperature lie in unstable and metastable regions of the phase diagram and hence these "critical temperatures" are unreal. We shall see later however that for large enough values of $(a\Delta\gamma - \Delta E)$ more than one critical temperature is possible. In the present case, using $n = 1$ in (23), (21) gives the single value of the reduced critical temperature, as defined in (14), to be

$$\tau_c = 1 - 4m \sin^2 (\pi/2(M+1)) \tag{24}$$

We see that for a single layer $\tau_c = 1 - 2m$ as should be the case for a 2-dimensional lattice and rises fairly rapidly toward 1 for increasing M .

The Perturbation Calculation.—The effect of small values of $(a\Delta\gamma - \Delta E)$ may be seen through a perturbation calculation. (A general treatment of the effect of a surface tension difference on T_c is given in Appendix IIb). The unperturbed expressions are given by eq. 20, 22, 23 with $n = 1$, (24) and $\lambda_c = 0$. The critical conditions corresponding to eq. A18 and A19 of the appendix are

$$0 = \sum_{j=1}^M \sin^2 \left(\frac{j\pi}{M+1} \right) \left\{ \xi_j^2 + \frac{\delta\tau_c}{4\tau_c} \right\} \tag{25}$$

$$0 = \sum_{j=1}^M \sin^3 \frac{j\pi}{M+1} \xi_j \tag{26}$$

where the notation $\xi_j = x_j - 1/2$ is used instead of δx_j . Trigonometrical analysis gives for (A7)

$$\xi_K = \xi_+ + \xi_- \cos \frac{kK}{M+1} + C \sin \frac{k\pi}{M+1} \tag{27}$$

where

$$\xi_+ = \frac{\xi_0 + \xi_{M+1}}{2}$$

$$\xi_- = \frac{\xi_0 - \xi_{M+1}}{2} \tag{28}$$

and C is determined by (26) to be

$$C = -\frac{16}{3} \frac{a}{M+1} \xi_+$$

$$a = \cos^3 \frac{\pi}{2(M+1)} / \sin \frac{3\pi}{2(M+1)} \tag{29}$$

Substituting (27) and (29) into (25), we get

$$\frac{\delta\tau_c}{\tau_c} = \left\{ 4 \left(\frac{64}{3} \frac{a^2}{(M+1)^2} - 1 \right) \xi_+^2 - \xi_-^2 \right\}$$

$$\simeq \{-0.16 \xi_+^2 - \xi_-^2\} \quad \text{for } M \geq 5 \tag{30}$$

Numerical values of T_c for the two cases, $\xi_+ = 0$ or $\xi_- = 0$ are given in Table I for the varying values of $|\xi_0|$ and M with $m = 0.25$, the value appropriate to a closed-packed lattice.

Exact values of the critical temperature also were calculated numerically in certain cases using an electronic computer, and are shown in brackets for comparison. Although the approximation becomes poor when $|\xi_0|$ increases beyond 0.3 and for large M , the following qualitative features are evident: (see also Appendix IIB for a general proof).

- (1) The critical temperature decreases with increase of the surface tension or adsorption energy difference, although the value of T_c for a given film thickness is not changed by an order of magnitude.
- (2) The fall of T_c appears to be more important in the case of an antisymmetrical distribution of ξ_K ($\xi_+ = 0$) which can take place when one surface of the system is adsorbed on a solid substrate, rather than for a symmetrical distribution of ξ_K for both surfaces free, or both in contact with the same type of solid substrate.

Discussion

As indicated above, we can expect only one critical temperature for a system when there is no surface tension difference between the pure components and no preferential adsorption on the solid surface.

When these conditions do not hold, however, the symmetry of the coexistence curve with respect to $x_j = 1/2$ is destroyed, and solutions of equation 17 for a critical temperature other than the largest may lie in a stable region and hence be real. It is of particular interest to decide whether any critical temperature may be associated with the surface layers independently of the bulk.

The simultaneous equations 6 are adopted

$$\frac{x_1}{1-x_1} = e^\lambda + \frac{4m}{\tau} x_0 - \frac{2}{\tau} [1 - 2x_1 + 2m(2x_1 - x_1)]$$

$$\frac{x_j}{1-x_j} = e^\lambda - \frac{2}{\tau} [1 - 2x_j + 2m(2x_j - x_{j+1} - x_{j-1})] \tag{31}$$

$$\frac{x_M}{1-x_M} = e^\lambda + \frac{4m}{\tau} x_{M+1} - \frac{2}{\tau} [1 - 2x_M + 2m(2x_M - x_{M-1})]$$

Consider a symmetrical case and assume that $x_0 = x_{M+1}$ is much larger than unity. Then, since the bracket terms in the argument of the exponential are of order unity, we find that x_1 and x_M are almost equal to unity except when $(-\lambda)$ is large enough to cancel the surface term of $(4m/\tau_0)x_0$ where, however, all other x_j 's are almost equal to zero. Hence we can assume either

$$(I) \quad x_1 = x_M \simeq 1$$

$$\text{or}$$

$$(II) \quad x_j \simeq 0, \quad j \neq 1, M \tag{32}$$

In other words, the concentration of the surface layers is practically independent of that of other layers, so that we can expect two critical tempera-

tures, one for the interior, and the other for the surface. In fact, in the former case, the coexistence curve for x_j is almost the same as that of x_{j-1} for the system of $(M - 2)$ layers with the boundary conditions $x_0 = x(M - 2) + 1 = 1$, and in the latter, the coexistence curve for x_1 is almost the same as that of the single layer system. The typical coexistence curves and the curves of λ as a function of x_j are shown in Fig. 1 for $j = 1, M$ and for $j \neq 1, M$. The criterion for the appearance of two critical temperatures is found to be

$$x_0 > \frac{1}{2} + \frac{M}{2(M-2)} > 1 \quad (33)$$

by calculating the summand of the grand partition function, with the approximation (32). Since in most actual cases the above criterion is satisfied, we may conclude that under the nearest neighbor approximation two critical temperatures, one at $\tau_c \simeq 1$ and the other at $\tau_c \simeq 1 - 2m$ will in principle exist, as was pointed out by Saraga and Prigogine, as long as the system retains the original lattice structure in this temperature range.

It should be noted that in Saraga and Prigogine's discussion, two critical temperatures for the surface and bulk phases exist irrespective of the value of the surface tension or adsorption energies of the two components, although they may not both be observable in practice since at the surface critical temperature the bulk will already be separated into two phases. However, in our case the surface critical temperature is obtained for a stable solution only when the surface tension or adsorption energy difference is sufficiently large. The case of solid solutions of the rare gas atoms may be of practical interest. The vapor pressures of solid solutions of A-Kr⁷, Kr-Xe⁸ and A-Xe⁹ have been measured and the critical solution temperatures either observed or inferred.

The surface tension difference will be large enough to satisfy the criterion (33), so that two critical temperatures could be observable as well as any effect of finite film thickness upon the critical temperature of the interior of the film. In the case of liquid solutions, the freezing point is usually above the surface critical temperature so as to mask it. Apart from the two solutions of the first critical condition connected with the two surfaces and one connected with the bulk, there remain $M - 3$ possible solutions. In the nearest neighbor approximation, however, these $M - 3$ solutions cannot be real since in the equivalent system of $(M - 2)$ layers the boundary conditions $x_0 = x_{M+1}$ do not satisfy the criterion (33). However, this is no longer the case if an adsorbing surface interacts with layers of the solution other than the first, *i.e.*, if we take into account the long-range character of these forces. In this case, still retaining the model of a regular solution, equation 6 becomes for $1 < j < M$

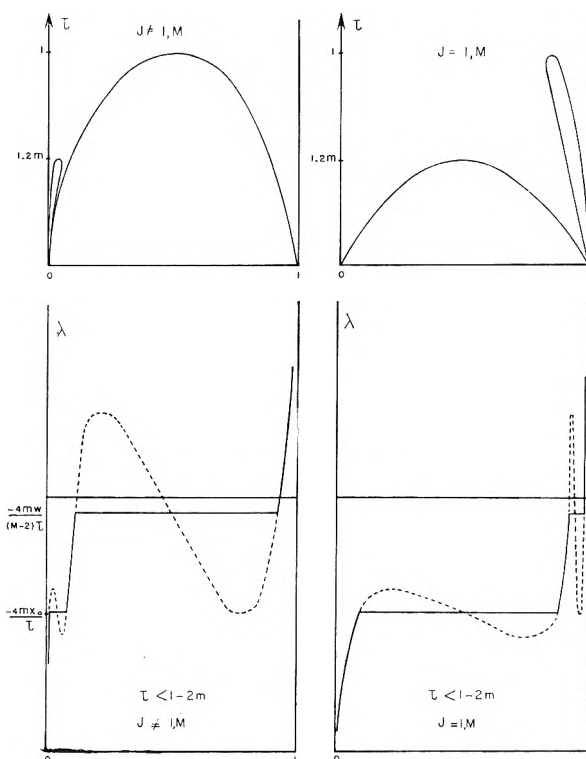


Fig. 1.—(a) (top) Coexistence curves for interior and surface layers. (b) (bottom) The absolute activity as a function of composition for interior and surface layers, showing the two “Bragg-Williams loops” which appear for a temperature below the “bulk” and “surface” critical temperatures.

$$\lambda = \frac{\lambda_j}{\tau} + \ln \frac{x_j}{1 - x_j} + \frac{2}{[(1 - 2x_j) + 2m(2\tau_j - x_{j+1} - x_{j-1})]}$$

$$j = 1, \quad \lambda = \frac{\lambda_1}{\tau} + \ln \frac{x_1}{1 - x_1} + \frac{2}{[(1 - 2x_1) + 2m(2x_1 - x_2 - \frac{1}{2})]} \quad (34)$$

$$j = M, \quad \lambda = \frac{\lambda_M}{\tau} + \ln \frac{x_M}{1 - x_M} + \frac{2}{[(1 - 2x_M) + 2m(2x_M - x_{M-1} - \frac{1}{2})]}$$

If $|\lambda_j|$ is sufficiently larger than unity, then the j th layer will behave almost independently of other layers for the same reason as above, and there will be a reduced critical temperature corresponding to the j th layer, which will again be of order $(1 - 2m)$. On the other hand, if $|\lambda_j|$ is smaller than unity, there will not be any critical temperature associated with this particular layer. However, it can be shown that in the limit of low temperatures ($\tau \ll \lambda_j$), a distinct phase separation becomes observable for each layer. Using the cube law¹⁰ for the fall-off of the surface potential, it is reasonable to suppose that $|\lambda_j|$ will have the form of

$$|\lambda_j| \simeq \pm \frac{|\lambda_1|}{j^3} \pm \frac{|\lambda_M|}{(M+1-j)^3} \quad (35)$$

so that if $|\lambda_1|$ and $|\lambda_M|$ are of order 5 or 10, only a

(7) J. F. Walling and G. D. Halsey, *J. Phys. Chem.*, **62**, 752 (1958); R. Heastie, *Proc. Phys. Soc.*, **73**, 490 (1959).
 (8) M. P. Freeman and G. D. Halsey, *J. Phys. Chem.*, **60**, 119 (1956).
 (9) R. Heastie and C. Lefebvre, *J. Phys. Soc.*, **76**, 180 (1960).

(10) T. L. Hill, *J. Chem. Phys.*, **17**, 590 (1949).

few layers will have their own critical temperatures.

At this point, we apply our discussion to the adsorption isotherm of gases on a solid substrate by considering a particle-hole system. The phase separation associated with a single layer corresponds to the Langmuir adsorption, and the "collective" phase separation to the B.E.T. adsorption. Since in this case $|\lambda_i|$ will be of order ten, (35) indicates that about two surface layers may show the phase separation associated with single layer. However, as the temperature decreases, more single layer phase separations appear and the adsorption isotherm will become step-wise similar to that discussed by Halsey¹¹ and Hill.¹²

Finally we add that our model may also be applicable to the Lennard-Jones-Devonshire model of melting and to the lattice model of the liquid He(I)-He(II) phase transition. In either case, a lowering of the phase-transition temperature appears to be predicted by the present theory.

Acknowledgments.—We wish to thank Mr. M. Banville of the Mathematics Department of this University for his guidance in the computer calculations. We are also most grateful to the Paint Research Institute for grants in support of this work and to the National Research Council for a scholarship to K.N. during part of the year.

Appendix I

Treatment of the Critical Conditions.—By expansion of (16), we get

$$D_K(u, v) = \sum_{j=1}^K (-1)^{j+K} \Delta_{j-1}(u) \Delta_{K+1M}(u) v_j + \sum_{j=K+1}^M (-1)^{j+K} \Delta_{jK-1}(u) \Delta_{j+1M}(u) v_j \quad (A1)$$

where we define

$$\Delta_{j-1}(u) = 1, \Delta_{j-2}(u) = 0 \quad (A2)$$

Noting that (A1) is valid for any u and v and considering (15) as a special case of (16), we have

$$\Delta_{1M}(u) = \Delta_{1K-1}(u) \{ u \Delta_{K+1M}(u) - \Delta_{K+2M}(u) \} \quad (A3)$$

or, using the identities

$$\Delta_{jK}(u) = u_K \Delta_{jK-1}(u) - \Delta_{jK-2}(u) = u_j \Delta_{j+1K}(u) - \Delta_{j+2K}(u) \quad (A4)$$

for $j + 2 \leq K$

we may write

$$\Delta_{1M}(u) = \Delta_{1K-1}(u) \Delta_{KM}(u) - \Delta_{1K-2}(u) \Delta_{1K+1}(u) \quad (A5)$$

Now we apply the critical condition (15') to (A5) and get

$$\frac{\Delta_{1K-1}(u)}{\Delta_{K+1M}(u)} = \frac{\Delta_{1K-2}(u)}{\Delta_{KM}(u)} = \dots = \Delta_{1M-1}(u) = \frac{1}{\Delta_{2M}(u)} \quad (A6)$$

Using (A6) in (A1) we have

$$\Delta_K(u, v) = \Delta_{2M}(u) (-1)^{K-1} \Delta_{1K-1}(u) \left\{ \sum_{j=1}^M v_j (-1)^{j-1} \Delta_{1j-1}(u) \right\} \quad (A7)$$

or from the second critical condition (16')

$$\sum_{j=1}^M v_j (-1)^{j-1} \Delta_{1j-1}(u) = 0 \quad (A8)$$

Now from eqs. 9 and A7

$$\frac{\delta x_j}{\delta x_1} = \frac{D_j(u, 1)}{D_1(u, 1)} = (-1)^{j-1} \Delta_{1j-1}(u) \quad (A9)$$

and substituting (A9) into v_j in (A8) we get

$$\sum_{j=1}^M \frac{2x_{j-1}}{x_j^2(1-x_j)^2} [(-1)^{j-1} \Delta_{1j-1}(u)]^3 = 0 \quad (A10)$$

The critical conditions may be presented in a somewhat more useful way by introducing the function $F_K(u)$ as defined in (19). From (19) and (A4) we can show easily that

$$F_K(u) = (-1)^K \Delta_{1K}(u) \quad \text{for } -1 \leq K \leq M \quad (A11)$$

so that the critical conditions may be written as in (17) and (18).

Appendix II

A General Consideration of the Critical Temperature.—(A). The value of T_c as a function of film thickness. From the definitions (19) and (12) we find that

$$\begin{aligned} [F_K(u) - F_{K-1}(u)] - [F_{K-1}(u) - F_{K-2}(u)] \\ = (-2 - u_K) F_{K-1}(u) \\ = \frac{1}{n} \left[\frac{\tau}{4x_K(1-x_K)} - 1 \right] F_{K-1}(u) \\ \geq \frac{1}{n} \frac{2kT}{w} \end{aligned} \quad (A13)$$

where

$$\tau = \frac{2kT}{w} \quad (A14)$$

Since $F_0(u) - F_1(u) > 0$ and $F_0(u) > 0$, (A13) shows that $F_K(u)$ is always positive for $\tau \geq 1$. Thus the first critical condition (17) requires that $\tau_c < 1$.

As τ decreases from unity, $F_M(u)$ will also decrease and at $\tau = \tau_c$, $F_M(u)$ becomes zero. It may be shown generally that at the highest critical temperature (which is the real bulk critical temperature, as discussed in the main text) all $F_k(u)$ for $-1 < k < M$ become positive, from which we may conclude the following: (1) At the highest critical temperature if there are any x_j 's for $(1 \leq j \leq M)$ which are larger than one-half, there are others which are smaller, and *vice versa*. (2) The highest critical temperature will decrease as film thickness decreases, provided that other conditions are unchanged.

(B) The value of T_c as a function of surface tension difference or difference of adsorption potential.

Let

$$\{ \tau_c, \lambda_c, x_1, x_2, \dots, x_M \} \quad (A15)$$

be the solution corresponding to the highest critical temperature under the given boundary conditions x_0 and x_{M+1} and with $x_0 > 1/2$. Changing the boundary conditions by infinitesimal amounts δx_0 and δx_{M+1} , but with x_0/x_{M+1} constant, gives a corresponding change of (A15) denoted by

$$\{ \delta \tau_c, \delta \lambda_c, \delta x_1, \dots, \delta x_M \} \quad (A16)$$

These $(M + 2)$ variables are determined by M equilibrium conditions (A17), and the two critical conditions (A18) and (A19)

(11) G. D. Halsey, *J. Chem. Phys.*, **16**, 931 (1948).
 (12) T. L. Hill, *ibid.*, **15**, 767 (1947).

$$\delta x_0 w_j = u_j \delta x_j + \delta x_{j+1} + \delta x_{j-1} \quad (A17)$$

$$j = 1, 2, \dots, M$$

$$0 = \delta F_M(u) = \sum_{j=1}^M \frac{\partial F_M(u)}{\partial u_j} \left\{ \frac{\partial u_j}{\partial x_j} \delta x_j + \frac{\partial u_j}{\partial \tau_c} \delta \tau_c \right\}$$

$$= - \sum_{j=1}^M \frac{\partial F_M(u)}{\partial u_j} \left\{ v_j' \delta x_0 + \frac{1}{4m x_j (1-x_j)} \delta \tau_c \right\}$$

$$= \sum_{j=1}^M \frac{[F_{j-1}(u)]^2}{F_{M-1}(u)} \left\{ v_j' \delta x_0 + \frac{1}{4m x_j (1-x_j)} \delta \tau_c \right\} \quad (A18)$$

$$0 = \delta \left\{ \sum_{j=1}^M \frac{2x_j - 1}{x_j^2 (1-x_j)^2} [F_{j-1}(u)]^3 \right\} \quad (A19)$$

where w_j and v_j' are defined by

$$w_j = - \frac{\tau_c}{4m} \frac{\delta \lambda_c}{\delta x_0} - \frac{1}{4m} \left\{ \lambda_c - \ln \frac{x_j}{1-x_j} \right\} \frac{\delta \tau_c}{\delta x_0} \quad (S20)$$

$$v_j' = \frac{\tau_c}{4m} \frac{2x_j - 1}{x_j^2 (1-x_j)^2} \frac{\delta x_j}{\delta x_0} \quad (A21)$$

and in deriving the last expression of (A18) use was made of the relation

$$\frac{\partial F_M(u)}{\partial u_j} = (-1)^M \frac{\partial \Delta_{1M}(u)}{\partial u_j} =$$

$$- (-1)^{j-1} \Delta_{1j-1}(u) (-1)^{M-j} \Delta_{j+1M}(u)$$

$$= - \frac{[F_{j-1}(u)]^2}{F_{M-1}(u)} \quad (A22)$$

We first note that the solution of (A17)

$$\frac{\delta x_K}{\delta x_0} = \frac{D_K(u, \bar{w})}{\Delta_{1M}(u)} \quad (A23)$$

$$\bar{w}_j = w_j - \left[\delta_{j,1} + \delta_{j,M} \frac{\delta x_{M+1}}{\delta x_0} \right] \quad (A24)$$

diverges except for a special value of $\delta \lambda_c$ due to the first critical condition $\Delta_{1M}(u) = 0$. This divergence, however, has no meaning since in such a case the higher order terms neglected in (A17) may play an important role. Further the divergence gives no contribution to $F_M(u)$ due to the second critical condition (18). However, there is a divergence difficulty in (A19), because there is no "third" critical condition to cancel divergent terms there. Hence, (A19) requires (23) to be finite. This determines $\delta \lambda_c / \delta x_0$ except for the order of $F_M(u)$ which is sufficient for the proposed object.

Using eq. A5, we find

$$(-1)^{M-K} \Delta_{K+1M}(u) = \frac{F_{K-1}(u)}{F_{M-1}(u)} [1 + \epsilon_K] \quad (A25)$$

where

$$\epsilon_K = F_M(u) F_{M-1}(u) \sum_{j=K+1}^M \frac{1}{F_{j-1}(u) F_{j-2}(u)} \quad (A26)$$

Substituting (A25) into the expansion of (A23), (see (A1))

$$\frac{\delta x_K}{\delta x_0} = - \frac{F_{K-1}(u)}{F_{M-1}(u) F_M(u)} \left\{ \sum_{j=1}^K F_{j-1}(u) [(1 + \epsilon_K) \bar{w}_j + \right.$$

$$\left. \sum_{j=K+1}^M F_{j-1}(u) (1 + \epsilon_j) \bar{w}_j \right\}$$

$$= - \frac{F_{K-1}(u)}{F_{M-1}(u) F_M(u)} \left\{ \sum_{j=1}^M F_{j-1}(u) (1 + \epsilon_j) \bar{w}_j + \right.$$

$$\left. \sum_{j=1}^K F_{j-1}(u) (\epsilon_K - \epsilon_j) \bar{w}_j \right\} \quad (A27)$$

The requirement that (A27) be finite gives

$$\sum_{j=1}^M F_{j-1}(u) \bar{w}_j = 0 \{F_M(u)\}$$

or, substituting (A24)

$$\frac{\tau_c}{4m} \sum_{j=1}^M F_{j-1}(u) \frac{\delta \lambda_c}{\delta x_0} + \frac{1}{4m} \sum_{j=1}^M F_{j-1}(u) \left[\lambda_c - \ln \frac{x_j}{1-x_j} \right]$$

$$\frac{\delta \tau_c}{\delta x_0} + \left\{ 1 + F_{M-1}(u) \frac{\delta x_{M+1}}{\delta x_0} \right\} = 0 \{F_M(u)\} \quad (A28)$$

Before substituting into (A18), we note that the first term of this expression can be written as

$$-v_j' \delta x_0 = \left(\frac{\partial u_j}{\partial x} \right)_{\tau_c} \left(\frac{\partial x_j}{\partial x_0} \right)_{\tau_c} \delta x_0 + \left(\frac{\partial u_j}{\partial x} \right)_{\tau_c} \left(\frac{\partial x_j}{\partial \tau_c} \right)_{x_0} \delta \tau_c \quad (A29)$$

of which the contribution of the second term to $F_M(u)$ is very small due to condition (18). We may therefore write

$$\delta F_M(u) \simeq \sum_{j=1}^M \frac{\partial F_M(u)}{\partial u_j} \left\{ \left(\frac{\partial u_j}{\partial x} \right)_{\tau_c} \left(\frac{\partial x_j}{\partial x_0} \right)_{\tau_c} \delta x_0 + \left(\frac{\partial u_j}{\partial \tau_c} \right)_{x_j} \delta \tau_c \right\} \quad (A30)$$

Now, making use of (A27) and (A28) in (A30), we finally obtain

$$0 = \sum_{k=1}^M [F_{K-1}(u)]^3 \frac{2x_K - 1}{x_K^2 (1-x_K)^2} [\rho_K \delta x_0 + \mu_K \delta \tau_c] \quad (A31)$$

where

$$\rho_K = \frac{1}{4m} \sum_{k=1}^M \frac{1}{F_{j-1}(u) F_j(u)} \sum_{l=1}^j F_{l-1}(u) \left[\ln \frac{x_l}{1-x_l} - \ln \frac{x}{1-x} \right] \quad (A32)$$

$$\mu_K = \frac{x_K (1-x_K)}{\tau_c (2x_K - 1)} \frac{1}{F_{K-1}(u)} \quad (A33)$$

$$\ln \frac{x}{1-x} = \sum_{l=1}^H \ln \frac{x_l}{1-x_l} F_{l-1}(u) / \sum_{l=1}^M F_{l-1}(u) \quad (A34)$$

Noting (18), and taking a reasonable dependence of x_K on K , we can show that both coefficients of δx_0 and $\delta \tau_c$ in (A31) are positive definite, from which we may finally conclude that

$$\left(x_0 - \frac{1}{2} \right) \frac{\partial \tau_c}{\partial x_0} < 0$$

for x_0/x_{M+1} constant, or that the critical temperature is lowered by an increase in the surface tension and/or adsorption energy difference.

THE PHOTOCHEMISTRY OF THE IODIDE ION IN AQUEOUS SOLUTION

BY JOSHUA JORTNER, RAPHAEL LEVINE, MICHAEL OTTOLENGHI AND GABRIEL STEIN

*Department of Physical Chemistry, Hebrew University, Jerusalem, Israel**Received February 9, 1961*

The photochemistry of evacuated potassium iodide solutions at 2537 Å. was investigated. The dependence of the initial quantum yields on pH, iodide ion concentration and light intensity was investigated. The nature of the residual pH independent yield at pH > 3 is discussed. The pH dependence of the initial quantum yields could be represented by a linear dependence on the square root of H⁺ ion concentration. It is shown that this is in agreement with a mechanism based on the theory of diffusion controlled scavenging. The H⁺ ion acts as an electron scavenger for a species (electrons or H atoms) formed in the photochemical cage and yield H atoms in the bulk of the solution. The reactivity of H atoms photochemically produced in solution was investigated, and evidence for a pH dependent oxidation mechanism of I⁻ by H atoms is presented, which may involve the H₂⁺aq ion as the actual oxidizing agent.

Introduction

In the ultraviolet region aqueous solutions of iodide show an intense absorption¹ $\epsilon_{2562} = 1.32 \times 10^4$ at 25°, characterized by a high oscillator strength $f = 0.25$. This band has been classified as a charge transfer spectrum.^{2,3} For the alkali halides in aqueous solutions the absorption band is typical of the anion and no spectroscopic evidence for ion pair formation has been found.⁴ The nature of the excited state has been a matter of controversy.^{4,5a,5b}

As has been well known for a long time⁶ aerated aqueous iodide solutions liberate free iodine on illumination. More recently the same was shown to occur in deaerated solution.^{7,8} The photochemical wave length threshold was shown to coincide with the absorption band onset.⁷ Farkas and Farkas⁹ showed that the quantum yield was pH dependent, a conclusion supported by Franck and Platzman,¹⁰ who suggest a competition between the decay of the excited state and its interaction with H₃O⁺ ion as the reason for the pH dependence. On the other hand Rigg and Weiss⁸ conclude that the pH dependence arises out of the competition in bulk between the back reaction of H + I and H₂⁺ formation by the reaction between H + H⁺. The two theories thus differ in their interpretation of radical formation and the relatively low quantum yield.

Recently the system has been investigated in the whole pH region in the presence of N₂O,¹¹ and by flash photolysis technique,^{12,13} where the existence of the I₂⁻ ion as intermediate was demonstrated.

The purpose of the present work was to investigate the mechanism of primary radical formation

in this system, and the possible specific role of the H₃O⁺ ion in this process. Another aspect of this work is the investigation of the chemistry of radicals photochemically produced. It was postulated by Weiss¹⁴ that H atoms in aqueous solutions may act as an oxidizing agent through the intermediate formation of H₂⁺. The occurrence of such oxidation reactions is now well established. Using H atoms externally generated it was shown¹⁵ that in the case of the I⁻ ion the results are consistent with the view that the actual oxidant is the H₂⁺ ion. Further independent investigation of this problem appeared desirable in the case of the photochemistry of I⁻.

Experimental

Light Source.—The light source was a low pressure mercury lamp operated at 1000 v. drawn from a step up transformer fed from stabilized mains. The current through the lamp (30–150 ma.) was varied by means of a Variac in the primary circuit of the lamp transformer. The output of the lamp was monitored by an I.P. 21 photomultiplier tube connected to a Photovolt instrument. About 90% of the light output is at 2537 Å.

The radiation was filtered through a 5 cm. quartz cell containing KI-I₂ aqueous solution permitting the isolation of the strong Hg 2537 Å. line.

Actinometry was carried out by means of the uranyl oxalate actinometer.¹⁶ The chemical change was linear in light intensity as determined by the monitoring photocell. As a check a ferri oxalate actinometer¹⁷ was used. In a typical experiment we obtained for the light intensity, J

$$J(\text{uranyl oxalate}) \quad J = 6.35 \times 10^{-7} \text{ einstein l.}^{-1} \text{ sec.}^{-1}$$

$$J(\text{ferri oxalate}) \quad J = 6.20 \times 10^{-7} \text{ einstein l.}^{-1} \text{ sec.}^{-1}$$

Agreement between the results was satisfactory.

Reaction Cell.—The reaction cell was adapted from a 4 cm. quartz absorption cell with flat optical windows of 3 cm. optical length for light absorption at 2537 Å. and 4 cm. optical length for spectrophotometry. It was connected to a vacuum system through a valve. The cell orientation relative to the light source was held fixed during all experiments. In this cell 13 cc. of solution was used for each irradiation. Another cell was employed for gasometric analysis, consisting of quartz cylindrical cell with flat optical windows as basis, and 5 cm. optical length holding 60 cc. of solution.

Analysis.—Hydrogen was determined by a microgasometric method. The pressure was determined by a McLeod gauge.

Iodine was determined by its absorption as I₃⁻. The spectrophotometric light source was an ordinary 6V 3A tungsten hot wire bulb, with a cut off filter above 400 mμ. An empirical calibration was carried out by introducing a

- (1) J. Franck and G. Scheibe, *Z. physik. Chem.*, **A139**, 22 (1928).
- (2) E. Rabinowitch, *Rev. Mod. Phys.*, **14**, 118 (1942).
- (3) L. E. Orgel, *Quart. Rev.*, **8**, 422 (1954).
- (4) G. Stein and A. Treinin, *Trans. Faraday Soc.*, **55**, 1086, 1091 (1959).
- (5) (a) R. L. Platzman and J. Franck, *Z. Physik*, **138**, 411 (1954); (b) M. Smith and M. C. R. Symons, *Disc. Faraday Soc.*, **24**, 206 (1957).
- (6) W. H. Ross, *J. Am. Chem. Soc.*, **28**, 788 (1906).
- (7) K. Butkowiak, *Z. Physik*, **62**, 71 (1930).
- (8) T. Rigg and J. Weiss, *J. Chem. Soc.*, 4198 (1952).
- (9) A. Farkas and L. Farkas, *Trans. Faraday Soc.*, **34**, 1120 (1938).
- (10) R. L. Platzman and J. Franck, "Farkas Memorial Volume," Jerusalem, 1952, p. 21.
- (11) F. S. Dainton and S. A. Sills, *Nature*, **186**, 879 (1960).
- (12) L. I. Grossweiner and M. S. Matheson, *J. Phys. Chem.*, **61**, 1098 (1957).
- (13) F. H. C. Edgecombe and R. G. W. Norrish, *Proc. Roy. Soc. (London)*, **A253**, 154 (1959).

- (14) J. Weiss, *Nature*, **165**, 728 (1950).
- (15) G. Czapski, J. Jortner and G. Stein, *J. Phys. Chem.*, **63**, 1769 (1959).
- (16) E. J. Bowen, "The Chemical Aspects of Light," Oxford University Press, New York, N. Y., 1946.
- (17) C. A. Parker, *Proc. Roy. Soc. (London)*, **A220**, 104 (1953).

known amount of I_2 in aqueous iodide solutions, into the reaction cell, and measuring optical densities by means of the IP 21 photomultiplier and the Photovolt instrument. It was found that the optical density was independent of iodide ion concentration above $10^{-2} M$ and a linear dependence of D on the iodine concentration up to 1.2×10^{-5} mole liter $^{-1}$ was found with an apparent molar absorption coefficient $\epsilon = 9 \times 10^3$ mole $^{-1}$ liter cm. $^{-1}$ (compared to $\epsilon_{350} = 26500$ mole $^{-1}$ liter cm. $^{-1}$). At lower I^- concentrations a similar procedure was employed. The lower limit of iodine detected is about 2×10^{-7} mole liter $^{-1}$ and the upper limit was 2.3×10^{-5} mole liter $^{-1}$. This technique enabled an accurate determination of initial reaction yields.

Materials.—All chemicals used were of Analar grade. Solutions were prepared in triply distilled water (ordinary distillation followed by distillation from alkaline permanganate and phosphoric acid). Control experiments were carried out using water purified by irradiation with 200 kv. X-rays and decomposition of the H_2O_2 thus formed by irradiation with the 2537 Å. line of a low pressure Hg lamp. These experiments yielded the same results as obtained in triply distilled water.

Procedure.—A known amount of freshly prepared neutral potassium iodide solution or solid KI was introduced into the reaction vessel and the acid or buffer were added from a separate container, after evacuation, to avoid thermal oxidation. No thermal oxidation could be detected. Erratic results were obtained in solutions containing initial iodine concentration higher than $5 \times 10^{-6} M$ causing a decrease of the initial yield. This effect was most important at high pH and low I^- concentration. The pH below 3.5 was adjusted by H_2SO_4 and above pH 3.5 by KH_2PO_4 - Na_2HPO_4 buffer ($10^{-3} M$). The pH was determined at the end of each run.

The contents of the reaction cell were stirred continuously by a Teflon coated magnetic stirrer. For experiments on deaerated solutions the reaction cell was connected to the vacuum system for 20 seconds every five minutes until, after approximately 3.5 hours, its equilibrium vapor pressure was $1-2 \times 10^{-5}$ mm. The small reaction cell was kept in a thermostated brass compartment in which water was circulated. Experiments were carried out at $25 \pm 0.2^\circ$.

At suitable intervals after the beginning of irradiation a mechanical shutter separating the cell and the lamp was closed and the amount of free iodine determined. Hydrogen was determined at the end of each run in the large irradiation vessel. These iodine and hydrogen determinations were in satisfactory agreement of about 10%.

Results and Discussion

Dependence of Initial Yields on pH and Light Intensity.—An initial quantum yield γ_i was obtained from the expression

$$\gamma_i = \frac{1}{J} \left(\frac{d[I_2]}{dt} \right)_0$$

where J is the light intensity. The dependence of γ_i in evacuated solutions on pH, iodide ion concentration and light intensity was investigated.

Figure 1 presents the dependence of the yield of I_2 at constant light intensity on irradiation time. The initial slopes could be determined and hence γ_i was approximately evaluated.

The pH dependence of γ_i is shown in Fig. 2. Above pH 3.5 a residual pH independent quantum yield is observed. This is consistent with recent observations.¹³ The pronounced dependence of γ_i in acid solutions is in qualitative agreement with previous investigations.⁸

The initial quantum yield is independent of light intensity. This observation was confirmed with reasonable accuracy for a low pH region (pH 0.8). These data are presented in Fig. 3, and are consistent with other recent results.¹¹

The Nature of the Absorption Act and Primary Products.—There is good agreement between the

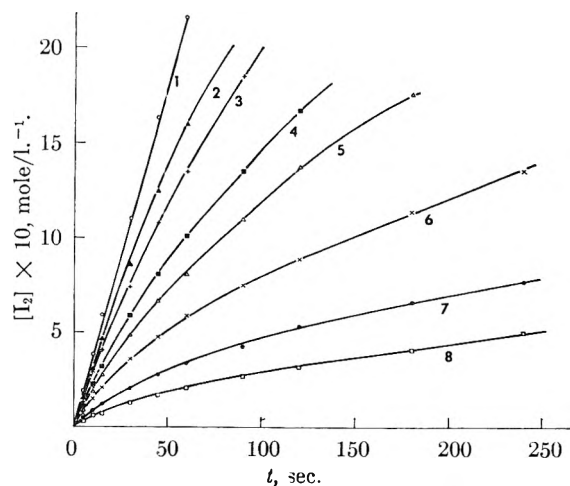


Fig. 1.—Photo-oxidation yields of iodide solutions at constant light intensity, $I^- = 0.15 M$, $J = 9.7 \times 10^{-1}$ einstein liter $^{-1}$ sec. $^{-1}$: Curve 1, $0.74 M H_2SO_4$; 2, pH 0.65; 3, pH 0.90; 4, pH 1.10; 5, pH 1.36; 6, pH 1.78; 7, pH 2.2; 8, pH 2.6.

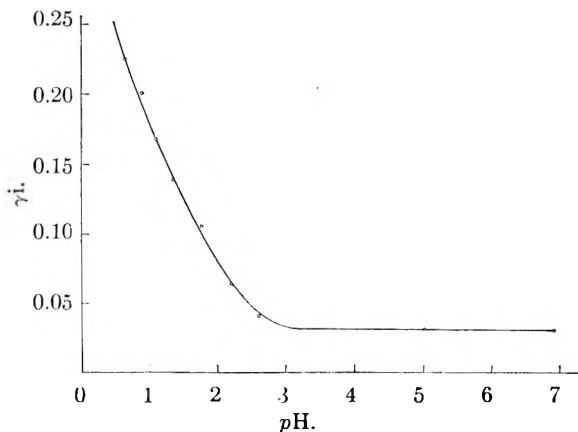


Fig. 2.—The pH dependence of the initial quantum yields.

experimental spectroscopic results and their recent theoretical interpretations regarding the nature of the primary absorber. Both the theory of Smith and Symons^{18,19} and that of Stein and Treinin^{4,20} agree in that they postulate as did Platzman and Franck⁵ a symmetrical excited state in which the electron is not bound to a single solvent molecule⁹ but rather is bound in the field formed by the oriented water molecules of the solvent medium. In spite of detailed differences, concerning the structure of the excited level, both groups recently have concluded^{19,20} that in the excited state the electron probably is confined to the first hydration layer of water molecules.

The restrictions imposed by the Franck-Condon principle on the optical electron transfer process have to be considered. The life time of the spherically symmetrical excited state of the iodide ion,⁵ is of the order of the relaxation time of the solvent molecules. After a period of 10^{-10} to 10^{-11} sec. an iodine atom and an electron are formed. There is no experimentally observed fluorescence in aqueous iodide solutions. The life time of an

(18) M. Smith and M. C. R. Symons, *Trans. Faraday Soc.*, **54**, 338 (1958).

(19) T. R. Griffiths and M. C. R. Symons, *ibid.*, **56**, 1125 (1960).

(20) G. Stein and A. Treinin, *ibid.*, **56**, 1393 (1960).

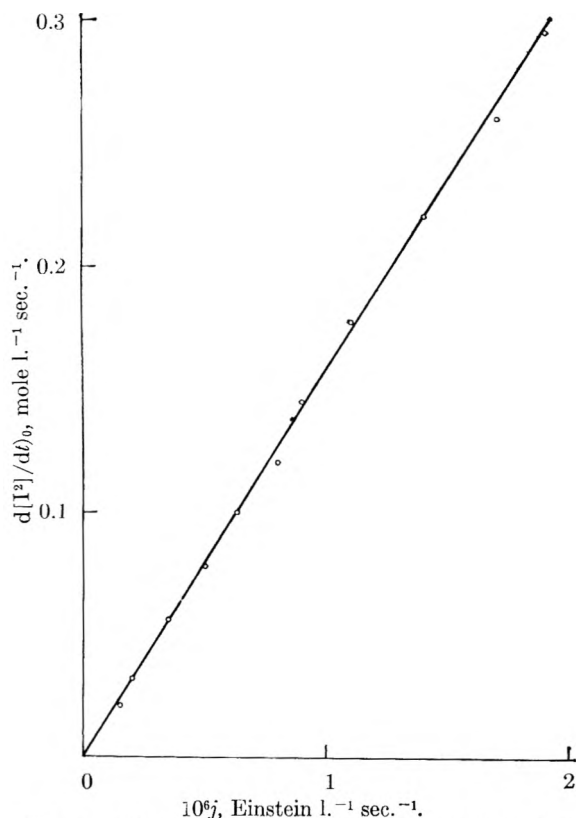
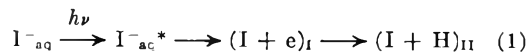


Fig. 3.—The dependence of the initial photo-oxidation yields of $5 \times 10^{-2} M$ KI solutions on light intensity at pH 0.8.

excited state required before fluorescent radiative transition to the ground state occurs is of the order of 10^{-8} sec. or longer. Therefore in systems like that of aqueous iodide after 10^{-11} to 10^{-10} sec. the process of thermal degradation of the excited state may lead to an intermediate state, in which the electron is less confined, and may undergo a quasi random walk process in the vicinity of the iodine atom over the water molecules. A dissociative electron capture of this electron by a water molecule may result in the formation of an H atom by a pH independent mechanism. This may occur by localization of the electronic charge on a prestretched H—OH bond. The kinetic scheme will be presented in the form



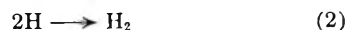
where () represents the solvent cage. The radical pairs in I or in II may undergo primary recombination, which is kinetically equivalent to a thermal deactivation of the excited state. The radical pairs which escape primary recombination may undergo diffusive secondary recombination with their original partners.²¹ The radicals escaping recombination diffuse into the bulk. The residual pH independent yield observed in evacuated solutions above pH 3.5 indicates the operation of this mechanism. This model for the "residual yield" is actually a modification of the original

(21) J. C. Roy, W. H. Hamill and R. R. Williams, *J. Am. Chem. Soc.*, **77**, 2953 (1955).

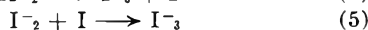
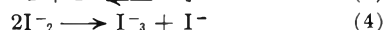
(22) J. Franck and F. Haber, *Sitzungsber. Preuss. Akad. Wiss.*, 250 (1931).

Franck-Haber mechanism,²² taking into account the Franck-Condon principle.

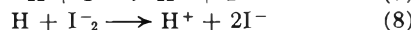
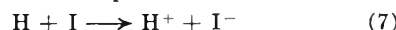
The Residual Yield.—Independent evidence derived from the investigation of the chemistry of hydrogen atoms in iodide solutions¹⁵ indicates that at pH above 3 no oxidation reaction of I^- ion by H atoms occurs. Thus in this pH region the possible reactions of the radicals in bulk will be hydrogen atom recombination



and iodine formation by the mechanism proposed by Grossweiner and Matheson¹²



These back reactions are possible



As these experiments were carried out at relatively high $[I^-]$ concentration, it is reasonable to assume that every iodine atom introduced into the bulk is converted into the I^-_2 ion. This assumption is consistent with the results of Grossweiner and Matheson.¹² Including reactions 2,3,4 and 8 in the kinetic scheme the steady-state treatment for the intermediates I, I^-_2 and H readily leads to

$$\left(\frac{d[I_2]}{dt}\right)_0 = \frac{k_4 \alpha J}{2k_4 + k_8(k_4/k_2)^{1/2}} \quad (I)$$

where α is the quantum yield for the introduction of radicals into the bulk.

The relation between the experimental residual yield γ_i^r and α will be considered for two limiting cases

$$(a) \quad k_2 = k_4 = k_8 \quad \gamma_i^r = \frac{1}{3} \alpha$$

$$(b) \quad k_3 = k_4 \gg k_8 \quad \gamma_i^r = \frac{1}{2} \alpha$$

As both reactions 2 and 4 are diffusion controlled^{23,24} these are the relevant cases. Thus α is of the order of $2\gamma_i^r - 3\gamma_i^r$.

In Fig. 4 the photochemical curves at various I^- concentrations at pH 5.5 are presented. From the initial slopes the residual yield is obtained $\gamma_i^r = 0.03 \pm 0.005$. The initial residual yield is independent of I^- concentration.

Graphical Evaluation of Initial Yields.—In the photochemical system the iodine yield *versus* time curves (Fig. 1) are departing from linearity indicating an efficient back reaction. This effect causes a considerable inaccuracy in the estimation of the initial quantum yields. This difficulty is mainly manifested at high pH and low I^- concentrations.

The initial yields were calculated on the basis of the assumption, to be discussed later, that at relatively low pH below 2.0 hydrogen atoms in the bulk act as oxidizing agents for I^- ions; or alternatively may reduce I_2 . Disregarding for the moment the actual oxidation and reduction mech-

(23) N. Davidson, *J. Chem. Phys.*, **19**, 1311 (1951).

(24) H. L. Friedman and A. H. Zeltman, *ibid.*, **28**, 1113 (1958).

anisms the rate of formation of I_2 can be represented by

$$\frac{d[I_2]}{dt} = \frac{\alpha J}{2} \left(1 + \frac{k_{ox}[I^-] - k_r[I_2]}{k_{ox}[I^-] + k_r[I_2]} \right) = \frac{\alpha J k_{ox}[I^-]}{k_{ox}[I^-] + k_r[I_2]} \quad (\text{II})$$

where k_{ox} and k_r are the composite rate constants for oxidation of I^- and reduction of I_2 by H atoms. In the pH region below 2 it is assumed that the rate of introduction of radicals into the bulk is equal to the initial photo-oxidation yield.

Integration of equation II for the initial stages of the reaction experimentally investigated when I^- can be considered as effectively constant, leads to the result

$$\frac{t}{[I_2]} = \frac{1}{\alpha J} + \frac{1}{2\alpha J} \frac{k_r}{k_{ox}[I^-]} [I_2] \quad (\text{III})$$

The plots of $t/[I_2]$ versus $[I_2]$ are presented in Fig. 5 and 6 for various H^+ and I^- concentrations. The plots are linear up to $[I_2] = 2 \times 10^{-5} M$, in good agreement with equation III.

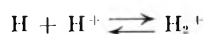
From the intercepts in Fig. 5 and 6 the initial photo-oxidation yields are obtained. The initial quantum yields at various pH obtained by this method are presented in Table I. These results are compared with the initial yields obtained directly from the initial slopes of the curves in Fig. 1. The results thus obtained by the extrapolation method are about 5–20% higher, although they show the same general pH dependence as the initial yields directly obtained. These results clearly indicate that in the low pH region the initial quantum yield is pH dependent.

TABLE I

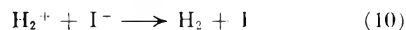
INITIAL QUANTUM YIELDS FOR PHOTO-OXIDATION OF EVACUATED 0.15 M KI SOLUTIONS

pH	γ_i	
	From Fig. 1	From intercepts of Fig. 5
0.65	0.226	0.240
0.9	.200	.212
1.1	.167	.187
1.36	.139	.163
1.78	.105	.138

The pH Dependence of γ_i .—The pH dependence of the initial quantum yield in the region below pH 3.5 may be due to either of the causes: (a) Interaction of the H^+ ion with the excited state of the iodide or with one of the species participating in the secondary recombination in the photochemical cage. These possible mechanisms will lead to a pH dependent rate of introduction of radicals into the bulk. (b) It was proposed by Rigg and Weiss⁸ that a scavenging reaction of H atoms occurs



followed by



These reactions are assumed to compete with the back reactions 7 and 8.

In this mechanism⁸ no clear cut distinction between secondary cage recombination and bulk recombination was presented. However, the treatment is based on conventional steady-state ki-

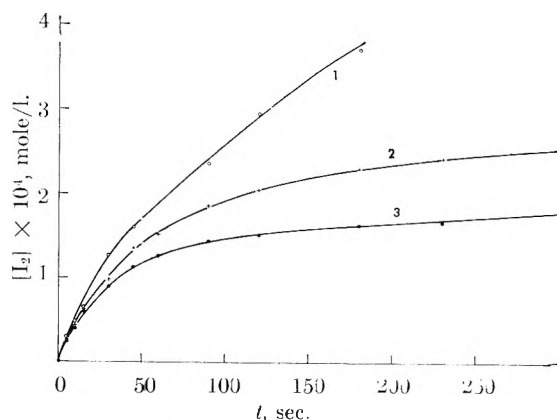


Fig. 4.—Photo-oxidation curves at various I^- concentrations at pH 5.5, $J = 9.7 \times 10^{-7}$ einstein liter⁻¹ sec.⁻¹ (1) $I^- = 0.6 M$, (2) $I^- = 0.3 M$, (3) $I^- = 0.15 M$.

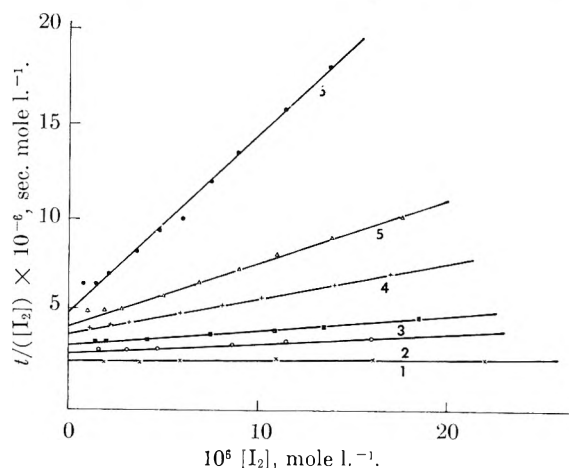


Fig. 5.—Graphical determination of initial yields at different pH values: $I^- = 0.15 M$; curve numbers the same as in Fig. 1

netics⁸ leading to the dependence of the initial photo-oxidation rate on $J^{2/3}$. These results for bulk scavenging are inconsistent with the independence of the quantum yield of light intensity. Thus the pH dependence is attributed to mechanism (a) which, however is not unique. Farkas and Farkas²⁵ postulated the direct interaction of the excited electron with the H^+ ion. This idea was supported by Franck and Platzman¹⁰ who reported a linear dependence of γ_i on H^+ which is in variance with our experimental results. The independence of γ_i of light intensity is consistent either with Farkas' mechanism or with a model of radical scavenging by H^+ from a photochemical cage, this scavenging reaction competing efficiently with secondary recombination. By investigating the pH dependence of γ_i we intended to distinguish between these possibilities.

Our experimental results can be represented by the equation

$$\gamma_i = \eta + W[H^+]^{1/2} \quad (\text{IV})$$

where at 25°

$$\eta = 0.092 \pm 0.005$$

$$W = 0.33 \pm 0.02$$

This equation is satisfactorily fulfilled in the pH

(25) A. Farkas and L. Farkas, *Trans. Faraday Soc.*, **34** 1113 (1938).

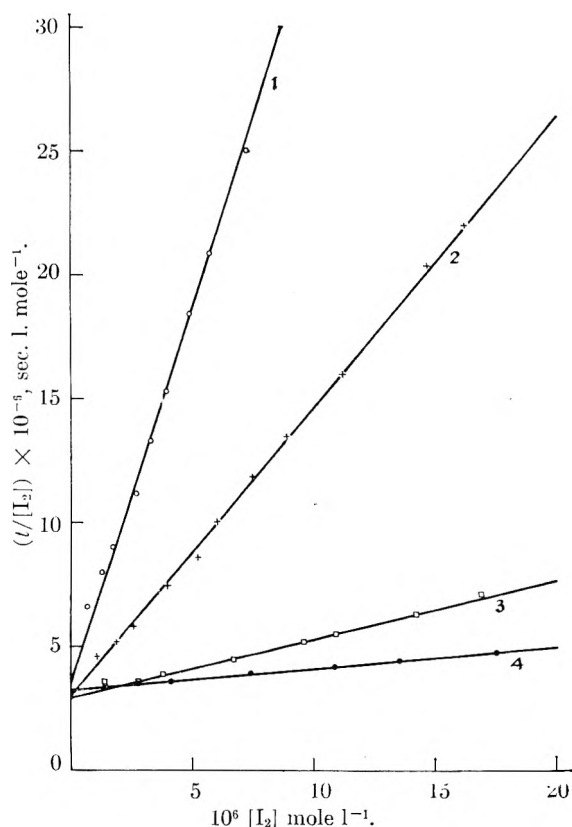


Fig. 6.—Graphical determination of initial yields at various I^- concentrations: (1) pH 0.87, $I^- = 5 \times 10^{-3} M$; (2) pH 0.87, $I^- = 1.5 \times 10^{-2} M$; (3) pH 0.87, $I^- = 5 \times 10^{-2} M$; (4) pH 0.90, $I^- = 1.5 \times 10^{-1} M$.

region up to pH 2.0 and I^- concentrations under investigation. The square root law is presented in Fig. 7. In this plot we have used the initial quantum yields obtained by the extrapolation method. The intercept of the line in Fig. 7 yields the value of 0.092 ± 0.005 which is equal to $3\gamma_r$ in good agreement with the prediction of equation I.

At pH > 2 deviations from linearity in the linear plot of Fig. 7 occur due to the change in reaction mechanism. At low pH below 0.7 the deviations are predicted by the theory of diffusion controlled scavenging. Theoretical predictions for efficient scavenging reactions competing with secondary recombinations predict such a functional dependence on scavenger concentrations.²⁶

Application of the Theory of Diffusion Controlled Scavenging.—The square root law was derived by application of two models: a continuous model²⁷ and random walk in three dimensions.²⁸ The approach developed by Noyes^{26,28} will be applied here.

Denoting by β' the total probability of two original partners to react and by $h(t)dt$ the probability of these radicals to react between the time t and $t + dt$, then

$$\beta' = \int_0^{\infty} h(t)dt \quad (V)$$

The residual yield for the introduction of the radicals into the bulk is

$$\alpha^r = \Gamma(1 - \beta') \quad (VI)$$

where Γ is the cross-section for primary photodissociation followed by the formation of radical pair in a solvent cage.

In the presence of a scavenger the probability of a radical to escape geminate recombination is^{26,28}

$$\begin{aligned} \int h(t)(1 - e^{-k[S]t}) dt &= \beta' - \int h(t) e^{-k[S]t} dt = \\ \beta' - \int_0^{\infty} 4a^2/\beta'^2 at^{-3/2} e^{-k[S]t} dt &= \\ 2a(\pi k[S])^{1/2} - \frac{8a^2k}{\beta'} [S] \end{aligned} \quad (VII)$$

where k is the long time bulk rate constant for the scavenging reaction,²⁸ $[S]$ the scavenger concentration, and a is a parameter defined by Noyes.²⁶

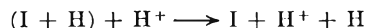
The integration of $h(t)$ is valid according to this approximation only after a certain period corresponding to the formation of distinct chemical species and subsequent few diffusive displacements. This period is selected as the relaxation time of the solvent molecules 10^{-11} sec. Thus we set $4a^2/\beta'^2 = 10^{-11}$ sec. and as $\beta' \sim 1$ hence $4a^2 \sim 10^{-11}$ sec. The theoretical expression for relatively low scavenger concentrations is thus given by

$$\alpha = \alpha_r + 2a\Gamma(\pi k[S])^{1/2} \quad (VIII)$$

Fitting our experimental results into this scheme using the value of $W = 0.33$ obtained from Fig. 3 we obtain $k = 3 \times 10^8 M^{-1} \text{ sec.}^{-1}$ as an upper limit, assuming $\Gamma = 1$.

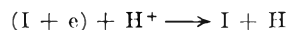
The nature of the scavenging reaction will now be considered. A plausible mechanism for hydrogen atom scavenging by H^+ is that of H_2^+ formation according to reaction 9.⁸ However independent experimental work¹⁵ indicates that the rate constant of H_2^+ formation is relatively low, $k_9 \sim 10^3 M^{-1} \text{ sec.}^{-1}$, a result which is much lower than the scavenging rate constant. Thus we are forced to conclude that H_2^+ formation is not involved in the scavenging reaction. The magnitude of the rate constant k shows that the scavenging process involves electron transfer. However at present we cannot decide whether it is an H atom or an electron which undergoes the random walk process in the photochemical cage and which interacts with H^+ .

Thus the scavenging mechanisms may involve the charge transfer process



Theoretical estimates²⁹ indicate the efficiency of this reaction at relatively large separations.

Alternatively the scavenging reaction may involve thermal electron capture by the hydroxonium ion, which may be an efficient process. The



possibility of specific reactions of thermalized electrons was considered in detail in radiation chemistry.^{30,31} Recently the question of the distinction between hydrogen atoms and related species was raised. Thus Barr and Allen³² postu-

(29) W. F. Libby, *J. Phys. Chem.*, **56**, 863 (1952).

(30) H. Frohlich and R. L. Platzman, *Phys. Rev.*, **92**, 1152 (1953).

(31) D. Armstrong, E. Collinson, F. S. Dainton, D. M. Donaldson, E. Hayon, N. Miller and J. Weiss, *Proc. 2nd Int. Conf. Peaceful Uses of Atomic Energy, Geneva*, **29**, 80 (1958).

(26) R. M. Noyes, *J. Am. Chem. Soc.*, **77**, 2042 (1955).

(27) L. Monchick, *J. Chem. Phys.*, **24**, 381 (1956).

(28) R. M. Noyes, *J. Am. Chem. Soc.*, **74**, 5486 (1956).

lated the existence of two forms of H atoms in aqueous solutions. One of these probably is the thermalized electron.^{33,34}

Dependence of γ_i on I^- Concentration.—The experimental results presented in Fig. 6 indicate that the initial quantum yield is independent of initial iodide concentration in the concentration region 5×10^{-3} to $0.15 M$ at low pH. These results were obtained under conditions of total light absorption which hold up to the lower I^- concentration employed. These results are in variance with previously reported experimental data⁸ and indicate that contrary to previous suggestions^{8,11} the iodide ion concentration does not affect the rate of introduction of radicals into the bulk.

Radical Reactions in the Bulk.—As a result of the scavenging reaction, or by diffusion away from original partners, hydrogen and iodide atoms are introduced into the bulk. At relatively low pH below 2.0 hydrogen atoms act as oxidizing agents for the iodide ion. Recently this fact was demonstrated by oxidation of the iodide ion by H atoms externally generated, and it was shown that the results are consistent with an oxidation mechanism involving H_2^+ as the actual oxidizing species.¹⁵ In this low pH region the initial rate of introduction of H atoms into the bulk is equal to the initial photo-oxidation rate.

The nature of the oxidation reaction of I^- by atomic hydrogen in the photochemical system was investigated by considering the compound rate constants ratio k_r/k_{ox} . This value was obtained from the ratio of slope to intercept from Figs. 5 and 6. The accuracy of the rate constants obtained is about 5%. These data are presented in Table II.

TABLE II

THE DEPENDENCE OF k_r/k_{ox} ON pH AND IODIDE ION CONCENTRATIONS

pH	I^-, M	$1/H^+, M^{-1}$	$10^{-4} \frac{k_r}{k_{ox}}$
0.65	1.5×10^{-1}	4.15	0.58
.87	5×10^{-3}	...	0.89
.87	1.5×10^{-2}	...	1.0
.87	5×10^{-2}	...	0.76
.9	1.5×10^{-1}	7.7	0.71
1.1	1.5×10^{-1}	11.9	1.46
1.36	1.5×10^{-1}	23.3	2.25
1.78	1.5×10^{-1}	57.0	5.20

The ratio of the rate constants is found to be pH dependent. A plot of this ratio as a function of $1/[H^+]$ is a straight line, with a positive intercept. (Fig. 8). The experimental results can be fitted by the expression

$$\frac{k_r}{k_{ox}} = 1.5 \times 10^3 + \frac{900}{[H^+]} \quad (IX)$$

No dependence of k_r/k_{ox} on I^- could be detected up to $1.5 \times 10^{-1} M$. For higher iodide concentrations the results were not accurate enough to establish this point.

(32) N. F. Barr and A. O. Allen, *J. Phys. Chem.*, **62**, 928 (1958).

(33) J. T. Allen and G. Scholes, *Nature*, **187**, 226 (1960).

(34) G. Czapski, J. Jortner and G. Stein, *J. Phys. Chem.*, **65**, 964 (1961).

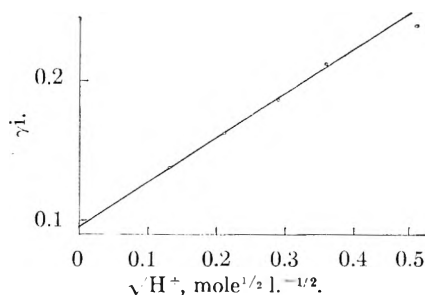


Fig. 7.—The dependence of initial quantum yields on the square root of H^+ ion concentration.

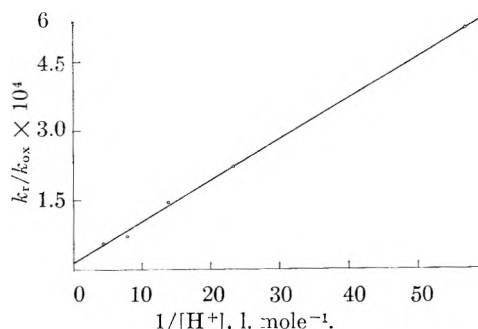
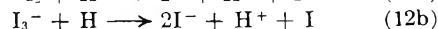
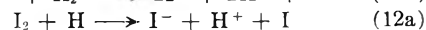
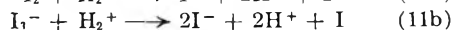
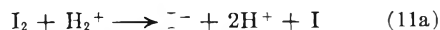


Fig. 8.—The dependence of the compound rate constants ratio k_r/k_{ox} on $1/H^+$ for $0.15 M I^-$.

We wish to show that these results are consistent with the oxidation mechanism involving H_2^+ . We assume that oxidation of the I^- ion proceeds by reactions 9 and 10. The possible reaction

$$H_2^+ + I_2^- \longrightarrow H_2 + I_2$$

is not introduced because of the low steady state concentrations I_2^- compared with that of I^- . The reduction reaction of iodine and I^- may proceed by

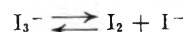


Under our experimental conditions iodine is present mainly as I_3^- . However the pronounced dependence of the reduction yield of iodine on I^- concentration at pH 5.5 (Fig. 4) indicates that triiodide ions are more stable toward reduction compared with free I_2 .

The concentration of free I_2 can be obtained from the expression

$$[I_2] = \frac{K_e [I_2]_t}{K_e + [I^-]} \cong \frac{K_e [I_2]_t}{[I^-]}$$

where $K_e = 1.4 \times 10^{-3}$ at 25° is the equilibrium constant for the reaction



and $[I_2]_t$ is the total iodine concentration. Application of steady state treatment to the bulk reactions 9, 10, 11 and 12 leads to the result

$$\frac{d[I_2]_t}{dt} = \frac{\alpha J}{2} \left(1 + \frac{X[I^-] - Y[I_2]}{X[I^-] + Y[I_2]} \right) \quad (X)$$

where $X = k_9 k_{10} [H^+]$.

$$Y = k_9 k_{11} [H^+] + k_{-9} k_{12} + k_{10} k_{12} [I^-] + k_{11} k_{12} [I_2]$$

$$k_{11} = k_{11}^0 + \frac{k_{11}^0 K_e}{[I^-]}$$

$$k_{12} = k_{12}^a + \frac{k_{12}^b K_o}{[I^-]}$$

Thus we obtain

$$\frac{k_r}{k_{ox}} = \frac{k_{11}}{k_{10}} + \frac{k_{12}(k_{-9}/k_{10} + [I^-])}{k_9[H^+]} + \frac{k_{11}k_{12}}{k_9k_{10}} [I_2] \quad (\text{XI})$$

For relatively low I_2 concentrations the linear term in I_2 can be neglected. This is indicated from Figs. 5 and 6 where no deviations from linearity were observed.

The pH dependence of the ratio of the rate constants is consistent with the oxidation mechanism involving H_2^+ . The oxidation mechanism involving abstraction of H atoms from the hydration layer³⁵ requires that the ratio of the rate constants should not be dependent on pH, while the triple

(35) N. Uri, *Chem. Revs.*, **50**, 376 (1952).

collision mechanism³⁶ requires that the intercept in Fig. 8 should be zero. Neither of these conditions is fulfilled.

It should be pointed out however that while the photochemical data indicate a pH dependent mechanism for the oxidation of I^- by H atoms, these results by themselves do not yield absolute evidence for the oxidation mechanism involving H_2^+ . The main effect of H^+ ion on the photochemistry is due to the pH dependence of the rate of introduction of radicals into the bulk. The difficulties of the detection of the dependence of k_{ox}/k_r on I^- ion concentration which probably cancels out due to opposite effects remain to be elucidated.

(36) J. P. Ethier and F. Haber, *Naturwiss.*, **18**, 266 (1930).

THE NATURE OF THE CHROMIUM(VI)-1,5-DIPHENYLCARBOHYDRAZIDE REACTION. II. THE CHROMIUM(II)-DIPHENYLCARBAZONE REACTION^{1,2}

BY IVAN E. LICHTENSTEIN AND THOMAS L. ALLEN

Department of Chemistry, University of California, Davis, California

Received February 6, 1961

Chromium(II) reacts with diphenylcarbazone in aqueous solution to give an intense magenta color. A molar absorptance index of 3.6×10^4 (based on chromium(II) concentration) has been obtained at 546 $m\mu$. The absorption spectrum is very similar to that of the magenta product of the aqueous chromium(VI)-1,5-diphenylcarbohydrazide reaction. It is concluded that the same colored substance, a chromium complex, is formed in both reactions.

Introduction

In several previous investigations³⁻⁵ it has been found that chromium(II) reacts with diphenylcarbazone (phenylazofornic acid-2-phenylhydrazide) in aqueous media to give an intense magenta color, similar to that arising from the aqueous chromium(VI)-1,5-diphenylcarbohydrazide reaction. Very recently, however, Babko and Get'man⁶ have reported that chromium(II) does not react with diphenylcarbazone. They attribute the results of previous investigators to the use of chromous acetate. Since they have found that diphenylcarbazone in acetic acid has the same color whether chromium(II) is present or not, Babko and Get'man conclude that the color observed by previous workers must have resulted from the side reaction of diphenylcarbazone with acetic acid.

Because of the doubt thrown on the existence of the chromium(II)-diphenylcarbazone reaction, which had seemed to be closely related to the chromium(VI)-1,5-diphenylcarbohydrazide reaction, we have made a detailed investigation of this and related systems.

(1) This work was assisted by a research grant from the National Science Foundation.

(2) Abstracted in part from the Ph.D. Dissertation of Ivan E. Lichtenstein, University of California, Davis, 1960.

(3) M. Bose, *Anal. Chim. Acta*, **10**, 201, 209 (1954).

(4) R. T. Pflaum and L. C. Howick, *J. Am. Chem. Soc.*, **78**, 4862 (1956).

(5) B. Das Sarma and J. N. Ray, *Sci. and Culture (India)*, **21**, 477 (1956).

(6) A. K. Babko and T. E. Get'man, *Zhur. Obshch. Khim.*, **29**, 2416 (1959).

Experimental

Materials.—Pure diphenylcarbazone was obtained from its double compound with 1,5-diphenylcarbohydrazide by the method of Krumholz and Krumholz.⁷ The diphenylcarbazone was recrystallized from 1:2 EtOH- H_2O , m.p. 123–126°; lit.⁷ 125°. *Anal.* Calcd. for $C_{18}H_{12}N_2O$: C, 64.97; H, 5.03; N, 23.32. Found: C, 64.80; H, 4.91; N, 23.49. The double compound was recrystallized from 1:1 EtOH- H_2O , m.p. 154–157°; lit.⁷ 156–158°. Eastman 1,5-diphenylcarbohydrazide, lot 42, m.p. 173–174°, was used directly. Acetone was Eastman Spectro grade. Matheson prepurified nitrogen and "bone-dry" CO_2 were used. Other substances were reagent grade.

Solutions.—A 1 *M* chromium(II) solution, used in the qualitative expts., was prepared by reduction of a chromic chloride solution with zinc amalgam. The deep blue solution was stored under CO_2 . For the quantitative expts. a more dilute chromous solution was prepared by the method of Stone⁸ and stored under nitrogen. The all-glass apparatus used to store and dispense the solution was similar to the gravity type of apparatus described by Stone.⁸ Chromium(II) was determined both iodometrically⁹ and potentiometrically.¹⁰ The average of four such determinations was $1.17(\pm 0.02) \times 10^{-3}$ *M*. This solution also contained significant amounts of chromium(III). The presence of chromium(III) should not interfere with a study of the chromium(II)-diphenylcarbazone reaction, as chromium(III) does not react with diphenylcarbazone or 1,5-diphenylcarbohydrazide under the conditions of these expts.³ Nevertheless, blanks containing appropriate amounts of chromium(III) were used. The chromium(III) stock solution contained 0.018 *M* $CrCl_3$ and 0.2 *M* HCl . Zinc(II) also was added to the blanks, since the chromous solution contained this species owing to its manner of preparation. The zinc(II) stock solution contained 0.5 *M* $ZnCl_2$ and 0.1 *M* HCl .

(7) P. Krumholz and E. Krumholz, *Monatsh.*, **70**, 431 (1937).

(8) H. W. Stone, *Anal. Chem.*, **20**, 747 (1948).

(9) H. W. Stone and R. L. Eichelberger, *ibid.*, **23**, 868 (1951).

(10) J. J. Lingane and R. L. Pecsok, *ibid.*, **20**, 425 (1948).

Apparatus.—Absorption spectra were measured with a Beckman DU spectrophotometer at 25° using 1.000 cm. fused silica cells. A Beckman Model G pH meter was used to determine pH.

Qualitative Experiments.—One drop of 1 M chromium(II) solution was added to an acidified water-acetone solution of diphenylcarbazone or double compound. After dilution to a suitable volume, the absorption spectrum of the solution (relative to a reagent blank) was measured.

Quantitative Experiments.—In the first expt. listed in Table I, 50 mg. of diphenylcarbazone was dissolved in 40 ml. of acetone, and then 80 ml. of water and 12 ml. of 1 M HCl were added. The solution was divided in half, and nitrogen was bubbled through each portion for one hour. Then 10.55 ml. of the dilute chromium(II) solution was added to one portion; 5.0 ml. of the chromium(III) solution and 0.2 ml. of the zinc(II) solution were added to the other. Oxygen was excluded prior to and during this step, and for five minutes thereafter. The solutions then were diluted to 200 ml. with water. For the spectrophotometric measurements 5.00-ml. aliquots were diluted to 25.0 ml. In the second expt. 3.07 ml. of the chromium(II) solution was used, and the spectrophotometric measurements were made after dilution to 200 ml. The third expt. was similar to the second, except that the water used to dilute the diphenylcarbazone solution was "air equilibrated" by bubbling air through it for several hours, and the solution was not flushed out with nitrogen. In the fourth expt. the 12 ml. of 1 M HCl were omitted; otherwise it was identical with the second. (The fairly low pH resulted from the acidity of the chromous solution.)

For comparison it was necessary to determine the absorption spectrum of the colored product of the chromium(VI)-1,5-diphenylcarbohydrazide reaction. Appropriate amounts of the organic reagent in acetone, dilute HCl, and a solution of chromium(VI) were mixed. The final solution contained 10% acetone by volume and had a pH of 2.3. The absorption spectra of solutions of diphenylcarbazone in glacial acetic acid and in 10 vol. % acetic acid also were determined.

Results

The qualitative expts. showed that chromium(II) and diphenylcarbazone give an intense magenta color despite the absence of acetic acid and acetates. Both the position of the absorption maximum (545 m μ) and the shape of the absorption curve (half-maxima at 500 and 590 m μ) are identical, within the experimental error, with those of the colored product of the chromium(VI)-1,5-diphenylcarbohydrazide reaction (maximum at 546 m μ , half-maxima at 495 and 590 m μ). The reagent blank, containing diphenylcarbazone and zinc(II), had slight absorption and no maximum in this region. Its absorption spectrum was essentially the same as that of diphenylcarbazone in aqueous solution at pH 1.5.⁴ It was also found, in a separate expt., that the absorption of an appropriate blank containing zinc(II) and 1,5-diphenylcarbohydrazide was negligible in the visible region.

Chromium(II) likewise reacts with the double compound of diphenylcarbazone and 1,5-diphenylcarbohydrazide to give a magenta solution with the same absorption spectrum. The absorption of the reagent blank was again slight in the region of interest.

The salient features of the quantitative studies are shown in Table I. In each expt. the absorbancy of the solution increased slowly to a maximum value. The table lists both the time at which the absorbancy reached its maximum value, and the molar absorbancy index based on the maximum absorbancy at 546 m μ (relative to the reagent blank) and the formal concentration of chromium(II). A comparison of the first and second expts. shows

that increasing the mole ratio of diphenylcarbazone to chromium(II) substantially increases the value of $(a_M)_{\text{max}}$ and reduces t_{max} . The third expt. shows that when oxygen is present in the diphenylcarbazone solution prior to addition of chromium(II) maximum color is sharply reduced, probably because of the reaction of oxygen with chromous ion. In the fourth expt. the effect of pH was investigated. It is seen that increasing the pH increases both the rate and quantity of color development. The opposite effect occurs in the chromium(VI)-1,5-diphenylcarbohydrazide reaction.¹¹

TABLE I

THE CHROMIUM(II)-DIPHENYLCARBAZONE REACTION

Mole ratio of reactants ^a	pH	t_{max} , hr. ^b	$(a_M)_{\text{max}}$ ^c
8:1	1.5 ^d	40	2.8×10^4
28:1	1.5	14	3.3×10^4
28:1	1.5	14	1.1×10^{4e}
28:1	2.8	2	3.6×10^4

^a Diphenylcarbazone:chromium(II). ^b Time at which the absorbancy reached a maximum. ^c Maximum value of the molar absorbancy index at 546 m μ . ^d Before taking aliquots. ^e Oxygen not excluded.

The solution of diphenylcarbazone in glacial acetic acid was found to have an intense purple color. Its absorption spectrum shows a peak at 550 m μ , with half-maxima at 500 and 585 m μ . The molar absorbancy index at 550 m μ , based on diphenylcarbazone, is 6.7×10^3 . On dilution with water the color fades to a light orange, and the spectrum of diphenylcarbazone in 10% acetic acid has only a weak plateau in the 520–540 m μ region. A comparison of the absorption spectra of diphenylcarbazone in various solvents will be reported elsewhere.

Discussion

The results presented above show that the magenta substance which is formed by mixing solutions containing diphenylcarbazone and chromium(II) is a product of a reaction between these reagents, and not a product of some side reaction. It has been reported that zinc(II) forms colored products with diphenylcarbazone and 1,5-diphenylcarbohydrazide.¹² However, the blank tests have shown that colored substances are not formed by zinc ion and either reagent at the concentration level used in these expts. It also has been shown that the presence of acetic acid or acetates is not necessary for color development. Furthermore, the presence of small amounts of acetic acid in a diphenylcarbazone solution is not in itself sufficient to produce the magenta color. Hence the strong absorption at 540 m μ reported by earlier workers^{3,4} cannot be attributed to their use of chromous acetate.

For each of the chromium(II)-diphenylcarbazone systems studied it was found that the absorption spectrum had essentially the same form as that of the chromium(VI)-1,5-diphenylcarbohydrazide system. Logarithmic graphs of absorbancy vs. wave length for the two systems were superimposable

(11) T. L. Allen, *Anal. Chem.*, **30**, 447 (1958).

(12) F. J. Welcher, "Organic Analytical Reagents," Vol. III, D. J. Van Nostrand Co., Inc., New York, N. Y., 1947, pp. 431 and 456.

within the experimental uncertainty.¹³ Under the most favorable conditions employed (the last expt. in Table I), the molar absorptivity index at 546 $m\mu$ is 3.6×10^4 based on chromium(II). This is substantially larger than the value of 2.5×10^4 (at 540 $m\mu$) obtained by Pflaum and Howick.⁴ It seems likely that when the reaction is carried out under optimum conditions the molar absorptivity index will be the same as that of the magenta product of the chromium(VI)-1,5-diphenylcarbohydrazide reaction, which is $(4.17 \pm 0.04) \times 10^4$ at 546 $m\mu$ based on chromium(VI).¹¹

Extraction studies of the latter substance have shown that it is a chromium complex.¹⁴ As the

(13) We are indebted to Dr. A. I. Popov for pointing out this method.

(14) I. E. Lichtenstein and T. L. Allen, *J. Am. Chem. Soc.*, **81**, 1040 (1959). In this article the complex was inadvertently called an organometallic complex. Although the word organometallic commonly indicates that the metal is bonded directly to a carbon atom, such an implication was not intended, inasmuch as the complex is probably a chelate in which chromium is bonded to oxygen and/or nitrogen atoms.

colored substance and chromium were extracted in the same proportion, all of the chromium must have been complexed. The close similarity of the magenta product of the chromium(II)-diphenylcarbazone reaction, both in the form of its absorption spectrum and in its molar absorptivity index, suggests that it is the same substance, and that here too all of the chromium is complexed.

The absorption spectrum of the chromium complex in aqueous solution is rather similar to that of diphenylcarbazone in glacial acetic acid (or, to a lesser extent, in certain other solvents). It is markedly different from that of diphenylcarbazone in dilute acetic acid and other aqueous solutions. Previous investigators^{4,5} have obtained evidence that the complex contains diphenylcarbazone and chromium(III). Because of the similarity in spectra, it is reasonable to suppose that diphenylcarbazone has a similar structure in the complex and in glacial acetic acid; complexing with chromium(III) makes this structure stable with respect to the form normally present in aqueous solution.

THERMODYNAMICS OF SOLUTION OF HIPPURIC ACID IN WATER AND IN VARIOUS SODIUM CHLORIDE SOLUTIONS^{1,2}

BY RICCI J. LARESE AND WILLIAM J. CANADY

West Virginia University Medical Center, Department of Biochemistry, Morgantown, West Virginia

Received February 10, 1961

In view of the fact that hippuric acid is a compound of considerable biological importance, and since crystallization is used as a step in the quantitative determination of hippuric acid, the solubility of hippuric acid as a function of temperature and ionic strength has been studied. The solvents varied from pure water to 3.0 *m* sodium chloride solution. Variations of the free energies, heats and entropies of solution with ionic strength are presented. The free energy of solution at 25° is linear with ionic strength, while the heat of solution varies very little with ionic strength. The variation of the change in heat capacity for the solution process with salt concentration may be explained in a rough qualitative manner in terms of the iceberg theory of Frank and Evans. The variation of the entropy change with salt concentration is very slight at 25° but when extrapolated to lower temperatures it tends to increase with an increase in ionic strength as would be expected from iceberg theory.

The solubility of hippuric acid in water and in salt solutions has been of practical interest for a number of years, since crystallization is used as a step in the quantitative determination of hippuric acid.³⁻⁵

Very little work to date has had to do with the temperature dependence of the solubility of hippuric acid or the effect of added neutral salts upon this dependence.

Equilibrium was studied from both undersaturation and oversaturation. Solvents ranged from pure water to three molal salt solution; seven temperatures were investigated, ranging from approximately 15 to approximately 45°.

Experimental

Equipment.—Constant temperature was maintained by means of a Sargent thermistor controlled water-bath. The temperature may be maintained within $\pm 0.01^\circ$. The

temperature was measured with two EXAX solid point thermometers having temperature ranges of 0 to 30° and 20 to 50°, respectively, in increments of 0.1°. These thermometers were calibrated against a Leeds and Northrup platinum resistance thermometer over the entire experimental range. The platinum resistance thermometer had been previously calibrated by the U.S. Bureau of Standards. A Beckman DUUV Spectrophotometer was used for the photometric determinations.

Materials.—The hippuric acid was obtained from the Fisher Corporation and was the "highest purity" grade. It was recrystallized twice from water and its melting point remained unchanged at 187.2°. The water was doubly distilled through all glass apparatus. The sodium chloride used was J. T. Baker C.P. grade.

Procedure.—For equilibrium approached from under saturation, one gram of hippuric acid was placed in a 100 ml. screw cap Pyrex erlenmeyer flask along with 80-90 ml. of solvent. Water-proofed corks were placed around the necks of the flasks and this whole assembly was wired to lead sinkers. The lengths of wire linking them with the lead sinkers at the bottom of the bath were arranged so that the flasks would float with a gentle bobbing, rotating motion due to the brisk circulatory flow of water in the bath, but were not allowed to move about freely.

For equilibrium approached from oversaturation, the procedure was similar to that described above except that the flasks containing hippuric acid crystals and solvent were maintained at approximately 55° for six hours before being placed in the bath.

Samples were removed at various times from both the

(1) This investigation was supported by a grant from the National Science Foundation.

(2) Abstracted from a thesis by R. J. Larese in partial fulfillment of the requirements for the M.S. degree, West Virginia University.

(3) A. J. Quick, *Am. J. Med. Sci.*, **185**, 630 (1933).

(4) A. J. Quick, *Am. J. Clin. Path.*, **10**, 222 (1940).

(5) T. E. Weichselbaum and J. G. Probststein, *J. Lab. Clin. Med.*, **24**, 636 (1939).

under and oversaturated flasks. For the studies with pure water 25 ml. was removed; for the studies with salt solutions the samples consisted for 10 ml. In each case care was exercised to avoid taking up any solid. The aliquot was transferred to a volumetric flask which was held in the same bath. After a 15-minute equilibration, the volume was adjusted exactly to the mark. This made it possible to be certain that no appreciable volume change took place from the slight warming or cooling effect introduced by removal of the sample. The flasks then were stoppered and weighed. The contents of each volumetric flask were diluted in such a way as to produce a solution ranging from $2-5 \times 10^{-5} M$ in hippuric acid for spectrophotometric determination at 230 $m\mu$. Serial dilutions were found to follow Beer's law. All readings were compared to a standard curve derived by least squares from known solutions of hippuric acid.

Results

The results obtained from undersaturation did not differ significantly from those obtained from oversaturation. Approximately half of the experiments were done in each way. The average deviation from the mean at each temperature for 281 determinations was 1.13%.

The logarithm of the solubility, s , expressed as molality, was plotted against the reciprocal of the absolute temperature on large scale graph paper. A smooth curve was drawn and the values read at various values of $1/T$. These smoothed values are listed in Table I. The smoothed data were fitted to an equation of the form

$$\ln s = \frac{\Delta H_0}{RT} + \frac{\Delta C_p}{R} \ln T + C \quad (1)$$

where

$$\Delta H = \Delta H_0 + \Delta C_p T$$

It is assumed that the conventional activity coefficient is independent of concentration.

TABLE I

LOGARITHMS OF THE SOLUBILITIES OF HIPPURIC ACID IN WATER AND NaCl SOLUTIONS AT VARIOUS TEMPERATURES
Concentrations are expressed as molalities

T, °K.	H ₂ O	0.2	0.5	1.0	2.0	3.0
288.1	1.8690	1.9160	1.9980	2.1590	2.3335
288.8	1.8213
292.1	1.7580	1.7970	1.8415	1.9220	2.0820	2.2540
298.1	1.6840	1.7210	1.7641	1.8435	1.9978	2.1638
303.1	1.6030	1.6360	1.6810	1.7609	1.9172	2.0815
308.1	1.5215	1.5523	1.5947	1.6782	1.8361	1.9978
313.1	1.4372	1.4645	1.5080	1.5919	1.7522	1.9190
318.1	1.3470	1.3745	1.4194	1.5033	1.6720	1.8400

Some thermodynamical quantities of interest are listed in Table II. The standard free energy change ΔF^0 is written as equal to $-RT \ln s$. In addition ΔH , the change in heat content, ΔS^0 , the entropy change and ΔC_p , the change in heat capacity, are also listed. All values given are for a temperature of 25°, except for the change in heat capacity, which is essentially independent of temperature over the range studied. The relative activity coefficient γ at 25° defined as Molality in water/Molality in salt solution is given as well.

It should be noted that the solubility measured in water at 25° agrees well, within one per cent., with the result of Larsson.⁶ It should be noted that ΔC_p in 0.2 m sodium chloride is larger than the value

for pure water. Since these terms vary considerably with small experimental errors, it is doubtful that this is significant.

The constants appearing in eq. 1 are given in Table III so that the solubility may be calculated for any temperature within the experimental range. A linear relationship is found when ΔF^0 is plotted against ionic strength. Since the logarithms of the solubility of many non-electrolytes produce a linear result when plotted against ionic strength, the linearity of the free energy plot is not surprising. A plot of relative activity coefficient, γ , against ΔC_p , the change in heat capacity, results in a fairly good straight line.

TABLE II

NaCl concn.	ΔF , cal.	ΔH , cal.	ΔS , e. u.	ΔC_p , cal./°C.	γ
0.0	2293	6264	13.3	103.7	1.00
.2	2342	6421	13.7	104.6	1.09
.5	2401	6485	13.7	100.1	1.20
1.0	2511	6479	13.3	91.0	1.44
2.0	2723	6561	12.9	54.4	2.07
3.0	2949	6813	13.0	21.1	3.03

TABLE III

CONSTANTS OF EQUATION 1

NaCl concn.	ΔH_0	$\frac{\Delta C_p}{R}$	$-C$
0.0	-24647.60292	52.18857	342.84110
.2	-26112.56126	54.92649	360.99648
.5	-23371.88995	50.41238	330.74994
1.0	-20651.03184	45.80447	300.08691
2.0	-9672.34056	27.40730	177.08581
3.0	+513.62820	10.63547	64.70971

Discussion

A relatively small variation of the heat of solution at 25° with ionic strength was observed. If the heat of solution is calculated for higher temperatures, e.g., 45°, the effect becomes even smaller, while at lower temperatures considerable variation is observed. The variation of ΔC_p might be interpreted in terms of the "iceberg theory" of Frank and Evans.⁷ Clausen and Polglase⁸ have suggested that the large changes in the heat capacities which they observed for the solution of aliphatic hydrocarbons in water might be due to the large amount of energy required to crack this shell of relatively demobilized water molecules surrounding the solute molecules. It is possible that in the case of hippuric acid, "melting" of such a sheath by added electrolyte might take place; hence ΔC_p would be expected to decrease with increasing ionic strength which is indeed observed. Rather large negative entropy changes would be expected also. It must be kept in mind, of course, that hippuric acid is a crystalline solid and that any thermodynamic terms associated with its solution also include destruction of the crystal as well as hydration of the solute molecules. It may be seen that the entropy changes are positive as might be expected in going from the highly ordered solid to the more disordered solution; this effect would seem to swamp out any "iceberg" contribution. Also to be noted is the

(7) H. S. Frank and M. W. Evans, *J. Chem. Phys.*, **13**, 519 (1945).

(8) W. F. Clausen and M. F. Polglase, *J. Am. Chem. Soc.*, **74**, 4817 (1952).

(6) E. Larsson, *Z. physik. Chem.*, **127**, 233 (1927).

fact the entropy change at 25° is almost independent of ionic strength, probably indicating a cancellation of effects, since the simple iceberg concept mentioned would predict that ΔS^0 would tend to become more positive as the "ice" layer around the solute is "melted." This lack of change in ΔS^0 might be ascribed to the increasing relative importance of a solute-ion interaction term or terms as the temperature is raised. It is of interest how-

ever, that at temperatures considerably lower than 25°, ΔS^0 does become more positive with increasing salt concentration as would be expected if iceberg formations were being broken up.

Acknowledgment.—The authors are indebted to the National Science Foundation for their support of this work, and to Dr. James B. Hickman, Department of Chemistry, West Virginia University, for the calibration of our thermometers.

THE CONDUCTANCE OF HYDROCHLORIC ACID AT 25°

BY R. H. STOKES

*Department of Physical and Inorganic Chemistry of the University of New England,
Armidale, New South Wales, Australia*

Received February 24, 1961

A new method of analysis of hydrochloric acid involving conductimetric determination of the concentration of a sodium chloride solution prepared from the acid is found to give very high accuracy. The conductance of hydrochloric acid is redetermined up to 1 *N* at closer intervals of concentration than those of existing data. Elimination of errors due to adsorption in flasks and cells, and to the Soret effect on placing the cells in the thermostat, makes the reproducibility $\pm 0.005\%$. Deviation-functions are tabulated which make interpolation within this accuracy possible, so that the results may be used for direct conductimetric analysis of hydrochloric acid solutions. The results are used to test the Fuoss-Onsager theory of conductance, and indicate a limiting equivalent conductance for hydrochloric acid, $\Lambda^0 = 426.50 \text{ cm}^2 \text{ ohm}^{-1} \text{ equiv.}^{-1}$ at 25°. The Fuoss-Onsager equation is exact only up to about 0.004*N*, whereas the earlier and very similar equation of Pitts holds exactly up to 0.92 *N*.

Introduction

The standardization of hydrochloric acid solutions is frequently required operation in chemical laboratories. In many research laboratories today, high-precision equipment for measuring electrolytic conductance is available, and the simple operation of measuring a conductance is much to be preferred to chemical standardization in such cases. The data of Shedlovsky¹ cover the range up to 0.1 *N* at 25° and those of Owen and Sweeton² go to 12 *N*, overlapping with Shedlovsky's. The concentration-intervals at which these investigators worked are however rather wide for convenient interpolation, and at some concentrations agreement between them is not as good as the precision of either set of measurements. The recent prediction by Agar³ that the Soret effect may cause systematic errors in conductance measurement, and its experimental verification in this Laboratory,⁴ have made it possible to obtain conductance measurements of such high reproducibility that a fresh series of measurements covering the range up to 1 *N* at closer intervals seemed worthwhile.

Another justification for the work is that it should provide a searching test of the validity of the Fuoss-Onsager extension of the Debye-Hückel-Onsager theory to higher concentrations, for hydrochloric acid solutions are virtually unaffected by solvent corrections to the conductance, both the self-dissociation of water and the ionization of dissolved carbon dioxide being repressed by the solute.

Experimental

1. **Purification and Analysis of Hydrochloric Acid Solutions.**—Analytical reagent quality hydrochloric acid was

diluted to about 5.8 molal with conductance water and distilled in Pyrex apparatus. Though constant-boiling hydrochloric acid is an often recommended primary standard, it was not used as such in this work. The reasons for its rejection need stating: After the original work of Hulett and Bonner in 1909,⁵ Foulk and Hollingsworth⁶ made in 1923 a careful reinvestigation covering the pressure range 730–780 mm. They noted a slight dependence of composition on the rate of distillation. Their values near 760 mm. have been reliably confirmed. In 1930 Bonner and Wallace⁷ extended the range of pressures covered. They quote the compositions to five significant figures, but mention that the accuracy of their silver chloride determinations was such that the deviation of duplicates or triplicates from the mean was $\pm 0.05\%$ in some cases! They also failed to confirm Foulk and Hollingsworth's observation on the effect of rate of distillation; a failure which is not surprising, for their method of seeking the effect was nothing more than a measurement of the density of the distillate to an accuracy of 1 in 10,000. They seem to have been under the impression that this accuracy in density measurement would give the same accuracy in the composition of the acid, whereas a variation of 1×10^{-3} in density corresponds to a relative error of 0.1% in the composition of the constant-boiling acid. Since the data of Bonner and Wallace are the only ones available at the atmospheric pressure of 680 mm. prevailing in this Laboratory, other means of analysis were necessary.

The most satisfactory solid base for acidimetric titration appears to be borax, provided that its hydrate composition can be definitely established as the decahydrate. A weighed 15-g. sample of analytical reagent borax was equilibrated in a platinum basin for several days in an evacuated desiccator over a solution saturated with respect to both sucrose and sodium chloride,⁸ the desiccator being immersed in a 25° thermostat. At the end of this period the sample was reweighed, the change being only 0.004%. This established that it was the decahydrate. A stock of 4 liters of approximately 1 molar acid was prepared from the distilled material and stored in a vessel from which it could be drawn by a siphon-tube. The container was thoroughly shaken before any sample was drawn off, to eliminate concentration-vari-

(1) T. Shedlovsky, *J. Am. Chem. Soc.*, **54**, 1411 (1932).

(2) B. B. Owen and F. H. Sweeton, *ibid.*, **63**, 2811 (1941).

(3) J. N. Agar, *Trans. Faraday Soc.*, **56**, 776 (1960).

(4) R. H. Stokes, *J. Phys. Chem.*, **65**, 1277 (1961).

(5) G. A. Hulett and W. D. Bonner, *J. Am. Chem. Soc.*, **31**, 390 (1909).

(6) C. W. Foulk and M. Hollingsworth, *ibid.*, **45**, 1220 (1923).

(7) W. D. Bonner and R. E. Wallace, *ibid.*, **52**, 1747 (1930).

(8) H. Menzel, *Z. anorg. allgem. Chem.*, **224**, 10 (1935).

tions arising from the condensation of vapor on the walls above the solution during nocturnal cooling of the laboratory. Solution which had stood for any length of time in the siphon-tube was discarded. As a further precaution against change, the conductance of this stock solution was measured at the beginning and end of the work with agreement to 0.005%. All analyses were made by transferring the stock acid directly from the siphon into a weight-buret, whence it was weighed out on a Mettler balance accurate to 0.1 mg. The weights of acid taken for analysis were never less than 30 g., so that weighing-errors of even 1 mg. would not exceed 0.003%.

For the borax analyses, 10–15 g. portions of borax were dissolved in conductance water and sufficient of the stock acid was weighed in to form an excess of 0.3 to 1% over the stoichiometric requirement. This excess was then back titrated volumetrically with 0.02 *N* carbonate-free sodium hydroxide (prepared from sodium amalgam), using a glass-electrode *pH* meter to follow the course of the titration. The end-point was taken as the point of inflection of the curve of *pH* vs. volume of sodium hydroxide. It should be noted that this point can be demonstrated, by consideration of the equilibria involved, to be the true equivalence-point in this titration, which is effectively that of hydrochloric acid against sodium hydroxide in the presence of boric acid. This was also confirmed by titration of a small amount of dilute hydrochloric acid with sodium hydroxide in the presence of the appropriate weighed amounts of pure sodium chloride and boric acid, in a volume equal to the final volume in the borax titrations. Other analyses were made by weight-titration against a 1 *M* sodium hydroxide solution (also prepared from sodium amalgam), which was in turn standardized by titration against potassium hydrogen phthalate. Gravimetric silver chloride determinations also were made.

It was considered, however, that none of these methods was quite up to the precision aimed at. The method on which most reliance finally was placed is given:

Weight-titrations of the stock acid were made against the 1 *M* sodium hydroxide, in an argon atmosphere, using brom thymol blue indicator, and with a differential volumetric finish with 0.02 *M* sodium hydroxide. The end-point was determined readily within 0.05 ml. of the 0.02 *M* sodium hydroxide, and since the weight of 1 *M* hydrochloric acid stock titrated was about 50 g., the end-point was known to 0.002%. The solution of sodium chloride left at the end of the titration was diluted by weight in the titration-flask so as to fall in the range 0.12–0.25 *M*. Its conductance was then measured. A "solvent-correction" (not exceeding 0.01% of the total conductance) was obtained by a blank titration on the same amount of indicator in the same volume. (The indicator blank titration was less than 0.05 ml. of the 0.02 *N* sodium hydroxide.) Now the conductance of sodium chloride solutions in the range 0.1–0.3 *M* is very accurately known from the work of Shedlovsky, *et al.*,⁹ and of Chambers.¹⁰ A graph of the deviation-function $\Lambda + 35\sqrt{c}$ against *c* (Fig. 1) shows that differences between the two investigations are less than 0.01% and the smooth curve through them is probably reliable to 0.005%. By a simple process of successive approximations using this deviation-function, the concentration of the sodium chloride then can be determined from its conductance within this accuracy. This method of course amounts to using the conductance of sodium chloride as the primary standard for acidimetry; the justification of this is that sodium chloride is a substance capable of preparation in extreme purity, and of exact weighing as a solid, and that conductance measurements with modern equipment can exceed in accuracy almost any standard analytical technique. [This being the case, why not simply analyze the hydrochloric acid conductimetrically by comparison with the data of Shedlovsky and of Owen and Sweeton? The reason is that, good though the measurements of these workers certainly are, they differ in places by up to 0.02%. It will in fact be shown later that the present results for the conductance of hydrochloric acid agree with Shedlovsky's within 0.005% between 0.1 and 0.005 *M*.]

The analytical results, expressed as moles of hydrogen

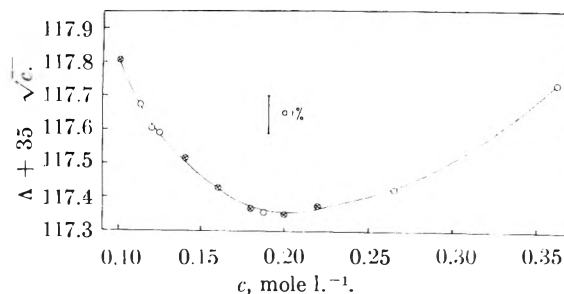


Fig. 1.—Interpolation function for the conductance of sodium chloride at 25° in the range 0.1–0.35 *N*: O, Chambers, ref. 10; X, Shedlovsky, Brown and MacInnes, ref. 9.

chloride per kg. of stock solution *in vacuo*, are summarized in Table I. The greatest weight is attached to the sodium chloride conductance method, and the least to the phthalate standardization of the sodium hydroxide, since the purity of the phthalate was not guaranteed to be better than 99.95%. The over-all mean of 0.97925 mole/kg. is also the mean of the three sodium chloride conductance determinations, and this figure was used for calculating concentrations of all solutions in the conductance measurements. Two liters of 0.1 *M* solution was prepared by weight-dilution of the 1 *M* stock, using a balance accurate to 5 mg. for weighing the diluted solution, and a 1 kg. capacity Mettler balance for weighing the large weight-buret of 1 *M* stock. Both the containers used for storage of these stocks had been used previously for the same purpose for a long time, so that surface reaction with the acid would be minimized.

TABLE I
SUMMARY OF ANALYSES OF HYDROCHLORIC ACID STOCK

Method	Moles HCl/kg. of soln. <i>in vacuo</i>
NaCl conductance, final soln. 0.135 <i>M</i>	0.9792 ₈
NaCl conductance, final soln. 0.208 <i>M</i>	.9792 ₂
NaCl conductance, final soln. 0.244 <i>M</i>	.9792 ₄
Borax weight-titration, 15 g. of borax	.9792 ₂
Borax weight-titration, 8 g. of borax	.9792 ₁
Silver chloride gravimetric	.9791
Weight-titration against NaOH standardized by potassium hydrogen phthalate	.9794 ₆
Over-all mean	.9792 ₅

The dilutions of the stock solutions were made by weight in the vessel shown in Fig. 2. For all solutions below 0.05 *M*, the following precaution against loss of acid by adsorption on the flask walls was taken: The stock solution was weighed into the tared clean dry flask (without the delivery-tube) from a weight-buret, the appropriate amount (500 to 600 ml.) of conductance water was added, and the flask and solution were weighed on the 1 kg. Mettler balance to 1 mg. The solution was then thoroughly mixed and allowed to stand in the flask for about half an hour, with occasional shaking to wet the whole surface. This solution (A) was then poured away and the mouth of the flask was dried with filter paper. The wet flask was reweighed, and contained 1 to 2 g. of the solution A on its wet surface. A fresh lot of stock acid then was weighed into the wet flask and diluted by weight to a concentration near that of solution A. The concentration of solution B then was calculated from the weight of stock acid and the small weight of solution A still in the wet flask. Now, suppose that solution A had lost 0.1% in concentration through adsorption on the flask walls: then since solution A contributed no more than one part in 300 of the total solute in the final solution B, the adsorption error in solution B would not exceed 0.0003%. This "rinsing" technique incidentally eliminates any errors due to contamination of the flask in cleaning and drying. Steaming-out is unnecessary, and the only washing required is a few rinses with conductance water. The flask need not be dried except when a check on the tare is con-

(9) T. Shedlovsky, A. S. Brown and D. A. MacInnes, *Trans. Electrochem. Soc.*, **66**, 165 (1934).

(10) J. F. Chambers, J. M. Stokes and R. H. Stokes, *J. Phys. Chem.*, **60**, 985 (1956).

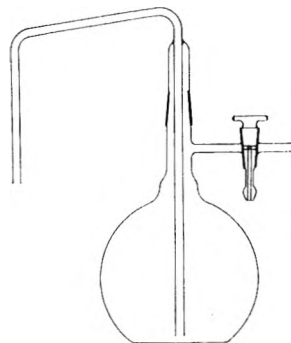


Fig. 2.—Weight-dilution vessel and delivery tube.

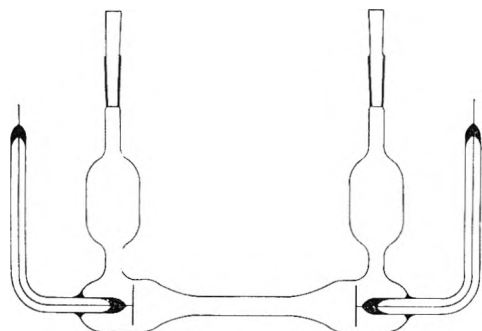


Fig. 3.—Conductance cell with mixing bulbs to permit elimination of error due to Soret effect.

sidered necessary, and even an error in the tare is largely self-cancelling. Another interesting point is: when a stock solution has to be weighed, it is delivered into the flask from a weight-buret. If it is delivered into a clean *dry* flask, the increase in weight of the flask is very appreciably less than the loss of solution from the weight-buret, *e.g.*, by 10 mg. This discrepancy is not due to evaporation in the ordinary sense, for the flask (having a narrow neck) may be left on the automatic balance and seen to have a constant weight for many minutes. It is due to the fact that when the liquid is run into the dry flask, it saturates the relatively dry air in the flask, so that more air is displaced from the flask than would be displaced by the liquid alone. If the liquid is weighed into a wet flask, the air within which is already saturated, the discrepancy disappears, and the weighing of the flask then forms a useful check on the weight-buret figure. In the weight-buret itself, of course, room air enters and becomes saturated, but since the new space formed is only equal to the volume of liquid run out, the error here is not significant. This is a point to be watched for whenever a liquid is weighed into a container many times the volume of the liquid.

Solution B was used for the conductance measurements proper, solution A being used, if at all, only for preliminary rinsing of conductance cells. A few measurements were made on both solutions, and it was found as expected that solution A gave lower conductances, especially with very dilute solutions, in accordance with the adsorption explanation. For example, with a 0.005 *N* solution, solution A gave a result 0.06% low.

Conductance water was prepared by passing the laboratory distilled water through a mixed-bed ion-exchange resin column. The water leaving the column was monitored by conductance measurements; a few hundred ml. was run to waste before using the water, by which time its conductance was below 1×10^{-7} ohm⁻¹ cm.⁻¹. The water was passed through the bed fairly rapidly (200–300 ml. per minute) to reduce the chance of colloidal matter being picked up from the resin; no visible or weighable residue was left on evaporation. At the time this work was done, many hundreds of liters of water had been passed through the bed, so that most of the accessible colloidal material had probably already gone. The residual conductance (only about twice that due to the self-dissociation of water) was tentatively ascribed to residual carbon dioxide, and therefore no solvent corrections were applied to the conductances of hydrochloric acid

made by dilution with this water. In the measurements above 0.002 *N*, no attempt was made to protect the water or the solutions from the atmosphere, as at these acid concentrations the ionization of carbon dioxide in equilibrium-water is suppressed to the point where it can contribute no more than 0.001% to the total conductance. For the 0.001 and 0.00036 *N* solutions however it was considered desirable to exclude atmospheric carbon dioxide, since in the latter solution the contribution of ionized carbon dioxide might be nearly 0.01%. These two solutions were therefore prepared and introduced into the cells under the protection of CO₂-free argon presaturated with water vapor; appropriate corrections were applied to the weighings of argon-filled containers.

The conductance bridge was a Leeds and Northrup Jones-Dike bridge. Calibrations of the resistance coils had been made and were applied where significant. A variable-frequency oscillator, tuned amplifier, and C.R.O. detector were used. The oscillator output was kept below 1 volt, as it was shown that higher outputs caused detectable ohmic heating of the cells. The cells were thermostated at 25° in an 80-liter oil thermostat. The control was within $\pm 0.002^\circ$, and the actual temperature was established as within 0.003° of 25° by a platinum resistance thermometer and Smiths' Difference Bridge.

Conductance Cells.—The four Pyrex cells used were of the pattern shown in Fig. 3, the dimensions of the central tubular section being varied to give cell constants of approximately 3.5, 4.5, 20 and 300 cm.⁻¹. The electrodes were lightly platinized, so that frequency-dependence over the range 1–4 kc./sec. was less than 0.01%. This small dependence was extrapolated out by plotting *R* against $1/\sqrt{f}$. The resistances of the internal leads and the cell-to-bridge leads were determined by measuring a standard 1000 ohm resistance first connected to the bridge by short heavy leads, and then connected in series with the leads and the cell filled with mercury. The contribution of the mercury to the resistance being less than 0.002 ohm (except in the capillary cell of constant 296 cm.⁻¹) the leads resistances were easily determined to 0.001 ohm. The largest was 0.15 ohm. The cells were calibrated with the Jones and Bradshaw¹¹ 0.1 demal potassium chloride solution, prepared from three times recrystallized analytical reagent potassium chloride, dried *in vacuo* and then at 400°.

For all the measurements below 0.1 *M*, at least two and often three cells were used; above 0.1 *M* the capillary cell with constant 296 cm.⁻¹ was used exclusively, as the resistances were too low for optimum accuracy with the other cells; below 0.003 *M* only the two cells of constants 3.5 and 4.5 cm.⁻¹ were used, the resistance in the cell of constant 21 cm.⁻¹ being too high for convenience. In filling the cells, the delivery tube from the solution flask was put well down into the filling tube of the cell so that no evaporation loss could occur after the cell had been rinsed once with solution. The cells were rinsed six times with solution before filling, and the ground joints at the end of the filling tubes were wiped dry with filter paper before inserting the stoppers. The cells were thermostated for half an hour, then the solution was sucked up into the mixing bulb on the side-arm, and forced back, until no further change in resistance occurred. In the case of the most dilute solutions where an argon atmosphere was present in the cells, mixing was performed by inversion of the cells without removing the stoppers.

The time of half an hour allowed for temperature equilibration was proved to be more than adequate by a study of the rate of change of resistance with time in a cell calibration. The cell, previously warmed or cooled above or below 25°, was placed in the thermostat at zero time and its resistance read every half-minute. The resistances were converted to effective temperatures, which were found to change in accordance with Newton's law of heat transfer. The rate constant of the heat transfer process was such that the cell contents must be within 0.001° of the bath temperature after 18 minutes. Further evidence of the adequacy of the equilibration time was provided by the fact that the same resistance value was attained for equilibration periods of 20 minutes or several hours, provided that the Soret effect was eliminated by mixing the cell contents at the end of the equilibration period. After mixing, the resistance was un-

(11) G. Jones and B. C. Bradshaw, *J. Am. Chem. Soc.*, **55**, 1780 (1933).

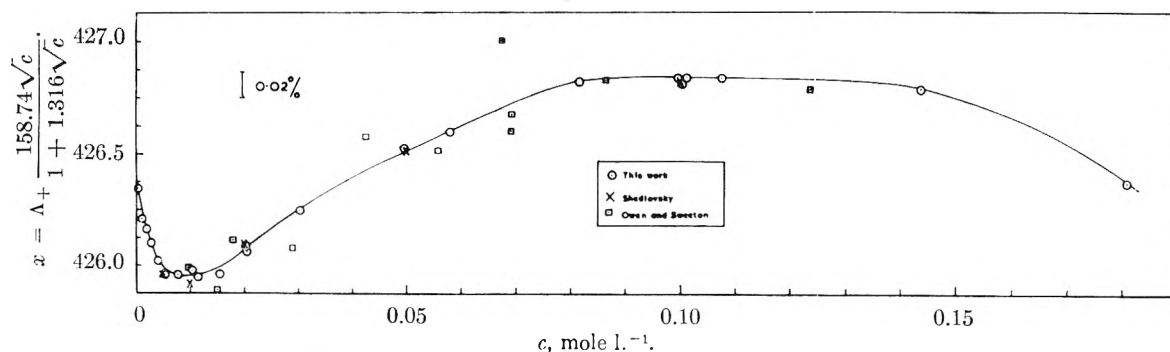


Fig. 4.—Interpolation function for conductance of hydrochloric acid at 25° in the range 0–0.18 N : $x = \Lambda + 158.74\sqrt{c}/(1 + 1.316\sqrt{c})$; \circ , this work; \times , Shedlovsky, ref. 1; \square , Owen and Sweeton, ref. 2.

changed for many hours. To eliminate adsorption effects on the black electrodes, the cells after measurement were refilled with the same solution and the measuring process (with mixing) was repeated. If any change greater than 0.005% was noted, the filling was repeated until constancy was found. Such changes were significant only when the cells previously had been used for a solution of considerably different concentration. The same procedure was followed in the cell calibrations. Agreement between duplicate or triplicate measurements in different cells was within 0.01%, and the mean values reported are probably correct within 0.005%.

The results are summarized in Table II. In order to test these data for smoothness, and for comparison with other work, a deviation plot on which variations of 0.002% can be detected is needed. Such a plot is provided by the function

$$z = \Lambda_{\text{obs}} + \frac{158.74\sqrt{c}}{1 + 1.316\sqrt{c}}$$

which lies in the extremely narrow range 426.06–426.86 between $c = 0$ and $c = 0.18 M$.

For the concentrations between 0.1 and 1 N another deviation function was necessary; this was chosen as

$$y = \Lambda_{\text{obs}} + 49.5\sqrt{c} + 27.9c$$

Values of these two deviation functions are included in Table II.

TABLE II

CONDUCTANCES OF AQUEOUS HYDROCHLORIC ACID AT 25°, AND VALUES OF INTERPOLATION FUNCTIONS

c in mole l.⁻¹; Λ in cm.² int. ohm⁻¹ g. equiv.⁻¹

$$x = \Lambda + 158.74\sqrt{c}/(1 + 1.316\sqrt{c})$$

$$y = \Lambda + 49.5\sqrt{c} + 27.9c$$

10^2c	Λ	x	10^2c	Λ	z
0.35938	423.44	426.38	20.3166	407.10	426.15
1.02493	421.39	426.27	30.302	403.82	426.30
1.81756	419.83	426.23	49.898	399.13	426.52
2.6749	418.49	426.18	57.934	397.56	426.58
4.0733	416.77	426.12	81.504	393.82	426.76
5.3061	415.52	426.07	99.505	391.39	426.77
7.7094	413.58	426.07	100.196	391.28	426.75
10.1149	411.98	426.08	100.759	391.23	426.77
11.3555	411.22	426.06	107.295	390.44	426.77
15.4732	409.11	426.07	143.213	386.63	426.73
20.1515	407.18	426.17	180.616	383.14	426.40
c	Λ	y	c	Λ	y
0.10730	390.44	409.64	0.44469	364.32	409.74
.14321	386.63	409.36	.51084	360.19	409.82
.180616	383.14	409.22	.81933	342.27	409.94
.32975	371.81	409.42	.99345	332.68	409.74

In Figs. 4 and 5 the x and y values of Table II are plotted along with the values derived from the work of Shedlovsky¹ and of Owen and Sweeton.² These comparisons are made only for solutions from 0.01 N upwards; the more dilute

solutions appear in Fig. 7 where the horizontal scale is more expanded. The points from the present work lie within 0.005% of the smooth curve throughout; those of Shedlovsky above 0.01 N are equally close to it; and those of Owen and Sweeton show slightly greater departures of up to 0.03% from it. It seems reasonable therefore to assert that the conductances of Table II are reliable within 0.005%, and that interpolations carried out on plots of the deviation function x and y of Table II may be used to determine the concentration of any pure hydrochloric acid solution up to 1 N from measurement of its conductance, with a similar accuracy.

The best procedure to adopt in converting a measured specific conductance to a concentration of hydrochloric acid is to make successive approximations based on the relation

$$c = \frac{1000K_{\text{sp}}}{\Lambda} \quad (1)$$

First assume as a very rough first approximation the value $\Lambda_1 = 400$, and obtain from equation 1 a first approximation c_1 . Evaluate the quantity

$$x = \frac{158.74\sqrt{c_1}}{1 + 1.316\sqrt{c_1}} \text{ from Fig. 4, or}$$

$$y = 49.5\sqrt{c_1} + 27.9c_1 \text{ from Fig. 5}$$

thus obtaining a better approximation Λ_2 , which yields in turn from equation 1 a second approximation c_2 . Repetition of this process gives values of c which converge rapidly to constancy, and are reliable to within 0.005%. The process may be shortened by one or two stages if the concentration is previously known within a few per cent., but even if the only information available is the specific conductance and the fact that the concentration is not greater than 1 N , the process does not require more than four successive approximations. Above 1 N , as the data of Owen and Sweeton clearly show, the specific conductance is less useful as a measure of concentration; it passes through a flat maximum at about 6 N , and near this concentration it is quite useless. If it is necessary to analyze such solutions they should be diluted to below 1 N before measurement of the conductance. If weight-concentrations rather than volume-concentrations are required, the density at 25° may be computed with the necessary accuracy by the equation¹²

$$d = 0.99707 + 0.00490w$$

where d is the density in g. ml.⁻¹ and w is the percentage of hydrogen chloride by weight.

Tests of Theories of Concentration Dependence of Conductance.—The quantitative interpretation of conductance data in dilute solutions involves the calculation of the electrophoretic effect and the relaxation effect from the ionic distribution function and the expression for the potential near an ion. The result can be written in the general form

$$\Lambda = (\Lambda^0 - f_2)(1 - f_1) \quad (2)$$

(12) From data in "International Critical Tables," Vol. III, McGraw-Hill Book Co., New York, N. Y., 1928, p. 54. The data of H. E. Wirth, *J. Am. Chem. Soc.*, **62**, 1118 (1940), are more accurate and convenient as the density at various molar concentration is given.

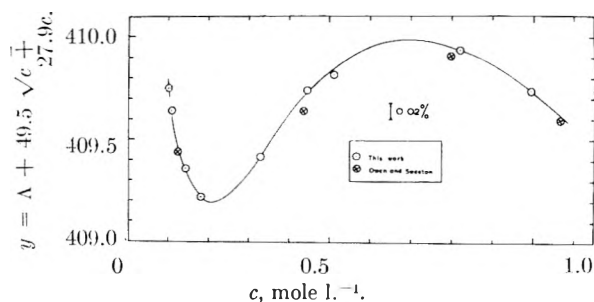


Fig. 5.—Interpolation function for the conductance of hydrochloric acid at 25° in the range 0.1–1 *N*: $y = \Lambda + 49.5 \sqrt{c} + 27.9c$; ○, this work; ⊗, Owen and Sweeton, ref. 2.

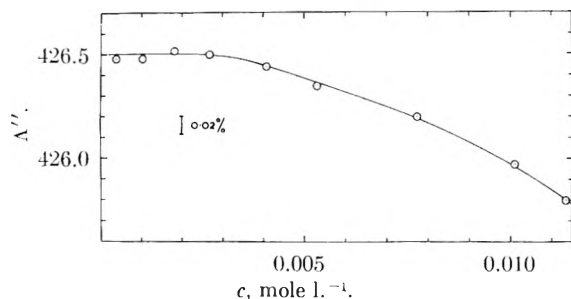


Fig. 6.—Fuoss-Onsager extrapolation for hydrochloric acid at 25°: $\Lambda'' = \Lambda + S \sqrt{c} - E c \log c - J c$; $S = 158.68$, $E = 206.3$, $J = 606$.

where f_2 gives the electrophoretic effect and f_1 is the ratio of the relaxation field to the applied field.

The following discussion of these two effects refers to the case of 1:1 electrolytes only.

Onsager's original limiting theory gives

$$f_1 = \frac{e^2}{ekT(3\sqrt{2} + 6)} \kappa$$

and

$$f_2 = (I^2/3\pi\eta N)\kappa$$

These values on multiplying out (2) and neglecting the cross-product $f_1 f_2$ give the Onsager limiting law

$$\Lambda = \Lambda^0 - (B_1 \Lambda^0 + B_2) \sqrt{c} \equiv \Lambda^0 - S \sqrt{c} \quad (3)$$

For 1:1 electrolytes in water at 25°, with c expressed in mole liter⁻¹ and Λ in cm² ohm⁻¹ equiv⁻¹, $B_1 = 0.2300$ and $B_2 = 60.65$. Hence, with most 1:1 salts, where $\Lambda^0 = 100$ to 150 units, the electrophoretic term is responsible for most of the observed change, being about twice the magnitude of the relaxation term. For acids on the other hand, where $\Lambda^0 \approx 400$ units, the relaxation term is the larger. The conductance of hydrochloric acid therefore provides a particularly good test of theories of the relaxation effect.

In recent years there have been several attempts to extend the range of validity of the theory by replacing the point-charge model of Onsager by a model in which the ions are treated as hard spheres of effective diameter a . In the case of the electrophoretic effect this is not difficult, and leads to the result

$$f_2 = (I^2/3\pi\eta N) \frac{\kappa}{1 + \kappa a} \quad (4)$$

when the standard Debye-Hückel potential is employed.¹³⁻¹⁶ Pitts,¹⁷ employing the Gronwall-La Mer-Sandved¹⁸ ex-

pression for the potential, obtained the result (4) plus a small additional term of order c , and Mirtskhulava¹⁹ almost simultaneously gave a similar treatment.

The relaxation term has proved less tractable. Falkenhagen, *et al.*,¹³ made the first attempt, but later work showed that their treatment lacked a transcendental term involving the exponential integral function, which remains important even at low concentrations. Robinson and Stokes¹⁴ combined an approximate form of the Falkenhagen expression with equation 4 to yield the equation

$$\Lambda = \Lambda^0 - S \sqrt{c}/(1 + \kappa a) \quad (5)$$

which gives a useful ($\pm 0.1\%$) but not exact account of conductance for fully dissociated 1:1 electrolytes up to about 0.1 *N* with reasonable choices of the parameter a . The deviation-function x shown in Fig. 4 is in fact merely a transposition of equation 5; if the equation were exact, x would have the constant value Λ^0 . The sharp rise in the region below 0.005 *N* is due to the neglect of the higher transcendental terms in the relaxation field expression.

Pitts¹⁷ in 1953 gave the first full treatment of the relaxation effect for finite ion size; he evaluated the transcendental terms and expressed them as functions of κa in tables. His complete equation including both the relaxation effect and the electrophoretic effect may be written

$$\Lambda = \Lambda^0 - P_1 - P_2 - P_3 + P_4 \quad (6)$$

$$\text{where } P_1 = \frac{B_1 \Lambda^0 \sqrt{c}}{(1 + \kappa a)(1 + \kappa a/\sqrt{2})}; \quad P_2 = \frac{B_2 \sqrt{c}}{1 + \kappa a}$$

$$P_3 = b^2(\kappa a)^2 S_1/3; \quad P_4 = \frac{b P_2 \kappa a}{3} \left[\left(\frac{\sqrt{2} - 1}{\sqrt{2} + \kappa a} \right) + T_1 \right]$$

$b = e^2/(\epsilon kTa)$; and S_1 and T_1 are functions involving *inter alia* three terms containing exponential integral functions, and are tabulated for $\kappa a = 0.02$ to $\kappa a = 0.50$ at intervals of 0.02 in Pitts' Table I. In using Pitts' equation, it is more convenient to have values of $(\kappa a)^2 S_1/3$ and $\kappa a/3 \times [\sqrt{2} - 1/\sqrt{2} + \kappa a + T_1]$. These are given in Table III, and make calculations by equation 6 fairly straightforward.

Fuoss and Onsager^{15,16} in 1955 gave a very similar treatment, but used the standard Debye-Hückel expression for the potential. Their equations also contain transcendental terms derived from exponential integral functions, but owing to differences in the methods of presentation it is not easy to point out specific differences between their result and that of Pitts. The Fuoss-Onsager treatment has been further expounded by Fuoss and Accascina in a book²⁰ which gives more detail, and replaces the exponential integral functions by series expansions which give a term in $\kappa a \ln(\kappa a)$ in the final conductance expression. In this simplified version, the Fuoss-Onsager equation is written

$$\Lambda = \Lambda^0 - S \sqrt{c} + E c \log c + J c \quad (7)$$

where S is the coefficient of the Onsager limiting law; E is a coefficient calculable from Λ^0 and solvent properties; the linear coefficient J is calculable from Λ^0 , solvent properties, and the ion size parameter a . Both Pitts' and Fuoss and Onsager's equations are expected to hold up to $\kappa a = 0.2$; a comparison of their predictions for hydrochloric acid follows.

In Fig. 6, equation 7 is employed to evaluate Λ^0 from the data of Table II. The value $a = 4 \text{ \AA}$. is selected to make $J = 606$, since this value makes the extrapolation-function

$$\Lambda'' = \Lambda_{\text{obs.}} + S \sqrt{c} - E c \log c - J c \quad (7a)$$

constant up to about 0.004 *N*. The values $S = 158.68$ and $E = 206.3$ were computed from the equations given by Fuoss and Accascina,²⁰ using as a "trial value" of Λ^0 Shedlovsky's figure $\Lambda^0 = 426.16$. The resulting final value for Λ^0 is 426.50. The range of good fit of equation 7 is however disappointingly small; the concentration 0.004 *N* corresponds only to $\kappa a = 0.083$, and thereafter departures from the theory are rapid.

In Fig. 7, another value of J is tried in an attempt to obtain a slightly worse fit over a wider range with equation 7; with $J = 562$ the deviations do not exceed 0.03% up to 0.012 *N* ($\kappa a = 0.12$) but they are clearly not random, the quantity Λ'' displaying marked curvature. In the expectation that this curvature might arise from the neglect

(19) I. A. Mirtskhulava, *Zhur. Fiz. Khim. (USSR)*, **27**, 840 (1953).

(20) R. M. Fuoss and F. Accascina, "Electrolytic Conductance," Interscience Publishers, New York, N. Y., 1959.

(13) H. Falkenhagen, M. Leist and G. Kelbg, *Ann. Physik*, [0] **11**, 51 (1952).

(14) R. H. Stokes, *J. Am. Chem. Soc.*, **76**, 1988 (1954); R. A. Robinson and R. H. Stokes, *ibid.*, **76**, 1991 (1954).

(15) R. M. Fuoss and L. Onsager, *Proc. Natl. Acad. Sci.*, **41**, 274 (1955).

(16) R. M. Fuoss and L. Onsager, *J. Phys. Chem.*, **61**, 668 (1957).

(17) E. Pitts, *Proc. Roy. Soc. (London)*, **4217**, 43 (1953).

(18) I. H. Gronwall, V. K. La Mer and K. Sandved, *Physik. Z.*, **29**, 3508 (1928).

TABLE III
TRANSCENDENTAL FUNCTIONS OF EQUATION 6

κa	$10^3(\kappa a)^2 S_1/3$	$\left[\frac{\sqrt{2}-1}{\sqrt{2}-\kappa a} + T_1 \right] \frac{\kappa a}{3}$
0.02	0.0735	0.00998
.04	.2072	.01671
.06	.3693	.02224
.08	.5342	.02701
.10	.6997	.03152
.12	.8575	.03566
.14	1.0030	.03904
.16	1.1465	.04242
.18	1.2702	.04532
.20	1.3852	.04831
.22	1.4886	.05061
.24	1.5813	.05346
.26	1.6634	.05616
.28	1.7360	.05854
.30	1.7994	.06069

of terms of order $c^{3/2}$ in the numerous series expansions involved in obtaining equation 7 from the more exact form, the full expression given by Fuoss and Onsager (equation 7.7 of ref. 16) also was tried: the value $a = 4 \text{ \AA}$. gave a somewhat better fit, but curvature was still apparent, and the limit of fit within 0.03% was extended only to 0.015 N .

On the other hand, Pitts' equation 6 holds within experimental accuracy up to 0.02 N , the average deviation of the function

$$\Lambda''' = \Lambda + P_1 + P_2 + P_3 - P_4$$

from the constant value $\Lambda^0 = 426.50$ being only 0.005% up to 0.02 N , as shown in the lower part of Fig. 6. The value of a needed in this case is 3.67 \AA . Furthermore, Pitts' equation continues to give a very good representation of the conductance up to 0.1 N ; the deviations are only 0.05% at 0.05 N and 0.37% at 0.1 N . It is difficult to see why Pitts' equation should show such marked superiority, for the only essential difference between his treatment and that of Fuoss and Onsager lies in his use of the Gronwall-La Mer-Sandved potential expression, and experience with the application of this expression to activity data shows that for strong 1:1 electrolytes in water the differences between its predictions and those of the Debye-Hückel potential expression can be accommodated by small changes in the a parameter. Conductance data, because of their higher precision, are of course a more severe test than activity data.

The whole of this critique of the fine structure of conductance theory is based on the quantitative interpretation of very small differences; in this connection the writer treasures a letter written by a well-known firm of electrical instrument manufacturers, in which the manager "does not imagine that any conductance measurements on solutions could require an accuracy greater than $\pm 0.5\%$." If this were only true, how simple conductance theory would be!

The earlier data for hydrochloric acid below 0.006 N are shown in Fig. 8, where the function plotted is Λ of equation 7a. Their scatter (0.06%) is such that no significant comparison of the theoretical equations is possible; the superior smoothness of the present results, as well as their close correspondence with the theoretical equations, are reasonable justification for preferring them.

Grateful acknowledgment is made of the assistance of Dr. R. A. Robinson, and in particular of his moral support during that baffling stage of the work before the importance of errors due to the Soret effect was realized, when it seemed

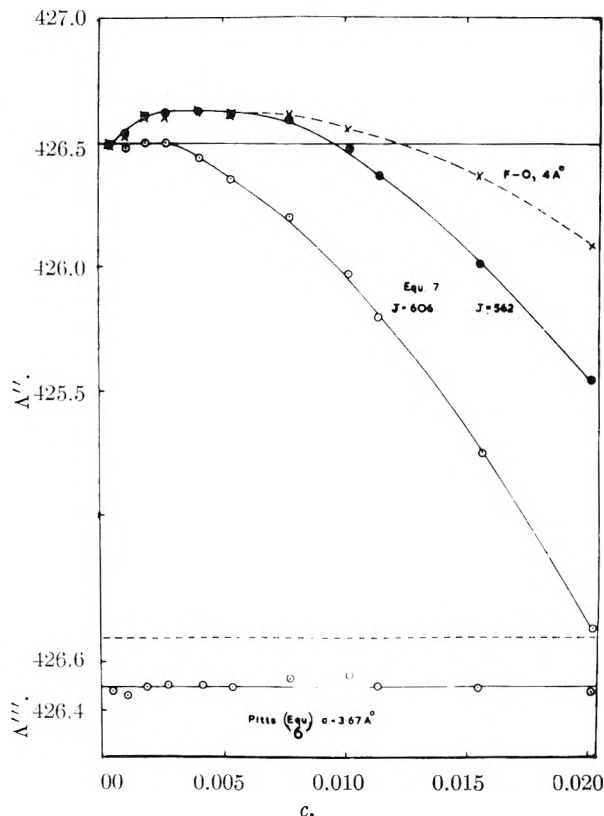


Fig. 7.—Tests of the Fuoss-Onsager and Pitts equations for hydrochloric acid at 25°: \times , full Fuoss-Onsager function (eq. 7.7 of ref. 16, with $a = 4 \text{ \AA}$.); \bullet , equation 7a, this paper, with $J = 562$; \circ (upper diagram), equation 7a with $J = 606$; \circ (lower diagram), Pitts function (eq. 6a of this paper) with $a = 3.67 \text{ \AA}$.

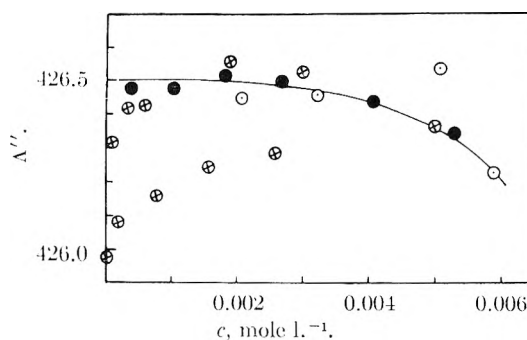


Fig. 8.—Comparison of conductance data for hydrochloric acid at 25° in dilute solutions: \bullet , this work; \circ , Owen and Sweton, ref. 2; \otimes , Shedlovsky, ref. 1. The function plotted is Λ''' of equation 7a, i.e., the Fuoss-Onsager extrapolation function with $J = 606$.

that the results depended on the weather. (In fact, this was the case; one gets a different result on putting a cell into the 25° thermostat on a cold day from that on a hot day, unless the Soret effect is eliminated.)

CHLORIDE COMPLEXES OF IRON(III) IONS AND THE KINETICS OF THE CHLORIDE-CATALYZED EXCHANGE REACTION BETWEEN IRON(II) AND IRON(III) IN LIGHT AND HEAVY WATER^{1a, b}

BY N. SUTIN, J. K. ROWLEY AND R. W. DODSON

Chemistry Department, Brookhaven National Laboratory, Upton, Long Island, New York

Received April 17, 1961

The association of iron(III) ions with chloride ions and the kinetics of the electron exchange between iron(II) ions and the chloride complexes of iron(III) ions have been studied in H₂O and D₂O. From spectrophotometric measurements the equilibrium constant, K_1 , for the reaction $\text{Fe}^{3+} + \text{Cl}^- \rightleftharpoons \text{FeCl}^{2+}$ is 2.0 times larger in D₂O than in H₂O. The value of K_1 (H₂O) is 4.4 and ΔH_1 (H₂O) is 5.0 kcal. mole⁻¹ at 25° and an ionic strength of 0.50. A small difference in the temperature coefficient of K_1 is found in the two solvents. The exchange reaction between FeCl^{2+} and Fe^{2+} proceeds 2.5 times more rapidly in H₂O than in D₂O. The kinetic isotope effect is nearly the same as that found in the Fe^{2+} to Fe^{3+} and Fe^{2+} to FeOH^{2+} exchanges. The isotope effects are discussed in terms of an electrostatic model.

Introduction

The electron exchange between ferrous and ferric iron in acid perchlorate media goes through two paths, one involving ferric ion, the other hydrolyzed ferric ion. The specific rate of the second path is about 1000-fold greater than that of the first.² It was suggested³ that the exceptional reactivity of FeOH^{2+} might derive from the operation of a hydrogen atom transfer mechanism in this path, and that this idea might be tested by measurements in heavy water. Such measurements were carried out,⁴ with the finding that both paths are slowed down equally in D₂O. Hence it was concluded that the intervention of a hydrogen atom transfer mechanism does not account for the special reactivity of the hydrolyzed ion. On the other hand, since both reactions are retarded by a factor 2 in D₂O, it was suggested that hydrogen atom transfer may prevail in both.

When chloride is present, the rate law indicates that additional reaction paths come into play.² In these, ferrous ion reacts with the chloride complexes of ferric iron. The present work was undertaken to ascertain whether a D₂O effect would be found in these reaction paths. If the exchange with the chloride complexes proceeds via an activated complex with a chloride bridge, D₂O might have a quite different effect than it does on the other reactions which may involve water or hydroxyl bridging.

We have made rate measurements in D₂O media containing chloride. To analyze the kinetic data it was necessary to have information about the equilibria, so measurements on the complexing of ferric iron by chloride ions in H₂O and D₂O were carried out.

Experimental

Materials.—The ferrous perchlorate was obtained from the G. Frederick Smith Chemical Co. and purified by recrystallization from perchloric acid. A stock solution of ferric perchlorate for use in the spectrophotometric measurements was prepared from the recrystallized ferrous per-

chlorate by fuming with perchloric acid. The iron was estimated spectrophotometrically as the tris-(2,2'-dipyridine) complex according to the procedure of Moss and Mellon.⁵ The perchloric acid (70%) and the hydrochloric acid (37.8%) were obtained from the J. T. Baker Chemical Co., and were standardized by titration with sodium hydroxide. The heavy water (>99.7% D₂O) was obtained from the Stuart Oxygen Co., San Francisco.

For the kinetic measurements a stock solution of ferric perchlorate was prepared from a hydrochloric acid solution of Fe^{56} according to the procedure of Silverman and Dodson.² This method involves the extraction of iron(III) chloride into isopropyl ether, back-extraction into water and repeated precipitations of ferric hydroxide with ammonia. The ferric hydroxide then was dissolved in perchloric acid and standardized.

Procedure.—The equilibrium was studied spectrophotometrically according to the procedure described by Rabinowitch and Stockmayer.⁶ The spectra were measured on a Beckman DU spectrophotometer with 1 cm. Corex cells. The spectrophotometer was fitted with a circulating thermostat. Measurements were made in the 330–400 m μ range, at temperatures ranging from 16.5 to 35.5°. In a given series of measurements the chloride concentration was kept constant while the iron(III) concentration was varied. The spectra of the solutions containing added chloride were measured against solutions of the same iron(III) and hydroxide ion concentrations. In all cases the ionic strength of the solution was adjusted to 0.50 with perchloric acid.

The solutions in heavy water were prepared by adding D₂O to relatively concentrated solutions of the reagents in H₂O. The D₂O content of the final solution was ~97%.

The experimental procedure followed in the kinetic measurements was similar to that used in previous work.² The reaction was quenched by complexing the ferrous ion with 2,2'-dipyridine. The iron(III) then was precipitated as ferric hydroxide with ammonia; and the activity of the precipitate was measured with a proportional counter. The procedure was checked by measuring the exchange rate in H₂O. The Silverman and Dodson values were reproduced to within 2%.

Results

Equilibrium Studies.—The absorbances of the solutions in H₂O and D₂O at different iron(III) concentrations and temperatures are presented in Tables I and II. The spectra of these solutions are similar and show a broad maximum at 336 m μ . As a first approximation the absorbance will be assumed to be due solely to the species FeCl^{2+} . From the relations $A = \epsilon_1(\text{FeCl}^{2+})$ and $K_1 = [(\text{FeCl}^{2+})/(\text{Fe}^{3+})(\text{Cl}^-)]$, it follows that

$$\frac{(\text{Fe}^{3+})(\text{Cl}^-)_0}{A} = \frac{1}{\epsilon_1 K_1} + \frac{(\text{Fe}^{3+})}{\epsilon_1} \quad (1)$$

(1) (a) Research performed under the auspices of the U. S. Atomic Energy Commission; (b) Presented in part at the 136th meeting of the American Chemical Society, Atlantic City, New Jersey, 1959.

(2) J. W. Silverman and R. W. Dodson, *J. Phys. Chem.*, **56**, 846 (1952).

(3) R. W. Dodson, *J. Phys. Chem.*, **56**, 852 (1952); R. W. Dodson and N. Davidson, *ibid.*, **56**, 866 (1952), remarks in discussion at the 1952 ACS Symposium at Notre Dame.

(4) J. Hudis and R. W. Dodson, *J. Am. Chem. Soc.*, **78**, 911 (1956).

(5) M. L. Moss and M. G. Mellon, *Ind. Eng. Chem., Anal. Ed.*, **14**, 862 (1942).

(6) E. Rabinowitch and W. Stockmayer, *J. Am. Chem. Soc.*, **64**, 335 (1942).

In these expressions A is the measured absorbance, ϵ_1 the extinction coefficient of FeCl^{2+} , and $(\text{Cl}^-)_0$

where $[\text{Fe(III)}]$ is the total concentration of ferric ion.

TABLE I

ABSORBANCES IN H_2O AT AN IONIC STRENGTH OF 0.50 AS A FUNCTION OF IRON(III) CONCENTRATION AND TEMPERATURE; $(\text{Cl}^-)_0 = 2.00 \times 10^{-3}F$

$T, ^\circ\text{C.}$	$\text{Fe(III)} F \times 10^3$	$\lambda, \text{m}\mu$						
		330	336	340	350	366	380	400
16.5	21.56	0.237	0.240	0.234	0.197	0.113	0.055	0.015
	19.40	.218	.226	.217	.182	.104	.052	.013
	17.25	.195	.198	.194	.162	.092	.045	.012
	15.09	.171	.173	.170	.142	.081	.041	.011
	12.94	.148	.150	.146	.123	.068	.033	.009
8.624	.100	.101	.099	.083	.047	.023	.006	
20.8	21.56	.260	.265	.259	.220	.126	.064	.018
	19.40	.242	.245	.239	.203	.117	.059	.017
	17.25	.214	.217	.213	.180	.103	.051	.014
	15.09	.188	.191	.187	.157	.091	.046	.012
	12.94	.163	.166	.162	.137	.078	.038	.010
8.624	.110	.111	.108	.092	.053	.025	.007	
25.0	21.56	.286	.292	.285	.244	.143	.072	.021
	19.40	.265	.269	.264	.224	.130	.066	.018
	17.25	.237	.240	.235	.200	.115	.059	.016
	15.09	.209	.211	.208	.177	.103	.052	.015
	12.94	.181	.183	.180	.152	.087	.044	.012
8.624	.121	.124	.121	.103	.059	.030	.008	
29.6	21.56	.318	.325	.319	.273	.160	.083	.024
	19.40	.293	.299	.294	.250	.147	.076	.022
	17.25	.261	.266	.261	.224	.130	.067	.018
	15.09	.230	.234	.231	.198	.116	.060	.017
	12.94	.202	.205	.201	.172	.100	.050	.014
8.624	.135	.139	.136	.116	.068	.035	.010	
35.5	21.56	.362	.371	.366	.316	.188	.099	.030
	19.40	.335	.341	.337	.288	.172	.091	.026
	17.25	.301	.307	.301	.259	.154	.079	.023
	15.09	.265	.270	.266	.230	.137	.071	.021
	12.94	.232	.237	.233	.200	.118	.062	.018
8.624	.157	.160	.158	.132	.081	.043	.013	

TABLE II

ABSORBANCES IN D_2O AT AN IONIC STRENGTH OF 0.50 AS A FUNCTION OF IRON(III) CONCENTRATION AND TEMPERATURE; $(\text{Cl}^-)_0 = 2.00 \times 10^{-3}F$

$T, ^\circ\text{C.}$	$\text{Fe(III)} F \times 10^3$	$\lambda, \text{m}\mu$						
		330	336	340	350	366	380	400
16.5	21.56	0.566	0.573	0.566	0.484	0.279	0.140	0.039
	17.25	.465	.476	.470	.401	.231	.144	.033
	12.94	.363	.372	.365	.311	.181	.092	.027
	8.624	.249	.254	.250	.212	.122	.060	.019
	4.312	.128	.131	.128	.110	.064	.032	.009
20.8	21.56	.607	.622	.610	.523	.303	.153	.043
	17.25	.500	.515	.504	.433	.251	.125	.036
	12.94	.388	.399	.392	.334	.196	.100	.031
	8.624	.267	.273	.268	.230	.132	.068	.020
	4.312	.137	.141	.138	.119	.069	.034	.010
25.0	21.56	.659	.679	.666	.574	.337	.171	.049
	17.25	.543	.560	.550	.472	.277	.141	.040
	12.94	.424	.436	.429	.368	.216	.113	.034
	8.624	.292	.300	.295	.253	.148	.077	.024
	4.132	.150	.153	.150	.130	.075	.039	.011
29.6	21.56	.716	.741	.730	.630	.373	.194	.057
	17.25	.592	.609	.601	.519	.308	.157	.047
	12.94	.461	.474	.467	.406	.241	.126	.038
	8.624	.321	.329	.325	.280	.168	.087	.026
	4.312	.165	.170	.168	.145	.087	.044	.013
35.5	21.56	.805	.831	.818	.716	.432	.225	.069
	17.25	.668	.691	.683	.597	.358	.188	.059
	12.94	.519	.539	.534	.463	.280	.147	.046
	8.624	.361	.373	.369	.321	.195	.103	.032
	4.312	.188	.195	.193	.168	.101	.054	.015

the total concentration of the chloride ion. If $[\text{Fe(III)}] \gg (\text{Cl}^-)_0$ equation 1 becomes

$$\frac{[\text{Fe(III)}](\text{Cl}^-)_0}{A} = \frac{1}{\epsilon_1 K_1} + \frac{[\text{Fe(III)}]}{\epsilon_1} \quad (2)$$

Approximate values of ϵ_1 and K_1 were determined by plotting $[\text{Fe(III)}](\text{Cl}^-)_0/A$ vs. $[\text{Fe(III)}]$. The values of K_1 obtained then were used to calculate (Fe^{3+}) from the relation

$$[\text{Fe(III)}] = (\text{Fe}^{3+})[1 + K_1(\text{Cl}^-) + (K_h/(\text{H}^+))] \quad (3)$$

where K_h is the hydrolysis constant of the ferric ion. The measured absorbances also were corrected for differences in the ferric ion concentration of the chloride-containing solution and of the blank solution using the approximate values of K_1 and ϵ_1 and the relation

$$A_{\text{corr.}} = \frac{A \left[1 + \frac{K_h}{(\text{H}^+)} \right]}{\left[1 + \frac{K_h}{(\text{H}^+)} - \frac{\epsilon_3}{\epsilon_1} - \frac{\epsilon_2 K_h}{\epsilon_1 (\text{H}^+)} \right]} \quad (4)$$

where ϵ_2 is the extinction coefficient of the hydrolyzed ferric ion and ϵ_3 that of the ferric ion.^{7,8} The values of K_h , ϵ_2 and ϵ_3 were assumed to be the same in D_2O and H_2O . The slopes and intercepts of plots of $(\text{Fe}^{3+})(\text{Cl}^-)_0/A_{\text{corr.}}$ vs. (Fe^{3+}) then were obtained by the method of least squares. Plots of the data in H_2O and D_2O at 336 $\text{m}\mu$ and 25° are shown in Fig. 1.

While this procedure gives good values for the product $\epsilon_1 K_1$, data of very high precision are required to evaluate ϵ_1 and K_1 separately.

Extinction Coefficients.—The extinction coefficients, particularly those at the longer wave lengths, showed some variation with temperature. At 350 $\text{m}\mu$ no systematic variation of the extinction coefficient with temperature was observed, and in treating the data we have assumed the extinction coefficient at 350 $\text{m}\mu$ to be temperature independent. This assumption, although somewhat arbitrary, is consistent with the measurements of Lister and Rivington⁹ on the effect of temperature on the extinction coefficients of FeSCN^{2+} . They found that with increasing temperature, the extinction coefficient at the maximum (460 $\text{m}\mu$) decreased 1% in 10° while at 520 $\text{m}\mu$ it increased 4%. In the same temperature interval, the extinction coefficient at ~485 $\text{m}\mu$ did not change significantly.

In order to obtain a self-consistent set of extinction coefficients, values of the extinction coefficient at 350 $\text{m}\mu$ were calculated by multiplying the extinction coefficients at 330, 336 and 340 $\text{m}\mu$ (and 366 $\text{m}\mu$ in D_2O) by the ratio of the absorbances at 350 $\text{m}\mu$ to those at these wave lengths. The average values of the extinction coefficients at 350 $\text{m}\mu$ obtained in this way are $1.44 \pm 0.15 \times 10^3$ in H_2O and $1.85 \pm 0.15 \times 10^3$ in D_2O . The value in H_2O is in excellent agreement with that reported by Connick and Coppel.¹⁰ From these values of the extinction coefficient at 350 $\text{m}\mu$, the extinction coefficients at the other wave lengths were calculated from the ratio of the absorbances at these wave lengths to that at 350 $\text{m}\mu$. The extinction

(7) R. M. Milburn and W. C. Vosburgh, *J. Am. Chem. Soc.*, **77**, 1352 (1955).

(8) R. C. Turner and K. E. Miles, *Can. J. Chem.*, **35**, 1002 (1957).

(9) M. W. Lister and D. E. Rivington, *ibid.*, **33**, 1572 (1955).

(10) R. E. Connick and C. P. Coppel, *J. Am. Chem. Soc.*, **81**, 6389 (1959).

coefficients calculated in this manner are presented in Table III.

TABLE III

EXTINCTION COEFFICIENTS ($\times 10^{-3}$) OF FeCl_2^{2+} IN H_2O AND D_2O

$T, ^\circ\text{C}.$	Solvent	$\lambda, \text{m}\mu$						
		330	336	340	350	366	380	400
16.5	H_2O	1.73	1.76	1.72	1.44	0.82	0.40	0.11
	D_2O	2.16	2.21	2.17	1.85	1.07	0.54	0.16
20.8	H_2O	1.71	1.74	1.70	1.44	0.83	0.41	0.11
	D_2O	2.15	2.20	2.16	1.85	1.07	0.54	0.16
25.0	H_2O	1.70	1.73	1.69	1.44	0.83	0.42	0.12
	D_2O	2.13	2.19	2.15	1.85	1.08	0.56	0.16
29.6	H_2O	1.68	1.71	1.68	1.44	0.84	0.43	0.12
	D_2O	2.11	2.17	2.14	1.85	1.10	0.57	0.17
35.5	H_2O	1.66	1.70	1.67	1.44	0.85	0.45	0.13
	D_2O	2.08	2.15	2.13	1.85	1.12	0.59	0.18

Equilibrium Constants.—The equilibrium constants calculated from the extinction coefficients listed in Table III and the intercepts from the least

TABLE IV

COMPARISON OF SPECTROPHOTOMETRIC ESTIMATES OF THE FeCl_2^{2+} ASSOCIATION IN H_2O AND D_2O AT 25° AND IONIC STRENGTH OF 0.50

K_1^a	ΔG_1^0 kcal. mole $^{-1}$	ΔH_1 kcal. mole $^{-1}$	ΔS_1 cal. deg. $^{-1}$ mole $^{-1}$	Source
4.6	-2.1	8.5 ^b	35	Rabinowitch and Stockmayer ¹
5.3	-2.2	Olerup ^c
...	...	6.0 ^d	...	Connick and Coppel ¹¹
2.6	-1.8	3.8 ^e	19	Coll, Nauman and West ^f
4.4	-2.1	5.0 ^g	24	This work
8.7 ^h	...	4.2 ^g	...	This work

^a K_1 was corrected to $\mu = 0.50$ and $T = 25^\circ$ using the Rabinowitch and Stockmayer semi-empirical relation between K_1 and μ and our value of ΔH_1 . ^b $\mu = 0.61$. ^c H. Olerup, *Svensk. Kem. Tidskr.*, **55**, 324 (1943). ^d $\mu = 1.38$. ^e $\mu = 3.0$. ^f H. Coll, R. V. Nauman and P. W. West, *J. Am. Chem. Soc.*, **81**, 1284 (1959). ^g $\mu = 0.50$. ^h In D_2O .

squares treatment are presented in Table IV together with the values of $K_1(\text{H}_2\text{O})$ obtained by other investigators. Table IV also includes values of ΔG_1^0 , ΔH_1 and ΔS_1 . ΔH_1 was calculated from a plot of $\log K_1$ vs. $(1/T)$ and ΔG_1^0 from the equilibrium constant corrected to zero ionic strength using the semi-empirical relation⁶

$$\log_{10} K_1(\mu = 0) = \log_{10} K_1(\mu) + \frac{3\mu^{1/2}}{1 + 1.5\mu^{1/2}} - 0.295\mu$$

The values of ΔH_1 reported by Rabinowitch and Stockmayer and by Connick and Coppel were determined at 400 and 370 $\text{m}\mu$, respectively, and are based on the assumption that the extinction coefficients at these wave lengths are temperature independent. Our data show that this assumption is not, in general, a good one, and is particularly poor at 400 $\text{m}\mu$. Indeed the higher values of ΔH_1 reported can be largely accounted for in terms of the increase in the extinction coefficients with temperature. A value of $\Delta H_1 = 4.3$ kcal. mole $^{-1}$ determined by a potentiometric method in H_2O ¹¹ is further evidence that the earlier spectrophotometric determinations are too high. The value of ΔH is very sensitive to the assumptions made about the temperature dependence of the extinction coefficients. If the extinction coefficients at 336 $\text{m}\mu$ are temperature-independent, a value of $\Delta H_1 = 4.7$ kcal. mole $^{-1}$ would be obtained in H_2O , instead of

the 5.0 kcal. mole $^{-1}$ which is found when temperature independence at 350 $\text{m}\mu$ is assumed. With the temperature dependence of ϵ at 370 $\text{m}\mu$ found in the present work, the data of Connick and Coppel give a ΔH_1 of 5.5 kcal. mole $^{-1}$, in closer agreement with our value. The difference between the values of $\Delta H_1(\text{H}_2\text{O})$ and $\Delta H_1(\text{D}_2\text{O})$ is just outside the experimental error of the measurements.

Kinetic Studies.—The effect of chloride ion on the rate of the $\text{Fe(II)}-\text{Fe(III)}$ exchange in H_2O has been investigated by Silverman and Dodson. Their measurements can be described in terms of the rate law:

$$R = k_1(\text{Fe}^{2+})(\text{Fe}^{3+}) + k_2(\text{Fe}^{2+})(\text{FeOH}^{2+}) + k'(\text{Fe}^{2+})(\text{FeCl}_2^{2+}) + k''(\text{Fe}^{2+})(\text{FeCl}_2^+)$$

from which it follows that

$$\frac{k[1 + K_1(\text{Cl}^-) + K_1K_2(\text{Cl}^-)^2] - k_0}{(\text{Cl}^-)} = \frac{k'K_1 + k''K_1K_2(\text{Cl}^-)}{(\text{Cl}^-)} \quad (5)$$

where k is the over-all second order rate constant in the presence of chloride ion, and k_0 the rate constant in the absence of chloride, both at the same acidity. k' and k'' are the rate constants for the reaction of Fe^{2+} with FeCl_2^{2+} and FeCl_2^+ , respectively. K_2 is the equilibrium constant for the reaction $\text{FeCl}_2^{2+} + \text{Cl}^- = \text{FeCl}_2^+$. Hence, provided K_1 and K_2 are known, k' and k'' can be calculated from the intercepts and slopes of plots of

$$\frac{k[1 + K_1(\text{Cl}^-) + K_1K_2(\text{Cl}^-)^2] - k_0}{(\text{Cl}^-)} \text{ vs. } (\text{Cl}^-)$$

The dependence of the $\text{Fe(II)}-\text{Fe(III)}$ exchange rate on the chloride ion concentration in D_2O is given in Table V. It will be seen that the rate increases with increasing chloride concentration. Plots of the data in H_2O and D_2O are shown in Fig. 2.

TABLE V

RATE DEPENDENCE ON CHLORIDE CONCENTRATION IN D_2O AT AN IONIC STRENGTH OF 0.50;

$T, ^\circ\text{C}.$	$(\text{Cl}^-), F$	$t_{1/2}, \text{sec.}$	$k, F^{-1} \text{sec.}^{-1}$
10	0	798	1.82
	0.047	544	2.68
	.121	344	4.23
	.242	235	6.20
	.300	188	7.66
	.353	168	8.67
20	0	302	4.82
	0.047	230	6.33
	.121	138	10.6
	.242	108	13.5
	.353	87	16.7

In order to determine the values of k' and k'' in H_2O , Silverman and Dodson used the values of K_1 , K_2 , ΔH_1 and ΔH_2 reported by Rabinowitch and Stockmayer. Since our measurements show that this value of ΔH_1 is too large, it is necessary to recalculate k' and k'' . We have not determined K_2 , but since our value of $K_1(\text{H}_2\text{O})$ agrees well with that of Rabinowitch and Stockmayer, we will use their value of $K_2(\text{H}_2\text{O})$ at 25° . The isotope effect on K_2 probably is not as large as that on K_1 and we shall

assume it to be 1.5. In addition we shall assume that the temperature dependence of K_2 is the same as that of K_1 . The values of k' and k'' together with the activation energy determined from a plot of $\log k'$ vs. $(1/T)$ is shown in Table VI. The values of ΔS^* calculated from the expression

$$k = \frac{eRT}{Nh} e^{\Delta S^*/R} e^{-E_{act.}/RT}$$

are also included in this table. In view of the uncertainty in the values of k'' we do not feel justified in calculating an activation energy or isotope effect for the exchange path involving FeCl_2^+ . The difference in the activation energy of the exchange path involving FeCl^{2+} in H_2O and D_2O lies within the experimental error of the measurements.

Discussion

The D_2O effect gives no obvious indication of differences in the mechanism of the exchange of ferrous ions with Fe^{3+} , FeOH^{2+} and FeCl_2^+ .

The possibility remains that all three reactions proceed via a hydrogen atom transfer mechanism. However, this is not very likely for the following reasons. (1) The equilibrium isotope effect is of the same order of magnitude as the kinetic effects originally taken as support for hydrogen atom transfer. The equilibrium does not involve any net hydrogen atom or proton transfer. (2) Kinetic isotope effects of similar magnitude occur in other oxidation-reduction systems which do not seem to involve hydrogen atom transfer.

In a general way, the isotope effects arise from differences in the free energies of solvation in the two solvents. Obvious factors to be considered are the interactions of the coordinated water molecules or hydroxide ions with the ions, the release of water molecules to the bulk solvent, or their removal, and the "structure breaking" action of the various species in relation to the differing degrees of structure in the two solvents.

TABLE VI

CATALYSIS OF THE Fe(II)-Fe(III) EXCHANGE REACTION BY CHLORIDE IONS

T, °C.	F ⁽¹⁾	k' sec. ⁻¹	E _a kcal. mole ⁻¹	ΔG* kcal. mole ⁻¹	ΔS* cal. deg. ⁻¹ mole ⁻¹
0		5.4			
10		10.9			
20		22.8	11.5	15.3	-15.0
			D ₂ O		
10		4.1			
20		9.1	13.2	15.6	-10.2

Bigeleisen has pointed out¹² that with highly charged positive ions, the action of the coulomb field on the hydrogen-oxygen bonds of the water molecules in the first coordination spheres may be of considerable importance. The positive charge repels the protons, thus tending to weaken the O-H bonds. From the usual zero point energy con-

(11) E. L. King, M. J. M. Woods and P. K. Gallagher, as presented at the 136th meeting of the American Chemical Society, Atlantic City, New Jersey, 1959.

(12) Private communication from J. Bigeleisen, see also J. Bigeleisen, *J. Chem. Phys.*, **32**, 1583 (1960).

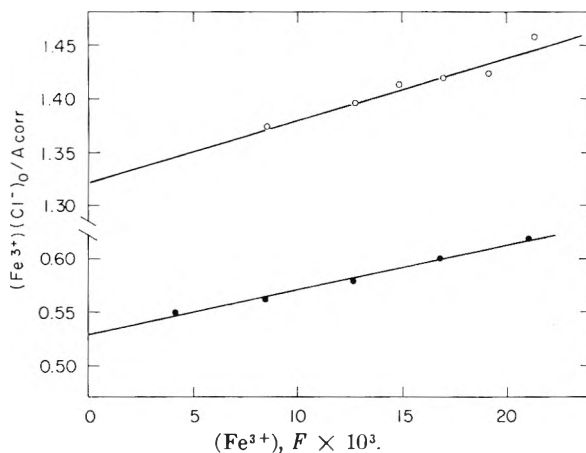


Fig. 1.—Variation of $(\text{Fe}^{3+})(\text{Cl}^-)_0/A_{\text{corr.}}$ with ferric ion concentration: ● in D_2O ; ○ in H_2O .

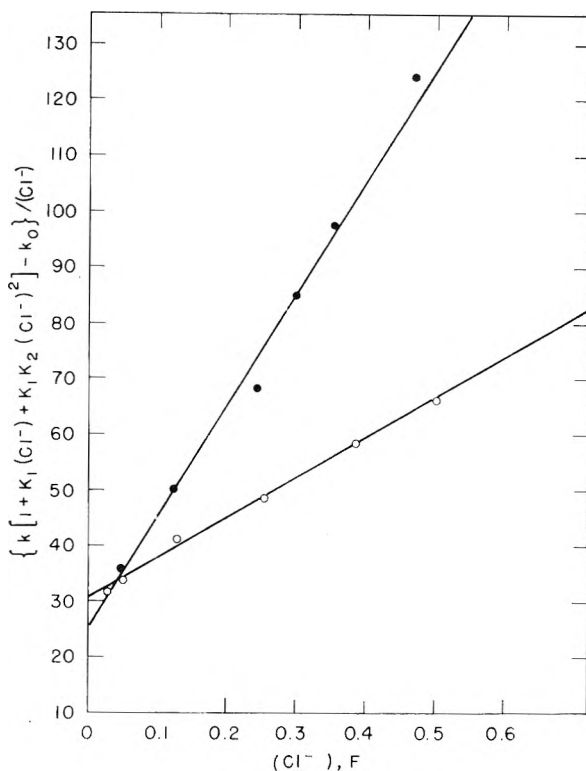


Fig. 2.—Analysis of the chloride ion catalysis of the exchange reaction: ● in D_2O ; ○ in H_2O .

siderations, a reaction which tends to weaken the bond will be favored with hydrogen, as compared with deuterium.

By considering the differences in the frequencies of the internal stretching vibrations of a water molecule in the inner coordination sphere of a cation and in the bulk solvent, Bigeleisen¹² has calculated that the inner sphere complex formed between a tripositive cation and a singly charged anion will be more stable in D_2O by 340 cal./mole. This is an appreciable part of the increased stability of FeCl_2^+ in D_2O . In a similar way, the reaction of two positive ions to form an activated complex containing water will be favored in H_2O , which is the general trend observed.

Equilibrium Isotope Effects.—The effect of D_2O

on a number of equilibria is shown in Table VII. Reactions (1) and (3) are both favored in D₂O. In the iron(III) reaction the present argument attributes most of the D₂O effect to the strengthening of the OH bonds when the charge on the cation is reduced from three to two. It is expected that the D₂O effect is less for the cobalt(III) reaction since there is only one coordinated water molecule instead of the six presumed to be on the ferric ion. Also the weakening of the OH bond in the (NH₃)₅-Co₂H₂O³⁺ ion is less than in the Fe(H₂O)₆³⁺ ion, since it is a much weaker acid by a factor of 10³.¹³

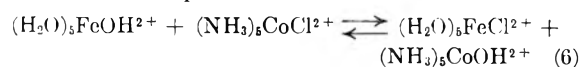
TABLE VII

D₂O EFFECTS ON VARIOUS EQUILIBRIA

Equilibrium	$\frac{K(D_2O)}{K(H_2O)}$	Reference
1) (H ₂ O) ₅ FeH ₂ O ³⁺ + Cl _{aq.} ⁻ ⇌ (H ₂ O) ₅ FeCl ²⁺ + H ₂ O	2.0	This work
2) (H ₂ O) ₅ FeH ₂ O ³⁺ ⇌ (H ₂ O) ₅ FeCH ²⁺ + H _{aq.} ⁺	1.0	4
3) (NH ₃) ₅ CoH ₂ O ³⁺ + Cl _{aq.} ⁻ ⇌ (NH ₃) ₅ CoCl ²⁺ + H ₂ O	1.5	a
4) (NH ₃) ₅ CoH ₂ O ³⁺ ⇌ (NH ₃) ₅ CoOH ²⁺ + H _{aq.} ⁺	1/1.5	b

^a H. Taube, *J. Am. Chem. Soc.*, **82**, 524 (1960). ^b D. J. Bearcroft, D. Sebera, A. Zwickel and H. Taube, to be published.

The hydrolytic reactions, (2) and (4), cannot be discussed directly on the foregoing basis because of the appearance of the aquated proton. This difficulty may be partially circumvented by rewriting the reactions so as to have hydroxide displacing the coordinated water. For substitution by hydroxide, the $K(D_2O)/K(H_2O)$ ratios become 6.5 for the iron(III) and 4.5 for the cobalt(III). Again the effect of the anion is to favor the reaction in D₂O and again the effect is less with cobalt than with the iron. The fact that the effects with hydroxide are about three times as large as with chloride show that the specific properties of the anion, which are doubtless important both when it is aquated and when it is in the complex cannot be ignored. The problem of the aquated anion disappears when we consider reaction (6) which represents the exchange of hydroxide for chloride between the two positive ions.



The simple electrostatic arguments would say that the $K(D_2O)/K(H_2O)$ ratio for this reaction should be unity. By combining reactions (1) to (4) this ratio is found to be 0.9, which is rather close to unity. This suggests that the ratio of the effects associated with chloride on the two tripositive ions is nearly equal to the ratio of those associated with hydroxide, and that the electrostatic arguments give a consistent interpretation of the two systems.

Kinetic Isotope Effects.—A few of the known solvent isotope effects on the rates of oxidation-reduction reactions involving iron, cobalt, chromium and vanadium are shown in Table VIII. The first two reactions illustrate a significant point

(13) A. Zwickel and H. Taube, *J. Am. Chem. Soc.*, **81**, 1288 (1959).

in this discussion: when there is no water in the first coordination spheres of the reactants no isotope effect is observed. All the other reactions go faster in H₂O, as expected from the electrostatic argument presented above. It is not inconsistent that the isotope effects in the iron(II)-iron(III) reactions are about the same when a ferric ion brings an anion into the activated complex as when it brings only water. The reason is that the anion has already exerted its effect on the water molecules coordinated to the ferric ion, so that its effect is partially cancelled in the activated complex.

TABLE VIII

D₂O EFFECTS ON VARIOUS REACTION RATES

Reactants	k_{H_2O}/k_{D_2O}	Reference
(1) Co(phen) ₃ ³⁺ + Co(phen) ₃ ²⁺	1.0	a
(2) Co(NH ₃) ₆ ³⁺ + Cr(dipy) ₃ ²⁺	1.0	b
(3) Fe(H ₂ O) ₆ ³⁺ + Fe(H ₂ O) ₆ ²⁺	2.1	4
(4) (H ₂ O) ₅ FeOH ²⁺ + Fe(H ₂ O) ₆ ²⁺	2.1	4
(5) (H ₂ O) ₅ FeCl ²⁺ + Fe(H ₂ O) ₆ ²⁺	2.5	This work
(6) (NH ₃) ₅ CoH ₂ O ³⁺ + Cr(H ₂ O) ₆ ²⁺	3.8	13
(7) (NH ₃) ₅ CoH ₂ O ³⁺ + Cr(dipy) ₃ ²⁺	2.6	b
(8) (NH ₃) ₅ CrCl ²⁺ + Cr(H ₂ O) ₆ ²⁺	1.3	c
(9) (NH ₃) ₅ CoH ₂ O ³⁺ + V _{aq.} ²⁺	2.6	14
(10) (NH ₃) ₅ CoCl ²⁺ + V _{aq.} ²⁺	2.2	14

^a B. R. Baker, F. Basolo and H. M. Neuman, *J. Phys. Chem.*, **63**, 371 (1959). ^b A. Zwickel and H. Taube, *J. Am. Chem. Soc.*, **81**, 2915 (1959). ^c A. E. Ogard and H. Taube, *ibid.*, **80**, 1084 (1958).

The isotope effect of 3.8 observed in reaction (6) of Table VIII appears too large to be accounted for by the simple electrostatic arguments used above. It is tempting to associate this large effect with the water bridge in the activated complex.¹³ The isotope effect of reaction (8) which also proceeds via a bridged activated complex is only 1.3. From a comparison of the isotope effects of reactions (6) and (8) Zwickel and Taube¹³ concluded that the replacement of a bridging water molecule by a bridging chloride ion leads to a marked decrease in the isotope effect of the oxidation-reduction reaction. If this conclusion applies to all oxidation-reduction reactions proceeding via bridged activated complexes, the similarity of the isotope effects observed in reactions (3) and (5) suggests that the oxidation of Fe(H₂O)₆²⁺ ions by Fe(H₂O)₆³⁺ or (H₂O)₅FeCl²⁺ ions does not proceed via a bridged activated complex. In an analogous manner, the similar isotope effects of reactions (9) and (10) and other comparisons have led Zwickel and Taube¹⁴ to propose that the oxidation of V_{aq.}²⁺ by the Co(III) complexes probably proceeds via an activated complex which approximates to the outer sphere type.

This discussion has been limited largely to the examination of one possible reason for the rates and equilibria of ionic reactions being different in H₂O and D₂O, namely, electrostatic influences on water molecules in the first coordination sphere. It is by no means implied that this is a unique or sufficient way to look at the problem, but we feel that it may be a useful point of view.

(14) A. Zwickel and H. Taube, *ibid.*, **83**, 793 (1961).

FARADAIC RECTIFICATION AND ELECTRODE PROCESSES. II

BY MITSUGI SENDA,^{1a} HIDEO IMAI^{1b} AND PAUL DELAHAY

Coates Chemical Laboratory, Louisiana State University, Baton Rouge, Louisiana

Received February 6, 1961

The correlation between the mean rectification voltage ($\Delta \bar{E}_\infty$) and mean rectification current (\bar{I}_r) and the influence of the circuit resistance are discussed quantitatively. Time variations of the rectification current are analyzed and two methods for the determination of $\Delta \bar{E}_\infty$ are proposed: (a) comparison of \bar{I}_r - t curves with the I - t curves in the potentiostatic voltage-step method (Barker) and (b) direct calculation of $\Delta \bar{E}_\infty$. A double pulse method is described in which the time for charging of the double layer is decreased and the drift of potential due to heating of the electrolyte is minimized at very high frequencies. Experimental data are given and equipment which has been quantitatively tested up to 51 Mc. and which could possibly be used up to 144 Mc. is briefly described.

A rather general treatment of faradaic rectification and its application to electrode kinetics was developed in a previous paper from this Laboratory.² We consider here two additional problems, namely (a) the correlation between measurements of the rectification voltage and the rectification current and (b) the use of a double pulse method to shorten the time required for charging of the double layer in rectification voltage measurements. Instrumentation for measurements up to very high frequencies (possibly 144 Mc.) is briefly described.

Experimental

Cell and Synchronization Device.—A dropping mercury electrode with a low head of mercury was fitted with a magnetic hammer. The signal for the hammer was obtained from an amplifier connected to a drum with contacts rotating at constant speed. The drum also provided a pulse which modulated the a.c. signal generator as described below. The drop time, as controlled by the hammer, was 5 sec. (in comparison with the "natural" drop time of approximately 12 sec. at open circuit in 1.1 *M* HClO₄) and the a.c. pulse could be applied for drop lives as short as 0.12 sec. and as long as 5 sec. Electrode areas as small as 0.004 cm.² could be obtained, and a.c. power consumption at very high frequencies was kept to a minimum. The cell was in a metal cabinet to minimize interference with radiobroadcasting. The lead from the terminal of the coaxial cable to the mercury reservoir was as short as possible (about 2 cm.) to minimize inductance.

A.C. Signal Generation and Modulation.—A signal generator (50 kc. to 65 mc.) with 100% modulation (G4 in Fig. 1) was used at frequencies up to a few megacycles. The output signal fed into a power amplifier. Available power above a few megacycles was too low and a transmitter (T) was substituted for the signal generator. Square-wave modulation was achieved as follows: one of the contact of the synchronization drum (see preceding section) generated a 45 v. pulse which triggered a sawtooth generator (G1). The resulting signal was transformed (G2) into a square-wave pulse which modulated the output of generator G4. The transmitters used above a few megacycles were set in the "key" position, and the output was modulated by means of relay RL1, the latter being triggered with the signal from G2. The transmitter signal was applied to a 100-ohm potentiometer connected to a two-section L-C filter (0.001 and 0.00035 microfarad and 2 × 30 millihenries) to eliminate 60 cycle hum.

Rectification Voltage and Current Measurements.—Rectification voltages were measured with the oscilloscope CRO from the ohmic drop across resistance R2, the high-frequency component being eliminated with the low-pass filter F. Potentiometer P, set at zero voltage in this work, provided a known voltage to be applied to the cell. The output of the voltage divider VD was set at zero except when the voltage-step method was applied (see below).

The low-pass filter was composed of the following elements: (a) A 50 microhenry inductance connected to the cell. (b) A 3-section L-C filter (3 × 2.5 millihenry R.F. transmitter coil, 3 × 0.05 microfarad.); the sections were individually shielded; the axis of the coils were perpendicular to each other to minimize coupling. (c) A shielded 9-section L-C filter composed of capacitors of either 100 or 200 micromicrofarad and 6 or 7 turn coils (22 mm. diameter, 3 mm. spacing between turns, gauge 18 wire); coil axes were perpendicular to each other in each group of 3 coils; L and C varied from one section to another to minimize resonance. (d) A terminal filter composed of 500 microhenries and 0.001 microfarad. Careful design was essential to avoid spurious rectification by the oscilloscope preamplifier as a result of leak of the high frequency signal through the filter by capacitive coupling. This filter could be used in the range 200 Kc. to 51 Mc. It was not tested at higher frequencies but it still might be effective.

Resistance R2 was usually set at 1 megohm in rectification voltage measurements and was varied from 100 to 4000 ohms in rectification current measurements.

Voltage-Step Method.—The voltage step was generated across a 0.9 ohm resistance of a conventional voltage divider (VD). The voltage applied to VD was controlled by relay RL2, the latter being triggered by the signal from G2. The amplitude of the voltage step was determined by means of the oscilloscope OSC.

Double Pulse Method.—A square wave pulse from G3 was applied to the cell simultaneously with the modulated a.c. signal. The amplitude of the pulse was controlled with G3 and by adjustment of R1.

Measurement of A.C. Signal across the Cell.—A Tektronix oscilloscope, model 531, with plug-in unit, type G, sufficed up to a few megacycles. At higher frequencies, the a.c. signal was rectified before application to the oscilloscope. The rectification unit was a set of 10 silicon diodes in series. Ten one megohm resistors were in parallel with the 10 diodes as voltage divider. The terminal stage was connected to a 25 micromicrofarad capacitor. The rectifier unit was calibrated with a Hewlett-Packard vacuum tube voltmeter, model 410B, having a flat response up to 700 Mc. A Tektronix oscilloscope, model 585 was used at a later stage.

Correlation between Rectification Voltage and Current.—In a previous paper² from this Laboratory it was pointed out that two types of control of the d.c. component must be considered in faradaic rectification: control of the mean current (in general $\bar{I} = 0$) or the mean potential (in general $\bar{E} = E_e$, E_e being the equilibrium potential). It was further shown that the mean rectification current density for the electrode reaction $O + ne = R$ (O and R being soluble) is

$$\bar{I}_r = \frac{\Delta \bar{E}_\infty}{\tau + \frac{1}{I_a^0} \frac{RT}{nF}} \exp(\lambda^2 t) \operatorname{erfc}(\lambda t^{1/2}) \quad (1)$$

with

$$\lambda = \frac{1}{nF \left(\frac{1}{I_a^0} + \frac{nF}{RT} \tau \right)} \left(\frac{1}{C_0^0 D_0^{1/2}} + \frac{1}{C_R^0 D_R^{1/2}} \right) \quad (2)$$

(1) (a) Postdoctoral research associate January 1960–March 1961; on leave from Department of Agricultural Chemistry, Kyoto University, Kyoto. (b) Postdoctoral research associate 1960–1962; on leave from Minami College, Hiroshima University, Hiroshima.

(2) P. Delahay, M. Senda and C. H. Weis, *J. Am. Chem. Soc.*, **83**, 312 (1961). See references to previous works therein.

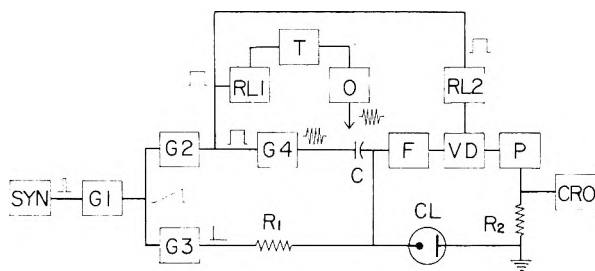


Fig. 1.—Equipment for faradaic rectification. SYN, synchronization device; G1, Tektronix sawtooth generator, model 162; G2 and G3, Tektronix square-wave generator, model 161; G4, Hewlett-Packard signal generator, model 606A and Hewlett-Packard amplifier, model 460 AR loaded with a 620 ohm resistance; T, Heathkit transmitters "Apache," model TX1 (3.5, 7, 14, 21 and 28 Mc.), or "Seneca," model VHF-1 (51 and 144 Mc.); O, output filter and voltage divider; RL1 and RL2, Clare mercury relay, type HG 1001; F, low-pass filter; VD, voltage divider; P, 0-3 volt 50 ohm potentiometer; CRO, Tektronix oscilloscope model 535 with plug-in unit type E, R1 adjustable from 0.1 to 5.7 megohms; R2 adjustable from 0 to 1 megohm; C in general 0.003 microfarad, but could be adjusted; CL cell with dropping mercury electrode and mercury pool.

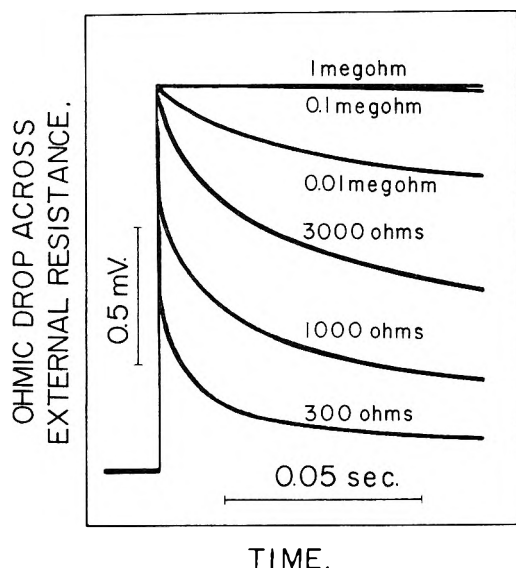


Fig. 2.—Influence of external resistance (R_2 of Fig. 1) for the discharge of $0.63 \text{ mM Hg}_2^{++}$ in 1.1 M HClO_4 on mercury at 1 Mc. and 30° . Curves are tracings of oscillograms. Electrode area, 0.0041 cm.^2 ; circuit resistance except R_2 , 120 ohms ; a.c. peak to peak voltage applied to the cell, 1.6 v. The shift of E is negative.

There the C^0 's are the bulk concentrations, the D 's the diffusion coefficients; r is the total resistance of the d.c. cell circuit for the measurement of the rectification current density; I_a^0 is the apparent exchange current density (not corrected for double layer effects, etc.); R , T and F have their usual significance; t is the time elapsed since the application of the a.c. signal; and $\Delta \bar{E}_\infty$ is the mean rectification voltage that would be observed for control of the mean current instead of the mean potential, the a.c. signal being the same in both cases. Note that $\Delta \bar{E}_\infty$ is expressed for $t \rightarrow \infty$ to allow for charging of the double layer.

Equation 1 is identical to the equation for current-time variations in the potentiostatic voltage-step

method³ provided $\Delta \bar{E}_\infty = -\Delta V$, ΔV being the voltage step. Hence, the mean rectification voltage can be measured indirectly by comparison of the \bar{I}_r-t curve with the $I-t$ curve obtained by the voltage-step method, the voltage step ΔV being adjusted so that $\bar{I}_r = I$ at any given time. This method which was originally developed and extensively used by Barker⁴ finds its full justification in eq. 1. Barker did not consider \bar{I}_r-t curves in detail and he did not make a detailed analysis of the correlation between measurements of \bar{I}_r and $\Delta \bar{E}_\infty$. This matter is taken up below.

It follows from eq. 1 that when $r \gg (1/I_a^0)$ (RT/nF) and $\lambda t^{1/2} \ll 1$, i.e., when

$$r \gg \frac{RT}{n^2 F^2} \left(\frac{1}{C_O^0 D_O^{1/2}} + \frac{1}{C_R^0 D_R^{1/2}} \right) t^{1/2} \quad (3)$$

one has $\bar{I}_r = \Delta \bar{E}_\infty / r$. If the cell resistance and the resistances of the elements F , VD and P (Fig. 1) in series are much smaller than R_2 , the ohmic drop across R_2 is for all practical purposes equal to the rectification voltage when the above conditions are fulfilled. Control of \bar{I} at zero is practically achieved. There is consequently a progressive transition from control of $\bar{I} = 0$ toward $\bar{E} = E_c$ as the total resistance of the cell circuit decreases (Fig. 2).

The identity of \bar{I}_r-t and $I-t$ curves when $\Delta V = -\Delta \bar{E}_\infty$ was verified for the discharge of mercurous ions on mercury by direct measurements of $\Delta \bar{E}_\infty$ and determination of ΔV for which $\bar{I}_r = I$ at any given time. Results are given in Fig. 3 for large values of the argument in eq. 1 ($\lambda t^{1/2} > 7$) for which this equation reduces to

$$\bar{I}_r = \Delta \bar{E}_\infty \frac{n^2 F^2}{RT} \left(\frac{1}{C_O^0 D_O^{1/2}} + \frac{1}{C_R^0 D_R^{1/2}} \right)^{-1} (\pi t)^{-1/2} \quad (4)$$

regardless of the value of r . \bar{I}_r is then diffusion controlled. Note that the linearity of \bar{I}_r with $t^{-1/2}$ is verified in Fig. 3.

Rectification voltages can also be calculated directly from \bar{I}_r-t curves without comparison with $I-t$ curves obtained by the voltage-step method by the following method. It follows from eq. 4 that the quantity $\bar{I}_r t^{1/2} / \Delta \bar{E}_\infty$ should approach the constant value

$$\frac{n^2 F^2}{RT} \left(\frac{1}{C_O^0 D_O^{1/2}} + \frac{1}{C_R^0 D_R^{1/2}} \right)^{-1} \pi^{-1/2}$$

for large values of t corresponding to diffusion control. This quantity is readily calculated and, since \bar{I}_r and t are measured, $\Delta \bar{E}_\infty$ is directly obtained. The experimental value of $\bar{I}_r t^{1/2} / \Delta \bar{E}_\infty$ for pure diffusion control is $6.6 \times 10^{-3} \text{ amp. cm.}^{-2} \text{ sec.}^{1/2} \text{ volt}^{-1}$ for the data of Fig. 3 vs. 7.5×10^{-3} for the value calculated for the polarographic diffusion coefficient, $D_{\text{Hg}_2^{++}} = 0.9 \times 10^{-5} \text{ cm.}^2 \text{ sec.}^{-1}$.

The double layer charging was not considered in the derivation of eq. 1. The more general problem was set up and solved in the form of Laplace transformation. Inverse transformation, however, appeared very complex and only

(3) (a) W. Vielstich and P. Delahay, *ibid.*, **79**, 1874 (1957). (b) For a review of this and other relaxation methods in electrode kinetics, see P. Delahay, Chap. 5 in "Advances in Electrochemistry and Electrochemical Engineering," Vol. 1, edited by P. Delahay, Interscience Publishers, Inc., New York, N. Y., in course of publication.

(4) G. C. Barker, "Transactions of Symposium on Electrode Processes," E. Yeager, editor, John Wiley and Sons, Inc., New York, N. Y., in course of publication.

two extreme cases were examined: (a) $rc_1 \ll t$, τ being the resistance of eq. 1 and c_1 the differential double layer capacity per unit area; eq. 1 then holds and the charging current becomes vanishingly small before the rectification current is measured. (b) When $rc_1 \gg t$, the time constant of the external circuit is much larger than the time constant for the circuit composed of the double layer capacity in parallel with the faradaic impedance for the mean circuit; the double layer charging current is almost entirely supplied by the electrode reaction and not by the external circuit; this case was treated in a previous paper (see eq. 18 in ref. 2).

Double Pulse Method for Very High Frequencies.—The full rectification voltage $\Delta\bar{E}_\infty$ does not appear across the cell immediately after application of the a.c. signal because of charging of the double layer. This effect was previously examined² by theory and experiment, and it was shown that the rectification voltage approaches $\Delta\bar{E}_\infty$ for $t \rightarrow \infty$. The time at which $\Delta\bar{E}_\infty$ is practically reached can easily exceed 0.01 sec., especially when the polarization resistance is high, and the a.c. signal must be applied for a relatively long time. Heating of the electrolyte then interferes because of the drift of potential. Heating is particularly serious at high frequencies because of the power required to maintain a few millivolts across the double layer. The upper usable frequencies can be increased by the following method which is inspired for the galvanostatic double pulse method^{5,6}: a square wave pulse of short duration is applied to the cell simultaneously with the a.c. signal, and the time variation of the rectification voltage is determined (Fig. 4). The curve with a rectification voltage independent of time corresponds to $\Delta\bar{E}_\infty$.

When the duration of the current pulse is sufficiently small in comparison with the time scale for the measurement of the rectification voltage, the potential vs. time curve is given by an equation identical to eq. 18 in ref. 2 except for the coefficient ($\Delta\bar{E}_\infty - \Delta\bar{E}_i$) of the second term which is now replaced by $(\Delta\bar{E}_\infty - \Delta\bar{E}_i - \Delta\bar{E}_p)$, $\Delta\bar{E}_p$ being the potential variations caused by the current pulse at the beginning of a.c. signal application.

Measurements of $\Delta\bar{E}_\infty$ by this method could be made for the reduction of 10^{-2} mM Hg_2^{++} on mercury in 1 M HClO_4 at frequencies up to 28 Mc., the a.c. pulse not exceeding 0.5 – 1 millisecc. and the square wave pulse being 10 microsecc. long or even shorter.

Comparison of Methods.—The determination of rectification voltages with control of \bar{I} at zero has several advantages: it is the most direct method; duration of the a.c. pulse can be quite short (1 millisecc. or less) with the double pulse method; and the sensitivity of the oscilloscope need not be as high as in rectification current measurements. There is one disadvantage, namely, that generation *in situ* of one reactant by a polarographic technique does not appear practical. Conversely, generation *in situ* is quite simple in rectification current measurements. Application of one or the other

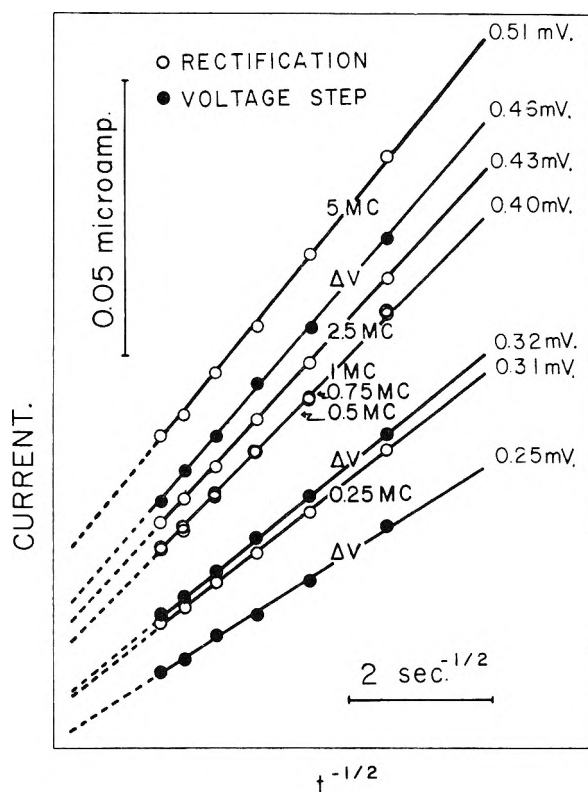


Fig. 3.—Analysis of current-time curves for faradaic rectification and the potentiostatic voltage-step method for the discharge of 0.3 mM Hg_2^{++} on mercury in 1.15 M HClO_4 at 30°. The frequency (in megacycles per sec.) and rectification voltage or voltage step are indicated on each line. The zero of coordinates is common for all lines. ΔV is positive and $\Delta\bar{E}_\infty$ negative, and the current is anodic. Electrode area, 0.0053 cm.²; cell resistance, 150 ohms; a.c. peak to peak voltage applied to cell: 0.4, 0.8, 1.2, 1.6, 4.2, 8.4 v. for 0.25, 0.5, 0.75, 1, 2.5 and 5 Mc., respectively.

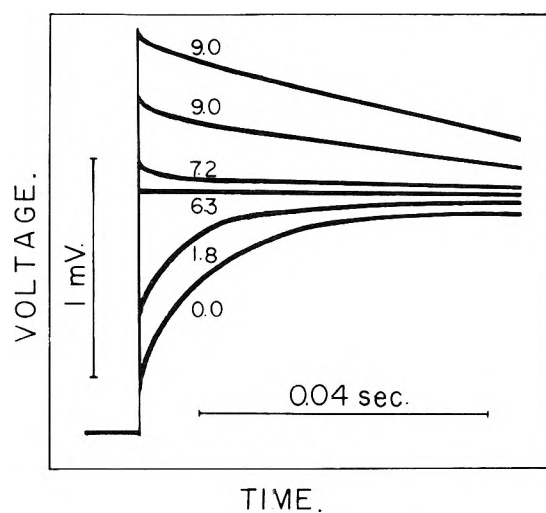


Fig. 4.—Tracings of voltage-time curves for the double pulse method for the discharge of 0.012 mM Hg_2^{++} on mercury in 1.1 M HClO_4 at 0.5 Mc. and 30°. Electrode area, 0.0041 cm.²; cell resistance, 81 ohms; a.c. peak to peak voltage applied to the cell 1.2 v.; duration of square-wave pulse, 30 microsecc. except for the upper curve for which the pulse was 40 microsecc. long. Amplitude of the current square-wave is indicated in microamp. on each curve. The shift of \bar{E} is negative.

(5) (a) H. Gerischer and M. Krause, *Z. physik. Chem., N.F.*, **10**, 264 (1957); (b) **14**, 184 (1958).

(6) H. Matsuda, S. Oka and P. Delahay, *J. Am. Chem. Soc.*, **81**, 5077 (1959).

method thus depends on the system being studied. At any rate, the same general equipment is used in both methods.

Acknowledgment.—The investigation was supported in part by the Office of Naval Research and by the National Science Foundation.

KINETICS OF THE REACTION BETWEEN Pu(VI) AND Sn(II) IN CHLORIDE-PERCHLORATE SOLUTION¹

BY S. W. RABIDEAU AND B. J. MASTERS

University of California, Los Alamos Scientific Laboratory, Los Alamos, New Mexico

Received January 25, 1961

A study has been made of the kinetics of the reaction, $\text{Pu(VI)} + \text{Sn(II)} \rightarrow \text{Pu(IV)} + \text{Sn(IV)}$. In mixed chloride-perchlorate media, the rate of Pu(VI) reduction is first-order dependent upon the concentration of each reactant, strongly dependent upon the chloride ion concentration and independent of the hydrogen ion concentration. These observations are consistent with a parallel path mechanism in which the reaction proceeds primarily through activated complexes having the formulas $(\text{PuO}_2\text{SnCl}_3)^+$ and $(\text{PuO}_2\text{SnCl}_4)^0$. Thermodynamic quantities for the activation processes have been obtained for these two reaction paths, and the correlation between charge and entropy has been found to apply to these activated complexes of charge +1 and zero. The experimental observation that the reduction of Pu(VI) by Sn(II) occurs much more rapidly than does the reduction of Pu(V) by Sn(II) has been interpreted as evidence that the Pu(VI)-Sn(II) reaction proceeds through a single step mechanism which involves the transfer of two equivalents of charge.

Introduction

Kinetic studies of the reactions of plutonyl ion with various reducing agents such as, for example, Ti(III),^{2a} V(III)^{2b} and U(IV)³ have been made not only because of the variety of mechanistic possibilities offered by these systems and the desire to provide a background of chemical information for this actinide element, but also because there appear to be opportunities provided by the study of these reactions to focus attention upon factors which may aid in the correlation of the relative rates of the chemical reactions.

In the reductions of Fe(III)⁴ and Pu(IV)⁵ with Sn(II), it has been observed that although the reaction rate is very slow in perchlorate solution, in the presence of chloride ion a marked acceleration in rate is found. This observation has also been found to be applicable to the Pu(VI)-Sn(II) system in the present work. It appears that the introduction of chloride ions into the activated complex provides a much more effective path for the oxidation-reduction process than is available in perchlorate solution even under conditions of low acidity.

Experimental

Materials.—Stock solutions of 1.3×10^{-3} to 1.1×10^{-2} M stannous chloride in hydrochloric acid were prepared from Baker and Adamson reagent grade crystalline $\text{SnCl}_2 \cdot 2\text{H}_2\text{O}$. These solutions were protected from atmospheric oxygen with the use of a vessel fitted with stopcocks through which was directed a stream of Oxsorbent-scrubbed argon. Plutonium(VI) perchlorate solutions were prepared from weighed samples of high-purity metal. After dissolution of the metal in a weighed quantity of standardized 70% perchloric acid, the solution was ozonized overnight. Prior to use, this stock solution was subjected to an additional period of ozonization to ensure quantitative conversion of the plutonium to the plutonyl form. The residue of dissolved ozone was removed by prolonged flushing with purified argon. The purification of the water, sodium perchlorate and the sodium

chloride and the standardization of the hydrochloric and perchloric acids followed procedures described previously.⁵

Analyses.—Solutions of Fe(III) in hydrochloric acid were prepared from C.P. grade Fe_2O_3 and were standardized volumetrically against potassium permanganate with the use of the Zimmermann-Reinhardt procedure. Standard iron wire was carried through the analysis procedure as a control. Stock solutions of Sn(II) were analyzed by the addition of the sample to a slight excess of an argon-flushed 2 M hydrochloric acid solution of Fe(III). The stannous ion concentration in the stock solution was computed from the spectrophotometrically observed decrease in ferric ion concentration. At the reagent concentrations used, a significant time was required for essentially complete reaction. The kinetics of the reaction between Fe(III) and Sn(II) in hydrochloric acid solution has been studied.⁶ All spectrophotometric measurements were made with the Cary Model 14 instrument. A molar extinction coefficient of 2,350 was measured for Fe(III) in 2 M hydrochloric acid at 3350 Å. with a slit width of 0.10 mm.

The concentration of Pu(VI) was followed in the rate measurements as a function of time from optical density measurements at a wave length of 8298 Å. and a slit width of 0.10 mm. Molar extinction coefficients of standard Pu(VI) solutions were measured in each experiment under varied conditions of solution composition and temperature.

The contribution to the optical densities at 8298 Å. by Sn(II), Sn(IV), Pu(III) and Pu(IV) was considered to be negligible at the concentrations of metal ions used in these experiments.

In experiments in which the concentration of Pu(V) was followed as a function of time, the sharp absorption peak at 5674 Å. in dilute hydrochloric-perchloric acid solution was used.

Procedure and Apparatus.—It was necessary to flush the spectrophotometer cell and all reagent solutions with purified argon to reduce the atmospheric oxidation of the Sn(II) to negligible proportions. With this precaution, 10^{-4} M solutions of stannous chloride could be used without loss of titer because of air oxidation. Weight aliquots of the Pu(VI) stock solution were added to one leg of the double-chambered spectrophotometer cell. The Sn(II) solution together with appropriate quantities of acid and salt solutions were added to the second leg. Prior to mixing the solutions in the two compartments, thermal equilibrium was attained by the solutions in a water thermostat. The cell was then placed in a water-thermostated compartment within the Cary instrument. The total volume of mixed solutions was computed for each rate run from the measured solution densities and the weights of the component solutions.

(1) This work was done under the auspices of the United States Atomic Energy Commission.

(2) (a) S. W. Rabideau and R. J. Kline, *J. Phys. Chem.*, **63**, 1502 (1959); (b) **62**, 414 (1958).

(3) T. W. Newton, *ibid.*, **62**, 943 (1958).

(4) M. H. Gorin, *J. Am. Chem. Soc.*, **58**, 1787 (1936).

(5) S. W. Rabideau, *J. Phys. Chem.*, **64**, 1491 (1960).

(6) F. R. Duke and R. C. Pinkerton, *J. Am. Chem. Soc.*, **73**, 3045 (1951).

Calculations.—As discussed in a previous paper,⁵ a least squares program has been prepared to treat second-order kinetic data with the use of the IBM-704 computer. From input data which consisted of optical densities *versus* time at 8298 Å., initial reactant concentrations, molar extinction coefficients, stoichiometric reaction coefficients and cell length, specific reaction rate constants were computed which corresponded to the least squares fit of the data. Input optical densities were used up to the point at which it was calculated that 1% of the Sn(II) had been consumed in the reduction of Pu(VI). This generally corresponded to about 50% reduction of the Pu(VI). Also, the associated uncertainties of the specific rate constants as reflected by their standard deviations constituted a part of the program print-out.

If the equation for the formation of the activated complex is written in terms of the uncomplexed reactant ions, then appropriate correction terms must be applied to the experimentally measured apparent rate constant obtained in chloride solutions to take into consideration the fact that a fraction of each of the metal ion species is present in the form of chloro-complexes. For stannous ion, the relationship between the uncomplexed form, Sn^{++} , and the total bivalent tin, Sn(II) , is given by the expression

$$[\text{Sn}^{++}] = [\text{Sn(II)}] / (1 + \beta_1[\text{Cl}^-] + \beta_2[\text{Cl}^-]^2 + \beta_3[\text{Cl}^-]^3) \quad (1)$$

where the β_n values represent the successive formation quotients for the stannous chloro-complexes containing one, two and three chlorides, respectively, and molar concentrations are enclosed by brackets. The general expression for the Sn(II) formation quotient is

$$\beta_n = [\text{SnCl}_n]^{+2-n} / [\text{Sn}^{++}] [\text{Cl}^-]^n \quad (2)$$

A report of the non-linear least squares procedure which was used to obtain the β -values for the Sn(II) chloro-complexes has been prepared.⁷ A portion of the Pu(VI) is also present in the solutions in the form of a chloro-complex or complexes and the apparent rate constant must be adjusted to reflect this fact if the true chloride ion dependence of the reaction rate is to be evaluated.

If it is considered that a single chloro-complex of Pu(VI) is present, the relationship between the uncomplexed plutonyl ion, PuO_2^{++} , and the total plutonyl ion concentration, Pu(VI) , is given by

$$[\text{PuO}_2^{++}] = [\text{Pu(VI)}] / (1 + \beta_1'[\text{Cl}^-]) \quad (3)$$

where the formation quotient, β_1' , is defined by the expression

$$\beta_1' = [\text{PuO}_2\text{Cl}^+] / [\text{PuO}_2^{++}] [\text{Cl}^-] \quad (4)$$

The expression

$$(\epsilon_0 - \bar{\epsilon}) / [\text{Cl}^-] = \beta_1'(\bar{\epsilon} - \epsilon_1) \quad (5)$$

can be derived with the assumption of a single Pu(VI) chloro-complex, where ϵ_0 , $\bar{\epsilon}$ and ϵ_1 correspond to the molar extinction coefficient values for PuO_2^{++} , Pu(VI) and PuO_2Cl^+ , respectively. Further, with the assumption of the invariance of ϵ_1 , ϵ_0 and β_1' , with changes in solution composition at constant ionic strength, values of β_n'' have been obtained from plots of $(\epsilon_0 - \bar{\epsilon}) / [\text{Cl}^-]$ vs. $\bar{\epsilon}$ between 2.4 and 29.6° at 8298 Å.

The spectrophotometric data for Pu(VI) in perchlorate-chloride media can also be explained by the assumption of successive chloro-complexes.^{8,9} If the relationship between PuO_2^{++} and Pu(VI) is written on the basis of a two chloro-complex model, it follows that

$$[\text{PuO}_2^{++}] = [\text{Pu(VI)}] / (1 + \beta_1''[\text{Cl}^-] + \beta_2''[\text{Cl}^-]^2) \quad (6)$$

where the formation quotients are given by

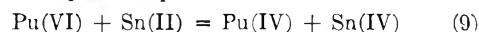
$$\beta_n'' = [\text{PuO}_2\text{Cl}_n]^{+2-n} / [\text{PuO}_2^{++}] [\text{Cl}^-]^n \quad (7)$$

In the present work, both the single and the two chloro-complex models of Pu(VI) have been considered. The relationship between the successive formation quotients for the two Pu(VI) chloro-complexes, β_1'' and β_2'' , and the formation quotient for the single Pu(VI) complex, β_1' , can be shown⁸ to be equal to

$$\beta_2'' = \beta_1'(\beta_1'' - \beta_1') \quad (8)$$

Results

Stoichiometry.—In chloride-perchlorate acid solutions, Pu(VI) is reduced rapidly by Sn(II). From measurements made at a wave length of 8298 Å. it was observed that the change in the concentration of Pu(VI) with the addition of known quantities of Sn(II) corresponded to the reduction of one mole of Pu(VI) for each mole of Sn(II). These stoichiometry measurements were made in solutions which contained chloride ion in the concentration of 0.5 M. Thus, it was concluded that the stoichiometry of the reaction can be represented by the equation



In the presence of chloride ion concentrations of approximately 1.5–2.0 M, less than one mole of Pu(VI) is reduced per mole of Sn(II) because of the effective competition of Pu(IV) for the Sn(II). The Pu(IV)-Sn(II) reaction makes a greater contribution to the observed stoichiometry at higher chloride ion concentrations because of its larger chloride ion dependence.⁵

Pu(V)-Sn(II) Reaction.—To determine whether Pu(V) is an intermediate product in the reduction of Pu(VI) with Sn(II), the rate of the Pu(V)-Sn(II) reaction was examined. Pu(V) was prepared in 0.1 M hydrochloric–0.1 M perchloric acid solution by the reduction of Pu(VI) with Pu(III). Essentially equimolar quantities of Pu(VI) and Pu(III) were used in the initial solution. The equilibrium reaction



was driven to the right by the extraction of Pu(IV) with 0.2% dibutyl phosphate in benzene. The aqueous layer was washed with benzene to remove traces of dibutyl phosphate. The procedure of Markin and McKay¹⁰ which accomplished the extraction of Pu(IV) from Pu(V) in nitric acid solution was found in the present work to be applicable in hydrochloric acid or in perchloric acid solutions also. Solutions of Pu(V) which were pinkish-violet in color and which contained small amounts of the other oxidation states of plutonium as revealed by spectrophotometric examination were produced by this extraction procedure. If Pu(V) were an intermediate step in the reduction reaction of Pu(VI) with Sn(II), then since the over-all reaction is rapid, it would be expected that the reduction of Pu(V) by Sn(II) would also be rapid. However, in 0.5 M HCl solutions containing about 2×10^{-3} M concentrations of each reactant and no added salt, the reduction of Pu(V) by Sn(II) is observed to proceed much more slowly than does the reaction between Pu(VI) and Sn(II). At 2.4°, if it is assumed that the disappearance of Pu(V) is attributable solely to the reaction with Sn(II), an upper limit for the apparent bimolecular rate constant of about $0.15 \text{ M}^{-1} \text{ sec}^{-1}$ is obtained.

Rate Law.—The rate of the reaction between Pu(VI) and Sn(II) has been found to be first order in each of the reactants. The initial molar concentration ranges used for the reactants were 1.6×10^{-4} to 3.1×10^{-4} M for the Pu(VI) and $1.6 \times$

(7) S. W. Rabideau and R. H. Moore, *J. Phys. Chem.*, **65**, 371 (1961).

(8) T. W. Newton and F. B. Baker, *ibid.*, **61**, 934 (1957).

(9) R. Krub, *J. Am. Chem. Soc.*, **76**, 4865 (1954).

(10) T. L. Markin and H. A. C. McKay, *J. Inorg. Nucl. Chem.*, **7**, 298 (1958).

10^{-4} to $1.1 \times 10^{-3} M$ for the Sn(II). Linear second-order plots were observed to approximately 30 to 80% of completion of reaction without taking into consideration the possibility of the reaction of the product, Pu(IV), with the Sn(II). With this consecutive reaction taken into consideration, the linear portion of the second-order plot increased to as much as 90%. In terms of the total concentration of the metal ion species, the rate law can be written as

$$-d[\text{Pu(VI)}]/dt = -d[\text{Sn(II)}]/dt = k_{\text{obsd}} [\text{Pu(VI)}][\text{Sn(II)}] \quad (11)$$

in solutions of constant chloride ion concentration.

In Table I are given a set of data for a typical experiment which were used as the input to the computer. From these data a value of $15.42 \pm 0.07 M^{-1} \text{ sec.}^{-1}$ was obtained for k_{obsd} .

TABLE I

INPUT DATA FOR REDUCTION OF Pu(VI) WITH Sn(II) AT 2.4° , $[\text{H}^+] = 2.0 M$, $\mu = 2.0$

$[\text{Pu(VI)}] = [\text{Sn(II)}] = 1.647 \times 10^{-4} M$; Pu(VI) molar extinction coefficient = 462

Time, sec.	Optical density	Time, sec.	Optical density
0	...	82.5	0.619
30	0.698	90	.610
37.5	.685	97.5	.600
45	.672	105	.591
52.5	.660	112.5	.582
60	.649	120	.574
67.5	.639	127.5	.566
75	.629	135	.558

Acidity Dependence.—From experiments conducted at 20.2° at a constant chloride ion concentration of $0.500 M$ and at an ionic strength of two, it was found that the rate of reaction between Pu(VI) and Sn(II) is hydrogen ion concentration independent. As shown in Table II, within a deviation of about 5% from the mean value, the values of k_{obsd} are unchanged over nearly a sixfold change in acidity. The standard deviation of the specific rate constant k_{obsd} in an individual experiment is given by σ .

TABLE II

ACIDITY DEPENDENCE OF Pu(VI)-Sn(II) REACTION AT 20.2° , $\mu = 2.0$, $[\text{Cl}^-] = 0.50 M$

$[\text{H}^+], M$	$k_{\text{obsd}}, M^{-1} \text{ sec.}^{-1}$	σ
2.000	19.45	0.09
1.504	17.07	.10
1.002	19.45	.08
0.574	18.89	.10
0.344	17.61	.04

Mean 18.49

Chloride Ion Dependence.—The specific rate constant, k_{obsd} , defined by equation 11, includes a functional dependence upon the chloride ion concentration. If the rate law is written in terms of the uncomplexed metal ion species, and it is desired to obtain the appropriate chloride ion dependence for the rate law expressed in this manner, then it is necessary as mentioned in the Experimental section of this paper to apply corrections for the chloro-complexes of the reactant metal ions. With the assumption of a *single* chloro-complex of

Pu(VI) and with the use of the formation quotients of Sn(II) as derived from least squares calculations,⁷ the rate law can be written as

$$-d[\text{Pu(VI)}]/dt = -d[\text{Sn(II)}]/dt = k_{\text{obsd}} [\text{PuO}_2^{++}] [\text{Sn}^{++}] (1 + \beta_1' [\text{Cl}^-]) (1 + \beta_1 [\text{Cl}^-] + \beta_2 [\text{Cl}^-]^2 + \beta_3 [\text{Cl}^-]^3) \quad (12)$$

With the substitution of

$$k' = k_{\text{obsd}} (1 + \beta_1' [\text{Cl}^-]) (1 + \beta_1 [\text{Cl}^-] + \beta_2 [\text{Cl}^-]^2 + \beta_3 [\text{Cl}^-]^3) \quad (13)$$

in equation 12, the rate law can be simplified to

$$-d[\text{Pu(VI)}]/dt = -d[\text{Sn(II)}]/dt = k' [\text{PuO}_2^{++}] [\text{Sn}^{++}] \quad (14)$$

The formation quotients β_1' and β_n have been defined by equations 4 and 2, respectively, and the values of these quantities used in the present work are given in Table III.

TABLE III

FORMATION QUOTIENTS FOR CHLORO-COMPLEXES OF Pu(VI) AND Sn(II), $\mu = 2.0$

$t, ^\circ\text{C.}$	β_1'	β_1	β_2	β_3
2.4	0.39	7.75	34.4	15.5
10.2	.46	9.01	39.8	19.8
15.0	.50	9.80	43.7	23.3
20.2	.56	10.6	48.2	27.7
29.6	.67	12.2	57.2	37.6

A mean value of 3.3 kcal./mole was computed for ΔH for the reaction



from the results given in Table III.

Through the use of the formation quotients β_1' and β_n , corrections have been applied for the chloro-complexes of the metal ion reactants; however, the specific rate constant, k' , as expressed by equation 14, is dependent upon the chloride ion concentration. The object of applying the corrections for the chloro-complexing of the metal ion reactants has been to define this dependence. In Table IV are given the experimentally obtained values of the specific rate constants as functions of both temperature and chloride ion concentration together with their associated standard deviations. Also included are the values of k' , the specific rate constant corrected for chloro-complexing of Pu(VI) and Sn(II).

In plots of $\log k'$ vs. $\log [\text{Cl}^-]$, straight lines of average slopes 3.54 appear to fit the data satisfactory at each temperature. Equation 14 may be written to include explicitly the chloride ion concentration dependence as

$$-d[\text{Pu(VI)}]/dt = -d[\text{Sn(II)}]/dt = k_1 [\text{PuO}_2^{++}] [\text{Sn}^{++}] [\text{Cl}^-]^3 + k_2 [\text{PuO}_2^{++}] [\text{Sn}^{++}] [\text{Cl}^-]^4 \quad (16)$$

where

$$k' = k_1 [\text{Cl}^-]^3 + k_2 [\text{Cl}^-]^4 \quad (17)$$

Equations 16 and 17 suggest the involvement of parallel paths in the rate-determining steps which are dependent upon the third and upon the fourth powers of the chloride ion concentrations. Values of k_1 and k_2 were obtained by the use of a weighted least squares computer fit of the polynomial expression given in equation 17. Because of the ex-

TABLE IV
SPECIFIC RATE CONSTANTS FOR Pu(VI)-Sn(II) REACTION,
 $\mu = 2.0$, $[H^+] = 2.0 M$

Initial reactant concentrations about $1.7 \times 10^{-4} M$				
t , °C.	$[Cl^-]$, M	k_{obsd} , $M^{-1} \text{sec.}^{-1}$	σ	k' , $M^{-1} \text{sec.}^{-1}$
2.4	1.752	28.27	0.14	9,684
	1.002	15.42	.07	1,269
	0.751	9.59	.04	407
	.501	5.37	.02	99.2
	.250	1.735	.004	10.1
10.2	1.754	56.37	.31	25,080
	1.003	29.32	.12	3,001
	0.752	18.98	.07	989
	.497	11.19	.04	244
	.248	3.36	.01	22.4
15.0	1.754	66.03	.51	34,520
	1.003	33.70	.23	3,961
	0.751	20.49	.17	1,209
	.501	13.38	.08	332
	.250	4.56	.02	33.6
20.2	1.753	105.9	.9	66,530
	1.002	50.09	.32	6,875
	0.750	29.58	.27	2,006
	.501	16.80	.16	472
	.250	6.20	.03	50.2
29.6	0.747	55.61	.29	4,812
	.501	36.33	.12	1,271
	.250	12.85	.05	123

tremely large range in the individual values of k' , it is considered that weights applied in proportion to $(1/k')^2$ gave a more satisfactory fit of the data. The values of these parameters are given in Table V.

TABLE V
TEMPERATURE COEFFICIENTS OF SPECIFIC RATE CONSTANTS
FOR PARALLEL PATHS^a

t , °C.	k_1	σ_1	k_2	σ_2
2.4	433	37	768	55
10.2	893	56	2068	88
15.0	1376	265	2507	394
20.2	1534	573	5136	934
29.6	6056	407	7574	850

^a Single Pu(VI) chloro-complex model assumed.

The least squares values of the slopes of plots of $\ln k_1$ and $\ln k_2$ vs. $1/T$ were obtained with computer methods. With the aid of the method of propagation of errors, it can be shown that the statistical weighting factors for these plots are $(k_1/\sigma_{k_1})^2$ and $(k_2/\sigma_{k_2})^2$, respectively. With reference to the expressions from the transition state theory,¹¹ values of the free energy, heat and entropy of activation were computed for the parallel paths in which three and four chlorides are involved in the formation of the activated complex. In Table VI, these results are given along with the entropy of the activated complex.¹² These calculations are predicated upon the single chloro-complex model for Pu(VI). The values of S^* were computed with the use of ΔS^* and values

of +13.2, -5.9 and -27 e.u. for Cl^- , Sn^{++} and PuO_2^{++} , respectively.^{13,14}

TABLE VI
THERMODYNAMIC ACTIVATION QUANTITIES FOR PARALLEL
REACTION PATHS IN THE REDUCTION OF Pu(VI) WITH
Sn(II) AT 25°

Process	ΔF^\ddagger , kcal./ mole	ΔH^\ddagger , kcal./ mole	ΔS^\ddagger , e.u.	S^\ddagger , e.u.
$PuO_2^{++} + Sn^{++} + 3Cl^- \rightarrow$ $(PuO_2 \cdot Sn \cdot Cl_3)^+$	12.3	15.7	11.3	18
$PuO_2^{++} + Sn^{++} + 4Cl^- \rightarrow$ $(PuO_2 \cdot Sn \cdot Cl_4)^0$	12.3	13.5	4.2	24

The effect of chloride ion on the absorption spectrum of Pu(VI) was determined at eight different wave lengths by Newton and Baker.⁸ We have referred to their conclusions that with various qualifying assumptions, the spectrophotometric data can be explained nearly equally well with either the single or the two chloro-complex Pu(VI) model. The treatment of the kinetic data for the Pu(VI)-Sn(II) reaction has been discussed in the preceding paragraphs with the assumption of the single chloro-complex of Pu(VI). It was a matter of interest to determine the magnitude of the effects which the assumption of a two chloro-complex model for Pu(VI) would have upon the results of the calculations.

With a procedure similar to that outlined previously,⁸ the values of β_1'' and β_2'' have been obtained as a function of temperature and are given in Table VII. These quantities have been defined in equation 7. These formation quotient values reproduce the molar extinction coefficients obtained at 8298 Å. between 2.4 and 29.6° within the limit of experimental error. These values also are consistent with the measurements made at 4300, 8303 and 8373 Å. at a temperature of 25°.⁸

TABLE VII
TEMPERATURE DEPENDENCE OF FORMATION QUOTIENTS FOR
TWO CHLORO-COMPLEX MODEL FOR Pu(VI)

t , °C.	β_1''	β_2''
2.4	0.92	0.21
10.2	1.00	.25
15.0	1.06	.28
20.2	1.15	.33
29.6	1.30	.43

Equation 13 is modified in the two chloro-complex treatment of the kinetic data by the substitution of the term $(1 + \beta_1''[Cl^-] + \beta_2''[Cl^-]^2)$ for $(1 + \beta_1''[Cl^-])$. The specific rate constant corrected for chloro-complexing in this fashion is designated as k'' . Plots of $\log k''$ vs. $\log [Cl^-]$ indicate a slightly greater power for the chloride ion dependence in the rate expression than was found in the single Pu(VI) chloro-complex model. An average slope of 3.76 was obtained in this plot in contrast to the 3.54 average slope obtained in the plots of $\log k'$ vs. $\log [Cl^-]$. Thus, both models

(11) S. Glasstone, K. Laidler and H. Eyring, "The Theory of Rate Processes," McGraw-Hill Book Co., Inc., New York, N. Y., 1941, p. 417.

(12) T. W. Newton and S. W. Rabideau, *J. Phys. Chem.*, **63**, 365 (1959).

(13) W. M. Latimer, "Oxidation Potentials," 2nd Ed., Prentice-Hall, Inc., New York, N. Y., 1952.

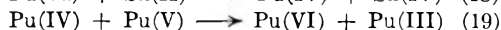
(14) J. J. Katz and G. T. Seaborg, "The Chemistry of the Actinide Elements," Methuen and Co., Ltd., London, 1957 (also John Wiley and Sons, Inc., New York, N. Y.).

indicate that the kinetic data for the Pu(VI)-Sn(II) reaction may be interpreted on the basis of parallel paths in which three and four chloride ions are involved.

In the evaluation of the thermodynamic quantities for the reaction from the kinetic data based upon corrections applied with the two chloro-complex model for Pu(VI), the same procedures as described above for the single chloro-complex were used. For the two chloro-complex model the heats and entropies of activation for the k_1 and k_2 paths have been found to be 17.5 and 13.2 kcal./mole and 16.1 and 4.4 e.u., respectively. With the use of the same values for the entropies of the individual ions as were used in Table VI, the entropies of the activated complexes with charges of +1 and zero were found to be 22.8 and 24.3 e.u., respectively. These latter results represent changes of +4.8 and +0.3 e.u. with respect to the corresponding quantities listed in Table VI.

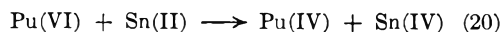
Discussion

Pu(V)-Sn(II) Reaction.—The value obtained for the apparent rate constant in the Pu(V)-Sn(II) reaction corresponds to approximately one-eighth of the value of the Pu(VI)-Sn(II) apparent rate constant under comparable conditions. However, Pu(VI) was known to be present in small amount during the Pu(V)-Sn(II) rate measurements, and it appears probable that some induced reaction, such as that represented by the chain mechanism

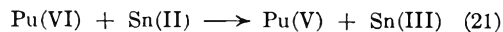


may have contributed appreciably to the observed rate of Pu(V) disappearance. Consequently, the actual value of the Pu(V)-Sn(II) apparent rate constant may be very much smaller than the observed upper limit of $0.15 M^{-1} \text{ sec.}^{-1}$ at 2.4° . In any event, it may be concluded that the Pu(V)-Sn(II) reaction rate is much too slow to be of importance in the reduction of Pu(VI) and Sn(II).

Pu(VI)-Sn(II) Reaction.—The two-equivalent transfer mechanism



is in accord with both the observed rate law and the stoichiometry requirement, and seems to represent the most likely of several alternative mechanisms for the reduction of Pu(VI) by Sn(II). If we wish to consider as a possible rate-determining step the one equivalent transfer process



then in order to satisfy the stoichiometric equation, reaction 21 must be followed by a rapid reaction sequence in which either (a) reduction of a second Pu(VI) ion by Sn(III) followed by disproportionation of Pu(V); (b) reduction of a second Pu(VI) ion by Sn(III) is accompanied by reduction of Pu(V) by Sn(II); or (c) Pu(V) is further reduced by Sn(III). Possibility (a) may be excluded from consideration because of the relative slowness of the Pu(V) disproportionation reaction, the rate of which has been observed in chloride solutions in the present work. In view of the measured slowness of the Pu(V)-Sn(II) reaction observed in this

study, case (b) may also be eliminated. In possibility (c), it must be assumed that Pu(V) and Sn(III) undergo rapid reaction, even when present at very low steady state concentrations. However, if these intermediates are indeed capable of rapid reaction, it would appear more likely that they should undergo reaction before diffusing out of the "solvent cage" following the reaction step shown in equation 21, and in this event, the over-all process would become indistinguishable from the mechanism shown in equation 20.

The strong chloride ion concentration dependence observed for the Pu(VI)-Sn(II) reaction has been observed in the stannous reduction of many other reducible cations; for example, Fe(III) and Pu(IV). It seems to be well established that the species of tin(II) which is responsible for the reduction process is the chloro-complex or complexes; the inclusion of chloride ions into the activated complex apparently provides a more favorable configuration for the oxidation-reduction process than is capable of being formed in perchlorate media.

In studies of the reduction of uranyl, neptunyl and plutonyl ions with various cations in perchlorate media, the observed rate expressions often exhibit an inverse hydrogen ion concentration dependence which implies that one or more hydrogen ions are lost in the formation of the activated complex. In the present study, there appears to be an exception to this generalization inasmuch as it has been found that the reduction of plutonyl with stannous ion is hydrogen ion independent. However, in this latter case, chloride ion was present in appreciable concentration and tin(II) is rather strongly complexed by this anion. Also, in contrast with some of the other reductants, stannous ion is little hydrolyzed in the range of acidities used in the present experiments. It seems likely that in chloride solution the other actinide -yl ion types may also show a zero order hydrogen ion concentration dependence with Sn(II) and other relatively little hydrolyzed reductants with the chloride ion apparently assuming the function which hydroxyl ion (or oxide ion) performs in the formation of the activated complexes in perchlorate solutions.

Entropy of Activated Complexes.—In the study of the influence of charge upon the entropy of the activated complex, it has been observed that a decreased positive charge corresponds to a more positive entropy of the complex.^{12,5} This conclusion is supported in the present work with activated complexes of charge +1 and zero. The latter represents an extension of previously recorded information to an additional charge type.

It is of interest to note that although it is not possible to distinguish between a single or a two chloro-complex model for Pu(VI) on the basis of the analysis of spectrophotometric data, it is of little consequence insofar as its effect upon the interpretation of the kinetic data is concerned. With both models it is concluded that parallel paths in which three and four chloride ions are involved constitute the rate-determining steps. Also, independent of the model choice, the entropies

of the correspondingly charged activated complexes are essentially equal within experimental error.

Acknowledgment.—The authors wish to express

their appreciation to Drs. J. F. Lemons and C. E. Holley, Jr., for helpful discussions and to the statistical section at LASL for assistance in the computer treatment of the data.

MEASUREMENT OF ADSORPTION ISOTHERMS AND SURFACE AREAS BY CONTINUOUS FLOW METHOD¹

BY P. E. EBERLY, JR.

Esso Research Laboratories, Esso Standard, Division of Humble Oil & Refining Co., Baton Rouge, Louisiana

Received December 19, 1960

Previous work has shown the possibility of measuring adsorption isotherms by a continuous flow technique. Basically this method involves the transport of a continuous stream of adsorbate vapor through a packed column of adsorbent by an inert, non-adsorbable carrier gas stream. After saturation of the column, the adsorbed material is eluted by the carrier gas stream alone. From analysis of the effluent gas, it is possible to calculate the adsorption isotherm provided all diffusional effects are eliminated and the adsorption equilibrium is rapidly established. This method is ideally suited for study of high temperature adsorption because the low contact times afforded by the flow method tend to minimize the decomposition of the adsorbate. Also, the adsorption equilibrium can be expected to be rapidly established at these conditions. To verify the theoretical principles, experiments were made with *n*-butane on silica gel at 48° covering a wide range of partial pressures. Good agreement was observed between the flow and equilibrium isotherms. The technique was then extended to the measurement of ammonia isotherms on both fresh and steam-deactivated SiO₂-Al₂O₃ cracking catalyst, SiO₂ gel and γ -Al₂O₃ at 260 to 482°. Both a reversible and irreversible adsorption occur on the catalysts and γ -Al₂O₃. The amount adsorbed decreases with temperature. The steam-deactivated catalyst adsorbs considerably less than the fresh material. Little difference is seen in the adsorption behavior of fresh SiO₂-Al₂O₃ and the non-catalytic γ -Al₂O₃. Silica gel exhibits only a negligible amount of reversible and no irreversible adsorption even at the lowest temperature.

I. Introduction

Advantages for studying catalytic materials under conditions approaching as closely as possible those used in the actual reaction have recently been emphasized by Heinemann.² One of the most extensively used methods for studying catalytic surfaces has been that of adsorption. Since a majority of reactions in the petroleum industry occur at high temperature, adsorption measurements in static systems have been difficult to make because of decomposition. To avoid this, flow systems can be used to decrease the contact time and thus minimize decomposition.

The purpose of this investigation was to determine whether reasonably accurate adsorption isotherms could be determined in a flow system according to the principles of Wilson,³ de Vault⁴ and Glueckauf.⁵ Basically, the method consists in transporting a continuous stream of adsorbate through a column of initially unsaturated adsorbent by means of an inert, non-adsorbable carrier gas. This continuous flow method is to be distinguished from that of pulse flow reported previously.^{6,7} After saturation, the adsorbed material is eluted by the pure carrier gas alone. From an analysis of the composition of the effluent stream as a function of time, the adsorption isotherm can be calculated provided that (1) diffusional effects are kept to a minimum and (2) the adsorption equilibrium is rapidly established. These conditions

can be expected to be essentially fulfilled at high temperatures.

Figure 1 illustrates the method of calculation for a system exhibiting a Langmuir-type isotherm. Here, the concentration of adsorbate (*c*) in the effluent stream is plotted as a function of time. If the two previously mentioned conditions are met, the adsorption front will be sharp whereas the desorption branch will be diffuse in nature. From a knowledge of the "break-through" time of the adsorption front, the amount of material adsorbed at the concentration, *c*₀, of the incoming stream can be determined. This is proportional to the area ABDO. The desorption branch of the curve can be used to calculate the amount adsorbed at any desired concentration from zero up to the maximum concentration, *c*₀. This is done by means of the equation

$$x = \frac{n\bar{c} + y\bar{c}}{m} \times 1000$$

where

x = amount adsorbed at concn. \bar{c} (Point G in Fig. 1) in mmoles/g.

n = moles of pure carrier gas passed after shutting off the adsorbate stream. This corresponds to the amount passed in the time interval, H-E, in Fig. 1

\bar{c} = concn. of adsorbate at Point G in moles of adsorbate/mole of carrier gas

Thus, the term *n* \bar{c} is proportional to the area EFGH in Fig. 1.

y \bar{c} = the amount of adsorbate remaining in the column when the concn. is *c*. This corresponds to the area GHI

m = grams of adsorbent

In this manner, many points on the isotherm can be determined from only a single flow curve. Gregg and Stock⁸ showed reasonably good agreement between isotherms measured in this manner

(1) Paper presented at A.C.S. Southwest Regional Meeting, Oklahoma City, Oklahoma, December 1-3, 1960.

(2) H. Heinemann. Sec. International Congress on Catalysis, Paris, France, July 4-9, 1960.

(3) J. N. Wilson, *J. Am. Chem. Soc.*, **62**, 1583 (1940).

(4) D. deVault, *ibid.*, **65**, 532 (1943).

(5) E. Glueckauf, *J. Chem. Soc.*, 1302 (1947).

(6) P. E. Eberly, Jr., *J. Phys. Chem.*, **65**, 68 (1961).

(7) P. E. Eberly, Jr., and E. H. Spencer, *Trans. Faraday Soc.*, **57**, 289 (1961).

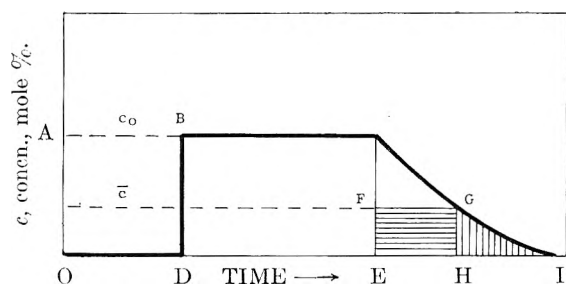


Fig. 1.—Diagram illustrating calculation of adsorption isotherm from continuous flow data. This plot shows the concentration of adsorbate (c) in the effluent gas as a function of time. The symbols, c_0 and \bar{c} represent, respectively, the inlet adsorbate concentration and the concentration corresponding to points F and G in the diagram.

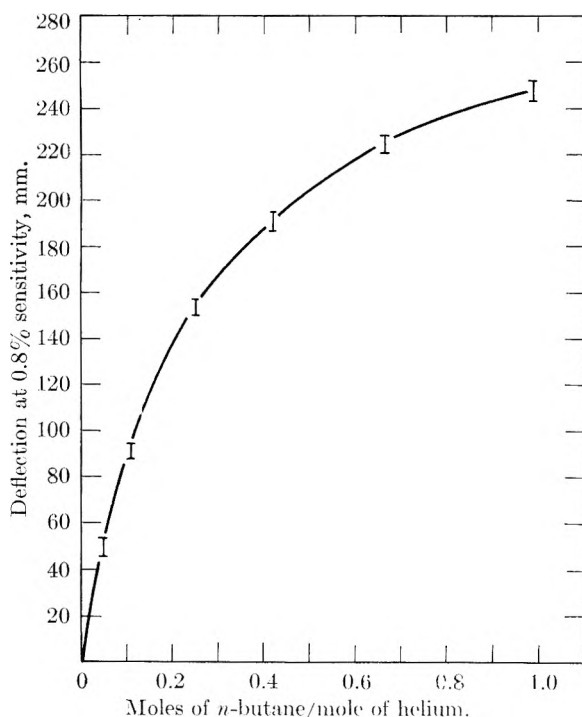


Fig. 2.—Cell response as a function of n -butane concentration.

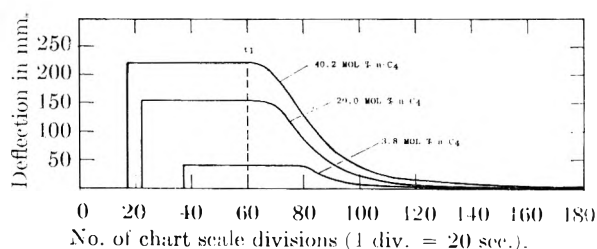


Fig. 3.—Continuous flow curves of n -butane on silica gel at 48° . The column consisted of 4.2 g. of silica gel packed into standard $1/4$ " stainless steel tubing resulting in bed length of 28 cm. The combined flow rate of n -butane and helium was 50 cc./min. at room temperature and pressure. Time, t_1 , represents the time when the introduction of n -butane to the column was discontinued.

and those determined in a static system. From these flow isotherms, corresponding surface areas can be estimated by the BET method.

(8) S. J. Gregg and R. Stock, Sec. Symposium on Gas Chromatography, May 19–23, 1953. Preprints published by Butterworth's Sci. Publ. (London), 1953.

To verify the theoretical principles, experiments were made with n -butane on silica gel at 48° covering a wide range of partial pressures. The technique was then extended to the study of ammonia adsorption on both fresh and steam-deactivated $\text{SiO}_2\text{-Al}_2\text{O}_3$ cracking catalysts at temperatures of 260, 371 and 482° . For comparative purposes, measurements were also made on $\eta\text{-Al}_2\text{O}_3$ and SiO_2 gel.

II. Experimental

The apparatus consisted essentially of a gas injection system connected in series to a packed column of adsorbent and a thermal conductivity cell. To avoid unnecessary diffusional effects, every attempt was made to minimize extraneous void volumes. The gas injection system for permitting the instantaneous introduction of a stream of constant composition to the column has been described previously.⁹ Helium was selected as the carrier gas and the adsorbate, n -butane or ammonia, was introduced into the helium stream by insertion of a hypodermic needle through a silicone rubber disc. For helium and n -butane, flow rates were measured by observing the movement of a soap film through a buret. Ammonia flow rates were measured with a rotameter.

The columns were constructed of $1/4$ " stainless steel tubing (i.d. = 0.18 in.). The solid adsorbents were prepared in a 48–60 mesh particle size. Particles much smaller than this create excessive pressure drops which distort the shape of the curve. Also, if the particle size becomes too large, diffusional effects may create some distortion. For our lower temperature work with n -butane, the column was maintained at a constant temperature by use of a water-bath. A fluidized-sand bath similar to that described by Adams, Gernand and Kimberlin¹⁰ was used for our high temperature work with ammonia.

Concentrations of adsorbate in the effluent stream were measured by a Perkin-Elmer thermal conductivity cell which has a fast time constant of less than 0.5 second. With n -butane concentrations up to 50 mole %, the response of the cell at a given sensitivity was not linear with concentration. The calibration curve to convert cell response to concentration is shown in Fig. 2. The length of the vertical lines shows the variability at various concentration levels. The deflection of the cell with ammonia was linear up to maximum concentration of ~ 7 mole %.

The source and physical properties of the porous materials are shown in Table I. The gases were obtained from the Matheson Co. The purities of helium, n -butane and ammonia were 99.99, 99.85 and 99.99%, respectively.

TABLE I

Porous material	Source	Surface area, m. ² /g.	Pore volume, cc./g.
Fresh 13% Al_2O_3			
87% SiO_2	Davison Chem. Co.	499	0.35
Steamed 13% Al_2O_3			
87% SiO_2^a	Davison Chem. Co.	283	.33
$\eta\text{-Al}_2\text{O}_3$	Nat. Aluminate Corp.	236	.42
SiO_2 gel	Davison Chem. Co.	585	.31

^a Steamed for 24 hours at 538° and 1 atm.

III. Results

a. n -Butane on Silica Gel at 48° .—The column consisted of 4.2 g. (5 cc.) of silica gel packed into a 0.18 in. i.d. stainless steel tube resulting in a bed length of 28 cm. Prior to the adsorption measurements, dry helium was allowed to flow through the column for a period of 16 hours at 48° .

Six flow curves were obtained with streams containing 3.8, 9.6, 20.0, 28.9, 40.2 and 49.7 mole %

(9) P. E. Eberly, Jr., *Trans. Faraday Soc.*, **57**, 1169 (1961).

(10) C. E. Adams, M. O. Gernand and C. N. Kimberlin, Jr., *Ind. Eng. Chem.*, **46**, 2458 (1954).

n-butane. Three of these curves are shown in Fig. 3. In these experiments, the respective individual flow rates prior to injection were so adjusted so that the total combined rate was always maintained at 50 cc./min. The ordinate represents the deflection in mm. at 0.8% sensitivity of the conductivity cell. The abscissa is the number of chart scale divisions (one division being equal to 20 seconds). The time, t_1 , represents the time when the injection of *n*-butane was discontinued.

The absence of diffusional effects and rapid establishment of adsorption equilibrium are indicated by the sharpness of the adsorption "break-through" curve. The amount adsorbed at the maximum concentration (c_0) for each of the six runs was calculated from these "break-through" times.¹¹ This represents the equilibrium isotherm and is represented by the circled points in Fig. 4. To further substantiate that equilibrium had been established, several determinations were made at a lower combined flow rate of 30 cc./min. These results agreed with the isotherm measured at 50 cc./min.

The area under the desorption curves of Fig. 3 is considerably larger than that of the adsorption front. This is due to the non-linearity of the cell response. By use of the calibration curve in Fig. 2, the desorption curves are replotted to yield curves of concentration *vs.* time. The amount of *n*-butane desorbed was thus found to be equal to the amount adsorbed. This was true for every run except that using 49.7 mole % *n*-butane. The discrepancy can be attributed to a lack of sufficient precision in the cell calibration curve at high partial pressures of *n*-butane.

Flow isotherms determined from the desorption curves of the five remaining runs are shown in Fig. 4 and compared with the equilibrium isotherm. Extremely good agreement was observed with the exception of the isotherm calculated from the 40.2 mole % *n*-butane flow curve. The deviation was 7% higher than the equilibrium isotherm at the highest partial pressure. This can be attributed to the variability in the calibration curve.

Since the curves were in such good agreement, it was thought interesting to determine the surface area of the silica gel from this isotherm. The data were replotted in the BFT manner. The resulting surface area is listed in Table II and compared with the area obtained with *n*-butane at 0° in a static system. The values are of the same order of magnitude. The surface area from the static isotherms is about 80 m.²/g. higher which is due to the increased severity of degassing the sample under vacuum at 300°. It has been found that the area obtained from a butane isotherm must be multiplied by a correction of 1.5 to make it agree with the one obtained from the nitrogen isotherm.¹² This value of 570 m.²/g. shown in parenthesis in Table II and was calculated from the static isotherm.

Since many points on the isotherm can be determined from only a single flow curve, this method

(11) From runs with argon, a non-adsorbable gas, the correction for flow through the dead space was found to be negligible.

(12) P. H. Emmett. "Catalysis I," Reinhold Publ. Corp., New York, N. Y., 1954, Chapt. II.

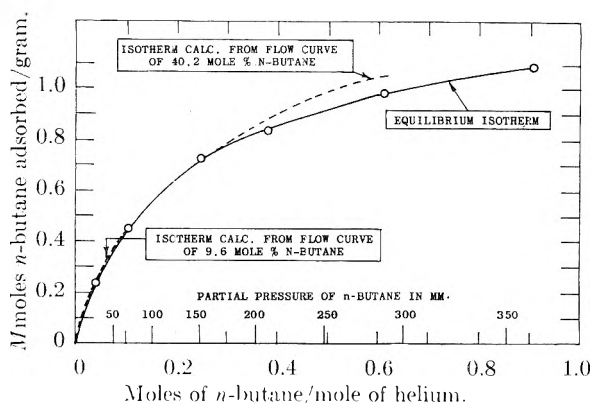


Fig. 4.—Comparison of calculated isotherms with equilibrium isotherm of *n*-butane on silica gel at 48°. The isotherms calculated from the flow curves of 3.8, 20.0 and 28.9 mole % *n*-butane coincided with the equilibrium curve.

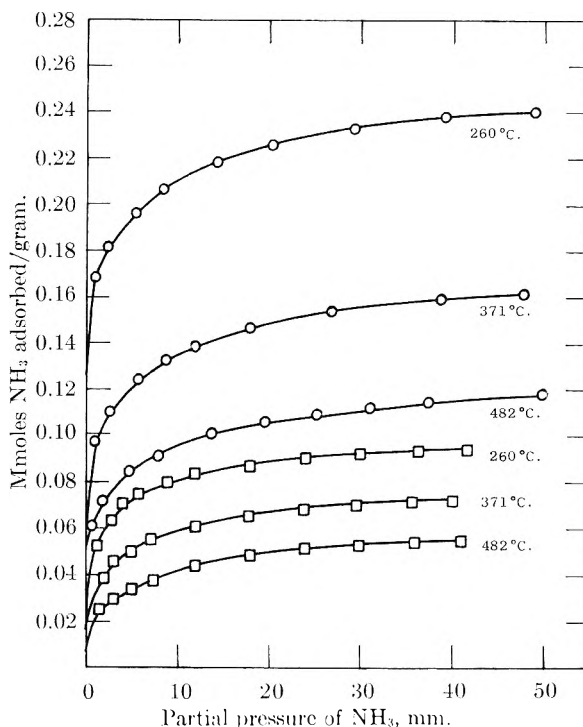


Fig. 5.—Adsorption isotherms of NH_3 on fresh and steam-deactivated $\text{SiO}_2\text{-Al}_2\text{O}_3$ cracking catalyst. The circles and squares represent data with the fresh and steam-deactivated silica-alumina cracking catalysts.

TABLE II

	N_M , mmoles/ g.	Area of <i>n</i> -butane molecule, Å. ²	Surface area, m. ² /g.
<i>n</i> -C ₄ Flow isotherm at 48°	1.299	38.0	300
<i>n</i> -C ₄ Static isotherm at 0°	1.765	35.7	380 (570)
N ₂ Static isotherm at -196°	5.99	16.2	585

^a Sample outgassed at 300° for 8 hours. ^b Obtained by multiplying surface area of *n*-butane (static method) by correction factor of 1.5.

may show some advantage over a static system for routine measurement of surface areas.

b. Ammonia on $\text{SiO}_2\text{-Al}_2\text{O}_3$, SiO_2 Gel and $\gamma\text{-Al}_2\text{O}_3$ at 260–482°.—The method discussed in the previous section was applied to the study of ammonia adsorption at high temperatures on silica-alumina cracking catalysts and related solids.

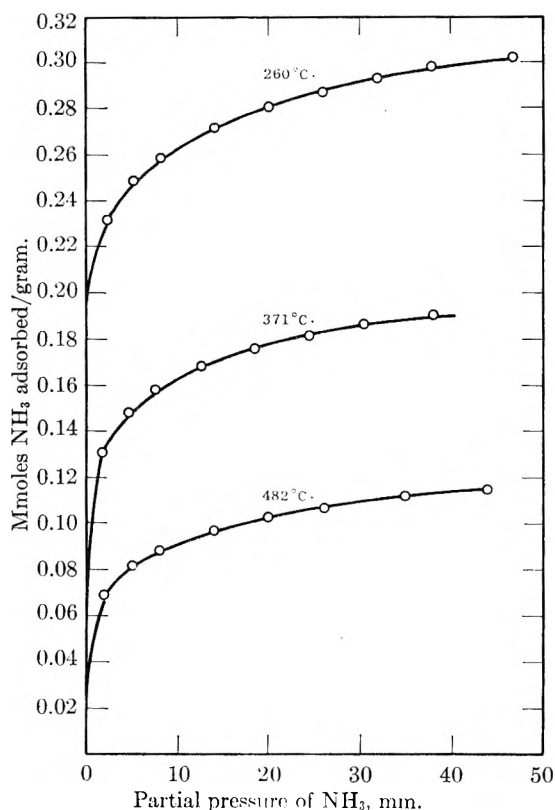


Fig. 6.—Adsorption isotherm of NH_3 on $\eta\text{-Al}_2\text{O}_3$.

Many papers have appeared on the correlation of catalytic activity with surface acidity as measured by various methods. Such investigators include among other Tamele,¹³ Benesi,^{14,15} and Mills, Boedeker, Oblad and Milliken.^{16,17} Very little work, however, has been done on ammonia adsorption at high temperatures. It was thought that flow adsorption isotherms of NH_3 might be useful in elucidating the nature of catalytic activity at high temperatures.

For fresh $\text{SiO}_2\text{-Al}_2\text{O}_3$, the column consisted of 4.099 g. (5 cc.) packed into 0.18 in. i.d. stainless steel tubing resulting in a bed length of about 30 cm. The particle size was 48–60 mesh. Prior to the adsorption experiments, the column was flushed with helium at 50 cc./min. for a period of 16 hours at 538°. The temperature was then lowered to 482° and ammonia injected at a partial pressure of about 40 mm. After steady-state had been reached, the injection was discontinued and the adsorbed material was eluted from the column by the helium stream alone. After flushing for an hour, no more ammonia could be detected in the effluent stream. The portion remaining on the surface at this time was defined as the amount of irreversible adsorption. The temperature was then lowered successively to 371 and 260° and the ammonia injection performed at each temperature.

Since we are dealing with at least two types of

(13) M. W. Tamele, *Disc. Faraday Soc.*, **8**, 270 (1950).

(14) H. Benesi, *J. Am. Chem. Soc.*, **78**, 5490 (1956).

(15) H. Benesi, *J. Phys. Chem.*, **61**, 970 (1957).

(16) G. A. Mills, E. R. Boedeker and A. G. Oblad, *J. Am. Chem. Soc.*, **72**, 1554 (1950).

(17) T. H. Milliken, G. A. Mills and A. G. Oblad, *Disc. Faraday Soc.*, **8**, 279 (1950).

adsorption, reversible and irreversible, the adsorption isotherm can only be evaluated if we make the assumption that the amount of irreversible adsorption is independent of ammonia pressure. If this is done, one obtains the Langmuir-type isotherms shown in Fig. 5. The data in this figure and subsequent Fig. 6 represent the total adsorption including both reversible and irreversible as a function of partial pressure. In Table III, the amount of the two adsorptions at the three temperatures is listed.

Adsorbent	Temp., °C.	Mmoles of NH_3 adsorbed/g.		Total
		Irrev.	Rev.	
Fresh $\text{SiO}_2\text{-Al}_2\text{O}_3$	482	0.035	0.081	0.116
	371	.066	.094	.160
	260	.127	.111	.238
Steamed $\text{SiO}_2\text{-Al}_2\text{O}_3$	482	0	.055	.055
	371	0.010	.063	.073
	260	.024	.070	.094
$\eta\text{-Al}_2\text{O}_3$	482	.032	.082	.114
	371	.104	.087	.191
	260	.182	.116	.298
SiO_2	482	0	.009	.009
	371	0	.010	.010
	260	0	.012	.012

A similar set of experiments was performed on an identical column of silica-alumina which had been steamed for 24 hours at 538° and 1 atm. pressure. After steaming, the column was flushed with dry helium for 16 hours at 538°. Results of the ammonia adsorption are shown in Fig. 5 and Table III. With the steamed catalyst, no irreversible adsorption was observed at 482°. At the lower temperatures, however, it did occur. The amount was still much smaller than observed with the fresh catalyst. At 260°, for instance, the amount of irreversible adsorption was only $1/6$ of that of the fresh material.

Determinations were also made on a similar column of $\eta\text{-Al}_2\text{O}_3$. These results are shown in Fig. 6. The data in Table III show that the amount of irreversible ammonia adsorption on alumina is comparable to that on fresh silica-alumina. Since alumina is much less active as a catalytic cracking catalyst, this adsorption must be different in nature from that on silica-alumina.

Silica gel exhibited no irreversible adsorption at even the lowest temperature. Reversible adsorption was also very small in spite of the fact that the gel had the highest surface area among the porous materials.

From the variation of the amount of adsorption with temperature, one may calculate an apparent heat of adsorption. For the reversible portion, the heat of adsorption for the cracking catalysts and η -alumina was roughly one kcal./mole. This is of the same order of magnitude as the extrapolated value of the heat of vaporization of ammonia. However, these surfaces may be decidedly different from that of silica gel since the latter had only a negligible capacity in comparison to the other solids even at the lowest temperature.

Within the precision of our data, the irreversible

adsorption of the alumina cannot be distinguished from that of silica-alumina by the temperature-dependence of the amount adsorbed. All three solids exhibit a heat of about 5 kcal./mole.

IV. Discussion

From the results of this work, and that reported previously,⁸ it has been found that sufficiently accurate adsorption isotherms can be determined from continuous flow curves. As such, it holds promise as a useful tool for investigating catalytic surfaces at temperatures close to those where the actual reaction occurs. As pointed out by Heinemann,² this is an area which needs to be investigated more thoroughly. Use of flow isotherms may also hold some promise for routine measurement of surface areas since many points on the isotherm can be determined from only a single flow curve. Care must be taken, however, to avoid diffusional effects and to ensure rapid establishment of equilibrium.

The results of high temperature ammonia adsorption on silica-alumina cracking catalyst are in essential agreement with previous work using quinoline at 315°. ^{16,17} The steamed catalyst which is known to be less active shows a smaller degree

of irreversible adsorption than the fresh material. Also, the non-catalytic silica gel shows no irreversible adsorption.

The results with alumina, however, do not fit the general picture. From ammonia adsorption data, it would be difficult to distinguish this material from fresh silica-alumina. A plausible explanation is that the alumina contains a distinctly different proportion of the so-called Lewis and Bronsted acid sites. The data reported here are not sufficient to distinguish between these two types of acidity.

The reversible portion of adsorption, however, cannot be completely ignored. If it were independent of the nature of the surface, we would expect the silica gel, having the largest surface area, to exhibit the greatest amount of reversible adsorption. Since, however, it had only a very small capacity, the comparatively large reversible adsorption associated with alumina and silica-alumina may be of significance in catalysis.

V. Acknowledgment.—The author wishes to express his sincere appreciation to Esso Research and Engineering Co. for their kind permission to publish this work.

LOW TEMPERATURE HEAT CAPACITY, ENTROPY AND HEAT OF FORMATION OF CRYSTALLINE AND COLLOIDAL FERRIC PHOSPHATE DIHYDRATE

BY EDWARD P. EGAN, JR., ZACHARY T. WAKEFIELD AND BASIL B. LUFF

Division of Chemical Development, Tennessee Valley Authority, Wilson Dam, Alabama

Received December 5, 1960

The low temperature heat capacities of strengite, $\text{FePO}_4 \cdot 2\text{H}_2\text{O}(c)$, and amorphous $\text{FePO}_4 \cdot 2\text{H}_2\text{O}$ were measured between 8 and 310°K. The respective entropies at 298.16°K. are 40.93 and 45.07 e.u.—the enthalpies, 6607 and 7121 cal. mole⁻¹. The heat capacity curve for strengite shows a peak with a maximum at or below 7.5°K. A peak in the curve for the amorphous material is less pronounced. The heats of formation, as determined in a solution calorimeter, and calculated solubility products are -451.5 kcal. mole⁻¹ and $\log K_{sp} = -34.56$ for strengite, -444.1 kcal. mole⁻¹ and $\log K_{sp} = -30.02$ for amorphous $\text{FePO}_4 \cdot 2\text{H}_2\text{O}$.

Compounds associated with the phosphorus status of soils command the attention of soil scientists—chemists and agronomists alike. Ferric phosphate dihydrate, $\text{FePO}_4 \cdot 2\text{H}_2\text{O}$, is such a compound. Although interest centers mainly on strengite, the crystalline form, even semiquantitative distinctions between the respective properties of crystalline and colloidal $\text{FePO}_4 \cdot 2\text{H}_2\text{O}$ are noteworthy.

Presented here are measurements of the heat capacities of crystalline and colloidal $\text{FePO}_4 \cdot 2\text{H}_2\text{O}$ at 7.5 to 300°K., entropies and heat contents at 298.16°K. derived therefrom, the heats of formation as determined by a method of solution calorimetry.

Materials and Apparatus.—Crystalline and colloidal $\text{FePO}_4 \cdot 2\text{H}_2\text{O}$ were prepared by methods that have been described.^{1,2} The crystals of strengite averaged 10 μ in length. Their surface area (by glycerol adsorption) was 0.79 sq. m./g.—an area considered unlikely to introduce

significant surface energy effects into the heat capacity measurements.

Although the crystals were dried at 105° without significant loss in weight below the dihydrate composition, they lost part of their water of hydration when dried under vacuum at room temperature. Hence in the helium-displacement of air from the low temperature calorimeter preparatory to sealing it, the calorimeter was evacuated as rapidly as was feasible to < 1 mm., helium was admitted to 1 atm., the evacuation was repeated, and helium was admitted to 0.3 atm.

The colloidal phosphate was vacuum desiccated to lower its water content to 2 moles. Its surface area (by glycerol adsorption) was 60 sq. m./g. Although similarities have been noted in the properties of the crystalline and colloidal forms of ferric phosphate dihydrate,^{1,2} there is no conclusive evidence that the thermodynamic values reported here for the colloidal material would have been obtained with the strengite had its surface area been increased to 60 sq. m./g. Electron diffraction patterns for the colloid showed a structural orderliness suggestive of strengite.²

The calorimeter was charged with the colloidal material in a nitrogen-filled dry box. Samples taken immediately before and immediately after filling the calorimeter showed a slight dehydration in the dry box, and the average composition was assumed to represent the calorimeter charge

(1) W. E. Cate, E. C. Huffman and M. E. Deming, *Soil Sci.*, **88**, 130 (1959).

(2) E. O. Huffman, W. E. Cate and M. E. Deming, *ibid.*, **90**, 8 (1960).

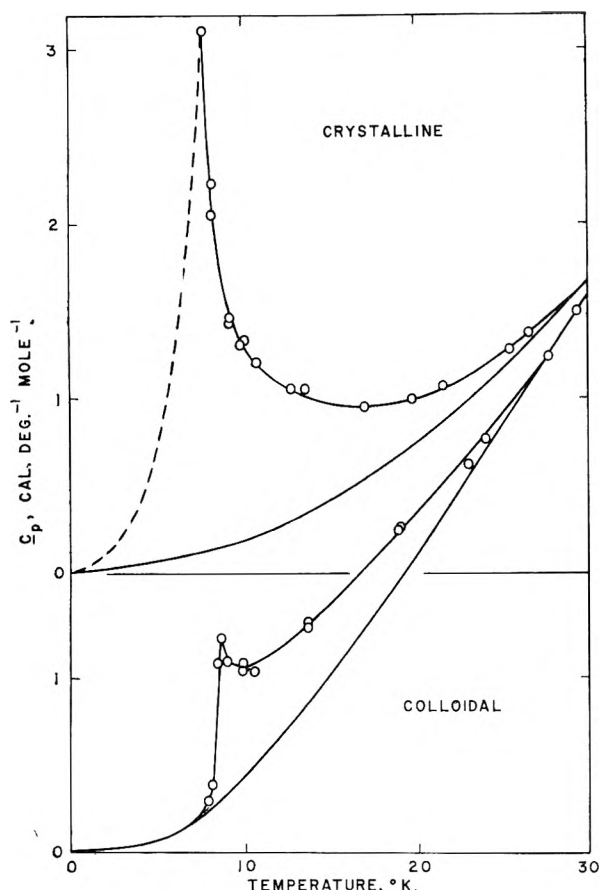


Fig. 1.—Low temperature heat capacity peaks for $\text{FePO}_4 \cdot 2\text{H}_2\text{O}$.

	Fe_2O_3	P_2O_5	H_2O
Before	42.77	38.06	19.17
After	42.85	38.12	19.03
Average	42.81	38.09	19.10
Theory	42.73	37.98	19.29

Anhydrous ferric chloride was prepared³ in a closed system. The product contained 34.46% Fe and 65.09% Cl (stoichiometric values, 34.43 and 65.57%). The final trap was transferred to a dry box for filling thin-walled, glass bulbs. The only chance for exposure of the hygroscopic salt to moist air was during the moment required to connect a bulb to a drying train preliminary to sealing of the neck.

Phosphoric acid ($\text{H}_3\text{PO}_4 \cdot 1.0055\text{H}_2\text{O}$ by chemical analysis) was prepared by dilution of the hemihydrate crystallized from reagent grade phosphoric acid.

Hydrochloric acid ($\text{HCl} \cdot 7.9935\text{H}_2\text{O}$ by chemical analysis) was prepared by dilution of the reagent acid.

The low temperature calorimeter^{4,5} and the solution calorimeter⁶ have been described.

Each measurement of a heat of solution was made in 850 ml. of solvent. Electrical calibrations were made over the same temperature interval immediately before and after each measurement.

Temperatures were measured to four decimal places for calculation of small differences, then were rounded to two places for tabulation. The defined calorie was taken as 4.1840 abs. j., the ice point as 273.16°K. The calorimeter resistance thermometers were calibrated by NBS to 10°K.;

(3) Betty Rapp Tarr in "Inorganic Syntheses," Vol. III, edited by L. F. Audrieth, McGraw-Hill Book Co., New York, N. Y., 1950, p. 191.

(4) E. P. Egan, Jr., Z. T. Wakefield and K. L. Elmore, *J. Am. Chem. Soc.*, **73**, 5579, 5581 (1951).

(5) E. P. Egan, Jr., and Z. T. Wakefield, *J. Phys. Chem.*, **64**, 1953 (1960).

(6) E. P. Egan, Jr., and B. B. Luff, *ibid.*, **65**, 523 (1961).

for measurements at lower temperatures, the NBS temperature-resistance tables at 1° intervals were extended to 7°K. by smooth extrapolation of first and second differences.

Low Temperature Heat Capacities. Strengite.—The calorimeter contained 52.616 g. (vacuum) or 0.28158 mole of $\text{FePO}_4 \cdot 2\text{H}_2\text{O}(c)$. The heat capacity measurements above 30°K. followed the conventional pattern for solids. At the lowest measured temperature, 7.75°K., a distinct peak appeared, and it was in evidence up to 30°K. Cooling of the full calorimeter below 7.5°K. was not possible in a reasonable time with all the refrigeration available from the helium cryostat. The temperature range from 7.5 to 30°K. was covered three times with reproducible results. The measured peak at 7.75°K. was 3.06 cal. mole⁻¹ deg.⁻¹. Neither the maximum height of the peak nor the span of its base in the direction of lower temperatures was established.

The peak is thought to represent a magnetic effect—possibly an antiferromagnetic transition.^{7,8} The observed heat capacities between 30 and 50°K. plotted against T^2 as a straight line passing through the origin. This straight line was used to establish the "normal" heat capacities. The side of the peak between 0 and 7.75°K. was filled in arbitrarily. The observed area under the peak, drawn as shown in Fig. 1, is 1.76 e.u.

The observed molal heat capacities are given in Table I. Smoothed heat capacities, entropies and enthalpies at integral temperatures are shown in Table II.

The entropy of $\text{FePO}_4 \cdot 2\text{H}_2\text{O}(c)$ at 298.16°K., excluding the area under the peak, is 39.17 e.u. The area under the peak, 1.76 e.u., makes a total entropy of 40.93 e.u. The accuracy is not estimated because of uncertainty about the area under the peak. The heat content ($H^0 - H_0^0$) at 298.16°K., on the assumption that the measured solid represents the ideal state, is 6592 cal. mole⁻¹, and the ΔH under the peak is 15 cal. mole⁻¹; total heat content, 6607 cal. mole⁻¹.

The calculations were made on an IBM 704 computer.⁵ The average deviation of the observed from the smoothed heat capacities was less than 0.1% above 30°K. At 7.75°K., the deviation was 20%, largely because of the rapidly changing slope in this region.

Colloidal $\text{FePO}_4 \cdot 2\text{H}_2\text{O}$.—The calorimeter contained 28.532 g. (vacuum) or 0.15269 mole of the colloidal material (assumed formula weight, 186.857 g.). The peak in the heat capacity was much less pronounced than for the strengite. The "normal" heat capacities were established by plotting the observed heat capacities between 29 and 50°K., divided by the temperature, against T^2 . The resulting curve was extrapolated smoothly to 0°K. The peak (Fig. 1) began at about 7°K., went through a maximum of 1.23 cal. deg.⁻¹ mole⁻¹ at 8.75°K., and joined the "normal" curve smoothly at 29°K. The observed molal heat capacities are given in Table III. Smoothed values of heat capacity, entropy and enthalpy at integral tem-

(7) E. F. Westrum, Jr., and F. Grønvald, *J. Am. Chem. Soc.*, **81**, 1777 (1959).

(8) E. F. Westrum, Jr., and C. Chou, *J. Chem. Phys.*, **30**, 761 (1959).

TABLE I

OBSERVED HEAT CAPACITY OF $\text{FePO}_4 \cdot 2\text{H}_2\text{O}(c)$, CAL. DEG.⁻¹ MOLE⁻¹

T , °K.	ΔT	C_D	T , °K.	ΔT	C_D
7.75	0.23	3.095	127.46	8.26	19.87
8.23	1.34	2.055	131.96	8.57	20.74
8.27	0.50	2.288	135.79	8.40	21.35
9.21	0.51	1.429	140.34	8.19	22.13
9.32	1.12	1.460	144.25	8.54	22.82
9.88	0.60	1.309	148.58	8.39	23.59
10.01	1.47	1.320	153.30	8.67	24.37
10.74	0.77	1.203	157.28	9.02	25.00
12.81	3.82	1.055	161.82	8.37	25.71
13.60	0.22	1.055	165.92	8.24	26.37
17.02	4.30	0.950	170.06	8.11	27.02
19.79	4.90	0.991	174.48	8.88	27.72
21.61	4.66	1.069	178.49	8.75	28.32
25.43	5.98	1.288	182.81	7.77	28.96
26.58	5.07	1.382	186.70	7.67	29.52
31.10	5.22	1.828	189.65	5.92	29.93
31.73	5.00	1.904	193.46	5.85	30.43
37.09	6.70	2.597	196.37	3.56	30.82
37.54	6.54	2.660	198.25	7.05	31.10
43.05	4.42	3.469	202.24	8.19	31.59
43.30	5.64	3.518	206.07	8.60	32.14
48.27	5.97	4.382	210.35	8.02	32.66
49.37	6.46	4.581	214.30	7.86	33.22
53.17	3.79	5.288	218.29	7.86	33.69
55.01	4.79	5.632	222.09	7.71	34.22
56.07	3.17	5.831	226.08	7.72	34.69
56.42	5.23	5.908	229.73	7.57	35.19
59.58	3.84	6.515	233.73	7.58	35.66
61.77	5.46	6.976	237.24	7.45	36.12
64.09	5.17	7.451	241.24	7.45	36.60
67.32	5.63	8.102	244.62	7.32	37.05
69.74	6.14	8.565	248.63	7.33	37.52
73.02	5.79	9.221	251.88	7.20	37.91
75.58	5.54	9.759	255.91	7.22	38.37
78.87	5.91	10.47	259.58	7.59	38.77
82.02	5.01	11.13	262.59	7.13	39.15
83.49	8.14	11.43	267.07	7.98	39.66
88.37	7.67	12.41	270.17	8.03	40.05
91.62	8.12	13.04	276.39	6.37	40.73
95.74	7.08	13.84	280.15	7.50	41.16
99.11	6.84	14.51	283.53	7.91	41.56
103.23	7.90	15.31	287.60	7.39	42.00
106.68	8.31	15.97	291.12	7.28	42.39
111.19	8.01	16.83	295.45	8.32	42.85
115.02	8.38	17.55	299.12	8.71	43.26
119.26	8.13	18.36	306.26	5.57	44.01
123.44	8.46	19.13	311.56	5.02	44.56

peratures are shown in Table IV. The average deviation of the observed from the smoothed heat capacities was 0.1% or less above 30°K.

The entropy at 298.16°K. of the colloidal $\text{FePO}_4 \cdot 2\text{H}_2\text{O}$, from the heat capacities represented by the "normal" curve, is 44.58 e.u. The area under the peak contributes 0.49 e.u., making a total entropy of 45.07 e.u. The heat content ($H^0 - H_0^0$) at 298.16°K., from the "normal" heat capacities, is 7115 cal. mole⁻¹; the area under the peak contributes 6 cal. mole⁻¹, making a total heat content of 7121 cal. mole⁻¹.

The difference in entropy of the crystalline and colloidal materials, as used, was 4.1 e.u. At 30°K., the measured heat capacity for the colloid was about

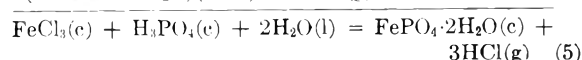
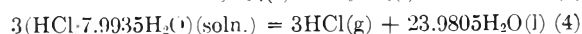
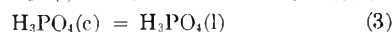
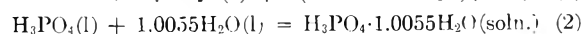
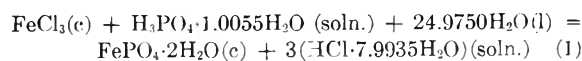
TABLE II

MOLAL THERMODYNAMIC FUNCTIONS OF $\text{FePO}_4 \cdot 2\text{H}_2\text{O}(c)$ (INCLUDING PEAK)

T , °K.	C_p , cal. deg. ⁻¹	S_p^0 , cal. deg. ⁻¹	$H^0 - H_0^0$, cal.
10	1.301	1.45	9.49
15	0.972	1.89	14.96
20	1.004	2.17	19.79
25	1.258	2.42	25.36
30	1.725	2.68	32.69
35	2.318	2.99	42.77
40	3.005	3.34	56.03
45	3.803	3.74	73.01
50	4.687	4.19	94.20
60	6.618	5.21	150.6
70	8.612	6.38	226.7
80	10.71	7.67	323.3
90	12.73	9.04	440.5
100	14.68	10.49	577.6
110	16.54	11.98	733.9
120	18.55	13.50	909.3
130	20.43	15.06	1104
140	22.02	16.63	1316
150	23.81	18.21	1543
160	25.44	19.80	1792
170	27.01	21.39	2054
180	28.54	22.98	2332
190	29.97	24.56	2625
200	31.32	26.13	2931
210	32.63	27.69	3251
220	33.93	29.24	3584
230	35.21	30.78	3930
240	36.46	32.30	4288
250	37.68	33.82	4659
260	38.85	35.32	5041
270	40.01	36.80	5436
280	41.15	38.28	5842
290	42.26	39.74	6259
300	43.35	41.19	6687
273.16	40.37	37.27	5563
298.16	43.15	40.93	6607

twice that for the crystals; at 200°K. and above, the difference was about 5%. The difference was approximately constant at 2 cal. deg.⁻¹ mole⁻¹ at all temperatures above 30°K.—the region above the peak. The percentage difference is greater than that reported for MgO .⁹ The higher entropy for the colloid probably includes a zero-point entropy which is difficult to estimate from the information available on iron phosphates.

Heats of Formation. Strengite.—The heat of formation of strengite was determined from appropriate measurements of heats of solution with 4.036 molal hydrochloric acid as the solvent. The measurements were based on the reaction scheme



The heats of solution for reactants and products

(9) W. F. Gianque, *J. Am. Chem. Soc.*, **71**, 3192 (1949).

TABLE III

OBSERVED HEAT CAPACITY OF COLLOIDAL $\text{FePO}_4 \cdot 2\text{H}_2\text{O}$, CAL. DEG.⁻¹ MOLE⁻¹

T , °K.	ΔT	C_p	T , °K.	ΔT	C_p
7.97	1.19	0.293	132.04	6.68	22.58
8.23	0.98	.392	136.00	8.23	23.19
8.52	.67	1.088	139.95	9.14	23.86
8.71	1.51	1.226	144.09	7.95	24.49
9.04	1.57	1.096	148.41	7.79	25.23
9.94	2.04	1.043	152.17	8.20	25.80
9.94	0.86	1.081	156.34	8.08	26.47
10.66	1.61	1.045	160.27	8.00	27.06
13.77	5.36	1.288	164.55	8.35	27.74
13.77	6.66	1.313	168.93	7.77	28.41
18.96	4.75	1.844	172.56	7.67	28.93
19.09	3.92	1.864	176.83	8.04	29.59
23.07	4.01	2.284	180.62	8.44	30.13
24.02	5.31	2.367	185.05	8.40	30.77
27.61	4.99	2.837	189.41	9.15	31.43
29.33	5.26	3.096	193.57	8.66	31.99
32.65	5.06	3.630	197.95	6.09	32.56
34.94	5.93	4.041	201.32	6.43	33.12
38.57	6.76	4.705	204.49	7.00	33.49
40.94	6.07	5.141	208.18	7.30	34.09
44.58	5.24	5.841	211.92	7.86	34.49
47.25	6.53	6.383	215.91	8.14	35.11
49.95	5.50	6.940	219.71	7.73	35.51
53.04	3.43	7.549	224.36	7.53	36.27
55.24	5.38	7.986	227.87	8.57	36.63
57.77	6.04	8.484	232.30	8.35	37.31
60.74	5.63	9.108	236.36	8.41	37.70
63.44	5.25	9.694	240.81	8.67	38.37
66.46	5.82	10.34	245.18	9.24	38.79
69.25	6.32	10.86	249.62	8.99	39.43
72.37	6.00	11.44	254.34	9.08	39.94
75.27	5.73	12.02	258.98	9.74	40.52
78.45	6.16	12.69	263.80	9.83	41.09
81.97	8.27	13.42	264.47	5.79	41.16
85.71	7.07	14.19	267.55	7.42	41.60
89.86	7.52	14.96	270.67	6.62	42.03
93.24	7.99	15.59	275.42	4.53	42.47
97.15	7.05	16.28	277.25	6.55	42.83
100.98	7.48	17.01	278.11	6.29	42.85
104.64	7.93	17.68	280.83	6.29	43.18
108.58	7.71	18.41	284.59	6.67	43.64
112.37	7.52	19.08	287.53	7.11	44.01
116.10	7.33	19.77	291.44	7.04	44.48
120.00	7.75	20.46	295.04	7.91	44.93
124.13	8.74	21.20	299.08	8.26	45.41
127.88	8.01	21.83	303.34	8.69	45.78

in equation 1 were measured directly. Heats of reaction for equations 2, 3 and 4 were known.

The heat of solution of H_2O , 2.6 to 8.4 g., in 850 ml. of HCl solution was -66.7 ± 1.9 cal. mole⁻¹ (av. of 5 determinations). The heat of solution of $\text{H}_3\text{PO}_4 \cdot 1.0055\text{H}_2\text{O}$, 3.1 to 3.8 g., in HCl solution to which had been added the stoichiometric quantity of water was -1713.8 ± 5.5 cal. mole⁻¹ H_3PO_4 (av. of 4 determinations). The heat of solution of FeCl_3 , 4.3 to 5.2 g., in HCl solution to which had been added the stoichiometric quantities of water and phosphoric acid was $-25,022 \pm 25$ cal. mole⁻¹ (av. of 4 determinations).

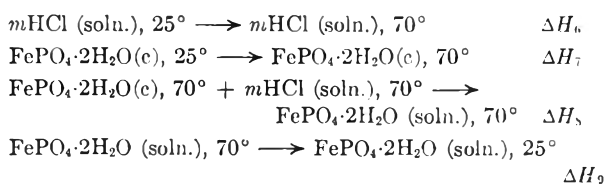
Because of the small supply of strengite, an amorphous ferric phosphate of approximately the composition of strengite was used in exploration

TABLE IV

MOIAL THERMODYNAMIC FUNCTIONS OF COLLOIDAL $\text{FePO}_4 \cdot 2\text{H}_2\text{O}$ (INCLUDING PEAK)

T , °K.	C_p , cal. deg. ⁻¹	S_p° , cal. deg. ⁻¹	$H^\circ - H_0^\circ$, cal.
10	1.066	0.326	2.558
15	1.425	.814	8.633
20	1.947	1.294	17.04
25	2.507	1.788	28.17
30	3.229	2.306	42.43
35	4.046	2.864	60.57
40	4.961	3.463	83.05
45	5.935	4.103	110.3
50	6.931	4.780	142.4
60	8.972	6.226	221.9
70	11.00	7.758	321.8
80	13.02	9.359	441.9
90	15.00	11.01	582.0
100	16.79	12.68	741.1
110	18.68	14.37	918.5
120	20.46	16.37	1114
130	22.18	17.78	1327
140	23.88	19.49	1558
150	25.46	21.19	1805
160	27.03	22.88	2067
170	28.56	24.57	2345
180	30.05	26.24	2638
190	31.48	27.90	2946
200	32.90	29.55	3268
210	34.28	31.19	3604
220	35.62	32.82	3953
230	36.96	34.43	4316
240	38.21	36.03	4692
250	39.42	37.62	5080
260	40.64	39.19	5481
270	41.88	40.74	5893
280	43.09	42.29	6318
290	44.31	43.82	6755
300	45.47	45.34	7204
273.16	42.27	41.23	6026
298.16	45.27	45.07	7121

of the dissolution in 4.036 *m* HCl at room temperature. When the time came to make the measurements on the crystals, however, less than 1 g. would dissolve in the HCl solution at room temperature; to get about 5 g. in solution for a satisfactory temperature change, the temperature had to be raised to 70°. The average of five determinations at 70° of the heat of solution of 4.7 to 5.0 g. of strengite was 7901 ± 40 cal. mole⁻¹. This value was corrected to 25° according to the scheme



Specific heat data for HCl solutions at the desired concentrations and temperatures were somewhat meager in the literature.^{10,11}

Specific heats were measured at 25, 40, 55 and

(10) G. Åkerlöf and J. W. Teare, *J. Am. Chem. Soc.*, **59**, 1855 (1937).

(11) "International Critical Tables," Vol. V, McGraw-Hill Book Co., New York, N. Y., p. 115.

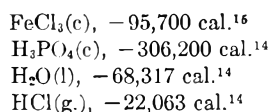
70° for a solution representing the average final solution resulting from dissolution of 4.7 to 5.0 g. of strengite in 822 g. of 4.036 *m* HCl solution. The measured specific heats in cal./g. solution between 25 and 70° were represented by the equation $c = 0.7863 + 0.0006988t - 0.00002893t^2$ with a precision of 0.0006 cal./g. These specific heats were used in the calculation of ΔH_6 and ΔH_9 on the assumption that straight HCl solution had the same specific heats.

The measured heat capacity of strengite, as extrapolated from 25 to 70°, was used in the calculation of ΔH_7 . The average corrected heat of solution for $\text{FePO}_4 \cdot 2\text{H}_2\text{O}(c)$ at 25°, represented by the summation ΔH_{6-9} , was 3127 cal. mole⁻¹.

The average heat of solution of $\text{HCl} \cdot 7.9935\text{H}_2\text{O}$, 12 to 17 g., in HCl solution representing the average composition of the solution after dissolution of the strengite was -271.7 ± 7.0 cal. mole⁻¹ HCl.

Substitution of the measured heats of solution in equation 1 yielded a heat of reaction of $-29,181$ cal. The heat of reaction for equation 2, as calculated from the heat of formation¹² of liquid H_3PO_4 and the heat of dilution⁶ of H_3PO_4 , is -1983 cal. mole⁻¹ H_3PO_4 . The heat of reaction for equation 3 is 3086 cal. mole⁻¹ H_3PO_4 .¹³ (This value represents the heat of fusion at the melting point, 315.51°K.; the absence of a correction to 298.16°K. introduces a much smaller error than the uncertainties in some of the heats of formation.) The heat of reaction for equation 4 is 48,948 cal.—a value derived from the heat of formation of $\text{HCl}(g)$ ¹⁴ ($-22,063$ cal. mole⁻¹) and the heat of formation of $\text{HCl} \cdot 7.9935\text{H}_2\text{O}$ as calculated by fitting a cubic equation to part of the heat of dilution data¹⁴ for HCl.

A summation yields for equation 5 a heat of reaction of 22,365 cal. Substitution into equation 5 of the molal heats of formation from the elements at 298.16°K.



yields -451.5 ± 1.0 kcal. mole⁻¹ as the heat of formation of $\text{FePO}_4 \cdot 2\text{H}_2\text{O}(c)$ from the elements at 25°—a value that may be compared with the value¹⁴ -440.8 kcal. mole⁻¹, which presumably was calculated from the heat of formation of $\text{FePO}_4(c)$ ¹⁶ and the dissociation pressure of $\text{FePO}_4 \cdot 2\text{H}_2\text{O}(c)$.¹⁷

Colloidal $\text{FePO}_4 \cdot 2\text{H}_2\text{O}$.—The heat of formation of colloidal $\text{FePO}_4 \cdot 2\text{H}_2\text{O}$ was determined also from pertinent heat of solution measurements in 4.036 *m* HCl as the solvent. The only additional measurements required were the heats of solution

(12) T. D. Farr, Tennessee Valley Authority, *Chem. Eng. Rept.*, No. 8 (1950).

(13) E. P. Egan, Jr., and Z. T. Wakefield, *J. Phys. Chem.*, **61**, 1500 (1957).

(14) National Bureau of Standards Circular 500, U. S. Govt. Printing Office, Washington, D. C., 1952.

(15) M. F. Koehler and J. P. Coughlin, *J. Phys. Chem.*, **63**, 605 (1959).

(16) W. A. Roth, A. Meichsner and H. Richter, *Arch. Eisenhuttentw.*, **8**, 239 (1934/5).

(17) K. Sano, *J. Chem. Soc. Japan*, **69**, 1066 (1938).

of the colloidal phosphate, which dissolved readily at 25°.

The colloidal preparation, in equilibrium with atmospheric moisture, was vacuum-desiccated in the thin-walled glass sample bulbs until the weight loss indicated removal of the water in excess of the stoichiometric $\text{FePO}_4 \cdot 2\text{H}_2\text{O}$. Dissolution of the product in the hydrochloric acid solvent gave -4256 , -4230 , -4336 and -4184 (av., -4252 ± 45) cal. mole⁻¹ $\text{FePO}_4 \cdot 2\text{H}_2\text{O}$ at 25°.

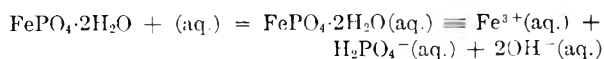
The relatively wide spread in the measured heats of solution indicated that dehydration of the samples through the narrow filling tube may not have been uniform—that the samples may have been mixtures of over- and under-dehydrated material. We have noted that the amorphous material may be dried to a constant composition approximating $\text{FePO}_4 \cdot 1.1\text{H}_2\text{O}$.

Dissolution of the colloidal $\text{FePO}_4 \cdot 2\text{H}_2\text{O}$ undoubtedly included a heat of wetting of a fine powder. Three additional samples were brought to constant weight over a saturated solution of K_2HPO_4 (92% relative humidity). (Soil samples equilibrated at relative humidities above 90% showed practically no heat effect when wetted by water.¹⁸) The weight corresponded to the composition $\text{FePO}_4 \cdot 6.38\text{H}_2\text{O}$. Dissolution of 4.1 to 5.8 g. of this material gave -158 , -135 and -129 (av., -141 ± 11) cal. mole⁻¹ $\text{FePO}_4 \cdot 2\text{H}_2\text{O}$ at 25°. The difference between -141 and -4252 leaves -4111 cal. mole⁻¹ for the heat of wetting.

The heat of reaction for equation 1 with colloidal $\text{FePO}_4 \cdot 2\text{H}_2\text{O}$ substituted for the crystalline strengite is $-21,802$ cal., which combines with the values for equations 2, 3 and 4 to yield a heat of reaction for summary equation 5 of 24,137 cal. mole⁻¹ $\text{FePO}_4 \cdot 2\text{H}_2\text{O}$. Substitution of the known heats of formation in equation 5, as was done for strengite, leads to a heat of formation of colloidal $\text{FePO}_4 \cdot 2\text{H}_2\text{O}$ of -444.1 kcal. mole⁻¹ at 25°, which includes the heat of wetting.

A measurement of the heat of solution of colloidal $\text{FePO}_4 \cdot 2\text{H}_2\text{O}$ in the HCl solvent at 70° would have provided a second thermodynamic path as a check on the 70-to-25° extrapolation of the solution data for strengite. The supply of the colloidal phosphate was exhausted, however, in futile attempts to measure its heat of solution at 70°. The fragile sample bulbs were ruptured prematurely, presumably by the water vapor pressure resulting from further dehydration of the solid at 70°.

Solubility Products.—Solubility product constants for strengite and amorphous $\text{FePO}_4 \cdot 2\text{H}_2\text{O}$ at 298.16°K. were calculated on the assumption that both ionize according to the scheme



$$\Delta F(\text{aq.} - c) = \Delta H(\text{aq.} - c) - T\Delta S(\text{aq.} - c)$$

$$\Delta F = -RT \ln K_{sp}$$

The heats of formation and entropies of the ions were taken from reference 14. Substitution of the corresponding heat of formation and entropy for each of the indicated species yielded for strengite a

(18) A. N. Puri and R. C. Hoan, *Soil Sci.*, **47**, 415 (1939).

value of $\log K_{sp} = -34.56$ and for amorphous $\text{FePO}_4 \cdot 2\text{H}_2\text{O}$ a value of $\log K_{sp} = -30.02$. These values may be compared with the value of -33.5 reported by Chang and Jackson¹⁹ as a median of

(19) S. C. Chang and M. L. Jackson, *Soil Sci. Soc. Am., Proc.*, **21**, 265 (1957).

values (-32 to -35) obtained in direct measurements on ferric phosphate dihydrate.

Acknowledgment.—W. E. Cate and M. E. Deming prepared the ferric phosphates. Inez Jenkins Murphy and J. W. Williard made the chemical analyses.

NOTES

X-RAY DIFFRACTION OBSERVATIONS OF THE Pd-H₂ SYSTEM THROUGH THE CRITICAL REGION¹

BY ARNULF J. MAELAND AND THOMAS R. P. GIBB, JR.

Department of Chemistry, Tufts University, Medford, Mass.

Received November 4, 1960

The occlusion of hydrogen by palladium has been studied extensively (*cf.* ref. 2). Two solid phases, both with a f.c.c. structure, have been identified by X-ray diffraction.³⁻⁶ The α -phase is formed by the absorption of small amounts of hydrogen, the maximum composition is about $\text{PdH}_{0.03}$ at room temperature, and it has a lattice parameter only slightly larger than that of pure palladium (3.889 Å.). As hydrogen is further absorbed, the α -phase becomes unstable and the lattice suddenly expands to about 4.018 Å. ($\text{PdH}_{0.6}$) to form the β -phase. Additional hydrogen uptake is accompanied by a gradual expansion of the α -phase lattice. X-Ray diffraction studies of the Pd-H₂ system have, for the most part, been performed at room temperature on samples prepared either electrolytically or at elevated temperatures. Either procedure involves some uncertainty as to what may occur in the specimen between the time it is charged and the time the X-ray exposure is made. Recognizing this problem, Owen and Jones⁷ and Owen and Williams⁸ charged the specimen from the gaseous phase and made the X-ray exposures while the specimen was maintained at a definite temperature and constant hydrogen pressure.

The present investigation is an extension of the investigation of Owen and Williams to higher temperatures and pressures. Six evolution isotherms, from 206 to 346°, have been traced from 33 atm. to zero pressure.

Experimental

Apparatus.—The high temperature assembly used has been described previously.⁹ The specimen temperature was

measured with an accuracy of $\pm 3^\circ$ or better. All diffraction patterns were obtained with the Straumanis type G.E. powder camera and with nickel-filtered copper radiation.

Materials.—The palladium metal was of 99.8% (specified) purity and was obtained from A. D. Mackay, Inc. Commercially available hydrogen was purified by passing it through a Deoxo purifier, then through a column of Drierite, and finally through a hot uranium getter.

Experimental Procedure.—Two methods of charging the specimen with hydrogen were employed. In method (1) the hydrogen was admitted at room temperature into the evacuated system to the desired pressure. The temperature was then raised to its proper value (the temperature of the isotherm under study). Both temperature and pressure were kept constant one hour or more before making the exposure. After the exposure, the specimen was allowed to cool to room temperature. Before the next exposure was made, the specimen was heated to the temperature of the isotherm, the pressure changed and maintained at this new value. In method (2) the hydrogen was admitted as in (1) and the temperature adjusted to the value of the isotherm. After each exposure the pressure was changed and maintained constant for one hour; this was done, however, *without cooling* the specimen to room temperature. Both methods gave similar results.

Lattice Parameter Calculation.—The lattice constants were obtained by the extrapolation method of Bradley and Jay,¹⁰ using the 422, 420, 311 and 400 lines. In some cases, the broad diffraction bands, caused by the beryllium sample holder, completely masked the 422 and 420 lines. In these instances care was taken not to alter the position of the specimen during a series of isothermal exposures at different pressures. It was assumed that the absorption and asymmetry errors similarly affected the reflections from a particular plane (331) at the various pressures, and the extrapolation method could therefore be used (assuming constant slope).

Results

Parameter values for the hydrogen charged specimen, held at 206, 258 and 346°, are listed in Table I, along with the various pressures employed. Figure 1 is a plot of the lattice parameter *versus* hydrogen gas pressure for each of the six isotherms traced. In the favorable cases, *i.e.*, when the 422, 420, 311 and 400 reflections were unmasked, the broadened lines of the β -phase yielded parameters with an accuracy of ± 0.004 Å., while the parameters of the α -phase are less accurate due to the very diffuse appearance of the lines. At the higher temperatures the lines appeared to be partially resolved and the accuracy for the 346° isotherm is ± 0.003 Å. In the few instances when the α -phase and the β -phase coexisted, the lines of the α -phase were so weak that measurement was impossible. The presence of the α -phase is indicated in the table, however, so that it may be known when the two phases coexisted.

(10) A. J. Bradley and A. A. Jay, *Proc. Phys. Soc. (London)*, **44**, 583 (1932).

(1) This research was supported by the U. S. Atomic Energy Commission.

(2) D. P. Smith, "Hydrogen in Metals," Univ. of Chicago Press, Chicago, 1948.

(3) L. W. McKeehan, *Phys. Rev.*, **21**, 334 (1923).

(4) J. O. Linde and G. Borelius, *Ann. Physik*, **84**, 747 (1927).

(5) F. Kruger and G. Gehm, *ibid.*, **16**, 174 (1933).

(6) G. Rosenhall, *ibid.*, **18**, 150 (1933).

(7) E. A. Owen and J. I. Jones, *Proc. Phys. Soc. (London)*, **49**, 587 (1937); **49**, 603 (1937).

(8) E. A. Owen and E. St. J. Williams, *ibid.*, **56**, 52 (1944).

(9) E. J. Goon, J. T. Mason and T. R. P. Gibb, Jr., *Rev. Sci. Instr.*, **28**, 342 (1957).

TABLE I

ISOTHERMAL VARIATION OF LATTICE PARAMETER OF PAL-LADIUM HYDRIDE WITH HYDROGEN GAS PRESSURE

206° Isotherm		258° Isotherm		346° Isotherm			
Pres- sure, atm.	Parameter, Å.	Pres- sure, atm.	Parameter, Å.	Pres- sure, atm.	Param- eter, Å.		
22.3	...	4.043	23.3	...	4.035	33.7	3.997
13.3	...	4.040	19.4	...	4.031	31.7	3.986
5.1	Faint	4.022	16.8	...	4.027	30.8	3.971
4.5	Faint	4.020	11.8	...	4.022	28.6	3.961
4.2	Faint	4.015	11.3	...	4.021	26.9	3.951
3.8	3.916	4.013	10.5	...	4.021	25.5	3.941
2.7	3.914	...	10.3	...	4.021	22.0	3.937
1.7	3.909	...	9.9	...	4.020	19.4	3.933
5.1	Faint	4.025	9.9	...	4.019	17.3	3.929
5.0	Faint	4.022	9.5	...	4.020	15.2	3.927
4.8	Faint	4.022	9.4	Faint	4.016	11.3	3.923
4.4	Faint	4.019	9.3	Faint	4.017	7.9	3.919
14.6	...	4.038	9.2	3.934	...	4.1	3.916
7.8	...	4.034	7.8	3.928
5.8	...	4.029	7.1	3.926
5.1	...	4.027	4.4	3.916
4.8	Faint	4.027	2.0	3.912
4.4	Faint	4.025
4.1	Faint	4.023
3.7	Faint	4.022
3.4	3.920
0.0	3.903

Discussion

From a consideration of Fig. 1 it is evident that, in crossing the two-phase region, the 206° isotherm exhibits some unusual features not observed for the other three isotherms studied below the critical solution temperature. Starting with the β -phase at high pressure, it is seen that the lattice parameter of the β -phase decreases gradually with decreasing hydrogen pressure. The rate of change in lattice parameter increases as the two-phase region is approached. When the pressure has been lowered to 5.1 atm., the α -phase makes its appearance. Both the α - and the β -phase continue to coexist as the pressure is further diminished, the α -phase continuously increasing in amount. When the pressure is decreased beyond 3.7 atm., the β -phase disappears entirely and the parameter of the α -phase then decreases linearly with decreasing pressure. It should be pointed out that the lattice constants of both the α - and the β -phase decrease in crossing the ($\alpha + \beta$) region when the pressure is lowered (*cf.* ref. 8). This is contrary to what is expected in a two-phase region of an alloy system in a state of thermal equilibrium. In such a case the parameters (concentrations) of the two phases remain constant within the ($\alpha + \beta$) field. It would seem, therefore, that the system is not in a state of equilibrium. Owen and Williams⁸ arrived at the same conclusion from their investigation of the 60, 80, 100 and 120° isotherms. The 206° isotherm is of the same form as those investigated by these authors.

Figure 1 shows that at 206° two different sets of parameters were obtained for the β -phase in the region where the α - and the β -phases coexist. The difference is believed to be due to the previous history of the sample. This is a form of hysteresis

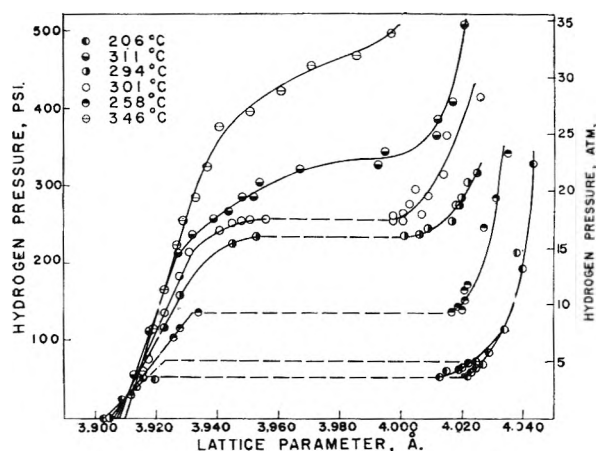


Fig. 1.—Hydrogen evolution isotherms.

which is also observed in dissociation pressure measurements. The runs are listed in Table I in the order in which they were made.

All diffraction patterns taken at 206° of the β -phase contained broadened lines in the back reflection region. Prolonged heat treatment at the temperature of the isotherm did not improve the definition of the lines. When the α -phase appeared on diminishing the pressure, its presence was first indicated by the appearance of low angle lines. On further decrease of pressure high angle lines were produced, but these were more diffuse than the β -phase lines. The definition of the lines improved somewhat with rising temperature. Thus, the patterns taken at 346° gave moderately sharp lines in the back reflection region. The crossing of isotherms in the lower left-hand region of Fig. 1 is, of course, due to the opposing effect of H-content and thermal expansion.

The parameters of the α - and β -phases where they coexist are plotted in Fig. 2 for each temperature investigated. The results from Owen's and William's investigation are also included. When the two phases coexist over a range of pressures at one particular temperature, the parameters recorded are those measured at the pressure when the β -phase disappears with decreasing pressure. From Fig. 2 it is evident that the parameter for the β -phase when it disappears is approximately the same at all temperatures from 60° to about 230°. The parameter of the α -phase, however, (measured when the β -phase disappears) increases gradually with temperature. From temperature-concentration measurements, it is known that the concentration of hydrogen in the β -phase, measured at the right-hand end of the plateaus, decreases with increasing temperature. Since the β -phase lattice contracts when hydrogen is removed from it, it appears that up to about 230° this contraction is exactly balanced by the thermal expansion of the lattice. For temperatures higher than about 230° the contraction due to decreasing hydrogen concentration in the β -phase lattice dominates. The data indicate a critical solution temperature of 308° in fair agreement with the value of 295.3° estimated by Gillespie and Galstaun.¹¹

(11) L. J. Gillespie and L. S. Galstaun, *J. Am. Chem. Soc.*, **58**, 2565 (1936).

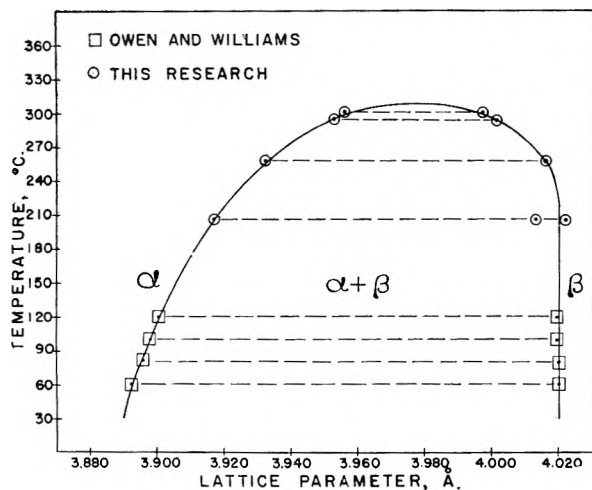


Fig. 2.

The reaction occurring in the plateau region can, if we neglect non-stoichiometry, be written



The heat of this reaction, $[\Delta H]$, then can be calculated from the integrated form of the van't Hoff equation. A logarithmic plot of P vs. $1/T$ using the evolution plateau pressures from Table II yields a straight line and a value of -9.5 kcal./

TABLE II

PLATEAU PRESSURES AT VARIOUS TEMPERATURES			
Temp., °C.	$P_{1/2}$, cm.	$1/T \times 10^3$	
80	8.0	2.83	8
100	14.0	2.68	8
120	30.0	2.54	8
206	279	2.09	This work
258	709	1.88	This work
294	1215	1.76	This work
301	1334	1.74	This work

mole for ΔH . Nace and Aston recently reported -9.6 kcal./mole from calorimetric absorption measurements at 30° .¹² Extrapolation of the data to the critical solution temperature (308°) gives a value of 19.7 atm. for the critical solution pressure in agreement with the value reported by Gillespie and Galstaun (ref. 11). Above the critical temperature a homogeneous transition occurs between the α - and the β -phase. Whether or not this transformation requires a complex rearrangement cannot be asserted, since the positions of the hydrogens in the α -phase have as yet not been established. Worsham,¹³ *et al.*, have shown by neutron diffraction studies that the hydrogen atoms occupy octahedral sites in the face-centered cubic palladium lattice to give a NaCl type structure. They were unable to determine the hydrogen positions in the α -phase because of the very small hydrogen concentration in this phase at room temperature. Extension of the neutron diffraction experiments to higher temperatures and pressures (higher hydrogen concentrations in the α -phase) should furnish results indicative of the hydrogen positions in this phase.

(12) D. M. Nace and J. G. Aston, *J. Am. Chem. Soc.*, **79**, 3619 (1952).

(13) J. E. Worsham, M. K. Wilkinson and C. G. Schull, *J. Phys. Chem. Solid*, **3**, 303 (1957).

The further absorption of hydrogen in the β -phase may be visualized as occupation by hydrogen of vacant lattice sites in the hydride lattice. If the sites are smaller than the hydrogen atoms or ions, the entry of the latter would result in a distension of the lattice such as is observed in Fig. 1. An alternate interpretation, which agrees with other properties of the system, *e.g.*, dissociation pressure, is that the vacancies attract one another more than do the hydrogens. The lattice energy of the defect structure is slightly higher and the lattice parameter slightly lower than that of the perfect structure. As hydrogens occupy vacant sites, therefore, the lattice expands.

In contrast to palladium hydride, no contraction of the uranium hydride lattice is observed at a fixed temperature when the hydrogen pressure is decreased.⁹ The difference in behavior between UH_3 and PdH_x may be due to the large difference in the number of hydrogen vacancies that the two hydride lattices can tolerate. In uranium hydride the attractive energy between vacancies (E_{vv}) is 6.6 kcal./mole and the corresponding value for palladium hydride is about 2.1 kcal./mole.¹⁴ Libowitz points out that the greater the value of E_{vv} , the smaller the concentration of vacancies required to break down the lattice.¹⁵ The increase in concentration of vacancies when hydrogen is removed from uranium hydride presumably is too small to produce an observable decrease in the lattice parameter before the hydride phase breaks down. In palladium hydride, however, the increased concentration of vacancies is much larger and the lattice parameter is observed to decrease (Fig. 1).

(14) G. G. Libowitz, NAA-SR-3452.

(15) G. G. Libowitz, *J. Chem. Phys.*, **27**, No. 2, 514 (1957).

ADSORPTION OF CONGO RED BY HYDROUS THORIUM OXIDE

BY RAMESHWAR PRASAD AND ARUN K. DEY

Chemical Laboratories, University of Allahabad, Allahabad (India)

Received December 16, 1960

In earlier communications¹⁻⁴ we have described the precipitation of samples of hydrous thorium oxide of different amphoterism and have studied the adsorption of inorganic ions by the different samples. The hydrous oxide precipitated with a deficient amount of alkali behaves as basic in character and thus adsorbs anions in preference to cations. On the other hand, the sample precipitated with an excess of alkali behaves as acidic in nature and has a preferential adsorptive capacity for cations. It is well known that insoluble metallic hydroxides have an affinity to adsorb dye molecules and are, therefore, used as mordants.

Extensive studies⁵⁻⁸ on the adsorption of dye-

(1) R. Prasad and A. K. Dey, *Proc. Natl. Acad. Sci. India*, **27A**, 350 (1959).

(2) R. Prasad and A. K. Dey, *Vijāna Pari. Anu. Patrika*, **3**, 155 (1960).

(3) R. Prasad and A. K. Dey, *J. Ind. Chem. Soc.*, **37**, 747 (1960).

(4) R. Prasad and A. K. Dey, *J. Sci. Ind. Res., India* (communicated).

(5) A. K. Dey and S. Ghosh, *Proc. Natl. Acad. Sci. India*, **15A**, 143 (1946).

stuffs by precipitated hydrous oxides have been carried out in these laboratories. Tewari, Dey and Ghosh⁹ from a consideration of adsorption of dyestuffs by hydrous oxides attempted to elucidate the mechanism of aging of metal hydroxides.

This paper records our observations on the association of the acid dye, congo red, with samples of hydrous thorium oxide obtained by different methods.

Experimental

Materials.—Aqueous solutions of thorium chloride (BDH LR), sodium hydroxide (BDH AnalaR) and congo red were prepared and standardized.

Apparatus.—The absorbance of the dye was studied with a Unicam SP 500 spectrophotometer operated on 220 volts/50 cycles single phase, a.c. mains with the help of a Doran stabilized mains unit. The measuring cells were glass of 10 mm. thickness, supplied with the instrument. The experiments were conducted in an air-conditioned room maintaining 20°.

Colorimetric measurements were done by using Klett-Summerson's photoelectric colorimeter operated on the same mains using color filter no. 50 (transmission 470 to 530 m μ) chosen after ascertaining the region of maximum absorption of the dye.

pH measurements were done with an L. and N. pH indicator operated on the same mains with a glass-calomel electrode system.

Color of the Dye at Different pH.—It was found that the absorbance of the dye at 500 m μ remains constant at pH 5.8 to 8.9 and all determinations were done at pH 6.8.

Validity of Beer's Law.—Beer's law was valid in the range 4 to 12 p.p.m. of the dye and hence colorimetric estimations were done in this range of concentration.

Preparation of Samples of the Hydrous Oxide.—Samples A, B, C and D of the hydrous oxide were obtained by adding calculated amounts of a standard solution of sodium hydroxide to 500 ml. of 0.25 M thorium chloride solution at 25°

- A precipitated with 10% deficient sodium hydroxide
- B precipitated with equivalent sodium hydroxide
- C precipitated with 5% excess sodium hydroxide
- D precipitated with 10% excess sodium hydroxide

The samples were thoroughly washed with water till the washings were free from thorium (where present), hydroxyl and chlorine ions. The precipitates were suspended in water, vigorously shaken in a Microid Flask Shaker and the final volumes were raised by dilution with water to 10 g. of ThO₂ per liter.

Adsorption Experiments.—To 1 ml. of the suspension (0.01 g.), varying amounts of the dye were added and the volumes were raised to 100 ml. The systems were allowed to equilibrate for 24 hours. In the supernatant liquid, the concentration of congo red was estimated by the colorimeter.

Discussion

The results show that the adsorptive capacities of the samples decrease with rise in temperature. Among the four samples A, B, C and D, the basic character of the hydrous oxide diminishes in the order above mentioned, on account of the increasing amounts of alkali used for their precipitation. Hence, it is expected that an acid should be adsorbed most by sample A and least by sample D. The order of adsorption as noted in this paper is A > B > D > C, showing thereby that C has the least adsorptive capacity.

It is well known that amphoteric bodies depend on environmental conditions to display their acidic or basic characters. It may be concluded that in

this case the acidic and the basic characters of the hydrous oxide more nearly neutralize each other in sample C than in others and its adsorptive power is least both for acidic and basic dyes. It will be of interest to note that Dey and Ghosh³ studied the amphoteric behavior of hydrous stannic oxide and found that at the isoelectric point, the hydrous oxide showed the minimum adsorption for both acidic and basic dyes. In this case sample C appears to approach an isoelectric sample more nearly than others, and has the least capacity to adsorb congo red which is further confirmed by adsorption of basic dyes also.¹⁰ The other samples, A, B and D show the adsorption in the same order depending on their diminishing basic character and the observations are explainable on the amphotericism of the hydrous oxide.

It is also to be mentioned that congo red is adsorbed considerably by all the samples of hydrous thorium oxide as has been seen from the high values of x/m in the experiments. The solutions at equilibrium become very faint in color and the adsorbents assume an orange color due to the association of the dye.

Acknowledgment.—The authors express their gratitude to the Council of Scientific and Industrial Research, India, for supporting the work and for granting an assistantship to R.P.

(10) R. Prasad and A. K. Dey (unpublished work).

ELECTRIC MOMENTS OF SOME ADDITION COMPOUNDS OF ZINC CHLORIDE WITH ORGANIC BASES

BY M. JUDITH SCHMELZ,¹ M. ANN GERTRUDE HILL¹ AND COLUMBA CURRAN

Department of Chemistry, University of Notre Dame, Notre Dame, Indiana

Received December 29, 1960

The determination of electric dipole moments of coordination compounds of zinc chloride with organic bases has been hindered by the low solubility of most of these complexes in non-polar solvents. Dioxane was observed to have adequate solvent properties for the complexes of zinc chloride with pyridines and the picolines for dielectric constant measurements, and benzene is a suitable solvent for dichlorobis-(triethylphosphine)-zinc. The moments of these addition compounds along with that of boron trichloride-pyridine have been determined for comparison with values previously obtained for other metal complexes. Dielectric constant measurements also were made on dioxane solutions of the complexes of zinc chloride with aniline and the toluidines but these are not reported, as spectroscopic measurements reveal that these complexes are partially dissociated in this solvent.

Experimental

The pyridine and picoline complexes were prepared by the addition of freshly distilled ligand to aqueous solutions of zinc chloride in mole ratios of 2:1. The addition compounds were recrystallized from ethanol and dried over sulfuric acid.

(1) Sister Mary Judith Schmelz, R.S.M., and Sister M. Ann Gertrude Hill, O.S.U. Supported under AEC Contract AT(11-1)-38, Radiation Laboratory of the University of Notre Dame.

(6) S. N. Tewari, *Kolloid-Z.*, **128**, 19 (1952).

(7) R. B. Hajela and S. Ghosh, *Proc. Natl. Acad. Sci. India*, **28A**, 59, 118, 130 (1959).

(8) S. N. Tewari and S. Ghosh, *ibid.*, **21A**, 29, 41 (1952).

(9) S. N. Tewari, A. K. Dey and S. Ghosh, *Z. anorg. Chem.*, **271**, 150 (1953).

TABLE I
 POLARIZATIONS AND ELECTRIC MOMENTS AT 25°

Compound	% Cl		Solvent	100wf ₂	ΔD/wf ₂	Δd/wf ₂	P _∞	P _D	μ _i Debyes
	Calcd.	Found							
ZnCl ₂ (C ₆ H ₅ N) ₂	24.08	23.90	D	0.17-0.56	36.2	0.32	1807	74	9.20 ± 0.04
ZnCl ₂ (α-CH ₃ C ₅ H ₄ N) ₂	21.99	21.45	D	.18-.43	30.7	.24	1695	85	8.86 ± .04
ZnCl ₂ (β-CH ₃ C ₅ H ₄ N) ₂	21.99	21.90	D	.18-.86	35.5	.26	1948	85	9.54 ± .04
ZnCl ₂ (γ-CH ₃ C ₅ H ₄ N) ₂			B	.50-.79	31.0	.35	1943	85	9.53 ± .04
ZnCl ₂ (γ-CH ₃ C ₅ H ₄ N) ₂	21.99	21.70	D	.35-.86	37.0	.22	2030	85	9.75 ± .1
ZnCl ₂ (Et ₃ P) ₂	19.03	19.17	B	.33-1.06	17.1 ^a	.32	1285	110	7.57 ± .1
BCl ₃ (C ₆ H ₅ N)	54.18	53.58	B	.30-0.93	31.5 ^a	.35	1200	51	7.50 ± .04

^a Extrapolated values (wf₂ = 0).

Boron trichloride-pyridine was prepared by mixing carbon tetrachloride solutions of pyridine and boron trichloride. The product was dissolved in benzene and reprecipitated by the addition of petroleum ether. Triethylphosphine was prepared by the reaction of ethylmagnesium bromide with phosphorus trichloride; after hydrolysis the product was distilled in an atmosphere of nitrogen and added to an aqueous solution of zinc chloride to yield dichlorobis-(triethylphosphine)-zinc. The precipitate was washed with ether and dried over sulfuric acid. C.P. benzene was refluxed over phosphoric anhydride and distilled. Dioxane was purified by the method described by Fieser.² The product was distilled from sodium.

Dielectric constant and density measurements and calculations of electric moments were carried out as in previous work.³ With the exceptions noted, the dielectric constant/weight fraction ratios listed in Table I are average values. The refractions were taken as the sum of the values for the base and the metal chloride. A value of 19 ml. was estimated for zinc chloride from the refractions listed for magnesium, cadmium and mercury chlorides in Landolt-Börnstein.⁴ The distortion polarizations were taken as 1.10 MRD.

Discussion

The agreement between the values obtained for the moment of dichlorobis-(β-picoline)-zinc in benzene, 9.53, and in dioxane, 9.54, indicates that dioxane exerts no specific solvent effect on the moments of these addition compounds. The moments of the zinc chloride complexes are in the expected order: γ-picoline > β-picoline > pyridine > α-picoline. The difference between the moments obtained for the α-picoline and pyridine complexes, 0.55 Debye, is equal to the calculated difference for these tetrahedral molecules. It is not possible to make quantitative calculations of the moments of the α- and β-picoline complexes as these values depend on the favored (unknown) relative orientations of the pyridine rings, which are affected by the steric requirements of the methyl groups.

The moment observed for dichlorobis-(triethylphosphine)-zinc, 7.57, compares to the value 10.7 reported by Jensen⁵ for dichlorobis-(triethylphosphine)-platinum(II). Taking into account the configurations of these complexes, tetrahedral for zinc and *cis* square planar for platinum, the sum of the R₃P-Zn and Zn-Cl moments is 6.58, compared to 7.57 for the sum of the R₃P-Pt and Pt-Cl vectors. This difference, 1.0 Debye, is not surprising in the light of the greater stability of the platinum complexes compared to those of zinc. It is expected that the P-Pt σ-bond

(2) L. Fieser, "Experiments in Organic Chemistry," D. C. Heath and Co., Boston, Mass., 1941, p. 369.

(3) C. Curran, P. A. McCusker and H. S. Makowski, *J. Am. Chem. Soc.*, **79**, 5188 (1957).

(4) Landolt-Börnstein, "Physikalisch-Chemische Tabellen," Edwards Bros., Ann Arbor, Mich., 1943, vol. 2.

(5) K. A. Jensen, *Z. anorg. allgem. Chem.*, **229**, 225 (1936).

will have a greater covalent character and therefore a greater polarity than the P-Zn bond. The difference suggests that there is no appreciably greater double bond character (which decreases bond polarity) in the phosphorus-to-platinum than in the phosphorus-to-zinc bond.

The moments obtained reveal an anomaly in the relative polarities of zinc complexes and boron complexes. The moments of boron trichloride-trimethylamine and boron trichloride-triethylphosphine are 6.23 and 7.03, respectively.⁶ These values indicate that the P-B bond is more polar than the N-B bond. It is not possible to determine the moment of a dichlorobis-(trialkylamine)-zinc complex because of solubility limitations. The moment of boron trichloride-pyridine is 1.27 Debyes larger than that of boron trichloride-trimethylamine. If this difference (multiplied by 1.15 for the tetrahedral bis complex) holds also for the addition compounds of zinc chloride, the moment of dichlorobis-(triethylamine)-zinc is expected to be 7.8, compared to the observed moment of dichlorobis-(triethylphosphine)-zinc, 7.57. This indicates that the P-Zn bond is slightly less polar than the N-Zn bond. Partial P=Zn double bond character could account for this, but zinc is not expected to use electrons from its completed third shell in forming π-bonds.

(6) G. M. Phillips, J. S. Hunter and L. E. Sutton, *J. Chem. Soc.*, 146 (1945).

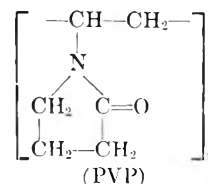
THE EFFECT OF UREA ON THE CONFIGURATION OF POLYVINYLPIRROLIDONE

BY IRVING M. KLOTZ AND JOEL W. RUSSELL

Department of Chemistry, Northwestern University, Evanston, Illinois

Received January 6, 1961

The synthetic polymer polyvinylpyrrolidone (PVP) mimics protein behavior in a number of



respects. For example it forms complexes with many types of small molecule,¹⁻³ although with

(1) H. Bennhold and R. Schubert, *Z. ges. Exptl. Med.*, **113**, 722 (1943).

(2) C. Wunderly, *Arztl. Forsch.*, **4**, I, 29 (1950).

(3) W. Scholtan, *Makromol. Chem.*, **11**, 131 (1953).

only about one-third the affinity shown by serum albumin.⁴ Likewise it shifts the pK_a of a covalently-linked acid-base substituent in the same direction as is observed with corresponding protein conjugates.⁵ Furthermore, with the PVP conjugate, as with those of proteins, the addition of urea to the aqueous solution decreases markedly the shift in acidity constant.⁵

Urea is a well-known protein denaturant and produces marked changes in macromolecular configuration of proteins. The intrinsic viscosity of ovalbumin (molecular weight 44,000) for example, changes from 0.043 (g./100 cc.)⁻¹ for the native protein⁶ to 0.24 for the protein in 7.5 *M* urea.⁷ It seemed of interest, therefore, to examine the effect of urea on the viscosity and hence configuration, of polyvinylpyrrolidone.

Experimental

Viscosities were measured in a standard Ostwald viscometer whose water outflow time was 110 sec. Before each measurement the viscometer was cleaned with warm chromic acid solution, rinsed thoroughly with distilled water and dried with a stream of dry air. It was mounted carefully with the same clamp in the same position in a water-bath at 25° and its vertical alignment was checked with a plumb line. Outflow times for a given solution checked within ± 0.03 sec. or better.

Stock solutions were prepared containing 4% polyvinylpyrrolidone in water and in 8 *M* urea, respectively. These were diluted with corresponding solvent to prepare more dilute solutions of the polymer. All solutions were filtered before use. Five-ml. samples were added carefully at the bottom of the bulb of the viscometer to prevent the formation of bubbles. Densities of the solutions were measured with a Westphal balance.

Measured viscosities, η , were converted to reduced viscosities η_{red} , according to the equation

$$\eta_{red} = \frac{(\eta/\eta_0) - 1}{c}$$

where η_0 is the viscosity of the solvent free of polymer and c is the concentration of polymer in g. per 100 ml. of solution. Reduced viscosities for polyvinylpyrrolidone in water and in urea are plotted in Fig. 1.

Discussion

It is of interest to note first that the intrinsic viscosity $[\eta]$, where

$$[\eta] = \lim_{c \rightarrow 0} (\eta_{red})$$

for polyvinylpyrrolidone in water is 0.225 (g./100 ml.)⁻¹ which is of the same order of magnitude as that of denatured ovalbumin.⁷ The average molecular weight of the sample of polyvinylpyrrolidone used is 40,000,⁸ compared to 44,000 for ovalbumin. Hence even in water, polyvinylpyrrolidone is in a relatively loose configuration.

It is not surprising therefore that urea has very little effect on the intrinsic viscosity of polyvinylpyrrolidone, the value dropping slightly, to 0.215. Such a drop is small and probably within experimental error, but it is of interest to note that the change with urea is in the direction to be expected

(4) I. M. Klotz and J. Ayers, unpublished experiments.

(5) I. M. Klotz and V. H. Stryker, *J. Am. Chem. Soc.*, **82**, 5169 (1960).

(6) A. Polson, *Kolloid Z.*, **88**, 51 (1939).

(7) H. K. Frensdorff, M. T. Watson and W. Kauzmann, *J. Am. Chem. Soc.*, **75**, 5157 (1953).

(8) "PVP, Polyvinylpyrrolidone," Bulletin P-100, General Aniline and Film Corp., New York, N. Y., 1951.

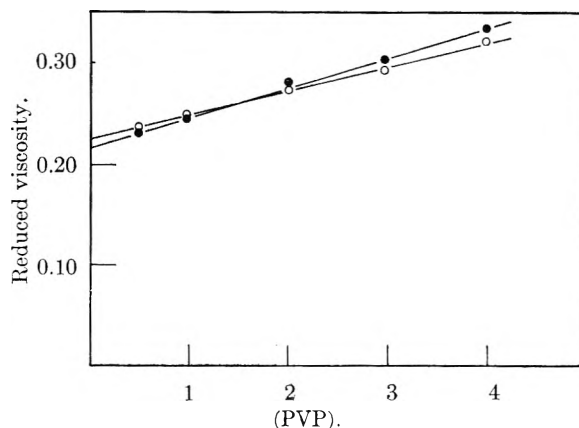


Fig. 1.—Reduced viscosity of polyvinylpyrrolidone as a function of concentration in g. per 100 ml.: ○, in water; ●, in 8 *M* urea in water.

for a decrease in the degree of hydration of the macromolecule.

In regard to comparisons of the behavior of proteins with that of polyvinylpyrrolidone, these viscosity experiments lead to two interesting conclusions. First it is evident that interactions such as binding of ions or masking of the reactions of conjugated groups can occur with a macromolecule having a relatively random configuration such as is found for PVP. Secondly urea may perturb these interactions of PVP even though it does not produce a major change in macromolecular configuration. These observations are directly relevant to the molecular interpretation of corresponding interactions of protein macromolecules.⁵

THE DISSOCIATION PRESSURE OF GALLIUM ARSENIDE

By V. J. LYONS AND V. J. SILVESTRI

IBM Research Laboratory, Poughkeepsie, New York

Received January 7, 1961

Gallium arsenide thermally dissociates to the constituent elements and two previous investigations of the reaction equilibria have been reported. The solid-liquid-vapor equilibria were studied by van den Boomgaard and Schol¹ over the range 781 to 1237°. Goldfinger and Drowart² have reported a mass spectrometric study of the vapor species resulting from thermal dissociation of the compound in the range 758 to 863°. The purpose of this work was to re-examine the reaction in a temperature range below the compound melting point because of the inconsistency in the reported data.

Since the vapor pressure of arsenic is several orders of magnitude greater than that of gallium the dissociation pressure of GaAs is essentially equal to the arsenic pressure in equilibrium with the compound. The method used to measure the equilibrium arsenic pressure was the visual observation of the arsenic dew-point in a sealed tube containing solid GaAs. The applicability of the method to decomposing solids has been demonstrated, and the more general details of the experimental procedures have been described

(1) J. van den Boomgaard and K. Schol, *Phillips Res. Rep.*, **12**, 127 (1957).

(2) P. Goldfinger and J. von Drowart, *J. Chem. Phys.*, **55**, 721 (1958).

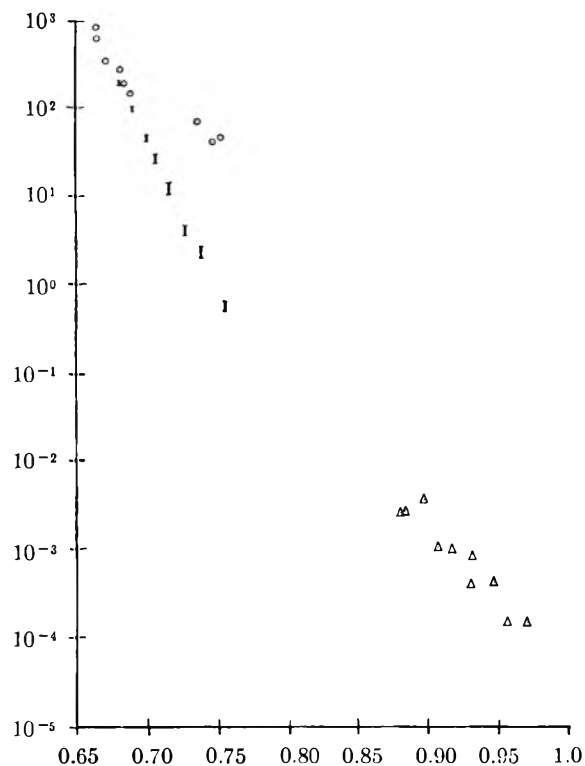


Fig. 1.—Comparison of three determinations of the dissociation pressure of GaAs: (1) circles are data of Boomgaard and Schol; (2) triangles are data of Goldfinger and Drowart; (3) vertical lines represent this work.

elsewhere.^{3,4,5} For this experiment, ten grams of high purity monocrystalline GaAs was broken into small pieces and sealed in an evacuated quartz tube 34 cm. long and 20 mm. in diameter. The end of the tube containing the compound was inserted into a 6 cm. well in a cylindrical stainless steel block 8.5 cm. long. A thermocouple well drilled through the opposite end of the block permitted a thermocouple to be positioned adjacent to the reaction tube. This assembly was placed in the center of a 32 cm. long Hoskins furnace. The opposite end of the tube was enclosed by a separately controlled furnace fabricated by winding nichrome ribbon on a quartz tube. This furnace extended into the Hoskins furnace to ensure against cold spots occurring at the junction of the two heating elements. The entire construction provided (1) isothermal regions over the GaAs sample and the thermocouple well at the opposite end of the tube, (2) independent temperature control of the two regions, (3) a monotonically increasing temperature gradient in the region between the thermocouple well (dew-point temperature) and the GaAs sample, and (4) visibility of the thermocouple well. The temperature of the Hoskins furnace was maintained to within $\pm 3^\circ$ by a proportioning Wheelco controller while a Variac operating from a constant voltage transformer controlled the dew point furnace. Temperatures were measured with Pt-Pt, 10% Rh calibrated thermocouples and the potentials were read on a Leeds & Northrup Potentiometer, Model 8662.

Each experimental point was measured in the following manner. The decomposition furnace was heated to a temperature in the range 1051 to 1196°, while the dew-point furnace was heated to approximately 650°. Equilibration times of 15–71 hours were allowed. In practice, the area around the thermocouple well was heated to temperatures slightly higher than 650°, through the use of a radiation shield, because of the gradual condensation of a GaAs film at the color end of the tube. Identification of this film was made by X-ray diffraction powder analysis. By using the shield, the GaAs film was caused to condense on the tube wall between the decomposition furnace and the thermo-

couple well; thus the film did not interfere with the dew-point observations. After equilibration, the radiation shield was removed and the temperature of the cooler furnace was lowered. Dew-points then were observed in the manner described in earlier papers. The dissociation pressure of the compound thus was measured over the range 1051 to 1196°. The data, which are presented in Table I and plotted in Fig. 1, can be fitted to the equation

$$\log P_{\text{mm}} = -\frac{34,500}{T^\circ\text{K.}} + 25.8 \quad (1)$$

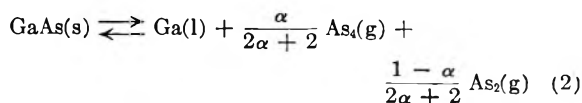
Calculations based on the experimental conditions showed that 0.05 to 1.0% of the sample had dissociated during the measurements. Evidence of a liquid phase on parts of the sample was observed after removing the GaAs from the reaction tube. These data show that the pressures were measured along the three-phase line and therefore describe, in part, the boundary of compound stability.

TABLE I

GaAs <i>T</i> , °C.	Total pressure, ^a mm.	<i>P</i> _{As₄} ^b	<i>P</i> _{As₂} ^b
1051	0.5–0.6	0.03	0.52
1079	2.0–2.6	0.24	2.06
1100	3.5–4.2	0.44	3.41
1124	10–13	2.36	9.1
1142	22–28	7.6	17.5
1158	43–47	15.1	29.9
1176	88–92	36.4	53.3
1196	185–195	92.4	97.6

^a From dew-points. ^b Calculated from average total pressure.

The measured arsenic pressures were considered equivalent to the total arsenic pressure over solid GaAs for the following reason. The reaction tube was heated by a two-zone furnace so that approximately one-third of the tube was heated to the decomposition temperature and one-third was heated to the dew-point temperature. Hence, a significant length of the tube (approximately 10 cm.) was maintained at the dew-point temperature. The tabulated data of Stull and Sinke⁶ show that the species As₄ would predominate in the dew-point range of temperatures while two species, As₄ and As₂, would be measurably present in the decomposition temperature range. From considerations of the temperature distribution in the reaction tube and the mean free path of the arsenic molecules it was concluded that, at equilibrium, the As₂ molecules would completely recombine to give only As₄ molecules at the dew-point temperatures. Thus, the measured pressures and the values of the equilibrium constant for the reaction $\text{As}_4 \rightleftharpoons 2\text{As}_2$ were used to calculate the pressure of each species in equilibrium with solid GaAs. The over-all reaction equilibrium at each experimental point may be represented by the chemical equation



where α is the As₄ fraction of the vapor. The pressures of As₄ and As₂ calculated from each experimental point are given in Table I.

A comparison of this work and that of van den Boomgaard and Schol shows good agreement at the higher temperatures. It is thought that the

(3) K. Weiser, *J. Phys. Chem.*, **61**, 513 (1957).

(4) V. J. Lyons, *J. Phys. Chem.*, **63**, 1142 (1959).

(5) V. J. Lyons and V. J. Silvestri, *ibid.*, **64**, 266 (1960).

(6) D. R. Stull and G. C. Sinke, "Thermodynamic Properties of the Elements," *Advances in Chemistry Series*, No. 8, 1956.

experimental difficulties encountered in attempting to extend the triple-point method to lower pressures and more dilute solutions (*i.e.*, the slow establishment of the equilibrium) led to their observation of higher pressure values at the lower temperatures. Extrapolations of the Goldfinger-Drowart data and this work show reasonably good agreement when considering the range of pressures measured.

The authors express their thanks to Dr. K. Weiser and Dr. G. A. Silvey for valuable discussions.

THE SORET EFFECT AS A SOURCE OF ERROR IN CONDUCTANCE MEASUREMENTS

By R. H. STOKES

Department of Physical and Inorganic Chemistry, University of New England, Armidale, N.S.W., Australia

Received January 10, 1961

Agar,¹ in a paper on the rate of attainment of Soret equilibrium, recently predicted that "there will be small transient changes of composition in a conductivity cell when it is transferred from the ambient temperature into a thermostat." The reality and considerable importance of this effect are demonstrated by the findings now reported.

Two conductance-cells were used. Cell A consisted of two electrode-bulbs about 2.5 cm. in diameter, joined by 6 cm. of tubing of 6 mm. internal diameter; its cell constant was 20.71 cm.⁻¹. Cell B, of constant 4.595 cm.⁻¹ was of similar construction except that the central section was only about 1 cm. long. Filling tubes were attached to both electrode-bulbs, and the leads to the electrodes were carried through glass side-arms well separated from the filling-tubes and each other. After the detection of the effect reported below, the filling-tubes were fitted with mixing-bulbs to facilitate the mixing of the cell contents without removal of the cell from the thermostat. The electrodes were lightly coated with platinum-black; frequency-dependence in the range 1-4 kc./sec. was less than 0.002% with cell A and 0.008% with cell B. This small residual dependence was extrapolated out by an R vs. f plot. The lead resistances were measured by filling the cells with mercury, and calibrations were made with the Jones and Bradshaw 0.1 demal potassium chloride standards at 25°. The cells were filled with 0.01 *M* hydrochloric acid and heated in a thermostat to 50°; at this temperature their contents were thoroughly mixed. They were then transferred quickly to a thermostat held at 25 ± 0.001°. Here the resistances were measured over a period of several hours by a calibrated Jones bridge. It was established by a previous study that the contents of the cell must be within 0.001° of the thermostat temperature after 20 minutes; hence any changes occurring after this time cannot be ascribed to temperature changes. Results such as those shown in Table I were consistently observed.

TABLE I

APPARENT SPECIFIC CONDUCTANCES IN OHM⁻¹ CM.⁻¹ AT 25° AT VARIOUS TIMES FOLLOWING PREVIOUS HEATING OF CELLS TO 50°

Time, hr.	Cell A	% low	Cell B	% low
0.58	0.0043969	0.304	0.0044067	0.077
1.58	.0043974	.295	.0044075	.059
5.42	.0043991	.254	.0044082	.043
After mixing at 25°	.0044103	.000	.0044101	.000

The results from the two cells at all times differed far more than could be ascribed to measuring or calibration errors. *But when the cell contents*

(1) J. N. Agar, *Trans. Faraday Soc.*, **56**, 776 (1960).

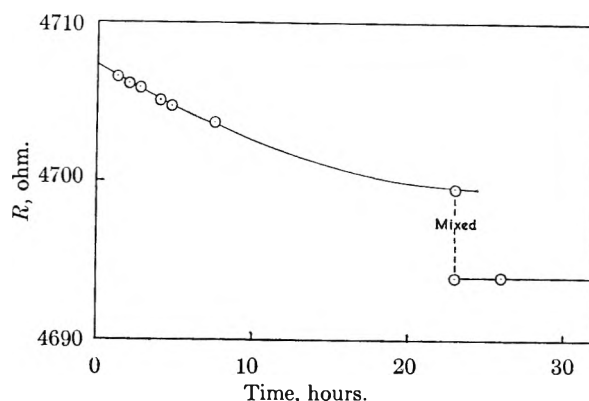


Fig. 1.—Change of resistance with time in cell A containing approximately 0.01 *N* hydrochloric acid. Cell thermostated at 50°, then transferred to 25° thermostat at zero time. Temperature equilibrium is known to be attained before the time of the first point plotted.

were thoroughly mixed at 25°, agreement was immediately established, and no further drift in readings then occurred for several days. Furthermore, the results after the mixing were in agreement with Shedlovsky's values² within 0.01%.

Exactly the opposite effect was observed on moving the cells from a 25 to 50° thermostat: the results again differed considerably, but this time both cells showed *higher* conductances than the final true values attained after mixing of the cell contents. In another experiment, cell A was heated to 50° in a water-bath, and its contents were mixed at this temperature. The bath and cell were then allowed to cool *slowly* to 25°, over a period of about 1.5 hours. The cell was then transferred to the 25° oil-thermostat for measurement. On reaching temperature equilibrium, the resistance was 4696.4 ohm, and on mixing the cell contents this value changed only to 4696.1 ohm, *i.e.*, 0.007%. The effect, then, evidently arises from *sudden* changes in cell temperature, and is therefore not to be ascribed to differences in adsorption of hydrochloric acid at the electrodes at different temperatures. An explanation in terms of adsorption also seems to be ruled out by the fact that the effect is of much the same relative magnitude for a wide range of hydrochloric acid concentrations.

It seems clear that the effect arises from thermal diffusion of hydrochloric acid into or out of the central portion of the cell during the period of rapid temperature change—*i.e.*, the first few minutes at the new temperature, while there are large temperature gradients between adjacent parts of the cell. The persistent nature of the resulting concentration-disturbance is at first sight surprising, though once again it is in accordance with Agar's predictions.¹ In Fig. 1 is plotted another series of measurements on cell A, which were followed this time for 24 hours before the cell contents were mixed; after this time, isothermal diffusion had only reduced the original disturbance to half its initial value, and it seems likely that at least a week would be needed to get a result correct within 0.01%, unless provision is made for thorough mixing of the cell contents as soon as temperature-equilibrium is reached. The initial disturbance is

apparently at the ends of the central tube, and diffuses away both outwards into the bulbs and inwards to the center of the cell; thus in cell A with its long central tube the effect lasts much longer than in cell B, where density-gradients would help to produce uniformity.

That the effect is so large with hydrochloric acid is due to its large Soret coefficient; with potassium chloride, the effect is still found but is smaller. Thus with 0.1 *M* KCl in cell A, the initial error found on rapidly transferring the cell from 25 to 50° was 0.09%. It is also still significant with hydrochloric acid even with the small temperature-rise from a room temperature of 22 to a 25° thermostat; here the initial error with 0.01 *N* HCl was 0.016% for cell A. Dr. J. N. Agar has pointed out to me that the sign of the observed effect is unexpected. One would expect the central tube to cool down more rapidly than the bulbs, so that in the early stages of the temperature-change hydrochloric acid should diffuse into the ends of the tube, with a consequent increase in the apparent conductance. The effect is perhaps due to differences in wall thickness, for in the region where the central tube joins the bulb the glass is certainly thinner.

It seems likely that many published conductance measurements at temperatures far removed from room temperature may have suffered from this error, for the usual criterion of temperature equilibrium is constancy of the resistance within about 0.01% over a period of an hour or two: Table I and Fig. 1 make it clear that constancy within this limit may be observed while the Soret disturbance is still present to an extent which causes several tenths of 1% error. The error would not be significant (a) where "flask cells" with attached conductivity cells are used, and the solution is passed into and out of the cell section several times between measurements; (b) where the cell temperature is changed only slowly, as will be the case if the cell is put into a thermostat at room temperature and this is then heated up to the measuring temperature, or (c) where the solution is first thermostated and then driven over into the empty cell. The ordinary form of cell used here is, however, extremely convenient to use; it is also convenient in work involving several temperatures to have a separate thermostat for each temperature and move the cell to each in succession. This can be done without Soret error provided the cell is fitted with mixing bulbs so that its contents can be mixed while it is completely immersed in the thermostat. I have recently used such cells to measure the conductance of hydrochloric acid with, I believe, an accuracy of 0.005%; the results will shortly be published. The possibility of using a conductance-cell deliberately designed to enhance the effect, for the measurement of Soret coefficients, is also being examined.

(2) T. Shedlovsky, *J. Am. Chem. Soc.*, **54**, 1411 (1932).

THE LEAD SALT-THIOUREA REACTION

By MARRINER K. NORR

U. S. Naval Ordnance Laboratory, White Oak, Silver Spring, Maryland

Received January 19, 1961

When solutions of sodium hydroxide, a lead salt and thiourea are mixed, lead sulfide gradually forms, first as a colloid and later as a precipitate. Studies of the reaction have been made by Brückmann,¹ Pick² and Whitcher,³ using lead acetate. In addition, it has been discussed by Sahasrabudhey and Krall⁴ and Kicinski.⁵ The mechanism and even the stoichiometry of the reaction have been debated. It is the purpose here to offer evidence shedding some light on the former and establishing the latter, using lead nitrate.

Experimental

Reagents.—Powdered lead sulfide was prepared by the lead nitrate-thiourea reaction. The sodium bromate was recrystallized reagent grade material, dried at 175°. Concentrated solutions of thiourea contained a small amount of insoluble impurity that was removed by filtration through a fine porosity, sintered-glass büchner funnel. All chemicals were reagent grade.

Procedures for Making Runs. Series 1,2,3.—Solutions containing sodium hydroxide (0.4–1.0 *M*), lead nitrate (0.01–0.06 *M*) and thiourea (0.1–0.4 *M*) were prepared by mixing the appropriate stock solutions in that order. In Series 1, the initial lead concentration was varied, keeping the thiourea and hydroxide ion concentrations constant; in Series 2, the initial thiourea concentration was varied; and in Series 3, the initial hydroxide ion concentration was varied. The runs were made at 23.00 ± 0.02°. The reaction was followed by periodically withdrawing samples, quenching them in excess perchloric acid to stop the reaction (final pH ca. 1.5), and analyzing them to determine the amount of hydroxide ion and lead consumed during the reaction. The lead sulfide present was removed by filtration prior to the lead determination.

Series 4.—Two solutions having the initial concentrations, 0.7 *M* NaOH, 0.035 or 0.060 *M* Pb(NO₃)₂ and 0.2 *M* (NH₂)₂CS were prepared. Periodically, samples were withdrawn, quenched in excess acetic acid, and filtered to remove the lead sulfide present. A portion of the filtrate was analyzed for lead. A second portion was analyzed for thiourea after lead had been removed as the sulfate (lead interfered with the thiourea determination).

Series 5.—Three identical solutions having the initial concentrations 0.7 *M* NaOH, 0.035 *M* Pb(NO₃)₂ 1.0 g. of powdered PbS/250 ml. of the solution, and 0.2 *M* (NH₂)₂CS were prepared. Periodically, samples were withdrawn and quenched in excess perchloric acid. The amount of hydroxide ion used up during the reaction was determined, and from this the amount of the lead remaining was calculated.

Series 6.—Four solutions having the initial concentrations, 0.6 *M* NaOH, 0.054 *M* Pb(NO₃)₂, 0, 0.50, 1.00 or 2.00 g. of powdered PbS/50 ml. of the solution and 0.3 *M* (NH₂)₂CS were prepared. Samples were withdrawn from the solutions and 5.2 min. after the beginning of the reaction they were quenched in perchloric acid. The amount of hydroxide ion used up was determined and, from this, the amount of lead remaining was calculated.

Series 7.—Two groups of solutions were prepared. In the first group (0.7 *M* NaOH, 0.035 *M* Pb(NO₃)₂, 0.2 *M* (NH₂)₂CS) half of the solutions were prepared from sodium hydroxide that had been stored for varying lengths of time in a Pyrex bottle and half from that stored similarly in a polyethylene bottle. In the second group (0.8 *M* NaOH, 0.048 *M* Pb(NO₃)₂, 0.3 *M* (NH₂)₂CS) half of the solutions were stirred for 12 min. and the other half for only 0.3 min. At a fixed time (for each group) after the beginning of the reaction, one sample was withdrawn from each run and quenched in perchloric acid. The amount of hydroxide ion used up was determined and, from this, the amount of lead remaining was calculated.

Alkaline Decomposition of Thiourea.—A 0.3 *M* thiourea–0.7 *M* sodium hydroxide solution was prepared and allowed

(1) G. Brückmann, *Kolloid-Z.*, **65**, 1 (1933).

(2) H. Pick, *Z. Physik*, **126**, 12 (1949).

(3) S. Whitcher, CML-TN-P9, Chicago Midway Laboratories, University of Chicago, Chicago, Ill., 1954.

(4) R. Sahasrabudhey and H. Krall, *J. Indian Chem. Soc.*, **21**, 63 (1944).

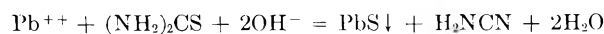
(5) F. Kicinski, *Chemistry & Industry (London)*, 54 (1948).

to stand for two hours at room temperature. It then was neutralized to the brom cresol green end-point with perchloric acid, and a solution of lead nitrate was added. No lead sulfide was formed, thus indicating that the formation of sulfide ions by the alkaline decomposition of thiourea was negligible under these conditions.

Analyses.—Hydroxide, lead⁶ and thiourea⁷ were determined by standard procedures. The hydroxide ion concentration of the samples was determined by back-titrating the excess perchloric acid quenching solution with sodium hydroxide to the brom cresol green end-point. Lead was titrated (in the presence of tartrate ions and ammonium hydroxide) with disodium ethylenediaminetetraacetate to the eriochrome black T end-point. The thiourea was treated with bromine (generated by sodium bromate, sodium bromide and hydrochloric acid), the excess bromine was removed with potassium iodide, and the iodine thus formed was determined by titration with sodium thiosulfate.

Results and Discussion

From the analytical determinations of Series 1-3, the ratio of the number of moles of hydroxide ion to the number of moles of lead consumed during the reaction was calculated. Its value was consistently a little below 2.0, but by an amount that (for most runs) was within the experimental error. The value was independent of the extent to which the reaction had proceeded. From the analyses of Series 4, the ratio of the number of moles of thiourea to the number of moles of lead consumed was calculated to be a little below 1.00 for both runs. The value was within the limits of the experimental error for the run having the lower initial lead concentration and just outside these limits for the other run. The values were independent of the extent to which the reaction had proceeded. These ratios help to confirm the following equation which had been postulated previously by several authors²⁻⁴



Brückmann,¹ Sahasrabudhey and Krall⁴ and Pick,² suggested that the reaction involved the formation and breakdown of a lead-thiourea intermediate compound, while Whitcher³ believed that it involved the formation of sulfide ions by the alkaline decomposition of thiourea. The negligible formation of sulfide ions during the two hour alkaline treatment of thiourea (see under Experimental) seems unfavorable to Whitcher's mechanism.

"Lead concentration *vs.* time" curves, drawn using the analytical data of Series 1-4, showed that the reaction rate was initially slow, then increased to a relatively constant value, and finally tapered off. The addition of lead sulfide powder to the runs of Series 5 completely removed the induction period (*i.e.*, the initial period of slow rate). In Series 6, it was found that the average rate during the first 5.2 min. was roughly proportional to the weight of the lead sulfide powder added. From these observations it was concluded that the colloidal lead sulfide formed by the reaction was acting as a surface catalyst. As the amount of lead sulfide grew, the reaction rate increased until the lowered concentrations of the reactants and/or the coagulation of the catalyst reversed the trend.

Using the "lead concentration *vs.* time" curves of the runs of Series 1-3, an attempt was made to

obtain the reaction orders from the rates at corresponding stages of the reaction and from the half times of the reaction. The orders with respect to lead, thiourea and the hydroxide ion were found to change as the reaction progressed. In addition, solutions prepared from different batches of sodium hydroxide reacted at anomalously different rates, and the reaction rates of the solutions decreased with the age of the sodium hydroxide solution from which they were prepared when the latter had been stored in Pyrex, but not when it had been stored in polyethylene (see Series 7).

In the second group of runs of Series 7, it was found that stirring decreased the average reaction rate: in the solutions stirred for 0.3 min., the reaction was 51% complete after 14.3 min., while in those stirred for 12 min., it was only 32-33% complete. The samples taken from the latter were markedly more transparent, indicating that considerably less colloidal lead sulfide was present. These results can be explained by the hypothesis that the lead sulfide formed by the reaction is acting as a surface catalyst and that stirring assists in its coagulation, thus reducing its effective surface area and therefore its catalytic effect.

Acknowledgment.—The author wishes to express thanks to Dr. Robert F. Brebrick for his helpful advice and encouragement.

THE IONIZATION CONSTANT OF HYDROXYLAMINE

By R. A. ROBINSON AND V. E. BOWER

National Bureau of Standards, Washington, D. C.

Received February 17, 1961

Although hydroxylamine has been known for nearly a century, its ionization constant is not well determined. The conductance work of Ross¹ gives pK 6.1 at 18° using his data at higher concentrations ($\sim 0.2 N$); the colorimetric measurements of Ölander² at 20° give pK 6.09 while there are three determinations at 25°; from conductance data Winkelblech³ obtained pK 5.8, the glass electrode work of Ishikawa and Aoki⁴ gave pK 6.60 but Hagiwara,^{5,6} also using the glass electrode, found pK 5.98. We now report some spectrophotometric measurements which support the results of Ölander and Hagiwara.

If a solution of hydroxylamine hydrochloride is partially neutralized by addition of sodium hydroxide so that a portion is present as the hydrochloride, S, and a portion as the free base, B, and if the solution contains also a "colored" indicator, such as 3,4-dinitrophenol, the equilibria are given by

$$pK = pH - \log (D - D_1)/(D_2 - D) - \log \gamma$$

for the indicator and

$$pK_a = pH - \log [B]/[S] + \log \gamma$$

(1) W. H. Ross, *Proc. Trans. Nova Section Inst. Sci.*, **11**, 95 (1905).

(2) A. Ölander, *Z. physik. Chem.*, **129**, 1 (1927).

(3) K. Winkelblech, *ibid.*, **36**, 546 (1901).

(4) F. Ishikawa and I. Aoki, *Bull. Soc., Inst. Phys. Chem. Res. Tokyo*, **19**, 136 (1940).

(5) H. Hagiwara, *ibid.*, **20**, 251 (1941).

(6) "Stability Constants," Part II, The Chemical Society, London, 1958, p. 51.

(6) J. L. Pinkston and C. T. Kenner, *Anal. Chem.*, **27**, 446 (1955).

(7) American Cyanamid Company, Technical Data Sheet T01-1055-02, Bound Brook, N. J. (no date).

TABLE I^a

	[S], mole/l.	[B], mole/l.	[S]/ [B]	Indicator, mole/l.	IONIZATION CONSTANTS OF HYDROXYLAMINE AT 20, 25 AND 30°					
					D_1			D_2		
					20°	25°	30°	20°	25°	30°
A	0.2834	0.1452	1.952	6.8×10^{-5} DNP	0.027	0.024	...	0.924	0.925	...
B	0.3238	0.0732	4.423	5.6×10^{-5} DNP	0.025	0.023	...	0.764	0.768	...
C	0.3430	0.1095	3.132	5.6×10^{-5} DNP	...	0.022	0.022	...	0.761	0.761
D	0.1061	0.1074	0.988	1.7×10^{-4} NCP	...	0.090	0.717	...

^a S = hydroxylamine hydrochloride, B = hydroxylamine, DNP = 3,4-dinitrophenol, NCP = 2-nitro-4-chlorophenol. The four stock solutions contained S and B at the concentrations recorded and sodium chloride at the same concentration as B; x ml. of stock were made up to 100 ml. The diluted stock contained indicator at the concentration recorded. To obtain D_1 and D_2 , solutions of the same indicator concentration were made in 0.01 *N* HCl and 0.01 *N* NaOH, respectively. The following values of D were obtained:

Series	°C.	$x \rightarrow$	5	10	15	20	25	50
A	20	0.682	0.688	0.699	0.708	0.721
	25	0.656	...	0.671	0.678	0.688	0.694	0.711
B	20	0.444	0.448	0.456	0.479
	25	0.401	...	0.420	0.430	0.438	0.442	0.461
C	25	0.458	...	0.471	0.481	0.491	0.498	0.512
	30	0.431	...	0.449	0.456	0.462	0.469	0.485
D	25	0.277	0.283	0.297

Measurements in series A, B and C were made at 400 $m\mu$ and in series D at 420 $m\mu$. The average pK_a values were:

Series	20°	25°	30°
A	6.03	5.96	...
B	6.05	5.97	...
C	...	5.95	5.84
D	...	5.93	...

where K_a is the acid ionization constant of the hydroxylammonium ion. D is the optical density of the solution, D_1 that of a solution of the same stoichiometric concentration of the phenol containing sufficient hydrochloric acid to give $pH \sim 2$ and D_2 that in a solution containing sodium hydroxide at $pH \sim 12$; γ is calculated as $-\log \gamma = A\sqrt{I}/(1 + \sqrt{I}) - 0.2I$. Hence

$$pK_a = pK - \log [B]/[S] + \log (D - D_1)/(D_2 - D) + 2 \log \gamma$$

The first term on the right already has been measured⁷ at 25°; it has been redetermined and the value of pK 5.42 confirmed. The second term is known from the composition of the solution and the third is found by spectrophotometric measurements.

Experimental

Hydroxylamine hydrochloride (Fisher's Certified Reagent) was recrystallized from aqueous ethanol and dried *in vacuo* over "Drierite." The drying was a very slow process, not complete even after six weeks when electrometric titration gave an assay of 99.8%. Measurements were made with a Beckman Model DU instrument, the cell compartment being maintained at constant temperature, $\pm 0.05^\circ$, by circulating water from a thermostat. Three series of measurements with different [B]/[S] ratios were made at 25° using 3,4-dinitrophenol as indicator and a fourth series was run with 2-nitro-4-chlorophenol as indicator. The pK of the latter has been measured recently.⁸ Details of the measurements are given in Table I. Much difficulty was experienced from the instability of the solutions and no reliable result could be obtained from a solution which was more than a few hours old; the instability was more marked with solutions of low concentration and high pH .

The ionization constants of 3,4-dinitrophenol at 20 and 30° were needed; measurements at these temperatures are reported in Table II. With these data, further spectro-

photometric measurements (Table I) gave the ionization constants of hydroxylamine at 20 and 30°.

The ionization constants of 3,4-dinitrophenol are: 20°, pK 5.46, 25°, pK 5.42; 30°, pK 5.38.

The average values for hydroxylamine are: 20°, pK_a 6.04; 25°, pK_a 5.96; 30°, pK_a 5.84.

TABLE II^a

IONIZATION CONSTANTS OF 3,4-DINITROPHENOL AT 20 AND 30°

Buffer	D	pK
20°, 400 $m\mu$, $D_1 = 0.025$, $D_2 = 0.764$		
f	0.394	5.47
g	.416	5.46
h	.440	5.44
30°, 400 $m\mu$, $D_1 = 0.022$, $D_2 = 0.761$		
f	0.427	5.38
g	.440	5.39
h	.467	5.37

^a The molarity of 3,4-dinitrophenol was 5.6×10^{-6} throughout. Buffer f, g and h were mixtures of xM sodium hydrogen succinate and xM sodium succinate where $x = 0.05$, 0.025 and 0.01, pH 5.348, 5.406 and 5.477 at 20°, pH 5.343, 5.403 and 5.474 at 30° and $-\log \gamma = 0.117$, 0.102 and 0.077 at 20° and 0.119, 0.104 and 0.078 at 30°, respectively.

A comparison of its thermodynamic properties with those of the ammonium ion⁹ gives the following data:

Hydroxylammonium ion	Ammonium ion
ΔG° 34,000	52,780 j. mole ⁻¹
ΔH° 34,000	52,200 j. mole ⁻¹
ΔS° -6 to +8	-1.87 j. deg. ⁻¹ mole ⁻¹

The basic ionization constants of hydroxylamine are: 20°, pK_b 8.13; 25°, pK_b 8.04; 30°, pK_b 7.99; so that hydroxylamine is a very much weaker base than ammonia.

(7) C. M. Judson and M. Kilpatrick, *J. Am. Chem. Soc.*, **71**, 3110 (1949); R. A. Robinson, M. M. Davis, M. Paabo and V. E. Bower, *J. Research Nat. Bur. Standards*, **64A**, 347 (1960).

(8) V. E. Bower and R. A. Robinson, *J. Phys. Chem.*, **64**, 1078 (1960).

(9) R. G. Bates and G. D. Pinching, *J. Research Nat. Bur. Standards*, **42**, 419 (1949); *J. Am. Chem. Soc.*, **72**, 1393 (1950).

Announcing . . . 1959 EDITION

American Chemical Society
DIRECTORY of
GRADUATE RESEARCH

INCLUDES: Faculties, Publications, and Doctoral Theses in Departments of Chemistry, Biochemistry, and Chemical Engineering at United States Universities.

- All institutions which offer Ph.D. in chemistry, biochemistry, or chemical engineering
 - Instructional staff of each institution
 - Research reported at each institution for past two years
 - Alphabetical index of approximately 3,000 faculty members and their affiliation; alphabetical index of 258 schools.
-

The ACS Directory of Graduate Research, prepared by the ACS Committee on Professional Training, is the only U.S. Directory of its kind. The 4th edition includes all schools and departments, known to the Committee, which are concerned primarily with chemistry, biochemistry, or chemical engineering, and which offer the Ph.D. degree.

The Directory is an excellent indication not only of research reported during the last two years by the staff members at these institutions but also of research done prior to that time. Each faculty member reports publications for 1958-59; where these have not totaled 10 papers, some articles prior to 1958 are reported. This volume fully describes the breadth of research interest of each member of the instructional staff.

Because of the indexing system, access to information is straightforward and easy—the work of a moment to find the listing you need. Invaluable to anyone interested in academic or industrial scientific research and to those responsible for counseling students about graduate research.

Compared to the 1957 edition, this new volume will contain 118 more pages, list approximately 200 additional faculty members, and include 22 additional schools.

Special Offer: Save \$2.50. Copies of the 1957 edition of the Directory, formerly \$3.50 each, may be purchased in combination with the current edition for a total price of \$5.00 for the two volumes. Possession of both copies provides continuity of reference information. Orders for 1957 editions only will be billed at the regular \$3.50 rate.

Paper bound.....752 pages.....\$4.00

ORDER FROM: Special Issues Sales

American Chemical Society
1155 - 16th Street, N.W. • Washington 6, D.C.

Announcing the second edition of . . .

THE RING INDEX

**A List of Ring Systems
Used in Organic Chemistry**

by **AUSTIN M. PATTERSON**
LEONARD T. CAPELL
DONALD F. WALKER

Until this book first appeared in 1940 there was no single source in any language where structural formulas, names and numberings of the thousands of parent organic ring systems could be found.

FEATURES

This new edition of the Ring Index lists 7727 organic ring systems—almost a hundred percent increase over the first edition. The book now has been enlarged to 1456 pages to cover the abstracted literature through 1956. Each ring system contains: (1) A structural formula showing the standard numbering system in accord with the 1957 Rules for Organic Chemistry of the IUPAC. (2) Other numberings that have appeared in the literature. (3) A serial number which identifies the system. (4) The preferred name and other names given to the system. (5) Identifying references to the original literature.

ARRANGEMENT

The ring systems are arranged from the simplest to the most complex, beginning with single rings, then systems of two rings and so on up to twenty-two ring complexes.

USES

The Ring Index is an indispensable reference work for organic chemists and for others who have to do with cyclic organic compounds. Some of its uses are: (1) Determining accepted structure of a ring system. (2) Finding name or names of the system if structure is known. (3) Finding the numbering of a system. (4) Identifying a system if there are two or more isomeric forms. (5) Discovering what systems have been reported in the literature and where. (6) Naming and numbering a newly discovered ring system. (7) As a reference book in teaching.

Cloth bound 1456 pages \$20.00

Order from

Special Issues Sales Department, American Chemical Society
1155 Sixteenth Street, N.W., Washington 6, D. C.